

**Amidate and Ureate Complexes of Nickel: Harnessing Ligand Design to Understand the
Mecha(Ni)Sm of C-H Bond Activation**

by

Douglas Dawson Beattie

BScE., Queen's University, 2014

A THESIS SUBMITTED IN PARTIAL FULFILLMENT OF
THE REQUIREMENTS FOR THE DEGREE OF

DOCTOR OF PHILOSOPHY

in

THE FACULTY OF GRADUATE AND POSTDOCTORAL STUDIES

(Chemistry)

THE UNIVERSITY OF BRITISH COLUMBIA

(Vancouver)

June 2019

© Douglas Dawson Beattie, 2019

The following individuals certify that they have read, and recommend to the Faculty of Graduate and Postdoctoral Studies for acceptance, the dissertation entitled:

Amidate and Ureate Complexes of Nickel: Harnessing Ligand Design to Understand the Mecha(Ni)Sm of C-H Bond Activation

submitted by Douglas Dawson Beattie in partial fulfillment of the requirements for

the degree of Doctor of Philosophy

in Chemistry

Examining Committee:

Prof. Laurel L. Schafer

Co-supervisor

Prof. Jennifer A. Love

Co-supervisor

Michael Fryzuk

Supervisory Committee Member

Mark MacLachlan

University Examiner

Mark Martinez

University Examiner

Additional Supervisory Committee Members:

Supervisory Committee Member

Supervisory Committee Member

Abstract

This thesis examines the use of hemi-labile amidate and ureate ligands on nickel metal centers in their (+1) and (+2) oxidation states. These 1,3-N,O-chelating ligands were studied both for their coordination chemistry on nickel and their propensity to undergo bond activations, specifically with carbon-hydrogen bonds.

In Chapter 1 we discuss the mechanisms of C-H bond activation for nickel centers of different oxidation states. We highlight important works for each oxidation state, with a focus on computational and mechanistic work. The Chapter is broken down by oxidation state.

In Chapter 2, we investigate the mechanism of Ni(II) C(sp³)-H bond activation. Using ureas as model substrates, we map the rates of C-H bond activation at Ni(II). We also characterize the nickellated products and investigate the role of additives on the rates of reaction. Comparisons to computational data from the literature are made where appropriate.

In Chapter 3 we discuss amides as ligands for low-coordinate Ni(I) organometallics. Using a variety of ligands, we show that substitution of the ligand at both the nitrogen and the carbon backbone dramatically affects the binding mode at Ni(I). We also discuss reactivity with radical species and investigate the mechanism of disproportionation of these complexes.

In Chapter 4 we discuss a new method for nickel catalyzed cyanation of aryl chlorides using a simple protocol. The reaction runs at room temperature and is among the mildest conditions to date. We show that XantPhos ligands are the best ligands to this end.

Lay Summary

Organic molecules are ubiquitous in all living things and are found in myriad commercial products. In organic molecules there are many bonds between carbon and hydrogen (C-H bonds) that are generally difficult to chemically change. Recent work has brought to light how elements in the middle of the periodic table (transition metals) can transform C-H bonds into valuable carbon-element bonds (element = oxygen, nitrogen, carbon, etc.). Such transformations are tools for product diversification in agricultural and pharmaceutical chemistry.

Work in this field uses precious metals such as palladium, rhodium, and iridium. Although effective, these metals are unsustainable (and expensive) and must be replaced with transition metals with a high earth abundance and lower CO₂ footprint.

My thesis explains how nickel, a sustainable and cheap metal, activates C-H bonds, including effects of different reaction variables. These studies inform the inorganic and organic chemical communities on the mechanism of how nickel can be used for sustainable chemical transformations.

Preface

All the work herein was completed with the support of my supervisors Prof. Jennifer A. Love, and Prof. Laurel L. Schafer. The experimental work was nearly exclusively carried about by me. However, some work was done in collaboration. Prof. Pierre Kennepohl and his group performed all EPR experiments:

Anna C. Grunwald synthesized and characterized compounds **2.1**, **2.2**, **2.5**, and **2.9** for the first time. Thibaut Perse also contributed, synthesizing and characterizing compound **2.10**. Both individuals also screened countless catalytic conditions to try to adapt the C-H activation of ureas to a catalytic variant. Eric G. Bowes completed all the DFT analysis from Chapter 3. Prof. Marcus Drover and Dr. Brian Patrick helped collect and refine some of the X-ray crystal structures in Chapter 3. Dr. Thomas Schareina synthesized, isolated, and characterized compounds **4.15b**, **4.24b**, and **4.25b** from catalytic reactions. He was also extremely helpful for discussions during my time in Germany. Dr. Nicholas Rotta-Loria synthesized pre-catalysts **4.1**, **4.3**, **4.5**, and **4.6**. Dr. Erica Lui synthesized and characterized compounds **5.1** and **5.7**. Matt Tewkesbury synthesized and characterized compounds **5.2**, **5.3**, and **5.4**.

Data in Chapter 2 was published in the *Journal of the American Chemical Society* as: **Beattie, D.D.**; Grunwald, A.C.; Perse, T.; Schafer, L.L.; Love, J.A. “Understanding Ni(II) Mediated C(sp³)-H Activation: Tertiary Ureas as Model Substrates.” *J. Am. Chem. Soc.*, **2018**, *140*, 12602-12610.

Data in Chapter 3 was published in *Angewandte Chemie International Edition* and *Organometallics* as: **Beattie, D.D.**; Bowes, E.G.; Drover, M.W.; Love, J.A.; Schafer, L.L. “Oxidation State Dependent Coordination Modes: Accessing an Amidate-Supported Nickel(I) δ -bis(C-H) Agostic Complex” *Angew. Chem. Int. Ed.* **2016**, *55*, 13290-13295.; and **Beattie, D.D.**;

Lascoumettes, G.; Kennepohl, P.; Love, J.A.; Schafer, L.L. “Disproportionation Reactions of an Organometallic Ni(I) Amidate Complex: Scope and Mechanistic Investigations” *Organometallics* **2018**, *37*, 1392-1399.

Data from Chapter 4 was published *Organic and Biomolecular Chemistry* as: **Beattie, D.D.**; Schareina, T.; Beller, M. “A Room Temperature Cyanation of (Hetero)Aromatic Chlorides by an Air Stable Nickel(II) Xantphos Precatalyst and Zn(CN)₂” *Org. Biol. Chem.* **2017**, *15*, 4291-4294.

All contributions to this and other theses during the period of **September 2014 – April 2019** are listed below by date.

1. Bowes, E.G.; **Beattie, D.D.**; Love, J.A. “The Importance of Phosphine Steric Bulk in Strained Chelate Formation” *Inorg. Chem. (ASAP)*, doi: 10.1021/acs.inorgchem.8b03514) (**PhD Work**)
2. Altus, K; Bowes, E.G.; **Beattie, D.D.**; Love, J.A. (Submitted Jan. 10, 2019) “Intermolecular Oxidative Addition of Aryl Halides to Platinum(II) Alkyl Complexes” *Submitted to Organometallics* (Manuscript ID: ja-2019-00120u) (**PhD Work**)
3. **Beattie, D.D.**; Grunwald, A.C.; Perse, T.; Schafer, L.L.; Love, J.A. Understanding Ni(II) Mediated C(sp³)-H Activation: Tertiary Ureas as Model Substrates. *J. Am. Chem. Soc.*, **2018**, *140*, 12602-12610. (Chapter 2)

4. **Beattie, D.D.**; Lascoumettes, G.; Kennepohl, P.; Love, J.A.; Schafer, L.L. “Disproportionation Reactions of an Organometallic Ni(I) Amidate Complex: Scope and Mechanistic Investigations” *Organometallics* **2018**, 37, 1392-1399. (Chapter 3)
5. **Beattie, D.D.**; Schareina, T.; Beller, M. “A Room Temperature Cyanation of (Hetero)Aromatic Chlorides by an Air Stable Nickel(II) Xantphos Precatalyst and Zn(CN)₂” *Org. Biol. Chem.* **2017**, 15, 4291-4294. (Chapter 4)
6. **Beattie, D.D.**; Bowes, E.G.; Drover, M.W.; Love, J.A.; Schafer, L.L. “Oxidation State Dependent Coordination Modes: Accessing an Amidate-Supported Nickel(I) δ -bis(C–H) Agostic Complex” *Angew. Chem. Int. Ed.* **2016**, 55, 13290-13295. (Chapter 3)

Table of Contents

Abstract.....	iii
Lay Summary	iv
Preface.....	v
Table of Contents	viii
List of Tables	xiv
List of Figures.....	xv
List of Schemes	xxvii
List of Abbreviations	xxxvi
List of Compound Numbers.....	xl
Acknowledgements	xlvi
Dedication	xlvii
Chapter 1: Introduction	1
1.1 General Introduction	1
1.2 Carbon-Hydrogen Activation.....	1
1.3 Nickel in C-H Activation Reactions	4
1.3.1 Agostic Compounds with Nickel	5
1.3.2 Mechanistic and Computational Studies of Nickel(0) in C-H Activation	7
1.3.2.1 Ni(0) Oxidative Addition Studies	7
1.3.3 Mechanistic Aspects of Ni(0) LLHT: The New Kid on the Block.....	8
1.3.4 Towards the Role of Nickel(I) in C-H Activation	12
1.3.5 Nickel(II) in C-H Activation: Concerted Metalation Deprotonation (CMD)	13
1.3.6 Mechanistic Studies of Nickel(III) and Nickel(IV) in C-H Activation	16

viii

1.3.6.1	Mirica <i>et al.</i> (April 2016).....	16
1.3.6.2	Sanford <i>et al.</i> (April 2017).....	18
1.3.6.3	Mézailles, Nebra, <i>et al.</i> (August 2017).....	20
1.4	Hemi-labile Ligands & 1,3- <i>N,O</i> -chelating Ligands.....	23
1.5	Scope of Thesis	24
Chapter 2: Understanding Ni(II) Mediated C(sp³)-H Activation: Ureas as Model Substrates		
.....		26
2.1	Introduction.....	26
2.2	Results and Discussion	30
2.2.1	Reaction Discovery	30
2.3	Reactivity of Cyclometalated (2.2-Ni).....	32
2.3.1	Validating the Relevancy of (2.2-Ni).....	32
2.3.2	Evaluation & Explanation of Side Products	33
2.4	Solvent Effects	35
2.4.1	Additive Effects	36
2.4.2	Kinetic Isotope Effects (KIEs).....	39
2.4.3	Substrates with 2° δ-C(sp ³)-H Bonds	43
2.4.4	Investigating Role of KOPiv.....	48
2.5	Catalytic Attempts	53
2.6	Conclusions.....	54
Chapter 3: Preparation of Low-Coordinate Ni(I) Amidate Complexes and Reactivity of Ni(I) Complexes Towards C(sp³)-H Activation.....		57
3.1	Introduction.....	57

3.2	Attempts to Synthesize of IPr-Ni(I)-Ureate Complexes	58
3.3	Synthesis of IPr-Ni(I)-Amidate Complexes.....	59
3.3.1	N-Dipp, C-aryl Amidate Ni(I) Complexes: N-Aryl Preferred.....	59
3.3.2	N-iPr, C-aryl Amidate Ni(I) Complexes: A Change in Binding Mode	61
3.3.3	N-iPr, C-(3°)alkyl Amidate Ni(I) Complexes: The First Ni(I) C(sp ³)-H Contacts ..	62
3.3.3.1	DFT Analysis of Structure and Bonding in Complex Ni(I)-3.5	65
3.3.4	N-iPr, C-(1,2°)alkyl Amidate Ni(I) Complexes: Linear 2-Coordinate Complexes..	66
3.4	Attempts Towards C-H Activation of Complex Ni(I)-3.5	68
3.4.1	Independent synthesis of Ni(II) C-H activated complex	69
3.4.2	Reactivity with Radical Reagents	72
3.4.2.1	Reaction with TEMPO.....	72
3.4.2.2	Reaction with Halide Reagents	76
3.4.2.3	Reaction with Gomberg's Dimer & SuperMesO.....	77
3.4.2.4	Reaction with [FeCp ₂][BAR ₄ ^F]	79
3.5	Reactivity with Lewis Basic & π-Acidic Ligands	80
3.5.1	Reaction with Phosphines and Isonitrile CNXyl	80
3.5.2	Independent Synthesis of (IPr)Ni(CNXyl) ₃	83
3.5.3	Independent Synthesis of Complex Ni(II)-(3.5) ₂	85
3.5.4	Reaction with Carbon Monoxide	87
3.5.5	Reaction with Alkenes	89
3.5.6	Mechanistic Studies	91
3.5.7	Reaction with <i>N</i> -chloroamide 3.15	92
3.5.8	Probing for Discrete Amidyl Radicals: Reactions with <i>N</i> -cyclopropyl Derivatives	93

3.5.9	Rate Law Studies	95
3.6	Additional Spectroscopic Studies of Agostic vs. Non-Agostic Complexes	96
3.6.1	EPR Spectroscopy.....	97
3.6.2	NMR Spectroscopy.....	98
3.7	Conclusions.....	101
Chapter 4: CREATE Sustainable Synthesis: Room Temperature Catalytic Cyanation of Aryl Chlorides using an Air-stable Ni(II)-XantPhos Pre-catalyst		103
4.1	Introduction.....	103
4.2	Results and Discussion	105
4.2.1	Screening of Reaction Conditions	105
4.2.2	Reaction Substrate Scope.....	107
4.2.3	Preliminary Mechanistic Investigations.....	110
4.2.3.1	Additive Effects	110
4.2.3.2	Proposal for Catalytic Cycle	110
4.3	Conclusion	112
Chapter 5: Conclusions & Future Work		113
5.1	Chapter 2: Understanding Ni(II) Mediated C(sp ³)-H Activation: Ureas as Model Substrates	113
5.1.1	Conclusions.....	113
5.1.2	Future Work & Preliminary Results – Directing Group Effects.....	115
5.1.2.1	Effect of Substituted of 8-Aminoquinolines	115
5.1.2.2	Pyridine Directing Groups	116
5.1.2.3	An Oxazoline Directing Group.....	117

5.2	Chapter 3: Preparation of Low-Coordinate Ni(I) Amidate Complexes and Reactivity of Ni(I) Complexes Towards C(sp ³)-H Activation	120
5.2.1	Conclusions.....	120
5.2.2	Future Work – Solid-State Reactions for Ni(I) C-H Activation	120
5.3	Chapter 4: CREATE Sustainable Synthesis: Room Temperature Catalytic Cyanation of Aryl Chlorides using an Air-stable Ni(II)-XantPhos Pre-catalyst	122
5.3.1	Conclusions.....	122
5.3.2	Future Work – Mechanistic Efforts	122
5.4	Summary	124
	Bibliography	125
	Appendices.....	144
	Appendix A - Experimental	144
A.1	General Considerations and Materials	144
A.2	Experimental Data for Chapter 2	146
A.3	Experimental Data for Chapter 3	210
A.4	Experimental Data for Chapter 4	262
A.5	Experimental Data for Chapter 5	272
	Appendix B Crystallographic Tables	303
B.1	Chapter 2: Understanding Ni(II) Mediated C(sp ³)-H Activation: Ureas as Model Substrates	303
B.2	Chapter 3: Preparation of Low-Coordinate Ni(I) Amidate Complexes and Reactivity of Ni(I) Complexes Towards C(sp ³)-H Activation	306
	Appendix C DFT Analysis.....	314

C.1	Chapter 3: Preparation of Low-Coordinate Ni(I) Amidate Complexes and Reactivity of Ni(I) Complexes Towards C(sp ³)-H Activation	314
-----	---	-----

List of Tables

Table 2.1 Effect of solvent on initial rates of formation of complex (2.2-Ni) ^a	36
Table 3.1 Distances and Angles of Agostic Complexes Ni(I)-3.4, Ni(I)-3.5, Ni(I)-3.6, and Ni(I)-3.8. *denotes value outside the accepted literature ranges.	65
Table 4.1 Ni-catalyzed cyanation of 2,4-dimethyl-chlorobenzene ^a	106

List of Figures

Figure 2.1 ORTEP depiction of the solid-state structure of complex (2.2-Ni) (ellipsoids at 50% probability, hydrogens and solvent omitted). Selected bond lengths (Å) and angles (°): C1-Ni1 1.923(2), N2-Ni1 1.855(2), N3-Ni1 1.972(2), C2-O1 1.238(3), C1-Ni1-N3 166.5(1), N1-C1-Ni1 109.8(2).....	32
Figure 3.1 (a) DFT-optimized structure of Ni(I)-3.5 (b) AIM contour map of the electron density in the Ni1-H1-C30 plane of Ni(I)-3.5 showing bcps as grey dots and bond paths as black lines.	66
Figure 3.2 ORTEP depiction of the solid-state structure of Ni(II)-3.12A (ellipsoids at 50% probability, hydrogens and solvent omitted). Selected average bond lengths (Å) and angles (°): Ni(1)-C(30) 1.921(3), C(30)-O(1) 1.266(6), C(30)-N(1) 1.323(6), C(30)-Ni(1)-Cl(1) 173.60(1).	71
Figure 3.3 Preliminary isotropic ORTEP depiction of the solid-state structure of Ni(II)-3.5-TEMPO(E) (ellipsoids at 50% probability, hydrogens omitted). Poor structure: geometry and connectivity only.....	74
Figure 3.4 VT ¹ H NMR spectra (400MHz, d ⁸ -tol, 223K) for the reaction shown in Scheme 3.10 performed at (a) 273K, and (b) below 223K, in a glovebox cold-well. The ¹³ C shift for the amide carbon is shown.	75
Figure 3.5 ORTEP depiction of the solid-state structure of Ni(I)-3.5-CNXyl (ellipsoids at 50% probability, hydrogens, second molecule of Ni(I)-3.5-CNXyl, solvent, and NHC(iPr) groups omitted) Selected bond lengths (Å) and angles (°): Ni1-Ni1 1.952(5), Ni1-C36 1.856(6), C36-N4 1.168(7), C1-Ni1-C36 105.1(2), C1-Ni1-N1 147.3(2).	82
Figure 3.6 ORTEP depiction of the solid-state structure of complex (IPr)Ni(CNXyl) ₃ (ellipsoids at 50% probability, hydrogens omitted). Selected bond lengths (Å) and angles (°): avg. N _(1,2,3) -	

C _(25,34,43) 1.18390(6), avg. Ni-C _(25,34,43) 1.82188(8), Ni-C1 1.96671(11), avg. C1-Ni-C _(25,34,43) 113.1678(30).....	84
Figure 3.7 cwEPR spectrum of complex Ni(I)-3.5-CO (-196 °C, toluene glass).	89
Figure 3.8 cwEPR spectrum of complexes Ni(I)-3.5 and Ni(I)-3.10 (8 K, toluene glass).	97
Figure 3.9 cwEPR spectrum of complexes Ni(I)-3.6 and Ni(I)-3.9 (8 K, toluene glass).	98
Figure 3.10 Variable temperature ¹ H NMR (400 MHz, C ₇ D ₈) of Ni(I)-3.6 and Ni(I)-3.7	100
Figure 5.1 ORTEP depiction of bis(benzoyleneureate)Ni(II) complex Ni-(5.7) ₂ . (ellipsoids at 50% probability, hydrogens and solvent omitted). Selected bond lengths (Å): C1-N2 1.3516, C1-O2 1.2383, N2-Ni1 1.9027.	119
Figure A.2.2. ¹ H NMR spectrum of (2.2-Ni) (400 MHz, d ₆ -DMSO, 298K). The ¹ H{ ³¹ P} NMR spectrum is shown in the inset.	157
Figure A.2.3. Stacked ¹ H NMR spectrum of (a) (2.2-Ni, denoted (\$)), and (b) compound (2.2); (400 MHz, d ₆ -DMSO, 298K).....	158
Figure A.2.4. ¹ H COSY NMR spectrum of (2.2-Ni) (400 MHz, d ₆ -DMSO, 298K)	158
Figure A.2.5. ¹ H COSY NMR spectrum (expanded) of (2.2-Ni) (400 MHz, d ₆ -DMSO, 298K)	159
Figure A.2.6. ¹ H COSY NMR spectrum (expanded) of (2.2-Ni) (400 MHz, d ₆ -DMSO, 298K)	159
Figure A.2.7. ¹ H NOESY NMR spectrum (expanded) of (2.2-Ni) (400 MHz, d ₆ -DMSO, 298K)	160
Figure A.2.8. ³¹ P{ ¹ H} NMR spectrum of (2.2-Ni) (162 MHz, d ₆ -DMSO, 298K)	160
Figure A.2.9. ¹ H- ³¹ P (HMBC) NMR spectrum of (2.2-Ni) (400 MHz, d ₆ -DMSO, 298K).....	161
Figure A.2.10. ¹³ C- ¹ H (HSQC-edited) NMR spectrum (expanded) of (2.2-Ni) (400 MHz, d ₆ -DMSO, 298K).....	161

Figure A.2.11. ^{13}C - ^1H (HSQC-edited) NMR spectrum (expanded) of (2.2-Ni) (400 MHz, d_6 -DMSO, 298K)	162
Figure A.2.12. ^{13}C - ^1H (HMBC) NMR spectrum (expanded) of (2.2-Ni) (400 MHz, d_6 -DMSO, 298K)	162
Figure A.2.13. ^{13}C - ^1H (HMBC) NMR spectrum (expanded) of (2.2-Ni) (400 MHz, d_6 -DMSO, 298K)	163
Figure A.2.14. $^{13}\text{C}\{^1\text{H}\}$ NMR spectrum of (2.2-Ni) (101 MHz, d_6 -DMSO, 298K)	163
Figure A.2.15. In situ ^1H NMR spectrum of (2.10) and (2.10-Ni) (400 MHz, d_6 -DMSO, 298K). The $^1\text{H}\{^{31}\text{P}\}$ NMR spectrum is shown in the inset.	164
Figure A.2.16. Stacked ^1H NMR spectrum of (a) in situ reaction mixture containing (2.10, denoted *) and (2.10-Ni, denoted \$), and (b) isolated compound (2.10); (400 MHz, d_6 -DMSO, 298K).	165
Figure A.2.17. In situ (expanded) ^1H COSY NMR spectrum of (2.10) and (2.10-Ni) (400 MHz, d_6 -DMSO, 298K)	165
Figure A.2.18. In situ ^1H COSY NMR spectrum of (2.10) and (2.10-Ni) (400 MHz, d_6 -DMSO, 298K)	166
Figure A.2.19. In situ $^{31}\text{P}\{^1\text{H}\}$ NMR spectrum of (2.10) and (2.10-Ni) (162 MHz, d_6 -DMSO, 298K)	166
Figure A.2.20. In situ ^1H - ^{31}P (HMBC) NMR spectrum of (2.10) and (2.10-Ni) (400 MHz, d_6 -DMSO, 298K)	167
Figure A.2.21. In situ ^{13}C - ^1H (HSQC-edited) NMR spectrum of (2.10), (2.10-Ni) (400 MHz, d_6 -DMSO, 298K)	167

Figure A.2.22. In situ ^{13}C - ^1H (HSQC) NMR spectrum of (2.10) and (2.10-Ni) (400 MHz, d_6 -DMSO, 298K).....	168
Figure A.2.23. In situ ^{13}C - ^1H (HMBC) NMR spectrum of (2.10) and (2.10-Ni) (400 MHz, d_6 -DMSO, 298K).....	168
Figure A.2.24. In situ ^1H NMR spectrum of (2.18) and (2.18-Ni) (400 MHz, d_6 -DMSO, 298K). The $^1\text{H}\{^{31}\text{P}\}$ NMR spectrum is shown in the inset.	169
Figure A.2.25. Stacked ^1H NMR spectrum of (a) in situ reaction mixture containing (2.18, denoted *) and (2.18-Ni, denoted \$), and (b) isolated compound (2.18); (400 MHz, d_6 -DMSO, 298K).	170
Figure A.2.26. In situ (expanded) ^1H COSY NMR spectrum of (2.18) and (2.18-Ni) (400 MHz, d_6 -DMSO, 298K).	170
Figure A.2.27. In situ ^1H COSY NMR spectrum of (2.18) and (2.18-Ni) (400 MHz, d_6 -DMSO, 298K)	171
Figure A.2.28. In situ $^{31}\text{P}\{^1\text{H}\}$ NMR spectrum of (2.18) and (2.18-Ni) (162 MHz, d_6 -DMSO, 298K).	171
Figure A.2.29. In situ ^{13}C - ^1H (HSQC-edited) NMR spectrum of (2.18), (2.18-Ni) (400 MHz, d_6 -DMSO, 298K).....	172
Figure A.2.30. In situ ^{13}C - ^1H (HSQC-edited) NMR spectrum of (2.18), (2.18-Ni) (400 MHz, d_6 -DMSO, 298K).....	172
Figure A.2.31. In situ ^{13}C - ^1H (HMBC) NMR spectrum of (2.18) and (2.18-Ni) (400 MHz, d_6 -DMSO, 298K).....	173
Figure A.2.32. In situ ^1H NMR spectra showing reaction progress of (2.2) converting to (2.2-Ni) (400 MHz, d_6 -DMSO, 298K).....	175

Figure A.2.33. Kinetic profile for conversion of (2.2) to (2.2-Ni) in d ₆ -DMSO over time (M/min).	176
Figure A.2.34. For (i) acid additives, 2.0 molar equivalents K ₂ CO ₃ , (ii) potassium salts, 1.75 molar equivalents K ₂ CO ₃ . <u>Legend</u> : ○ No additive, or K ₂ CO ₃ , ▲ K ₂ CO ₃ added (no additive); ● 2,4,6-trimethylbenzoic acid additive; ◆ 2,6-bis(trifluoromethyl)benzoic acid additive; ■ KO ₂ Piv additive.	177
Figure A.2.35. Kinetic profile for conversion of (2.2) to (2.2-Ni) over time (M/min).	178
Figure A.2.36. Kinetic profile for conversion of (2.10) to (2.10-Ni) over time (M/min).	178
Figure A.2.37. Kinetic profiles for conversion of (2.18) to (2.18-Ni) over time (M/min).	179
Figure A.2.38. [(PEt ₃)Ni(μ-OPiv) ₂] ₂ ; <i>paramagnetic</i> ¹ H NMR (400 MHz, C ₆ D ₆ , 298K)	181
Figure A.2.39. ¹ H NMR (300 MHz, d ₆ -DMSO, 298K)	182
Figure A.2.40. ¹ H paramagnetic NMR (300 MHz, d ₆ -DMSO, 298K).	182
Figure A.2.41. ¹ H NMR (300 MHz, d ₆ -DMSO, 298K)	182
Figure A.2.42. ¹ H NMR (300 MHz, C ₆ D ₆ , 298K)	183
Figure A.2.43. ¹ H paramagnetic NMR (300 MHz, C ₆ D ₆ , 298K).	183
Figure A.2.44. ³¹ P{ ¹ H} NMR (300 MHz, C ₆ D ₆ , 298K)	183
Figure A.2.45. ¹ H NMR (300 & 400 MHz, d ₆ -DMSO, 298K)	185
Figure A.2.46. paramagnetic ¹ H NMR (top spectrum 300 MHz, bottom spectrum 400 MHz, d ₆ -DMSO, 298K)	186
Figure A.2.47. ¹ H NMR of compound 2.8 from independent synthesis and from isolation.	189
Figure A.2.48. Compound (2.2); ¹ H NMR (400 MHz, CDCl ₃ , 298K).	192
Figure A.2.49. Compound (2.2); ¹³ C{ ¹ H} NMR (101 MHz, CDCl ₃ , 298K)	193
Figure A.2.50. Compound (2.3); ¹ H NMR (400 MHz, CDCl ₃ , 298K)	194

Figure A.2.51. Compound (2.3); $^{13}\text{C}\{^1\text{H}\}$ NMR (101 MHz, CDCl_3 , 298K)	195
Figure A.2.52. Compound (2.7); ^1H NMR (300 MHz, CDCl_3 , 298K)	196
Figure A.2.53. Compound (2.7); $^{13}\text{C}\{^1\text{H}\}$ NMR (75 MHz, CDCl_3 , 298K)	197
Figure A.2.54. Compound (2.8); ^1H NMR (300 MHz, CDCl_3 , 298K)	198
Figure A.2.55. Compound (2.10); ^1H NMR (300 MHz, CDCl_3 , 298K)	199
Figure A.2.56. Compound (2.10); $^{13}\text{C}\{^1\text{H}\}$ NMR (75 MHz, CDCl_3 , 298K)	200
Figure A.2.57. Compound (2.18); ^1H NMR (300 MHz, CDCl_3 , 298K)	201
Figure A.2.58. Compound (2.18); $^{13}\text{C}\{^1\text{H}\}$ NMR (101 MHz, CDCl_3 , 298K)	202
Figure A.2.59. Compound (2.21); ^1H NMR (400 MHz, CDCl_3 , 298K)	203
Figure A.2.60. Compound (2.21); $^{13}\text{C}\{^1\text{H}\}$ NMR (101 MHz, CDCl_3 , 298K)	204
Figure A.2.61. Compound (2.22); ^1H NMR (300 MHz, CDCl_3 , 298K)	205
Figure A.2.62. Compound (2.22); $^{13}\text{C}\{^1\text{H}\}$ NMR (75 MHz, CDCl_3 , 298K)	206
Figure A.2.63. Compound (2.2-Ni); ^1H NMR (400 MHz, $d_8\text{-tol}$, 298K)	207
Figure A.2.64. Compound (2.2-Ni); $^{31}\text{P}\{^1\text{H}\}$ NMR (162 MHz, $d_8\text{-tol}$, 298K)	208
Figure A.3.65. Example of ^1H NMR spectra (C_6D_6 , 400MHz, 298K) for kinetic run: Experiment (a) $[\text{I}_{\text{initial}}] = 0.02\text{M}$, $[\text{styrene}_{\text{initial}}] = 0.04\text{M}$, $[\text{TMB}] = 0.007\text{M}$	236
Figure A.3.66. Kinetic data for experiments (a)-(d). See description above for experimental procedure.....	237
Figure A.3.67. Plot of olefin equivalents vs rate of reaction. Error bars for each rate were determined through regression analysis of the raw data for duplicated runs.....	237
Figure A.3.68. Raw kinetic data for experiments (w)-(z). See description above for experimental procedure.....	238

Figure A.3.69. Plot of initial nickel concentration [Ni(I)-3.5] vs. rate of reaction. Error bars for each rate were determined through regression analysis of the raw data for duplicated runs.....	238
Figure A.3.70. ^1H NMR (400 MHz, 25°C, C_6D_6) of amide 3.12.	241
Figure A.3.71. ^1H NMR (300 MHz, 25°C, C_7D_8) of amide 3.12.	242
Figure A.3.72. ^{13}C NMR (101 MHz, 25°C, C_6D_6) of amide 3.12.	242
Figure A.3.73. ^1H NMR (400 MHz, 25°C, C_6D_6) of Ni(I)-3.2.....	243
Figure A.3.74. ^1H NMR (400 MHz, 25°C, C_6D_6) of Ni(I)-3.3.....	243
Figure A.3.75. ^1H NMR (400 MHz, 25°C, C_6D_6) of Ni(I)-3.4.....	244
Figure A.3.76. ^1H NMR (400 MHz, 25°C, C_6D_6) of Ni(I)-3.6.....	244
Figure A.3.77. ^1H NMR (400 MHz, 25°C, C_6D_6) of Ni(I)-3.7.....	245
Figure A.3.78. ^1H NMR (400 MHz, 25°C, C_6D_6) of Ni(I)-3.9.....	245
Figure A.3.79. ^1H NMR (400 MHz, 25°C, C_6D_6) of Ni(I)-3.11.....	246
Figure A.3.80. ^1H NMR (400 MHz, 25°C, C_6D_6) of Ni(II)-3.12A.....	246
Figure A.3.81. ^{13}C NMR (101 MHz, 25°C, C_6D_6) of Ni(II)-3.12A.	247
Figure A.3.82. ^1H - ^1H COSY NMR (400 MHz, 25°C, C_6D_6) of Ni(II)-3.12A.	247
Figure A.3.83. ^1H - ^{13}C HMBC NMR (400 MHz, 25°C, C_6D_6) of Ni(II)-3.12A.	248
Figure A.3.84. ^1H - ^{13}C HSQC NMR (400 MHz, 25°C, C_6D_6) of Ni(II)-3.12A.	248
Figure A.3.85. ^1H - ^{15}N HSQC NMR (400 MHz, 25°C, C_6D_6) of Ni(II)-3.12A.	249
Figure A.3.86. Variable temperature ^1H NMR (400 MHz, 25°C, C_6D_6) of Ni(II)-3.12A.....	250
Figure A.3.87. Variable temperature ^1H NMR (400 MHz, 25°C, C_6D_6) of Ni(II)-3.12A.....	251
Figure A.3.88. ^1H NMR (400 MHz, 25°C, C_6D_6) of Ni(II)-3.12B.....	252
Figure A.3.89. ^{13}C NMR (101 MHz, 25°C, C_6D_6) of Ni(II)-3.12B.....	252
Figure A.3.90. ^1H - ^{13}C HMBC NMR (400 MHz, 25°C, C_6D_6) of Ni(II)-3.12B.	253

Figure A.3.91. ^1H - ^{13}C HSQC NMR (400 MHz, 25°C, C_6D_6) of Ni(II)-3.12B.	253
Figure A.3.92. ^1H NMR (400 MHz, 25°C, C_6D_6) of Ni(II)-3.5-TEMPO(E/Z)	254
Figure A.3.93. ^1H NMR (400 MHz, 25°C, C_6D_6) of Ni(II)-3.5-TEMPO(E/Z/K)	254
Figure A.3.94. ^1H - ^1H NOESY NMR (400 MHz, 25°C, C_6D_6) of Ni(II)-3.5-TEMPO(E/Z)	255
Figure A.3.95. ^1H - ^1H NOESY NMR (400 MHz, 25°C, C_6D_6) of Ni(II)-3.5-TEMPO(E/Z)	255
Figure A.3.96. ^1H - ^{13}C HMBC NMR (400 MHz, 25°C, C_6D_6) of Ni(II)-3.5-TEMPO(E/Z)	256
Figure A.3.97. ^1H NMR (400 MHz, 25°C, C_6D_6) of Ni(II)-3.1-TEMPO	256
Figure A.3.98. $^{13}\text{C}\{^1\text{H}\}$ NMR (101 MHz, 25°C, C_6D_6) of Ni(II)-3.1-TEMPO	257
Figure A.3.99. ^1H - ^{13}C HMBC NMR (400 MHz, 25°C, C_6D_6) of Ni(II)-3.1-TEMPO	257
Figure A.3.100. ^1H NMR (300 MHz, 25°C, C_7D_8) of [Ni(II)-3.5-pyr][BAr4F].	258
Figure A.3.101. $^{11}\text{B}\{^1\text{H}\}$ NMR (96 MHz, 25°C, C_7D_8) of [Ni(II)-3.5-pyr][BAr4F].	258
Figure A.3.102. $^{19}\text{F}\{^1\text{H}\}$ NMR (282 MHz, 25°C, C_7D_8) of [Ni(II)-3.5-pyr][BAr4F].	259
Figure A.3.103. ^1H - ^1H COSY NMR (300 MHz, 25°C, C_7D_8) of [Ni(II)-3.5-pyr][BAr4F].	259
Figure A.3.104. ^1H - ^{13}C HSQC NMR (300 MHz, 25°C, C_7D_8) of [Ni(II)-3.5-pyr][BAr4F].	260
Figure A.3.105. ^1H - ^{13}C HMBC NMR (300 MHz, 25°C, C_7D_8) of [Ni(II)-3.5-pyr][BAr4F].	260
Figure A.3.106. ^1H NMR (400 MHz, 25°C, C_6D_6) of 3.15.	261
Figure A.3.107. ^{13}C NMR (101 MHz, 25°C, C_6D_6) of 3.15.	261
Figure A.4.108. ^1H NMR spectrum (300MHz, C_6D_6 , 298K) of complex 4.1.	267
Figure A.4.109. $^{31}\text{P}\{^1\text{H}\}$ NMR spectrum (121.5MHz, C_6D_6 , 298K) of complex 4.1.	267
Figure A.4.110. ^1H NMR spectrum (300 MHz, CDCl_3) of compound (4.8b)	268
Figure A.4.111. ^1H NMR spectrum (300 MHz, CDCl_3) of compound (4.19b)	269
Figure A.4.112. $^{13}\text{C}\{^1\text{H}\}$ NMR spectrum (75 MHz, CDCl_3) of compound (4.19b)	269
Figure A.4.113. $^{19}\text{F}\{^1\text{H}\}$ NMR spectrum (282 MHz, CDCl_3) of compound (4.19b)	270

Figure A.4.114. ^1H NMR spectrum (400 MHz, CDCl_3) spectrum of compound (4.21b)	270
Figure A.4.115. $^{13}\text{C}\{^1\text{H}\}$ NMR spectrum (101 MHz, CDCl_3) spectrum of compound (4.21b) .	271
Figure A.5.116. In situ ^1H NMR spectrum of (5.1) and (5.1-Ni) (400 MHz, $\text{d}_6\text{-DMSO}$, 298K).	278
Figure A.5.117. Stacked ^1H NMR spectrum of (a) in situ reaction mixture containing (5.1, denoted *) and (5.1-Ni, denoted \$), and (b) isolated compound (5.1); (400 MHz, $\text{d}_6\text{-DMSO}$, 298K).	279
Figure A.5.118. In situ $^{31}\text{P}\{^1\text{H}\}$ NMR spectrum of (5.1) and (5.1-Ni) (162 MHz, $\text{d}_6\text{-DMSO}$, 298K)	279
Figure A.5.119. In situ $^{13}\text{C}\text{-}^1\text{H}$ (HSQC-edited) NMR spectrum of (5.1) & (5.1-Ni) (400 MHz, $\text{d}_6\text{-DMSO}$, 298K).....	280
Figure A.5.120. In situ $^{13}\text{C}\text{-}^1\text{H}$ (HMBC) NMR spectrum of (5.1) and (5.1-Ni) (400 MHz, $\text{d}_6\text{-DMSO}$, 298K).....	280
Figure A.5.121. In situ ^1H NMR spectrum of (5.2) and (5.2-Ni) (400 MHz, $\text{d}_6\text{-DMSO}$, 298K).	281
Figure A.5.122. Stacked ^1H NMR spectrum of (a) in situ reaction mixture containing (5.2, denoted *) and (5.2-Ni, denoted \$), and (b) isolated compound (5.2); (400 MHz, $\text{d}_6\text{-DMSO}$, 298K).	282
Figure A.5.123. In situ $^{31}\text{P}\{^1\text{H}\}$ NMR spectrum of (5.2) and (5.2-Ni) (162 MHz, $\text{d}_6\text{-DMSO}$, 298K)	282
Figure A.5.124. In situ $^{13}\text{C}\text{-}^1\text{H}$ (HSQC-edited) NMR spectrum of (5.2) & (5.2-Ni) (400 MHz, $\text{d}_6\text{-DMSO}$, 298K).....	283

Figure A.5.125. In situ ^{13}C - ^1H (HMBC) NMR spectrum of (5.2) and (5.2-Ni) (400 MHz, d ₆ -DMSO, 298K).....	283
Figure A.5.126. In situ ^1H NMR spectrum of (5.3) and (5.3-Ni) (400 MHz, d ₆ -DMSO, 298K).	284
Figure A.5.127. Stacked ^1H NMR spectrum of (a) in situ reaction mixture containing (5.3, denoted *) and (5.3-Ni, denoted \$), and (b) isolated compound (5.3); (400 MHz, d ₆ -DMSO, 298K).	285
Figure A.5.128. In situ ^{13}C - ^1H (HSQC-edited) NMR spectrum of (5.3) & (5.3-Ni) (400 MHz, d ₆ -DMSO, 298K).....	285
Figure A.5.129. In situ ^{13}C - ^1H (HMBC) NMR spectrum of (5.3) and (5.3-Ni) (400 MHz, d ₆ -DMSO, 298K).....	286
Figure A.5.130. In situ ^1H NMR spectrum of (5.4) and (5.4-Ni) (400 MHz, d ₆ -DMSO, 298K).	287
Figure A.5.131. Stacked ^1H NMR spectrum of (a) in situ reaction mixture containing (5.4, denoted *) and (5.4-Ni, denoted \$), and (b) isolated compound (5.4); (400 MHz, d ₆ -DMSO, 298K).	288
Figure A.5.132. In situ ^{13}C - ^1H (HSQC-edited) NMR spectrum of (5.4) & (5.4-Ni) (400 MHz, d ₆ -DMSO, 298K).....	288
Figure A.5.133. In situ ^{13}C - ^1H (HMBC) NMR spectrum of (5.4) and (5.4-Ni) (400 MHz, d ₆ -DMSO, 298K).....	289
Figure A.5.134. In situ ^1H NMR spectrum of (5.6) and (5.6-Ni) (400 MHz, d ₆ -DMSO, 298K).	290

Figure A.5.135. Stacked ^1H NMR spectrum of (a) in situ reaction mixture containing (5.6, denoted *) and (5.6-Ni, denoted \$), and (b) isolated compound (5.6); (400 MHz, d_6 -DMSO, 298K).	291
Figure A.5.136. In situ paramagnetic ^1H NMR spectrum of (5.6) and (5.6-Ni) (400 MHz, d_6 -DMSO, 298K).	291
Figure A.5.137. In situ (expanded) ^1H -COSY NMR spectrum of (5.6) and (5.6-Ni) (300 MHz, d_6 -DMSO, 298K).	292
Figure A.5.138. In situ $^{31}\text{P}\{^1\text{H}\}$ NMR spectrum of (5.6) and (5.6-Ni) (162 MHz, d_6 -DMSO, 298K)	292
Figure A.5.139. In situ ^{31}P - ^1H HMBC NMR spectrum of (5.6) and (5.6-Ni) (162 MHz, d_6 -DMSO, 298K).	293
Figure A.5.140. In situ ^{13}C - ^1H (HSQC-edited) NMR spectrum of (5.6) and (5.6-Ni) (400 MHz, d_6 -DMSO, 298K)	293
Figure A.5.141. In situ ^{13}C - ^1H (HMBC) NMR spectrum of (5.6) and (5.6-Ni) (400 MHz, d_6 -DMSO, 298K).	294
Figure A.5.142 ^1H NMR (400 MHz, CDCl_3 , 298K) of 5.1	295
Figure A.5.143 ^{13}C NMR (101 MHz, CDCl_3 , 298K) of 5.1	295
Figure A.5.144 ^1H NMR (400 MHz, CDCl_3 , 298K) of 5.2	296
Figure A.5.145 ^{13}C NMR (101 MHz, CDCl_3 , 298K) of 5.2	296
Figure A.5.146 ^1H NMR (400 MHz, CDCl_3 , 298K) of 5.3	297
Figure A.5.147 ^{13}C NMR (101 MHz, CDCl_3 , 298K) of 5.3	297
Figure A.5.148 ^1H NMR (400 MHz, CDCl_3 , 298K) of 5.4	298
Figure A.5.149 ^{13}C NMR (101 MHz, CDCl_3 , 298K) of 5.4	298

Figure A.5.150 ^{19}F NMR (282 MHz, CDCl_3 , 298K) of 5.4	299
Figure A.5.151 ^1H NMR (400 MHz, CDCl_3 , 298K) of 5.5	299
Figure A.5.152 ^{13}C NMR (101 MHz, CDCl_3 , 298K) of 5.5	300
Figure A.5.153 ^1H NMR (400 MHz, CDCl_3 , 298K) of 5.6	300
Figure A.5.154 ^{13}C NMR (101 MHz, CDCl_3 , 298K) of 5.6	301
Figure A.5.155 ^1H NMR (400 MHz, CDCl_3 , 298K) of 5.7	301
Figure A.5.156 ^{13}C NMR (101 MHz, CDCl_3 , 298K) of 5.7	302
Figure B.1.157. ORTEP depiction of the solid-state structure of compound (2.2) (ellipsoids at 50% probability, hydrogens omitted). Selected bond lengths (\AA) and angles ($^\circ$): N1-C2 1.36153(7), C2-N2 1.38376(8), C2-O1 1.23146(10), C1-N1-C2 122.693(5), N1-C2-N2 114.660(6).....	303
Figure B.2.158. ORTEP depiction of the solid-state structure of Ni(II)-3.8-Cl (ellipsoids at 50% probability, hydrogens omitted). Selected bond lengths (\AA) and angles ($^\circ$): Ni1-C1 2.1779(7), Ni1-N1 1.942(2), Ni1-C28 2.322(3), C28-N1 1.301(3), C28-O1 1.311(3), N1-Ni1-C1 163.39(10), O1-Ni1-C11 171.21(5), O1-Ni1-N1 68.42(8).....	307
Figure B.2.159. ORTEP depiction of the solid-state structure of (Λ)- Ni(II)-(3.8) $_2$ (ellipsoids at 50% probability, hydrogens omitted).	308

List of Schemes

Scheme 1.1 The ideal C-H functionalization: a mild, selective, atom economic catalytic method.	3
Scheme 1.2 Examples of general mechanisms of C-H activation, modified from literature. ^[27,28]	4
Scheme 1.3 (a) Classifications of anagostic, H-bond, preagostic, and agostic complexes for d ⁸ -ML ₄ group 10 complexes – adapted from Scherer. ^[52] (b) Ni compounds with M ^{···} (E-H) interactions, prepared in the research groups of Hillhouse, ^[63,75] Spencer, ^[61] and Scherer. ^[51]	7
Scheme 1.4 Examples of oxidative addition of C-H bonds from Ni(0) complexes. ^[76,77,79,80]	8
Scheme 1.5 (a) Original report of hydroarylation of alkynes which was hypothesized to proceed through an oxidative addition mechanism. ^[83] (b) The seminal report of LLHT by Eisenstein and Perutz, showing that LLHT was more favorable in the hydroarylation of alkynes. ^[18] (c) A report by Sakaki and Eisenstein probing why zero valent group 10 metals prefer different mechanisms for C-H activation in isoelectronic systems. ^[81]	11
Scheme 1.6 A Ni(I) biaryl complex was postulated to undergo C-H activation through Ni(I). ^[70,89]	12
Scheme 1.7 Simplified scheme of concerted metalation deprotonation (CMD), modified from Fagnou et al. ^[25]	14
Scheme 1.8 Example of well-understood Ni(II) mediated C-H activation by a CMD mechanism (derived computationally): nickel(II) mediated C(sp ³)-H functionalization of 8AQ substituted amides. ^[126,130,131]	15
Scheme 1.9 The first report of high valent nickel's role in C-H activation by Mirica <i>et al.</i> ^[133]	18
Scheme 1.10 Report by Sanford <i>et al.</i> on Ni(IV) in C-H activation reactions. ^[132]	20
Scheme 1.11 Synthesis of Ni(II), Ni(III), and Ni(IV) fluoride complexes ligated to simple pyridine ligands. ^[134]	21

Scheme 1.12 The reaction of Ni(IV) (1.40) with 1,2-dichlorobenzene results in C-H activation and trifluoromethylation. The authors propose the Ni(III) (1.43 or [1.43] ₂) complexes are also proficient at this trifluoromethylation reaction. ^[134]	22
Scheme 1.13 A proposed comproportionation-disproportionation equilibrium between the Ni(II)-Ni(IV) and Ni(III) complexes may be responsible for the lowered reaction rates in the second kinetic regime.....	23
Scheme 1.14 Binding modes of amidate ligands to nickel. ^[144–153]	24
Scheme 2.1 (a) General scheme of nickel catalysis of amides bearing 8-aminoquinoline (8AQ) directing group; ^[28–58]	27
Scheme 2.2 Computationally derived mechanism of nickel(II) mediated C(sp ³)-H functionalization of 8AQ substituted amides. ^[62,63]	28
Scheme 2.3 Ureas as substrates for α-(C-H) functionalization of nitrogenous compounds; ^[156,157]	29
Scheme 2.4 A study of nickel(II) mediated C(sp ³)-H activation of ureas as models for amides.	29
Scheme 2.5 Synthesis of Ni(II) ureate 2.2-Ni by C(sp ³)-H activation of urea 2.2.	30
Scheme 2.6 Reactivity of complex (2.2-Ni) with a variety of coupling partners. Reactions in DMSO, yields are isolated; for reaction conditions, see appendix A.2 (¹ H NMR spectroscopic yields, Q = quinolin-8-yl).	33
Scheme 2.7 NMR Scale reaction of (2.2-Ni) with an alkyl electrophile. The demethylated product (2.7) is shown to the right.	34
Scheme 2.8 (a) Effect of additives: ^[166] For (i) acid additives, 2.0 molar equivalents K ₂ CO ₃ added, (ii) potassium salts, 1.75 molar equivalents K ₂ CO ₃ added. ^[171] <u>Legend:</u> ○ No additive, or K ₂ CO ₃ , □ KO ₂ Piv added (No K ₂ CO ₃), ▲ K ₂ CO ₃ added (no additive); ● 1-adamantyl carboxylic	

acid additive; ♦ KOAc additive; ■ KOPiv additive. (b) ● sum of (□ + ▲ + ○), combined traces from (a) showing that K ₂ CO ₃ and KOPiv work synergistically.	38
Scheme 2.9 Kinetic isotope effects for intra- and intermolecular C(sp ³)-H bond activation in ureas.	40
Scheme 2.10 Probing protonation of the Ni-C bond in (2.2-Ni) with (a) deuterated urea (2.2-d ₃), (b) an anilinium salt, and (c) 1-adamantyl carboxylic acid.	42
Scheme 2.11 Model validation, using ureas (2.2) and (2.10) for measuring the relative rates of C(sp ³)-H activation. Computational data based on the 8AQ-amide system. ^[130]	44
Scheme 2.12 Relative reaction rates for C-H activation of ureas (2.2, 2.5, 2.10, 2.12-2.20) to nickel products (2.2-Ni, 2.5-Ni, 2.10-Ni, (2.12-2.20)-Ni). ^[166]	46
Scheme 2.13 Hammett Plot showing rates of δ-C(sp ³)-H activation of <i>p</i> -benzyl substituted ureas (2.5, 2.12-2.16). ^[166]	47
Scheme 2.14 Attempts to use secondary ureas for nickel C-H activation studies.	48
Scheme 2.15 (a) Synthesis of [(PEt ₃)Ni(μ-OPiv) ₂] ₂ by two methods, and (b) ORTEP depiction of the solid-state structure of complex [(PEt ₃)Ni(μ-OPiv) ₂] ₂ (ellipsoids at 50% probability, hydrogens omitted). Selected bond lengths (Å) and angles (°): Ni-Ni 2.5875(3), O1-Ni1-P1 96.60(3).	49
Scheme 2.16 ¹ H paramagnetic NMR spectra for different reactions outlined in the general reaction scheme, and a table showing the reaction contents for reactions (I-VI, d ₆ -DMSO, 400 MHz, 298 K).	51
Scheme 2.17 Probing reactivity of (2.23) with nickel complex [(PEt ₃)Ni(μ-OPiv) ₂] ₂	52
Scheme 2.18 ESI-MS results (low resolution) for in situ generated complex (2.2-Ni-int).	53

Scheme 2.19 Attempts to functionalize urea 2.2 catalytically with a variety of cross-coupling partners.....	54
Scheme 2.20 Proposed mechanism for the Ni(II) mediated δ -C(sp ³)-H activation of substituted ureas.	55
Scheme 3.1 Retrosynthetic analysis for the preparation of Ni(I) ureate agostic complexes.	58
Scheme 3.2 Attempts to react Sigman's Dimer with ureate ligands.....	58
Scheme 3.3 (a) Accessing complexes Ni(I)-3.1, Ni(I)-3.2, and Ni(I)-3.3 from Sigman's Dimer by salt metathesis with Na(3.1-3.3). (b) ORTEP depiction of the solid-state structure of Ni(I)-3.1 ellipsoids at 50% probability, hydrogens omitted). Selected bond lengths (Å) and angles (°): Ni1-C33 2.195(2), Ni1-C34 2.166(2), Ni1-O1 1.9633(18), C33-C34 1.429(4), N1-C28 1.306(3), O1-C38 1.295(3), C1-Ni1-C33 171.82(9), C1-Ni1-C34 141.93(10), C1-Ni1-O1 107.90(8). (c) isotropic ORTEP depiction of the solid-state structure of Ni(I)-3.2. <i>Poor quality structure</i> . (d) ORTEP depiction of the solid-state structure of Ni(I)-3.3. Selected bond lengths (Å) and angles (°): Ni1-C37 2.1245(14), Ni1-O1 1.9937(11), N1-C28 1.2978(19), O1-C28 1.2936(18), C1-Ni1-C37 171.51(6), C1-Ni1-O1 109.44(6).	60
Scheme 3.4 Similar binding modes of Ni(I) NHC species in the literature, reported by Tatsumi ^[189] and Hillhouse. ^[188]	61
Scheme 3.5 (a) Accessing complex Ni(I)-3.4 from Sigman's Dimer by salt metathesis with Na(3.4). (b) Front view: ORTEP depiction of the solid-state structure of Ni(I)-3.4, disordered over two positions (ellipsoids at 50% probability, hydrogens and Dipp(iPr) groups omitted). Selected bond lengths (Å) and angles (°) averaged over both structures: Ni1-N1 1.920(18), N1-C28 1.33(3), O1-C28 1.26(2), C1-Ni1-N1 172.6(7). (c) Side view: ORTEP depiction of the solid-state structure of Ni(I)-3.4, disordered over two positions (ellipsoids at 50% probability,	

hydrogens and Dipp(iPr) groups omitted). Selected bond length (Å) averaged over both structures: Ni1-H4/8 (calc) 2.01(2)..... 62

Scheme 3.6 (a) Accessing complexes Ni(I)-3.5, Ni(I)-3.6, and Ni(I)-3.8 from Sigman's Dimer by salt metathesis with Na(3.5-3.8). (b) ORTEP depiction of the solid-state structure of Ni(I)-3.5 (ellipsoids at 50% probability, hydrogens omitted). H1 and H2 were freely located and refined from the electron density map. Selected bond lengths (Å) and angles (°): Ni1-C1 1.9119(9), Ni1-N1 1.9149(8), Ni1-C30 2.4476(10), Ni1-H1 2.024(15), Ni-H2 2.159(15), C28-N1 1.3392(13), C28-O1 1.2515(12), N1-Ni1-C1 172.12(4), C30-H1-Ni1 101.8(10), C30-H2-Ni1 94.3(10). (c) ORTEP depiction of the solid-state structure of Ni(I)-3.6. H1 and H2 were freely located and refined from the electron density map. Selected bond lengths (Å) and angles (°): Ni1-C1 1.89350(19), Ni1-N1 1.89980(19), Ni1-C30 2.4007(2), Ni1-H1 1.94(2), Ni-H2 2.15(2), C28-N1 1.33028(11), C28-O1 1.25036(12), N1-Ni1-C1 171.0550(12), C30-H1-Ni1 106.18(3), C30-H2-Ni1 92.60(8). (d) ORTEP depiction of the solid-state structure of Ni(I)-3.8. H1 and H2 were freely located and refined from the electron density map. Selected bond lengths (Å) and angles (°): Ni1-C1 1.89571(11), Ni1-N1 1.89054(9), Ni1-C30 2.5668(16), Ni1-H1 2.07(5), Ni1-H2 2.35(4), C28-N1 1.3417(19), C28-O1 1.247(2), N1-Ni1-C1 167.7872(7), C30-H1-Ni1 109.61(9), C30-H2-Ni1 91.32(9)..... 64

Scheme 3.7 (a) Accessing complexes Ni(I)-3.9, Ni(I)-3.10, and Ni(I)-3.11 from Sigman's Dimer by salt metathesis with Na(3.9-3.11). (b) ORTEP depiction of the solid-state structure of Ni(I)-3.9 (ellipsoids at 50% probability, hydrogens omitted). Selected bond lengths (Å) and angles (°): Ni1-N1 1.8871(12), N1-C28 1.3439(19), O1-C28 1.2496(18), H1-Ni1 2.53(2), C1-Ni1-N1 1.77.62(6). (c) ORTEP depiction of the solid-state structure of Ni(I)-3.10. Selected bond lengths (Å) and angles (°): Ni1-N1 1.85(2), N1-C28 1.381(19), O1-C28 1.255(13), H1-Ni1(calc) 2.295,

C1-Ni1-N1 169.0(5). (d) isotropic ORTEP depiction of the solid-state structure of Ni(I)-3.11.	
<i>Poor quality structure.</i>	68
Scheme 3.8 (a) Proposed synthesis of Ni(II)-3.12B via C-H activation by PCET from complex Ni(I)-3.5, (b) independent synthesis of complex Ni(II)-3.12B from complexes 3.14 and Ni(II)-3.12A.....	70
Scheme 3.9 Comparing chemical shifts of selected peaks in ^1H and ^{13}C NMR spectra of complex $\text{C}^{[206]}$ and Ni(II)-3.12B.	72
Scheme 3.10 Reaction of complex Ni(I)-3.5 with TEMPO to produce Ni(II)-3.5-TEMPO(E/Z/K). The ^{13}C shifts for the amidate carbons are shown.	73
Scheme 3.11 Reaction of complex Ni(I)-3.1 with TEMPO to produce Ni(II)-3.1-TEMPO(E). The ^{13}C shift for the amidate carbon is shown.	76
Scheme 3.12 (a) Reaction of Ni(I)-3.5 and Ni(I)-3.1 with radical reagents produces Ni(II)-3.5-X (X = Cl, I) and Ni(II)-3.5-Cl. These reactions are reversible in the presence of Na/Hg. ORTEP depictions (ellipsoids at 50% probability, hydrogens omitted selected bond lengths (Å) and angles (°)) of the solid-state structures of (b) Ni(II)-3.1-Cl: Ni1-Cl1 2.1563(4), Ni1-O1 1.9134(10), Ni1-N1 1.9215(12), C1-Ni1-N1 167.89(5), N1-Ni1-O1 68.48(5). (c) Ni(II)-3.1-Cl: - Ni1-Cl1 2.1600(6), Ni1-O1 1.9206(15), Ni1-N1 1.9280(17), C1-Ni1-N1 171.04(8), N1-Ni1-O1 68.58(7).....	78
Scheme 3.13 Reactivity of Ni(I)-3.5 with the trityl radical ($\text{Ph}_3\text{C}\cdot$) and SuperMesO \cdot phenoxyl radical.....	79
Scheme 3.14 Reactivity of Ni(I)-3.5 with the oxidant $[\text{FeCp}_2][\text{BAr}_4^{\text{F}}]$ in the presence of pyridine.	80

Scheme 3.15 Synthesis of complexes (IPr)Ni(CNXyl) ₃ and Ni(II)-(3.5) ₂ from complexes Ni(I)-3.5 and Ni(I)-3.5-CNXyl by coordination of CNXyl.	82
Scheme 3.16 Independent synthesis of (IPr)Ni(CNXyl) ₃ from Ni(COD) ₂ by subsequent addition of IPr (1 eq.) and CNXyl (3 eq.).	84
Scheme 3.17 (a) Independent synthesis of Ni(II)-(3.5) ₂ by salt elimination from [5]. (b) ORTEP depiction of the solid-state structure of (Λ)-Ni(II)-(3.5) ₂ (ellipsoids at 50% probability, hydrogens and solvent omitted). Selected (avg.) bond lengths (Å) and (avg.) angles (°): N(1,2)-C(1,2) 1.310(2), O(1,2)-C(1,2) 1.292(2), O(1)-Ni-O(2) 159.07(5), N(1,2)-Ni-O(1,2) 63.27(5) (c) VT paramagnetic ¹ H NMR spec. (400 MHz, d ₈ -tol) of complex Ni(II)-(3.5) ₂ at selected temperatures from 25°C to -81°C.	86
Scheme 3.18 Reaction of Ni(I)-3.5 with CO _(g) in the solution state produces (IPr)Ni(CO) ₃ and Ni(II)-(3.5) ₂ . The solid-state reaction proceeds through proposed intermediate Ni(I)-3.5-CO on way to (IPr)Ni(CO) ₃ and Ni(II)-(3.5) ₂ . ^a Complex Ni(I)-3.5 makes up the mass balance for this reaction.....	87
Scheme 3.19 Reaction of mono- and dialkenes with complex Ni(I)-3.5 produces complexes (IPr)Ni(CC) ₂ and Ni(II)-(3.5) ₂ with heating at 70°C	90
Scheme 3.20 Proposed Mechanism: Biomolecular electron transfer via nickel mediated amidyl transfer.	92
Scheme 3.21 Testing reaction of Ni(I)-3.5 with <i>N</i> -chloro- <i>N</i> -isopropylpivalamide 3.15.....	93
Scheme 3.22. (a) Ring-opening of an <i>N</i> -cyclopropyl amidyl radical, ^[227,228] (b) Complexes Ni(I)-3.8, Ni(I)-3.8-CNXyl, and Ni(II)-(3.8) ₂ ^[229] and (c) reaction of Ni(I)-3.8-CNXyl with CNXyl produces complexes (IPr)Ni(CNXyl) ₃ and Ni(II)-(3.8) ₂ . ^[230]	94

Scheme 3.23. Complexes which were investigated for solution structure. These are sets of agostic/non-agostic Ni(I) complexes synthesized in the previous sections.	96
Scheme 4.1 Examples of pharmaceuticals with Ar-CN moieties.	103
Scheme 4.2 Typical methods for the formation of aryl nitriles (a) Rosenmund-von Braun, and (b) palladium catalyzed methods, in this case a report by Buchwald et al. ^[241]	104
Scheme 4.3 Synthesis of Ni(II) diphosphine pre-catalysts 4.1-4.7. ^[254]	105
Scheme 4.4 Scope of nickel-catalyzed cyanation of aryl chlorides Isolated yields (average of two runs). Reaction conditions: aryl chloride (1.0 mmol), NMP (2.5 mL, 0.4 M), 24 h. ^b Approximate conversions of starting material are shown based on GC analysis). No rigorous quantitative analysis was completed.	109
Scheme 4.5 Additive effects to probe reaction mechanism of this nickel catalyzed method.	110
Scheme 4.6 (a) Activation of pre-catalyst (1a) and (b) mechanistic proposals.	111
Scheme 5.1 Proposed mechanism for the Ni(II) mediated δ -C(sp ³)-H activation of substituted ureas; as shown in Chapter 2.	114
Scheme 5.2 Hammett plot showing rates of δ -C(sp ³)-H activation of 8AQ-substituted ureas. ^[166]	116
Scheme 5.3 Investigating pyridyl directing groups for δ -C(sp ³)-H activation of ureas.	117
Scheme 5.4 Reaction of the oxazoline containing urea 5.7 with nickel, resulting in the rearrangement to a N-substituted benzoyleneureate Ni(II) complex Ni-(5.7) ₂ . The proposed mechanism is also shown.	119
Scheme 5.5 Proposed reaction of Ni(I)-3.5 with radical H-abstrating agents under ball mill conditions.	121

Scheme 5.6 (a) Hypothesis 1: Probing the rates of transmetalation of Ni(II) chloride and bromide salts. (b) Hypothesis 2: Probing the product ratio of nickel species upon oxidation of Ni(0) by aryl halides.	123
---	-----

List of Abbreviations

Å	angstrom (10^{-10} m)
AIM	atoms in molecules
Ar	aryl
Bn	benzyl
Boc	tert-butoxycarbonyl
Cal	calorie
COD	cyclooctadiene
conv.	Conversion
Cy	cyclohexyl
d	doublet
D	deuterium
δ	chemical shift
DCM	dichloromethane
DFT	density functional theory
ΔG^\ddagger	Gibbs free energy of activation
DMA	<i>N,N</i> -dimethylacetamide
DME	1,2-dimethoxyethane
DMF	<i>N,N</i> -dimethylformamide
DMSO	dimethylsulfoxide
EI	electron impact
equiv.	equivalents

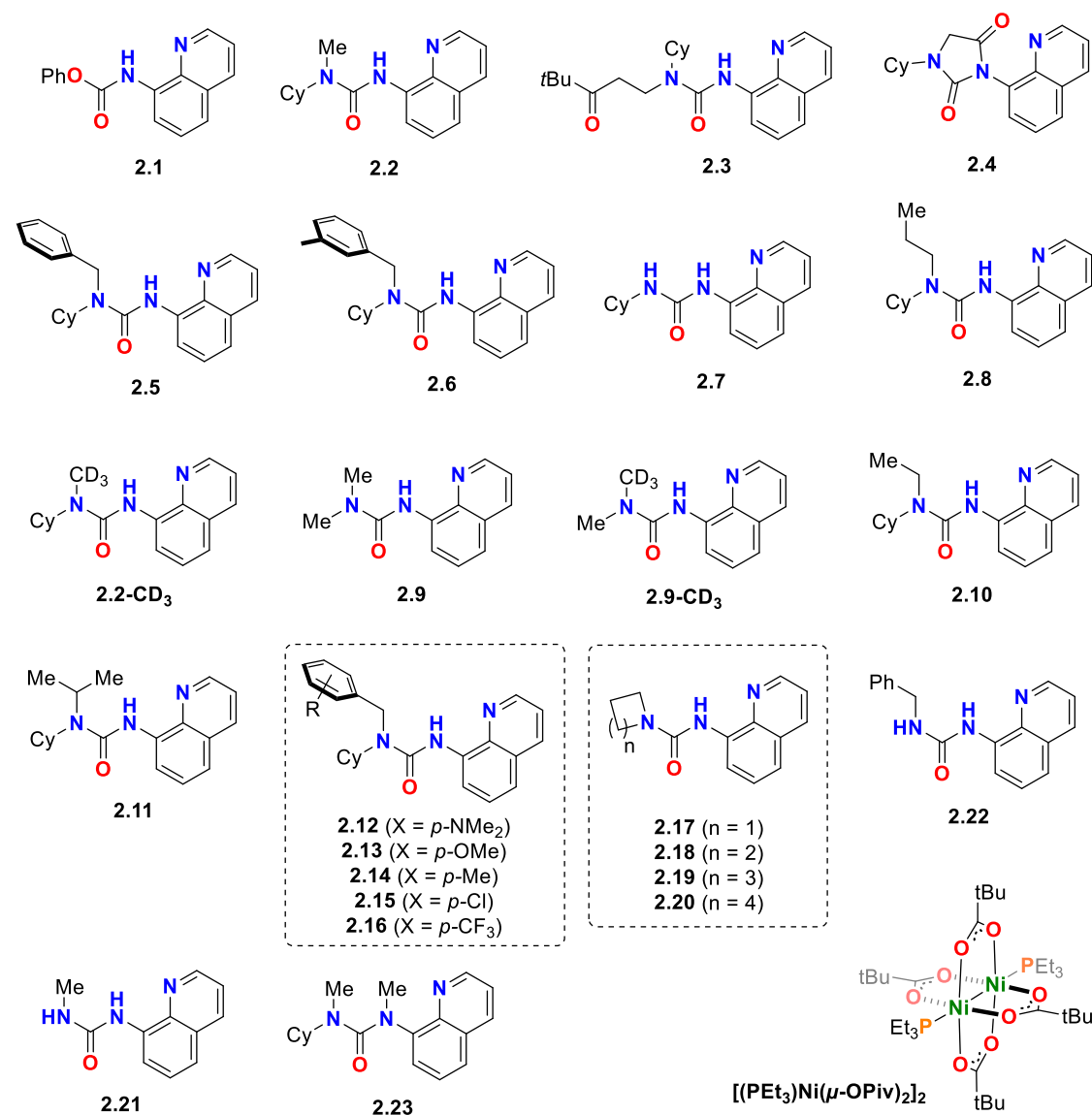
ESI	electrospray ionization
Et	ethyl
FGI	functional group interconversion
<i>gem</i>	geminal
HSAB	hard-soft acid-base
HMDS	hexamethyldisilazane
HRMS	high resolution mass spectroscopy
IMes	1,3-bis(2,4,6-trimethylphenyl)imidazol-2-ylidene
iPr	isopropyl
IPr	1,3-bis(2,6-diisopropylphenyl)imidazol-2-ylidene
IR	infrared
$^nJ_{X,Y}$	coupling constant between atoms X and Y, n bonds away
K_{eq}	equilibrium constant
KIE	kinetic isotope effect
k_n	rate constant
L	generic supporting ligand (neutral)
m	multiplet
<i>m</i>	meta
M	metal
M^+	molecular ion
μ	bridging ligand
Me	methyl
Mes	mesityl (2,4,6-trimethylphenyl)

MS	mass spectroscopy
m/z	mass-to-charge ratio
<i>o</i>	ortho
<i>p</i>	para
ν	frequency
NBO	natural bonding orbital
NMR	nuclear magnetic resonance spectroscopy
NBD	2,5-norbornadiene
NMP	<i>N</i> -methylpyrrolidone
ORTEP	Oak Ridge thermal ellipsoid plot
Ph	phenyl
ppm	parts per million
precat.	pre-catalyst
Py/py/pyr	pyridine
q	quartet
R	organic substituent
Reflns	reflections
Rpm	rotations per minute
r.t.	room temperature
s	singlet
sept.	septet
t	triplet
tBu	<i>tert</i> -butyl

tol	toluene
TEMPO	(2,2,6,6-tetramethylpiperidin-1-yl)oxyl
TFA	trifluoroacetic acid
THF	tetrahydrofuran
Ts	para-toluenesulfonyl (tosyl)

List of Compound Numbers

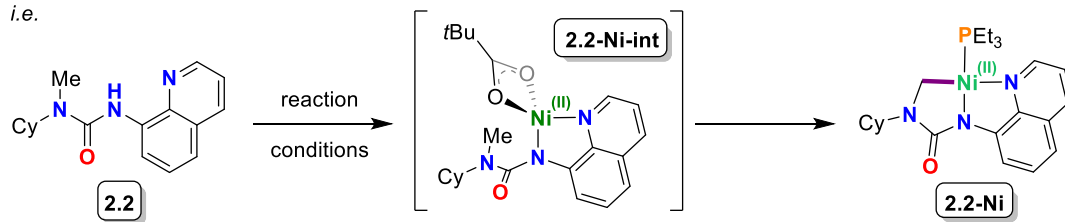
Chapter 2:



Nickel Compounds are numbered as below:

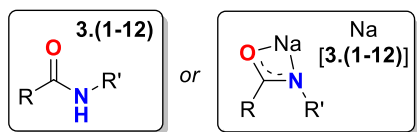
Proligand (**2.2**), intermediate N-H activated product (**2.2-Ni-int**) nickel compound (**2.2-Ni**)

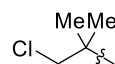
i.e.

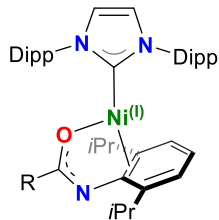


Chapter 3:

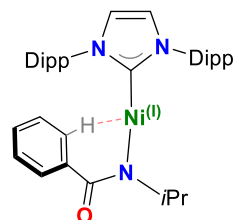
Amide Legend:



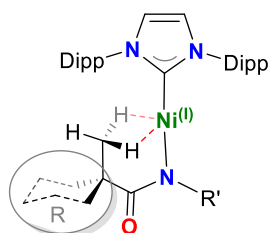
R	R'	Amide
<i>t</i> Bu	Dipp	3.1
Ph	Dipp	3.2
3,5-(CF ₃)Ph	Dipp	3.3
Ph	<i>i</i> Pr	3.4
<i>t</i> Bu	<i>i</i> Pr	3.5
(Me)Cy	<i>i</i> Pr	3.6
(CD ₃)Cy	<i>i</i> Pr	3.7
<i>t</i> Bu	cyclopropyl	3.8
Cy	<i>i</i> Pr	3.9
<i>i</i> Pr	<i>i</i> Pr	3.10
Et	<i>i</i> Pr	3.11
	<i>i</i> Pr	3.12

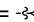


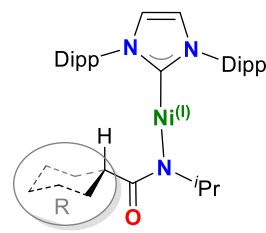
R = *t*Bu, **Ni(I)-3.1**
 R = Ph, **Ni(I)-3.2**
 R = 3,5-(CF₃)Ph, **Ni(I)-3.3**



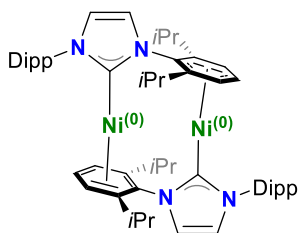
Ni(I)-3.4



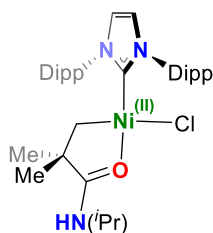
R' = *i*Pr, R = *t*Bu, **Ni(I)-3.5**
 R' = *i*Pr, R = MeCy, **Ni(I)-3.6**
 R' = , R = *t*Bu, **Ni(I)-3.8**



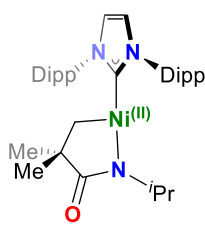
R = Cy, **Ni(I)-3.9**
 R = *i*Pr, **Ni(I)-3.10**
 R = Et, **Ni(I)-3.11**



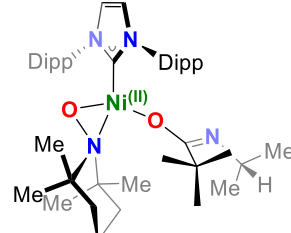
[(IPr)Ni]₂



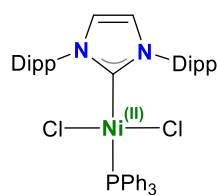
Ni(II)-3.12A



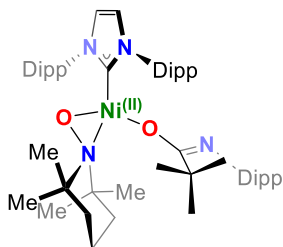
Ni(II)-3.12B



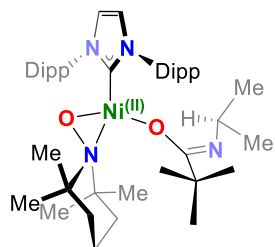
Ni(II)-3.5-TEMPO(E)



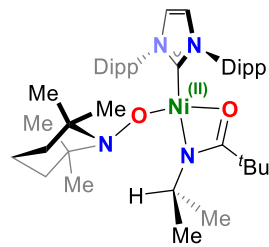
(IPr)NiCl₂PPh₃



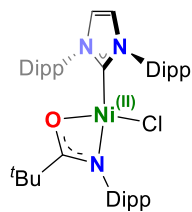
Ni(II)-3.1-TEMPO(E)



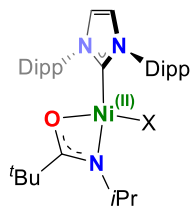
Ni(II)-3.5-TEMPO(Z)



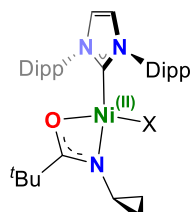
Ni(II)-3.5-TEMPO(K)



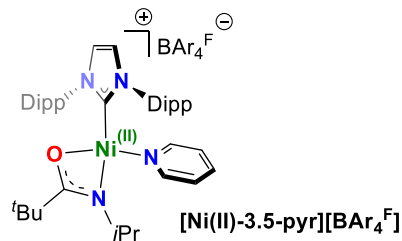
Ni(II)-3.1-Cl



Ni(II)-3.5-Cl/I



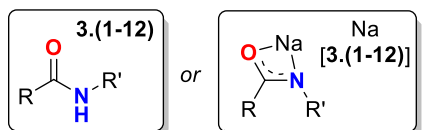
Ni(II)-3.8-Cl



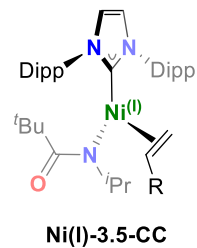
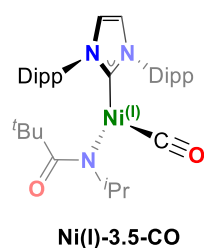
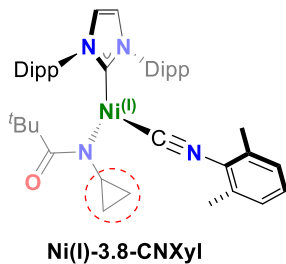
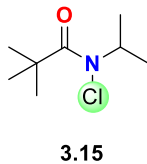
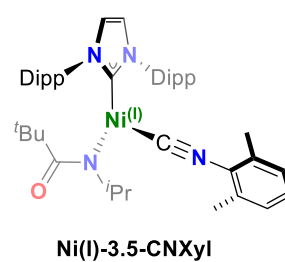
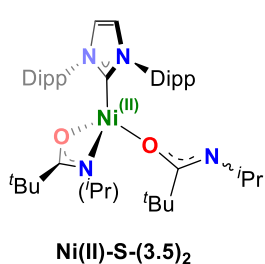
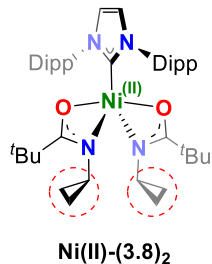
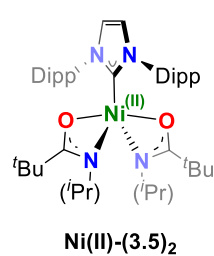
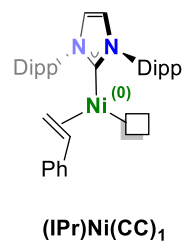
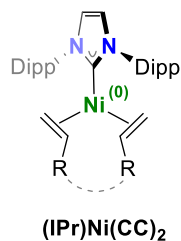
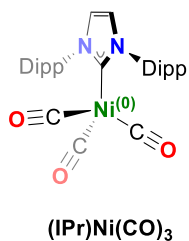
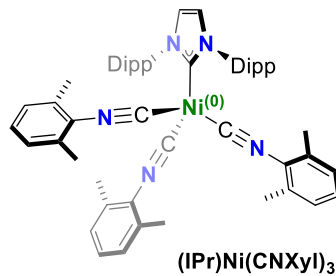
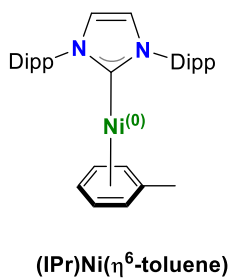
[Ni(II)-3.5-pyr][BAR₄F]

Chapter 3 continued...

Amide Legend:

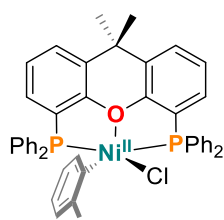


R	R'	Amide
<i>t</i> Bu	Dipp	3.1
Ph	Dipp	3.2
3,5-(CF ₃)Ph	Dipp	3.3
Ph	<i>i</i> Pr	3.4
<i>t</i> Bu	<i>i</i> Pr	3.5
(Me)Cy	<i>i</i> Pr	3.6
(CD ₃)Cy	<i>i</i> Pr	3.7
<i>t</i> Bu	cyclopropyl	3.8
Cy	<i>i</i> Pr	3.9
<i>i</i> Pr	<i>i</i> Pr	3.10
Et	<i>i</i> Pr	3.11
	<i>i</i> Pr	3.12

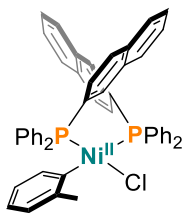


Chapter 4:

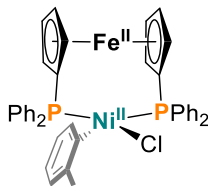
Nickel Pre-catalysts



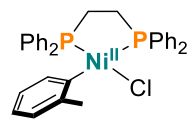
4.1
(XantPhos)



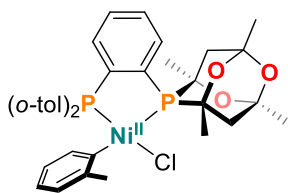
4.2
(BINAP)



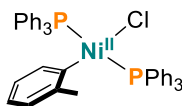
4.3
(dppf)



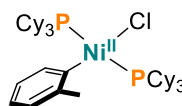
4.4
(dppe)



4.5
(PAd-DalPhos)

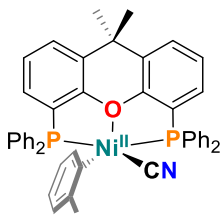


4.6
(PPh₃)

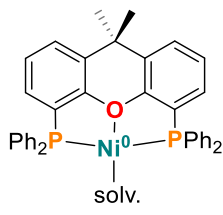


4.7
(PCy₃)

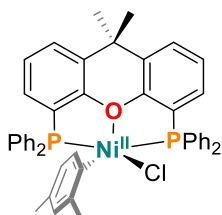
Nickel Intermediates (Proposed)



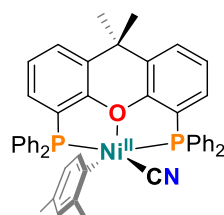
4.48



4.49



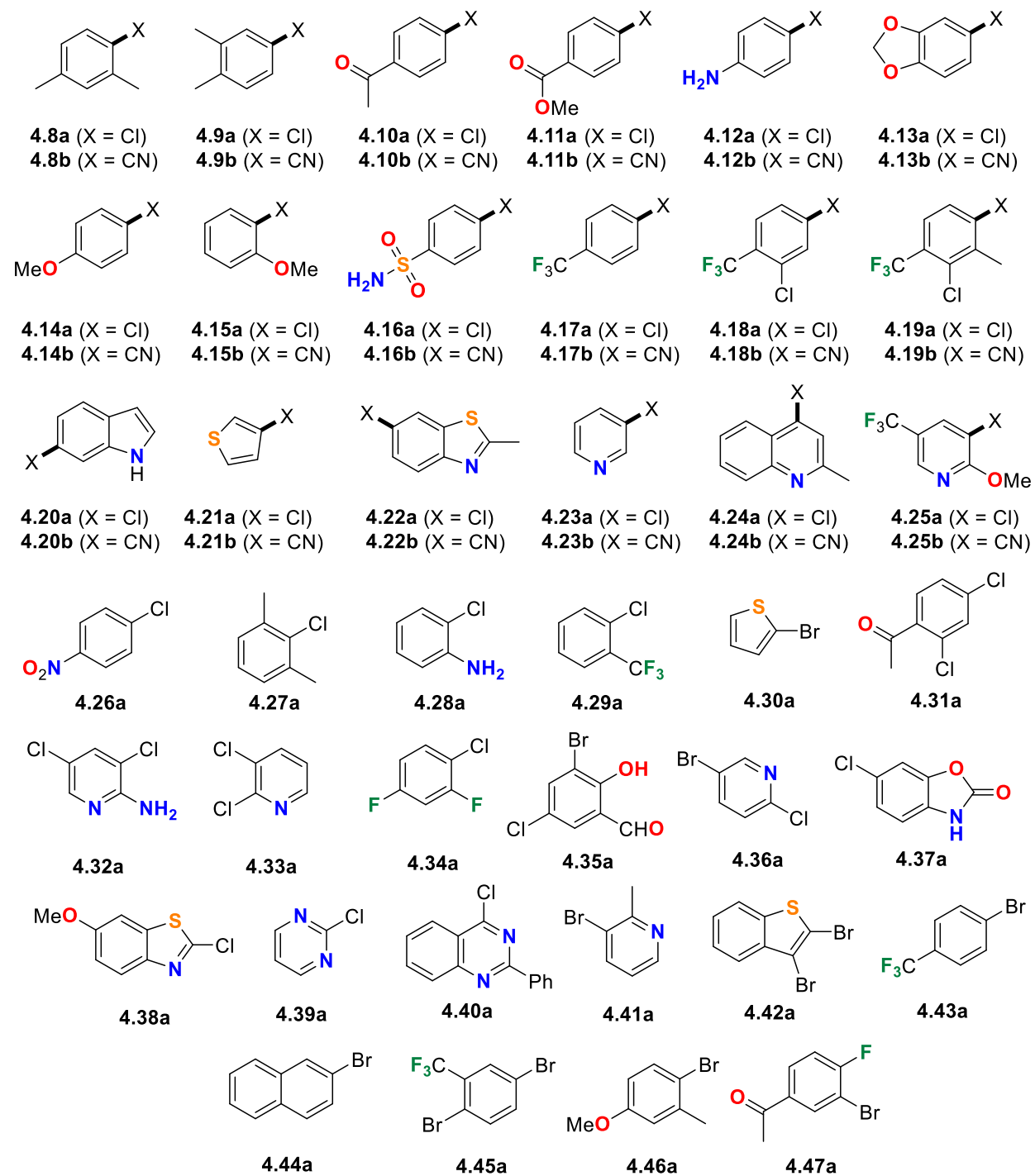
4.50



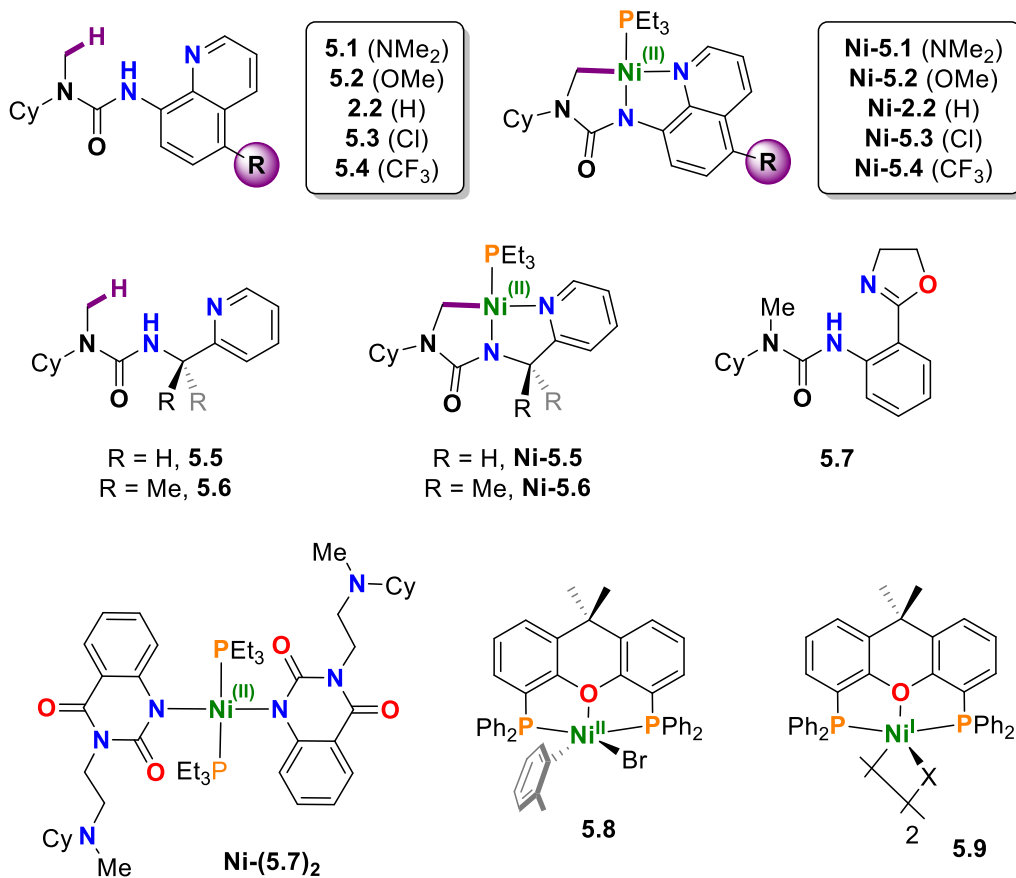
4.51

Chapter 4 continued...

Substrates (a) & Products (b)



Chapter 5:



Acknowledgements

First, I want to thank my supervisors, Prof. Laurel Schafer and Prof. Jennifer Love, who worked with me tirelessly to put together the science in this thesis. Jen, you put the ‘super’ back into supervisor: thanks for constantly having our backs and never, NEVER let those puns die! Laurel, I’ll never forget all the couch sessions and just talking about science. You two have done so much for me: I’ll miss you both!

To my committee, Profs. Perrin, Hudson, and Fryzuk, we did it! Thank-you for your time looking through documents and supporting me when I had questions or just needed to talk to someone in the department.

Thank-you to all my lab colleagues in both labs for being available to bounce ideas around. I’m especially grateful to Marcus Drover, Eric Bowes, Addison Desnoyer, Jason Brandt, Weiling Chiu, and Kris Altus for fielding my endless questions

Special thanks are owed to my parents and my family in Ontario, whose have supported me throughout my years of education, both morally and financially.

I would like to thank NSERC and UBC for funding my PhD here at UBC, without you I would not have been able to do the science within this thesis.

*This thesis is dedicated to Hope Kerby
for being a lighthouse of encouragement
during this doctoral degree.*

Without you, none of this would have been possible.

Chapter 1: Introduction

1.1 General Introduction

This thesis explores the coordination chemistry of anionic urea and amide ligands bound to nickel metal centers in the 1+ and 2+ oxidation states. These ureate and amidate nickel complexes are used as models in understanding nuances in the mechanisms of carbon-hydrogen (C-H) activation mediated by nickel. We anticipate our discoveries will inform the organic and inorganic chemistry communities of important considerations when designing catalytic cycles based on homogeneous catalysis using nickel. This thesis also describes a simple catalytic approach to the synthesis of benzonitriles using nickel catalysts in cross-coupling technology.

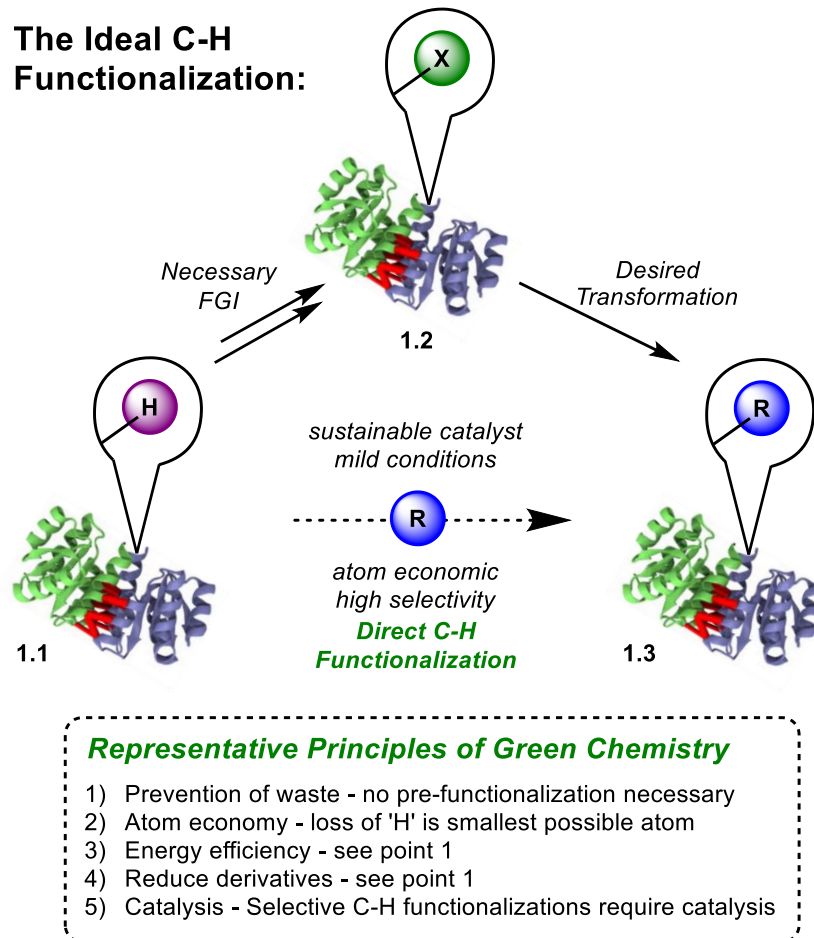
1.2 Carbon-Hydrogen Activation

The selective activation and functionalization of carbon-hydrogen (C-H) bonds by transition metals has long been a major research goal in the fields of organometallic chemistry and catalysis. Such reactions would permit the construction of functionalized molecules without prior activation of the coupling partners, improving step economy and minimizing waste.^[1] For example (Scheme 1.1), a representative organic compound **1.1** with ubiquitous C-H bonds would require multiple harsh functional group interconversions (FGIs) to convert some C-H group to a thermodynamically or kinetically leveraged C-X (X = leaving group) moiety **1.2**. This predetermined C-X group would be designed for a specific reactivity profile. From this C-X functional group, the desired transformation would proceed to produce the desired C-R functional group **1.3** (R ≠ H).

An alternative would be an idealized C-H functionalization reaction where the same C-H bond is *directly functionalized* to C-R in a single synthetic step using a sustainable catalyst. Further, the reaction should proceed under mild conditions, and with high atom economies and

reaction selectivity for the desired C-H bond (Scheme 1.1). These obvious advantages should make functionalization of C-H bonds the primary goal of site-selective catalytic transformations in synthetic chemistry.

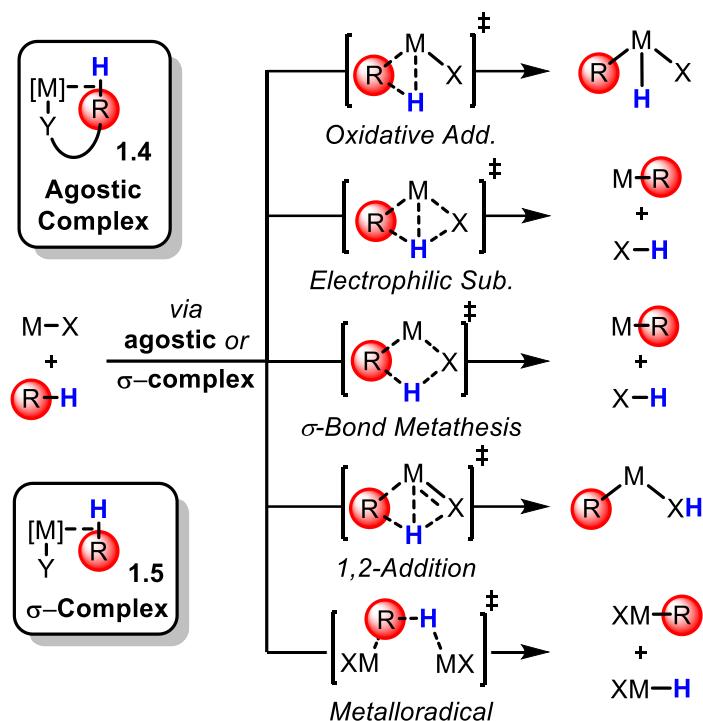
Unfortunately, these direct C-H functionalization reactions are challenging for several reasons: the main challenges are the low polarity (and thus low reactivity) of these bonds, and the difficulty of distinguishing between different C-H bonds. A number of strategies have been devised to overcome the inherent low reactivity, including: activated metal complexes,^[2–5] carefully selected base additives,^[6,7] and photo-redox methods.^[8–12] The challenge in selecting one C-H bond over another can be overcome by the use of directing groups,^[13–15] and in some cases judicious ligand selection.^[16,17]



Scheme 1.1 The ideal C-H functionalization: a mild, selective, atom economic catalytic method.

Transition metal-mediated C-H bond cleavage can occur through multiple reaction mechanisms (Scheme 1.2). Prior to the C-H activation step, the metal will interact with a $\sigma(\text{C-H})$ bond of the substrate. If the $\sigma(\text{C-H})$ interaction is made intramolecularly through use of some directing group, the donating $\sigma(\text{C-H})$ interactions are labeled ‘agostic contacts’ (**1.4**). If the contacts are intermolecular, the complex is called a ‘sigma (σ) complex’ (**1.5**). Metals in low oxidation states can activate C-H bonds by traditional oxidative addition pathways^[3,4] or by ligand-to-ligand hydrogen transfer (LLHT).^[18] Other metals cleave C-H bonds by radical pathways.^{17,18} Still others undergo redox neutral reactions such as sigma bond metathesis,^[21,22] concerted metalation deprotonation (CMD),^[6,13,23–25] or ambiphilic metal ligand activation (AMLA).^[22,26]

Even for a single transition metal complex, several mechanisms may be accessible, which can lead to competing processes and thus lower selectivity and reaction yield. As such, it is imperative to develop a detailed mechanistic understanding of these elementary reactions.



Scheme 1.2 Examples of general mechanisms of C-H activation, modified from literature.^[27,28]

1.3 Nickel in C-H Activation Reactions

Historically, the fields of catalysis and C-H activation have been dominated by noble metals such as palladium,^[29,30] platinum,^[29,30] rhodium,^[31,32] and iridium.^[33–36] However, interest has shifted toward understanding how the cheaper and most sustainable first-row metals (with 3d valence orbitals) can undergo the same classes of reactivity.^[37] In some cases, 3d metals can be used to advantage different sorts of reactivity that are not possible with noble metals (i.e. reactions with alkyls that resist β -hydride elimination).^[37,38]

Nickel in particular is an attractive metal for cross-coupling and other reactions.^[38] The ability for nickel to access a wide variety of oxidation states (-2,^[39,40] -1,^[41] 0,^[38] +1,^[42] +2,^[38] +3,^[43–45] +4^[46,47]) allows for variable reaction profiles. However, compared to group 10 noble metal homologues, much less is known about the ability of nickel to promote catalysis, and in particular C-H bond activation.^[37] Some progress has been made in this field; however, the mechanisms of which oxidation states of nickel may undergo C-H activation reactions are still not well understood.^[37,48] Here in this introduction we discuss mechanistic considerations with nickel in specific oxidation states, noting room for further development where appropriate.

The purpose of this introduction is not to contribute to the argument of whether oxidation state is an important (or unimportant) classification. Nor is its aim to comprehensively list all examples of catalytic C-H activation by nickel; this has been undertaken elsewhere.^[37] Rather it is to inform the reader of how formal oxidation state can be an important factor in predicting how nickel reacts with C-H bonds.

1.3.1 Agostic Compounds with Nickel

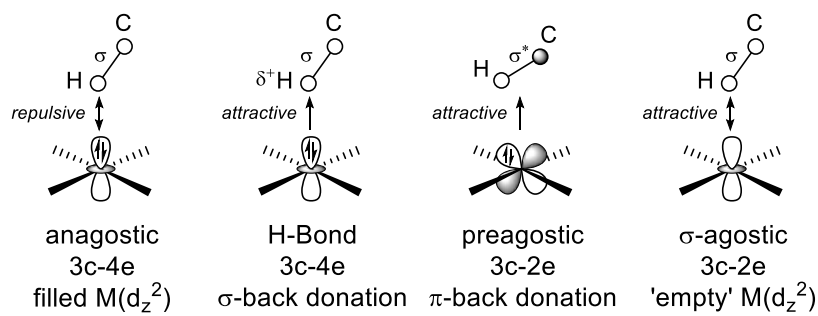
A discussion of bonding in agostic complexes is warranted for this thesis.^[27] Agostic and ‘anagostic’ interactions have been defined and redefined several times.^[49–52] We prefer the Scherer definition (Scheme 1.3a) where agostic interactions are defined by 3-center-2-electron (3c-2e) contacts. The $\sigma(\text{C-H})$ donates to an ‘empty’ orbital on the metal, which is an attractive interaction. Anagostic contacts are defined by a repulsive interaction, where the $\sigma(\text{C-H})$ is sterically predefined to interact with a ‘filled’ metal orbital. In some cases a $\text{M}_{\text{LP}} \rightarrow \sigma^*(\text{C-H})$ attractive interaction may also be possible. Other types of interactions also exist (i.e. H-bonding, and pre-agostic interactions – Scheme 1.3).

It is worth noting that complexes which exhibit ‘agostic’ or ‘anagostic’ interactions should nearly always be studied by a range of methods to experimentally define agostic or anagostic interactions. Some prefer to look only at bond distances and angles to confirm agostic or anagostic bonding.^[27] Others, like ourselves, prefer to examine these interactions by a combination of DFT, NMR spectroscopy, and X-ray crystallography.^[53,54]

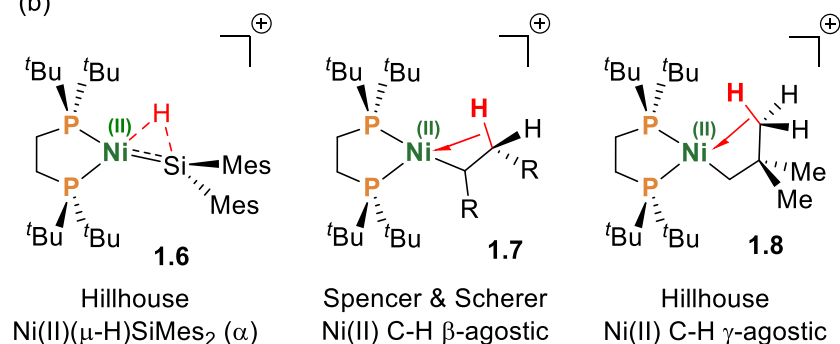
Nickel C-H agostic species are important species as they have been invoked in nickel catalyzed ethylene polymerizations,^[50,55,56] and β -elimination processes.^[57,58] Well-characterized C-H agostic complexes for Ni(0),^[59,60] and Ni(II)^[51,61–69] have been reported. For instance, Spencer,^[61] Hillhouse,^[63] and Scherer^[51] have shown that cationic Ni(II) C-H agostic complexes may be synthesized *via* protonation of Ni(0) olefin complexes (**1.6-1.8** – Scheme 1.3b). To our knowledge, there are no reports of C-H agostic or σ -type complexes of Ni(I), though such species have been proposed in aryl C-H bond activation using Ni(I).^[70]

Agostic and σ -complexes of other E-H (E = Si, B) bonds have been reported for Ni(I). McGrady and coworkers^[71] reported a Ni(I) $\eta^2:\eta^2$ -bis(B-H) borohydride σ -complex formed from salt metathesis with NaBH₄. Multinuclear nickel(I)-silyl complexes with Si-H agostic interactions have also been isolated.^[72–74] More recently, Uyeda and colleagues reported a dinickel(I) complex having geminal $\sigma_{\text{Si-H}}$ interactions, which are reactive intermediates in catalytic alkene hydrosilylation.^[74] These investigations of Ni(I) sigma complexes are important for understanding how Ni(I) can activate element-H bonds.

(a) d^8 - ML_4 Complexes



(b)



Scheme 1.3 (a) Classifications of anagostic, H-bond, preagostic, and agostic complexes for d^8 - ML_4 group 10 complexes – adapted from Scherer.^[52] (b) Ni compounds with $M \cdots (E-H)$ interactions, prepared in the research groups of Hillhouse,^[63,75] Spencer,^[61] and Scherer.^[51]

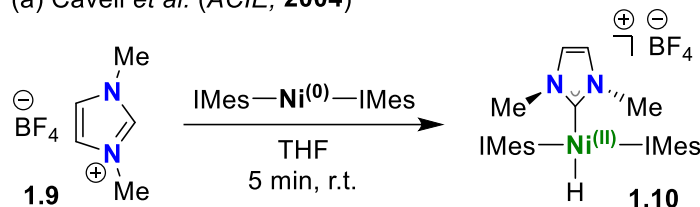
1.3.2 Mechanistic and Computational Studies of Nickel(0) in C-H Activation

1.3.2.1 Ni(0) Oxidative Addition Studies

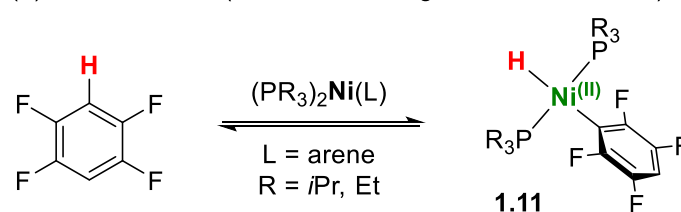
Low-valent late transition metals are well known to undergo oxidative addition of carbon-hydrogen bonds.^[33,34] Nickel in its zero oxidation state is no exception: concerted oxidative addition to Ni(0) has been directly observed to form aryl-bound Ni(II)-hydrides.^[76–80] Because the formation nickel(II) hydrides is thermodynamically unfavorable (and often reversible) due to the weak Ni-H bond, they are generally characterized in situ from C-H activation reactions.^[81]

In rare cases they have been isolated from well selected C-H synthons. For instance, oxidative addition of the imidazolium BF_4^- salt **1.9** (Scheme 1.4a) to $\text{Ni}(0)(\text{IMes})_2$ produced a tris(NHC)-Ni(II)-H complex **1.10**, which is stabilized by a new strong NHC-carbon bond (IMes = 1,3-bis(2,4,6-trimethylphenyl)imidazol-2-ylidene). In other examples, *ortho*-fluorinated aryls were selected because the resulting Ni-aryl bonds are strengthened by an increase in the ionicity,^[82] allowing for characterization of the kinetic Ni(II)-hydride products **1.11** and **1.12**.^[76–80]

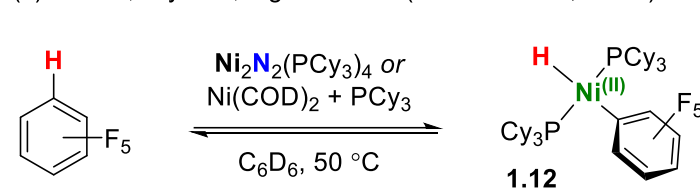
(a) Cavell *et al.* (*ACIE*, **2004**)



(b) Johnson *et al.* (*JACS*, **2008**; *Organometallics*, **2010**)



(c) Nakao, Hiyama, Ogoshi *et al.* (*Dalton Trans.*, **2010**)



Scheme 1.4 Examples of oxidative addition of C-H bonds from Ni(0) complexes.^[76,77,79,80]

1.3.3 Mechanistic Aspects of Ni(0) LLHT: The New Kid on the Block

Oxidative addition, however, is not the only C-H activation mechanism which occurs with Ni(0). Recently, the groups of Eisenstein and Perutz showed that in the presence of unsaturated hydrogen accepting ligands that Ni(0) can facilitate a ligand-to-ligand hydrogen transfer (LLHT)

which does not include discrete nickel(II)-hydride intermediates.^[18] In this seminal paper the authors computationally examined the mechanism of the hydroarylation of alkynes with fluorinated aryls. This study was based on an experimental report by the groups of Nakao and Hiyama, where the authors found that alkynes could be functionalized with fluoroarenes catalyzed by a Ni(0)-P(*c*-pentyl)₃ catalyst (Scheme 1.5a).^[83] Nakao hypothesized that C-H bond oxidative addition by a reducing Ni(0) metal center was the prevalent mechanism.

In a follow-up article, Nakao and his group showed that Ni(II)-hydrides are kinetically accessible through oxidative addition, and that alkyne insertion was the rate-determining step.^[79] (Scheme 1.5a) However, using a Ni(0) complex **1.13**, Eisenstein and Perutz found that instead of a concerted oxidative addition, the reactive Ni(0) species **1.13** prefers to directly transfer a hydrogen from the aryl ligand to the unsaturated neutral alkyne ligand to produce **1.14** (Scheme 1.5b).^[18] NBO analysis of the transition state **TS**_{13/14} does not show hydridic character of the transferring hydrogen.

In principle, this elementary step from **1.13** to **1.14** combines oxidative addition and insertion into a single step. Since the original account by the Eisenstein and Perutz groups,^[18] a range of reports have shown that Ni(0) often prefers to undergo LLHT type reactivity over oxidative addition of C-H bonds in the presence of unsaturated hydride-accepting molecules. Hydrogen acceptors have been shown to be alkenes,^[84,85] alkynes,^[86,87] and carbonyls.^[88]

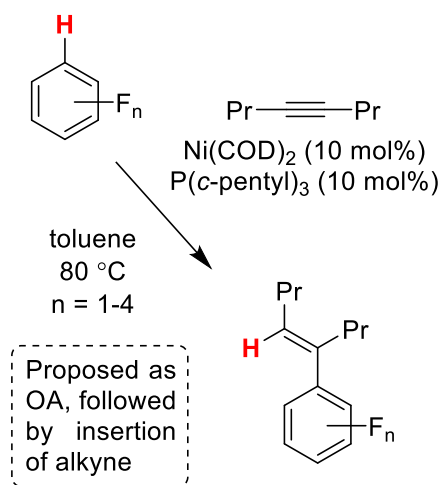
A related computational study by Sakaki and Eisenstein investigated why Ni(0) prefers LLHT over a concerted C-H oxidative addition (Scheme 1.5c). In short, the (i) smaller atomic radius of nickel and the (ii) comparatively low nickel-hydride bond strengths favor a change in mechanism compared to platinum and palladium. The smaller atomic radius of nickel results in a more congested coordination sphere. This brings the benzene and propene substituents closer in

proximity, and so a LLHT is more favorable in the transition state. This is visible in the transition state **TS**_{15/16} compared to **TS**_{17/18} (Scheme 1.5c) where in **TS**_{15/16} the alkene is close to the transferring hydrogen. In **TS**_{17/18} the alkene is much further from the forming hydride in **1.18**.

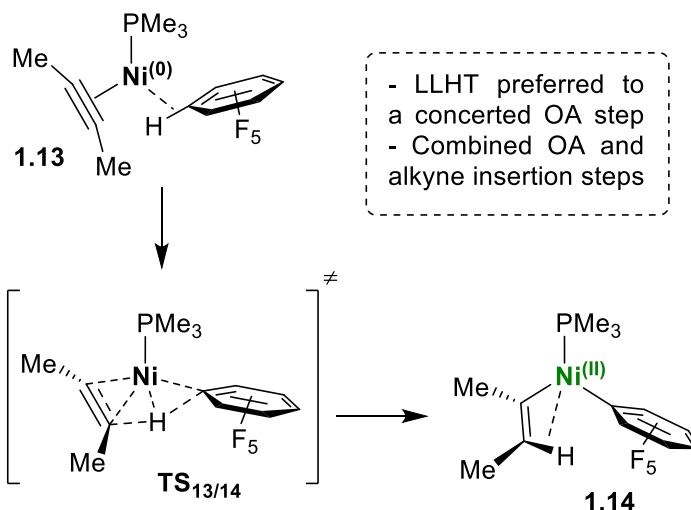
This was also shown by comparing the potential energy surfaces (PES) for the C-H activation of benzene for isoelectronic Ni(0), Pd(0), and Pt(0) complexes. While the PES of Pt and Pd showed increased electron density at the hydrides through the C-H activation step. On the reaction coordinate between **1.15** and **1.16** nickel held a steady electron density at the hydrogen undergoing LLHT (Scheme 1.5c). This contrasted the reaction coordinate between **1.17** and **1.18**, where platinum donated electron density to the hydrogen undergoing oxidative addition.

Both Ni(0) mediated C-H activation mechanisms (oxidative addition, LLHT) result in a 2e⁻ oxidation of the metal, however, the elementary steps differ significantly as outlined above. These differences should inform those designing catalytic cycles of how the choice of substrates and additives change mechanism and thus reaction selectivity.

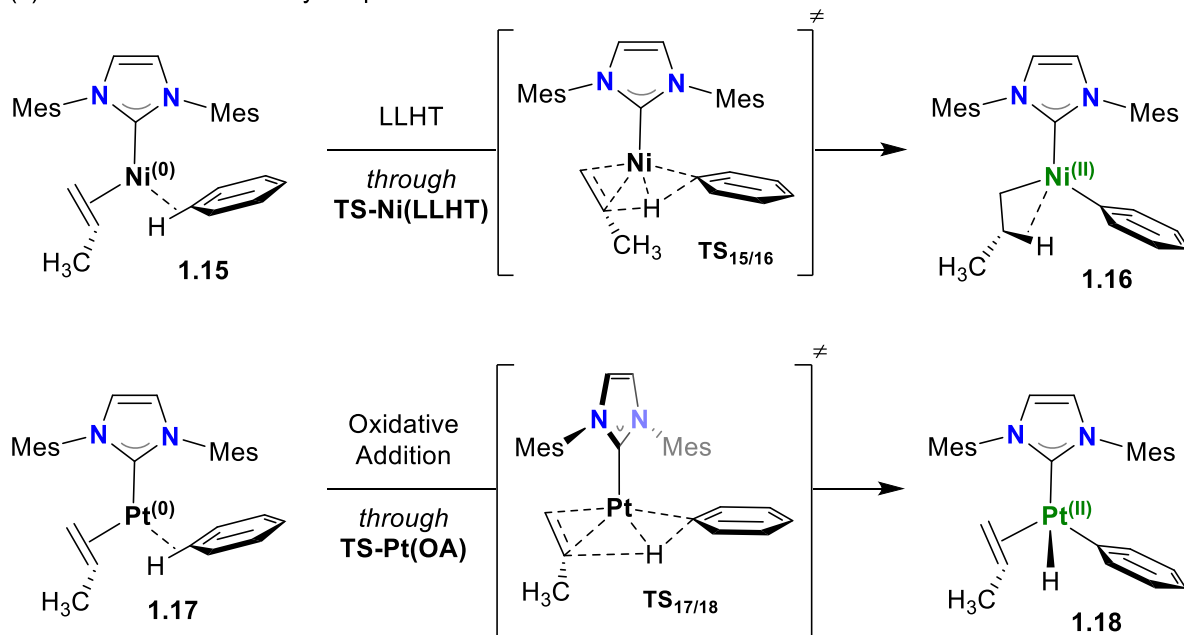
(a) Nakao, Hiyama *et al.* (JACS, 2008)



(b) Eisenstein and Perutz *et al.* (Organometallics 2012)



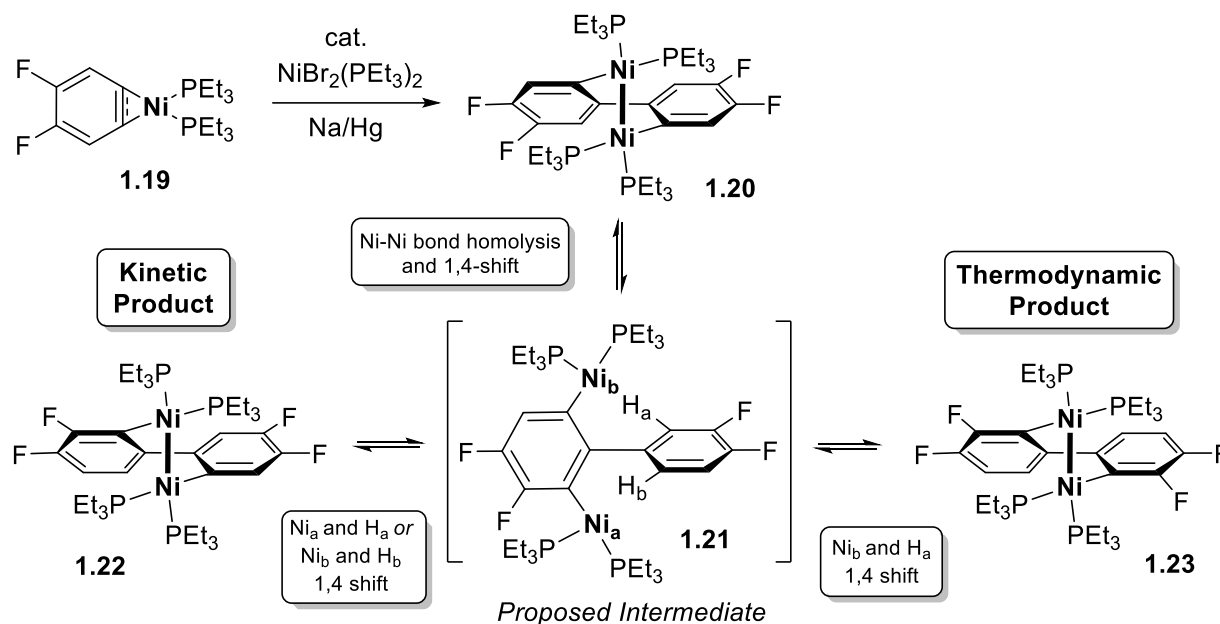
(c) Calculated Elementary Steps: Nickel vs. Platinum



Scheme 1.5 (a) Original report of hydroarylation of alkynes which was hypothesized to proceed through an oxidative addition mechanism.^[83] (b) The seminal report of LLHT by Eisenstein and Perutz, showing that LLHT was more favorable in the hydroarylation of alkynes.^[118] (c) A report by Sakaki and Eisenstein probing why zero valent group 10 metals prefer different mechanisms for C-H activation in isoleptic systems.^[81]

1.3.4 Towards the Role of Nickel(I) in C-H Activation

To our knowledge, there are no well-defined examples of Ni(I) complexes which facilitate C-H activation reactions. However, some progress has been made towards this end: the Johnson group reported a system which was proposed to undergo C-H activation with phosphine-ligated Ni(I) metal centers.^[70,89] From the di-Ni(I) biaryl complex **1.20**, the addition of catalytic $\text{NiBr}_2(\text{PEt}_3)_2$ and Na/Hg resulted in the isomerization to **1.22** and **1.23**. Complex **1.23** is the thermodynamic product because of the two *ortho*-fluoro substituents which increase M-C bond strengths.^[82] Based on (i) isolated nickel complexes (which were also observed as reaction intermediates), (ii) kinetic analyses, and (iii) product distribution analyses, the authors concluded that Ni(I) may be active in C-H activation from the common intermediate **1.21** (Scheme 1.6).



Scheme 1.6 A Ni(I) biaryl complex was postulated to undergo C-H activation through Ni(I).^[70,89]

Although the role of Ni(I) is certainly one possible explanation, there is no conclusive evidence to confirm this is true; the Johnson group alluded to this fact later on.^[48] For instance, Ni(I) is known to undergo facile disproportionation to Ni(0) and Ni(II) in the presence of π -acceptors (*See Chapter 3*).^[90] Moreover, the groups of Eisenstein, Perutz, and Johnson have confirmed that Ni(0) can undergo LLHT C-H activation reactions in the presence of strong π -acceptors. In the case of Johnson's report, benzyne could act as a hydrogen acceptor.

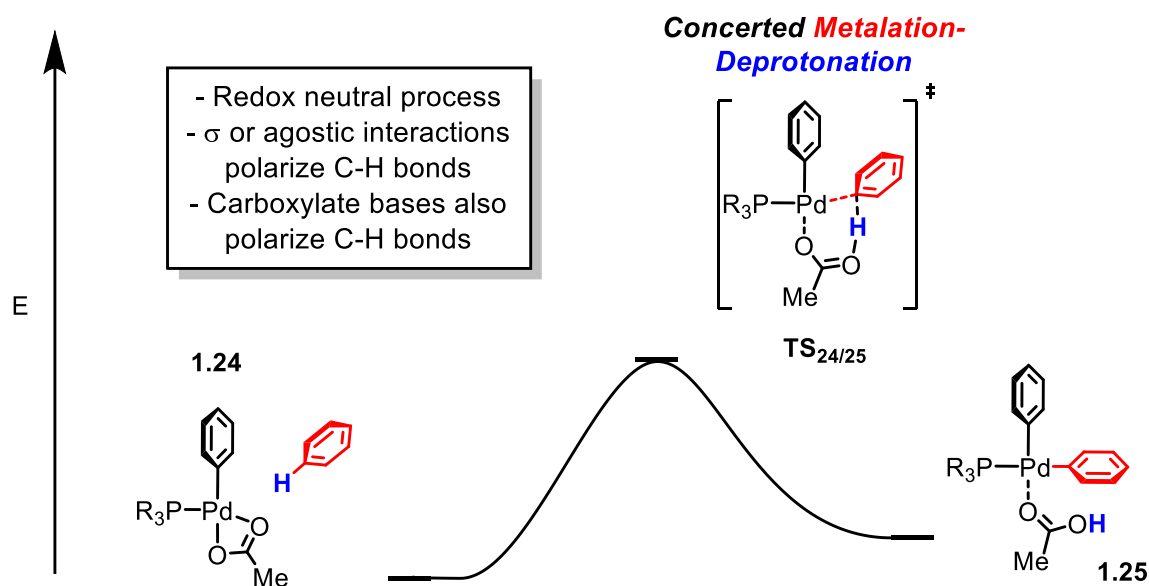
The lack of data suggesting that Ni(I) does or doesn't undergo C-H activation may be simply because this is an unfavorable reaction. However, the study of metaloradicals is difficult due to their paramagnetism. Additionally, the lack of a report should encourage inorganic chemists to investigate this chemical space to discover when Ni(I) may facilitate C-H bond activations. If these reactions were possible, which mechanism would be preferred?

1.3.5 Nickel(II) in C-H Activation: Concerted Metalation Deprotonation (CMD)

CMD (a.k.a. AMLA – see Scheme 1.2) is common in catalytic C-H activation with group 10 transition metal complexes in the 2+ oxidation state. In particular, the mechanism has been studied in depth for palladium(II) complexes.^[23–25,91,92] Computational reports by several research groups point to concerted deprotonation of the C-H bond during formation of the Pd-C bond.^[6,23,91] Bringing the C-H bond to the correct geometry for a strong C-H agostic interaction or $\sigma_{\text{C-H}}$ plays an important part in polarizing the C-H bond. Carboxylate ligands on palladium (**1.24** – Scheme 1.7) have been shown computationally to further polarize the C-H bond by a hydrogen-bonding type interaction.^[22,23,91] In the transition state **TS24/25**, the carboxylate ligand is bound κ^1 -O to palladium(II), and deprotonates the C-H bond to make the new Pd-C bond and the new O-H bond

in **1.25** (Scheme 1.7). In principle, this process can be reversible, leading to protonation of the Pd-C bond in **1.25**.

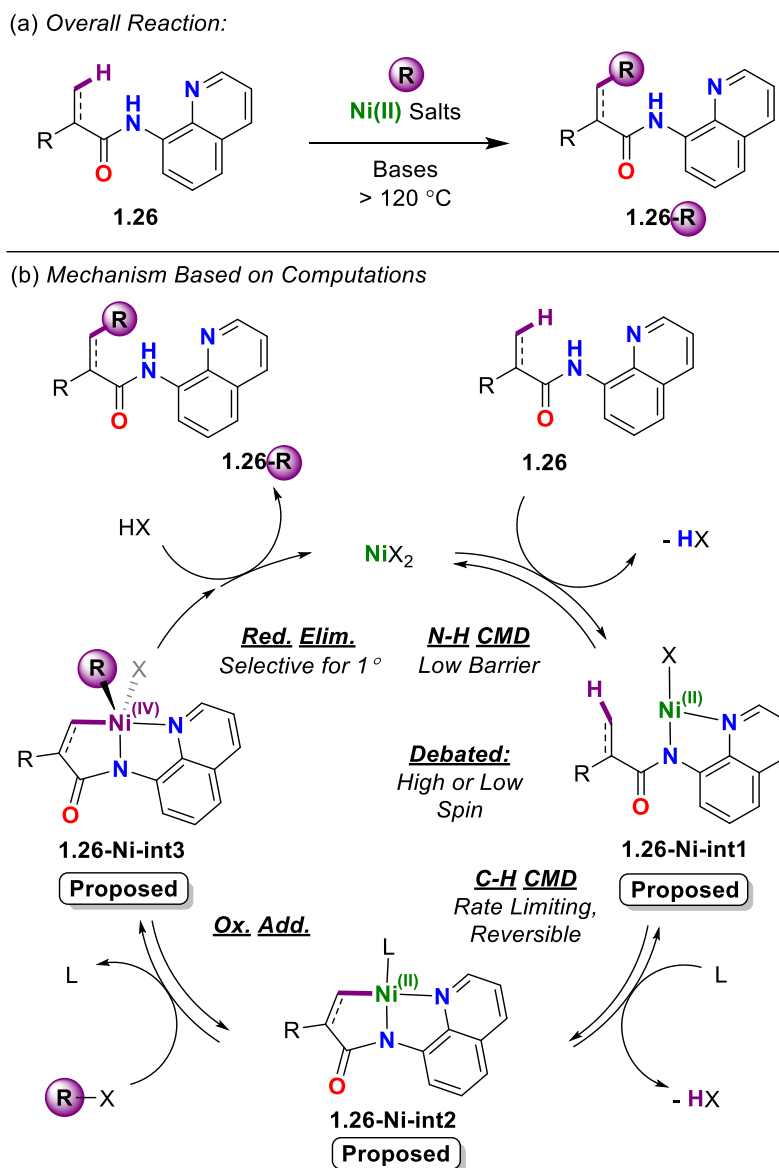
Related work on CMD reactions with palladium suggests that a combination of bases, typically carbonate and carboxylate bases, increases the reaction rate and yield of catalytic C-H functionalization methodologies. Elegant work by Rousseaux and Fagnou^[6] suggests that for Pd(II) C(sp³)-H activation of amides, hemi-labile carboxylates are integral to both lowering the CMD transition state energy and facilitating dissociation of phosphine from palladium(II) intermediates. Other related work from Tsuji and Fujihara *et al.* showed that bulky carboxylate bases can effect facile Pd(II) C-H activation.^[93]



Scheme 1.7 Simplified scheme of concerted metalation deprotonation (CMD), modified from Fagnou *et al.*^[25]

Compared to palladium, much less is known mechanistically about Ni(II) mediated CMD reactions, despite the increasing focus on Ni-based catalysis. The most well-studied examples are catalytic, and use Daugulis's 8-aminoquinoline (8AQ) directing group as in **1.26**^[94] (Scheme 1.8) to make new C-C,³⁰⁻⁵² C-N,^[95-97] C-O,^[98] C-S,^[99-103] and even C-X⁵⁹⁻⁶¹ [X = (pseudo)halide] cross

coupling products **1.26-R**. This strategy has been applied to β -C(sp²)-H^[28–32,40,43,44,49,50,56–60] and β -C(sp³)-H^[45,96–102,104,106,117–127] bonds in amides. Interestingly, reactions which couple these 8AQ-amides with alkynes have been shown to proceed through both Ni(0) LLHT pathways^[87] and Ni(II) CMD pathways.^[128,129] Calculations by Liu^[130] and Sunoj^[131] on the 8AQ-amide system confirm that CMD is the preferred pathway in the absence of alkyne coupling partners (Scheme 1.8).



Scheme 1.8 Example of well-understood Ni(II) mediated C-H activation by a CMD mechanism (derived computationally): nickel(II) mediated C(sp³)-H functionalization of 8AQ substituted amides.^[126,130,131]

To our knowledge, even for the catalytically well-developed 8AQ-amide system, there are no mechanistic studies that directly probe the factors (i.e. additives, solvents, etc.) that affect Ni(II) mediated C-H activation. Thus, experimental work must probes these factors and further compare experimental work to the computational reports noted above.

1.3.6 Mechanistic Studies of Nickel(III) and Nickel(IV) in C-H Activation

Significantly less is known about the role of nickel(III) and nickel(IV) in C-H activation reactions, especially compared to the literature surrounding the role of Ni(0) and Ni(II) metal centers. Recently, however, several groups have reported on the role of high valent nickel in C-H activation reactions: three groups have reported Ni(III) or Ni(IV) systems which they showed were capable of C-H activation.^[132–134] These reports are highly important works, giving new precedent to C-H activation mechanisms at nickel metal centers, especially with the recent understanding that high valent nickel is common in cross-coupling methodologies. We have chosen to talk about the Ni(III) and Ni(IV) sections together since some of these reports have not demonstrated that the nickel centers are perhaps in one oxidation state over the other.

1.3.6.1 Mirica *et al.* (April 2016)

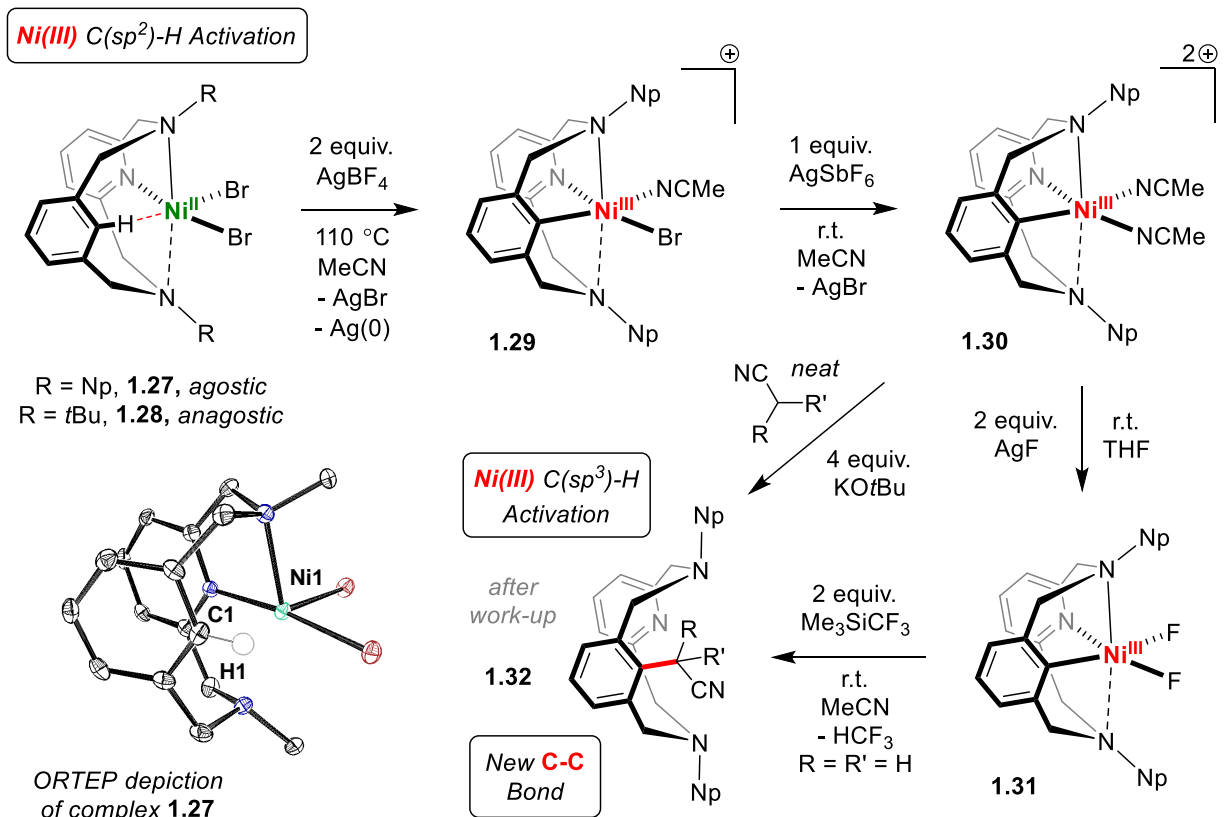
The first report of Ni(III)'s involvement in C-H activation was published by Mirica *et al.*, where they employed a modified pyridinophane ligand (Scheme 1.9), which is easily ligated to Ni(II) to produce the C(sp²)-H activation precursor **1.27** which exhibits a C-H agostic interaction in the solid-state. The Ni(1)-C(1), Ni(1)-H(1), and Ni(1)-C(1)-H(1) distances and angles (Scheme 1.9) are characteristic of classical C-H agostic interactions.^[49] The *t*Bu-substituted pyridinophane derivative **1.28** does not exhibit agostic interactions, rather anagostic.

The authors then subjected complex **1.27** to oxidative conditions, from which complex **1.29** was produced via an intramolecular C(sp²)-H activation event (albeit in poor yields - reported 20%). Interestingly the authors do not comment on the fate of the C(sp²)-H proton, which based on the low yield, could be mopped up by several possible bases (e.g. starting materials, side-products, etc.). The *t*Bu-substituted Ni(II) complex **1.28** does not undergo C(sp²)-H activation, suggesting that the steric profile of the ligand is important.

Although this report does not have DFT to back-up their proposal for Ni(III) mediated C-H activation, they do have some control experiments with different bases and oxidants. Some of these control results are unexpected; for instance, under standard conditions with added base (10 equiv. NEt₃ or 2 equiv. Na₂CO₃), no C-H activation product is observed. However, the authors do show that the C-H activation reaction is not solely promoted by traces of nickel or simple bases, which on the whole suggest that Ni(III) is involved in the C(sp²)-H activation step. Still, computational studies should be done to confirm these results.

Following some other simple transformations from complex **1.29**, the authors then show that their Ni(III)-pyridinophane complexes can promote intermolecular C(sp³)-H activation of nitriles, resulting in the quantitative functionalization of the pyridinophane ligand (Scheme 1.9). Notably, the authors show that primary, secondary, and tertiary C(sp³)-H bonds of nitriles are all amenable to C-H functionalization of the pyridinophane ligand.

In this first example of Ni(III) C(sp²)-H and C(sp³)-H activation studies, Mirica and his colleagues show that Ni(III) can promote the difficult activation and functionalization of secondary and tertiary C(sp³)-H nitriles. These proof-of-principle studies are exciting advances in high-valent nickel chemistry.



Scheme 1.9 The first report of high valent nickel's role in C-H activation by Mirica *et al.*^[133]

1.3.6.2 Sanford *et al.* (April 2017)

Researchers in the Sanford group are leading experts on high valent nickel chemistry, having reported synthetic examples of both Ni(III) and Ni(IV) complexes.^[47,135–137] Following up on their previous work, Sanford *et al.* reported on a bipyridal-triarylmethane (BP-TAM) ligand which promotes intramolecular C(sp²)-H activation at a Ni(IV) metal center (Scheme 1.10).

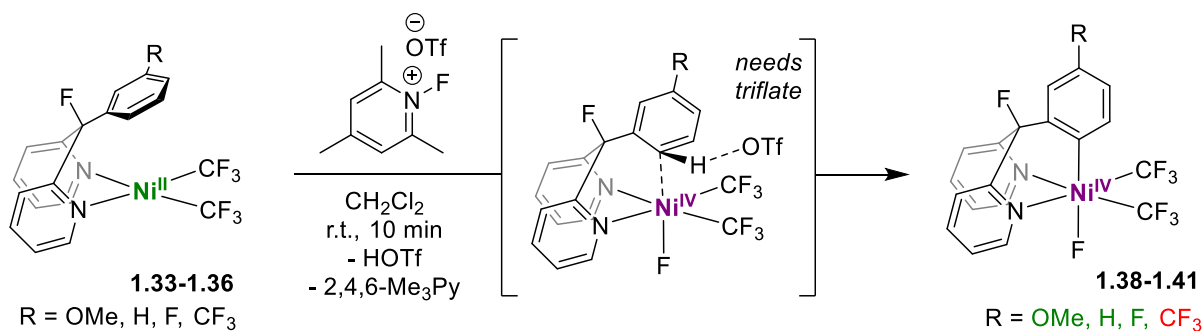
The Ni(II) BP-TAM complexes are synthesized from *cis*-Ni(II)(MeCN)₂(CF₃)₂ in dichloromethane. When the resulting complexes **1.33-1.36** are mixed with *N*-fluoro-2,4,6-trimethylpyridinium triflate, the nickel center is oxidized by 2-electrons, and Ni(IV) C(sp²)-H activated products **1.37-1.40** are isolated in good yields (reported 70-76%).

In collaboration with Canty, the Sanford group probed the reaction mechanism both experimentally and by DFT (Scheme 1.10b). Canty's calculations suggest that the rate limiting step has a low barrier (10.5 kcal/mol) and is the oxidative F⁺ transfer from the pyridinium reagent to nickel to produce **int-A**. The C-H activation step (**TS-E** – Scheme 1.10b) itself is characteristic of a S_EAr due to the highly electrophilic Ni(IV) metal center. Thus, breaking the C(sp²)-H bond is mediated by the acidic nickel center and the triflate ion, instead of relying on C-H bond polarization from a traditional agostic C-H contact. The authors explicitly note that agostic contacts were not found in the DFT studies.

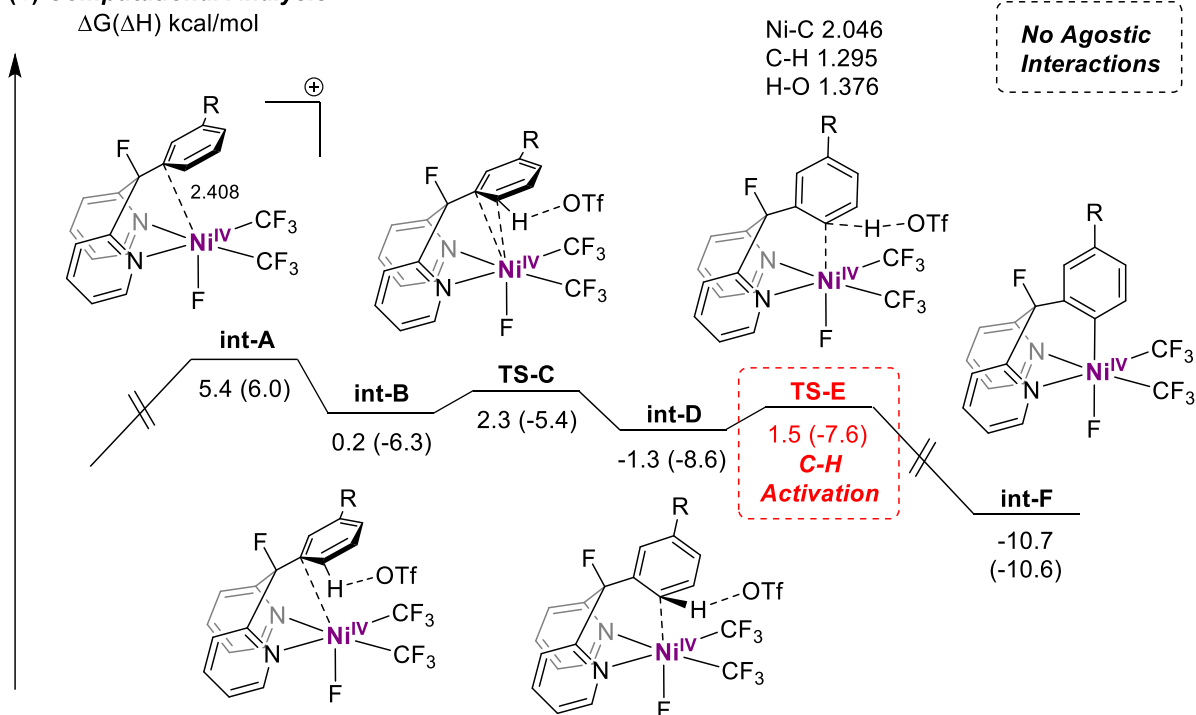
Experimentally, the reaction proceeds even at temperatures below 0 °C, and triflate was found to be critical for the reaction to proceed; this agrees with the low barrier and the role of the triflate ion in the C-H activation step between **int-D** and **int-F** found in the DFT analysis. Also consistent with the DFT is the electronic effect of the aryl ring in the C-H activation step. Electron rich and electron neutral substrates **1.33-1.35** proceed under the standard conditions, while the CF₃ substituted ring **1.36** did not undergo C-H activation, consistent with a S_EAr mechanism.

Notably, the authors admit that while the DFT supports a Ni(IV) mechanism, they cannot rule out the possible involvement of a Ni(III) metal center. It is thus surprising then that the authors do not comment on whether they probed the reaction by EPR spectroscopy, which may have given insight into this possibility. However, overall the DFT and experimental results are consistent with a Ni(IV) metal center promoting C(sp²)-H activation.

(a) Synthetic Results



(b) Computational Analysis



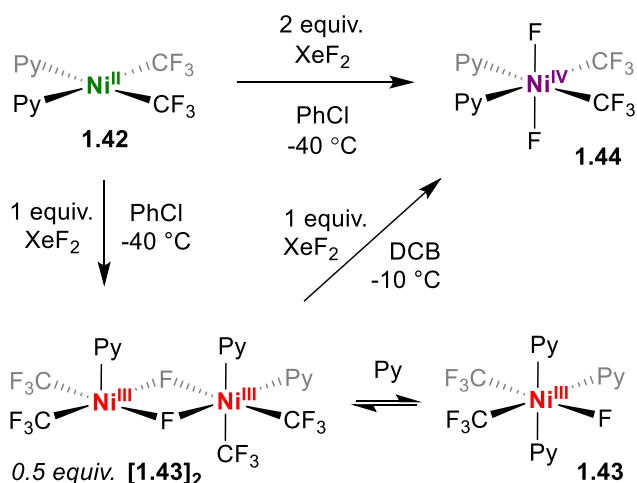
Scheme 1.10 Report by Sanford *et al.* on Ni(IV) in C-H activation reactions.^[132]

1.3.6.3 Mézailles, Nebra, *et al.* (August 2017)

Just over a year after Mirica *et al.* reported their Ni(III)-pyridinophane system (Scheme 1.11), Mézailles and Nebra, *et al.* reported simple pyridine ligated high valent nickel(III) and nickel(IV) complexes, which were reported to be capable of intermolecular C(sp²)-H activation/functionalization of both 1,2-dichlorobenzene (DCB) and pyridine with trifluoromethyl

groups.^[134] This was the first example of intermolecular C-H functionalization of unactivated species using high valent nickel (Mirica used activated nitriles), and is among some of the mildest trifluoromethylations to date.^[138,139]

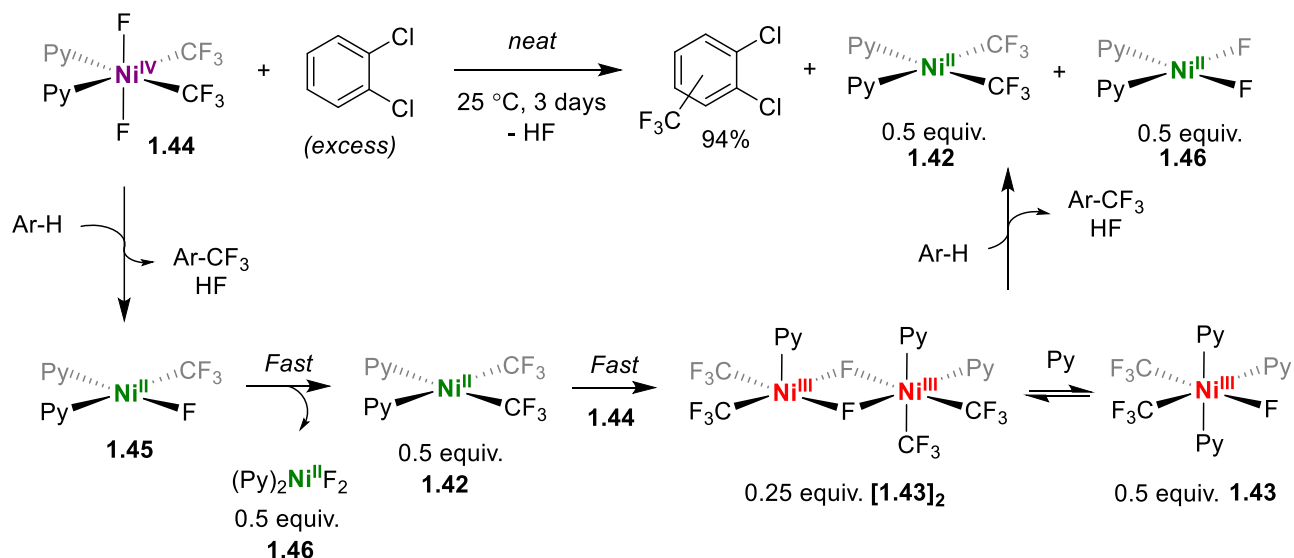
Starting from (Py)₂Ni(II)(CF₃)₂ **1.42**, the authors were able to successively prepare both Ni(III) (**1.43**) and Ni(IV) (**1.44**) complexes ligated by pyridine, fluoride, and trifluoromethyl ligands. In the case of the Ni(III) variant, a Ni(III) dimer is in equilibrium with a monomer Ni(III) complex (Scheme 1.11). The authors fully characterized the series of complexes by a variety of methods, including single crystal X-ray crystallography.



Scheme 1.11 Synthesis of Ni(II), Ni(III), and Ni(IV) fluoride complexes ligated to simple pyridine ligands.^[134]

When the Ni(IV) complex **1.44** was subjected to neat 1,2-dichlorobenzene, the aryl ring of 1,2-dichlorobenzene was cleanly trifluoromethylated in high yield over a period of 3 days (Scheme 1.12). The nickel products were found to be an equimolar amount of (Py)₂Ni(II)(CF₃)₂ **1.42** and (Py)₂Ni(II)F₂ **1.46**. As the trifluoromethylation progressed to approximately 60% conversion in two hours, the authors then note a sharp decrease in the rate of reaction. The explanation given by the authors is that as (Py)₂Ni(II)(CF₃)₂ is produced from C-C reductive elimination, the Ni(IV)

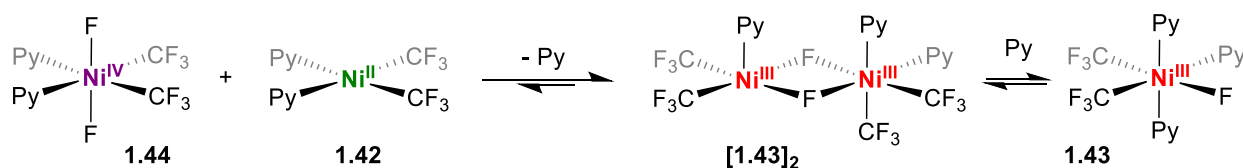
material comproportionates to give the Ni(III) dimer **[1.43]₂**. The authors also showed that this reaction occurs when the Ni(II) and Ni(IV) complexes (**1.42** and **1.44**) are mixed independently. Reaction with DCB then reaches a second kinetic region where it is produced only slowly for the next three days.



Scheme 1.12 The reaction of Ni(IV) (**1.40**) with 1,2-dichlorobenzene results in C-H activation and trifluoromethylation. The authors propose the Ni(III) (**1.43** or **[1.43]₂**) complexes are also proficient at this trifluoromethylation reaction.^[134]

The presence of Ni(III) in the reaction and slow production of trifluoromethylated DCB convinced the authors that the Ni(III) dimer **[1.43]₂** (or monomer **1.43**) is also active in the trifluoromethylation of DCB. This is certainly one possible explanation; however, we propose another: We believe that Ni(III) products **1.43** and **[1.43]₂** are being produced as the reaction progresses, the EPR spectroscopic data is clear. Moreover, from the independent reaction of **1.44** and **1.42** we know that the equilibrium favors the right-hand side of the comproportionation

equilibrium (Scheme 1.13). However, as more $(\text{Py})_2\text{Ni}(\text{II})(\text{CF}_3)_2$ (**1.42**) is produced, the comproportionation equilibrium will shift even more sharply to the right following Le Chatelier's Principle. This means the concentration of $\text{Ni}(\text{IV})$ (**1.44**) in the reaction will be much lower, resulting in lower reaction rates with DCB. So, the decreased reaction rates might also be due to this equilibrium, and not because the $\text{Ni}(\text{III})$ complexes **1.43** and $[\text{1.43}]_2$ are also active in this reaction. Regardless, we find this report to be exciting chemistry and promising with respect to new reactivity with high valent nickel species in C-H activation reactions. Particularly exciting is the intermolecular C-H activation and trifluoromethylation of unactivated $\text{C}(\text{sp}^2)\text{-H}$ bonds in DCB and pyridine.

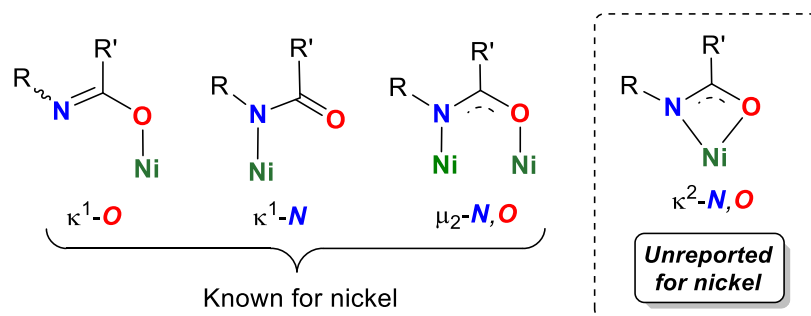


Scheme 1.13 A proposed comproportionation-disproportionation equilibrium between the $\text{Ni}(\text{II})$ - $\text{Ni}(\text{IV})$ and $\text{Ni}(\text{III})$ complexes may be responsible for the lowered reaction rates in the second kinetic regime.

1.4 Hemi-labile Ligands & 1,3-*N,O*-chelating Ligands

Recently, we have begun to explore the coordination chemistry of 1,3-*N,O* chelating ligands on late TMs. In particular, we have found that monoanionic LX-type amidates $[\text{RNCOR}']^-$ can be used to an advantage in the formation of square planar $\text{Rh}(\text{I})$ complexes that can access a range of new amidate coordination modes.^[140] In addition, we disclosed an unsaturated $\text{Cp}^*\text{Ir}(\text{III})$ phosphoramidate $[\text{RN}(\text{P}=\text{O})(\text{OR})_2]^-$ complex which promotes a range of E-H ($\text{E} = \text{H}, \text{B}, \text{C}, \text{Si}$) activation processes.^[141–143]

By examining the literature of nickel(II) mediated C-H activations, we observed that amides are common substrates. This is especially true for the quinoline-directed methods (Scheme 1.8). In light of these reports, we hypothesized that we might use our knowledge of 1,3-*N,O*-chelating ligands to understand how nickel activates C-H bonds in 8AQ-amides. We also hypothesized that amidates may stabilize low coordinate nickel amidate species which might also facilitate the activation of E-H bonds. To date, amidates are known ligands for Ni(II) and Ni(III),^[144–153] and the currently reported amidate binding modes for Ni are limited to $\kappa^1\text{-N}$,^[144–152] $\kappa^1\text{-O}$,^[148] and $\mu_2\text{-N,O}$ ^[153] (Scheme 1.14).



Scheme 1.14 Binding modes of amidate ligands to nickel.^[144–153]

1.5 Scope of Thesis

The central theme of this thesis is understanding mechanisms for nickel mediated processes. We focus heavily on the process of nickel in activating carbon-hydrogen bonds, however, we do also discuss and investigate disproportionation. The introduction Chapter highlights the state-of-the-art in the field of nickel mediated C-H activation with a particular focus on understanding mechanism as a function of formal oxidation state.

As we discuss in Chapter 1, much of the mechanistic work which probes the role of Ni(II) in C-H activations is purely computational. The work reported in Chapter 2 is the first experimental

study directly examining nickel's role in C(sp³)-H activation, using ureas as model substrates. We examine how reactions conditions (solvents, temperature) and additives affect the rates of C(sp³)-H activation of these ureas. We isolate some cyclometalated species and show that they are relevant for related catalytic methods. In addition, we examine the effects of substitution on the rates of C-H activation, and for the first time, map these rates. Comparisons are made to the literature where appropriate. We also examine the mechanisms of which additives affect reactions.

In Chapter 3, we investigate whether Ni(I) metal centers are capable of C-H activation. We isolate a range of Ni(I) amidate species and show that different N- and C-substitutions directly affect the preferred binding mode. We then examine the reactivity of some of these Ni(I)-amidate complexes and show that π -accepting ligands can promote disproportionation of monovalent nickel. Our conclusions are based on reaction scope studies, kinetic analyses, isolated intermediate studies, and independent syntheses.

Chapter 4 describes work which I completed abroad during my CREATE Sustainable Synthesis in the Beller Group at the Leibniz-Institut für Katalyse in Rostock, Germany. Working with Dr. Thomas Schareina, we developed a simple protocol for nickel catalyzed cyanation of aryl chlorides at room temperature.

In Chapter 5 we summarize each Chapter in this thesis, and discuss future work with respect to our discoveries, including some preliminary results. These results include ideas and extensions for future joint students between the Love & Schafer groups.

Chapter 2: Understanding Ni(II) Mediated C(sp³)-H Activation: Ureas as Model Substrates

2.1 Introduction

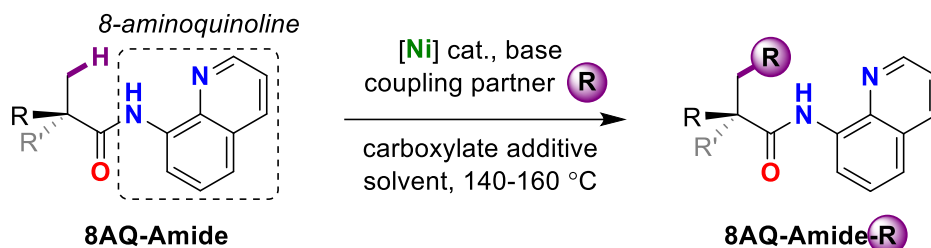
In Chapter 1, we discussed the role of nickel in different oxidation states to perform C-H activation reactions. Despite remarkable progress in understanding these reaction mechanisms, most studies that examine nickel's role are either catalytic or computational in nature. Catalytic studies, although extremely important, fundamentally shed limited light on elementary steps within a cycle. Computational studies are also extremely useful, they are not experimental in a physical sense. Ideally all experimental results would be analyzed computationally, and *vice versa*.

The mechanism of Ni(II) C-H activation is severely underdeveloped from an experimental perspective. Moreover, despite remarkable success in the coupling of unactivated aryl C(sp²)-H bonds,^[95,103–116] the functionalization of unactivated C(sp³)-H bonds remains difficult.^[45,96–102,104,106,117–127] Yet, there are no experimental studies determining the factors which contribute to the efficacy of C(sp³)-H activation at Ni(II).

As discussed in Chapter 1, the most well developed systems for Ni(II) C-H activation use 8AQ-directing groups to increase the effective concentration of nickel at a particular set of C-H bonds (Scheme 2.1, 2.2).^[15,61–94,109–115] However, because of the small radius of nickel, many of the catalytic variants of these reactions are limited to primary substrates. Calculations by the Liu^[130] and Sunoj^[131] groups on the 8AQ-amide system suggest that the activation of secondary C(sp³)-H bonds should be thermally accessible, however, the relative rates are projected to be lower than for primary substrates. This postulate is in contrast to the catalytic experimental observation that cyclic substrates with secondary C(sp³)-H bonds are readily functionalized.^[101,125,126] In some rare

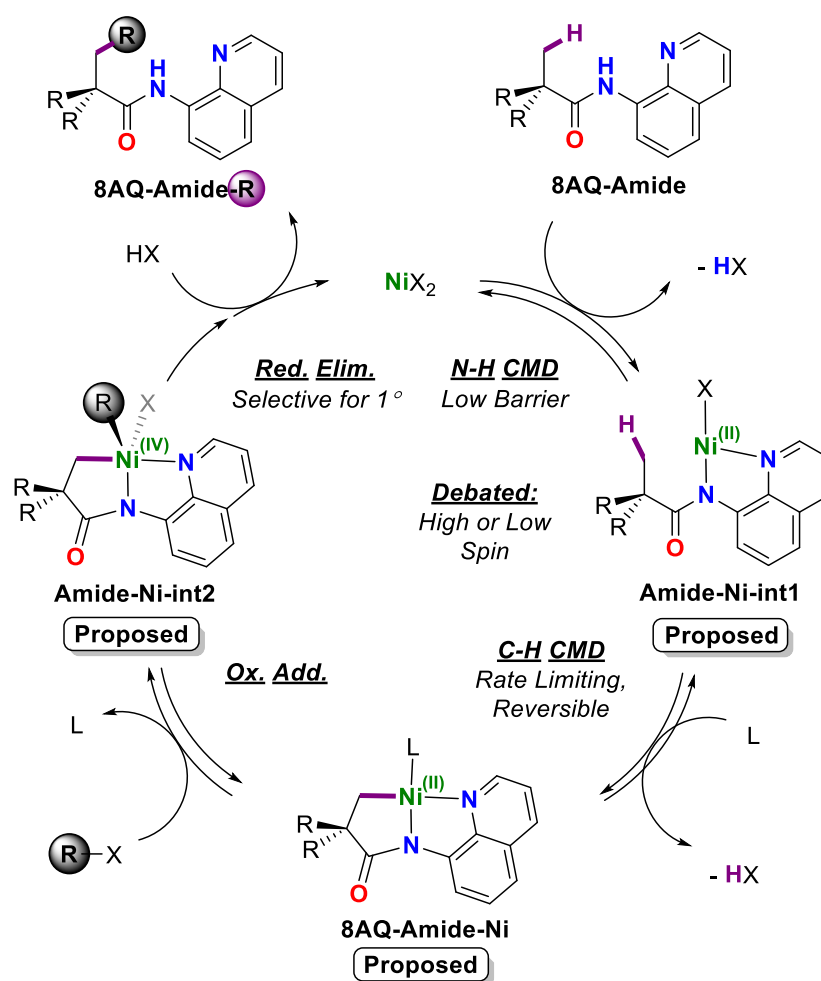
cases, products of acyclic secondary C(sp³)-H bond functionalizations have been isolated.^[97,104,106]

The regioselectivity of primary C(sp³)-H bonds is therefore due to the reductive elimination step, which is calculated to have higher barriers for secondary substrates.^[130]



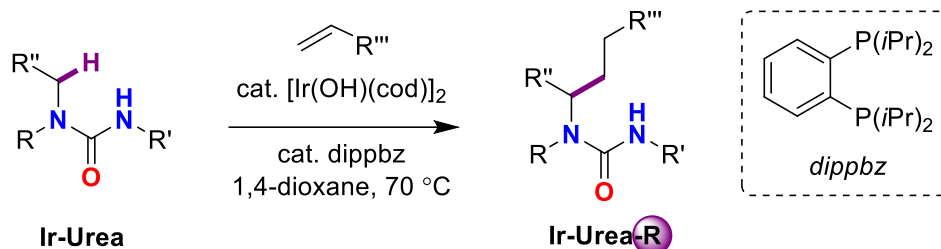
Scheme 2.1 (a) General scheme of nickel catalysis of amides bearing 8-aminoquinoline (8AQ) directing group;^[28-58]

There are some significant limitations in the above methodologies for the nickel catalyzed C(sp³)-H bond functionalization of 8AQ-amides: (i) substrates are generally limited to methyl, or cyclic alkyl derivatives; and (ii) each report uses different acid additives; there is no consensus on which carboxylates are optimal for C-H activation with Ni. Surprisingly, there are no experimental studies determining the factors which contribute to the efficacy of C(sp³)-H activation at Ni(II). Moreover, no intermediates in the C(sp³)-H functionalization of 8AQ-amides have been isolated. To push the boundaries of C-H functionalization methodologies using earth abundant nickel catalysts, we must aim to understand the mechanism of the C-H activation step itself.



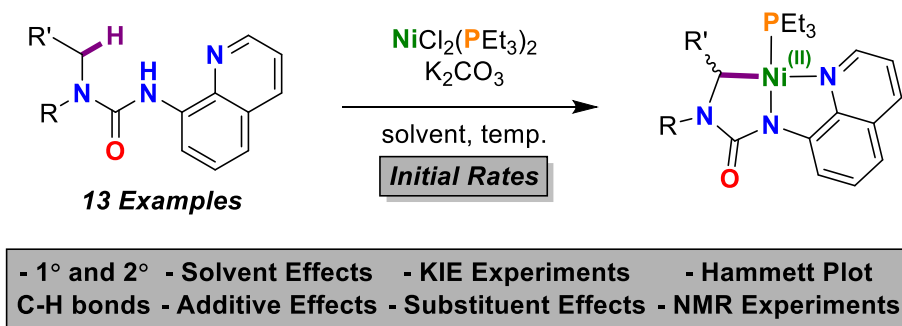
Scheme 2.2 Computationally derived mechanism of nickel(II) mediated C(sp³)-H functionalization of 8AQ substituted amides.^[62,63]

Recently, Nishimura *et al.* showed that secondary and tertiary ureas can be used as directing groups for iridium catalyzed C(sp³)-H bond alkylation alpha to a nitrogen atom (Scheme 2.3).^[156,157] The authors suggest that iridium facilitates this reaction through an oxidative addition pathway. Although the reaction has been extended to indoline derivatives, the authors were not able to functionalize other substrates with analogous secondary C(sp³)-H bonds.^[157]



Scheme 2.3 Ureas as substrates for α -(C-H) functionalization of nitrogenous compounds;^[156,157]

Our group has long been interested in the chemistry of nickel and group 10 metals.^[158–160] Inspired by the aforementioned Nishimura contribution, we imagined using 8-aminoquinoline-substituted tertiary ureas (Scheme 2.3) as more reactive models for the 8AQ-amide catalysis pioneered by Daugulis. We hypothesized that by using ureas instead of amides, that the C-H bond should have a higher effective concentration at the metal center due to the conformation imposed by the $\pi_{\text{N}}-\pi^*_{\text{CO}}$ bonding interaction. Additionally, we postulated that the increased acidity of C-H bonds alpha to a urea nitrogen atom would allow for trapping of the C-H activated intermediates by attenuating the basicity of the resulting Ni-C bond.



Scheme 2.4 A study of nickel(II) mediated C(sp³)-H activation of ureas as models for amides.

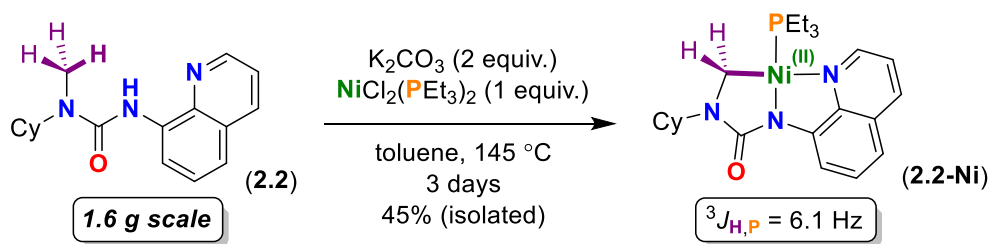
Herein, we show that by using simple nickel salts we can characterize, and in one case isolate, analogues of the previously proposed (*but not observed*) products of primary and

secondary δ -C(sp³)-H bond activation using 8AQ-substituted ureas as model substrates (Scheme 2.4). Through a series of kinetic and mechanistic experiments we show that C-H bond activation is rate determining and reversible. We also probe the kinetic consequences of different solvents and additives. Additionally, a Hammett analysis supports a transition state with an electrophilic metal center, as expected for a CMD pathway.

2.2 Results and Discussion

2.2.1 Reaction Discovery

We began by examining the C-H activation conditions of urea (**2.2**); (Me)(Cy)N(CO)N(H)(quinolin-8-yl). After screening a variety of conditions, we found that heating (**2.2**) in toluene in the presence of NiCl₂(PEt₃)₂ and K₂CO₃ led to the C(sp³)-H activation product [(PEt₃)Ni(κ^3 -C,N,N-(CH₂)N(Cy)(CO)N(quinolin-8-yl))] (**2.2-Ni**) in moderate yield (Scheme 2.5). Unfortunately, long reaction times are required; however, we were able to scale this reaction up to gram scales of (**2.2**) to isolate (**2.2-Ni**) in reasonable quantities. We characterized (**2.2-Ni**) by multinuclear and multidimensional NMR spectroscopy, X-ray diffraction (XRD), and elemental analysis.



Scheme 2.5 Synthesis of Ni(II) ureate **2.2-Ni** by C(sp³)-H activation of urea **2.2**.

In the ^1H NMR spectrum of (**2.2-Ni**) (d_8 -toluene, 298 K), a characteristic doublet assigned to the cyclometalated Ni-CH₂ [δ 2.67] displays phosphorus coupling through the nickel center [$^3J_{\text{H,P}} = 6.1$ Hz]. Coupling is not observed when phosphorus decoupling is employed. In the $^{31}\text{P}\{^1\text{H}\}$ NMR spectrum, the triethylphosphine signal is observed at [δ 18.9] as a sharp singlet. Additionally, in the $^{13}\text{C}\{^1\text{H}\}$ NMR spectrum the urea ($\text{C}=\text{O}$) carbonyl resonance shifts downfield by over 8 ppm relative to (**2.2**). Notably, in the presence of excess triethylphosphine the phosphine signal of (**2.2-Ni**) broadens significantly and the (PEt_3)-Ni-CH₂ [$^3J_{\text{H,P}}$] coupling disappears in the ^1H NMR spectrum; this suggests rapid phosphine exchange at room temperature.

We isolated XRD quality single crystals of (**2.2-Ni**) from toluene-hexamethyldisiloxane mixtures cooled to -35 °C. The solid-state molecular structure (Figure 2.1) reveals a square planar nickel center [$\Sigma\theta_{\text{Ni}} = 360.25(25)$]. The carbon-nickel bond [C(1)-Ni(1) = 1.923(2)] is shorter than other Ni(II)-C(sp³) bonds (see SI for list of other Ni(II)-C(sp³) bond lengths),^[161–164] likely due to the weak *trans*-influence of the quinoline nitrogen donor. Of note is the strain induced by the five-membered cyclometalated ring, where the angles made by (i) C(1)-N(1)-C(2) and (ii) N(1)-C(2)-N(2) are each reduced by five degrees compared to the solid-state structure of the proteoligand, (**2.2**) [$\Delta(^{\circ}) =$ (i) 5.1(2); (ii) 4.9(2)] (see Appendix D.2 for solid-state structure of (**2.2**)).

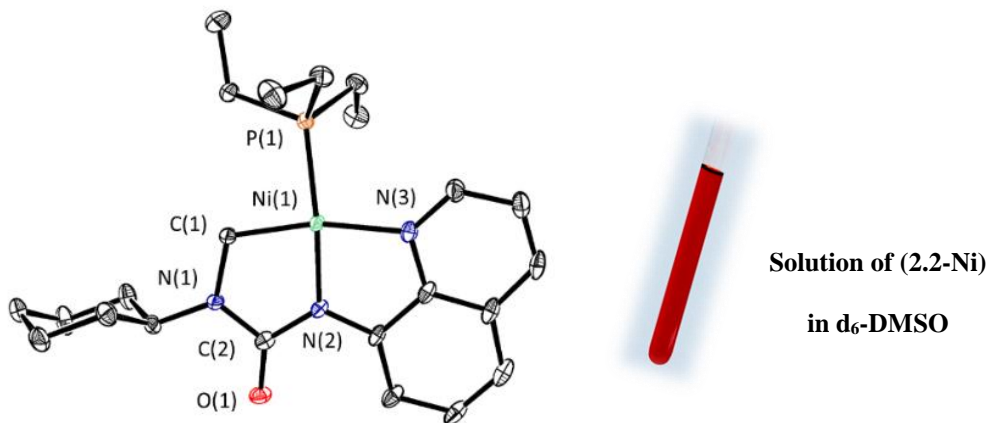
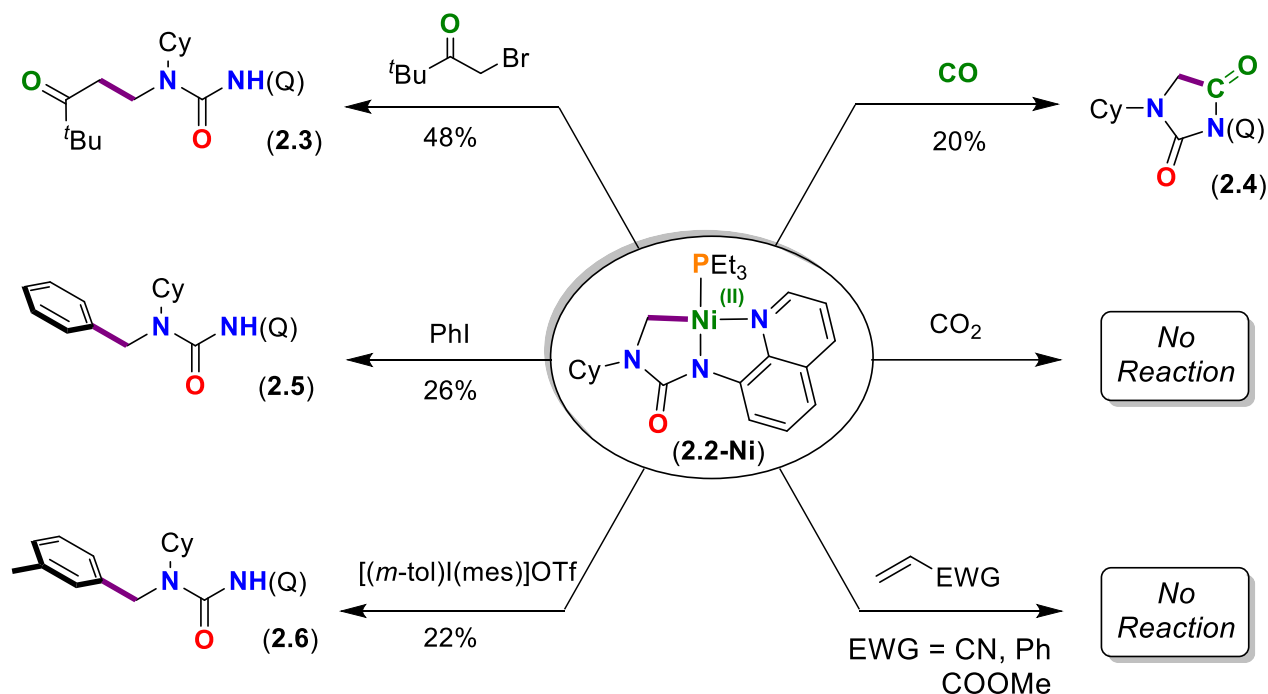


Figure 2.1 ORTEP depiction of the solid-state structure of complex (2.2-Ni) (ellipsoids at 50% probability, hydrogens and solvent omitted). Selected bond lengths (Å) and angles (°): C1-Ni1 1.923(2), N2-Ni1 1.855(2), N3-Ni1 1.972(2), C2-O1 1.238(3), C1-Ni1-N3 166.5(1), N1-C1-Ni1 109.8(2).

2.3 Reactivity of Cyclometalated (2.2-Ni)

2.3.1 Validating the Relevancy of (2.2-Ni)

With complex (2.2-Ni) in hand, we wished to see if cyclometalated (2.2-Ni) would undergo further reactivity to functionalize the C-Ni bond; this would suggest that (2.2-Ni) is a relevant intermediate in nickel mediated C(sp³)-H functionalization. We chose a variety of coupling partners to this end (Scheme 2.6). Addition of an α -bromoketone resulted in the formation of a new C-C bond to produce (2.3) in good yields. Likewise, we were also able to form new C-C bonds by additions of an aryl iodonium salt or PhI to produce (2.6) and (2.5) respectively. Insertion reactions of CO were also productive, resulting in the formation of new C-C and C-N bonds in the cyclized urea (2.4), which we prepared independently. In our hands, complex (2.2-Ni) did not react with either CO₂ or a range of activated olefins. These results suggest (2.2-Ni) is a relevant intermediate in nickel mediated C(sp³)-H functionalizations.



Scheme 2.6 Reactivity of complex **(2.2-Ni)** with a variety of coupling partners. Reactions in DMSO, yields are isolated; for reaction conditions, see appendix A.2 (¹H NMR spectroscopic yields, Q = quinolin-8-yl).

2.3.2 Evaluation & Explanation of Side Products

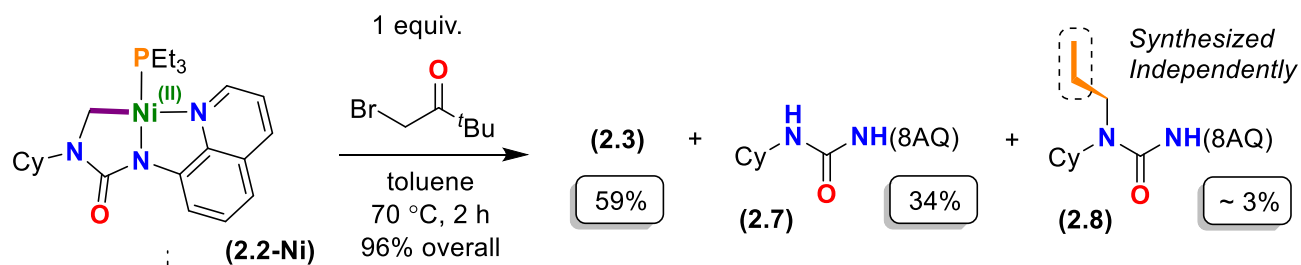
The yields of the functionalization reactions of **(2.2-Ni)** were found to be low in DMSO. Along with the major coupling products, we found that several side products were formed. We isolated these products from the reaction with 1-bromopinacolone (Scheme 2.7). The major side product is the demethylated urea **(2.7)**. We propose a mechanism for this reaction below (Scheme 2.7):

- Addition of 1-bromopinacolone to **(2.2-Ni)** may proceed through a one electron pathway, where nickel will oxidatively abstract the bromine atom, producing an alpha-ketyl radical.

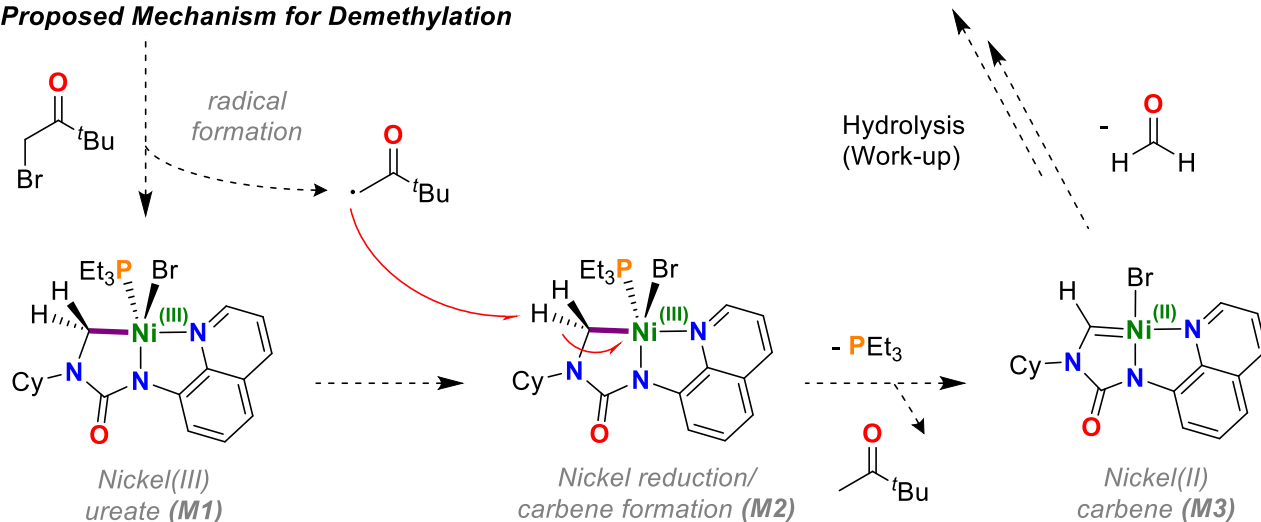
- ii) The alpha-ketyl radical may then abstract a proton from the Ni-CH₂ of the resulting Ni(III) ureate complex (**M1**) from step (i). This produces a Ni=CH fragment (**M3**).^[30,161]
- iii) Upon work-up with water, the carbene species will be hydrolyzed to formaldehyde, resulting in formation of demethylated urea (**2.7**).

The urea (**2.8**) is also produced as a minor side product via an ethylation step. We hypothesize this compound results from some phosphine substituent exchange process, as PEt₃ this is the only simple source of ethyl from the reaction mixture. Group 10 mediated phosphine substituent exchange has been reported recently.^[165]

NMR Scale Reaction



Proposed Mechanism for Demethylation



Scheme 2.7 NMR Scale reaction of (2.2-Ni) with an alkyl electrophile. The demethylated product (**2.7**) is shown to the right.

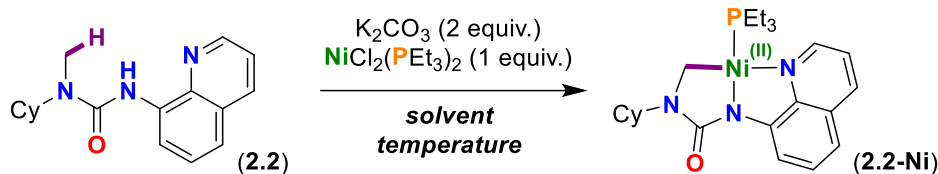
2.4 Solvent Effects

Having characterized **(2.2-Ni)** and verified its potential relevancy in C-H activation methodology, we sought to examine how solvent choice may affect the rate of C(sp³)-H activation. Six solvents, in three distinct temperature regimes ranging from 70-145 °C were chosen (Table 2.1). Reactions in d₆-DMSO (DMSO = dimethyl sulfoxide) heated to 145 °C converted nearly half of **(2.2)** to **(2.2-Ni)** in five hours (entry 2). Moreover, we found that **(2.2-Ni)** is produced appreciably even at 70 °C in DMSO (entry 5). Reactions in d₇-DMF (DMF = *N,N*-dimethylformamide) produced **(2.2-Ni)** at comparable rates to d₆-DMSO reactions, however, in our hands reactions in d₇-DMF suffered from a lack of reproducibility (See appendix A.2).

Reactions prepared in chlorinated solvents d₂-tetrachloroethane (entry 1) and CDCl₃ (entry 7) resulted in decomposition to myriad paramagnetic products. In contrast, reactions in deuterated tetrahydrofuran (entry 6), and acetonitrile (entry 4) did produce **(2.2-Ni)**, but were sluggish compared to reactions in DMSO. Reactions in acetonitrile also suffer from long induction periods.

These results show that coordinating polar aprotic solvents such as DMSO and DMF increase the rate of nickel mediated C(sp³)-H activation of **(2.2)**. We reason that coordinating solvents may be beneficial for stabilizing an electropositive nickel center in the reaction coordinate, or the solvent may assist with substitution of triethylphosphine for the quinoline directing group.

Table 2.1 Effect of solvent on initial rates of formation of complex (2.2-Ni)^a



Entry	Solvent	Temperature (°C)	Rate ^[166] (M/min)
1	d ₂ -TCE	145	decomposition ^a
2	d ₆ -DMSO	145	t _{1/2} ~ 5 hours
3	d ₆ -DMSO	90	(3.3 ± 0.1) x 10 ⁻⁵
4	CD ₃ CN	90	Complex (Appendix A.2)
5	d ₆ -DMSO	70	(6.9 ± 0.4) x 10 ⁻⁶
6	d ₈ -THF	70	negligible ^b
7	CDCl ₃	70	decomposition ^a

^aNo product is observed, and myriad paramagnetic peaks are detected

instead; ^bOver 36h, < 1% product formation by ¹H NMR spectroscopy.

2.4.1 Additive Effects

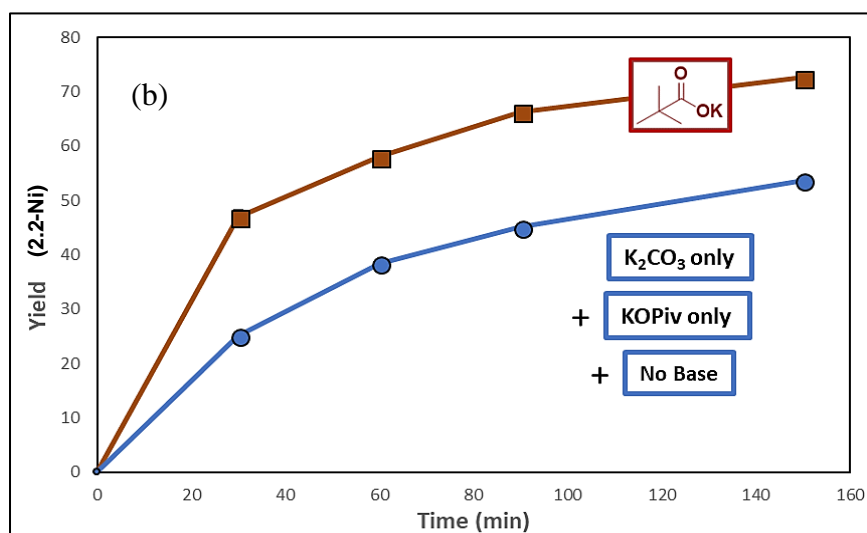
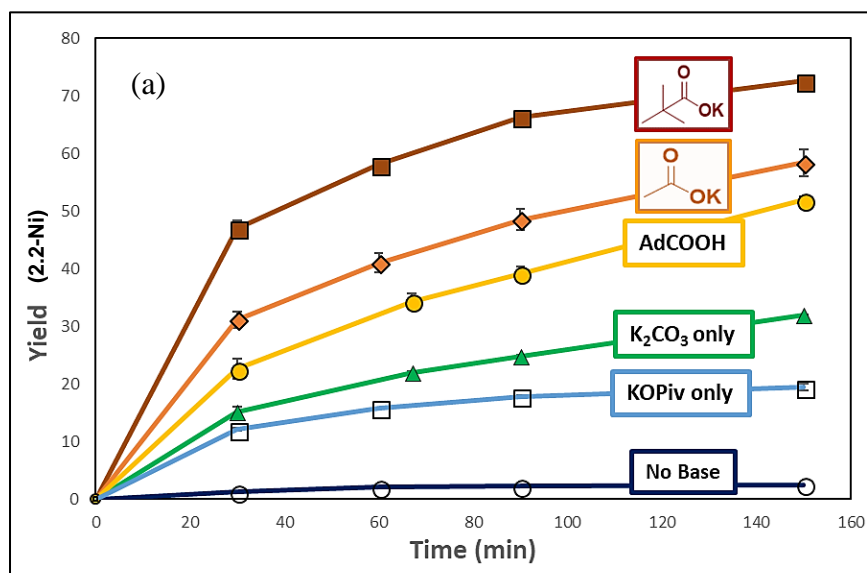
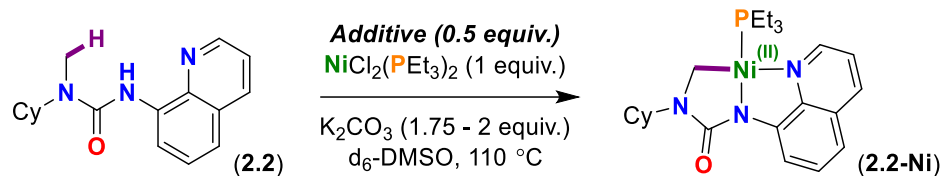
Using DMSO as our reaction solvent going forward, we screened different additives for their effects on the described C-H activation reaction (Scheme 2.8). In catalytic C-H functionalization methodologies, many research groups have found it advantageous to add bulky carboxylic acids or external bases. However, as noted before, there is no consensus throughout the nickel catalysis literature on what types of carboxylate additives are best for C-H activation. Thus, we screened a variety of carboxylate bases in the reaction of (2.2) to (2.2-Ni).^[167]

We first conducted a series of reactions to establish baseline reactivity (Scheme 2.8a). In the absence of carbonate base or additive, the reaction proceeds to ~2% yield after 150 minutes at 110 °C. The observation of product suggests that another component of the reaction (e.g. urea or phosphine) may facilitate C-H activation to some degree. It is likely that the acid which is produced

is neutralized by substrate quinoline or PEt_3 . When carbonate is present, the reaction proceeds slowly and levels off at low conversions. We postulate that this poor conversion is due to competitive substrate-phosphine binding as the reaction proceeds.

Addition of the bulky 1-admantyl carboxylic acid (AdCOOH) somewhat increased the rate of C-H activation compared to the control reactions without additives. However, the addition of the slightly smaller potassium pivalate (KOPiv) resulted in a more significant rate increase. Notably, these conditions at 110 °C in the presence of KOPiv exhibit reaction half lives of approximately thirty minutes at 110 °C; $t_{1/2} \sim 0.5$ h (*c.f.* Table 2.1, no additive, $t_{1/2} \sim 5$ h, 145 °C). KOAc does not promote the reaction to the same degree as KOPiv , but the rate is faster than with AdCOOH . It appears then, that for the additives there is an optimal steric profile, where the reaction proceeds at the highest rate.

From a strictly electronic perspective, adding 2,4,6-trimethylbenzoic acid has an insignificant effect on the reaction rate; however, addition of 2,6-bis(trifluoromethyl)benzoic acid slightly decreases the rate of C-H activation (see appendix A.2). The effect of carboxylate pK_a on CMD type reactions is complicated: in some cases more electron-donating substituents and higher pK_a result in faster reactions,^[168] while the opposite has also been observed.^[169] More studies would be needed to understand the origin of the rate difference in this case. Regardless, our results show that carbonate and carboxylate salts work synergistically to increase the rate of C-H activation (Scheme 2.8b).^[6,170]



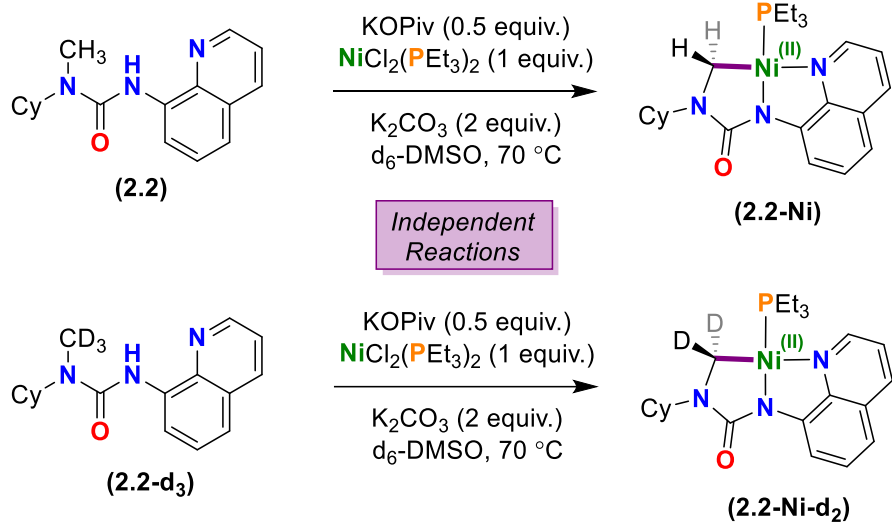
Scheme 2.8 (a) Effect of additives:^[166] For (i) acid additives, 2.0 molar equivalents K₂CO₃ added, (ii) potassium salts, 1.75 molar equivalents K₂CO₃ added.^[171] **Legend:** ○ No additive, or K₂CO₃, □ KOiPr added (No K₂CO₃), ▲ K₂CO₃ added (no additive); ● 1-adamantyl carboxylic acid additive; ◆ KOAc additive; ■ KOiPr additive. (b) ● sum of (□ + ▲ + ○), combined traces from (a) showing that K₂CO₃ and KOiPr work synergistically.

2.4.2 Kinetic Isotope Effects (KIEs)

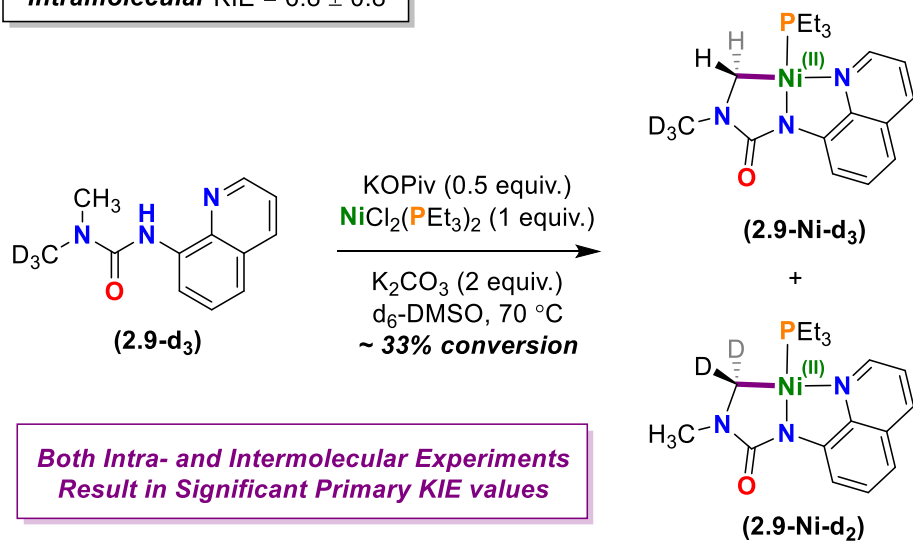
Next, we wished to determine if C-H activation was the rate determining step in this reaction. Calculations done on the 8AQ-amide system vary in whether C-H activation is rate-determining in catalytic reactions,^[130,131,172] although it has been shown that there can be difficulties when modelling additives.^[173] To address this point, we synthesized the tri-deutero urea (**2.2-d₃**) and the *N,N*-dimethyl substituted ureas (**2.9**, **2.9-d₃**) (Scheme 2.9). Only one methyl CH_3 signal is observed in the ^1H NMR spectra of (**2.9**) and (**2.9-d₃**), suggesting facile $\text{Me}_2\text{N}-\text{C}(=\text{O})$ bond rotation on the NMR spectroscopic timescale.

Using the optimized reaction conditions (solvent = d_6 -DMSO, additive = KOPiv), we compared the independent initial rates of C-H activation for (**2.2**) and (**2.2-d₃**), which resulted in a strong primary intermolecular KIE (7.2 ± 0.4), suggesting that $\text{C}(\text{sp}^3)\text{-H}$ bond activation step is rate limiting (Scheme 2.9). Our intramolecular KIE experiments with (**2.9-d₃**) also confirm a large primary KIE for $\text{C}(\text{sp}^3)\text{-H}$ bond activation (6.8 ± 0.8). The magnitudes of our primary KIEs are similar to the intermolecular KIE for a Pd catalyzed reaction with amide $\text{C}(\text{sp}^3)\text{-H}$ activation substrates [c.f. KIE = 6.5].^[6]

Intermolecular KIE = 7.2 ± 0.4



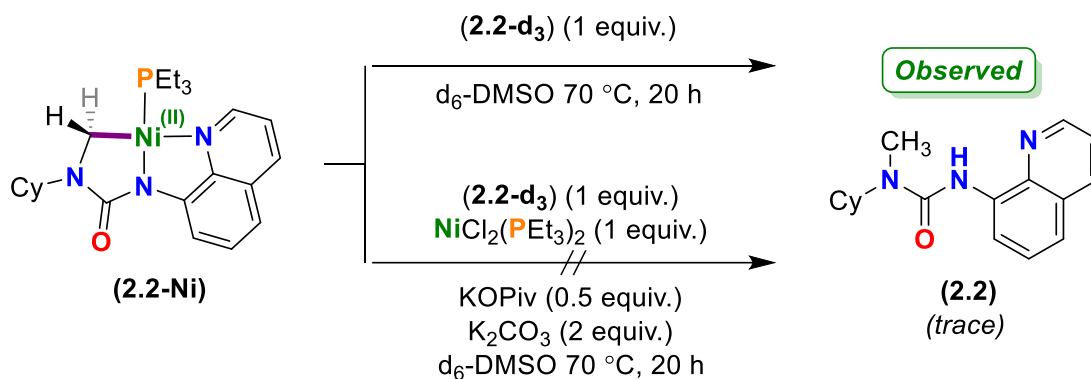
Intramolecular KIE = 6.8 ± 0.8



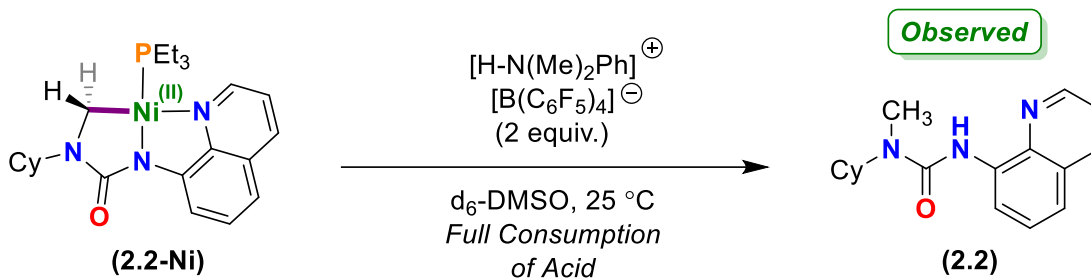
Scheme 2.9 Kinetic isotope effects for intra- and intermolecular C(sp³)-H bond activation in ureas.

We next wished to probe whether C-H activation was reversible in our system. To explore the question of reversibility we started by adding different proton sources to isolated complex (**2.2-Ni**) (Scheme 2.10). Upon heating the reaction at 70 °C in the presence of (**2.2-d3**) (Scheme 2.10a), we observed only trace amounts of (**2.2**) from the protonation of the cyclometalated (**2.2-Ni**), suggesting that the N-H in free urea (**2.2-d3**) can act as a proton source, but it is not significant. Interestingly, under standard reactions conditions with nickel and base, (**2.2**) is not observed, suggesting that the protonation of (**2.2-Ni**) is not from trace water. Adding the more acidic [HNMe₂Ph][B(C₆F₅)₄] leads to protonation of the Ni-C bond in (**2.2-Ni**) to give (**2.2**) even at room temperature (Scheme 2.10b). We next added the soluble carboxylic acid, AdCOOH, to probe whether carboxylate assisted CMD processes could, in principle, be reversible. No reaction is observed at room temperature, and heating to 70 °C for hours leads to only small amounts of protonation of (**2.2-Ni**) to give (**2.2**) (Scheme 2.10c). It appears then that C-H activation is *potentially* reversible under reaction conditions. However, only a small amount of free carboxylic acid would be produced; thus, we suggest that synthesis of (**2.2-Ni**) is essentially irreversible under these conditions.

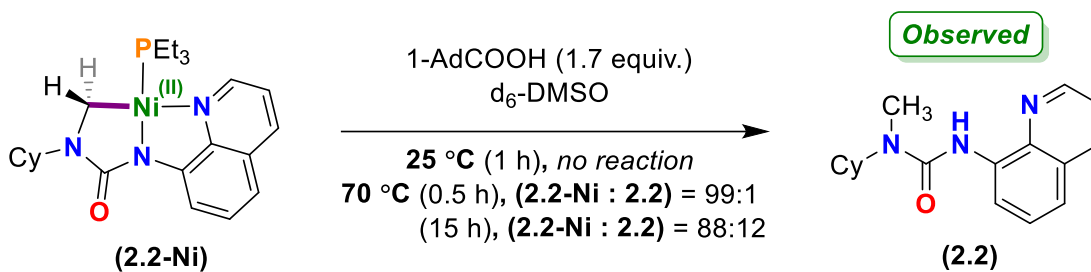
(a) Protonation with urea (N-H)



(b) Protonation with strong acid (N-H)



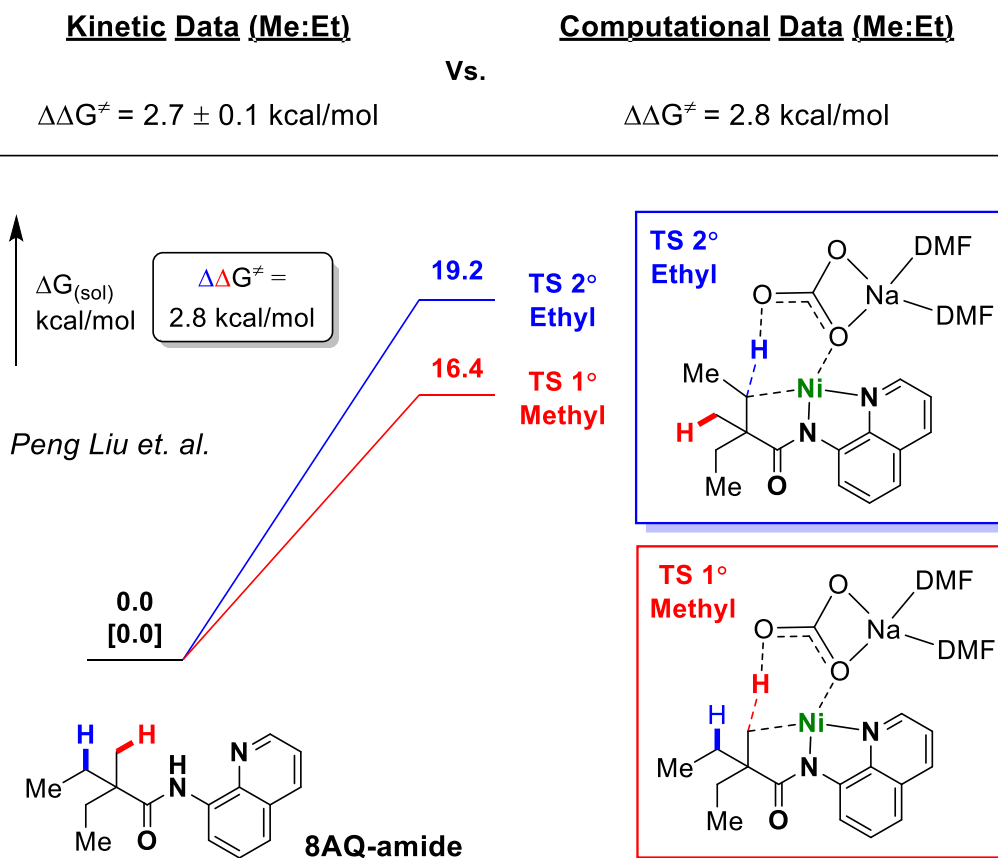
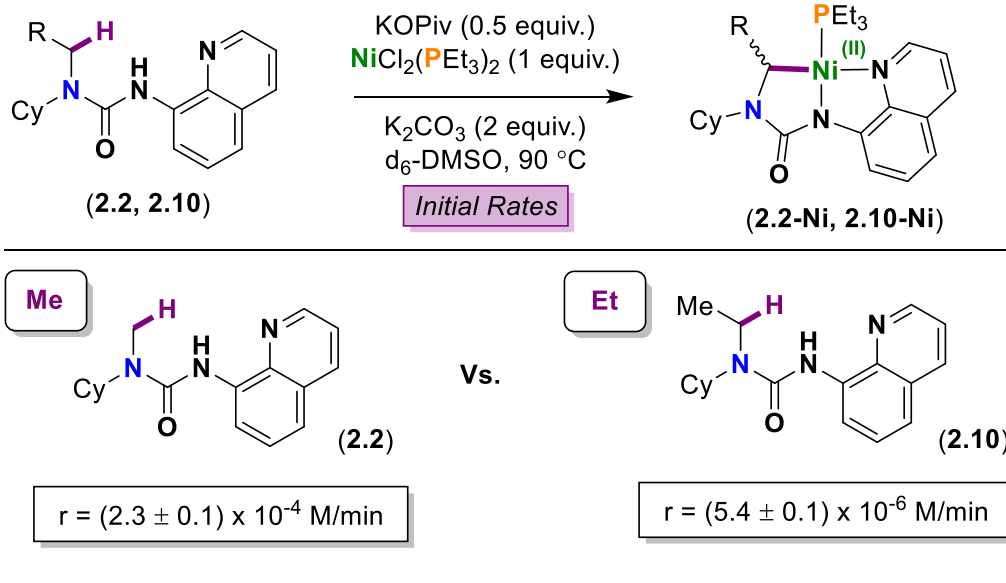
(c) Protonation with carboxylic acid (O-H)



Scheme 2.10 Probing protonation of the Ni-C bond in (2.2-Ni) with (a) deuterated urea (2.2-d₃), (b) an anilinium salt, and (c) 1-adamantyl carboxylic acid.

2.4.3 Substrates with 2° δ -C(sp³)-H Bonds

We next wished to test whether substituted ureas underwent similar reactivity to the methyl cyclohexyl urea (**2.2**) used thus far. To begin we chose the ethyl substituted variant (urea **2.10**) since the relative barriers of C-H activation have been calculated for methyl/ethyl 8AQ-substituted amides previously.^[130] Ethyl-substituted (**2.10**) undergoes C(sp³)-H activation, with a $k_{\text{rel}} \sim 2.4$ at 90 °C (k_{rel} of (**2.2**) was arbitrarily set to 100 for ease of comparison). *Via* Eyring analysis, we estimate the relative barriers to C-H activation for (**2.2**) versus (**2.10**) to be approximately [$\Delta\Delta G^\ddagger_{\text{exp}} = 2.7 \pm 0.1$ kcal/mol]. In a recent computational report by Omar and Lui,^[130] the authors compared the C-H activation barriers between a methyl and ethyl group for nickel mediated C(sp³)-H activation of 8AQ-amides [$\Delta\Delta G^\ddagger_{\text{calc}} = 2.8$ kcal/mol] (Scheme 2.11). Thus, our results agree nicely with calculations done on the 8AQ-amide chemistry.



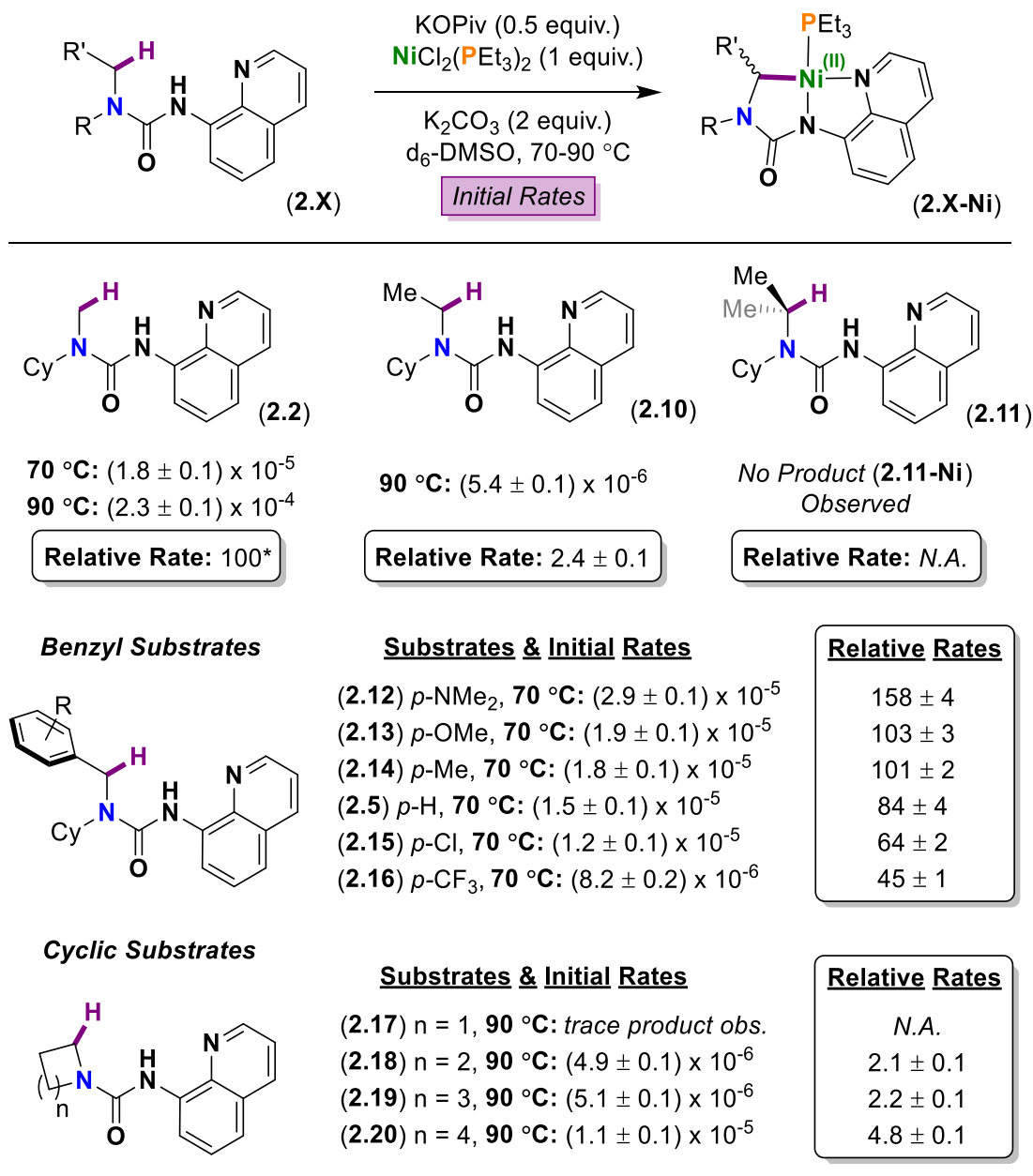
Scheme 2.11 Model validation, using ureas (2.2) and (2.10) for measuring the relative rates of C(sp³)-H activation. Computational data based on the 8AQ-amide system.^[130]

Our kinetic studies show that a range of other substrates (**2.5**, **2.10**, **2.12-2.20**) are susceptible to C-H activation under these conditions (Scheme 2.12). Each of the resulting organometallic species (**2.5-Ni**, **2.10-Ni**, (**2.12-2.20**)-Ni) was characterized by *in situ* NMR spectroscopy and display similar spectroscopic characteristics to (**2.2-Ni**). For instance, the products (**2.5-Ni**, **2.10-Ni**, (**2.12-2.20**)-Ni) each show a singlet in the $^{31}\text{P}\{^1\text{H}\}$ NMR spectrum between [δ 15.7-21.3] corresponding to a single PEt_3 . Like (**2.2-Ni**), the ^1H - ^{13}C HMBC NMR spectra show a shift [$\Delta(\text{ppm}) > 5$] of the urea carbonyl ($\text{C}=\text{O}$) resonance downfield upon cyclometalation.

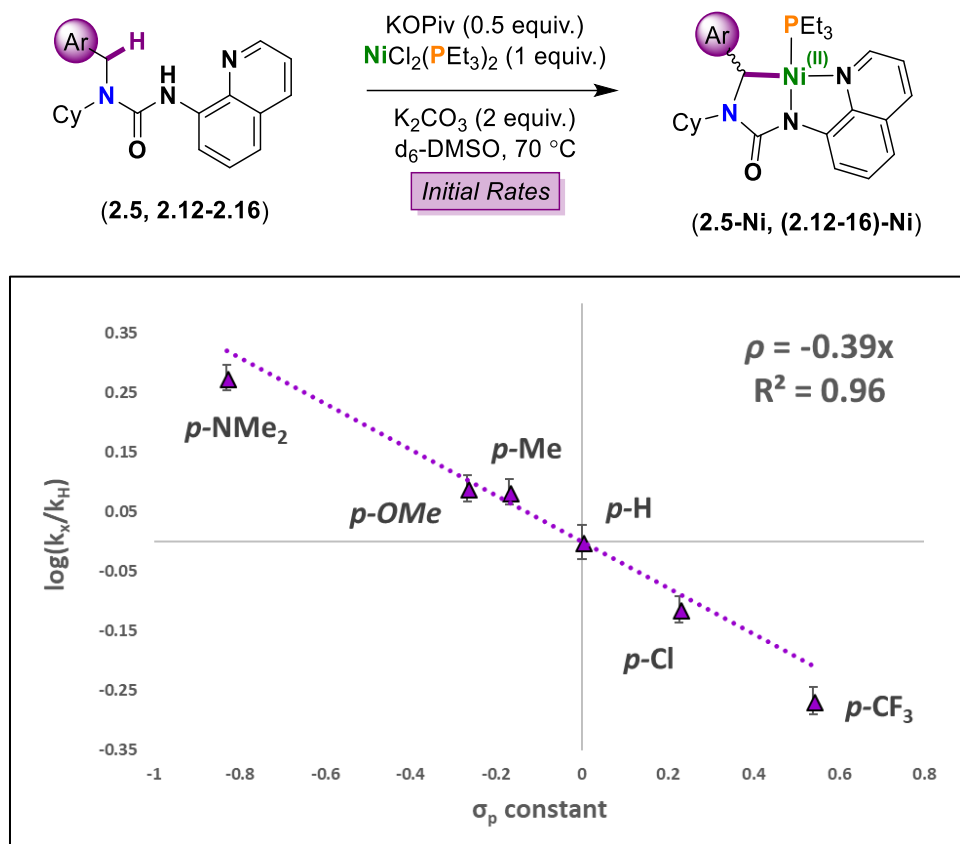
Substrate (**2.11**) bearing a isopropyl group is not amenable to C-H activation under these conditions, likely due to steric limitations. Reactions with benzyl substrates (**2.5**, **2.12-2.16**) display reaction rates that are comparable to (**2.2**) at 70 °C. The rate is highest for electron rich aryl rings adjacent to the reactive C-H bond. A Hammett analysis shows a linear correlation for substrates (**2.5**, **2.12-2.16**) (Scheme 2.13, $R^2 = 0.96$). Curiously, the effect of electronics on CMD type reactions can vary depending on the system and reaction conditions. In some cases, electron withdrawing substituents can result in increased rates of C-H activation,^[25,174] while in other cases electron donating substituents result in higher rates.^[175–177] The negative ρ value (-0.39), although small in magnitude, is consistent with an electrophilic C-H activation transition state (*c.f.* KIEs) that has a build-up of positive charge. We propose that increased C-H electron density leads to stronger C-H agostic interactions, increasing the rate of C-H activation.

Cyclic substrates derived from saturated *N*-heterocycles (**2.17-2.20**) also react at comparable rates to (**2.10**). The smaller azetidine derivative (**2.17**) does not form significant quantities of product (**2.17-Ni**) under these conditions. Our rate data suggest that larger rings react

faster than smaller rings. We attribute this effect to a decreased distance of the $\delta\text{-C}(\text{sp}^3)\text{-H}$ bond from the metal center, increasing the C-H effective concentration at the metal center.



Scheme 2.12 Relative reaction rates for C-H activation of ureas (2.2, 2.5, 2.10, 2.12-2.20) to nickel products (2.2-Ni, 2.5-Ni, 2.10-Ni, (2.12-2.20)-Ni).^[166]

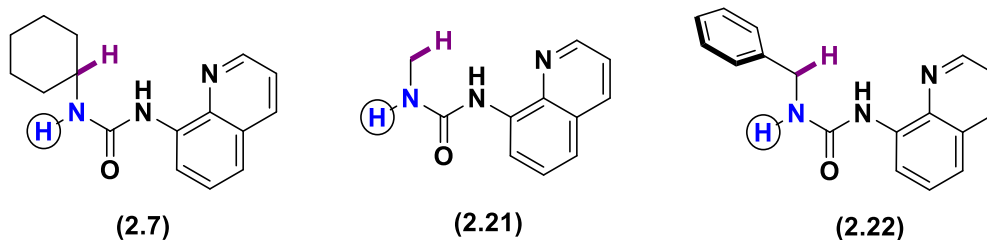
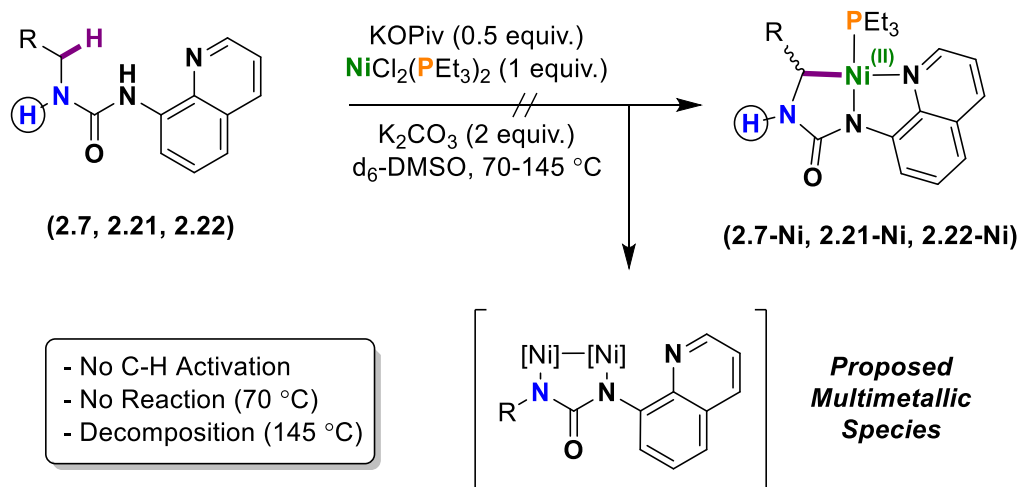


Scheme 2.13 Hammett Plot showing rates of δ -C(sp³)-H activation of *p*-benzyl substituted ureas (2.5, 2.12-2.16).^[166]

Having mapped the rates of C(sp³)-H activation of a range of tertiary ureas, we focused our attention to secondary ureas (Scheme 2.14). We chose to study -N(H)(R) (R = Me, Bn) ureas (**2.21**) and (**2.22**) respectively since methyl and benzyl substituents are readily activated in the analogous tertiary system. Under standard reaction conditions, we found that reactions with ureas (**2.21**) and (**2.22**) resulted in no C-H activation products, but instead formed an insoluble yellow solid and myriad organic products (by ¹H NMR spectroscopy). Urea (**2.7**) underwent similar reactivity; we

propose these ureas may be involved in producing multimetallic species as shown in Scheme 2.14.

Attempts with 2° Ureas

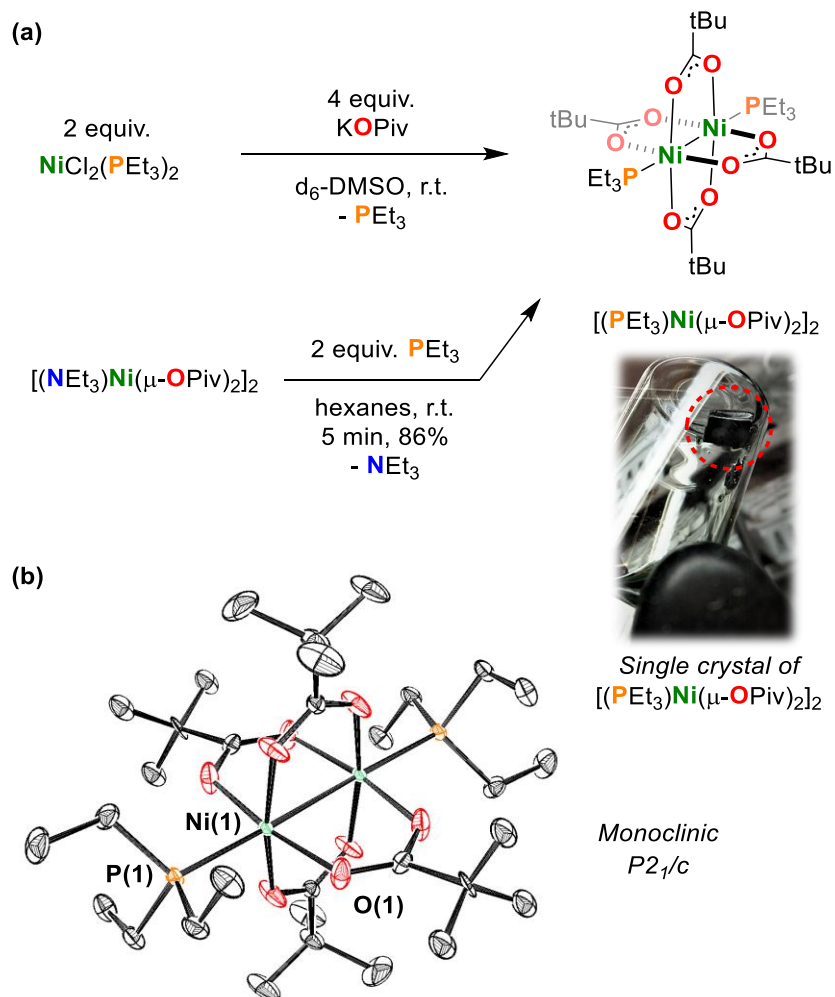


Scheme 2.14 Attempts to use secondary ureas for nickel C-H activation studies.

2.4.4 Investigating Role of KO piv

Encouraged by results with a large range of ureas, and the increased reaction rates with carboxylate additives, we began further mechanistic studies to determine the origins of increased reaction rates when pivalate is added to nickel. When KO piv is added to NiCl₂(PEt₃)₂ (Scheme 2.15), we observe new paramagnetic peaks in the ¹H NMR spectrum (d₆-DMSO, 298 K). Adding two equivalents of PEt₃ to a known Ni(II) paddlewheel dimer, [(NEt₃)Ni(μ-O piv)₂]₂ gave us the

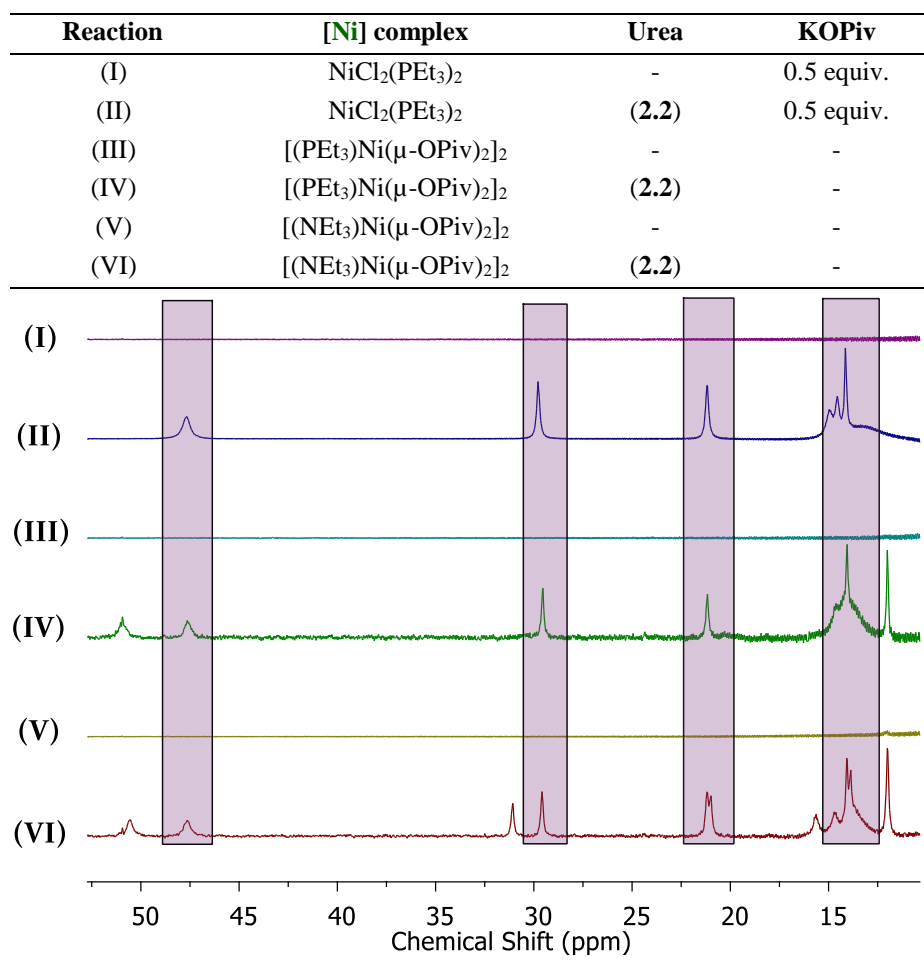
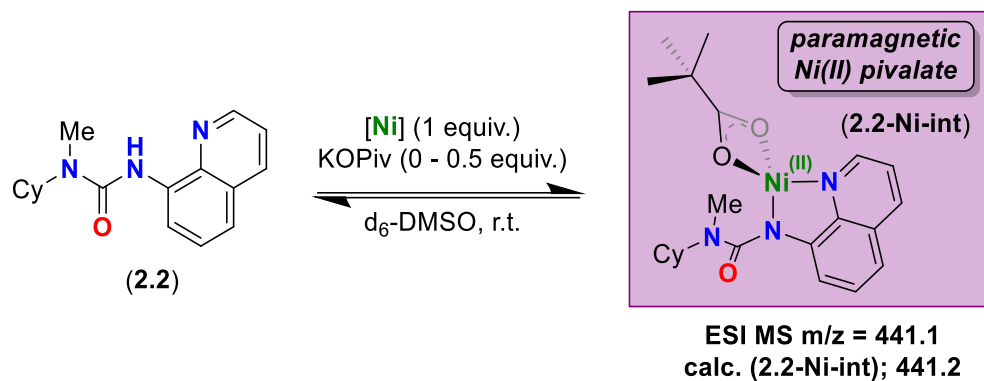
same paramagnetic resonances in the ^1H NMR spectrum. We reasoned the pivalate ions could promote dimerization of two nickel(II) centers, as is common in palladium(II) chemistry.^[14,178] Upon crystallization, we isolated paddlewheel complex, $[(\text{PEt}_3)\text{Ni}(\mu\text{-OPiv})_2]_2$, as large green-yellow iridescent crystals. We characterized $[(\text{PEt}_3)\text{Ni}(\mu\text{-OPiv})_2]_2$ by ^1H NMR spectroscopy, elemental analysis, the Evans method, and single crystal XRD.



Scheme 2.15 (a) Synthesis of $[(\text{PEt}_3)\text{Ni}(\mu\text{-OPiv})_2]_2$ by two methods, and (b) ORTEP depiction of the solid-state structure of complex $[(\text{PEt}_3)\text{Ni}(\mu\text{-OPiv})_2]_2$ (ellipsoids at 50% probability, hydrogens omitted). Selected bond lengths (Å) and angles (°): Ni-Ni 2.5875(3), O1-Ni1-P1 96.60(3).

In the solid-state, complex $[(\text{PEt}_3)\text{Ni}(\mu\text{-OPiv})_2]_2$ exhibits a paddlewheel type structure, where the nickel centers are bridged by four pivalate ions and capped by triethylphosphine ligands. Complex $[(\text{PEt}_3)\text{Ni}(\mu\text{-OPiv})_2]_2$ displays a shortened Ni-Ni distance [Ni-Ni; 2.5875(3) Å] relative to the related triethylamine derivative $[(\text{NEt}_3)\text{Ni}(\mu\text{-OPiv})_2]_2$ [c.f. Ni-Ni; 2.728(2)].^[179] Based on these results, we reasoned that pivalate-induced dimerization may be integral to increasing the rate of phosphine dissociation from Ni(II), much like in the case of Pd(II).^[6] Unfortunately, the poor solubility of $[(\text{PEt}_3)\text{Ni}(\mu\text{-OPiv})_2]_2$ in d_6 -DMSO prevents us from comparing the rates of C-H activation with urea (**2.2**). Moreover, if solutions of $\text{NiCl}_2(\text{PEt}_3)_2$ and KOiv are left overnight (d_6 -DMSO, 298 K), green solids crash out of the reaction, further suggesting formation of complex $[(\text{PEt}_3)\text{Ni}(\mu\text{-OPiv})_2]_2$ in situ.

We then examined the role of pivalate in the presence of ureas, pre-(C-H) activation. Upon addition of (**2.2**) to solutions of $\text{NiCl}_2(\text{PEt}_3)_2$ and KOiv (Scheme 2.16, reaction **II**), new paramagnetic peaks are observed in the ^1H NMR spectrum. These peaks are also observed upon the addition of (**2.2**) to $[(\text{PEt}_3)\text{Ni}(\mu\text{-OPiv})_2]_2$ (reaction **IV**), further supporting the formation of $[(\text{PEt}_3)\text{Ni}(\mu\text{-OPiv})_2]_2$ upon mixing $\text{NiCl}_2(\text{PEt}_3)_2$ and KOiv . These same paramagnetic peaks are observed when (**2.2**) is added to $[(\text{NEt}_3)\text{Ni}(\mu\text{-OPiv})_2]_2$ (reaction **VI**), suggesting that phosphine is not incorporated in the paramagnetic complex.

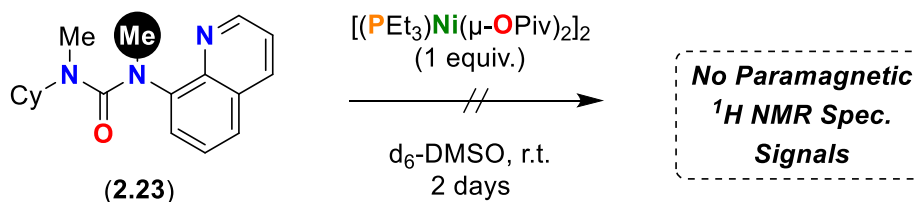


Scheme 2.16 1H paramagnetic NMR spectra for different reactions outlined in the general reaction scheme, and a table showing the reaction contents for reactions (I-VI, d_6 -DMSO, 400 MHz, 298 K).

Based on the above stoichiometric results, we proposed two possible paramagnetic nickel structures: (i) a simple Lewis base adduct of the urea quinoline *via* phosphine displacement, or (ii) the N-H activated product (**2.2-Ni-int**). We tested this hypothesis by synthesizing the quaternary urea (**2.23**), where the N-H is replaced by a N-CH₃ group. This substitution should not affect the Lewis base adduct but should stop the formation of an X-type Ni-N bond as in (**2.2-Ni-int**). Upon addition of (**2.23**) to complex (**4**) (Scheme 2.17), we observed no paramagnetic resonances after days of stirring, suggesting that the paramagnetic resonances belong to (**2.2-Ni-int**) and not the Lewis base adduct of the quinoline.

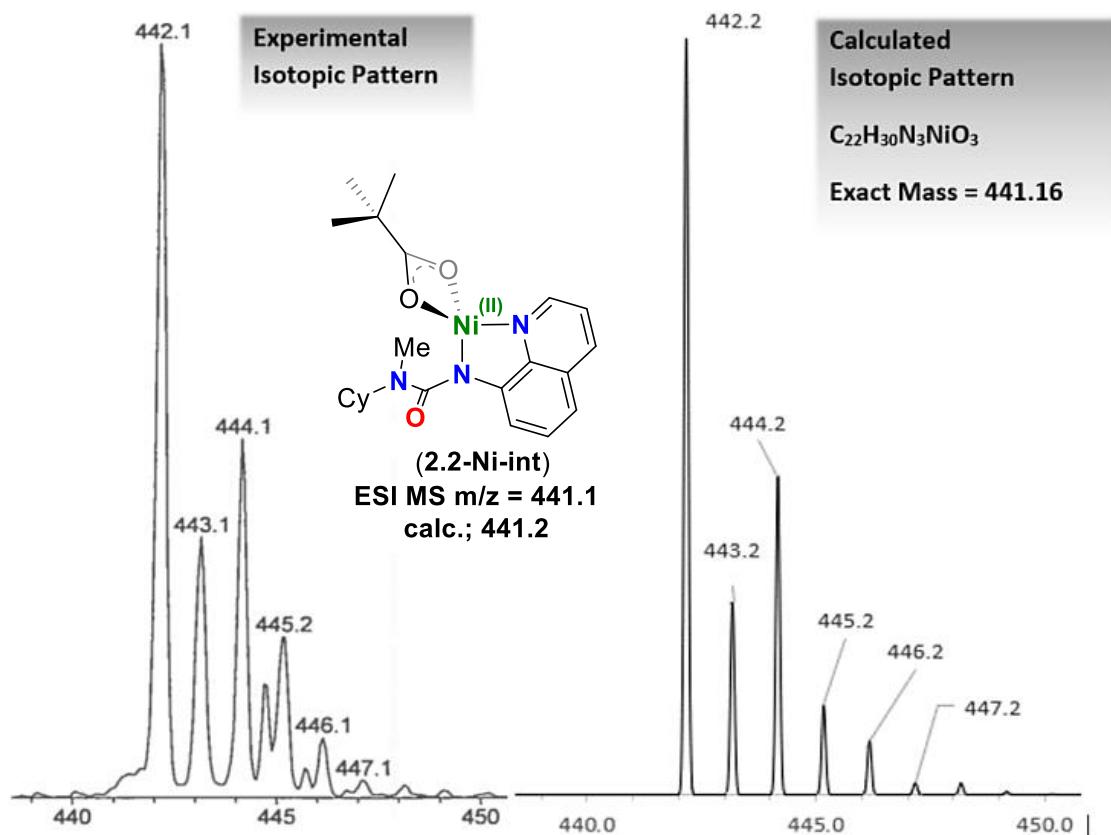
The above stoichiometric NMR scale reactions suggest that the Ni(II) ureate pre-(C-H) activation is a high spin complex, presumably tetrahedral or octahedral. At this time, we favor the idea that (**2.2-Ni-int**) is a monomer, although we cannot rule out dimer formation in solution. Electrospray-ionization mass spectrometry suggests the (**2.2-Ni-int**) is present in solution (Scheme 2.18), although we have not quantified the concentration of this product.

In the ¹H NMR spectra of reactions **II**, **IV**, and **VI** (Scheme 2.16) unbound (**2.2**) is visible but is significantly broadened. We propose an equilibrium between (**2.2**) and (**2.2-Ni-int**), among other probable nickel products. Additionally, the formation of (**2.2-Ni-int**) at room temperature suggests that N-H cleavage is facile. This has been previously proposed in computational studies of the analogous catalytic system with 8AQ substituted amides.^[130]



Scheme 2.17 Probing reactivity of (**2.23**) with nickel complex $[(\text{PEt}_3)\text{Ni}(\mu\text{-OPiv})_2]_2$.

ESI-MS (Low-Res) results:

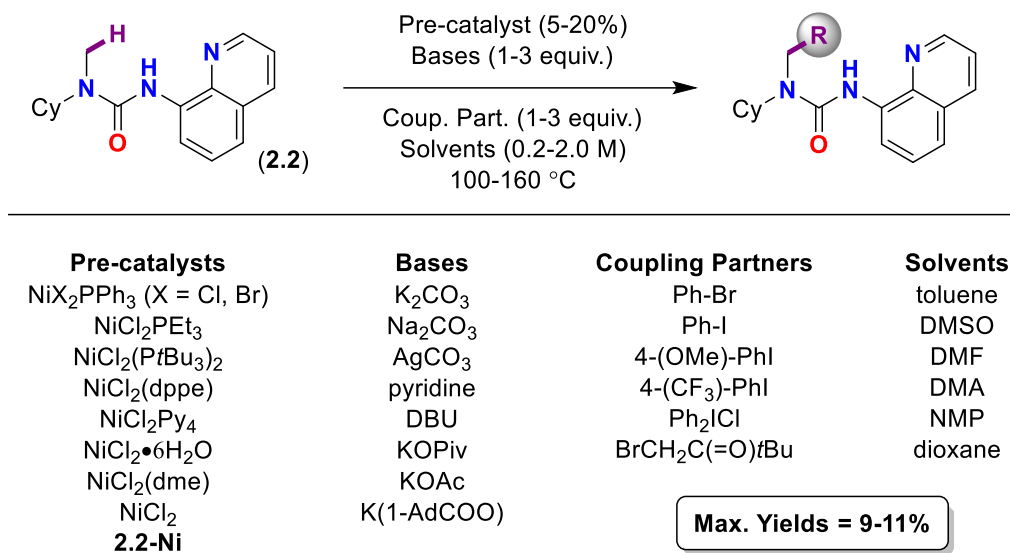


Scheme 2.18 ESI-MS results (low resolution) for in situ generated complex (2.2-Ni-int).

2.5 Catalytic Attempts

While concluding our stoichiometric studies we were also interested in developing a catalytic protocol for the $C(sp^3)$ -H activation of tertiary ureas. Below is a portion of the best results we obtained (Scheme 2.19). Using a wide variety of coupling partners, pre-catalysts, solvents, and bases, we were not able to catalytically functionalize substrate **2.2**. One explanation may be that the cyclometalated ureas are susceptible to radicals, as we hypothesized earlier (Scheme 2.7). If radicals are present in the reaction, perhaps they degrade some cyclometalated complexes before

they can undergo functionalization. Further studies are needed to understand our difficulties in developing this catalytic transformation.

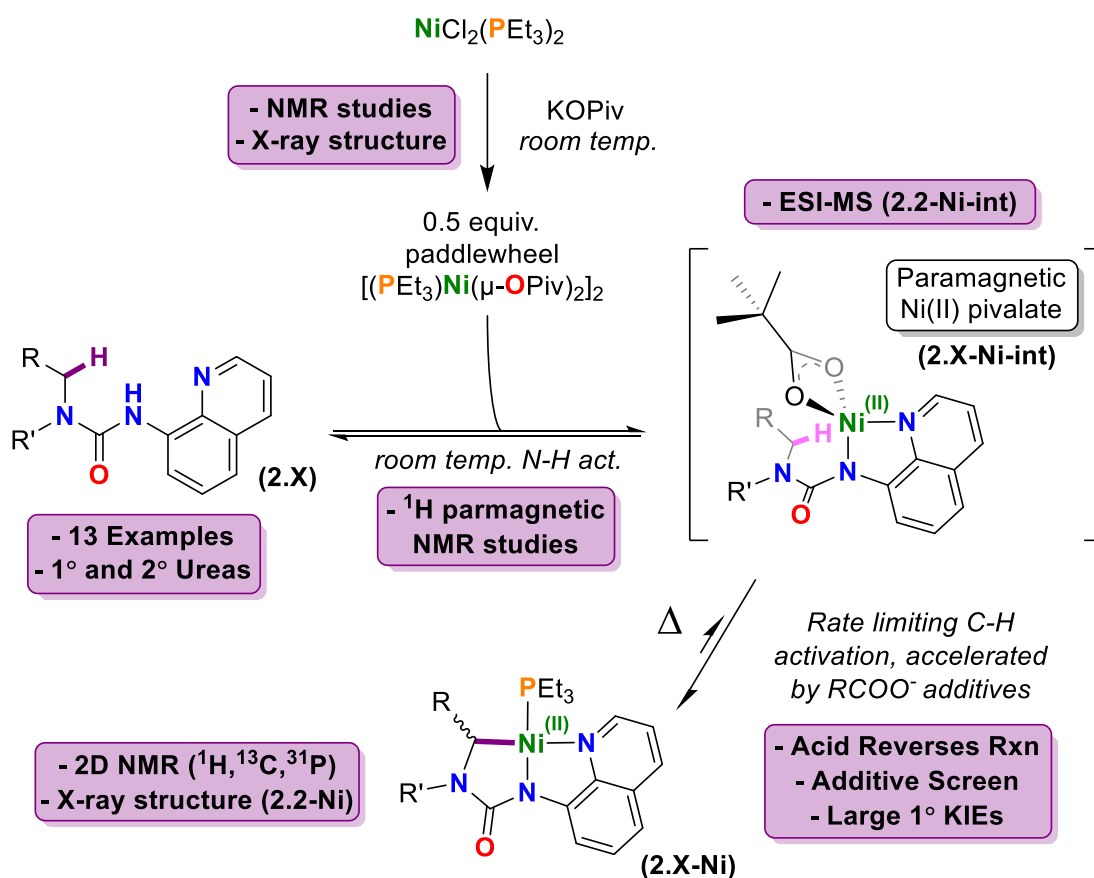


Scheme 2.19 Attempts to functionalize urea 2.2 catalytically with a variety of cross-coupling partners.

2.6 Conclusions

Based on the kinetic and mechanistic data we present in this Chapter, we suggest the following mechanism for C-H activation (Scheme 2.20). When KOPiv is added to NiCl₂(PEt₃)₂, a salt metathesis reaction produces [(PEt₃)Ni(μ-OPiv)₂]₂. NMR scale reactions (Schemes 2.15-2.18) suggest that pivalate is important for facile N-H activation, and dissociation of phosphine. Upon addition of urea (**2.2**), complex (**2.2-Ni-int**) is produced, which was shown by paramagnetic ¹H NMR studies (Schemes 2.15, 2.16) and supported by mass spectrometry. KIE experiments suggest then that the C-H activation step is rate limiting (Scheme 2.9), and protonation studies suggest reversibility is probable (Scheme 2.10). We isolated the C-H activation product (**2.2-Ni**, Scheme 2.4) and showed that different additives have a profound effect on the rate of product formation of (**2.2-Ni**) (Table 2.1). Namely, carboxylate additives (RCOO⁻) show a steric dependence on the

carboxylate R-group. We also showed that substrates (**2.5**, **2.9**, **2.10**, **2.12-2.20**) with secondary C(sp³)-H bonds may be C-H activated (Scheme 2.12), and these substrates are produced at a higher rate for more electron rich derivatives (Scheme 2.13). Finally, we show that (**2.2-Ni**) reacts with myriad electrophiles to afford C-C and C-N coupling products (Scheme 2.6), suggesting that (**2.2-Ni**) is a relevant intermediate in the nickel catalyzed C(sp³)-H functionalization of 8AQ-ureas.



Scheme 2.20 Proposed mechanism for the Ni(II) mediated δ-C(sp³)-H activation of substituted ureas.

We showed in this work that using ureas as model substrates, we can investigate the elementary steps of C(sp³)-H activation at nickel(II) centers. By using the 8AQ directing group, we measured the rates of C-H activation for primary and secondary C-H bonds and showed that

C-H activation is rate limiting prior to functionalization. Additionally, we investigated the role of carboxylate additives, showing that they increase the rate of phosphine dissociation, N-H activation, and C-H activation.

We anticipate this work will facilitate the discovery of important trends in nickel-catalyzed C-H activation, leading to the development of more efficient methodologies with broader scope. In addition, we have been focused on applying our discovery of nickel mediated urea C(sp³)-H bond activation to catalytic methodologies, which we anticipate may be used to advantage the alpha-functionalization of amide-directed amines.

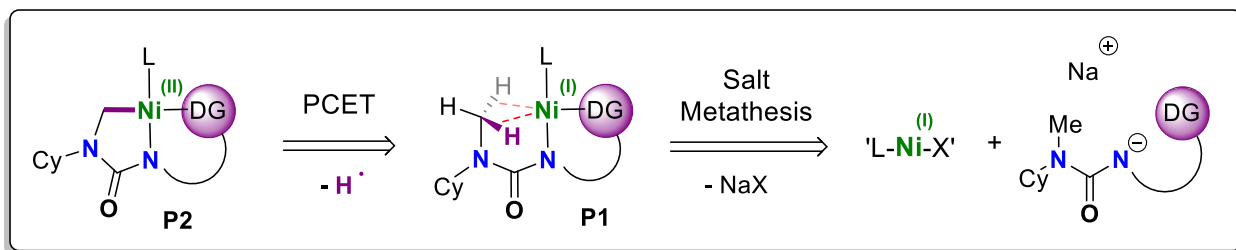
Experimental data for Chapter 2 begins on pg. 127

Chapter 3: Preparation of Low-Coordinate Ni(I) Amidate Complexes and Reactivity of Ni(I) Complexes Towards C(sp³)-H Activation

3.1 Introduction

Transition metal systems incorporating transient metal-centred unsaturation have proven ubiquitous for myriad catalytic transformations including olefin metathesis,^[180] olefin polymerization,^[181] cross-coupling,^[182,183] and hydrogenation.^[184] Thus, low-coordinate complexes are often targeted as highly reactive species. In the absence of other stabilizing contacts, coordinatively unsaturated complexes can interact with sigma (σ) bonds (e.g. C-H bonds)^[49,50,56] in a 3-center-2-electron (3c-2e) manner to form agostic or sigma complexes. From a mechanistic standpoint, understanding the interactions of σ -bonds with transition metals is critical, as it is understood that these interactions are requisite for productive bond activation processes.^[28,49]

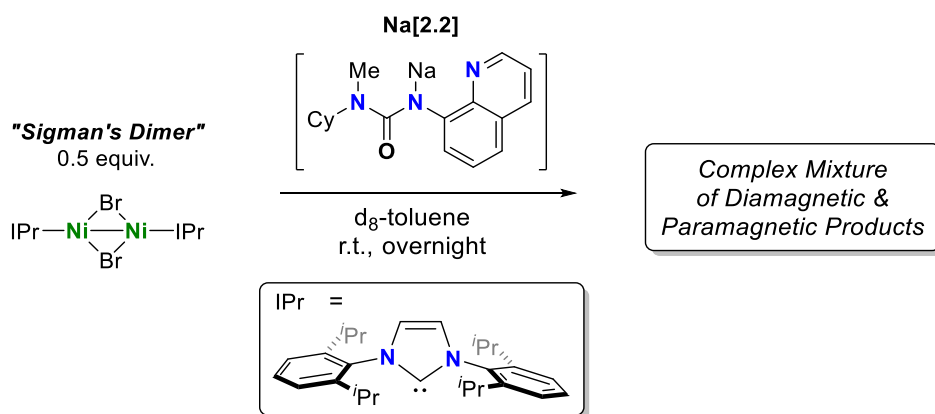
As was discussed in Chapter 1, the literature surrounding the role of Ni(I) complexes in C-H activation is essentially non-existent. Only one report claims Ni(I) can activate C-H bonds, however, their results are mechanistically not conclusive; at least with respect to oxidation state. We anticipated based on our results from Chapter 2 that we could prepare low coordinate ureate-Ni(I) complexes with C-H agostic interactions (Scheme 3.1), with the goal of probing the possible role of Ni(I) complexes in C-H activation. These low coordinate agostic complexes could be susceptible to hydrogen atom abstraction or proton coupled electron transfer (PCET), formally producing a Ni(II) cyclometalated complex as in Chapter 2 (c.f. **2.2-Ni**).



Scheme 3.1 Retrosynthetic analysis for the preparation of Ni(I) ureate agostic complexes.

3.2 Attempts to Synthesize of IPr-Ni(I)-Ureate Complexes

We began our study by attempting to use the same 8AQ ureas we used in Chapter 2, coupled with the low-coordinate Ni(I) synthon Sigman's Dimer, $[(IPr)Ni(\mu-Br)]_2$ (IPr = 1,3-bis(2,6-diisopropylphenyl)imidazol-2-ylidene).^[185,186] Reactions in toluene produced a range of products, which we were unable to characterize (Scheme 3.2). Based on the literature of Ni(I),^[42,75,187,188] we hypothesized that perhaps the 8AQ-ureas were not be amenable to this chemistry because Ni(I) often prefers to be lower coordinate. To remedy this issue, we began testing amides as alternative ligands for probing proposed Ni(I) C-H agostic contacts. We chose amides because of their modular synthesis.



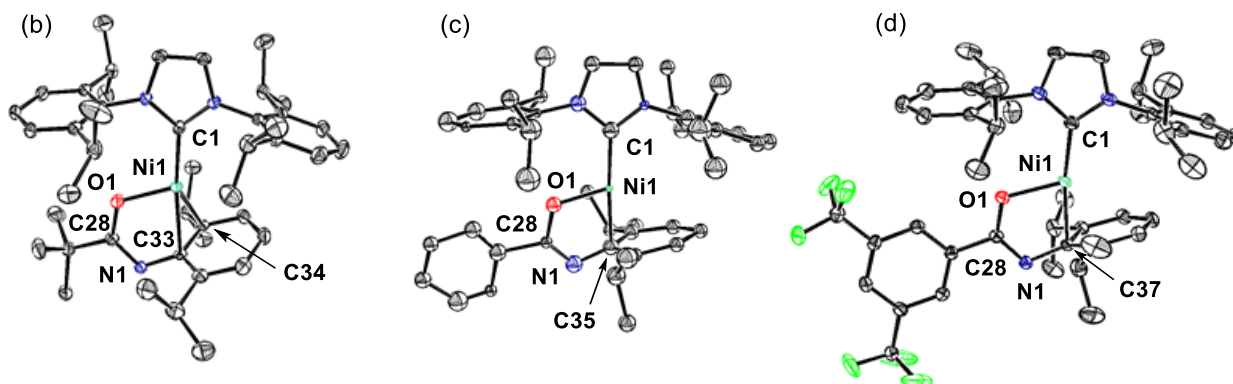
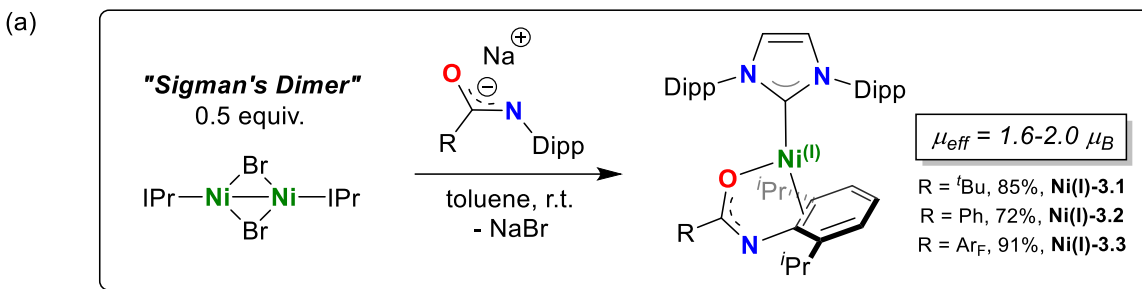
Scheme 3.2 Attempts to react Sigman's Dimer with ureate ligands

3.3 Synthesis of IPr-Ni(I)-Amidate Complexes

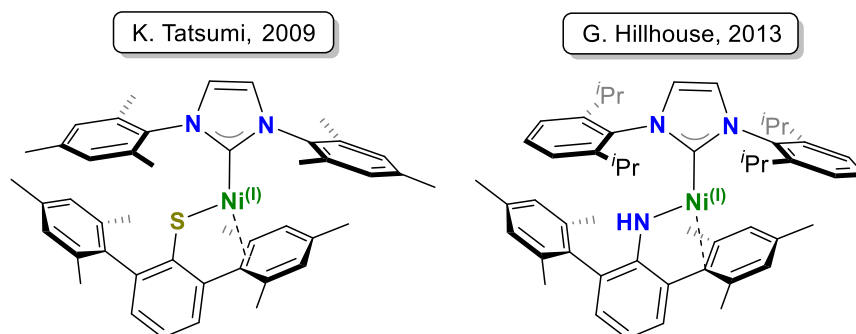
3.3.1 N-Dipp, C-aryl Amidate Ni(I) Complexes: N-Aryl Preferred

We began our investigation by examining amidate ligands with the sterically encumbered *N*-aryl Dipp group to encourage low coordination numbers at nickel. Our original amide (**3.1**) also incorporated a *tert*-butyl group to encourage agostic interactions. Reaction of Na(**3.1**) with Sigman's Dimer produced complex **Ni(I)-3.1**, which was isolated as a paramagnetic yellow crystalline solid in 85% yield (Scheme 3.3a). A C₆D₆ solution of **Ni(I)-3.1** displays a $\mu_{\text{eff}} = 1.71 \mu_{\text{B}}$ (Evans method, 25 °C), consistent with a one electron paramagnet [*c.f.* $\mu_{\text{SO}} = 1.73 \mu_{\text{B}}$]. Single crystal X-ray analysis of **Ni(I)-3.1** reveals a T-shaped $\kappa^1\text{-O}$, $\eta^2\text{-C=C}$ amidate binding mode (Scheme 3.3b), reminiscent of known Ni(I) thiolate^[189] and amide^[188] complexes (Scheme 3.4). In complex **Ni(I)-3.1**, bond lengths [C(28)-N(1) = 1.306(3) Å] and [C(28)-O(1) = 1.295(3) Å] are consistent with delocalization of charge throughout the amidate backbone. Bond distances [C(33)-C(34) = 1.429(4) Å] and [C(33)-C(38) = 1.432(3) Å] are elongated from the proteo-ligand [*c.f.* 1.403(3) Å, *see SI*], indicating some back-bonding into the aryl ring.

Based on the solid-state molecular structure of **Ni(I)-3.1** and structurally related complexes known in the literature, it seemed that this binding mode was preferred for IPr-Ni(I) complexes. We postulated that by changing the C-*t*Bu to a C-aryl that the Ni(I) metal center might choose to bind to the C-aryl group preferentially over the N-Dipp group. Complexes **Ni(I)-3.2** [C-Ph, N-Dipp] and **Ni(I)-3.3** [C-(3,5-bis(CF₃)Ph), N-Dipp] may be synthesized in good yields (72% and 91% respectively) from Sigman's Dimer (Scheme 3.3a). Surprisingly, both complexes adopt the same binding mode as complex **Ni(I)-3.1**. The electron-poor C-(3,5-bis(CF₃)Ph) moiety in **Ni(I)-3.3** is a far better π -accepting aryl when compared to the N-Dipp group. These results suggest the IPr-Ni(I) synthon prefers to be $\kappa^1\text{-O}$ and T-shaped if given the proper substituents.



Scheme 3.3 (a) Accessing complexes **Ni(I)-3.1**, **Ni(I)-3.2**, and **Ni(I)-3.3** from Sigman's Dimer by salt metathesis with Na(3.1-3.3). (b) ORTEP depiction of the solid-state structure of **Ni(I)-3.1** ellipsoids at 50% probability, hydrogens omitted). Selected bond lengths (Å) and angles (°): Ni1-C33 2.195(2), Ni1-C34 2.166(2), Ni1-O1 1.9633(18), C33-C34 1.429(4), N1-C28 1.306(3), O1-C38 1.295(3), C1-Ni1-C33 171.82(9), C1-Ni1-C34 141.93(10), C1-Ni1-O1 107.90(8). (c) isotropic ORTEP depiction of the solid-state structure of **Ni(I)-3.2**. *Poor quality structure*. (d) ORTEP depiction of the solid-state structure of **Ni(I)-3.3**. Selected bond lengths (Å) and angles (°): Ni1-C37 2.1245(14), Ni1-O1 1.9937(11), N1-C28 1.2978(19), O1-C28 1.2936(18), C1-Ni1-C37 171.51(6), C1-Ni1-O1 109.44(6).

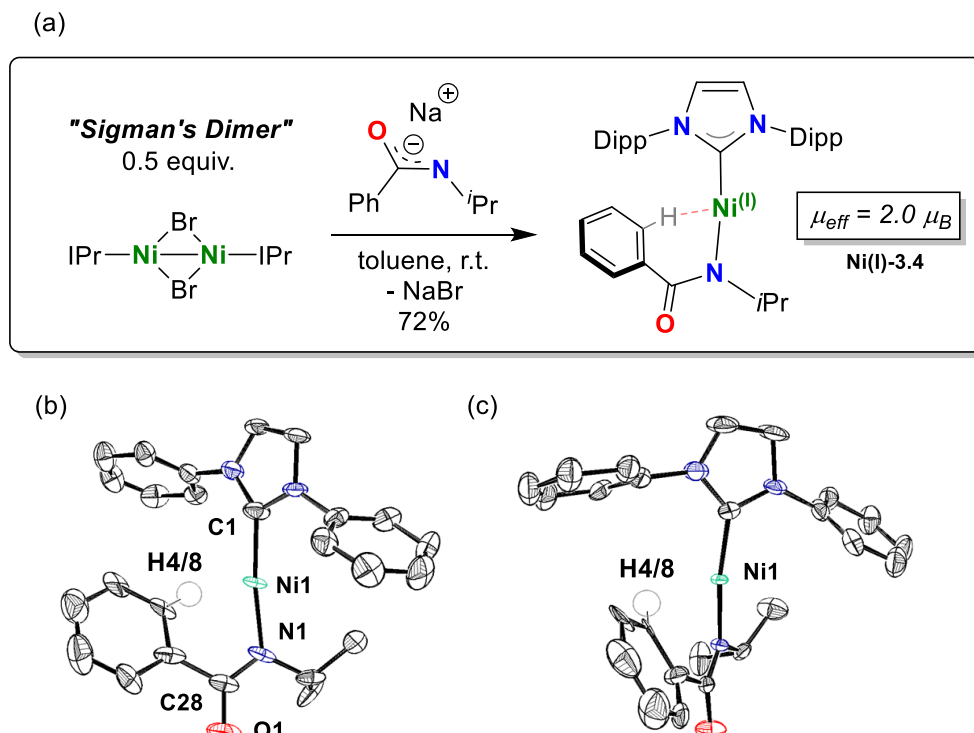


Scheme 3.4 Similar binding modes of Ni(I) NHC species in the literature, reported by Tatsumi^[189] and Hillhouse.^[188]

3.3.2 N-*i*Pr, C-aryl Amidate Ni(I) Complexes: A Change in Binding Mode

We then decided to substitute the π -stabilizing N-Dipp group from the amidate ligand. This structural substitution should render the amidate C-aryl available for backbonding. Complex **Ni(I)-3.4** [C-Ph, N-*i*Pr] may be synthesized in analogy to the other Ni(I)-amidate compounds from Sigman's Dimer (Scheme 3.5a). Single crystal X-ray diffraction of **Ni(I)-3.4** reveals what appears to be a Ni(I) C-H agostic complex, characterized by the binding mode $\kappa^2\text{-N,(C-H)}$ (Scheme 3.5b,c). The X-ray diffraction data is somewhat poor, however the calculated C-H agostic contacts are well within the expected distances for C-H agostic interactions.^[27] The amidate C-N [1.33(3) Å] and C-O [1.26(2) Å] suggest C-O double bond and C-N single bond character; delocalization is small compared to **Ni(I)-3.1**, **Ni(I)-3.2**, and **Ni(I)-3.3**.

These results show that amidates can be rationally designed to afford low-coordinate Ni(I) C-H agostic complexes as we hypothesized. Although these C(sp²)-H agostic interactions are the first of their kind for monovalent nickel, we were more interested in developing C(sp³)-H agostic derivatives to compare to our Chapter 2 results with ureas.



Scheme 3.5 (a) Accessing complex Ni(I)-3.4 from Sigman's Dimer by salt metathesis with Na(3.4). (b) Front view: ORTEP depiction of the solid-state structure of Ni(I)-3.4, disordered over two positions (ellipsoids at 50% probability, hydrogens and Dipp(iPr) groups omitted). Selected bond lengths (Å) and angles (°) averaged over both structures: Ni1-N1 1.920(18), N1-C28 1.33(3), O1-C28 1.26(2), C1-Ni1-N1 172.6(7). (c) Side view: ORTEP depiction of the solid-state structure of Ni(I)-3.4, disordered over two positions (ellipsoids at 50% probability, hydrogens and Dipp(iPr) groups omitted). Selected bond length (Å) averaged over both structures: Ni1-H4/8 (calc) 2.01(2).

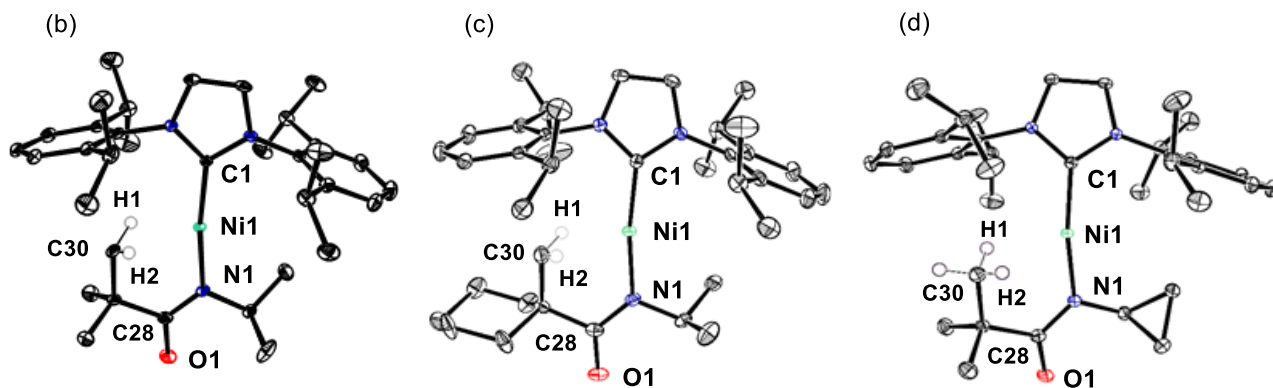
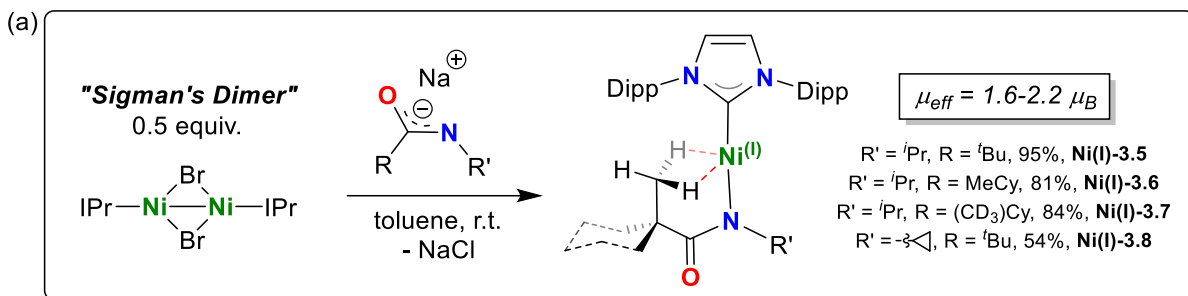
3.3.3 N-iPr, C-(3°)alkyl Amidate Ni(I) Complexes: The First Ni(I) C(sp³)-H Contacts

As in moving from complexes Ni(I)-(3.1, 3.2, 3.3) to Ni(I)-3.4, we became interested in substituting the amide aryl substituents with alkyl fragments. We anticipated the resulting Ni(I) structures might have weakly stabilizing C(sp³)-H agostic interactions in place of the C(sp²)-H contacts. Complex Ni(I)-3.5 [C-tBu, N-iPr], Ni(I)-3.6 [C-(1-methylcyclohexyl), N-iPr], Ni(I)-3.7

[C-(1-(d₃)-methylcyclohexyl), N-iPr] and **Ni(I)-3.6** [C-tBu, N-cyclopropyl] were synthesized by the same method with Sigman's Dimer (Scheme 3.6a).

Importantly, single crystal X-ray analyses indicate the formation of a κ^1 -N bound species, each structure having dual supporting σ -bis(C-H) agostic (or bifurcated η^3 -H₂C) contacts resulting in a pseudo-T-shaped geometry (Figure 3.6b,c,d). These bifurcated η^3 -H₂C interactions are rare for C(sp³)-H agostic complexes, but have been noted previously.^[190–193] To our knowledge, these complexes represent the first examples of Ni(I) C(sp³)-H agostic complexes. It is noteworthy that the X-ray data are of sufficient quality allowing for free location and refinement of the agostic hydrogen atoms, giving typical lengths and angles of C-H agostic donors (Table 3.1).

Unlike complexes **Ni(I)-3.1**, **Ni(I)-3.2**, and **Ni(I)-3.3**, the amidate bond lengths [C(28)-N(1) = 1.3392(13) Å] and [C(28)-O(1) = 1.2515(12) Å] in **Ni(I)-3.5** suggest localization of charge at N(1). Similar to related Ni(I) amido^[194] and alkyl^[186] structures, the C(1)-Ni(1)-N(1) angle 172.12(4)° indicates quasi-linearity. These structures should be described as essentially linear 2-coordinate Ni(I) complexes with weak δ -agostic interactions orthogonal to the amidate N-Ni bond. The H-Ni distances range from 1.94(2)-2.35(4) Å (see solid-state structures, Scheme 3.6b,c,d & Table 3.1). To confirm real bonding between the σ (C-H) and the nickel center, we analyzed **Ni(I)-3.5** by QT-AIM and NBO analyses.



Scheme 3.6 (a) Accessing complexes Ni(I)-3.5, Ni(I)-3.6, and Ni(I)-3.8 from Sigman's Dimer by salt metathesis with Na(3.5-3.8). (b) ORTEP depiction of the solid-state structure of Ni(I)-3.5 (ellipsoids at 50% probability, hydrogens omitted). H1 and H2 were freely located and refined from the electron density map. Selected bond lengths (Å) and angles (°): Ni1-C1 1.9119(9), Ni1-N1 1.9149(8), Ni1-C30 2.4476(10), Ni1-H1 2.024(15), Ni-H2 2.159(15), C28-N1 1.3392(13), C28-O1 1.2515(12), N1-Ni1-C1 172.12(4), C30-H1-Ni1 101.8(10), C30-H2-Ni1 94.3(10). (c) ORTEP depiction of the solid-state structure of Ni(I)-3.6. H1 and H2 were freely located and refined from the electron density map. Selected bond lengths (Å) and angles (°): Ni1-C1 1.89350(19), Ni1-N1 1.89980(19), Ni1-C30 2.4007(2), Ni1-H1 1.94(2), Ni-H2 2.15(2), C28-N1 1.33028(11), C28-O1 1.25036(12), N1-Ni1-C1 171.0550(12), C30-H1-Ni1 106.18(3), C30-H2-Ni1 92.60(8). (d) ORTEP depiction of the solid-state structure of Ni(I)-3.8. H1 and H2 were freely located and refined from the electron density map. Selected bond lengths (Å) and angles (°): Ni1-C1 1.89571(11), Ni1-N1 1.89054(9), Ni1-C30 2.5668(16), Ni1-H1 2.07(5), Ni-H2 2.35(4), C28-N1 1.3417(19), C28-O1 1.247(2), N1-Ni1-C1 167.7872(7), C30-H1-Ni1 109.61(9), C30-H2-Ni1 91.32(9).

Table 3.1 Distances and Angles of Agostic Complexes Ni(I)-3.4, Ni(I)-3.5, Ni(I)-3.6, and Ni(I)-3.8. *denotes value outside the accepted literature ranges.

<i>Literature</i> ^[49]	d(M-H) ~ 1.8-2.3 Å		M-C-H ~ 90-140 °	
Complex	Ni1-H1 (Å)	Ni1-H2 (Å)	C28-Ni1-H1 (°)	C28-Ni1-H1 (°)
Ni(I)-3.4	2.01(2) (calc)	-	115.4(4)	-
Ni(I)-3.5	2.159(15)	2.024(15)	101.8(10)	94.3(10)
Ni(I)-3.6	1.94(2)	2.15(2)	106.18(3)	92.60(8)
Ni(I)-3.8	2.07(5)	2.35(4)*	109.61(9)	91.32(9)

3.3.3.1 DFT Analysis of Structure and Bonding in Complex Ni(I)-3.5

The gas-phase geometry of **Ni(I)-3.5** was calculated and optimized using DFT (Figure 3.1a).^[195] The optimized geometry of **Ni(I)-3.5** differs from the X-ray structure in that the NHC imidazole and amidate O(1)-C(28)- N(1) planes deviate from coplanarity [29.3°],^[196] but the N(1)-Ni(1) [1.900 Å], C(1)-Ni(1) [1.922 Å] bond lengths and C(1)-Ni(1)-N(1) angle [172.6°] are consistent with solid-state observations. Two inequivalent C-H...Ni interactions are observed [$d(\text{H}(1)\cdots\text{Ni}(1)) = 2.119 \text{ Å}$; $d(\text{H}(2)\cdots\text{Ni}(1)) = 2.189 \text{ Å}$]. The elongation of the C(28)-H(1) and C(28)-H(2) bonds relative to those in the non-interacting ^{*t*Bu} groups was small [C(28)-H(1): 0.011 Å; C(28)-H(2): 0.006 Å], indicating the weak nature of the C-H...Ni interactions. Optimization of hydrogen atom positions in **Ni(I)-3.5** while constraining heavy atom positions to those determined by XRD did not result in significantly larger C-H bond elongation. NBO and AIM analysis were applied to **Ni(I)-3.5** to substantiate the putative bis- $\sigma_{\text{C-H}}$ bonding mode. Second order perturbation analysis performed in the NBO analysis reveals donation from the β -spin C-H σ -bond orbital to an *sd* hybrid on the Ni(I) centre [$E^{(2)}$: 5.7 kcal·mol⁻¹ (H1), 5.1 kcal·mol⁻¹ (H2)]. These interactions are non-negligible, but weak compared to those reported previously for Ni(II) agostic interactions.^[51] AIM theory is useful in cases where bonding modes are ambiguous, as searching

for bond critical points (bcps) in electron density maps provides a criterion for the presence of a chemical bond. The electron density topology in **Ni(I)-3.5** in the plane of the $\text{CH}_2\cdots\text{Ni}$ (Figure 3.1b). A bond critical point was located for the $\text{C(30)-H(1)}\cdots\text{Ni(1)}$ interaction, whereas no bcp was found between Ni and the more distal C(30)-H(2) bond. The H(1)-Ni(1) bond critical point properties are similar to those found for weak $\text{C-H}\cdots\text{Pd}$ interactions found in a series of unsaturated Pd(II) phosphine complexes by Hartwig and coworkers.^[197]

Despite the lack of a bcp, the similarity in $E^{(2)}$ values for the two $\text{C-H}\cdots\text{Ni}$ interactions suggests that the C(30)-H(2) bond is interacting with Ni in the same fashion, and the absence of bcps for agostic interactions is a phenomenon that has been noted previously.^[198] Taken together, the NBO and AIM data are consistent with our assignment of a bis- $\sigma_{\text{C-H}}$ binding motif.

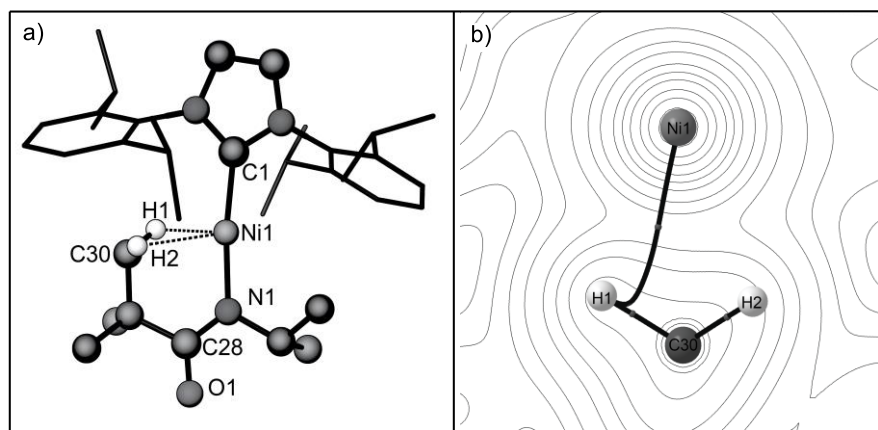


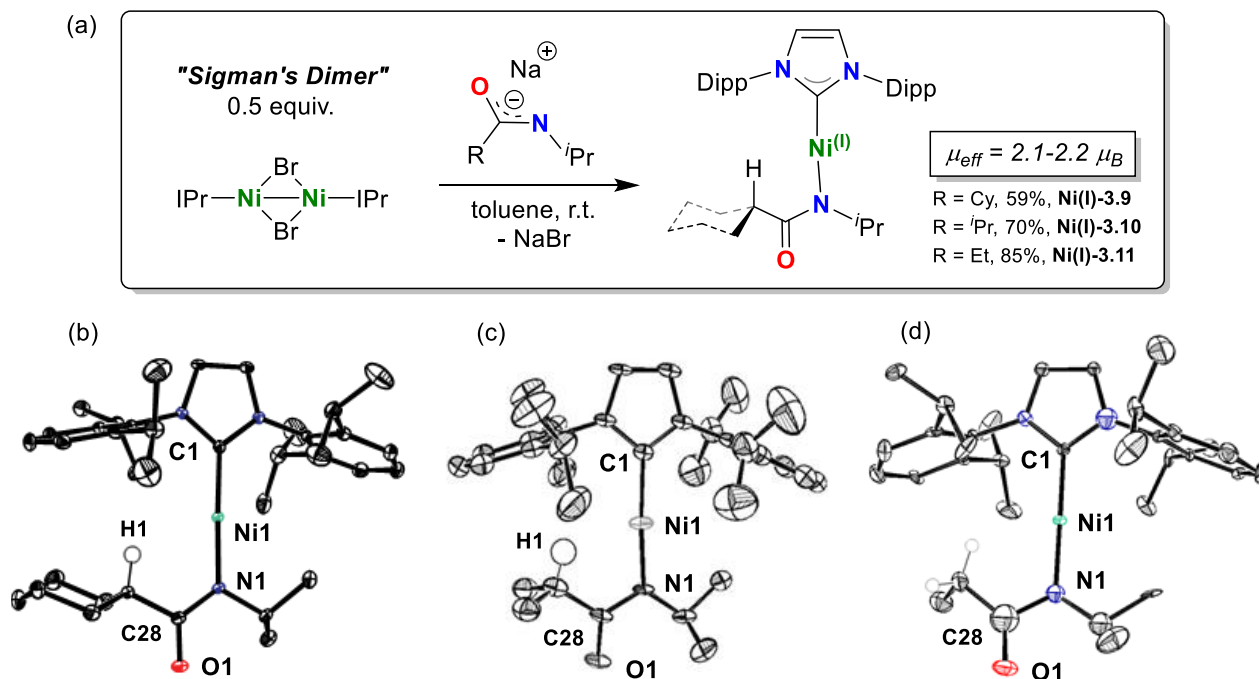
Figure 3.1 (a) DFT-optimized structure of Ni(I)-3.5 (b) AIM contour map of the electron density in the Ni1-H1-C30 plane of Ni(I)-3.5 showing bcps as grey dots and bond paths as black lines.

3.3.4 N-*i*Pr, C-(1,2°)alkyl Amidate Ni(I) Complexes: Linear 2-Coordinate Complexes

Crabtree has reported similar weak C-H agostic interactions to **Ni(I)-3.5** in an Ir(III) system when a ligand *t*Bu group was brought into close proximity.^[199] When an *i*Pr group was instead employed, the agostic interaction was no longer evident by NMR spectroscopy, nor in the solid-

state. To similarly probe the C-H agostic interactions in our system, we prepared amides **3.9** [C-Cy, N-iPr], **3.10** [C-iPr, N-iPr] and **3.11** [C-Et, N-iPr] (IPr)NHCOR. Combining Sigman's dimer (0.5 equiv) and Na[**3.9-3.11**] affords paramagnetic pale yellow crystals of **Ni(I)-3.9**, **Ni(I)-3.10**, and **Ni(I)-3.11** in 59%, 70%, and 85% yield respectively (Scheme 3.7a).^[200] Evans method measurements of these complexes (C₆D₆, 25 °C) are again consistent with a one-electron species. The large range of magnetic moments for two coordinate transition metal species has been addressed previously.^[201]

X-ray crystallographic analysis of **Ni(I)-3.9** and **Ni(I)-3.10** confirm structures (Scheme 3.7b,c) nearly identical to their agostic analogues **Ni(I)-3.6** and **Ni(I)-3.5** (Scheme 3.6c,b). However, in the absence of a quaternary carbon α to the carbonyl, a methine C-H bond is parallel to the nickel-nitrogen bond, eliminating any agostic contributions. Thus, **Ni(I)-3.9**, **Ni(I)-3.10**, and **Ni(I)-3.11** are formally two-coordinate Ni(I) species. This example illustrates an unusual case where the removal of steric bulk from complexes **Ni(I)-3.6** and **Ni(I)-3.5** to **Ni(I)-3.6** and **Ni(I)-3.5** results in a lower coordinate species.



Scheme 3.7 (a) Accessing complexes **Ni(I)-3.9**, **Ni(I)-3.10**, and **Ni(I)-3.11** from Sigman's Dimer by salt metathesis with **Na(3.9-3.11)**. (b) ORTEP depiction of the solid-state structure of **Ni(I)-3.9** (ellipsoids at 50% probability, hydrogens omitted). Selected bond lengths (Å) and angles (°): Ni1-N1 1.8871(12), N1-C28 1.3439(19), O1-C28 1.2496(18), H1-Ni1 2.53(2), C1-Ni1-N1 1.77.62(6). (c) ORTEP depiction of the solid-state structure of **Ni(I)-3.10**. Selected bond lengths (Å) and angles (°): Ni1-N1 1.85(2), N1-C28 1.381(19), O1-C28 1.255(13), H1-Ni1(calc) 2.295, C1-Ni1-N1 169.0(5). (d) isotropic ORTEP depiction of the solid-state structure of **Ni(I)-3.11**. *Poor quality structure.*

3.4 Attempts Towards C-H Activation of Complex **Ni(I)-3.5**

Having characterized the desired C(sp³)-H agostic compound **Ni(I)-3.5**, we wished to attempt C-H activation of these bifurcated 3-center-2-electron bonds. We envisioned a PCET (formal H atom abstraction) from one of the agostic C-H interactions by a bulky radical reagent to afford the cyclometallated species **Ni(II)-3.12B** (Scheme 3.8a). Such a reaction would be important for two reasons: (i) it could provide evidence of Ni(I) mediated C-H bond activation,

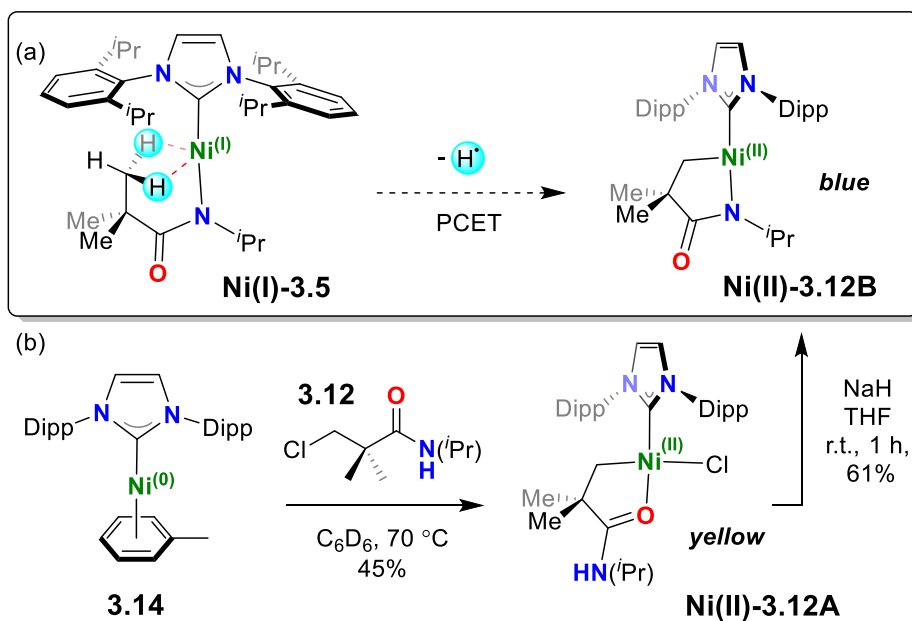
(ii) it would give precedent to eliminating the need for a double directing group as in Chapter 2 of this thesis. Below we describe the independent synthesis of complex **Ni(II)-3.12B**, the postulated product from hydrogen abstraction from complex **Ni(I)-3.5**. Furthermore, we report reactions of **Ni(I)-3.5** under a range of reducing and oxidizing conditions and show that reactions of **Ni(I)-3.5** do not produce complex **Ni(II)-3.12B**. Comparisons in reactivity are made between **Ni(I)-3.1** and **Ni(I)-3.5** where appropriate.

3.4.1 Independent synthesis of Ni(II) C-H activated complex

We began our investigations by independently synthesizing complex **Ni(II)-3.12B** (Scheme 3.8b). Complex **Ni(II)-3.12B** can be prepared in two steps from Ogoshi's two coordinate (IPr)Ni⁰(η^6 -toluene) complex **3.14**.^[202] Addition of the chlorinated amide^[203] **3.12** to complex **3.14** at room temperature affords complex **Ni(II)-3.12A** in 45% yield. Complex **Ni(II)-3.12A** was characterized by multinuclear NMR spectroscopy, electron impact mass spectrometry (EI-MS), elemental analysis (EA), and single crystal X-ray diffraction (XRD).

A ¹H-¹³C heteronuclear multiple bond correlation (HMBC) between the Ni-alkyl (CH_2) and the Ni-C_{NHC} support the formation of a Ni alkyl species in **Ni(II)-3.12A**. The ¹H NMR spectrum of **Ni(II)-3.12A** exhibits four methyl signals for the IPr isopropyl groups, suggesting limited rotation about the Ni-C_{NHC} bond (NHC = N-heterocyclic carbene). We propose the hydrogen atoms of the Ni-alkyl (CH_2) are responsible for this restricted rotation about the Ni-C_{NHC} bond. Variable temperature ¹H NMR studies show one pair of IPr isopropyl methyl signals coalesce between 308-314K (see ESI). In contrast, the second set does not coalesce until 325-331 K. Furthermore, nuclear Overhauser effect (NOE) ¹H NMR experiments show a correlation between the Ni-alkyl and the pair of more restricted IPr methyl peaks. Finally, the amide N-H is unambiguously

characterized by a one bond ^1H - ^{15}N heteronuclear single quantum correlation (HSQC). Our assignment is corroborated by single crystal XRD analysis (Figure 3.2). In the unit cell, four independent molecules are found, with all four connected by hydrogen bonding between the N-H and the Ni(1)-Cl(1) fragments. The Ni(1)-C(30) bond lengths [avg. 1.921(3) Å] are on average shorter than other Ni-C(sp³) bonds.^[204] Little delocalization is present in the amide N(1)-C(30)-O(1) fragment, characterized by the C(30)-O(1) [avg. 1.266(6) Å] and C(30)-N(1) [1.323(6) Å].



Scheme 3.8 (a) Proposed synthesis of **Ni(II)-3.12B** via C-H activation by PCET from complex **Ni(I)-3.5**, (b) independent synthesis of complex **Ni(II)-3.12B** from complexes **3.14** and **Ni(II)-3.12A**.

Addition of NaHMDS or NaH to yellow solutions of **Ni(II)-3.12A** results in slow formation of blue complex **Ni(II)-3.12B** (Scheme 3.8b). Reactions with NaH result in higher yields (61% NaH vs 26% NaHMDS). In our hands, complex **Ni(II)-3.12B** decomposes slowly in both solution or solid-state to afford an insoluble green-blue solid. We speculate that the unsaturated nature of **Ni(II)-3.12B** may make it susceptible to oligomerization. This phenomenon is known for related

cyclometallated amides at Ni(II) metal centers.^[205] Nevertheless, we were successful in fully characterizing **Ni(II)-3.12B** by multinuclear NMR spectroscopy, EI-MS, and EA. Repeated attempts to crystallize **Ni(II)-3.12B** led to analytically pure amorphous solids.

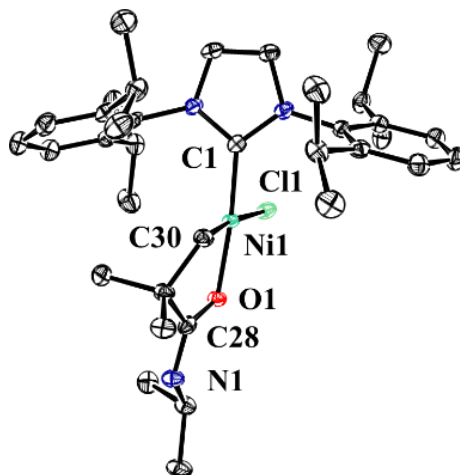
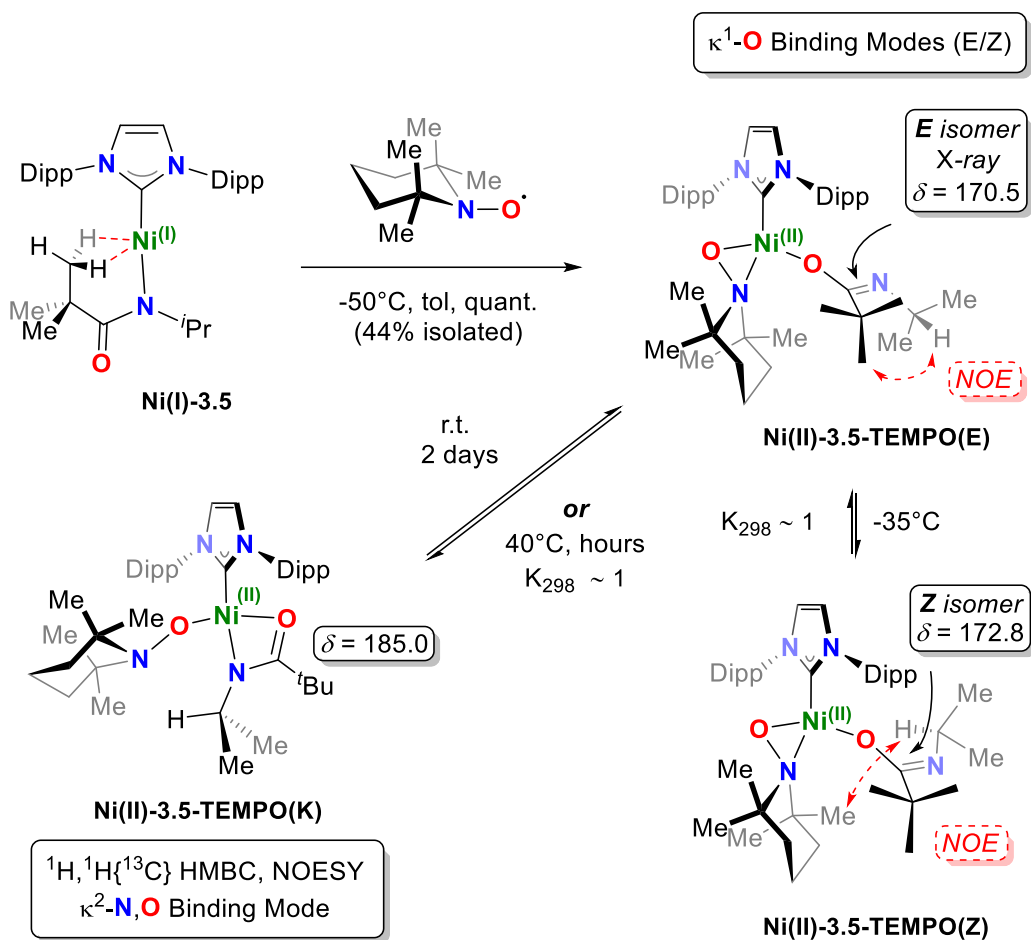


Figure 3.2 ORTEP depiction of the solid-state structure of **Ni(II)-3.12A** (ellipsoids at 50% probability, hydrogens and solvent omitted). Selected average bond lengths (Å) and angles (°): Ni(1)-C(30) 1.921(3), C(30)-O(1) 1.266(6), C(30)-N(1) 1.323(6), C(30)-Ni(1)-Cl(1) 173.60(1).

In contrast to **Ni(II)-3.12A**, the ^1H NMR spectrum of **Ni(II)-3.12B** suggests free rotation of the Ni-C_{NHC} bond as evident by only two distinct NHC methyl groups and a single methine resonance. The chemical shift for the Ni-alkyl (CH_2) is shifted considerably downfield [complex **Ni(II)-3.12B** δ 1.07; complex **Ni(II)-3.12A** δ 0.49] compared to **Ni(II)-3.12A**. The presence of the Ni-alkyl, like **Ni(II)-3.12A**, is confirmed by a ^1H - ^{13}C HMBC NMR experiment. Notably, Pelties and Wolf recently reported complex **C**, very structurally similar to **Ni(II)-3.12B** (Scheme 3.9).^[206] Not surprisingly, the blue solids **Ni(II)-3.12B** and complex **C** display comparable chemical shifts. Based on these comparisons we are confident in our assignment of monomolecular complex **Ni(II)-3.12B** based on NMR spectroscopy, in lieu of a solid-state molecular structure.

(Scheme 3.10). We propose these two structures are simple stereoisomers with amidate bound in a κ^1 -O mode. Thus, both *E* and *Z* amidates are visible by NMR spectroscopy. To our knowledge this would be the first example of κ^1 -O bound amidates where both the *E* and *Z* isomers are discernable by NMR spectroscopy.



Scheme 3.10 Reaction of complex **Ni(I)-3.5** with **TEMPO** to produce **Ni(II)-3.5-TEMPO(E/Z/K)**. The ^{13}C shifts for the amidate carbons are shown.

Our assignment is corroborated by single crystal XRD which shows the **Ni(II)-3.5-TEMPO(E)** isomer in the asymmetric unit. These crystals diffract well, however the structure is approximately 67% complete and is only used for atomic connectivity (see Appendix B.2). When

the same crystalline samples of **Ni(II)-3.5-TEMPO(E)** are dissolved at low temperature (glovebox cold-well, -50 °C), a 2:1 (*E* : *Z*) ratio is observed by ¹H NMR spectroscopy.

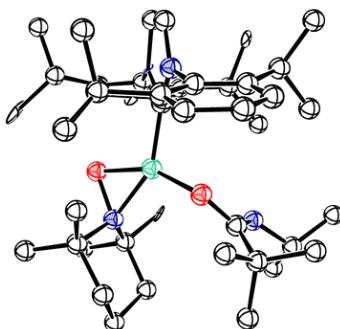


Figure 3.3 Preliminary isotropic ORTEP depiction of the solid-state structure of Ni(II)-3.5-TEMPO(E) (ellipsoids at 50% probability, hydrogens omitted). Poor structure: geometry and connectivity only.

Interestingly, we observed exclusive selectivity for **Ni(II)-3.5-TEMPO(E)**, i.e. the kinetic product, when solutions of TEMPO and **Ni(I)-3.5** were combined below 223K (Figure 3.4). Reactions done in a glovebox freezer (ca. 238K) showed some formation of **Ni(II)-3.5-TEMPO(Z)**. Thus, the equilibration of **Ni(II)-3.5-TEMPO(E)** to **Ni(II)-3.5-TEMPO(Z)** occurs between 223-238K.

If samples of **Ni(II)-3.5-TEMPO(E/Z)** are left at room temperature for days, **Ni(II)-3.5-TEMPO(K)** (Scheme 3.10) becomes visible by ¹H NMR spectroscopy. ¹H-¹³C HMBC experiments suggest the formation of the κ^2 -N,O bound Ni(II) amidate species; this binding mode has been observed with this amidate previously.^[207] We propose that **Ni(II)-3.5-TEMPO(K)** must be formed from **Ni(II)-3.5-TEMPO(E)** since forming **Ni(II)-3.5-TEMPO(K)** from **Ni(II)-3.5-TEMPO(Z)** requires isomerization of the nitrogen substituent. If solutions of **Ni(II)-3.5-TEMPO(E/Z/K)** are heated at 70°C for several days, **Ni(II)-3.5-TEMPO(K)** becomes the dominant product, thus we propose **Ni(II)-3.5-TEMPO(K)** is the thermodynamic product.

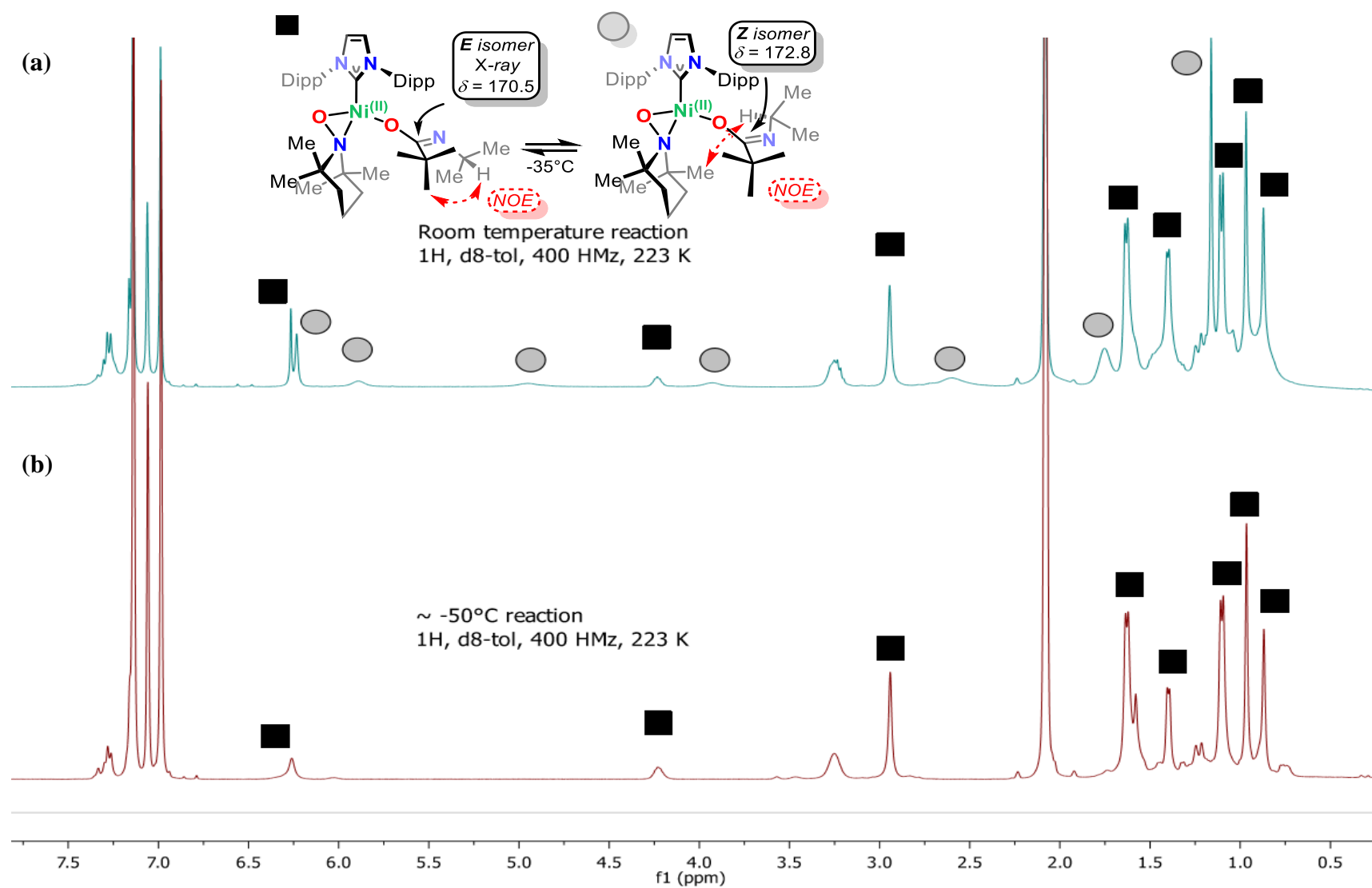
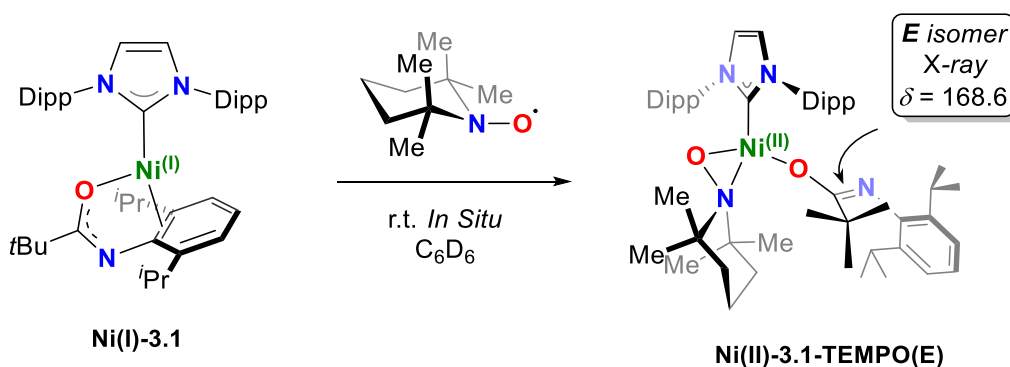


Figure 3.4 VT ^1H NMR spectra (400MHz, $\text{d}^8\text{-tol}$, 223K) for the reaction shown in Scheme 3.10 performed at (a) 273K, and (b) below 223K, in a glovebox cold-well. The ^{13}C shift for the amidate carbon is shown.

In contrast, reactions of **Ni(I)-3.1** and TEMPO result in a single species, which is likely **Ni(II)-3.1-TEMPO(E)** based on the increase in steric profile of the N-substituent. We did not isolate **Ni(II)-3.1-TEMPO(E)**, however we have characterized it by ^1H and ^{13}C NMR spectroscopy. In the $^{13}\text{C}\{^1\text{H}\}$ NMR spectrum, the amidate C=O resonance (Scheme 3.11) suggests the amidate is bound κ^1 through oxygen.^[208]



Scheme 3.11 Reaction of complex **Ni(I)-3.1** with TEMPO to produce **Ni(II)-3.1-TEMPO(E)**. The ^{13}C shift for the amidate carbon is shown.

3.4.2.2 Reaction with Halide Reagents

Next, we turned to halide reagents to see if halide radicals might produce complex **Ni(II)-3.12B**. Reaction mixtures of **Ni(I)-3.5** and chlorotriphenylmethane (Cl-CPh_3) or elemental iodine (I_2) react quickly in benzene and change from yellow to deep purple (Scheme 3.12). From these mixtures, the **Ni(II)** halide complexes **Ni(II)-3.5-X** ($\text{X} = \text{Cl}, \text{I}$) were characterized by ^1H and ^{13}C NMR spectroscopy. **Ni(I)-3.1** reacted similarly to give **Ni(II)-3.1-Cl** in the presence of Cl-CPh_3 in benzene. Independent syntheses of **Ni(II)-3.5-Cl** and **Ni(II)-3.1-Cl** from $\text{Ni}(\text{IPr})(\text{PPh}_3)_2\text{Cl}_2$ allowed for analytically pure samples to be prepared. Complexes **Ni(II)-3.1-Cl** and **Ni(II)-3.5-Cl**

were characterized by multinuclear NMR spectroscopy, elemental analysis (EA), EI-MS, and single crystal X-ray diffraction (XRD).

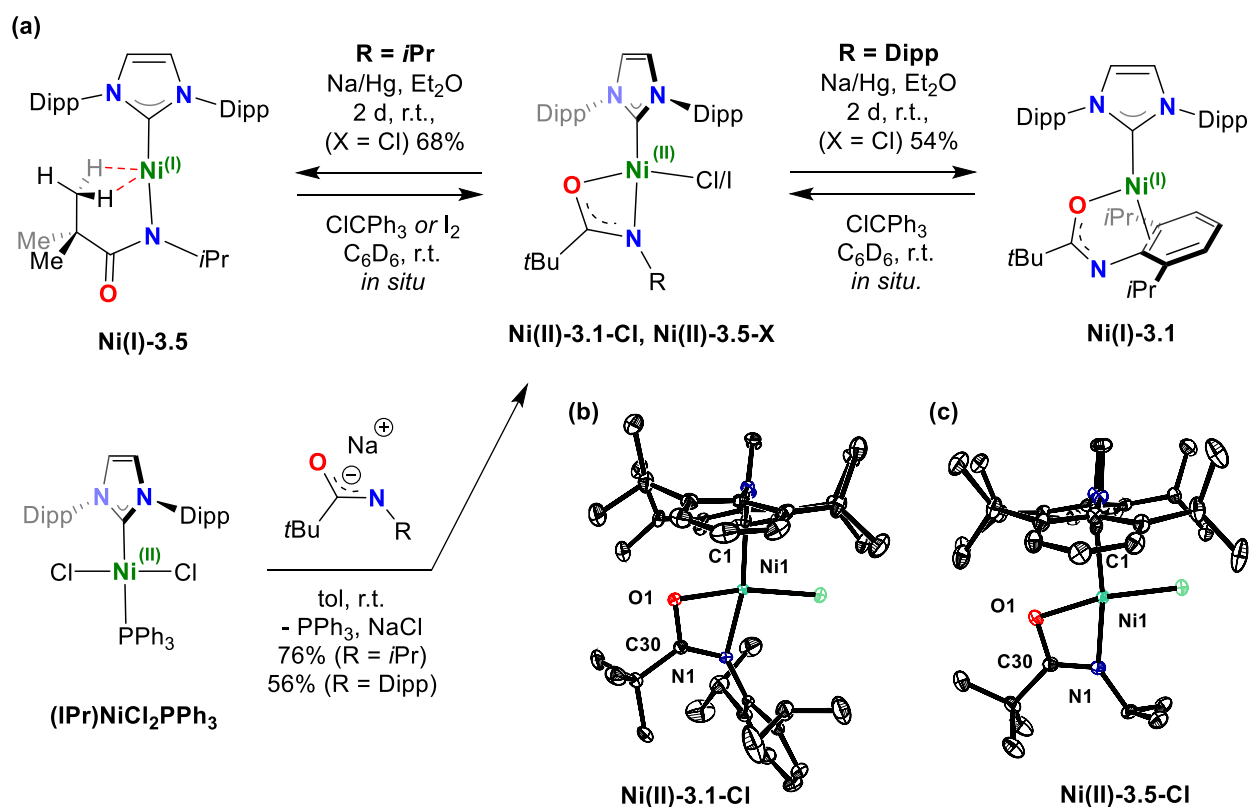
The solution $^{13}\text{C}\{^1\text{H}\}$ NMR spectra of **Ni(II)-3.1-Cl** and **Ni(II)-3.5-Cl** show carbonyl shifts ($\delta = 187.6$ and 186.5 , respectively) characteristic of $\kappa^2\text{-}N,O$ -amidate coordination.^[140,207,209] The $\kappa^2\text{-}N,O$ assignment is corroborated in the solid-state (Scheme 3.12b,c), wherein the amidate *N*-atom in both structures is oriented *trans* to the bulky IPr coligand; **Ni(II)-3.1-Cl** [C(1)-Ni(1)-N(1) $167.89(5)^\circ$] and **Ni(II)-3.5-Cl** [C(1)-Ni(1)-N(1) $171.04(8)^\circ$]. We propose that this isomer is favored due to the sterically demanding amidate *N*-substituent. The N-Ni-O bite angles of **Ni(II)-3.1-Cl** [N(1)-Ni(1)-O(1) $68.48(5)^\circ$] and **Ni(II)-3.5-Cl** [N(1)-Ni(1)-O(1) $68.58(7)^\circ$] are significantly strained from the ideal 90° for square planar complexes. Further analysis of the crystal structures of **Ni(II)-3.1-Cl** and **Ni(II)-3.5-Cl** reveals delocalization of charge through the O(1)-C(28)-N(1) π -system as seen by the similar O(1)-C(28) [**Ni(II)-3.1-Cl**, $1.3098(17)$ Å; **Ni(II)-3.5-Cl**, $1.321(2)$ Å] and N(1)-C(28) [**Ni(II)-3.1-Cl**, $1.3035(18)$ Å; **Ni(II)-3.5-Cl**, $1.305(3)$ Å] bond lengths. This data is consistent with our reports of $\kappa^2\text{-}N,O$ amidates bound to other TMs.^[140,207,209]

Combining **Ni(II)-3.1-Cl** or **Ni(II)-3.5-Cl** with 1.1 equiv. of (0.5%) Na/Hg amalgam results in the loss of NaCl and reformation of the Ni(I) derivatives **Ni(I)-3.1** and **Ni(I)-3.5** in good yields (Scheme 3.12 - 54% and 68% respectively). This is important since a change in oxidation state results in a complete change in the binding mode of amidates, with *N*-substitution playing the largest role in Ni(I) binding modes.

3.4.2.3 Reaction with Gomberg's Dimer & SuperMesO

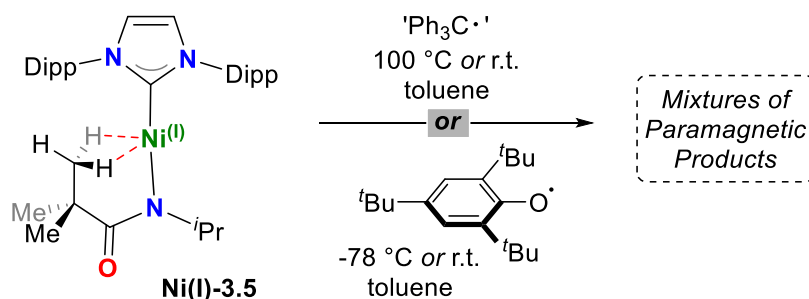
We next attempted to react complex **Ni(I)-3.5** with the trityl radical, Gomberg's Dimer (Scheme 3.13).^[210,211] Surprisingly, no reaction occurs at room temperature. Upon heating to 100°

C we did observe several new unknown paramagnetic peaks in the ^1H NMR spectrum, however, we do not observe the desired cyclometallation product (**Ni(II)-3.12B**). Similarly, reactions of **Ni(I)-3.5** with SuperMesO \cdot produced a mixture of paramagnetic products, but no **Ni(II)-3.12B** was observed by ^1H NMR spectroscopy (Scheme 3.13). Several attempts to crystallize the new paramagnetic products did not result in any X-ray quality crystals. Mass spectrometry was also ambiguous as the molecular ions for the expected Ni(II) products were not observed. We are currently investigating these reactions further.



Scheme 3.12 (a) Reaction of **Ni(I)-3.5** and **Ni(I)-3.1** with radical reagents produces **Ni(II)-3.5-X** (X = Cl, I) and **Ni(II)-3.5-Cl**. These reactions are reversible in the presence of Na/Hg. ORTEP depictions (ellipsoids at 50% probability, hydrogens omitted selected bond lengths (Å) and angles (°)) of the solid-state structures of (b) **Ni(II)-3.1-Cl**: Ni1-Cl1 2.1563(4), Ni1-O1 1.9134(10), Ni1-N1 1.9215(12), C1-Ni1-N1 167.89(5), N1-Ni1-O1

68.48(5). (c) Ni(II)-3.1-Cl: - Ni1-Cl1 2.1600(6), Ni1-O1 1.9206(15), Ni1-N1 1.9280(17), C1-Ni1-N1 171.04(8), Ni1-O1 68.58(7).



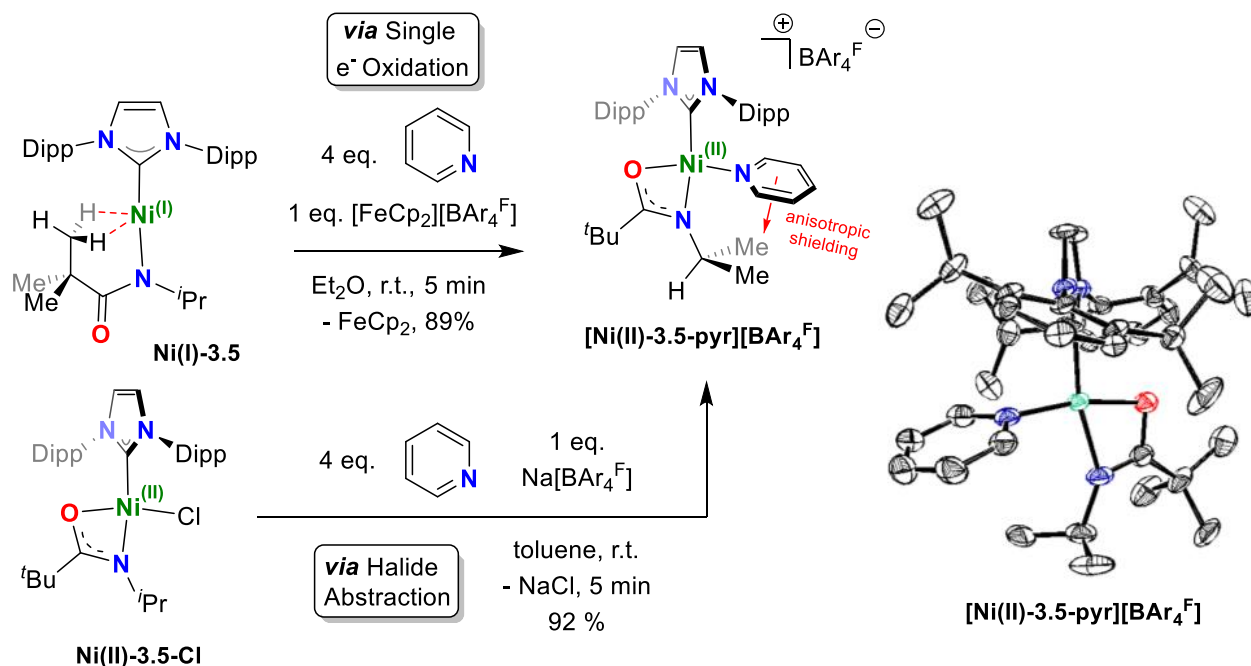
Scheme 3.13 Reactivity of Ni(I)-3.5 with the trityl radical ($\text{Ph}_3\text{C}\cdot$) and SuperMesO \cdot phenoxyl radical.

3.4.2.4 Reaction with $[\text{FeCp}_2][\text{BAR}_4^{\text{F}}]$

Single electron oxidation of complex **Ni(I)-3.5** with $[\text{FeCp}_2][\text{BAR}_4^{\text{F}}]$ in the presence of pyridine (Scheme 3.14) affords an orange solution containing ferrocene and the square-planar nickel(II) complex $[(\text{IPr})\text{Ni}(\kappa^2\text{-}N,O\text{-N}(\text{iPr})\text{C}(\text{O})^{\text{tBu}})(\text{pyridine})][\text{BAR}_4^{\text{F}}]$ (**[Ni(II)-3.5-pyr][BAR₄^F]**). Upon workup, complex **[Ni(II)-3.5-pyr][BAR₄^F]** is isolated as a diamagnetic orange solid in 89% yield. Alternately, **[Ni(II)-3.5-pyr][BAR₄^F]** can be prepared by salt elimination from complex **Ni(II)-3.5-Cl** in 92% yield by addition of 1 eq. of $\text{Na}[\text{BAR}_4^{\text{F}}]$ in the presence of pyridine. Complex **[Ni(II)-3.5-pyr][BAR₄^F]** was characterized by multinuclear (^1H , ^{13}C , ^{11}B , ^{19}F) NMR spectroscopy, high resolution electrospray mass spectrometry (HRESI-MS), single crystal XRD, and EA.

The ^{13}C resonance for the central amidate carbon is shifted significantly downfield with respect to complex **Ni(II)-3.5-Cl**, likely due to the cationic metal center. ^1H NMR spectroscopy suggests a *cis* arrangement of the two nitrogen donors (*N*-amidate, *N*-pyridine), as evident by the anisotropic shielding of the amidate isopropyl methyl groups ($\delta = -0.17$, c.f. **Ni(II)-3.5-Cl**: $\delta = 1.03$) by the pyridine ring current.^[212] This structural assignment is corroborated in the solid-state (Scheme 3.14), where the plane of the pyridine ring is between 2.51-2.63 Å from the closest methyl protons. Notably, the IPr ligand is severely distorted to accommodate coordination of pyridine.

Importantly, complex **Ni(II)-3.12B** is not observed in this reaction. Attempts to isolate the unsaturated Ni(II) complex in the absence of pyridine results in a mixture of paramagnetic products; all of which have resisted crystallization thus far.



Scheme 3.14 Reactivity of **Ni(I)-3.5** with the oxidant $[\text{FeCp}_2][\text{BAR}_4\text{F}]$ in the presence of pyridine.

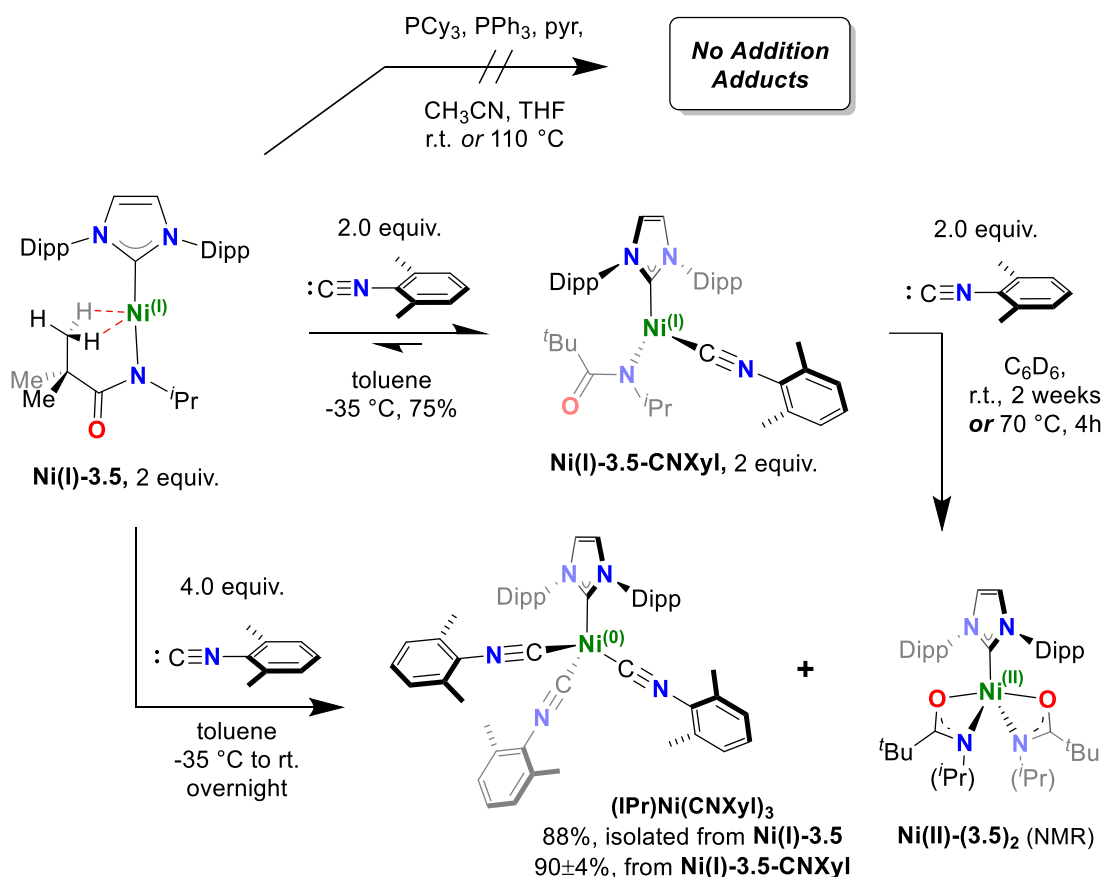
3.5 Reactivity with Lewis Basic & π -Acidic Ligands

3.5.1 Reaction with Phosphines and Isonitrile CNXyl

In an effort to displace the weak agostic contacts in **Ni(I)-3.5** to afford a three coordinate Ni(I) species, we next probed the reactivity of **Ni(I)-3.5** with two-electron donors. Markedly, no addition reaction was observed by NMR spectroscopy between **Ni(I)-3.5** and a variety of Lewis bases including THF, CH_3CN , pyridine, PPh_3 , and PCy_3 at room temperature or with extensive heating (Scheme 3.15). Moreover, recrystallization of **Ni(I)-3.5** at -35°C in the presence of excess THF, pyridine, PPh_3 , or PCy_3 did not result in an increase of coordination number to the Ni(I)

metal center. However, the joint σ -donating/ π -accepting isonitrile CNXyl (Xyl = 2,6-dimethylphenyl) was observed to rapidly react with **Ni(I)-3.5**, affording an orange solution of the three coordinate Ni(I) complex **Ni(I)-3.5-CNXYl** in 75% yield (Scheme 3.15).

Evans method measurements of **Ni(I)-3.5-CNXYl** ($\mu_{\text{eff}} = 1.58 \mu_{\text{B}}$, C_6D_6 , 25 °C) are consistent with a one-electron paramagnet. Amide distances [C(31)-N(1) = 1.324(8)] and [C(31)-O(1) = 1.276(7)] (Figure 3.5) suggest localization of charge at the amide N(1). The metal center back-donates to the isonitrile $\pi^*(\text{C}\equiv\text{N})$; evidenced by the lower [$\nu_{\text{CN}} = 2063 \text{ cm}^{-1}$] infrared stretching frequency [c.f. 2123 cm^{-1} ; free CNXyl]. The ready coordination of π -accepting CNXyl to the electron rich Ni(I) metal center points towards opportunities in small molecule activation.



Scheme 3.15 Synthesis of complexes $(\text{IPr})\text{Ni}(\text{CNXyl})_3$ and $\text{Ni}(\text{II})\text{-(3.5)}_2$ from complexes $\text{Ni}(\text{I})\text{-3.5}$ and $\text{Ni}(\text{I})\text{-3.5-CNXYl}$ by coordination of CNXYl.

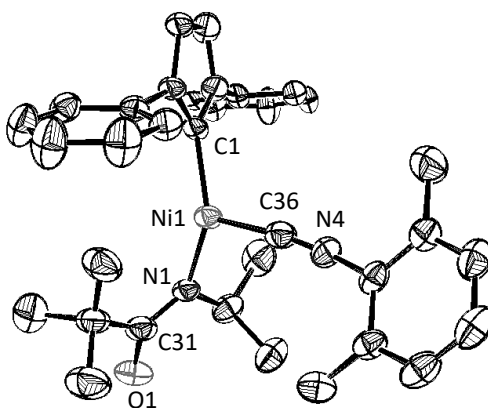


Figure 3.5 ORTEP depiction of the solid-state structure of $\text{Ni}(\text{I})\text{-3.5-CNXYl}$ (ellipsoids at 50% probability, hydrogens, second molecule of $\text{Ni}(\text{I})\text{-3.5-CNXYl}$, solvent, and $\text{NHC}(\text{iPr})$ groups omitted) Selected bond lengths (Å) and angles (°): Ni1-Ni1 1.952(5), Ni1-C36 1.856(6), C36-N4 1.168(7), C1-Ni1-C36 105.1(2), C1-Ni1-N1 147.3(2).

Notably, yields of $\text{Ni}(\text{I})\text{-3.5-CNXYl}$ are lower when the reaction is carried out at 25 °C.^[159] We hypothesized that the decreased yield might be due to a second addition of isonitrile CNXYl to $\text{Ni}(\text{I})\text{-3.5-CNXYl}$, to afford a four coordinate species $(\text{IPr})\text{Ni}(\kappa^1\text{-N}(\text{iPr})\text{CO}(\text{tBu}))(\text{CNXYl})_2$. Instead, adding 2 equiv. CNXYl to complex $\text{Ni}(\text{I})\text{-3.5}$ at -35 °C results in the new $\text{Ni}(0)$ complex $(\text{IPr})\text{Ni}(\text{CNXYl})_3$, and what we hypothesized was the $\text{Ni}(\text{II})$ complex $(\text{IPr})\text{Ni}(\kappa^2\text{-N,O-N}(\text{iPr})\text{CO}(\text{tBu}))(\kappa^1\text{-O-N}(\text{iPr})\text{CO}(\text{tBu}))$ $\text{Ni}(\text{II})\text{-(3.5)}_2$, based on (i) mass balance and (ii) the paramagnetic shifts observed in the ^1H NMR spectrum, as expected for a tetrahedral $\text{Ni}(\text{II})$ complex (Scheme 3.15). Likewise, addition of CNXYl to complex $\text{Ni}(\text{I})\text{-3.5-CNXYl}$ results in clean formation of $(\text{IPr})\text{Ni}(\text{CNXYl})_3$ and proposed $\text{Ni}(\text{II})\text{-(3.5)}_2$. These reactions are selective, and no other major nickel products are observed.

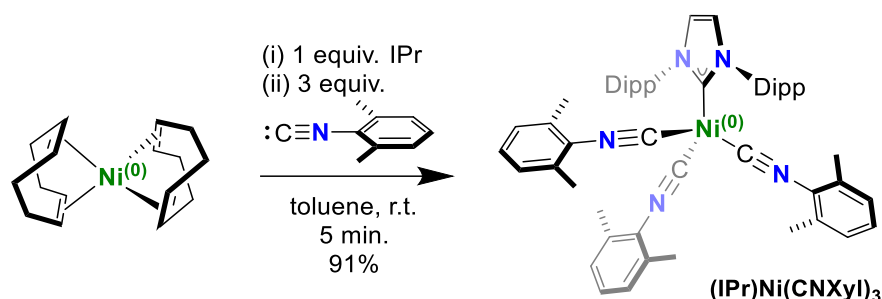
Many of the catalytic cycles proposed for nickel include disproportionation or comproportionation elementary reactions.^[43,213,214] These proposals are based on the propensity of nickel to undergo facile comproportionation-disproportionation in a variety of bond forming processes.^[213–217] Comproportionation is a commonly exploited route in the syntheses of Ni(I) complexes from Ni(II) and Ni(0) precursors. Surprisingly however, stoichiometric variants of disproportionation reactions are relatively unexplored. Furthermore, the generality of such reactions, and in particular, the ligand effects surrounding such transformations, is rarely the focus of inorganic reactivity studies.^[218] Such studies should provide insight to the catalysis community in the design of a particular nickel catalyzed methodology.

Below, we further explore the steric and electronic effects of reactions with various σ -donating- π -accepting ligands; namely, CO and a series of alkenes. These each result in clean disproportionation reactions from Ni(I) to Ni(0) and Ni(II). This work reports the characterization of the Ni(0) and Ni(II) products, and probes the mechanism of disproportionation using both kinetics and radical trapping experiments. The work points toward the propensity of Ni(I) to disproportionate readily in the presence of simple π -acid ligands.

3.5.2 Independent Synthesis of (IPr)Ni(CNXyl)₃

To confirm the proposed products of disproportionation, we initially completed the independent syntheses and characterization of complexes (IPr)Ni(CNXyl)₃ and Ni(II)-(3.5)₂. The new diamagnetic complex (IPr)Ni(CNXyl)₃ can be synthesized independently from Ni(COD)₂ by successive additions of IPr (1 equiv.) and CNXyl (3 equiv.) in 91% yield (Scheme 3.16). The ¹H NMR spectrum is consistent with a 3:1 ratio of CNXyl:IPr ligands, and only a single *ortho*-methyl peak is observed for the chemically equivalent isonitrile ligands (C₆D₆, 25°C). Likewise, only a

single IPr methine C-H is observed; taken together this suggests rapid Ni-C_{CNXyl} and Ni-C_{IPr} bond rotation on the ¹H NMR spectroscopic timescale. Chemical equivalence of the isonitrile ligands was corroborated in the solid-state by X-ray crystallography (Figure 3.6), which displays pseudo C_{3v} symmetry. The Ni(0) center takes part in significant Ni to π*(C≡N) back-donation, as revealed in the infrared (IR) spectrum [$\nu_{\text{CN}} = 1960 \text{ cm}^{-1}$] of complex (IPr)Ni(CNXyl)₃ [c.f. $\nu_{\text{CN}} = 2123 \text{ cm}^{-1}$, free CNXyl].



Scheme 3.16 Independent synthesis of (IPr)Ni(CNXyl)₃ from Ni(COD)₂ by subsequent addition of IPr (1 eq.) and CNXyl (3 eq.).

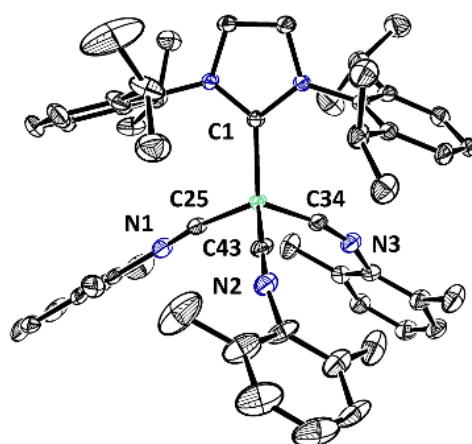


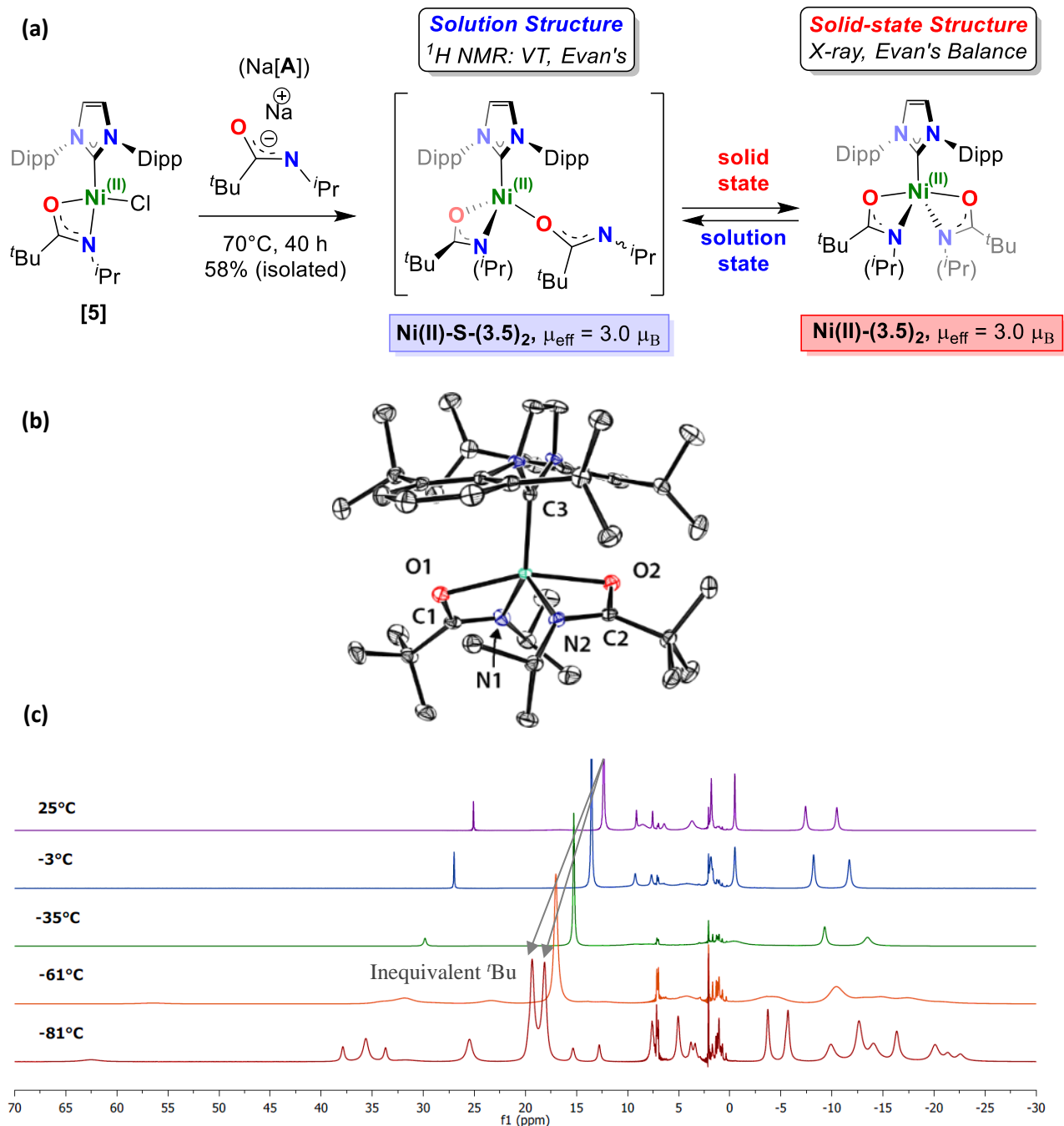
Figure 3.6 ORTEP depiction of the solid-state structure of complex (IPr)Ni(CNXyl)₃ (ellipsoids at 50% probability, hydrogens omitted). Selected bond lengths (Å) and angles (°): avg. N_(1,2,3)-C_(25,34,43) 1.18390(6), avg. Ni-C_(25,34,43) 1.82188(8), Ni-C1 1.96671(11), avg. C1-Ni-C_(25,34,43) 113.1678(30).

3.5.3 Independent Synthesis of Complex Ni(II)-(3.5)₂

We then turned our attention to the preparation of complex **Ni(II)-(3.5)₂** to confirm its structure. Gratifyingly, complex **Ni(II)-(3.5)₂** may be produced in moderate yield (58%) via salt elimination from **Ni(II)-3.5-Cl**^[159] (Scheme 3.17a). The high solubility of **Ni(II)-(3.5)₂** in a range of non-polar solvents (i.e. hexanes, pentanes, hexamethyldisiloxane) precluded the clean isolation of **Ni(II)-(3.5)₂** in high yield. Nevertheless, **Ni(II)-(3.5)₂** could be characterized by variable temperature (VT) paramagnetic ¹H NMR spectroscopy, solution and solid-state magnetic susceptibility measurements, elemental analysis (EA), and single-crystal X-ray diffraction (XRD).

Evan's method measurements ($\mu_{\text{eff}} = 3.0 \mu_{\text{B}}$, C₆D₆, 25 °C) are consistent with a high-spin Ni(II) complex ($S = 1$) with two unpaired electrons. VT paramagnetic ¹H NMR spectroscopy suggests complex **Ni(II)-S-(3.5)₂** has C₁ symmetry at low temperature, supporting a tetrahedral coordination geometry (Scheme 3.17c). We estimate the isomerization barrier of the two amidate ligands on nickel to be $\approx 9.2 \pm 0.1$ kcal/mol (see appendix A.2 for sample calculations).

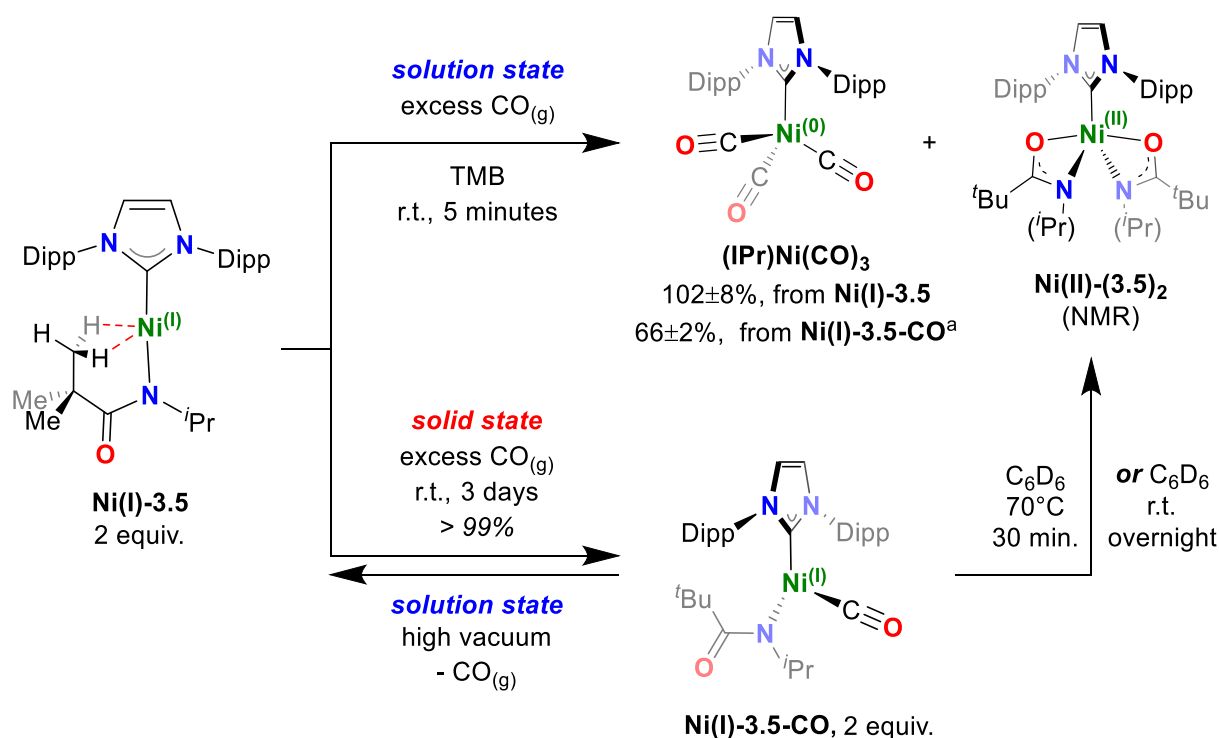
In contrast, the solid-state molecular structure of **Ni(II)-(3.5)₂** displays a pseudo C₂-symmetric five-coordinate complex, (IPr)Ni(κ^2 -*N,O*-N(iPr)CO(tBu))₂ (Scheme 3.17b). Both enantiomers (Δ/Λ) are found in the asymmetric unit, and Addison Tau values^[219] (0.275 Δ , 0.375 Λ) suggest that the 5-coordinate Ni(II) complex is best described as square-based pyramidal. The C-O and C-N bond lengths (Scheme 3.17b) are consistent with delocalization through the π -system; as has been reported for κ^2 -*N,O*-amidate ligands on Ni(II).^[159] The solid-state 5-coordinate complex is also paramagnetic ($\mu_{\text{eff}} = 3.2 \mu_{\text{B}}$, Evan's balance, 25 °C).



Scheme 3.17 (a) Independent synthesis of Ni(II)-(3.5)₂ by salt elimination from [5]. (b) ORTEP depiction of the solid-state structure of (A)-Ni(II)-(3.5)₂ (ellipsoids at 50% probability, hydrogens and solvent omitted). Selected (avg.) bond lengths (Å) and (avg.) angles (°): N(1,2)-C(1,2) 1.310(2), O(1,2)-C(1,2) 1.292(2), O(1)-Ni-O(2) 159.07(5), N(1,2)-Ni-O(1,2) 63.27(5) (c) VT paramagnetic ¹H NMR spec. (400 MHz, d₈-tol) of complex Ni(II)-(3.5)₂ at selected temperatures from 25°C to -81°C.

3.5.4 Reaction with Carbon Monoxide

Having characterized $(\text{IPr})\text{Ni}(\text{CNXyl})_3$ and $\text{Ni}(\text{II})\text{-(3.5)}_2$, we were interested in examining whether other σ -donating/ π -accepting ligands facilitate similar disproportionation reactions. By analogy, when solutions of $\text{Ni}(\text{I})\text{-3.5}$ are exposed to excess $\text{CO}_{(\text{g})}$, the quantitative disproportionation reaction to produce complexes $\text{Ni}(\text{II})\text{-(3.5)}_2$ and $(\text{IPr})\text{Ni}(\text{CO})_3$ ^[220] is observed within minutes by ^1H NMR spectroscopy (Scheme 3.18, internal standard (IS), TMB = 1,3,5-trimethoxybenzene).



Scheme 3.18 Reaction of $\text{Ni}(\text{I})\text{-3.5}$ with $\text{CO}_{(\text{g})}$ in the solution state produces $(\text{IPr})\text{Ni}(\text{CO})_3$ and $\text{Ni}(\text{II})\text{-(3.5)}_2$. The solid-state reaction proceeds through proposed intermediate $\text{Ni}(\text{I})\text{-3.5-CO}$ on way to $(\text{IPr})\text{Ni}(\text{CO})_3$ and $\text{Ni}(\text{II})\text{-(3.5)}_2$. ^aComplex $\text{Ni}(\text{I})\text{-3.5}$ makes up the mass balance for this reaction.

When crystalline $\text{Ni}(\text{I})\text{-3.5}$ is subjected to $\text{CO}_{(\text{g})}$ over a period of 3 days, the yellow crystals of $\text{Ni}(\text{I})\text{-3.5}$ slowly turn a bright green (Scheme 3.18). Crystal-to-crystal studies were unsuccessful,

and we have thus far been unable to crystallize this green solid. Upon dissolution, a new paramagnetic species is visible in the ^1H NMR spectrum, but resonances for **(IPr)Ni(CO)₃** and **Ni(II)-(3.5)₂** are not immediately observed. Overnight, however, these paramagnetic peaks disappear, and complexes **(IPr)Ni(CO)₃** (66±2%), **Ni(I)-3.5**, and **Ni(II)-(3.5)₂** become visible in the ^1H NMR spectrum.^[221] No other major nickel products are observed. Based on these observations, we postulate that the green solid is the CO-variant of **Ni(I)-3.5-CNXYl**; **(IPr)Ni(κ^1 -N(iPr)CO(*t*Bu))(CO) (Ni(I)-3.5-CO).**

In the solid-state, **Ni(I)-3.5-CO** does not lose CO under vacuum. However, if dissolved in organic solvent and exposed to high vacuum, the complex readily reverts to complex **Ni(I)-3.5**. Solid-state IR spectra (Nujol mull) of crude **Ni(I)-3.5-CO** reproducibly show the formation of four new CO stretches (ν_{CO} = 1997, 1992, 1978, 1970 cm^{-1}). Importantly, in our earlier work we observed two distinct geometric isomers of **Ni(I)-3.5-CNXYl** in the solid-state (i.e. trigonal planar vs. T-shaped).^[159] Thus, some of these additional CO stretches in **Ni(I)-3.5-CO** could be due to similar geometric isomers. Additionally, the ^1H NMR spectrum of **Ni(I)-3.5-CO** is very broad, not unlike complex **Ni(I)-3.5-CNXYl**.

cwEPR analysis of **Ni(I)-3.5-CO** (toluene glass, -196°C) shows rhombic symmetry (Figure 3.7). Holland et al. have prepared similar three coordinate Ni(I) carbonyl complexes.^[222] Our EPR parameters are analogous to theirs. Thus, based on our EPR, IR, and reactivity studies, we assign the structure of **Ni(I)-3.5-CO**.

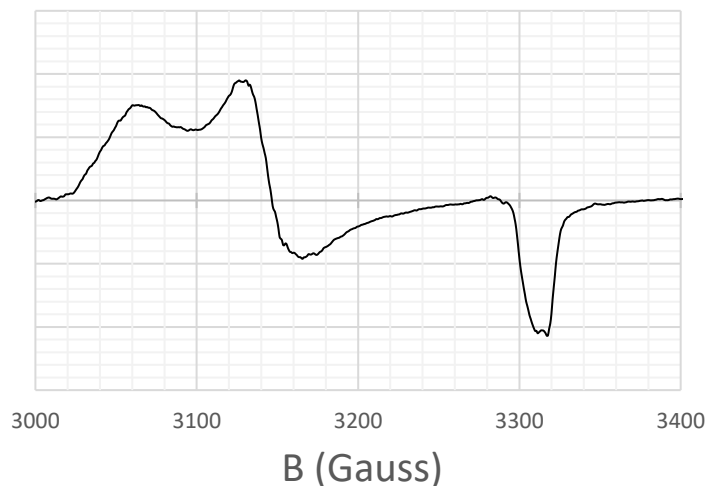


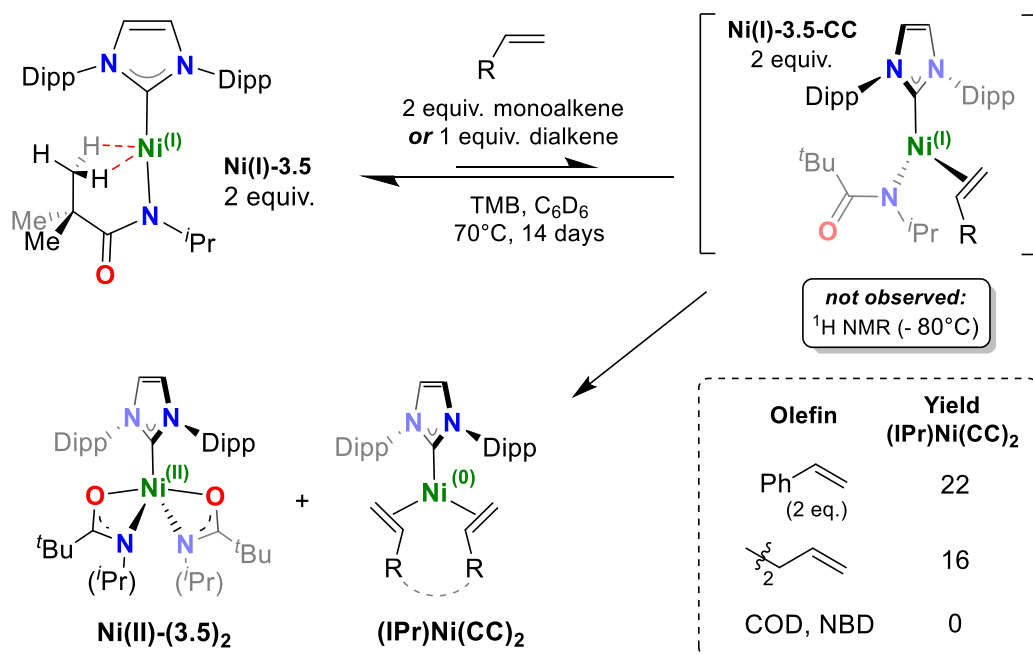
Figure 3.7 cwEPR spectrum of complex **Ni(I)-3.5-CO** (-196 °C, toluene glass).

3.5.5 Reaction with Alkenes

In order to explore other catalytically relevant small molecules, we turned our attention to alkenes to examine their propensity to promote the disproportionation of **Ni(I)-3.5**. Select alkenes can facilitate disproportionation of **Ni(I)-3.5** to Ni(0) and Ni(II), albeit at a much lower rate (Scheme 3.19). When solutions of **Ni(I)-3.5** are heated at 70°C with two equivalents of alkene, both **Ni(II)-(3.5)₂** and **(IPr)Ni(CC)₂** are visible by ¹H NMR spectroscopy albeit in low yields over 2 weeks [styrene (22%);^[223] 1,5-hexadiene (16%)^[224]]. Unreacted **Ni(I)-3.5** is also visible in the ¹H NMR spectrum. Reactions with norbornadiene (NBD) or 1,5-cyclooctadiene (COD) did not result in formation of **Ni(II)-(3.5)₂** or **(IPr)Ni(CC)₂**. Based on our yields with styrene versus 1,5-hexadiene, it seems then that an increased π -acidity leads to an increased rate of disproportionation. These observations taken together suggest the reaction with alkenes proceed through an intermediate complex **Ni(I)-3.5-CC** much like the reaction with CNXyl **Ni(I)-3.5-CNXYl** and CO_(g) **Ni(I)-3.5-CO**. However, low temperature ¹H NMR (-81°C, d₈-toluene) spectra of complex

Ni(I)-3.5 do not show new paramagnetic products in the presence of styrene. Moreover, attempts to isolate **Ni(I)-3.5-CC** by crystallizing **Ni(I)-3.5** from neat styrene produced crystals of **Ni(I)-3.5**, **(IPr)Ni(CC)₂**^[223] and **Ni(II)-(3.5)₂**. These results, along with the reaction of **Ni(I)-3.5** with carbon monoxide, suggest that this disproportionation reaction is relatively general to a variety of π -accepting ligands.

We hypothesize these disproportionation reactions are driven thermodynamically by the π -delocalization of metal electron density in the resulting Ni(0) products, each with strong π -acid ligands. The contrasting reactivity of 1,5-hexadiene and COD in this reaction show that the Ni(0) product must be stable for the reaction to proceed. Notably, steric effects may also play an important role, as pyridine and PPh₃ do not promote this disproportionation under the same reaction conditions.

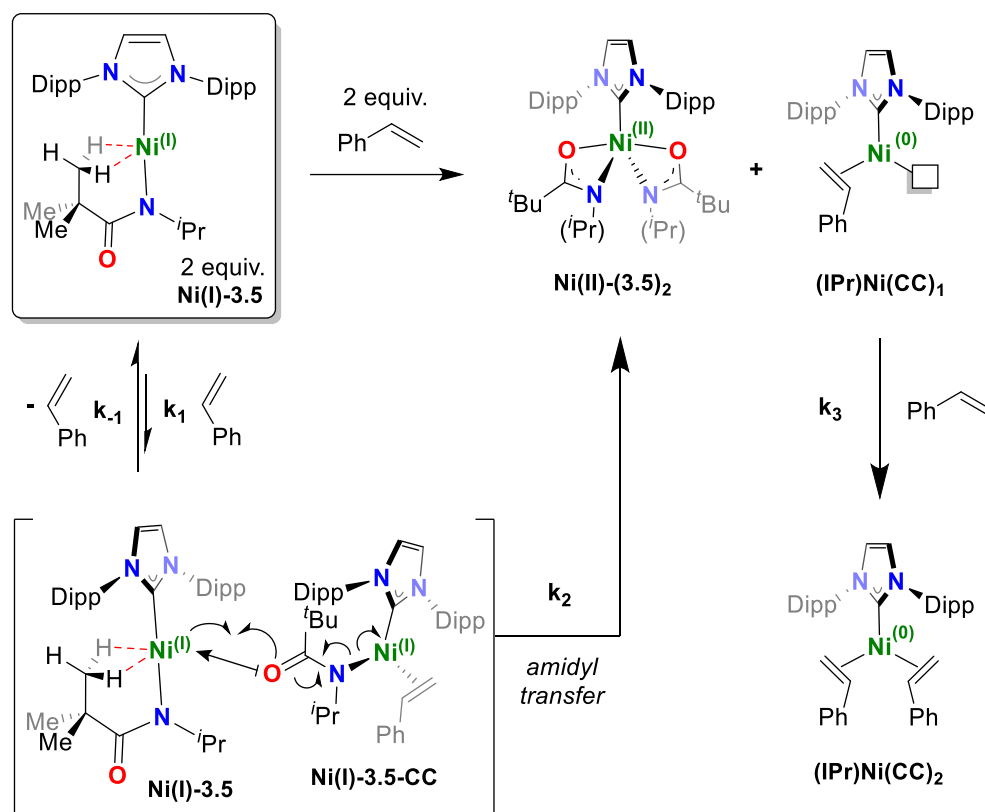


Scheme 3.19 Reaction of mono- and dialkenes with complex **Ni(I)-3.5** produces complexes **(IPr)Ni(CC)₂** and **Ni(II)-(3.5)₂** with heating at 70°C

3.5.6 Mechanistic Studies

We then aimed to understand the mechanism of this apparent disproportionation reaction. The reaction of **Ni(I)-3.5-CNXYl** with CNXYl (Scheme 3.15) to give complexes **(IPr)Ni(CNXYl)₃** and **Ni(II)-(3.5)₂** is slow, requiring weeks at room temperature. However, the reaction of **Ni(I)-3.5** with two equivalents of isonitrile results in the formation of **(IPr)Ni(CNXYl)₃** and **Ni(II)-(3.5)₂** overnight. Thus, we speculate that a second addition of CNXYl to complex **Ni(I)-3.5-CNXYl** may be involved in the disproportionation reaction pathway. Moreover, the product distribution in the decomposition of **Ni(I)-3.5-CO** and **Ni(I)-3.5-CNXYl** to complexes **Ni(I)-3.5**, **Ni(II)-(3.5)₂**, and **(IPr)Ni(CO)₃** and **(IPr)Ni(CNXYl)₃** (respectively) suggests π -acid ligand scrambling is prevalent (see reversibility in Schemes 3.15 and 3.18).

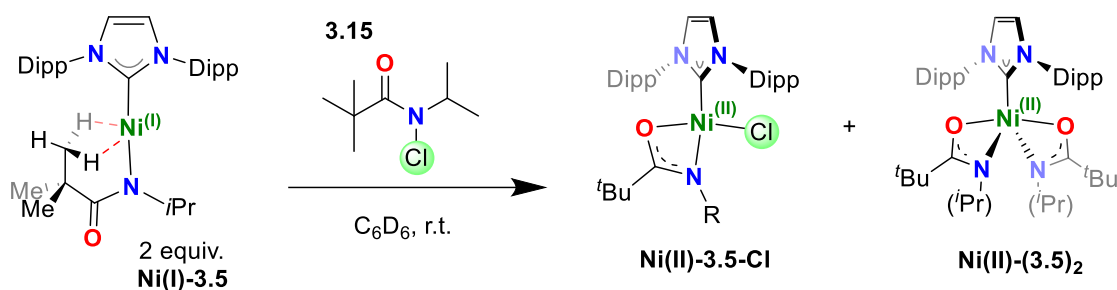
A bimolecular electron transfer mechanism is most likely (Scheme 3.20). In our proposed mechanism, an equivalent of alkene combines with **Ni(I)-3.5** to give the transient species **Ni(I)-3.5-CC**. Here, an amidate ligand may act as an electron transfer ligand via a metal-mediated radical process from **Ni(I)-3.5-CC** to **Ni(I)-3.5** to produce the Ni(II) complex **Ni(II)-(3.5)₂** and **IPrNi(η^2 -alkene)** (int. **(IPr)Ni(CC)₁**). Amidates, well known for their hemi-lability,^[225] are also known bridging ligands for electron transfer reactions.^[226] Moreover, the κ^1 -N binding mode of the starting complex **Ni(I)-3.5** could in principle allow for coordination of a second nickel(I) center and electron transfer through the N-C-O π -system. Finally, addition of a second alkene gives **(IPr)Ni(CC)₂** from int. **(IPr)Ni(CC)₁**.



Scheme 3.20 Proposed Mechanism: Biomolecular electron transfer via nickel mediated amidyl transfer.

3.5.7 Reaction with *N*-chloroamide **3.15**

We then sought to corroborate our amidyl-transfer mechanism. **Ni(I)-3.5-CC** was not observed by ^1H NMR spectroscopy because of either the transient or paramagnetic nature of this intermediate. Thus, we set out to demonstrate that complex **Ni(II)-(3.5)₂** could indeed be produced from a single-electron amidyl-addition to **Ni(I)-3.5**. Addition of *N*-chloro-*N*-isopropylpivalamide **3.15** to **Ni(I)-3.5** indeed results in clean formation to **Ni(II)-(3.5)₂** and **Ni(II)-(3.5)-Cl**, supporting our hypothesis (Scheme 3.21).^[159]

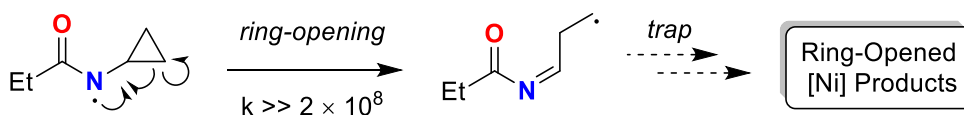


Scheme 3.21 Testing reaction of Ni(I)-3.5 with *N*-chloro-*N*-isopropylpivalamide 3.15.

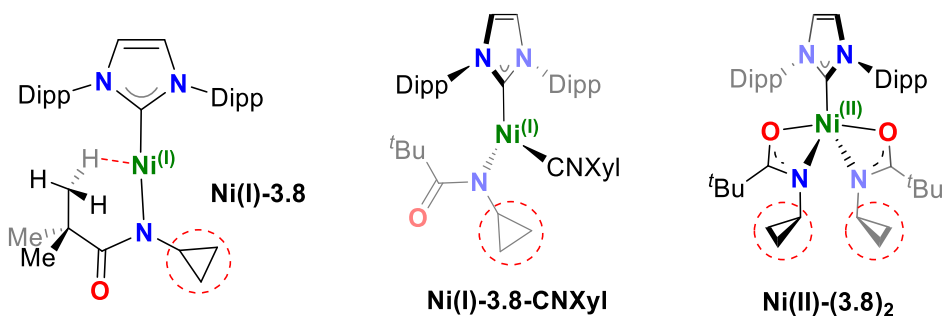
3.5.8 Probing for Discrete Amidyl Radicals: Reactions with *N*-cyclopropyl Derivatives

Another possible mechanistic pathway would feature amidate ligand redistribution via the formation of a discrete amidyl radical from homolytic Ni-N bond cleavage. If such a pathway were active, it should be possible to trap the amidyl radical with Ni(I) to form a Ni(II) species (i.e **Ni(II)-(3.5)₂**). To test the formation of discrete amidyl radicals we modified our amide *N*-R group to an *N*-cyclopropyl group. *N*-cyclopropyl amidyl radicals have been shown to undergo facile ($k \gg 2.0 \cdot 10^8 \text{ s}^{-1}$) ring-opening to form terminal *C*-bound radicals (Scheme 3.22a).^[227,228] We hypothesized that if amidyl radicals were indeed present, we could in principle trap a ring-opened cyclopropyl group with Ni(I). Thus, based on our previous synthesis of **Ni(I)-3.8**, we synthesized the *N*-cyclopropyl derivatives **Ni(I)-3.8-CNXYl**, and **Ni(II)-(3.8)₂**,^[229] (Scheme 3.22b) which are otherwise structurally identical to the *N*-isopropyl complexes **Ni(I)-3.5-CNXYl**, and **Ni(II)-(3.5)₂**. When 1 equiv. of CNXYl is added to complex **Ni(I)-3.8-CNXYl**, both **(IPr)Ni(CNXYl)₃** and **Ni(II)-(3.8)₂** are observed in the ¹H NMR spectrum (Scheme 3.22c).^[230] No ring-opened products are observed. Based on these results, we have illustrated that a mechanism involving the formation of amidyl radicals is unlikely to be the primary mechanism in these disproportionation reactions.

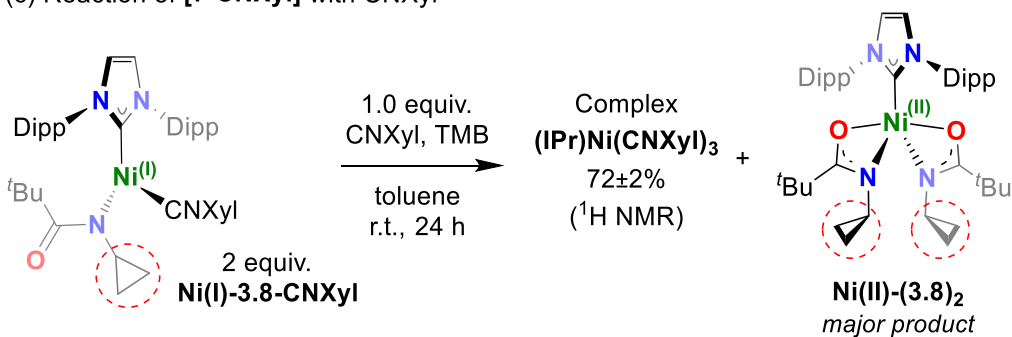
(a) Ring-opening of an *N*-cyclopropyl amidyl radical



(b) New nickel complexes containing an *N*-cyclopropyl amide (See ESI)



(c) Reaction of [7-CNXYl] with CNXYl



Scheme 3.22. (a) Ring-opening of an *N*-cyclopropyl amidyl radical,^[227,228] (b) Complexes **Ni(I)-3.8**, **Ni(I)-3.8-CNXYl**, and **Ni(II)-(3.8)₂**^[229] and (c) reaction of **Ni(I)-3.8-CNXYl** with CNXYl produces complexes **(IPr)Ni(CNXYl)₃** and **Ni(II)-(3.8)₂**.^[230]

3.5.9 Rate Law Studies

The kinetics of the alkene mediated disproportionation reaction was investigated. Careful initial rate investigations varying the concentrations of styrene and nickel afforded kinetic data which supports a second order reaction overall: first order in nickel, and first order in olefin (*See appendix A.2 for rate data*);

$$(1) \quad r_{\text{experimental}} = k_{\text{obs}}[\text{Ni(I)-3.5}][\text{styrene}]$$

Using the steady-state approximation, we derived the following rate law (Equation 2, *See pg. 220 for derivation, see Scheme 3.20 for reaction*). In the case of the alkene reactions we suggest this is a valid assumption; i.e. **Ni(I)-3.5-CC** is small and constant, and $k_1 \ll k_2 + k_{-1}$.^[231] Furthermore, we do not observe the transient (and likely reactive) complex **(IPr)Ni(CC)₁**, thus we assume the rate of production of **(IPr)Ni(CC)₁** is nearly equal to **(IPr)Ni(CC)₂**. Our equation then becomes:

$$(2) \quad r_{\text{theory}} = \frac{k_1 k_2 [\text{Ni(I)-3.5}]^2 [\text{styrene}]}{k_{-1} + k_2 [\text{Ni(I)-3.5}]}$$

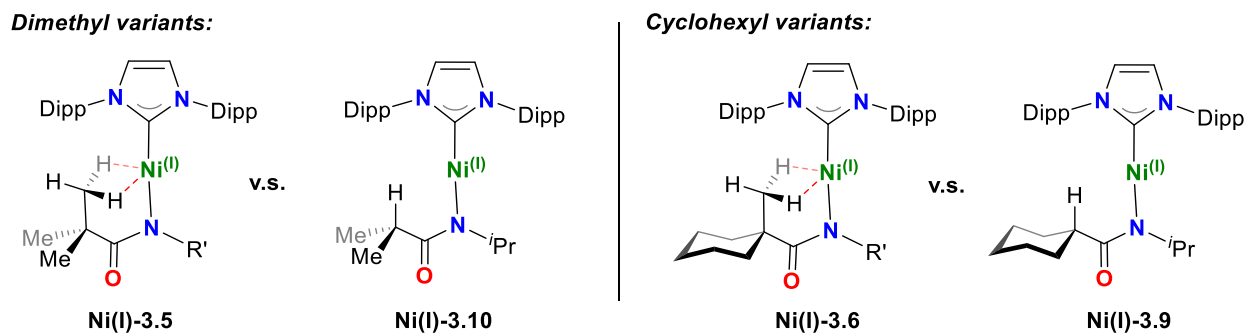
Our experimental and derived rate laws both incorporate a first order dependence on styrene. In contrast, the dependence on nickel appears relatively more complex. Two important situations should be considered to understand this apparent discrepancy between our derived and experimental rate laws: (i) for situations where $k_{-1} \geq k_2$, for a small regime of nickel concentrations the derived rate law may still appear relatively linear. In our study we were constrained to a small concentration regime due to solubility limitations of complex **Ni(I)-3.5**. Thus, our experimental rate law may appear first order in **Ni(I)-3.5**, however it may more closely resemble the dependence shown in equation (2). And (ii) if $k_2 \gg k_{-1}$, the derived rate law may resemble the simplified rate law shown in equation (3):

$$(3) \quad r_{theory} = k_{obs}[\text{Ni(I)-3.5}][\text{styrene}] = r_{experimental}$$

In this case, the derived rate law agrees with our experimental rate law for the disproportionation of complex **Ni(I)-3.5** in the presence of styrene. It would be difficult to show whether situation (i) or (ii) is operative in our system, however, both situations reasonably match with our experimental rate law.

3.6 Additional Spectroscopic Studies of Agostic vs. Non-Agostic Complexes

Having been unable to produce complex **Ni(II)-3.12B** from **Ni(I)-3.5**, we were determined to understand why the agostic C-H bonds in **Ni(I)-3.5** were not amenable to C-H activation reactions. We turned to EPR and NMR spectroscopies to understand the solution structures of these Ni(I) complexes. Specifically, we wished to compare the solution spectra of agostic/non-agostic sets of Ni(I) complexes **Ni(I)-3.5** vs **Ni(I)-3.10** and **Ni(I)-3.6** vs **Ni(I)-3.9** (Scheme 3.23).



Scheme 3.23. Complexes which were investigated for solution structure. These are sets of agostic/non-agostic Ni(I) complexes synthesized in the previous sections.

3.6.1 EPR Spectroscopy

We first examined the EPR spectra of the dimethyl variants **Ni(I)-3.5** vs **Ni(I)-3.10**. The solution state EPR spectrum of **Ni(I)-3.10** displays rhombic symmetry (Figure 3.7). **Ni(I)-3.5** also shows rhombic symmetry in its EPR spectrum, however an additional species with a small g_3 resonance is seen near ~ 3330 Gauss, which is similar in magnetic field strength to the peak at 3330 Gauss in **Ni(I)-3.10**. We reasoned this second species could be present due to fluxionality in **Ni(I)-3.5** in the solution state because of the agostic interactions. If this were true, the same phenomenon should be seen for the EPR spectral differences of **Ni(I)-3.6** vs **Ni(I)-3.9**. Indeed, we found that the EPR spectra of **Ni(I)-3.6** vs **Ni(I)-3.9** resulted in a second species in the EPR spectrum of **Ni(I)-3.6** but which appears similar to **Ni(I)-3.9**. In this case the second species seems to be in a higher ratio.

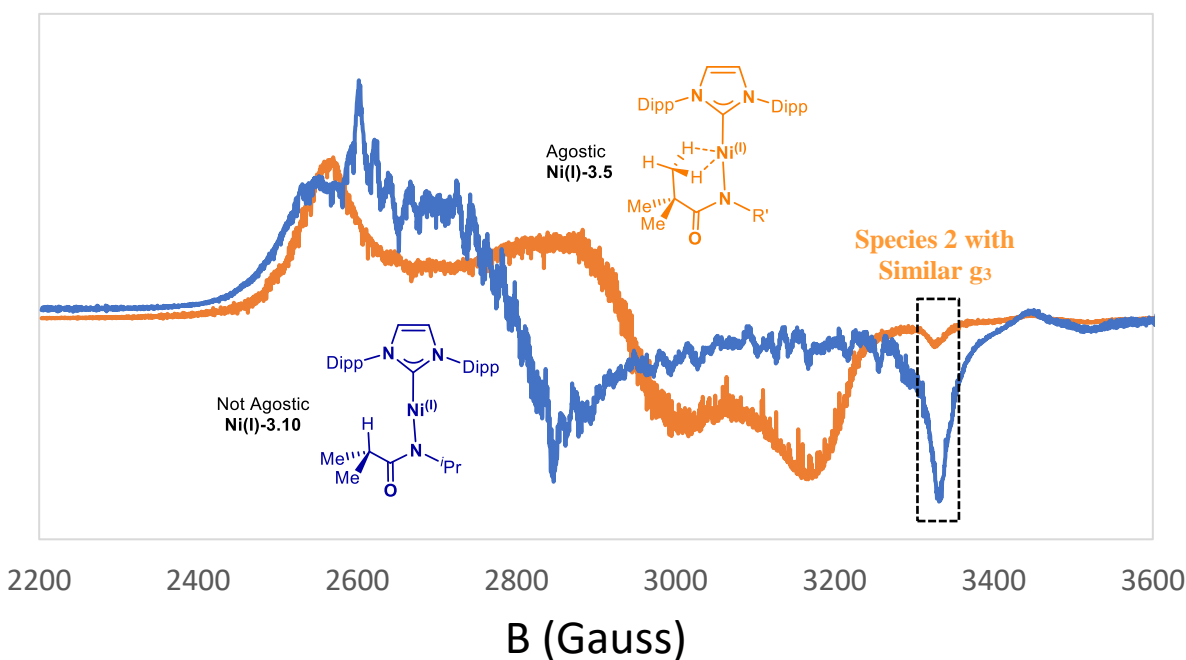


Figure 3.8 cwEPR spectrum of complexes **Ni(I)-3.5** and **Ni(I)-3.10** (8 K, toluene glass).

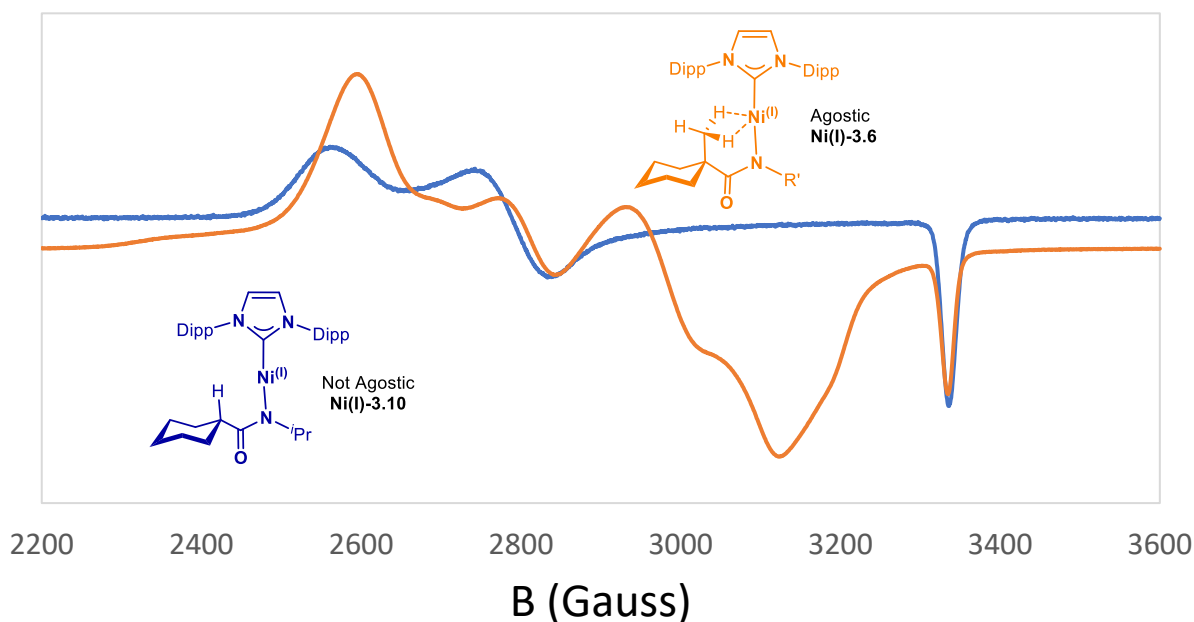


Figure 3.9 cwEPR spectrum of complexes **Ni(I)-3.6** and **Ni(I)-3.9** (8 K, toluene glass).

The nature of this additional species in solution for **Ni(I)-3.5** and **Ni(I)-3.6** is not known at this time. We speculate this species could be the $\kappa^2\text{-}N,O$ isomer in solution, although further experiments are needed to give evidence to this possibility.

3.6.2 NMR Spectroscopy

We then turned to NMR spectroscopy to see if we could identify the agostic CH_3 protons. We chose to examine the variable temperature ^1H NMR spectra of **Ni(I)-3.6** and **Ni(I)-3.7** to essentially look for missing peaks in the spectra of the deuterated variant **Ni(I)-3.7**. We measured the NMR spectra of **Ni(I)-3.6** and **Ni(I)-3.7** in toluene between 298 K and 198 K (Figure 3.10). Surprisingly, we found that solutions of **Ni(I)-3.6** and **Ni(I)-3.7** did not show any differences in

their VT-NMR spectra. This strongly suggests that the C-H agostic contacts are either very fluxional or they are not visible due to broadening from the unpaired electron at nickel.

At this point we tend to think the agostic contacts are fluxional in solution, and so are not viable candidates for solution-state reactivity of these agostic C-H bonds. The EPR and NMR both suggest this is true.

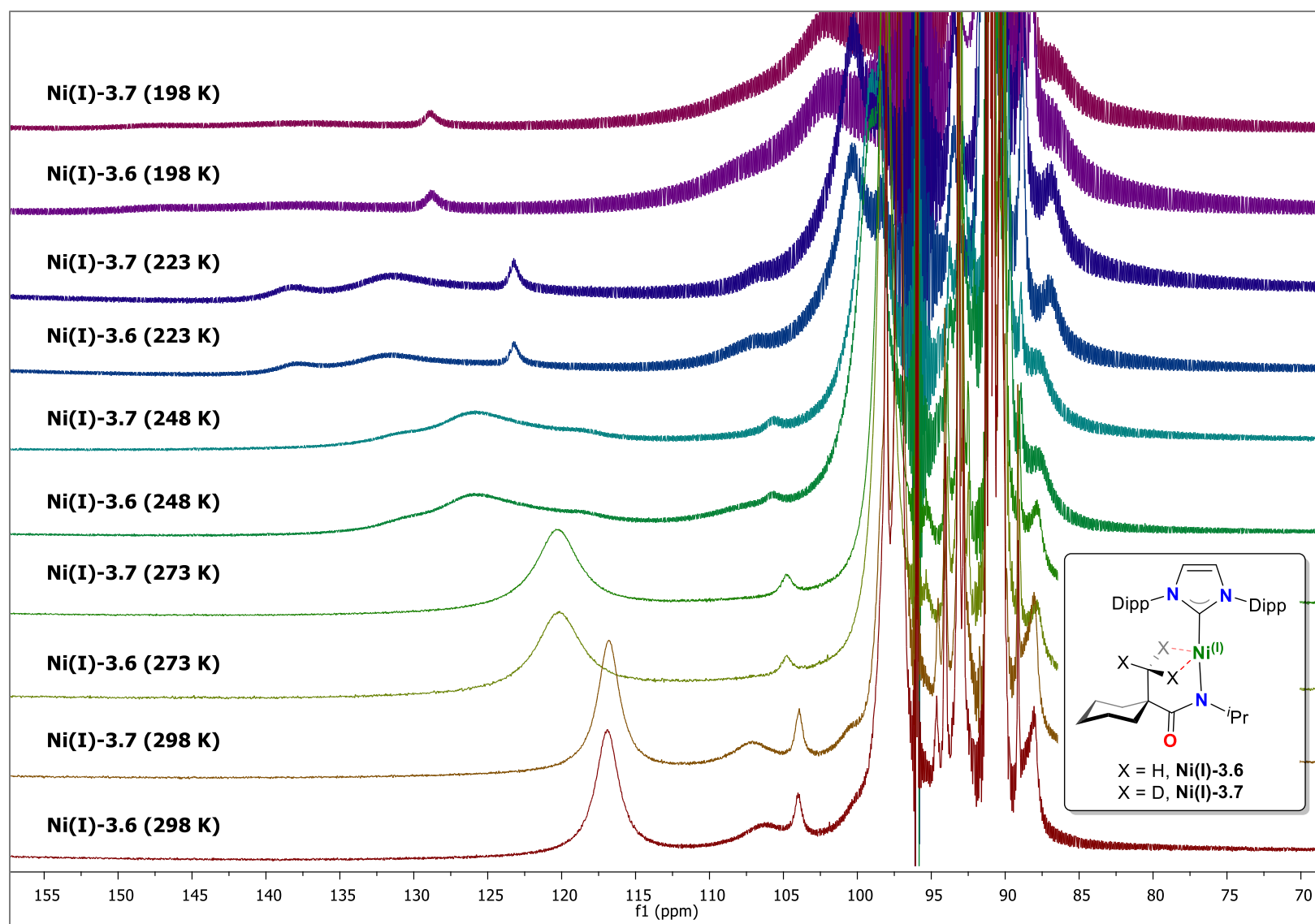


Figure 3.10 Variable temperature ^1H NMR (400 MHz, C_7D_8) of Ni(I)-3.6 and Ni(I)-3.7

3.7 Conclusions

We have synthesized a variety of nickel amidates in the +1 and +2 oxidation states. Our findings include the first examples of κ^2 -*N,O* amidate nickel complexes (**Ni(II)-3.1-Cl** and **Ni(II)-3.5-Cl**), the first rigorously characterized Ni(I) C-H agostic complexes (**Ni(II)-3.4,3.5,3.6,3.7,3.8**), and the related two-coordinate nickel complexes (**Ni(I)-3.9,3.10,3.11**). We also examined the reactivity of **Ni(I)-3.1** and **Ni(I)-3.5** with radical reagents, showcasing the hemi-lability of these ligands. Of importance is the difference in binding modes accessed for the simple amidate ligands, as well as the effect of oxidation state on these binding modes. These complexes highlight the coordinative flexibility of 1,3-*N,O* chelating ligands.

Additionally, we discussed a disproportionation reaction of the low-coordinate Ni(I) amidate complex **Ni(I)-3.5** with a variety of σ -donating/ π -accepting ligands: isonitrile CNXyl, CO_(g), and select alkenes. It appears the rate of the reaction increases in the presence of strongly π -acidic ligands. We propose the thermodynamic driving force is the resulting Ni(0) complex, which has increased metal-to-ligand π -delocalization for strongly π -acidic ligands. This is especially evidenced by the contrasting reactivity between 1,5-hexadiene and COD; the latter of which cannot form the analogous Ni(0) species due to unfavorable alkene-NHC steric congestion. Additionally, larger ligands hinder disproportionation, as evident by the lack of reaction with PPh₃. Notably, having π -ligands which bind strongly to Ni(I), and are slow to dissociate should favor more inert and isolable Ni(I) species, as evidenced by complexes **Ni(I)-3.5-CO**, **Ni(I)-3.5-CNXyl**, and **Ni(I)-3.9-CNXyl**.

We have shown the reaction does not proceed via a discrete amidyl radical pathway utilizing an *N*-cyclopropyl containing amidate derivative **Ni(I)-3.9**. We postulate the key step is a bimolecular ligand transfer through a bridging μ -*N,O* amidate ligand. These reactions are clean

and selective, allowing us to probe the mechanism of the rarely studied disproportionation of nickel. We expect this data will aid in the development and understanding of processes involving monovalent nickel.

Attempts to C-H activate Ni(I) C-H agostic contacts were not successful with a range of radical and oxidizing reagents. Using NMR, and EPR spectroscopy, we probed the nature of these agostic interactions to explain this lack of reactivity. The EPR and NMR data suggest that in solution the agostic complexes are fluxional. This may explain why we were unable to produce **Ni(II)-3.12B** from **Ni(I)-3.5** under several reaction conditions.

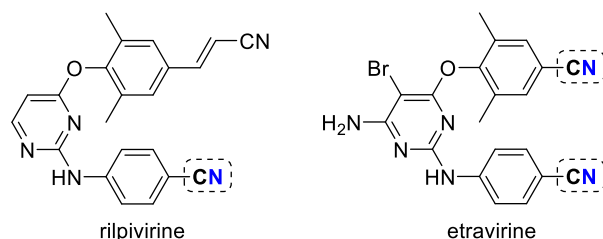
Experimental data for Chapter 3 begins on pg. 191

Chapter 4: CREATE Sustainable Synthesis: Room Temperature Catalytic Cyanation of Aryl Chlorides using an Air-stable Ni(II)-XantPhos Pre-catalyst

As part of the CREATE Sustainable Synthesis (CSS) program, I travelled to Rostock, Germany, to work with Prof. Matthias Beller at the Leibniz-Institut für Katalyse. Working with Dr. Thomas Schareina, I developed a nickel catalyzed protocol for producing aryl nitriles from aryl chlorides. Below are the results from this collaboration:

4.1 Introduction

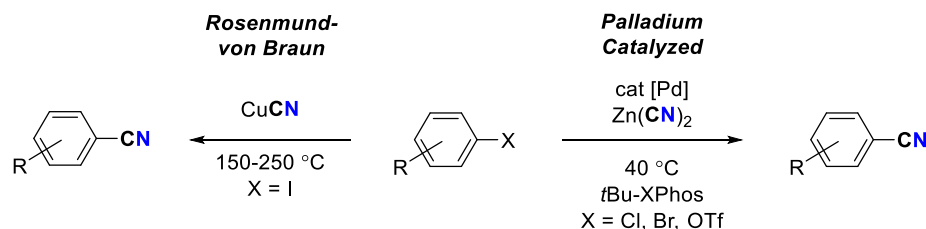
Arylnitriles are highly useful in organic synthesis due to their ability to undergo a variety of transformations. Important nitrile-containing molecules are found in both the pharmaceutical,^[232] and polymer^[233,234] industries. For example, etravirine and rilpivirine (Scheme 4.1) are both important pharmaceuticals for the treatment of the HIV infection.^[232]



Scheme 4.1 Examples of pharmaceuticals with Ar-CN moieties.

The formation of C(sp²)-CN bonds is accomplished classically using the Sandmeyer^[235,236] and Rosenmund-von Braun^[237,238] (RvB) reactions. These reactions employ stoichiometric reagents, and in the case of the RvB reaction, high temperatures are required (Scheme 4.1). Modern catalytic cyanation of C(sp²)-X (X = I, Br, Cl) is dominated primarily by palladium catalysis. These methodologies typically require the use of aryl bromides or iodides, high temperatures, and

significant catalyst loading. Although the cyanation of aryl chlorides has been reported,^[239–244] these reactions require special palladium catalysts and elevated temperatures (>70°C). On the other hand, the nickel-catalyzed cyanation of aryl chlorides is known,^[245–252] however the substrate scope is relatively unexplored.^[253] To our knowledge, no general methodology exists for the catalytic cyanation of aryl chlorides under ambient conditions.



Scheme 4.2 Typical methods for the formation of aryl nitriles (a) Rosenmund-von Braun, and (b) palladium catalyzed methods, in this case a report by Buchwald et al.^[241]

It is noteworthy that Cohen and Buchwald recently reported a mild cyanation of (hetero)aryl halides and triflates using a palladium pre-catalyst and Zn(CN)_2 (Scheme 4.2).^[241] However, the scope included only a single aryl chloride and electron-rich aryl chlorides gave poor conversions. Moreover, the applicability of this system is reduced by high Pd pre-catalyst loadings (2-5%).

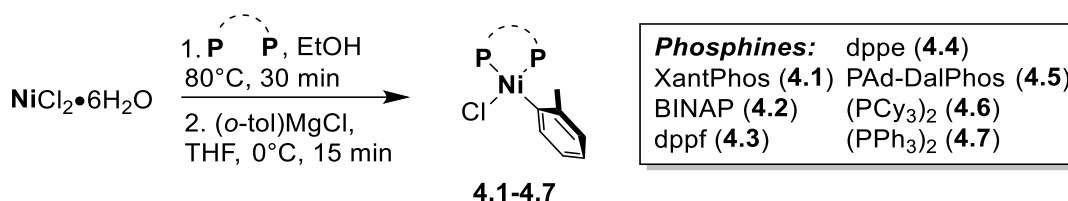
Herein, we communicate the first general, room temperature catalytic cyanation of (hetero)aryl chlorides. Our methodology employs an easily prepared, air stable nickel pre-catalyst^[254] which is based on the commercially available chelating diphosphine; 4,5-bis(diphenylphosphino)-9,9-dimethylxanthene (XantPhos). Advantageously, our system avoids the use of any additional base or reducing agents, and we utilize Zn(CN)_2 , a non-hygroscopic and

somewhat less toxic source of $[\text{CN}^-]$ (Intraperitoneal, $\text{LD}_{50} = 100 \text{ mg/kg}$)^[255] relative to alkali cyanides (NaCN , KCN , Intraperitoneal, $\text{LD}_{50} = 4.72\text{-}5.55 \text{ mg/kg}$).^[256]

4.2 Results and Discussion

4.2.1 Screening of Reaction Conditions

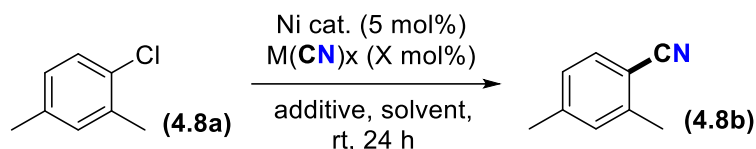
The general problem of both cyanide cross-coupling and hydrocyanation with nickel is the deactivation of the catalyst by coordination of multiple cyanide ligands to the metal center, which affords stable and unreactive $\text{M}(\text{CN})_x$ species.^[240,257] In some instances, these pathways have been suppressed by employing rigid bidentate phosphine ligands.^[258] Hence, we began our development of a room temperature cyanation catalyst using complex **4.1** (Scheme 4.3).^[254]



Scheme 4.3 Synthesis of Ni(II) diphosphine pre-catalysts **4.1-4.7**.^[254]

Using 2,4-dimethyl-chlorobenzene (**4.8a**), chosen as a sterically challenging substrate, with $\text{Zn}(\text{CN})_2$ in *N,N*-dimethylformamide (DMF) the desired product **4.8b** was observed in 38% yield (Table 1, entry 1). No other products were observed through GC-FID, and our GC-FID calibration curves suggest exclusive selectivity for the benzonitrile product. Solvent choice proved important, as only amide solvents (Table 4.1, entries 1-4) demonstrated conversion of the starting material; *N*-methylpyrrolidone (NMP) gave the highest (60%) yields (Table 4.1, entry 4).

Table 4.1 Ni-catalyzed cyanation of 2,4-dimethyl-chlorobenzene^a



Entry	Catalyst	Solvent	M(CN) _x (mol%)	Yield (%)
1	4.1	DMF	Zn(CN) ₂ (105)	38
2	4.1	DMA	Zn(CN) ₂ (105)	37
3	4.1-4.7	THF	Zn(CN) ₂ (105)	0
4	4.1	NMP	Zn(CN) ₂ (105)	60
5	4.1	NMP	NaCN (110)	0
6	4.1	NMP	KCN (110)	0
7	4.1	NMP	CuCN (105)	0
8	4.1	NMP	K ₄ [Fe(CN) ₆] (35)	0
9	4.1	NMP	Zn(CN) ₂ (50)	26
10	4.1	NMP	Zn(CN) ₂ (150)	50
11 ^b	NiCl₂(dme)	NMP	Zn(CN) ₂ (105)	36
12	4.2-4.7	NMP	Zn(CN) ₂ (105)	0
13 ^c	4.1	NMP	Zn(CNd) ₂ (105)	60
14^{d,e}	4.1	NMP	Zn(CN)₂ (105)	70
15 ^{d,f}	4.1	NMP	Zn(CN) ₂ (105)	59
16 ^{d,e}	-	NMP	Zn(CN) ₂ (105)	0

^aYields determined by GC-FID, reaction conditions: aryl chloride (0.2 mmol), nickel pre-catalyst (5 mol %), M(CN)_x (X mol%), NMP (1 mL, 0.2 M), 24 h, yields were determined by GC analysis using tetradecane as an internal standard.

^bNiCl₂dme (10 mol%), Zn(0) (20 mol%), XantPhos (10 mol%), ^c0.5 mL NMP used instead (0.4 M), ^dReaction run on a 1.0 mmol scale. Additives: ^ealuminum oxide (6.6 mol% from AlCl₃·6H₂O). ^fZnCl₂ (up to 50 mol%).

Zn(CN)₂ was the only metal cyanide source which afforded the desired product at low temperature (entries 4-8). Experiments varying the amount of Zn(CN)₂ showed that 105 mol% (Table 4.1, entries 4, 9, 10) gave optimal conversion. Although lower yields were achieved, we were able to produce the nitrile product with an *in situ* generated catalyst using XantPhos, NiCl₂(dme) (dme = 1,2-dimethoxyethane), and zinc metal (Table 4.1, entry 11). Other Ni(II) pre-catalysts^[254] **4.2-4.7** did not afford the product **4.8a** (Table 4.1, entry 12).

Surprisingly, we found that stirring rate was an important variable for the reaction conditions: the optimal rate was found to be 500-700 rotations per minute (rpm). Rates near 250 rpm or 900 rpm reproducibly gave yields closer to 35%. Since the $\text{Zn}(\text{CN})_2$ is poorly soluble in NMP, this dependence on stirring is likely related to particle size and thus concentration of dissolved cyanide ions. Cyanide ions are known to shut down nickel catalysis.^[257]

Lewis acids are known to improve the cyanation process by accelerating the transfer of cyanide from the solid to solution.^[248] Indeed, under our test reaction conditions, we observed a positive influence after the addition of an aluminium oxide solid (5% based on $\text{AlCl}_3 \cdot 6\text{H}_2\text{O}$ precursor)^[259] (Table 4.1, entry 14). The exact role of this Lewis acid in the reaction is not clear, but may be related to the formation of aluminium cyanides. Expectedly, reactions performed without the addition of nickel did not afford the benzonitrile product (Table 4.1, entry 16).

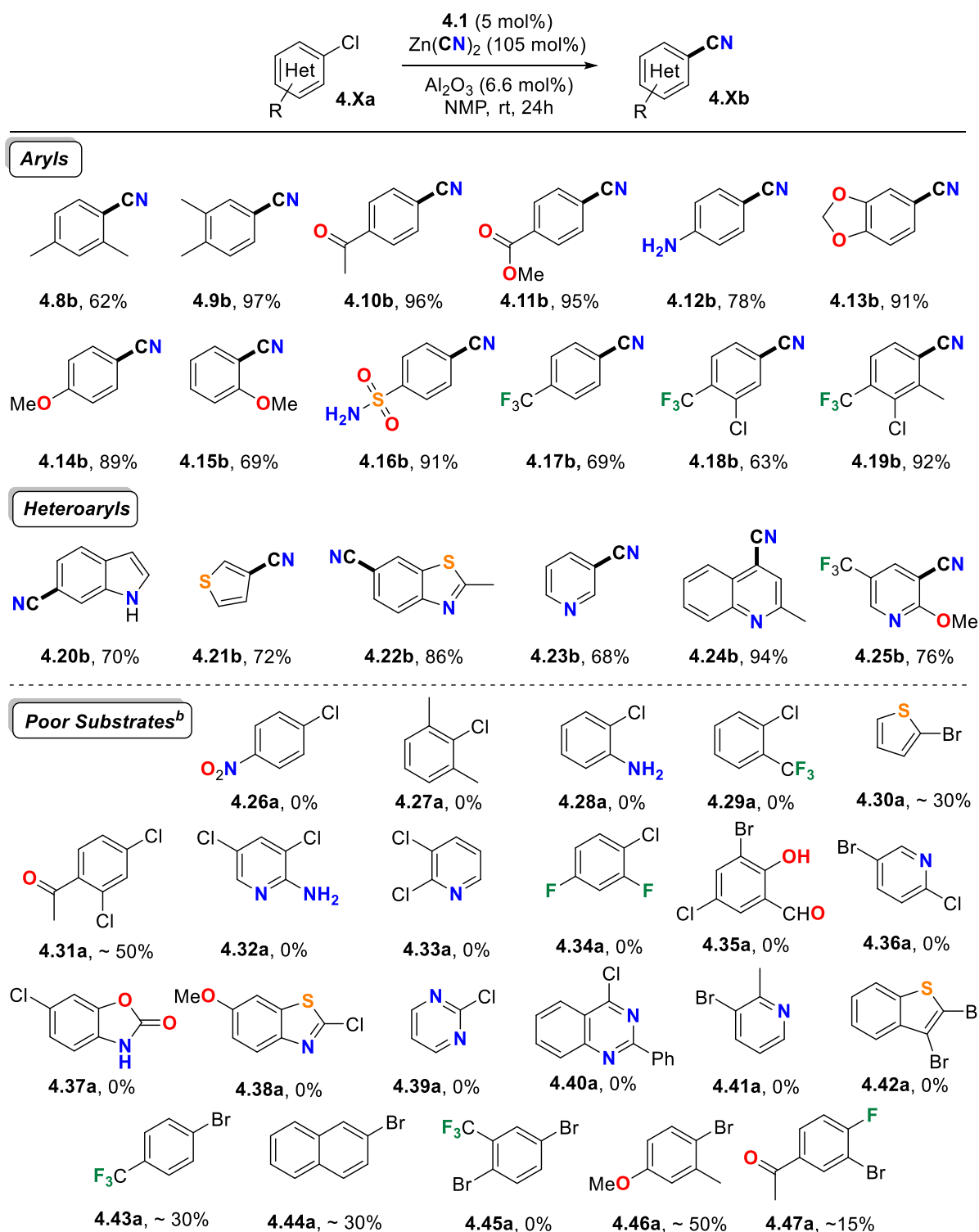
4.2.2 Reaction Substrate Scope

Having optimized conditions in hand, we applied our system to a range of aryl chlorides. Product **4.8b** is isolated in a fair yield (Scheme 4.4), while **4.9b** is produced in excellent yield. The poorer conversion of **4.8a** is most-likely attributed to steric effects. Products with ketone (**4.10b**), ester (**4.11b**), amine (**4.12b**), ether (**4.14b**), sulfonamide (**4.16b**), and trifluoromethyl (**4.17b**-**4.19b**) moieties at the *para*-position were also isolated in good to excellent yields. Interestingly, no Buchwald-Hartwig homocoupling products were detected by GC-FID in the preparation of the primary aniline **4.12b**. Product **4.13b**, containing a 1,3-benzodioxole functional group, was also isolated in excellent yield. Reactants **4.18a** and **4.19a**, which feature 1,3-dichloro substitution, react at a single site; selectively is realized at the less-sterically hindered chloride *para* to the trifluoromethyl group.

For the synthesis of bio-active compounds it is important that heteroaryl substrates were also tolerated under these reaction conditions (Scheme 4.4). Substrates based on indole (**4.20a**), thiophene (**4.21a**), and pyridine (**4.23a**) heteroaromatics afforded the corresponding products in good yields. Furthermore, thiazole (**4.22a**) and quinoline (**4.24a**) derivatives both allowed for isolation of the corresponding products in excellent yields.

Comparing **4.8** vs **4.9**, **4.12** vs **4.28**, **4.17** vs **4.29**, and **4.14** vs **4.15** showed that *ortho*-substitution is not well tolerated for both electron-poor and -rich substrates. When comparing the sterically similar substrates **4.8a** vs **4.19a**, the more electron-poor **4.19a** afforded the product in a much higher yield. The only functional group found not to be tolerant to our conditions was the nitro (-NO₂) moiety; *para*-nitrochlorobenzene (**4.26a**) did not show any desired product formation. The intolerance of nitro groups is proposed to be due to oxygen transfer from the nitro group to the phosphine ligand, which is well known for nickel phosphine species.^[260]

Surprisingly, comparing the cyanation of aryl chlorides and bromides under the same conditions, we found that conversion to the benzonitrile products in the latter case were lower. For example, comparing **4.17a** (69% yield) and **4.43a** (~ 30% conversion), the bromide analogue is clearly less useful in this transformation. Even the naphthyl derivative **4.44a** and the electron poor **4.45a** resulted in low conversions to the corresponding benzonitriles. We explain this unusual observation by the chloride induced stabilization of active nickel intermediates. It is also possible that under these reaction conditions, transmetalation of nickel intermediates to zinc proceeds at faster rates for nickel chloride relative to the nickel bromide intermediates.

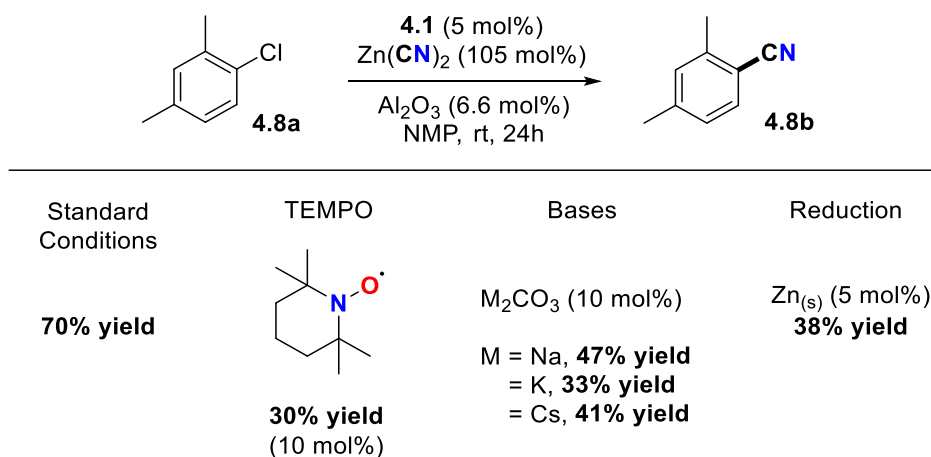


Scheme 4.4 Scope of nickel-catalyzed cyanation of aryl chlorides Isolated yields (average of two runs). Reaction conditions: aryl chloride (1.0 mmol), NMP (2.5 mL, 0.4 M), 24 h. ^bApproximate conversions of starting material are shown based on GC analysis). No rigorous quantitative analysis was completed.

4.2.3 Preliminary Mechanistic Investigations

4.2.3.1 Additive Effects

We then began some preliminary investigations into additive effects of this reaction. If one-electron pathways were operative at the metal center, adding TEMPO should significantly affect the reactivity. Under our optimized reaction conditions addition of TEMPO (10 mol%) did hamper reactivity but did not fully shut down the catalytic reaction (Scheme 4.5). This result suggests that the catalytic cycle is a two-electron cycle. Base additives did result in lower yields, perhaps inhibiting or interfering with the transmetalation step. Finally, reducing conditions also did not improve the yield, suggesting that catalyst death is not due to over-oxidation.



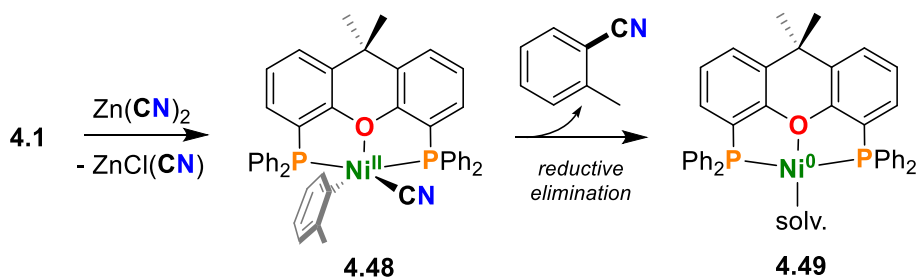
Scheme 4.5 Additive effects to probe reaction mechanism of this nickel catalyzed method.

4.2.3.2 Proposal for Catalytic Cycle

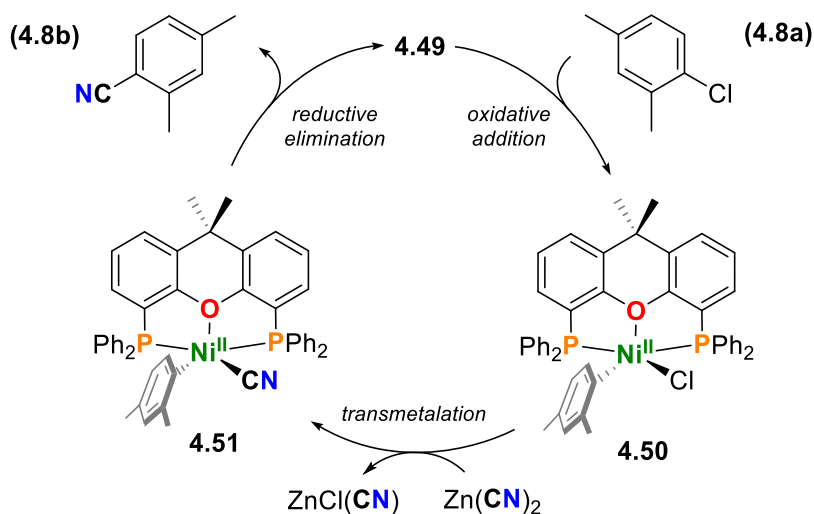
Based on the literature of nickel-catalyzed cyanations,^[38,248,261] we proposed a catalytic cycle for this transformation (Scheme 4.6). Initially, the pre-catalyst **4.1** undergoes transmetalation with Zn(CN)₂ to give **4.48**, which upon reductively eliminating *ortho*-methylbenzonitrile, gives the solvato complex **4.49**. We observed a small amount of *ortho*-methylbenzonitrile in all GC-FID

traces of reaction mixtures, in agreement with this proposal. The Ni(0) complex **4.49** undergoes oxidative addition with the aryl halide substrate to give complex **4.50**. Following transmetalation with $\text{Zn}(\text{CN})_2$ to give **4.51**, the desired benzonitrile is produced by reductive elimination from **4.51** to reconstitute complex **4.49**.

(a) Activation of pre-catalyst **1a**



(b) Proposed catalytic cycle for cyanation of aryl chlorides



Scheme 4.6 (a) Activation of pre-catalyst (**1a**) and (b) mechanistic proposals.

4.3 Conclusion

A general catalytic cyanation of (hetero)aryl chlorides under ambient conditions is described. This method uses an air and moisture stable nickel pre-catalyst with a commercially available bidentate phosphine ligand, XantPhos. This room temperature cyanation of (hetero)aryl chlorides proceeds smoothly in the presence of $\text{Zn}(\text{CN})_2$ and does not require drying of the cyanide source. Advantageously, the procedure does not require drying of the glassware, substrates, or the nickel pre-catalyst. Our simple and mild reaction conditions should allow for widespread use of this protocol.

Experimental data for Chapter 4 begins on pg. 243

Chapter 5: Conclusions & Future Work

5.1 Chapter 2: Understanding Ni(II) Mediated C(sp³)-H Activation: Ureas as Model Substrates

5.1.1 Conclusions

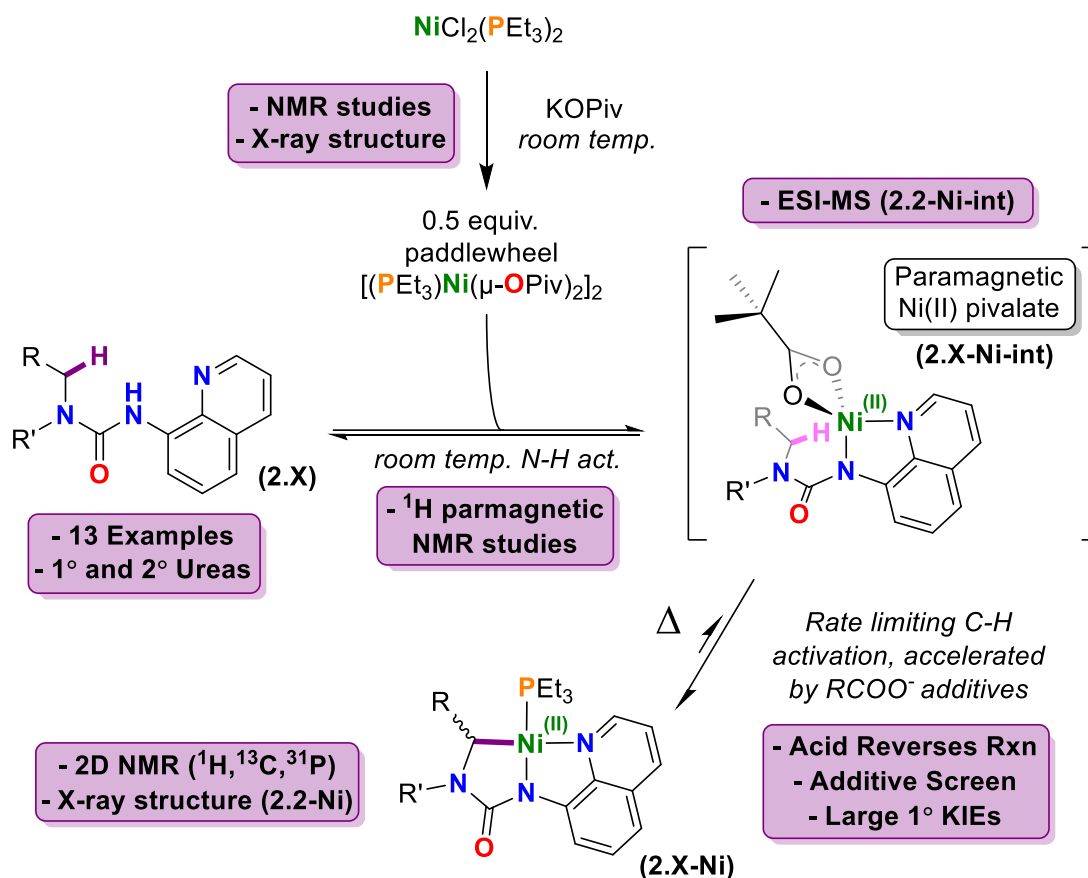
Work in Chapter 2 described the first examples of experimental mechanistic studies of nickel's role in activating C(sp³)-H bonds. Using the ubiquitous 8AQ directing group, we use tertiary ureas as model substrates to look at a variety of reaction variables (Scheme 5.1).

The best solvents for the C-H activation reactions that we studied seem to be polar aprotic solvents such as DMSO, DMF, and CH₃CN. In contrast, solvents such as THF and toluene result in impeded rates, and chlorinated solvents degrade the product. Additives also proved to be important, with carboxylate ligands giving the best results. In our hands pivalate was the best additive. 1-AdCOOH and KOAc were also effective additives for increasing the rate of C-H activation. Notably, this same trend is realized for more sterically encumbered reactions, as shown by additive studies with secondary C(sp³)-H activation events.

We showed that the carboxylate additives help with phosphine dissociation, and are also important for realizing facile N-H activation to give paramagnetic (likely tetrahedral) Ni(II) ureate intermediates (**2.X-Ni-int**), which we showed by mass spectrometry and N-substitution studies (Scheme 5.1). This paramagnetic intermediate is likely an intermediate along the reaction pathway. From this intermediate, rate-limiting C-H activation occurs (*recall* KIEs), which we showed to be potentially reversible through protonation studies. We also examined a range of substitutions at the C-H activation site, and for the first time we have determined the rates of C(sp³)-H activation at Ni(II) metal centers. Secondary C-H bonds react slower than primary C-H bonds while tertiary

substrates did not react. Using secondary ureas resulted in a range of products which we were unable to identify.

Lastly, we were able to show that the cyclometalated intermediate (**2.2-Ni**) was relevant for C-C coupling reactions with aryl halides, aryl iodonium salts, alkyl bromides, and carbon monoxide. These results, taken with others DFT studies, suggest that 8AQ-substituted ureas are good models for understanding nickel(II)'s role in C(sp³)-H activation.



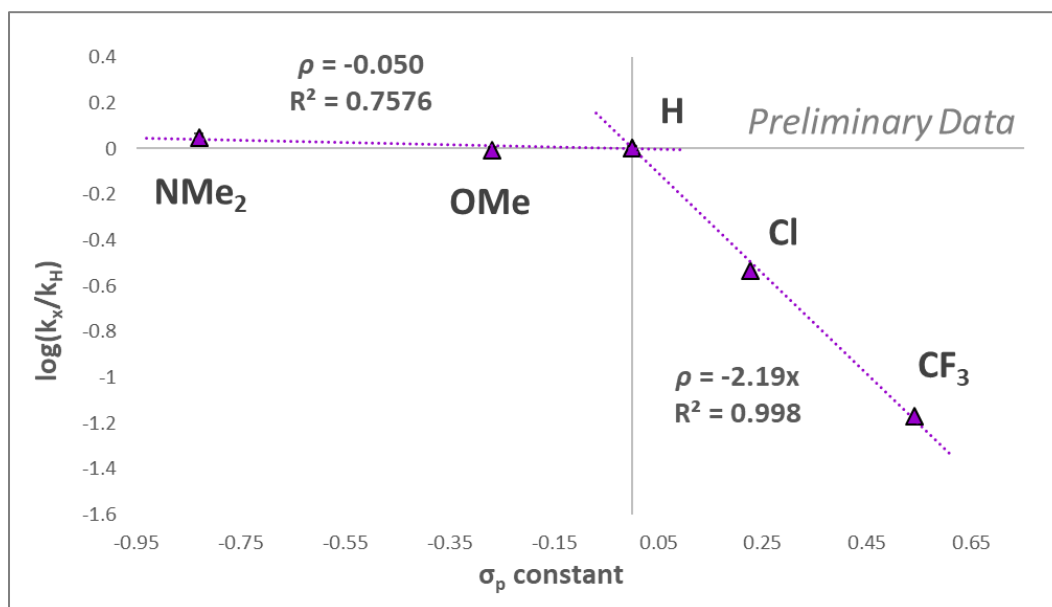
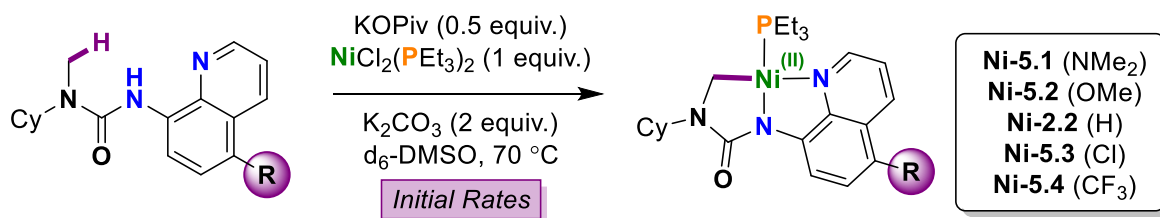
Scheme 5.1 Proposed mechanism for the Ni(II) mediated δ-C(sp³)-H activation of substituted ureas; as shown in Chapter 2.

5.1.2 Future Work & Preliminary Results – Directing Group Effects

In Chapter 2 we investigated the mechanism of C(sp³)-H activation at Ni(II) using 8AQ-substituted ureas as model substrates. Going forward we were interested in learning about the role of the directing group. In nickel catalyzed 8AQ-amide C(sp³)-H functionalization reactions, only the 8AQ derivatives promote productive catalysis. Several groups have unsuccessfully tried to use other directing groups in these reactions. Furthermore, there are no studies examining how the electronics of the 8AQ group affect rates of C-H activation at Ni(II). The results herein describe our initial attempts to (i) examine the electronic effects of 8AQ-substituted ureas on the rates of C-H activation, and (ii) understand if other directing groups can be used in place of 8AQ.

5.1.2.1 Effect of Substituted of 8-Aminoquinolines

We were first interested in examining the electronic effect of the 8AQ directing group. We synthesized the substituted ureas **5.1-5.4** in a similar method as we did in Chapter 2. Under standard reaction conditions found in Chapter 2 (Scheme 5.2), we found that electron poor directing groups resulted in lower rates of the formation of the C(sp³)-H activated products. In contrast, electron rich substrates did not result in faster rates. Rather, the preliminary Hammett plot has two regimes, which suggests a change in mechanism or a change in the rate-determining step. We speculate that the electron poor ligands may not be proficient at displacing phosphine, which may then be the rate determining step. In the case of the electron-neutral and -rich ligands, this displacement may be facile. However, we are currently investigating these results further.

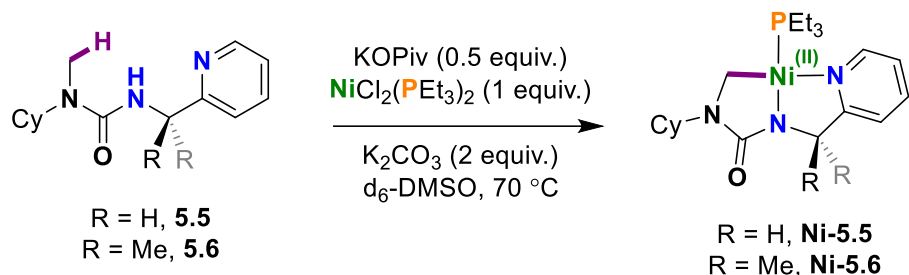


Scheme 5.2 Hammett plot showing rates of δ -C(sp³)-H activation of 8AQ-substituted ureas.^[166]

5.1.2.2 Pyridine Directing Groups

We also wished to examine other directing groups as substitutes for the 8AQ group. To our knowledge, no other directing group has been successfully used for nickel catalyzed C(sp³)-H activation. We began with pyridine directing groups: we chose to synthesize ureas **5.5** and **5.6** to examine the possible effect of substitution in the methylene backbone (Scheme 5.3). Under standard reaction conditions (Scheme 5.3), we found that both **5.5** and **5.6** react slowly to produce the C(sp³)-H activated cyclometalated complexes **Ni-5.5** and **Ni-5.6**. Although we have not quantified the rates by kinetic analysis, the dihydro-variant **5.5** reacts much slower than the urea with the dimethyl backbone (**5.6**). Upon synthesizing **2.2-Ni** from urea **2.2**, we observed a

reduction in angle on the directing group by $\sim 3\text{-}4^\circ$ (*c.f.* Chapter 2). Thus, we attribute the faster rate of cyclometallation of **5.6** over **5.5** to the thermodynamics of the product formation.



Scheme 5.3 Investigating pyridyl directing groups for $\delta\text{-C}(\text{sp}^3)\text{-H}$ activation of ureas.

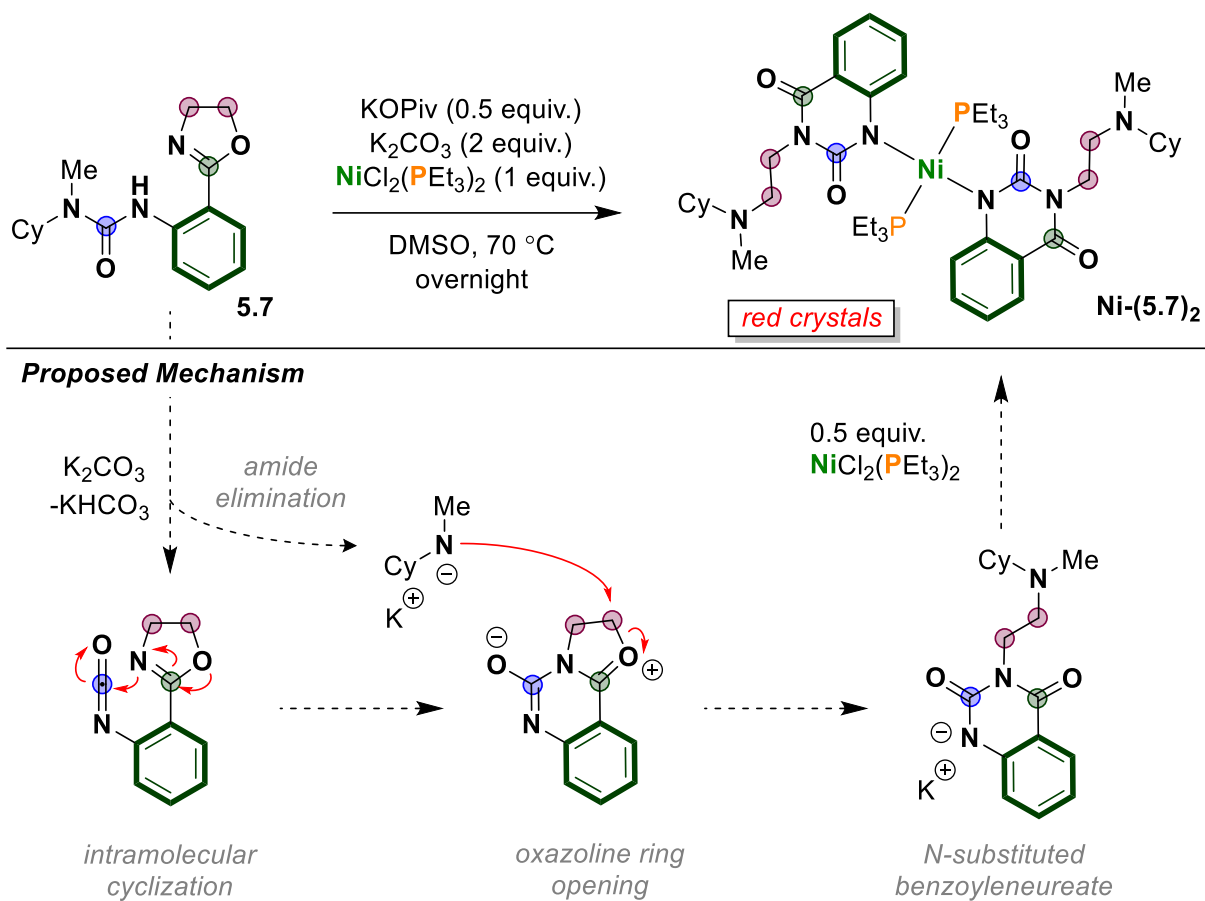
5.1.2.3 An Oxazoline Directing Group

In a theoretical report by Yu *et. al.*,^[172] the authors predicted that an oxazoline-amide directing group could be a potent substitute for the 8AQ-amide directing group used heavily throughout the literature of nickel mediated C(sp²)-H activation. Furthermore, the authors suggest that the barrier to C-H activation should in fact be lower for the oxazoline-amide functionality. However, to our knowledge, this directing group has not been applied experimentally to nickel mediated C-H activation catalysis.

To probe the feasibility of using oxazoline for C(sp³)-H activation with nickel, we synthesized the analogous urea **5.7** which contains the oxazoline directing group. By ¹H NMR spectroscopy, the oxazoline-urea did not undergo C-H activation as anticipated under standard reaction conditions. Instead, red crystals formed in the bottom of the heated NMR tube. Single crystal X-ray diffraction revealed that the organic fragments underwent a rearrangement reaction to produce a square planar bis(benzoyleneureate) Ni(II) complex **Ni-(5.7)₂** (Scheme 5.4). The ureates are located *trans* to one another, while the remaining two coordination sites are occupied by triethylphosphine ligands. In the X-ray crystal structure, the molecule exhibits C_i symmetry.

Based on the resulting atom connectivity and our knowledge of the reactivity of carbonyl compounds, we propose a mechanism for this reaction below (Scheme 5.4):

- i) Following deprotonation by K_2CO_3 , potassium *N*-methylcyclohexyl amide is eliminated from the urea, producing an oxazoline isocyanate.
- ii) This isocyanate may undergo facile intramolecular cyclization with the oxazoline nitrogen, resulting in the formation of a ureate-oxonium zwitterion. This oxonium character should render the adjacent methylene a potent electrophile at carbon.
- iii) The potassium *N*-methylcyclohexyl amide may then attack this electrophilic methylene, resulting in ring opening of the oxazoline fragment.
- iv) The potassium benzoyleneureate salt may then undergo salt metathesis with nickel. Of course, this process must repeat once more to afford the second equivalent of benzoyleneureate at nickel.



Scheme 5.4 Reaction of the oxazoline containing urea **5.7** with nickel, resulting in the rearrangement to a N-substituted benzoyleneureate Ni(II) complex **Ni-(5.7)₂**. The proposed mechanism is also shown.

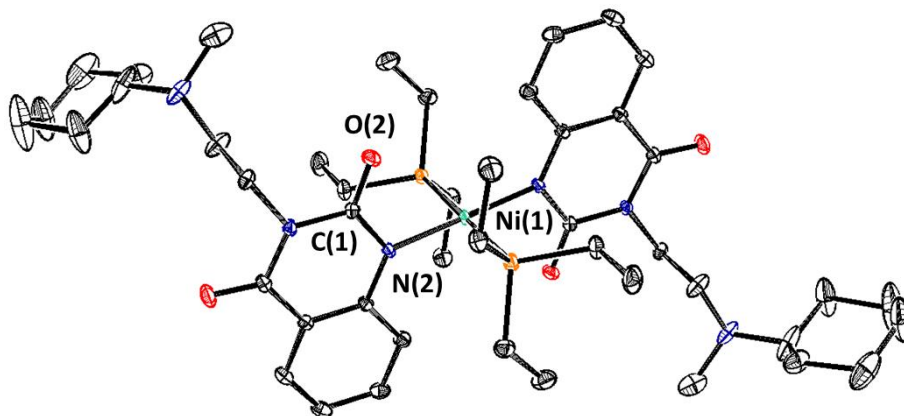


Figure 5.1 ORTEP depiction of bis(benzoyleneureate)Ni(II) complex **Ni-(5.7)₂**. (ellipsoids at 50% probability, hydrogens and solvent omitted). Selected bond lengths (Å): C1-N2 1.3516, C1-O2 1.2383, N2-Ni1 1.9027.

We are currently investigating this work further and will report our findings in due course. We anticipate this work will inform those in the catalysis community of alternate directing groups that could be used for Ni(II) catalyzed C(sp³)-H functionalization.

5.2 Chapter 3: Preparation of Low-Coordinate Ni(I) Amidate Complexes and Reactivity of Ni(I) Complexes Towards C(sp³)-H Activation

5.2.1 Conclusions

Work in Chapter 3 focused on the synthesis of Ni(I) amidate complexes. These complexes adopt a range of binding modes depending on the N-R and C-R substituents, showcasing the hemilability of amidates on nickel. In addition, we isolated the first examples of molecules displaying C(sp²)-H and C(sp³)-H agostic contacts at nickel(I) metal centers.

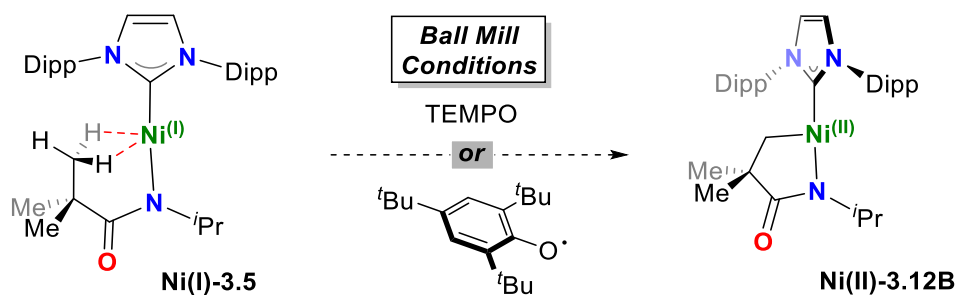
In subsequent studies we investigated the reactivity of these Ni(I) complexes with radical species and π -accepting ligands. In the radical studies, we observed oxidation of Ni(I) to Ni(II), and a change in amidate binding mode in all cases. In the studies with π -accepting ligands we probed the mechanism of disproportionation of Ni(I) to Ni(II) and Ni(0). We isolated reactive intermediates and showed through kinetics and substitution studies that the likely mechanism is a bimolecular ligand transfer of the amidate ligand.

5.2.2 Future Work – Solid-State Reactions for Ni(I) C-H Activation

Our EPR and NMR spectroscopic studies on agostic complexes **Ni(I)-3.5** and **Ni(I)-3.6** suggested that the agostic C-H contacts are either fluxional or perhaps non-existent when dissolved. However, solid-state crystal structures and DFT studies clearly showed that these

agostic interactions are present. It is therefore not surprising that **Ni(I)-3.5** did not engage in C-H activation, precluding further studies in solution.

As an alternative, we are interested in examining the reactivity of Ni(I) agostic complexes in the solid-state. By keeping the Ni(I) complexes in their solid-state, we hope to leverage the solid-state agostic contacts which may be more amenable to C-H activation reactions. We propose that ball-mill technology might work well for this purpose (Scheme 5.5). Simple grinding with a mortar and pestle may also be possible.



Scheme 5.5 Proposed reaction of **Ni(I)-3.5** with radical H-abstracting agents under ball mill conditions.

Of importance will be the stability of **Ni(II)-3.12B** to the proton (-OH) sources made during the proposed C-H activation reaction. With protonation studies we will also probe the stability of **Ni(II)-3.12B**. This will be integral for the purification step which inevitably will involve solubilizing reaction components. We hope this change from solution to solid-state conditions will address the issue of transient agostic interactions.

5.3 Chapter 4: CREATE Sustainable Synthesis: Room Temperature Catalytic Cyanation of Aryl Chlorides using an Air-stable Ni(II)-XantPhos Pre-catalyst

5.3.1 Conclusions

Work in Chapter 4 described research undertaken while on a CREATE Sustainable Synthesis internship. While working for Matthias Beller in Rostock, Germany, Thomas Schareina and I developed a simple protocol for the cyanation of aryl chlorides using a nickel catalyst and zinc cyanide. Notably, the reaction is the first example of catalytic cyanation of aryl chlorides at room temperature. Together with the absence of additives, these conditions are exceedingly mild. We propose that this method could be applied to complex systems due to the mild nature of the reaction conditions. This work is ongoing in the Beller lab.

5.3.2 Future Work – Mechanistic Efforts

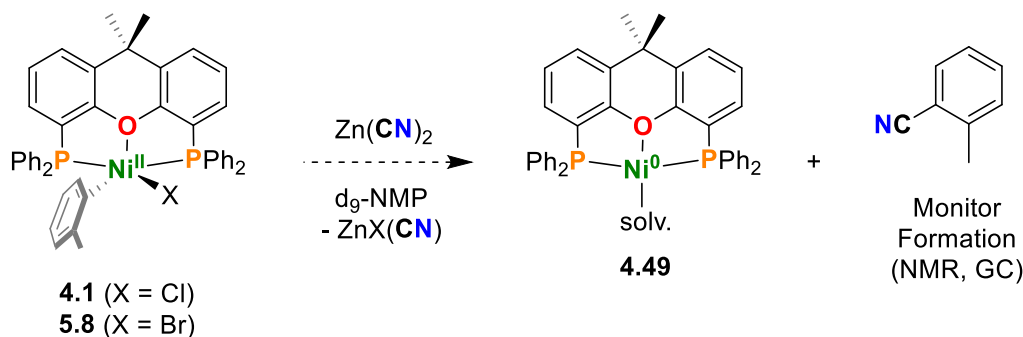
By probing the reaction with a substrate scope, we showed that our method is rather general; however, it does not translate well to aryl bromides or iodides. Although aryl chlorides are generally desirable substrates over their bromides and iodides, this result is strange from a mechanistic perspective. We offer two explanations: (1) The transmetalation of Ni(II)-Cl is faster. It is possible the transmetalation is the slowest step of the catalytic cycle, and thus perhaps Ni-Cl transmetalates more quickly with zinc. (2) The oxidative addition of Ar-Br and Ar-I to Ni(0) lead to Ni(I) species, which may be off-cycle species that are not conducive to catalytic turnover. From the literature we know that aryl bromides and iodides oxidatively add faster, but also give Ni(I) products in addition to the Ni(II) products.^[217,261]

In theory it should be possible to test both hypotheses by simple experiments (Scheme 5.6). The first hypothesis can be tested by examining the rate of cyanation product formation for both the nickel bromide and chloride intermediates **5.8** and **4.1** respectively. The organic product could

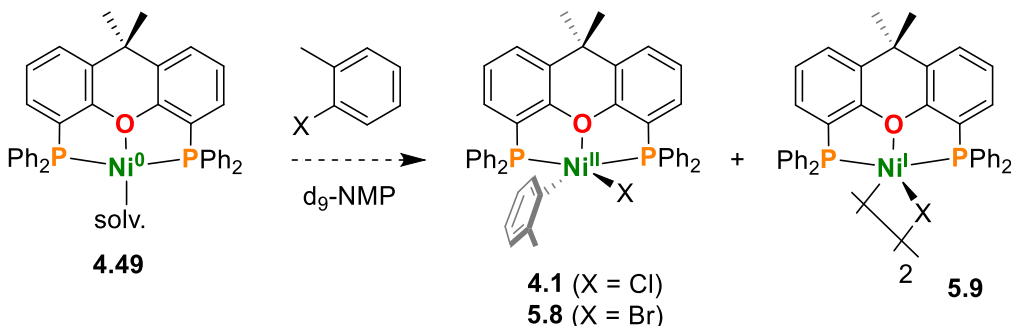
be monitored by either NMR spectroscopy or gas chromatography. Because stirring rate is an important factor in this method, we propose that standard reaction conditions (Schlenk flask, stirring, etc.) will be better than simple NMR scale stoichiometric reactions without stirring. Thus, gas chromatography may be a more effective method.

The second hypothesis can be tested by examining the ratio of nickel products from the stoichiometric reaction of Ni(0)-Xantphos (**4.49**) with aryl halides. The amount of Ni(I) products will be probed by EPR spectroscopy, and the Ni(II) products **5.8** and **4.1** will be probed by NMR spectroscopy. We hope these experiments will shed light not only on the mechanism of this catalytic method, but also explain the halide preferences we observed during our study.

(a) Testing Hypothesis 1: Transmetalation rates



(b) Testing Hypothesis 2: Ratio of nickel products from oxidation



Scheme 5.6 (a) Hypothesis 1: Probing the rates of transmetalation of Ni(II) chloride and bromide salts. (b)

Hypothesis 2: Probing the product ratio of nickel species upon oxidation of Ni(0) by aryl halides.

5.4 Summary

As summarized in the previous sections, this thesis focused on understanding the mechanisms of elementary reactions of homogeneous nickel compounds:

In Chapter 2 we investigated the mechanism of Ni(II) C(sp³)-H activation: the first and only experimental study of its kind. Our results using ureas as model substrates compare nicely to computational results of the amide variants that were already available. Our studies also map rates of C-H activation for different substituents, which had not been accomplished previously.

In Chapter 3 we examined a range of reduced Ni(I)-amidate species and determined the preferred binding modes based on nitrogen and carbon substituents. We also isolated the first examples of Ni(I) C-H agostic complexes, both C(sp²)-H and C(sp³)-H variants. These complexes were reacted with a range of molecules in an attempt to C-H activate the agostic contacts. Although these studies did not afford the desired reactivity, we learned that Ni(I) complexes disproportionate in the presence of π -acceptors.

In Chapter 4 we developed the first room temperature catalytic method for cyanation of aryl chlorides. This method is a simple protocol which does not require drying of any reagents. This study gives further insight into XantPhos as a practical ligand for nickel catalysis, and its ability to shield nickel from off-cycle pathways.

Experimental data for Chapter 5 begins on pg. 253

Bibliography

- [1] P. Anastas, N. Eghbali, *Chem. Soc. Rev.* **2010**, 39, 301–312.
- [2] K. M. Waltz, J. F. Hartwig, *Science* **1997**, 277, 211–213.
- [3] M. J. Wax, J. M. Stryker, J. M. Buchanan, C. A. Kovac, R. G. Bergman, *J. Am. Chem. Soc.* **1984**, 106, 1121–1122.
- [4] A. H. Janowicz, R. A. Periana, J. M. Buchanan, C. A. Kovac, J. M. Stryker, M. J. Wax, R. G. Bergman, *Pure Appl. Chem.* **1984**, 56, 13–23.
- [5] H. Chen, S. Schlecht, T. C. Semple, J. F. Hartwig, *Science* **2000**, 287, 1995–1997.
- [6] S. Rousseaux, S. I. Gorelsky, B. K. . W. Chung, K. Fagnou, *J. Am. Chem. Soc.* **2010**, 132, 10692–10705.
- [7] Y. Zhang, B. Shi, J. Yu, *J. Am. Chem. Soc.* **2009**, 131, 5072–5074.
- [8] M. H. Shaw, V. W. Shurtleff, J. A. Terrett, J. D. Cuthbertson, D. W. C. MacMillan, *Science* **2016**, 352, 1304–1308.
- [9] C. L. Joe, A. G. Doyle, *Angew. Chem. Int. Ed.* **2016**, 55, 4040–4043.
- [10] J. D. Cuthbertson, D. W. C. MacMillan, *Nature* **2015**, 519, 74–77.
- [11] A. McNally, C. K. Prier, D. W. C. MacMillan, *Science* **2011**, 334, 1114–1117.
- [12] Z. Zuo, D. T. Ahneman, L. Chu, J. A. Terrett, A. G. Doyle, D. W. C. MacMillan, *Science* **2014**, 345, 437–440.
- [13] L. V Desai, K. J. Stowers, M. S. Sanford, *J. Am. Chem. Soc.* **2008**, 13285–13293.
- [14] T. W. Lyons, M. S. Sanford, *Chem. Rev.* **2010**, 110, 1147–1169.
- [15] G. Rouquet, N. Chatani, *Angew. Chem. Int. Ed.* **2013**, 52, 11726–11743.
- [16] L.-C. Campeau, D. J. Schipper, K. Fagnou, *J. Am. Chem. Soc.* **2008**, 130, 3266–3267.
- [17] X.-C. Wang, W. Gong, L.-Z. Fang, R.-Y. Zhu, S. Li, K. M. Engle, J.-Q. Yu, *Nature* **2015**,

- 519, 334–338.
- [18] J. Guihaumé, S. Halbert, O. Eisenstein, R. N. Perutz, *Organometallics* **2012**, *31*, 1300–1314.
- [19] Q. Lu, F. Glorius, *Angew. Chem. Int. Ed.* **2017**, *56*, 49–51.
- [20] H. Yi, G. Zhang, H. Wang, Z. Huang, J. Wang, A. K. Singh, A. Lei, *Chem. Rev.* **2017**, *117*, 9016–9085.
- [21] R. Waterman, *Organometallics* **2013**, *32*, 7249–7263.
- [22] Y. Boutadla, D. L. Davies, S. A. Macgregor, A. I. Poblador-Bahamonde, *Dalton Trans.* **2009**, 5820–5831.
- [23] S. I. Gorelsky, D. Lapointe, K. Fagnou, *J. Org. Chem.* **2012**, *77*, 658–668.
- [24] D. Lapointe, K. Fagnou, *Chem. Lett.* **2010**, *39*, 1118–1126.
- [25] S. I. Gorelsky, D. Lapointe, K. Fagnou, *J. Am. Chem. Soc.* **2008**, *130*, 10848–10849.
- [26] We will refer to this heteroatom assisted c-h activation mechanism as cmd for the duration of this manuscript. We do so for ease of discussion, and we acknowledge other equally valid descriptions such as ambiphilic metal ligand activation.
- [27] M. Brookhart, M. L. H. Green, G. Parkin, *Proc. Natl. Acad. Sci.* **2007**, *104*, 6908–6914.
- [28] J. A. Labinger, J. E. Bercaw, *Nature* **2002**, *417*, 507–514.
- [29] X. Chen, K. M. Engle, D. Wang, J. Yu, *Angew. Chem. Int. Ed.* **2009**, *48*, 5094–5115.
- [30] R. Nakano, R. Jazzar, G. Bertrand, *Nat. Chem.* **2018**, *10*, 1196–1200.
- [31] D. A. Colby, R. G. Bergman, J. A. Ellman, *Chem. Rev.* **2010**, *110*, 624–655.
- [32] X. Qi, Y. Li, R. Bai, Y. Lan, *Acc. Chem. Res.* **2017**, *50*, 2799–2808.
- [33] A. H. Janowicz, R. G. Bergman, *J. Am. Chem. Soc.* **1982**, *104*, 352–354.
- [34] J. K. Hoyano, W. A. G. Graham, *J. Am. Chem. Soc.* **1982**, *104*, 3723–3725.

- [35] S. R. Klei, K. L. Tan, J. T. Golden, C. M. Yung, R. K. Thalji, K. A. Ahrendt, J. A. Ellman, T. D. Tilley, R. G. Bergman, *C-H Bond Activation by Iridium and Rhodium Complexes: Catalytic Hydrogen-Deuterium Exchange and C-C Bond-Forming Reactions*. **2004**, pp. 46–55.
- [36] S. Pan, T. Shibata, *ACS Catal.* **2013**, *3*, 704–712.
- [37] P. Gandeepan, T. Müller, D. Zell, G. Cera, S. Warratz, L. Ackermann, *Chem. Rev.* **2018**, *119*, 2192–2452.
- [38] S. Z. Tasker, E. A. Standley, T. F. Jamison, *Nature* **2014**, *509*, 299–309.
- [39] L. Nattmann, S. Lutz, P. Ortsack, R. Goddard, J. Cornella, *J. Am. Chem. Soc.* **2018**, *140*, 13628–13633.
- [40] K. Jonas, *Angew. Chem. Int. Ed. English* **1975**, *14*, 752–753.
- [41] R. H. Sloane, R. Press, *Proc. R. Soc. Ser. A.* **1938**, *168*, 284.
- [42] C.-Y. Lin, P. P. Power, *Chem. Soc. Rev.* **2017**, *46*, 5347–5399.
- [43] M. I. Lipschutz, T. D. Tilley, *Angew. Chem. Int. Ed.* **2014**, *53*, 7290–7294.
- [44] V. M. Iluc, A. J. M. Miller, J. S. Anderson, M. J. Monreal, M. P. Mehn, G. L. Hillhouse, *J. Am. Chem. Soc.* **2011**, *133*, 13055–13063.
- [45] X. Wang, P. Xie, R. Qiu, L. Zhu, T. Liu, Y. Li, T. Iwasaki, C. T. Au, X. Xu, Y. Xia, et al., *Chem. Commun.* **2017**, *53*, 8316–8319.
- [46] J. R. Bour, N. M. Camasso, M. S. Sanford, *J. Am. Chem. Soc.* **2015**, *137*, 8034–8037.
- [47] N. M. Camasso, M. S. Sanford, *Science* **2015**, *347*, 1218–1220.
- [48] S. A. Johnson, *Dalton Trans.* **2015**, *44*, 10905–10913.
- [49] M. Brookhart, M. L. H. Green, G. Parkin, *Proc. Natl. Acad. Sci.* **2007**, *104*, 6908–6914.
- [50] W. Scherer, G. S. McGrady, *Angew. Chem. Int. Ed.* **2004**, *43*, 1782–1806.

- [51] W. Scherer, V. Herz, A. Brück, C. Hauf, F. Reiner, S. Altmannshofer, D. Leusser, D. Stalke, *Angew. Chem. Int. Ed.* **2011**, *50*, 2845–2849.
- [52] W. Scherer, A. C. Dunbar, J. E. Barquera-Lozada, D. Schmitz, G. Eickerling, D. Kratzert, D. Stalke, A. Lanza, P. Macchi, N. P. M. Casati, et al., *Angew. Chem. Int. Ed.* **2015**, *54*, 2505–2509.
- [53] M. W. Drover, E. G. Bowes, L. L. Schafer, J. A. Love, A. S. Weller, *Chem. Eur. J.* **2016**, *22*, 6793–6797.
- [54] J. E. Barquera-Lozada, A. Obenhuber, C. Hauf, W. Scherer, *J. Phys. Chem. A* **2013**, *117*, 4304–4315.
- [55] M. P. Mitoraj, A. Michalak, T. Ziegler, *Organometallics* **2009**, *28*, 3727–3733.
- [56] C. Hall, R. N. Perutz, *Chem. Rev.* **1996**, *96*, 3125–3146.
- [57] B. Pudasaini, B. G. Janesko, *Organometallics* **2014**, *33*, 84–93.
- [58] N. Koga, S. Obara, K. Morokuma, *J. Am. Chem. Soc.* **1985**, *20*, 7109–7116.
- [59] T. a Ateşin, T. Li, S. Lachaize, W. W. Brennessel, J. J. García, W. D. Jones, *J. Am. Chem. Soc.* **2007**, *129*, 7562–7569.
- [60] W. J. Youngs, J. D. Kinder, J. D. Bradshaw, C. A. Tessier, *Organometallics* **1993**, *12*, 2406–2407.
- [61] F. M. Conroy-Lewis, L. Mole, A. D. Redhouse, S. A. Litster, J. L. Spencer, *J. Chem. Soc., Chem. Commun.* **1991**, *60*, 1601–1603.
- [62] O. P. Gladkikh, H. Inwood, D. Nicholls, D. C. Weatherburn, *Inorg. Chim. Acta* **2002**, *331*, 131–135.
- [63] K. D. Kitiachvili, D. J. Mindiola, G. L. Hillhouse, *J. Am. Chem. Soc.* **2004**, *126*, 10554–10555.

- [64] J. W. L. Martin, J. H. Johnston, N. F. Curtis, *J. Chem. Soc. Dalt. Trans.* **1978**, 68–76.
- [65] M. Schormann, S. Garratt, M. Bochmann, *Organometallics* **2005**, *24*, 1718–1724.
- [66] M. Sugimoto, J. Fujita, H. Ito, K. Toriumi, T. Ito, *Inorg. Chem.* **1983**, *22*, 955–960.
- [67] H. L. Wiencko, E. Kogut, T. H. Warren, *Inorganica Chim. Acta* **2003**, *345*, 199–208.
- [68] M. K. Yadav, G. Rajput, L. B. Prasad, M. G. B. Drew, N. Singh, *New J. Chem.* **2015**, *39*, 5493–5499.
- [69] M. Stępień, L. Latos-Grażyński, L. Szterenberga, J. Panek, Z. Latajka, *J. Am. Chem. Soc.* **2004**, *126*, 4566–4580.
- [70] A. L. Keen, M. Doster, S. A. Johnson, *J. Am. Chem. Soc.* **2007**, *129*, 810–819.
- [71] M. Kandiah, G. S. McGrady, A. Decken, P. Sirsch, *Inorg. Chem.* **2005**, *44*, 8650–8652.
- [72] R. Beck, S. A. Johnson, *Organometallics* **2012**, *31*, 3599–3609.
- [73] Y. Zhou, D. R. Hartline, T. J. Steiman, P. E. Fanwick, C. Uyeda, *Inorg. Chem.* **2014**, *53*, 11770–11777.
- [74] T. J. Steiman, C. Uyeda, *J. Am. Chem. Soc.* **2015**, *137*, 6104–6110.
- [75] V. M. Iluc, G. L. Hillhouse, *J. Am. Chem. Soc.* **2010**, *132*, 11890–11892.
- [76] N. D. Clement, K. J. Cavell, C. Jones, C. J. Elsevier, *Angew. Chem. Int. Ed.* **2004**, 1277–1279.
- [77] S. A. Johnson, C. W. Huff, F. Mustafa, M. Saliba, *J. Am. Chem. Soc.* **2008**, *130*, 17278–17280.
- [78] S. A. Johnson, E. T. Taylor, S. J. Cruise, *Organometallics* **2009**, *28*, 3842–3855.
- [79] K. S. Kanyiva, N. Kashiara, Y. Nakao, T. Hiyama, M. Ohashi, S. Ogoshi, *Dalton Trans.* **2010**, *39*, 10483.
- [80] J. A. Hatnean, R. Beck, J. D. Borrelli, S. A. Johnson, *Organometallics* **2010**, *29*, 6077–

6091.

- [81] S. Tang, O. Eisenstein, Y. Nakao, S. Sakaki, *Organometallics* **2017**, *36*, 2761–2771.
- [82] E. Clot, C. Mégret, O. Eisenstein, R. N. Perutz, *J. Am. Chem. Soc.* **2009**, *131*, 7817–7827.
- [83] Y. Nakao, N. Kashihara, K. S. Kanyiva, T. Hiyama, *J. Am. Chem. Soc.* **2008**, *130*, 16170–16171.
- [84] J. S. Bair, Y. Schramm, A. G. Sergeev, E. Clot, O. Eisenstein, J. F. Hartwig, *J. Am. Chem. Soc.* **2014**, *136*, 13098–13101.
- [85] N. Catalyzed, C. H. B. Silylation, M. R. Elsby, J. Liu, S. Zhu, L. Hu, G. Huang, S. A. Johnson, *Organometallics* **2018**, *38*, 436–450.
- [86] V. Singh, Y. Nakao, S. Sakaki, M. M. Deshmukh, *J. Org. Chem.* **2017**, *82*, 289–301.
- [87] K. Yamazaki, A. Obata, A. Sasagawa, Y. Ano, N. Chatani, *Organometallics* **2018**, *38*, 248–255.
- [88] Y. Yang, X. Hou, T. Zhang, J. Ma, W. Zhang, S. Tang, H. Sun, J. Zhang, *J. Org. Chem.* **2018**, *83*, 11905–11916.
- [89] A. L. Keen, S. A. Johnson, *J. Am. Chem. Soc.* **2006**, *128*, 1806–1807.
- [90] D. D. Beattie, G. Lascoumettes, P. Kennepohl, J. A. Love, L. L. Schafer, *Organometallics* **2018**, *37*, 1392–1399.
- [91] D. L. Davies, S. M. A. Donald, S. A. Macgregor, *J. Am. Chem. Soc.* **2005**, *127*, 13754–13755.
- [92] T. Lyons, M. Sanford, *Chem. Rev.* **2010**, 1147–1169.
- [93] Y. Tanji, N. Mitsutake, T. Fujihara, Y. Tsuji, *Angew. Chem. Int. Ed.* **2018**, *57*, 10314–10317.
- [94] V. G. Zaitsev, D. Shabashov, O. Daugulis, *J. Am. Chem. Soc.* **2005**, *127*, 13154–13155.

- [95] A. Obata, Y. Ano, N. Chatani, *Chem. Sci.* **2017**, *8*, 6650–6655.
- [96] X. Wu, Y. Zhao, H. Ge, *J. Am. Chem. Soc.* **2015**, *137*, 4924–4927.
- [97] X. Wu, Y. Zhao, H. Ge, *Chem. Eur. J.* **2014**, *20*, 9530–9533.
- [98] F. X. Luo, Z. C. Cao, H. W. Zhao, D. Wang, Y. F. Zhang, X. Xu, Z. J. Shi, *Organometallics* **2017**, *36*, 18–21.
- [99] X. Wang, R. Qiu, C. Yan, V. P. Reddy, L. Zhu, X. Xu, S.-F. Yin, *Org. Lett.* **2015**, *17*, 1970–1973.
- [100] X. Ye, J. L. Petersen, X. Shi, *Chem. Commun.* **2015**, *51*, 7863–7866.
- [101] C. Lin, W. Yu, J. Yao, B. Wang, Z. Liu, Y. Zhang, *Org. Lett.* **2015**, *17*, 1340–1343.
- [102] S.-Y. Yan, Y.-J. Liu, B. Liu, Y.-H. Liu, Z.-Z. Zhang, B.-F. Shi, *Chem. Commun.* **2015**, *51*, 7341–7344.
- [103] A. Yokota, N. Chatani, *Chem. Lett.* **2015**, *44*, 902–904.
- [104] Y. Aihara, N. Chatani, *ACS Catal.* **2016**, *6*, 4323–4329.
- [105] B. Khan, R. Kant, D. Koley, *Adv. Synth. Catal.* **2016**, *358*, 2352–2358.
- [106] T. Uemura, M. Yamaguchi, N. Chatani, *Angew. Chem. Int. Ed.* **2016**, *55*, 3162–3165.
- [107] L. C. Misal Castro, A. Obata, Y. Aihara, N. Chatani, *Chem. Eur. J.* **2016**, *22*, 1362–1367.
- [108] Y. Aihara, J. Wuelbern, N. Chatani, *Bull. Chem. Soc. Jpn.* **2015**, *88*, 438–446.
- [109] Y. Aihara, M. Tobisu, Y. Fukumoto, N. Chatani, *J. Am. Chem. Soc.* **2014**, *136*, 15509–15512.
- [110] A. Yokota, Y. Aihara, N. Chatani, *J. Org. Chem.* **2014**, *79*, 11922–11932.
- [111] J. Li, Z. Zheng, T. Xiao, P. F. Xu, H. Wei, *Asian J. Org. Chem.* **2018**, *7*, 133–136.
- [112] A. P. Honeycutt, J. M. Hoover, *ACS Catal.* **2017**, *7*, 4597–4601.
- [113] A. Sasagawa, M. Yamaguchi, Y. Ano, N. Chatani, *Isr. J. Chem.* **2017**, *57*, 964–967.

- [114] M. Iwasaki, N. Miki, Y. Tsuchiya, K. Nakajima, Y. Nishihara, *Org. Lett.* **2017**, *19*, 1092–1095.
- [115] Z. He, Y. Huang, *ACS Catal.* **2016**, *6*, 7814–7823.
- [116] Y. Cheng, Y. Wu, G. Tan, J. You, *Angew. Chem. Int. Ed.* **2016**, *55*, 12275–12279.
- [117] G. Tan, L. Zhang, X. Liao, Y. Shi, Y. Wu, Y. Yang, J. You, *Org. Lett.* **2017**, *19*, 4830–4833.
- [118] C. Wang, L. Zhang, J. You, *Org. Lett.* **2017**, *19*, 1690–1693.
- [119] C. Lin, Z. Chen, Z. Liu, Y. Zhang, *Org. Lett.* **2017**, *19*, 850–853.
- [120] Y.-J. Liu, Z.-Z. Zhang, S.-Y. Yan, Y.-H. Liu, B.-F. Shi, *Chem. Commun.* **2015**, *51*, 7899–7902.
- [121] S. Maity, S. Agasti, A. M. Earsad, A. Hazra, D. Maiti, *Chem. Eur. J.* **2015**, *21*, 11320–11324.
- [122] M. Li, Y. Yang, D. Zhou, D. Wan, J. You, *Org. Lett.* **2015**, *17*, 2546–2549.
- [123] X. Wang, L. Zhu, S. Chen, X. Xu, C. T. Au, R. Qiu, *Org. Lett.* **2015**, *17*, 5228–5231.
- [124] M. Li, J. Dong, X. Huang, K. Li, Q. Wu, F. Song, J. You, *Chem. Commun.* **2014**, *50*, 3944–3946.
- [125] M. Iyanaga, Y. Aihara, N. Chatani, *J. Org. Chem.* **2014**, *79*, 11933–11939.
- [126] Y. Aihara, N. Chatani, *J. Am. Chem. Soc.* **2014**, *136*, 898–901.
- [127] X. Wu, Y. Zhao, H. Ge, *J. Am. Chem. Soc.* **2014**, *136*, 1789–1792.
- [128] B. R. Dible, M. S. Sigman, A. M. Arif, *Inorg. Chem.* **2005**, *44*, 3774–3776.
- [129] X. Zhang, Q. Zhao, J. Fan, D. Chen, J.-B. Liu, *Org. Chem. Front.* **2019**, DOI 10.1039/C8QO01310A.
- [130] H. M. Omer, P. Liu, *J. Am. Chem. Soc.* **2017**, *139*, 9909–9920.

- [131] S. Singh, S. K. R. B. Sunoj, *J. Org. Chem.* **2017**, 82, 9619–9626.
- [132] E. Chong, J. W. Kampf, A. Ariafard, A. J. Canty, M. S. Sanford, *J. Am. Chem. Soc.* **2017**, 139, 6058–6061.
- [133] W. Zhou, S. Zheng, J. W. Schultz, N. P. Rath, L. M. Mirica, *J. Am. Chem. Soc.* **2016**, 138, 5777–5780.
- [134] F. D’Accriscio, P. Borja, N. Saffon-Merceron, M. Fustier-Boutignon, N. Mézailles, N. Nebra, *Angew. Chem. Int. Ed.* **2017**, 56, 12898–12902.
- [135] E. A. Meucci, N. M. Camasso, M. S. Sanford, *Organometallics* **2017**, 36, 247–250.
- [136] J. R. Bour, N. M. Camasso, M. S. Sanford, *J. Am. Chem. Soc.* **2015**, 137, 8034–8037.
- [137] J. R. Bour, N. M. Camasso, E. A. Meucci, J. W. Kampf, A. J. Canty, M. S. Sanford, *J. Am. Chem. Soc.* **2016**, 138, 16105–16111.
- [138] C. Alonso, E. Martínez de Marigorta, G. Rubiales, F. Palacios, *Chem. Rev.* **2015**, 115, 1847–1935.
- [139] O. A. Tomashenko, V. V Grushin, *Chem. Rev.* **2011**, 111, 4475–4521.
- [140] M. W. Drover, L. L. Schafer, J. A. Love, *Organometallics* **2015**, 34, 1783–1786.
- [141] M. W. Drover, H. C. Johnson, L. L. Schafer, J. A. Love, A. S. Weller, *Organometallics* **2015**, 34, 3849–3856.
- [142] M. W. Drover, J. A. Love, L. L. Schafer, *J. Am. Chem. Soc.* **2016**, 138, 8396–8399.
- [143] M. W. Drover, L. L. Schafer, J. A. Love, *Angew. Chem. Int. Ed.* **2016**, 55, 3181–3186.
- [144] K. V. Tan, J. L. Dutton, B. W. Skelton, D. J. D. Wilson, P. J. Barnard, *Organometallics* **2013**, 32, 1913–1923.
- [145] J. O. Campeciño, L. W. Dudycz, D. Tumelty, V. Berg, D. E. Cabelli, M. J. Maroney, *J. Am. Chem. Soc.* **2015**, 137, 9044–9052.

- [146] Y. W. Tang, W. Zhang, Z. Bo, X. Fang, J. L. Qin, *Chinese J. Struct. Chem.* **2014**, *3*, 325–332.
- [147] T. Corona, F. F. Pfaff, F. Acuña-Parés, A. Draksharapu, C. J. Whiteoak, V. Martin-Diaconescu, J. Lloret-Fillol, W. R. Browne, K. Ray, A. Company, *Chem. Eur. J.* **2015**, *21*, 15029–15038.
- [148] M. B. Jones, B. S. Newell, W. A. Hoffert, K. I. Hardcastle, M. P. Shores, C. E. MacBeth, *Dalton Trans.* **2010**, *39*, 401–410.
- [149] H. J. Kruger, G. Peng, R. H. Holm, *Inorg. Chem.* **1991**, *30*, 734–742.
- [150] M. R. Maurya, S. J. J. Titinchi, S. Chand, *Catal. Letters* **2003**, *89*, 219–227.
- [151] M. D. Santana, G. García, G. López, A. Lozano, C. Vicente, L. García, J. Pérez, *Polyhedron* **2007**, *26*, 1029–1036.
- [152] J. Shearer, *J. Inorg. Biochem.* **2013**, *129*, 145–149.
- [153] M. D. Santana, G. García, M. Julve, F. Lloret, J. Pérez, M. Liu, F. Sanz, J. Cano, G. López, *Inorg. Chem.* **2004**, *43*, 2132–2140.
- [154] S.-Y. Yan, Y.-J. Liu, B. Liu, Y.-H. Liu, Z.-Z. Zhang, B.-F. Shi, *Chem. Commun.* **2015**, *51*, 7341–7344.
- [155] M. Iyanaga, Y. Aihara, N. Chatani, *J. Org. Chem.* **2014**, *79*, 11933–11939.
- [156] D. Yamauchi, T. Nishimura, H. Yorimitsu, *Angew. Chem. Int. Ed.* **2017**, *56*, 7200–7204.
- [157] I. Nakamura, D. Yamauchi, T. Nishimura, *Asian J. Org. Chem.* **2018**, *7*, 1347–1350.
- [158] A. N. Desnoyer, E. G. Bowes, B. O. Patrick, J. A. Love, *J. Am. Chem. Soc.* **2015**, *137*, 12748–12751.
- [159] D. D. Beattie, E. G. Bowes, M. W. Drover, J. A. Love, L. L. Schafer, *Angew. Chem. Int. Ed.* **2016**, *55*, 13290–13295.

- [160] N. A. LaBerge, J. A. Love, *Eur. J. Org. Chem.* **2015**, 2015, 5546–5553.
- [161] D. V. Gutsulyak, W. E. Piers, J. Borau-Garcia, M. Parvez, *J. Am. Chem. Soc.* **2013**, 135, 11776–11779.
- [162] E. A. LaPierre, W. E. Piers, D. M. Spasyuk, D. W. Bi, *Chem. Commun.* **2016**, 52, 1361–1364.
- [163] J. A. Kessler, V. M. Iluc, *Dalton Trans.* **2017**, 46, 12125–12131.
- [164] M. Schultz, F. Eisenträger, C. Regius, F. Rominger, P. Hanno-Igels, P. Jakob, I. Gruber, P. Hofmann, *Organometallics* **2012**, 31, 207–224.
- [165] Z. Lian, B. N. Bhawal, P. Yu, B. Morandi, **2017**, 1063, 1059–1063.
- [166] NMR yields (1h): average of 2-3 runs, 1,3,5-trimethoxybenzene was used as an internal standard.
- [167] The central results are shown in scheme 2.8: for a detailed list of reaction additives tested, see appendix.
- [168] J. S. Cannon, L. Zou, P. Liu, Y. Lan, D. J. O’Leary, K. N. Houk, R. H. Grubbs, *J. Am. Chem. Soc.* **2014**, 136, 6733–6743.
- [169] Y. Boutadla, D. L. Davies, S. A. Macgregor, A. I. Poblador-Bahamonde, *Dalton Trans.* **2009**, 5887.
- [170] H. Xu, K. Muto, J. Yamaguchi, C. Zhao, K. Itami, D. G. Musaev, *J. Am. Chem. Soc.* **2014**, 136, 14834–14844.
- [171] A further 0.25 equivalents of K₂CO₂ are added for the reaction with addition of AdCOOH. This ensures similar base profiles to reactions with potassium carboxylate additives.
- [172] B. E. Haines, J.-Q. Yu, D. G. Musaev, *Chem. Sci.* **2018**, 9, 1144–1154.
- [173] D. L. Davies, S. A. Macgregor, C. L. McMullin, *Chem. Rev.* **2017**, 117, 8649–8709.

- [174] H. Y. Sun, S. I. Gorelsky, D. R. Stuart, L. C. Campeau, K. Fagnou, *J. Org. Chem.* **2010**, 75, 8180–8189.
- [175] D. E. Stephens, J. Lakey-Beitia, A. C. Atesin, T. A. Ateşin, G. Chavez, H. D. Arman, O. V. Larionov, *ACS Catal.* **2015**, 5, 167–175.
- [176] R. A. Alharis, Electronic Effect on C-H Activation at Half Sandwich Complexes of Ir, Rh, and Ru, University of Leicester, **2018**.
- [177] A. D. Ryabov, I. K. Sakodinskaya, A. K. Yatsimirsky, *J. Chem. Soc. Dalt. Trans.* **1985**, 2629.
- [178] I. G. Powers, C. Uyeda, *ACS Catal.* **2017**, 7, 936–958.
- [179] I. L. Eremenko, S. E. Nefedov, A. A. Sidorov, M. A. Golubnichaya, P. V. Danilov, V. N. Ikorskii, Y. G. Shvedenkov, V. M. Novotortsev, I. I. Moiseev, *Inorg. Chem.* **1999**, 38, 3764–3773.
- [180] M. S. Sanford, J. A. Love, R. H. Grubbs, *J. Am. Chem. Soc.* **2001**, 123, 6543–6554.
- [181] H. G. Alt, A. Köppl, *Chem. Rev.* **2000**, 100, 1205–1221.
- [182] U. Christmann, R. Vilar, *Angew. Chem. Int. Ed.* **2005**, 44, 366–374.
- [183] N. T. S. Phan, M. Van Der Sluys, C. W. Jones, *Adv. Synth. Catal.* **2006**, 348, 609–679.
- [184] R. H. Crabtree, H. Felkin, G. E. Morris, *J. Organomet. Chem.* **1977**, 141, 205–215.
- [185] B. R. Dible, M. S. Sigman, A. M. Arif, *Inorg. Chem.* **2005**, 44, 3774–3776.
- [186] C. A. Laskowski, D. J. Bungum, S. M. Baldwin, S. A. Del Ciello, V. M. Iluc, G. L. Hillhouse, *J. Am. Chem. Soc.* **2013**, 135, 18272–18275.
- [187] V. M. Iluc, G. L. Hillhouse, *J. Am. Chem. Soc.* **2014**, 136, 6479–6488.
- [188] C. A. Laskowski, G. R. Morello, C. T. Saouma, T. R. Cundari, G. L. Hillhouse, *Chem. Sci.* **2013**, 4, 170–174.

- [189] M. Ito, T. Matsumoto, K. Tatsumi, *Inorg. Chem.* **2009**, *48*, 2215–2223.
- [190] W. Baratta, C. Mealli, E. Herdtweck, A. Ienco, S. A. Mason, P. Rigo, *J. Am. Chem. Soc.* **2004**, *126*, 5549–5562.
- [191] I. M. Riddlestone, D. McKay, M. J. Gutmann, S. A. Macgregor, M. F. Mahon, H. A. Sparkes, M. K. Whittlesey, *Organometallics* **2016**, *35*, 1301–1312.
- [192] J. M. Cole, P. G. Waddell, A. E. H. Wheatley, G. J. McIntyre, A. J. Peel, C. W. Tate, D. J. Linton, *Organometallics* **2014**, *33*, 3919–3923.
- [193] S. H. Crosby, G. J. Clarkson, J. P. Rourke, *J. Am. Chem. Soc.* **2009**, *131*, 14142–14143.
- [194] C. A. Laskowski, G. L. Hillhouse, *J. Am. Chem. Soc.* **2008**, *130*, 13846–13847.
- [195] Calculations performed at the PBE0-D3/6-311+G(2d, p)//PBE0-D3/6-31G(d, p) level of theory using the SDD effective core potential plus a f-type polarization functional for Ni. For further details see the appendices.
- [196] Several different functionals were screened for the optimization of **6** and all provided a similar torsion angle between the NHC and amidate planes; For further details see the appendices.
- [197] J. P. Stambuli, C. D. Incarvito, M. Bühl, J. F. Hartwig, *J. Am. Chem. Soc.* **2004**, *126*, 1184–1194.
- [198] E.-L. Zins, B. Silvi, M. E. Alikhani, *Phys. Chem. Chem. Phys.* **2015**, *17*, 9258–9281.
- [199] E. Clot, O. Eisenstein, T. Dubé, J. W. Faller, R. H. Crabtree, *Organometallics* **2002**, *21*, 575–580.
- [200] Under an inert atmosphere slow decomposition of solutions or of crystals is evident by NMR spectroscopy; this pathway is suppressed when samples are stored at -35°C.
- [201] M. I. Lipschutz, T. D. Tilley, *Organometallics* **2014**, *33*, 5566–5570.

- [202] Y. Hoshimoto, Y. Hayashi, H. Suzuki, M. Ohashi, S. Ogoshi, *Organometallics* **2014**, *33*, 1276–1282.
- [203] K. Abbaspour Tehrani, N. De Kimpe, *Tetrahedron Lett.* **2000**, *41*, 1975–1978.
- [204] D. D. Beattie, A. C. Grunwald, T. Perse, L. L. Schafer, J. A. Love, *J. Am. Chem. Soc.* **2018**, *140*, 12602–12610.
- [205] T. Yamamoto, K. Sano, K. Osakada, S. Komiya, A. Yamamoto, Y. Kushi, T. Tada, *Organometallics* **1990**, *9*, 2396–2403.
- [206] S. Pelties, R. Wolf, *Organometallics* **2016**, *35*, 2722–2727.
- [207] P. Horrillo-Martinez, B. O. Patrick, L. L. Schafer, M. D. Fryzuk, *Dalton Trans.* **2012**, *41*, 1609–1616.
- [208] M. W. Drover, 1,3-N,O-Chelated Complexes of Rhodium and Iridium : Harnessing Metal-Ligand Cooperativity for Bond Activation Processes, University of British Columbia, **2016**.
- [209] P. Eisenberger, R. O. Ayinla, J. M. P. Lauzon, L. L. Schafer, *Angew. Chem. Int. Ed.* **2009**, *48*, 8361–8365.
- [210] M. Gomberg, *J. Am. Chem. Soc.* **1900**, *22*, 757–771.
- [211] A. J. Rosenthal, M. Devillard, K. Miqueu, G. Bouhadir, D. Bourissou, *Angew. Chem. Int. Ed.* **2015**, *54*, 9198–9202.
- [212] M. Baranac-Stojanović, *RSC Adv.* **2014**, *4*, 308–321.
- [213] I. Kalvet, Q. Guo, G. J. Tizzard, F. Schoenebeck, *ACS Catal.* **2017**, *7*, 2126–2132.
- [214] A. B. Dürr, H. C. Fisher, I. Kalvet, K.-N. Truong, F. Schoenebeck, *Angew. Chem. Int. Ed.* **2017**, *56*, 13431–13435.
- [215] H. Lee, J. Börgel, T. Ritter, *Angew. Chem. Int. Ed.* **2017**, *56*, 6966–6969.

- [216] K. Zhang, M. Conda-Sheridan, S. Cooke, J. Louie, S. R. Cooke, J. Louie, *Organometallics* **2011**, *30*, 2546–2552.
- [217] S. Bajo, G. Laidlaw, A. R. Kennedy, S. Sproules, D. J. Nelson, *Organometallics* **2017**, *36*, 1662–1672.
- [218] K. Matsubara, Y. Fukahori, T. Inatomi, S. Tazaki, Y. Yamada, Y. Koga, S. Kanegawa, T. Nakamura, *Organometallics* **2016**, *35*, 3281–3287.
- [219] A. W. Addison, T. N. Rao, J. Reedijk, J. van Rijn, G. C. Verschoor, *J. Chem. Soc., Dalton Trans.* **1984**, 1349–1356.
- [220] R. Dorta, E. D. Stevens, N. M. Scott, C. Costabile, L. Cavallo, C. D. Hoff, S. P. Nolan, *J. Am. Chem. Soc.* **2005**, *127*, 2485–2495.
- [221] As only a single CO ligand is present, the product may be produced in maximum 66% yield. Complex Ni(I)-3.5 makes up mass balance.
- [222] N. a Eckert, A. Dinescu, T. R. Cundari, P. L. Holland, *Inorg. Chem.* **2005**, *44*, 7702–7704.
- [223] M. J. Iglesias, J. F. Blandez, M. R. Frutos, A. Prieto, E. Álvarez, T. R. Belderrain, M. C. Nicasio, *Organometallics* **2012**, *31*, 6312–6316.
- [224] J. Wu, J. W. Faller, N. Hazari, T. J. Schmeier, *Organometallics* **2012**, *31*, 806–809.
- [225] M. W. Drover, J. A. Love, L. L. Schafer, *Chem. Soc. Rev.* **2017**, *46*, 2913–2940.
- [226] A. Haim, *Acc. Chem. Res.* **1975**, *8*, 264–272.
- [227] R. Sutcliffe, K. U. Ingold, *J. Am. Chem. Soc.* **1982**, *104*, 6071–6075.
- [228] E. E. J. Dekker, J. B. F. N. Engberts, T. J. de Boer, *Tetrahedron Lett.* **1969**, *10*, 2651–2654.
- [229] For syntheses and characterization of cyclopropyl relatives, see appendicies.
- [230] Importantly the starting material reacts with the Ni(II)-bis(amidate) product to give an

unknown diamagnetic nickel product. This can be probed independently by combining one equivalent of each. By ^1H NMR spectroscopy, the same product is observed. The yield is based on both of these products.

- [231] S. J. Meek, C. L. Pitman, A. J. M. Miller, *J. Chem. Educ.* **2016**, 93, 275–286.
- [232] E. B. Lansdon, K. M. Brendza, M. Hung, R. Wang, S. Mukund, D. Jin, G. Birkus, N. Kutty, X. Liu, *J. Med. Chem.* **2010**, 53, 4295–4299.
- [233] J. I. Mark, H.F., Bikales, N., Overberger, C.G, Menges, G., Kroschwitz, *Encyclopedia of Polymer Science and Engineering*, Wiley, New York, **1985**.
- [234] G. Henrici-Olivé, S. Olivé, in *Chemistry*, Springer Berlin Heidelberg, Berlin, Heidelberg, **1979**, pp. 123–152.
- [235] H. H. Hodgson, *Chem. Rev.* **1947**, 40, 251–277.
- [236] T. Sandmeyer, *Berichte der Dtsch. Chem. Gesellschaft* **1884**, 17, 2650–2653.
- [237] K. W. Rosenmund, E. Struck, *Berichte der Dtsch. Chem. Gesellschaft* **1919**, 52, 1749–1756.
- [238] J. v. Braun, G. Manz, *Justus Liebig's Ann. der Chemie* **1931**, 488, 111–126.
- [239] T. D. Senecal, W. Shu, S. L. Buchwald, *Angew. Chem. Int. Ed.* **2013**, 52, 10035–10039.
- [240] P. Anbarasan, T. Schareina, M. Beller, *Chem. Soc. Rev.* **2011**, 40, 5049–5067.
- [241] D. T. Cohen, S. L. Buchwald, *Org. Lett.* **2015**, 17, 202–205.
- [242] Y. Tu, Y. Zhang, S. Xu, Z. Zhang, X. Xie, *Synlett* **2014**, 25, 2938–2942.
- [243] T. Chatterjee, R. Dey, B. C. Ranu, *J. Org. Chem.* **2014**, 79, 5875–5879.
- [244] P. Y. Yeung, C. M. So, C. P. Lau, F. Y. Kwong, *Org. Lett.* **2011**, 13, 648–651.
- [245] L. Cassar, *J. Organomet. Chem.* **1973**, 54, C57–C58.
- [246] L. Cassar, M. Foà, F. Montanari, G. P. Marinelli, *J. Organomet. Chem.* **1979**, 173, 335–

- 339.
- [247] Y. Sakakibara, N. Yadani, I. Ibuki, M. Sakai, N. Uchino, *Chem. Lett.* **1982**, *11*, 1565–1566.
- [248] Y. Sakakibara, K. Sasaki, F. Okuda, A. Hokimoto, T. Ueda, M. Sakai, K. Takagi, *Bull. Chem. Soc. Jpn.* **2004**, *77*, 1013–1019.
- [249] Y. Sakakibara, Y. Ido, K. Sasaki, M. Sakai, N. Uchino, *Bull. Chem. Soc. Jpn.* **1993**, *66*, 2776–2778.
- [250] Y. Sakakibara, H. Enami, H. Ogawa, S. Fujimoto, H. Kato, K. Kunitake, K. Sasaki, M. Sakai, *Bull. Chem. Soc. Jpn.* **1995**, *68*, 3137–3143.
- [251] R. K. Arvela, N. E. Leadbeater, *J. Org. Chem.* **2003**, *68*, 9122–9125.
- [252] F. Burg, J. Egger, J. Deutsch, N. Guimond, *Org. Process Res. Dev.* **2016**, *20*, 1540–1545.
- [253] X. Zhang, A. Xia, H. Chen, Y. Liu, *Org. Lett.* **2017**, *19*, 2118–2121.
- [254] E. A. Standley, S. J. Smith, P. Müller, T. F. Jamison, *Organometallics* **2014**, *33*, 2012–2018.
- [255] P. Patnaik, *A Comprehensive Guide to the Hazardous Properties of Chemical Substances: Third Edition*, **2006**.
- [256] A. H. Hall, G. E. Isom, G. A. Rockwood, *Toxicology of Cyanides and Cyanogens: Experimental, Applied and Clinical Aspects*, Wiley, **2015**.
- [257] L. Bini, C. Müller, D. Vogt, *Chem. Commun.* **2010**, *46*, 8325–8334.
- [258] M. Kranenburg, P. C. J. Kamer, P. W. N. M. van Leeuwen, D. Vogt, W. Keim, *J. Chem. Soc. Chem. Commun.* **1995**, 2177–2178.
- [259] R. Naumann, D. Petzold, *J. Therm. Anal.* **1981**, *20*, 319–330.
- [260] R. S. Berman, J. K. Kochi, *Inorg. Chem.* **1980**, *19*, 248–254.

- [261] T. T. Tsou, J. K. Kochi, *J. Am. Chem. Soc.* **1979**, *101*, 6319–6332.
- [262] D. F. Evans, *J. Chem. Soc.* **1959**, 2003–2005.
- [263] E. M. Schubert, *J. Chem. Educ.* **1992**, *69*, 62.
- [264] M. Ganesh, D. Seidel, *J. Am. Chem. Soc.* **2008**, *130*, 16464–16465.
- [265] H. W. Liang, K. Jiang, W. Ding, Y. Yuan, L. Shuai, Y. C. Chen, Y. Wei, *Chem. Commun.* **2015**, *51*, 16928–16931.
- [266] W. N. Palmer, C. Zarate, P. J. Chirik, *J. Am. Chem. Soc.* **2017**, *139*, 2589–2592.
- [267] A. Arcelli, A. Bongini, G. Porzi, S. Rinaldi, *J. Phys. Org. Chem.* **2012**, *25*, 132–141.
- [268] E. K. J. Lui, D. Hergesell, L. L. Schafer, *Org. Lett.* **2018**, *20*, 6663–6667.
- [269] L. J. E. Stanlake, L. L. Schafer, *Organometallics* **2009**, *28*, 3990–3998.
- [270] S. Sharma, E. Park, J. Park, I. S. Kim, *Org. Lett.* **2012**, *14*, 906–909.
- [271] X. Wang, L. Zhu, S. Chen, X. Xu, C.-T. Au, R. Qiu, *Org. Lett.* **2015**, *17*, 5228–5231.
- [272] M. Li, Y. Yang, D. Zhou, D. Wan, J. You, *Org. Lett.* **2015**, *17*, 2546–2549.
- [273] S. Miyamura, M. Araki, T. Suzuki, J. Yamaguchi, K. Itami, *Angew. Chem. Int. Ed.* **2015**, *54*, 846–851.
- [274] C. Lorenc, J. T. Reeves, C. A. Busacca, C. H. Senanayake, *Tetrahedron Lett.* **2015**, *56*, 1280–1282.
- [275] L. Wiehemeier, M. Cors, O. Wrede, J. Oberdisse, T. Hellweg, T. Kottke, *Phys. Chem. Chem. Phys.* **2019**, *21*, 572–580.
- [276] B. Geukens, F. Meersman, E. Nies, *J. Phys. Chem. B* **2008**, *112*, 4474–4477.
- [277] B. J. Groendyke, D. I. AbuSalim, S. P. Cook, *J. Am. Chem. Soc.* **2016**, *138*, 12771–12774.
- [278] *Ullmann's Encyclopedia of Industrial Chemistry*, Wiley-VCH Verlag GmbH & Co. KGaA, Weinheim, Germany, **2000**.

- [279] Y. Zhu, M. Zhao, W. Lu, L. Li, Z. Shen, *Org. Lett.* **2015**, *17*, 2602–2605.
- [280] Y. Lin, Q. Song, *Eur. J. Org. Chem.* **2016**, *2016*, 3056–3059.
- [281] A. V. Ushkov, V. V. Grushin, *J. Am. Chem. Soc.* **2011**, *133*, 10999–11005.
- [282] J. Kim, J. Choi, K. Shin, S. Chang, *J. Am. Chem. Soc.* **2012**, *134*, 2528–2531.
- [283] G. Y. J. Im, S. M. Bronner, A. E. Goetz, R. S. Paton, P. H. Y. Cheong, K. N. Houk, N. K. Garg, *J. Am. Chem. Soc.* **2010**, *132*, 17933–17944.
- [284] P. Hrobárik, I. Sigmundová, P. Zahradník, *Synthesis* **2005**, *2005*, 600–604.
- [285] M. Sundermeier, A. Zapf, S. Mutyala, W. Baumann, J. Sans, S. Weiss, M. Beller, *Chem. Eur. J.* **2003**, *9*, 1828–1836.
- [286] M. L. Czyz, D. W. Lupton, A. Polyzos, *Chem. Eur. J.* **2017**, *23*, 14450–14453.
- [287] R. C. DiPucchio, S.-C. Roşca, L. L. Schafer, *Angew. Chem. Int. Ed.* **2018**, *57*, 3469–3472.
- [288] G. M. Sheldrick, *Acta Crystallogr. Sect. A Found. Crystallogr.* **2008**, *64*, 112–122.
- [289] O. V. Dolomanov, L. J. Bourhis, R. J. Gildea, J. A. K. Howard, H. Puschmann, *J. Appl. Crystallogr.* **2009**, *42*, 339–341.

Appendices

Appendix A - Experimental

A.1 General Considerations and Materials

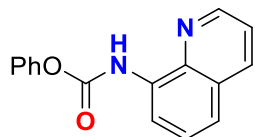
All experiments were carried out employing standard Schlenk techniques under an atmosphere of dry nitrogen employing degassed, dried solvents unless otherwise noted. 1,3,5-trimethoxybenzene (TMB), PEt_3 , and amines were purchased and used as received unless otherwise noted. K_2CO_3 , 1,3,5-trimethylbenzoic acid, 1-AdCOOH, 2,6-bis(trifluoromethyl)benzoic acid, KOiPr, and KOAc were dried on a Schlenk line under vacuum with heating ($>100^\circ\text{C}$). K_2CO_3 was ground in a mortar and pestle in a glovebox for all reactions in this manuscript. Celite[®] was dried in an oven at 180°C for at least 24 hours, then brought into a glove-box dried. d_6 -Benzene (C_6D_6) and d_8 -toluene (C_7D_8) were purchased from Cambridge Isotope Laboratories Inc., dried over sodium metal, and degassed by three freeze-pump-thaw cycles. d_6 -DMSO, d_7 -DMF, CD_3CN , CDCl_3 , and d_2 -TCE were dried over calcium hydride, distilled under vacuum, then degassing by three freeze-pump-thaw cycles. THF, Et_2O , and HMDSO were dried over sodium metal and degassed by three freeze-pump-thaw cycles. Hexanes and toluene were either dried over sodium metal or passed over activated alumina columns into Teflon sealed Schlenk flasks and degassed by three freeze-pump-thaw cycles. NMR spectra were recorded on 300, 400, or 600 MHz spectrometers. ^1H NMR spectra are reported in parts per million (ppm) and were referenced to residual solvent: $^1\text{H}(\text{THF-}d_8)$: δ 3.58; $^1\text{H}(\text{CD}_3\text{CN})$: δ 1.94; $^1\text{H}(\text{C}_6\text{D}_6)$: δ 7.16; $^1\text{H}(\text{CDCl}_3)$: δ 7.26; $^1\text{H}(\text{TCE-}d_2)$: δ 6.00; $^1\text{H}(\text{DMF-}d_7)$: δ 2.92; $^1\text{H}(\text{C}_7\text{D}_8)$: 2.08; $^1\text{H}(\text{d}_6\text{-DMSO})$: 2.50; $^{13}\text{C}(\text{C}_7\text{D}_8)$: 20.43; $^{13}\text{C}(\text{d}_6\text{-DMSO})$: 39.52; coupling constants are reported in Hz. The multiplicities are abbreviated as follows: app. = apparent, br = broad, s = singlet, d = doublet, dd = doublet of doublets, t = triplet, q = quartet, quin = quintet, sept = septet, m = multiplet. ^{13}C NMR spectra were performed as proton-decoupled

experiments and are reported in ppm. NMR spectra are shown using MestReNova 6.0.2 NMR processing software. Evans Method experiments^[262,263] were measured using coaxial inserts containing 1% cyclooctane in C₆D₆. High-resolution mass spectra were measured by the mass spectrometry and microanalysis service at the Department of Chemistry, University of British Columbia. Mass spectra were recorded on a Kratos MS-50 spectrometer using an electron impact (70 eV) source or a Bruker Esquire LC spectrometer using electrospray ionization source. Fragment signals are given in mass per charge number (m/z). Elemental analyses were recorded on a Carlo Erba EA 1108 elemental analyzer.

A.2 Experimental Data for Chapter 2

Synthesis of Carbamate (2.1)

phenyl quinolin-8-ylcarbamate (2.1)



Synthesized according to literature procedure.^[264] ¹H NMR spectrum match literature data:

¹H NMR (400 MHz, CDCl₃) δ 9.56 (br s, 1H), 8.85 (dd, *J* = 4.2, 1.6 Hz, 1H), 8.46 (d, *J* = 7.3 Hz, 1H), 8.18 (dd, *J* = 8.3, 1.6 Hz, 1H), 7.62-7.37 (m, 5H), 7.35-7.17 (m, 3H).

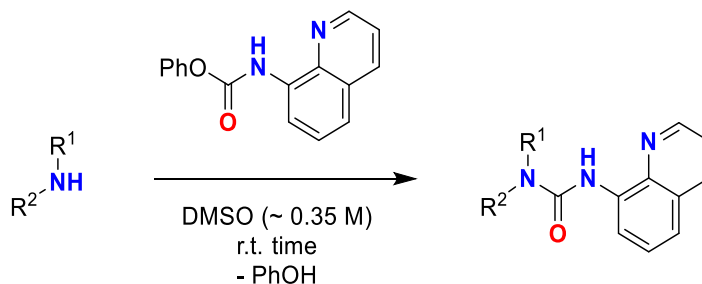
Synthesis of Ureas Derivatives

The majority of the ureas were synthesized according to one of the following four procedures (A-C). The purification of each urea is noted along with each compound's characterization data.

General Procedure A: An amine (1 equiv.)

was weighed and dissolved in DMSO (~0.35M). The resulting DMSO-amine solution was added to a 4 mL vial containing carbamate (2.1) (1 equiv.) and a stir bar. The contents were then stirred at room temperature and monitored

Procedure A:

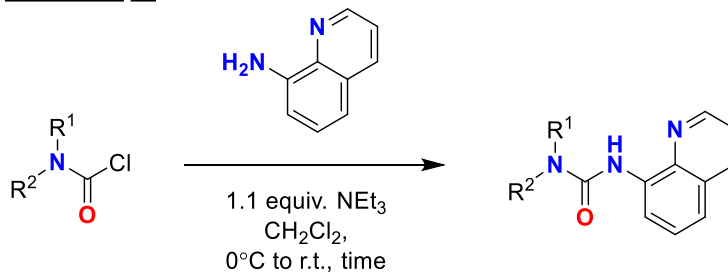


by thin layer chromatography (TLC). Upon reaction completion (30 min – 1 h), the contents were poured into a separatory funnel and diluted with ethyl acetate (30-40 mL per mL DMSO). The organic layer was then washed with successive aliquots of distilled water (5 x (10 mL per mL DMSO)) and brine (10 mL per mL DMSO). The organic layer was dried over MgSO₄ and filtered into a round-bottom flask. The contents were then dried in vacuo to afford the crude product.

General Procedure B: A carbamoyl chloride

(1.5 equiv.) was weighed into a round-bottom flask, dissolved in DCM, and the contents were cooled with an ice bath. 8-aminoquinoline derivative (1 equiv.) was weighed into a 20 mL vial, to which

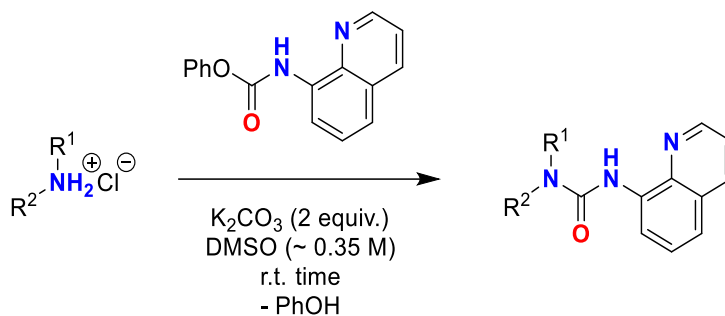
Procedure B:



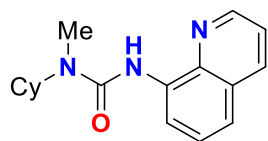
triethylamine (1.1 equiv.) and DCM were each added. The amines-DCM solution was then slowly added to the first solution while stirring. The contents were then stirred at room temperature and monitored by thin layer chromatography (TLC). Upon reaction completion, the contents were poured into a separatory funnel. The organic layer was then washed with successive aliquots of distilled water (3 x 20 mL) and brine (20 mL). The organic layer was dried over MgSO₄ and filtered into a round-bottom flask. The contents were then dried in vacuo to afford the crude product.

General Procedure C: See procedure A, but **Procedure C:**

additionally K₂CO₃ (2 equiv.) is added to the reaction mixture. The work-up procedure was also identical to procedure A.

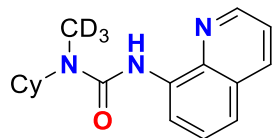


1-cyclohexyl-1-methyl-3-(quinolin-8-yl)urea (**2.2**)



Synthesis: Synthesized using procedure **A** with *N*-methylcyclohexyl amine (85.7 mg, 0.757 mmol) and carbamate (**2.1**) (200 mg, 0.757 mmol). **Purification:** sublimation of phenol (~20 mmHg, 80°C), and recrystallization from EtOAc/hexanes affords (**2.2**) as a white powder. **Yield** = 74% (159 mg, 0.560 mmol). **¹H NMR (400 MHz, CDCl₃)** δ = 9.37 (br s, 1H), 8.76 (dd, *J* = 4.2, 1.7 Hz, 1H), 8.59 (dd, *J* = 7.8, 1.1 Hz, 1H), 8.13 (dd, *J* = 8.3, 1.6 Hz, 1H), 7.51 (t, *J* = 8.0 Hz, 1H), 7.39 (ddd, *J* = 9.4, 8.3, 2.7 Hz, 2H), 4.32-4.18 (m, 1H), 3.04 (s, 3H), 1.93-1.75 (m, 4H), 1.74-1.63 (m, 1H), 1.55-1.38 (m, 4H), 1.23-1.05 (m, 1H). **¹³C NMR (101 MHz, CDCl₃)** δ = 155.3, 147.8, 138.7, 136.4, 136.4, 128.1, 127.8, 121.4, 119.4, 114.8, 54.1, 30.8, 28.6, 26.0, 25.8. **HRMS** (ESI) *m/z* calculated for C₁₇H₂₂N₃O [M+H]⁺: 284.1800; found: 284.1769. **Anal. Calcd.** for C₁₇H₂₁N₃O (283). C, 72.06%; H, 7.47%; N, 14.83%. Found: C, 71.84%; H, 7.40%; N, 14.77%.

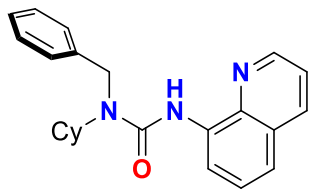
1-cyclohexyl-1-(methyl-d₃)-3-(quinolin-8-yl)urea (**2.2-d₃**)



Synthesis: Synthesized using procedure **A** with *N*-(methyl-d₃)cyclohexyl amine (**B-CD₃**) (88 mg, 0.757 mmol) and carbamate (**2.1**) (200 mg, 0.757 mmol). **Purification:** Sublimation of phenol (~20 mmHg, 80°C), and recrystallization from EtOAc/hexanes affords (**2.2-d₃**) as a white powder. **Yield** = 72% (156 mg, 0.545 mmol). **¹H NMR (300 MHz, CDCl₃)** δ = 9.36 (br s,

1H), 8.76 (dd, $J = 4.2, 1.7$ Hz, 1H), 8.59 (dd, $J = 7.8, 1.1$ Hz, 1H), 8.12 (dd, $J = 8.3, 1.6$ Hz, 1H), 7.51 (t, $J = 8.0$ Hz, 1H), 7.40 (dd, $J = 8.2, 4.2$ Hz, 1H), 7.37 (dd, $J = 8.2, 1.3$ Hz, 1H), 4.32-4.18 (m, 1H), 1.93-1.63 (m, 5H), 1.55-1.35 (m, 4H), 1.21-1.01 (m, 1H). **^2H NMR (61 MHz, CHCl_3)** $\delta = 3.02$. **^{13}C NMR (75 MHz, CDCl_3)** $\delta = 155.3, 147.8, 138.7, 136.4, 136.4, 128.1, 127.8, 121.4, 119.4, 114.8, 54.0, 30.8, 26.0, 25.8$. (CD_3 carbon resonance not observed). **HRMS** (ESI) m/z calculated for $\text{C}_{17}\text{H}_{19}\text{D}_3\text{N}_3\text{O}$ $[\text{M}+\text{H}]^+$: 287.1951; found: 287.1953.

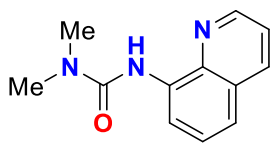
1-benzyl-1-cyclohexyl-3-(quinolin-8-yl)urea (2.5)



Synthesis: Synthesized using procedure **A** with *N*-benzylcyclohexylamine (462 mg, 2.44 mmol) and carbamate (**2.1**) (614 mg, 2.32 mmol). **Purification:** Recrystallize from hot hexanes for afford (**2.5**) as a crystalline white solid, **Yield** = 73% (610 mg, 1.70 mmol). **^1H NMR (400 MHz, CDCl_3)** δ 9.34 (br s, 1H), 8.57 (d, $J = 7.7$ Hz, 1H),

8.50 (d, $J = 2.4$ Hz, 1H), 8.06 (d, $J = 8.1$ Hz, 1H), 7.53-7.41 (m, 3H), 7.40-7.19 (m, 5H), 4.68 (s, 2H), 4.34 (s, 1H), 2.03-1.91 (m, 2H), 1.89-1.77 (m, 2H), 1.74-1.61 (m, 1H), 1.60-1.38 (m, 4H), 1.19-1.04 (m, 1H). **$^{13}\text{C}\{^1\text{H}\}$ NMR (101 MHz, CDCl_3)** δ 155.7, 147.5, 138.9, 138.7, 136.4, 136.2, 128.6, 128.0, 127.7, 127.2, 127.0, 121.3, 119.4, 114.9, 55.4, 46.7, 31.6, 26.2, 25.7. **HRMS** (ESI) m/z calculated for $\text{C}_{23}\text{H}_{26}\text{N}_3\text{O}$ $[\text{M}+\text{H}]^+$: 360.2076; found: 360.2077.

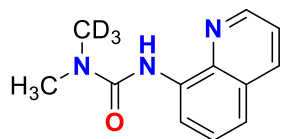
1,1-dimethyl-3-(quinolin-8-yl)urea (2.9)



Synthesis: Synthesized using procedure **B** with *N,N*-dimethylcarbamoyl chloride (1.49 g, 13.9 mmol) and 8-aminoquinoline (1.34 g, 9.29 mmol). **Purification:** Following removal of solvent in vacuo, aqueous KOH (1M, 20 mL) was added. The product was then

extracted with diethyl ether (3 x 100 mL) and the organic fractions were dried over magnesium sulfate. Following removal of the diethyl ether in vacuo, the organic residue was subject to column chromatography (Hex:EtOAc gradient, 6:1 to 2:1) to afford white crystals of compound (**2.9**). **Yield** = 63% (1.26 g, 5.85 mmol). NMR spectra match literature reports.^[265] **^1H NMR (300 MHz, CDCl_3)** δ 9.34 (s, 1H), 8.75 (dd, $J = 4.2, 1.7$ Hz, 1H), 8.57 (dd, $J = 7.7, 1.2$ Hz, 1H), 8.12 (dd, $J = 8.3, 1.6$ Hz, 1H), 7.50 (t, $J = 8.0$ Hz, 1H), 7.43-7.35 (m, 2H), 3.15 (s, 6H). **$^{13}\text{C}\{^1\text{H}\}$ NMR (75 MHz, CDCl_3)** δ 155.7, 147.87, 138.6, 136.4, 136.2, 128.1, 127.7, 121.4, 119.5, 114.8, 36.53. **HRMS** (ESI) m/z calculated for $\text{C}_{12}\text{H}_{14}\text{N}_3\text{O}$ $[\text{M}+\text{H}]^+$: 216.1137; found: 284.1137.

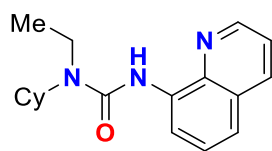
1-methyl-1-(methyl-d3)-3-(quinolin-8-yl)urea (2.9-d3)



Synthesis: Synthesized using procedure **C** with *N*-methyl-*N*-(methyl- d_3)amine hydrochloride (64 mg, 0.757 mmol) and carbamate (**2.1**) (200 mg, 0.757 mmol).

Purification: The DMSO reaction mixture is poured into a separatory funnel containing distilled water (30 mL) and EtOAc (30 mL). The organic layer was then washed with distilled water (3 x 30 mL). The product was then extracted into an aqueous layer with 1 M HCl (40 mL). The acid layer was then washed with Et₂O (3 x 20 mL). Finally, the acid aqueous layer was neutralized (pH > 8) and the product was extracted with EtOAc (2 x 20 mL). Removal of solvents in vacuo affords (**2.9-d₃**) as a crystalline white solid. **Yield** = 53% (88 mg, 0.403 mmol). **¹H NMR (400 MHz, CDCl₃)** δ 9.35 (s, 1H), 8.76 (dd, $J_{H,H}$ = 4.1, 1.3 Hz, 1H), 8.57 (dd, $J_{H,H}$ = 7.8, 0.7 Hz, 1H), 8.13 (dd, $J_{H,H}$ = 8.3, 1.2 Hz, 1H), 7.51 (apparent t, $J_{H,H}$ = 8.0 Hz, 1H), 7.37-7.45 (m, 2H), 3.16 (s, 3H). **²H NMR (61.4 MHz, CHCl₃)** δ = 3.14. **¹³C{¹H} NMR (101 MHz, CDCl₃)** δ 155.7, 147.8, 138.6, 136.5, 136.2, 128.1, 127.8, 121.5, 119.6, 114.8, 36.5. **HRMS** (ESI) m/z calculated for C₁₂H₁₁D₃N₃O [M+H]⁺: 219.1325; found: 219.1321.

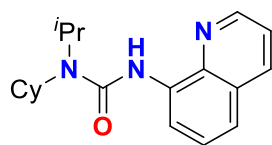
1-cyclohexyl-1-ethyl-3-(quinolin-8-yl)urea (**2.10**)



Synthesis: Synthesized using procedure **A** with *N*-ethylcyclohexylamine (96 mg, 0.757 mmol) and carbamate (**2.1**) (200 mg, 0.757 mmol). **Purification:** Following work-up, the crude product was subject to column chromatography (Hex:EtOAc gradient, 10:1) to

afford (**2.10**) as a white solid. **Yield** = 91% (205 mg, 0.689 mmol). **¹H NMR (300 MHz, CDCl₃)** δ 9.42 (br s, 1H), 8.76 (dd, J = 4.2, 1.4 Hz, 1H), 8.59 (d, J = 7.7 Hz, 1H), 8.13 (dd, J = 8.2, 1.3 Hz, 1H), 7.51 (apparent t, J = 7.9 Hz, 1H), 7.44-7.35 (m, 2H), 4.20 (m, 1H), 3.45 (quar, J = 7.1 Hz, 2H), 1.95-1.76 (m, 4H), 1.75-1.53 (m, 2H), 1.53-1.30 (m, 7H), 1.25-1.05 (m, 1H). **¹³C{¹H} NMR (75 MHz, CDCl₃)** δ 154.9, 147.9, 138.8, 136.5, 136.4, 128.2, 127.8, 121.4, 119.3, 114.8, 54.8, 37.4, 31.7, 26.2, 25.8, 16.1. **HRMS** (ESI) m/z calculated for C₁₈H₂₄N₃O [M+H]⁺: 298.1919; found: 298.1913.

1-cyclohexyl-1-isopropyl-3-(quinolin-8-yl)urea (**2.11**)

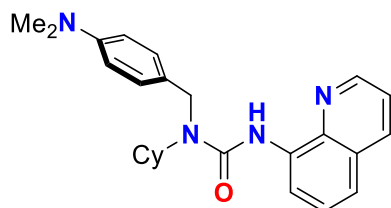


Synthesis: Synthesized using procedure **A** with *N*-isopropylcyclohexylamine (9 mg, 0.757 mmol) and carbamate (**2.1**) (200 mg, 0.757 mmol). **Purification:** Following work-up, the crude product was subject to column chromatography (Hex:EtOAc gradient, 10:1)

to afford (**2.11**) as a white solid. **Yield** = 72% (169 mg, 0.543 mmol). **¹H NMR (300 MHz, CDCl₃)** δ 9.36 (s, 1H), 8.77 (dd, J = 4.2, 1.7 Hz, 1H), 8.57 (dd, J = 7.7, 1.2 Hz, 1H), 8.12 (dd, J = 8.3, 1.6 Hz, 1H), 7.50 (t, J = 8.0 Hz, 1H),

7.40 (dd, $J = 8.3, 4.2$ Hz, 1H), 7.35 (dd, $J = 8.2, 1.2$ Hz, 1H), 4.18 (sept., $J = 6.9$ Hz, 1H), 3.85-3.68 (m, 1H), 2.08-1.57 (m, 8 H), 1.54-1.33 (m, 1H), 1.43 (d, $J = 6.9$ Hz, 6H), 1.32-1.14 (m, 1H). $^{13}\text{C}\{^1\text{H}\}$ NMR (75 MHz, CDCl_3) δ 154.8, 147.7, 138.8, 136.7, 136.4, 128.2, 127.9, 121.4, 119.1, 114.7, 54.8, 45.8, 31.6, 26.7, 25.7, 21.6. HRMS (ESI) m/z calculated for $\text{C}_{19}\text{H}_{26}\text{N}_3\text{O}$ $[\text{M}+\text{H}]^+$: 312.2076; found: 312.2073.

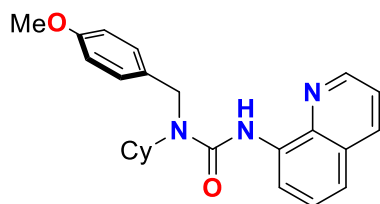
1-cyclohexyl-1-(4-(dimethylamino)benzyl)-3-(quinolin-8-yl)urea (**2.12**)



Synthesis: Synthesized using procedure **A** with 4-((cyclohexylamino)methyl)-*N,N*-dimethylaniline (176 mg, 0.757 mmol) and carbamate (**2.1**) (200 mg, 0.757 mmol). **Purification:** Following standard work-up, the organic residue was subject to column chromatography (Hex:EtOAc, 5:1) to afford (**2.12**) as

an off-white solid, **Yield** = 86% (262 mg, 0.651 mmol). ^1H NMR (300 MHz, CDCl_3) δ 9.36 (br s, 1H), 8.58 (dd, $J = 7.8, 1.2$ Hz, 1H), 8.53 (dd, $J = 4.2, 1.6$ Hz, 1H), 8.04 (dd, $J = 8.3, 1.6$ Hz, 1H), 7.48 (t, $J = 8.0$ Hz, 1H), 7.36-7.27 (m, 4H), 6.74 (d, $J = 8.7$ Hz, 2H), 4.57 (s, 2H), 4.35 (m, 1H), 2.92 (s, 6H), 2.04-1.75 (m, 4H), 1.75-1.61 (m, 1H), 1.61-1.35 (m, 4H), 1.21-1.01 (m, 1H). $^{13}\text{C}\{^1\text{H}\}$ NMR (75 MHz, CDCl_3) δ 155.9, 150.0, 147.5, 138.8, 136.6, 136.1, 128.0, 127.9, 127.7, 121.2, 119.2, 114.9, 112.9, 55.2, 46.3, 40.9, 31.6, 26.2, 25.8. HRMS (ESI) m/z calculated for $\text{C}_{25}\text{H}_{31}\text{N}_4\text{O}$ $[\text{M}+\text{H}]^+$: 403.2498; found: 403.2506.

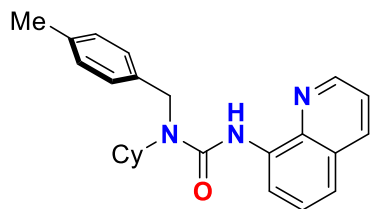
1-cyclohexyl-3-(quinolin-8-yl)-1-(4-(trifluoromethyl)benzyl)urea (**2.13**)



Synthesis: Synthesized using procedure **A** with *N*-(4-methoxybenzyl)cyclohexanamine (166 mg, 0.757 mmol) and carbamate (**2.1**) (200 mg, 0.757 mmol). **Purification:** Following work-up, the organic residue was subject to column chromatography (Hex:EtOAc, 8:1) to afford (**2.13**) as a

white solid, **Yield** = 68% (201 mg, 0.516 mmol). ^1H NMR (300 MHz, CDCl_3) δ 9.34 (br s, 1H), 8.57 (dd, $J = 7.8, 1.2$ Hz, 1H), 8.53 (dd, $J = 4.1, 1.7$ Hz, 1H), 8.06 (dd, $J = 8.3, 1.7$ Hz, 1H), 7.48 (t, $J = 8.1$ Hz, 1H), 7.41-7.30 (m, 4H), 6.92-6.85 (m, 2H), 4.61 (s, 2H), 4.33 (m, 1H), 3.77 (s, 3H), 2.03-1.75 (m, 4H), 1.75-1.60 (m, 1H), 1.55-1.38 (m, 4H), 1.19-1.02 (m, 1H). $^{13}\text{C}\{^1\text{H}\}$ NMR (75 MHz, CDCl_3) δ 158.9, 155.8, 147.5, 138.7, 136.4, 136.2, 130.8, 128.2, 128.0, 127.7, 121.3, 119.4, 114.9, 114.0, 55.4, 46.2, 31.6, 26.2, 25.8. HRMS (ESI) m/z calculated for $\text{C}_{24}\text{H}_{28}\text{N}_3\text{O}_2$ $[\text{M}+\text{H}]^+$: 390.2182; found: 390.2182.

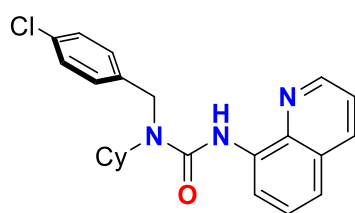
1-cyclohexyl-1-(4-methylbenzyl)-3-(quinolin-8-yl)urea (**2.14**)



Synthesis: Synthesized using procedure **A** with *N*-(4-methylbenzyl)cyclohexanamine (154 mg, 0.757 mmol) and carbamate (**2.1**) (200 mg, 0.757 mmol). **Purification:** Following standard work-up, the organic residue was subject to column chromatography (Hex:EtOAc gradient, 10:1 to

5:1) to afford (**2.14**) as a white solid, **Yield** = 69% (196 mg, 0.525 mmol). **¹H NMR (300 MHz, CDCl₃)** δ 9.34 (br s, 1H), 8.57 (dd, *J* = 7.8, 1.0 Hz, 1H), 8.51 (dd, *J* = 4.2, 1.5 Hz, 1H), 8.06 (dd, *J* = 8.3, 1.6 Hz, 1H), 7.48 (t, *J* = 8.0 Hz, 1H), 7.37-7.28 (m, 4H), 7.20-7.08 (m, 2H), 4.63 (s, 2H), 4.33 (m, 1H), 2.33 (s, 3H), 2.03-1.75 (m, 4H), 1.75-1.34 (m, 6H), 1.21-0.98 (m, 1H). **¹³C{¹H} NMR (75 MHz, CDCl₃)** δ 155.8, 147.5, 138.7, 136.8, 136.4, 136.2, 135.8, 129.3, 128.0, 127.7, 126.9, 121.3, 119.4, 114.9, 55.4, 46.5, 31.6, 26.2, 25.8, 21.2. **HRMS (ESI)** *m/z* calculated for C₂₄H₂₈N₃O₂ [M+H]⁺: 374.2232; found: 374.2230.

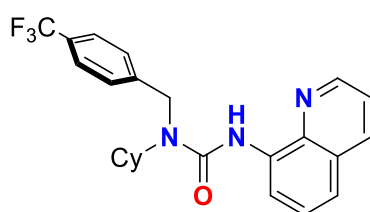
1-cyclohexyl-3-(quinolin-8-yl)-1-(4-chlorobenzyl)urea (**2.15**)



Synthesis: Synthesized using procedure **A** with *N*-(4-chlorobenzyl)cyclohexanamine (169 mg, 0.757 mmol) and carbamate (**2.1**) (200 mg, 0.757 mmol). **Purification:** Following work-up, the organic residue was subject to column chromatography (Hex:EtOAc, 10:1) to afford (**2.15**) as a white

solid, **Yield** = 62% (185 mg, 0.470 mmol). **¹H NMR (300 MHz, CDCl₃)** δ 9.34 (br s, 1H), 8.58-8.50 (m, 2H), 8.08 (dd, *J* = 8.3, 1.6 Hz, 1H), 7.49 (t, *J* = 8.1 Hz, 1H), 7.41-7.28 (m, 6H), 4.63 (s, 2H), 4.28 (m, 1H), 2.02-1.76 (m, 4H), 1.76-1.62 (m, 1H), 1.56-1.36 (m, 4H), 1.20-1.02 (m, 1H). **¹³C{¹H} NMR (75 MHz, CDCl₃)** δ 155.6, 147.6, 138.7, 137.7, 136.3, 136.1, 132.9, 128.8, 128.4, 128.0, 127.7, 121.4, 119.6, 115.0, 55.7, 46.1, 31.6, 26.1, 25.7. **HRMS (ESI)** *m/z* calculated for C₂₃H₂₅N₃OCl [M+H]⁺: 394.1686; found: 394.1682.

1-cyclohexyl-3-(quinolin-8-yl)-1-(4-(trifluoromethyl)benzyl)urea (**2.16**)

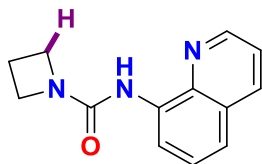


Synthesis: Synthesized using procedure **A** with *N*-(4-(trifluoromethyl)benzyl)cyclohexanamine (195 mg, 0.757 mmol) and carbamate (**2.1**) (200 mg, 0.757 mmol). **Purification:** Following work-up, the organic residue was subject to column chromatography (Hex:EtOAc, 10:1) to afford

(**2.16**) as a white solid, **Yield** = 87% (282 mg, 0.660 mmol). **¹H NMR (400 MHz, CDCl₃)** δ 9.36 (br s, 1H), 8.54 (dd, *J* = 7.7, 1.0 Hz, 1H), 8.52 (d, *J* = 3.4 Hz, 1H), 8.09 (dd, *J* = 8.3, 1.4 Hz, 1H), 7.61 (d, *J* = 8.3 Hz, 2H), 7.55 (d, *J* = 8.2

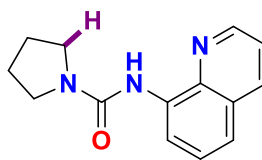
Hz, 2H), 7.50 (t, $J = 8.0$ Hz, 1H), 7.40-7.33 (m, 2H), 4.72 (s, 2H), 4.27 (m, 1H), 2.03-1.80 (m, 4H), 1.71 (m, 1H), 1.55-1.40 (m, 4H), 1.19-1.04 (m, 1H). $^{13}\text{C}\{^1\text{H}\}$ NMR (101 MHz, CDCl_3) δ 155.4, 147.6, 143.5, 138.5, 136.2, 136.0, 129.4 (q, $J = 32.5$ Hz), 127.9, 127.5, 127.2, 125.5 (q, $J = 3.6$ Hz), 124.3 (q, $J = 272.2$ Hz), 121.4, 119.6, 114.9, 55.8, 46.2, 31.6, 26.0, 25.5. $^{19}\text{F}\{^1\text{H}\}$ NMR (282 MHz, CDCl_3) δ 62.69. HRMS (ESI) m/z calculated for $\text{C}_{24}\text{H}_{25}\text{N}_3\text{OF}_3$ $[\text{M}+\text{H}]^+$: 428.1950; found: 428.1949.

N-(quinolin-8-yl)azetidine-1-carboxamide (**2.17**)



Synthesis: Synthesized using procedure **C** with azetidine hydrochloride (71 mg, 0.757 mmol) and carbamate (**2.1**) (200 mg, 0.757 mmol). **Purification:** Following work-up, the crude product was subject to column chromatography (Hex:EtOAc gradient, 5:1 to 1:1) to afford (**2.17**) as a crystalline white solid, **Yield** = 94% (161 mg, 0.708 mmol). ^1H NMR (300 MHz, CDCl_3) δ 8.81 (br s, 1H), 8.74 (dd, $J = 4.20, 1.6$ Hz, 1H), 8.55 (dd, $J = 7.7, 1.1$ Hz, 1H), 8.11 (dd, $J = 8.3, 1.6$ Hz, 1H), 7.50 (apparent t, $J = 7.9$ Hz, 1H), 7.43-7.35 (m, 2H), 4.21 (t, $J = 7.6$ Hz, 4H), 2.34 (quin, $J = 7.6$ Hz, 2H). $^{13}\text{C}\{^1\text{H}\}$ NMR (75 MHz, CDCl_3) δ 156.3, 147.9, 138.3, 136.4, 135.6, 128.1, 127.7, 121.5, 119.7, 114.6, 77.6, 77.2, 76.7, 49.3, 15.3. HRMS (ESI) m/z calculated for $\text{C}_{13}\text{H}_{14}\text{N}_3\text{O}$ $[\text{M}+\text{H}]^+$: 228.1137; found: 228.1142.

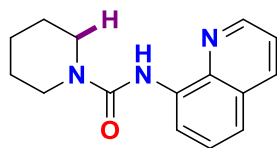
N-(quinolin-8-yl)pyrrolidine-1-carboxamide (**2.18**)



Synthesis: Synthesized using procedure **A** with pyrrolidine (108 mg, 1.51 mmol) and carbamate (**2.1**) (400 mg, 1.51 mmol). **Purification:** Following work-up, phenol was sublimed from the product at 100°C. Compound (**2.18**) was then recrystallized from DCM

layered with hexanes at room temperature. Crystals were collected after two days to afford (**2.18**) an off yellow solid, **Yield** = 93% (340 mg, 1.41 mmol). ^1H NMR (400 MHz, CDCl_3) δ 9.13 (br s, 1H), 8.76 (dd, $J = 4.2, 1.7$ Hz, 1H), 8.60 (dd, $J = 7.7, 1.1$ Hz, 1H), 8.13 (dd, $J = 8.3, 1.6$ Hz, 1H), 7.51 (apparent t, $J = 8.0$ Hz, 1H), 7.41 (dd, $J = 8.3, 4.2$ Hz, 1H), 7.38 (dd, $J = 8.3, 1.0$ Hz, 1H), 3.63 (m, 4H), 2.02 (m, 4H). $^{13}\text{C}\{^1\text{H}\}$ NMR (101 MHz, CDCl_3) δ 154.1, 147.8, 136.5, 136.2, 128.2, 127.8, 121.4, 119.4, 114.8, 45.9, 25.8. HRMS (ESI) m/z calculated for $\text{C}_{14}\text{H}_{16}\text{N}_3\text{O}$ $[\text{M}+\text{H}]^+$: 242.1293; found: 242.1292.

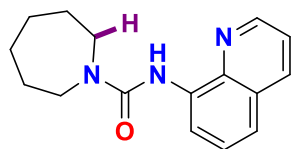
N-(quinolin-8-yl)piperidine-1-carboxamide (**2.19**)



Synthesis: Synthesized using procedure **A** with piperidine (65 mg, 0.757 mmol) and carbamate (**2.1**) (200 mg, 0.757 mmol). **Purification:** Following work-up, the crude product was subject to column chromatography (Hex:EtOAc gradient, 5:1) to afford

(**2.19**) as an off-yellow oil (This oil slowly crystallizes to give white crystals of **2m**), **Yield** = 98% (190 mg, 0.744 mmol). **¹H NMR (400 MHz, CDCl₃)** δ 9.41 (br s, 1H), 8.77 (dd, J = 4.2, 1.6 Hz, 1H), 8.56 (dd, J = 7.8, 1.1 Hz, 1H), 8.14 (dd, J = 8.3, 1.5 Hz, 1H), 7.51 (apparent t, J = 8.0 Hz, 1H), 7.42 (dd, J = 8.3, 4.2 Hz, 1H), 7.38 (dd, J = 8.3, 1.0 Hz, 1H), 3.61 (m, 4H), 1.68 (m, 6H). **¹³C{¹H} NMR (101 MHz, CDCl₃)** δ 154.78, 147.81, 138.68, 136.51, 136.21, 128.16, 127.82, 121.46, 119.48, 114.91, 45.30, 25.95, 24.66. **HRMS (ESI)** m/z calculated for C₁₅H₁₈N₃O [M+H]⁺: 256.1450; found: 256.1444.

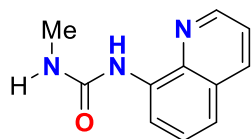
N-(quinolin-8-yl)azepane-1-carboxamide (**2.20**)



Synthesis: Synthesized using procedure **A** with azepane (75 mg, 0.757 mmol) and carbamate (**2.1**) (200 mg, 0.757 mmol). **Purification:** Following work-up, the crude product was subject to column chromatography (Hex:EtOAc gradient, 5:1) to afford

(**2.20**) as an off-yellow oil (This oil slowly crystallizes to give off-white crystals of **2.20**), **Yield** = 96% (195 mg, 0.723 mmol). **¹H NMR (400 MHz, CDCl₃)** δ 9.38 (br s, 1H), 8.76 (dd, J = 4.2, 1.7 Hz, 1H), 8.58 (dd, J = 7.8, 1.1 Hz, 1H), 8.13 (dd, J = 8.3, 1.7 Hz, 1H), 7.51 (apparent t, J = 8.1 Hz, 1H), 7.41 (dd, J = 8.3, 4.3 Hz, 1H), 7.38 (dd, J = 8.2, 1.1 Hz, 1H), 3.66 (m, 4H), 1.88 (m, 4H), 1.64 (m, 4H). **¹³C{¹H} NMR (101 MHz, CDCl₃)** δ 155.2, 147.8, 138.7, 136.5, 136.4, 128.2, 127.8, 121.4, 119.4, 114.9, 46.9, 28.7, 27.3. **HRMS (ESI)** m/z calculated for C₁₆H₂₀N₃O [M+H]⁺: 270.1606; found: 270.1601.

1-methyl-3-(quinolin-8-yl)urea (**2.21**)

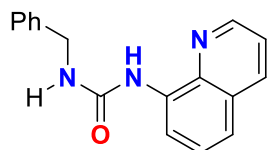


Synthesis: Synthesized using procedure **C** with methylamine hydrochloride (51.1 mg, 0.757 mmol) and carbamate (**2.1**) (200 mg, 0.757 mmol). **Purification:** Following work-up, the crude product was subject to column chromatography (Hex:EtOAc gradient, 5:1 to 2:1) to

afford (**2.21**) as an off-yellow solid, **Yield** = 92% (140 mg, 0.696 mmol). **¹H NMR (300 MHz, CDCl₃)** δ 9.03 (s, 1H), 8.74 (dd, J = 4.2, 1.6 Hz, 1H), 8.56 (dd, J = 7.7, 1.1 Hz, 1H), 8.13 (dd, J = 8.3, 1.6 Hz, 1H), 7.51 (apparent t, J = 7.9 Hz, 1H), 7.43-7.36 (m, 2H), 5.03 (br s, 1H), 2.95 (d, J = 4.9 Hz, 3H). **¹³C{¹H} NMR (75 MHz, CDCl₃)** δ 156.0, 147.7,

138.3, 136.6 136.0, 128.2, 127.8, 121.5, 119.7, 114.9, 27.3. **HRMS** (ESI) m/z calculated for $C_{11}H_{12}N_3O$ $[M+H]^+$: 202.0980; found: 202.0978.

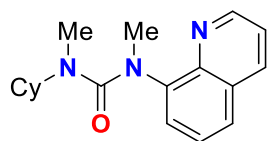
1-benzyl-3-(quinolin-8-yl)urea (**2.22**)



Synthesis: Synthesized using procedure **A** with benzyl amine (81.1 mg, 0.757 mmol) and carbamate (**2.1**) (200 mg, 0.757 mmol). **Purification:** Following work-up, the crude product was subject to column chromatography (Hex:EtOAc gradient, 9:1 to 1:1) to afford

(**2.22**) as a white solid, **Yield** = 92% (194 mg, 0.696 mmol). **1H NMR (400 MHz, $CDCl_3$)** δ 9.05 (br s, 1H), 8.69 (dd, J = 4.2, 1.4 Hz, 1H), 8.57 (d, J = 7.7 Hz, 1H), 8.12 (dd, J = 8.3, 1.4 Hz, 1H), 7.50 (apparent t, J = 8.0 Hz, 1H), 7.41-7.36 (m, 4H), 7.33 (m, 2H), 7.27 (m, 1H), 5.35 (t, J = 5.0 Hz, 1H), 4.54 (d, J = 5.7 Hz, 2H). **$^{13}C\{^1H\}$ NMR (101 MHz, $CDCl_3$)** δ 155.2, 147.7, 139.0, 138.2, 136.6, 135.9, 128.8, 128.2, 127.9, 127.8, 127.6, 121.5, 119.8, 115.0, 44.7. **HRMS** (ESI) m/z calculated for $C_{17}H_{16}N_3O$ $[M+H]^+$: 278.1293; found: 278.1291.

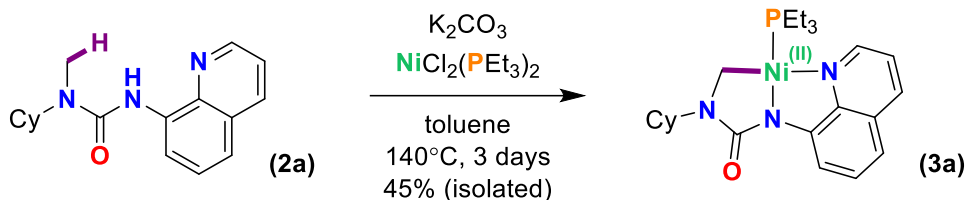
1-cyclohexyl-1,3-dimethyl-3-(quinolin-8-yl)urea (**2.23**)



Synthesis & Purification: In a glovebox, a Schlenk was charged consecutively with compound (**2.2**) (200 mg, 0.71 mmol), NaH (20 mg, 0.83 mmol), a stir bar, and THF (20 mL). The Schlenk was then sealed, removed from the glovebox, and introduced onto a

Schlenk line by established procedures. The contents were then stirred for 30 minutes at room temperature, at which point MeI (50 μ L, 114 mg, 0.80 mmol) was added slowly to the reaction contents at room temperature. The reaction was then stirred again for 30 minutes, followed by a quench with 1M aqueous NaOH (5 mL), and dilution with distilled water (30 mL). The organic products were then extracted from the aqueous layer with DCM (3 x 20 mL). Following removal of volatiles by rotary evaporation, the crude mixture was subject to column chromatography (Hex:EtOAc plug: 5:1 column volume, then elute product with 1:9.) to yield (**2.23**) as a clear oil. **Yield** = 81% (172 mg, 0.58 mmol). **1H NMR (300 MHz, $CDCl_3$)** δ = 8.98 (dd, J = 4.2, 1.7 Hz, 1H), 8.18 (dd, J = 8.3, 1.7 Hz, 1H), 7.68 (dd, J = 7.9, 1.6 Hz, 1H), 7.52-7.37 (m, 3H), 3.84 (tt, J = 11.5, 3.6 Hz, 1H), 3.29 (s, 3H), 2.31 (s, 3H), 1.67-1.52 (m, 2H), 1.52-1.40 (m, 1H), 1.40-1.28 (m, 2H), 1.28-0.78 (m, 5H). **^{13}C NMR (75 MHz, $CDCl_3$)** δ = 163.2, 150.2, 144.8, 143.6, 136.6, 129.8, 126.8, 126.2, 126.1, 121.6, 56.0, 39.8, 30.1, 29.9, 25.8, 25.7. **HRMS** (ESI) m/z calculated for $C_{18}H_{23}N_3O$ $[M+H]^+$: 298.1919; found: 298.1911.

Isolation of Cyclometalated Ni(II)-Ureate (2.2-Ni)



(PEt₃)Ni(κ^3 -C,N,N-(CH₂)CyN(C=O)N(N-8AQ) (2.2-Ni): In a glovebox, NiCl₂(PEt₃)₂ (2036 mg, 5.56 mmol), urea (2.2) (1600 mg, 5.65 mmol), and K₂CO₃ (1700 mg, 12.3 mmol) were each weighed into separate 20 mL vials. Each vial's contents were then added directly into a 100 mL Schlenk flask. Toluene (50 mL) and a stir bar were both added to the Schlenk flask, and the flask was then sealed with grease. The Schlenk was then removed from the glovebox and heated to 140°C in an oil bath for 2 days with stirring. After this time, the flask was introduced to a Schlenk line and the volatiles were removed in vacuo. Toluene (~ 30 mL) was then added to flask, and following sealing of the contents, the mixture was heated again to 140°C in an oil bath for 1 days with stirring. Once again, the flask was reconnected to a Schlenk line, and the volatiles were removed in vacuo. The Schlenk was then brought into a glovebox and the contents were washed with hexanes (3 x 50 mL), then partially dissolved in THF (50 mL). The resulting mixture was filtered through a Celite® plug into a new Schlenk flask to remove insoluble salts. The THF solution was then divided between three 20 mL scintillation vials and layered with Et₂O:hexanes (1:1, 4 mL), then hexanes (3 mL). The vials were cooled in a glovebox freezer (-35°C) to afford **(2.2-Ni)** as a semi-crystalline orange-brown solid. **N.B.** *These crystals require extensive drying under vacuum to remove THF/Et₂O from the crystal lattice. Additionally, vigorous washing with hexanes was required in some crystalline samples to remove sufficient solvent. Thus, important to check samples for purity by ¹H NMR to determine weight of solvent in sample.* **Yield:** 45% (1141 mg, 2.21 mmol; multiple crops). X-ray quality crystals were grown from toluene solutions of **(2.2-Ni)** layered with hexamethyldisiloxane, cooled to -35°C over several days.

¹H NMR (400 MHz, C₇D₈): δ = 9.81 (dd, $J_{\text{H,H}}$ = 8.0, 1.0 Hz, 1H), 7.79 (dd, $J_{\text{H,H}}$ = 4.9, 1.2 Hz, 1H), 7.50 (dd, $J_{\text{H,H}}$ = 8.2, 1.2 Hz, 1H), 7.42 (app. T, $J_{\text{H,H}}$ = 7.9 Hz, 1 H), 6.76 (dd, $J_{\text{H,H}}$ = 7.9, 0.9 Hz, 1H), 6.54 (dd, $J_{\text{H,H}}$ = 8.2, 4.9 Hz, 1H), 4.51-4.36 (m, 1H), 2.67 (d, $J_{\text{H,P}}$ = 6.1 Hz, 2H), 2.03-1.94 (m, 2H), 1.80-1.67 (m, 4H) 1.63-1.53 (m, 1H), 1.49-1.33 (m, 3H), 1.14 (pent, $J_{\text{H,H}}$ = 7.6, 6H) 0.85 (dq, $J_{\text{H,H}}$ = 7.6 Hz, 15.2 Hz, 9H).

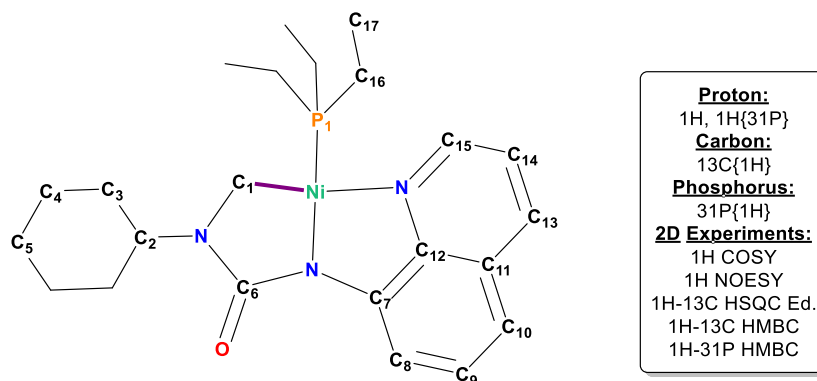
³¹P{¹H} NMR (162 MHz, 25°C, C₆D₆): 18.9 (s).

EI-MS (m/z): no characteristic fragments were observed.

Anal. Calcd. for C₂₃H₃₄N₃NiOP (458). C, 60.29%; H, 7.48%; N, 9.17%. Found: C, 60.49%; H, 7.55%; N, 8.92%.

Full (¹H, ¹³C, ³¹P) NMR Spec. Assignments of Ni(II)-Ureate (2.2-Ni) in d₆-DMSO

The cyclometalated ureates are characterized entirely *in situ*. As a comparison, we fully characterized complex (2.2-Ni) by a plethora of NMR spectroscopic experiments in d₆-DMSO. The NMR spectroscopic shifts of secondary nickelated complexes are analogous to those in (2.2-Ni).



¹H NMR (400 MHz, d₆-DMSO): δ = 8.55 (dd, *J* = 7.8, 0.7 Hz, **H8**: ¹H COSY to H10, H9, 1H), 8.44-8.40 (m, *partially eclipsed*, **H15**: ¹H-³¹P HMBC to P1, ¹H NOESY to H16, H17, 1H), 8.41-8.38 (m, *partially eclipsed*, **H13**: ¹H COSY to H14, ¹H NOESY to H10, 1H), 7.49 (dd, *J* = 8.2, 5.0 Hz, **H14**: ¹H COSY to H15, H13, 1H), 7.38 (app. t, *J* = 7.9 Hz, **H9**: ¹H COSY to H10, H8, 1H), 7.11 (d, *J* = 7.9 Hz, **H10**: ¹H NOESY to H13, ¹H COSY to H9, 1H), 3.59-3.49 (m, **H2**: weak ¹H NOESY to H1, ¹H COSY to H3, 1H), 2.35 (d, ³*J*_{H,P} = 4.4 Hz, **H1**: ¹H-³¹P HMBC to P1, ¹H NOESY to H2 (weak), H3, H16, 2H), 1.77-1.65 (m, *eclipsed*, **H4a**: ¹H COSY to H3, H5, H4b, ¹H NOESY to H1, ¹H-¹³C Ed. diastereotopic pair, 2H), ~ 1.75-1.65 (m, *partially eclipsed*, **H16**: ¹H-³¹P HMBC to P1, ¹H NOESY to H1, H15, 6H), 1.63-1.54 (m, **H5a**: ¹H COSY to H4, H5b, ¹H-¹³C Ed. diastereotopic pair, 1H), 1.53-1.41 (m, **H3**: ¹H COSY to H4a, H4b, 4H), 1.34-1.23 (m, *partially eclipsed*, **H4b**: ¹H COSY to H3, H4a, ¹H-¹³C Ed. diastereotopic pair, 2H), 1.23-1.12 (dt, *J* = 7.6 Hz, **H17**: ¹H COSY to H16, ¹H NOESY to H15, 9H), 1.12-0.94 (m, **H5b**: ¹H COSY to H5a, H4, ¹H-¹³C Ed. diastereotopic pair, 1H).

$^{13}\text{C}\{^1\text{H}\}$ NMR (400 MHz, $\text{d}_6\text{-DMSO}$): $\delta = 163.4$ (**C6**: ^1H - ^{13}C HMBC from H1, H2), 149.2 (**C15**: ^1H - ^{13}C HSQC from H15), 148.9 (**C7**: ^1H - ^{13}C HMBC from H9 (weak), H10, H8, *not* from H13-H15), 143.8 (**C12**: ^1H - ^{13}C HMBC from H8, H10, H13, H15, *not* from H9, H14), 138.0 (**C13**: ^1H - ^{13}C HSQC from H13), 128.9 (**C9**: ^1H - ^{13}C HSQC from H9), 128.9 (*fully eclipsed*, **C11**: ^1H - ^{13}C HMBC from H9, H14), 121.8 (**C14**: ^1H - ^{13}C HSQC from H14), 114.4 (**C8**: ^1H - ^{13}C HSQC from H8), 113.8 (**C10**: ^1H - ^{13}C HSQC from H10), 67.0 (*residual THF*), 53.3 (**C2**: ^1H - ^{13}C HSQC from H2), 29.5 (**C3**: ^1H - ^{13}C HSQC from H3), 25.6 (**C4**: ^1H - ^{13}C HSQC from H4a, H4b), 25.3 (**C5**: ^1H - ^{13}C HSQC from H5a, H5b), 25.1 (*residual THF*), 24.9 (d, $^2J_{\text{C,P}} = 22.2$ Hz, **C1**: ^1H - ^{13}C HSQC from H1), 14.0 (d, $^2J_{\text{C,P}} = 23.9$ Hz, **C16**: ^1H - ^{13}C HSQC from H16), 8.4 (**C17**: ^1H - ^{13}C HSQC from H17).

$^{31}\text{P}\{^1\text{H}\}$ NMR (162 MHz, $\text{d}_6\text{-DMSO}$): $\delta = 19.4$ (s, **P1**).

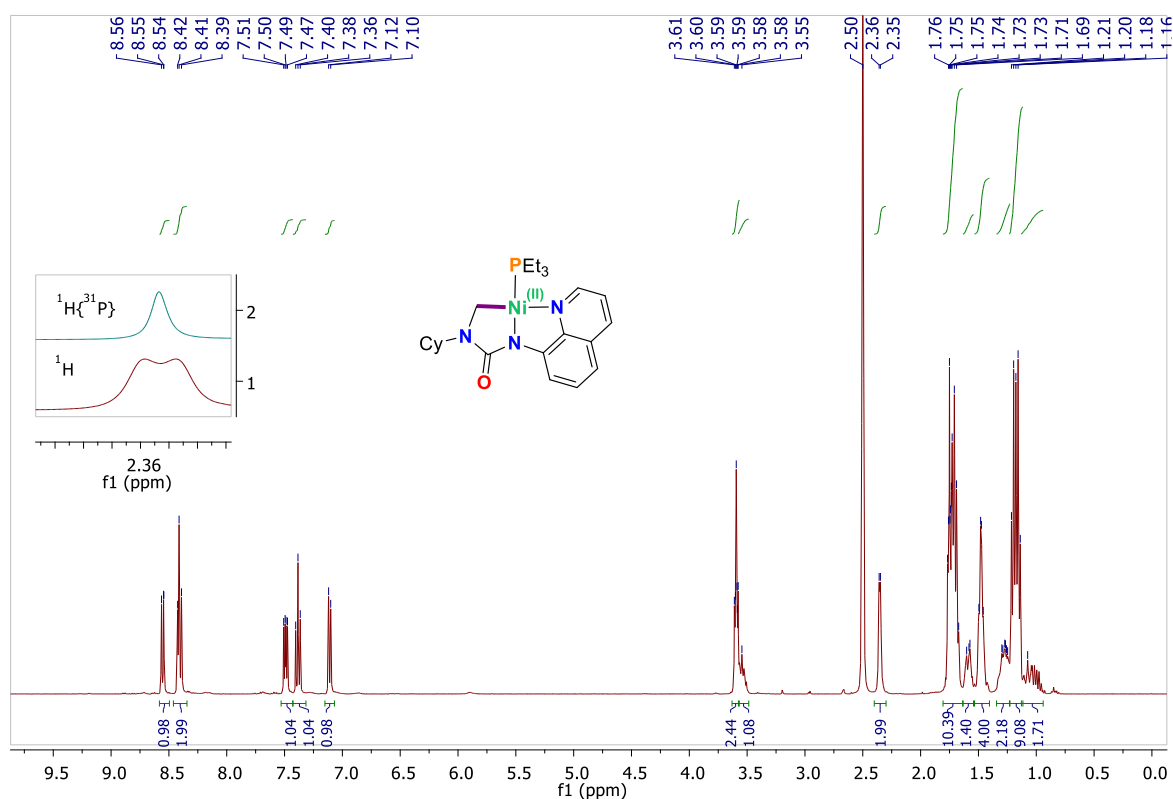


Figure A.2.1. ^1H NMR spectrum of (2.2-Ni) (400 MHz, $\text{d}_6\text{-DMSO}$, 298K). The $^1\text{H}\{^{31}\text{P}\}$ NMR spectrum is shown in the inset.

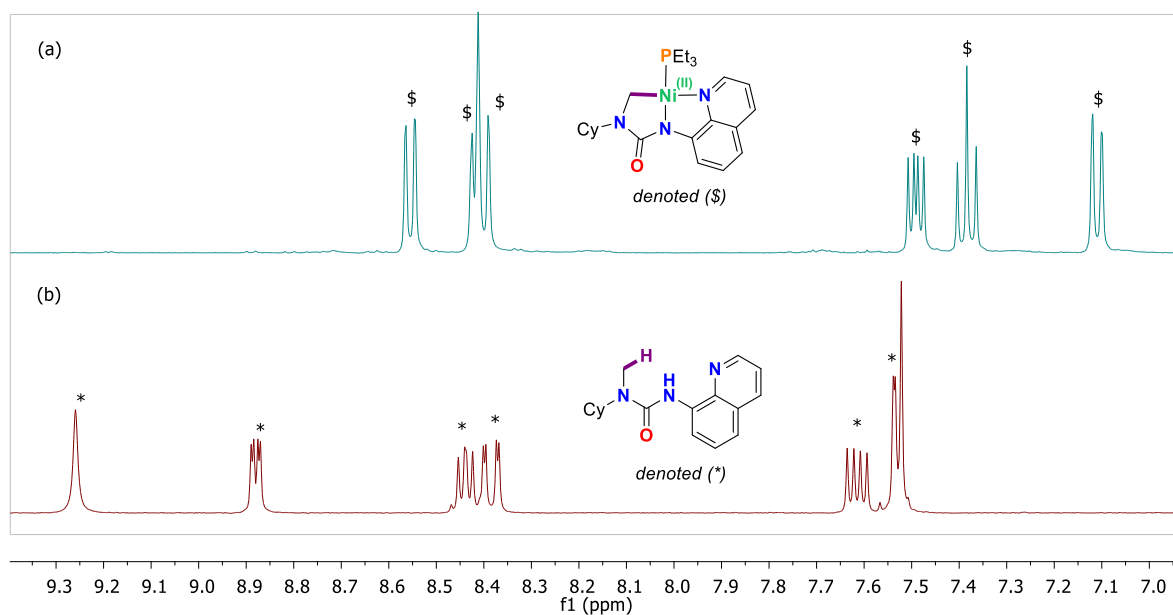


Figure A.2.2. Stacked ^1H NMR spectrum of (a) (2.2-Ni, denoted (\$)), and (b) compound (2.2); (400 MHz, d_6 -DMSO, 298K).

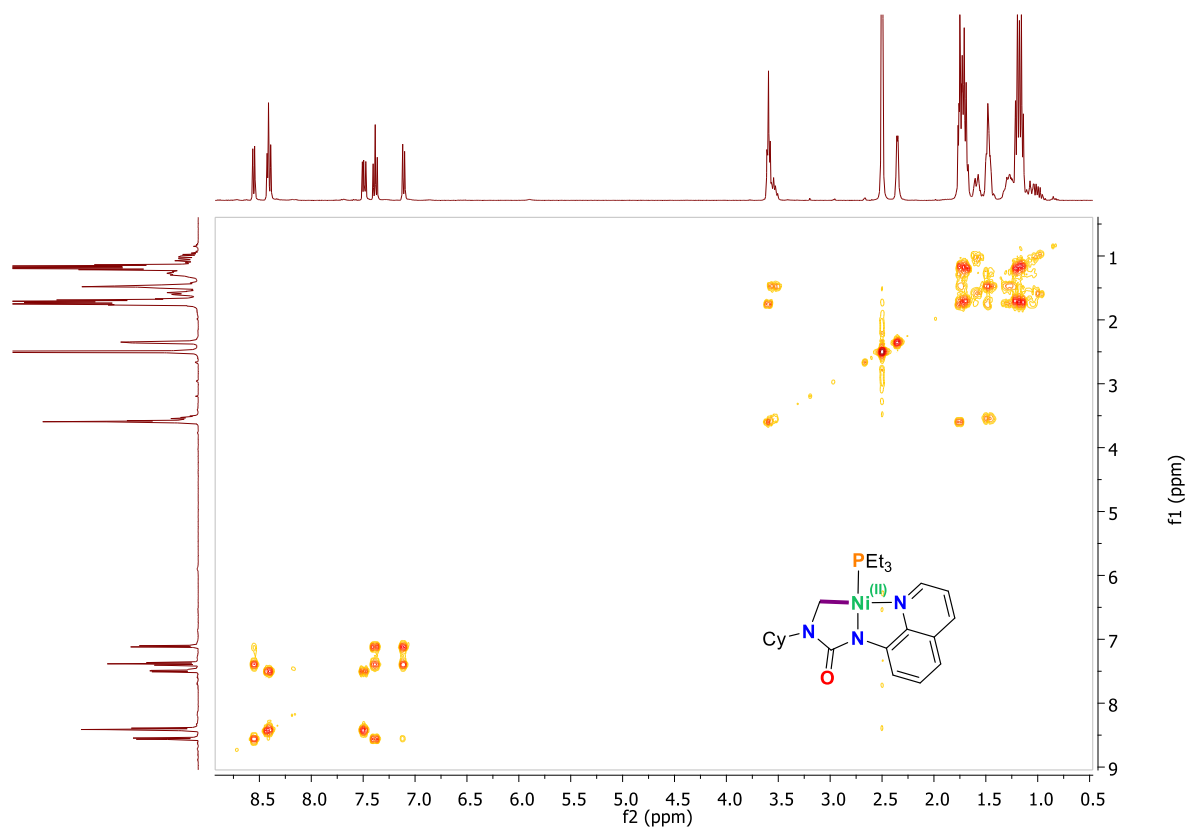


Figure A.2.3. ^1H COSY NMR spectrum of (2.2-Ni) (400 MHz, d_6 -DMSO, 298K)

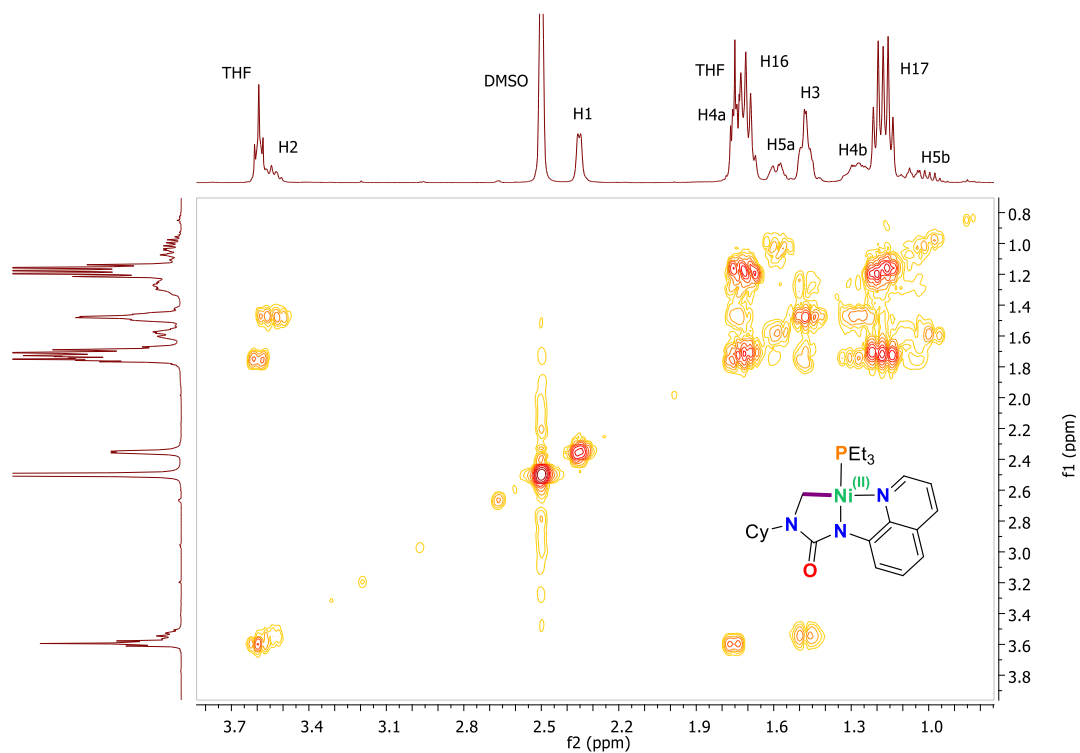


Figure A.2.4. ^1H COSY NMR spectrum (expanded) of (2.2-Ni) (400 MHz, $\text{d}_6\text{-DMSO}$, 298K)

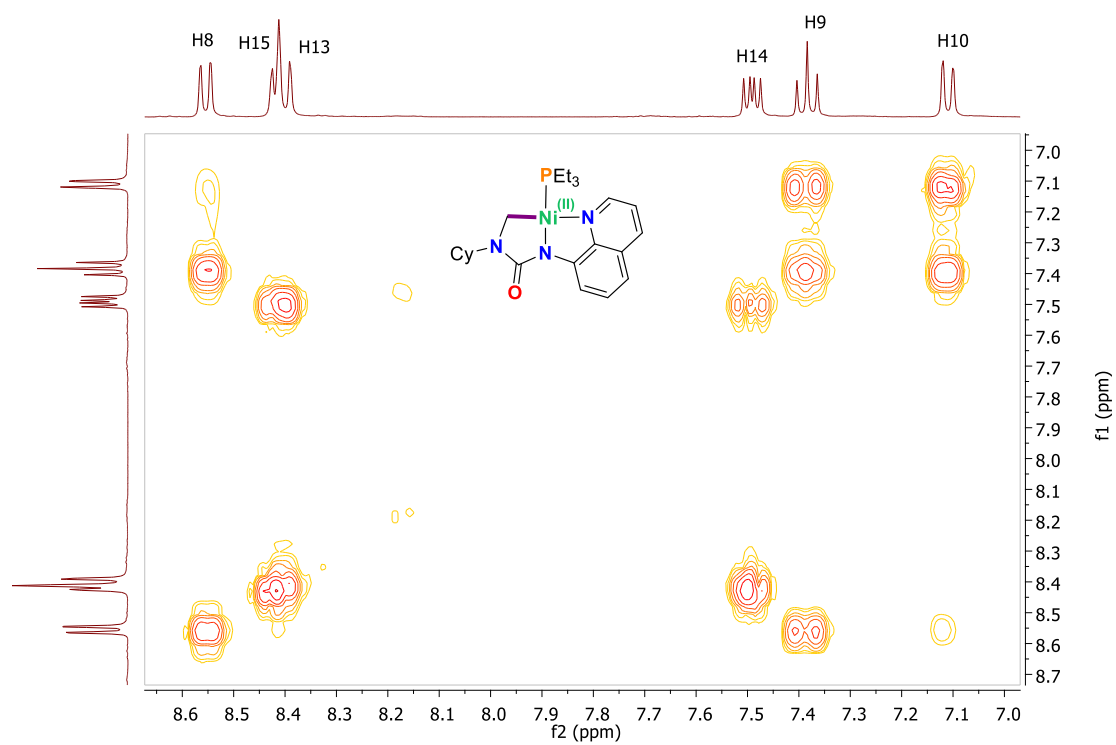


Figure A.2.5. ^1H COSY NMR spectrum (expanded) of (2.2-Ni) (400 MHz, $\text{d}_6\text{-DMSO}$, 298K)

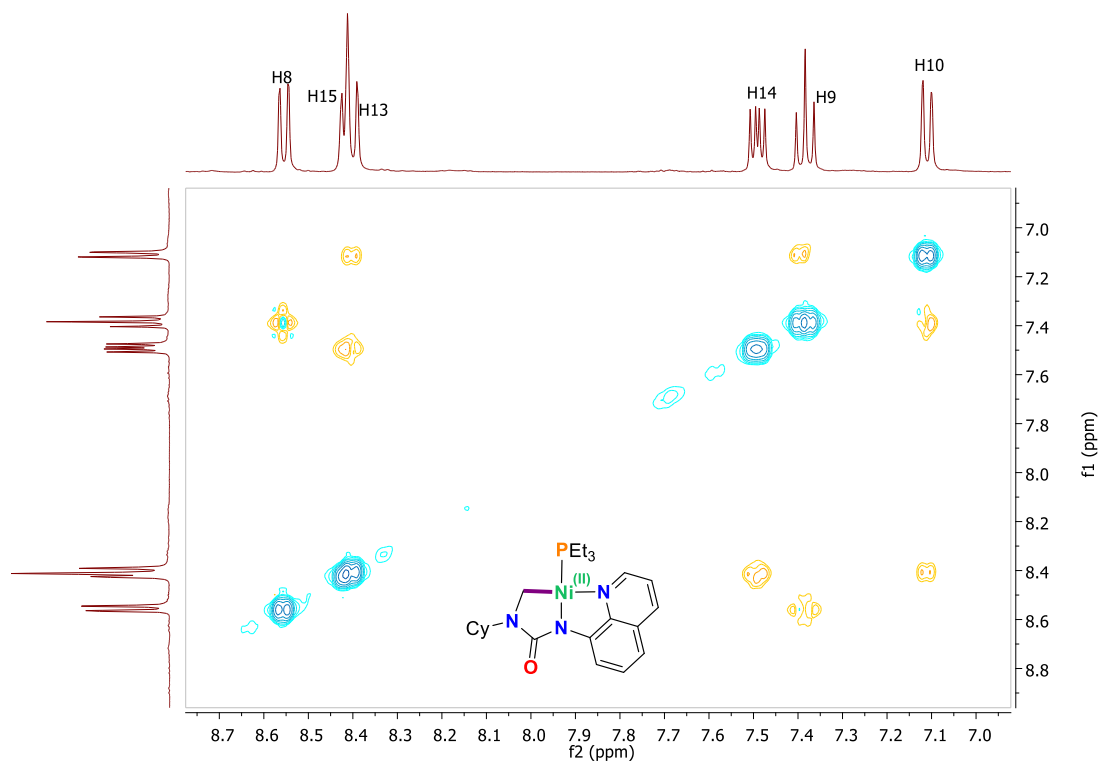


Figure A.2.6. ^1H NOESY NMR spectrum (expanded) of (2.2-Ni) (400 MHz, $\text{d}_6\text{-DMSO}$, 298K)

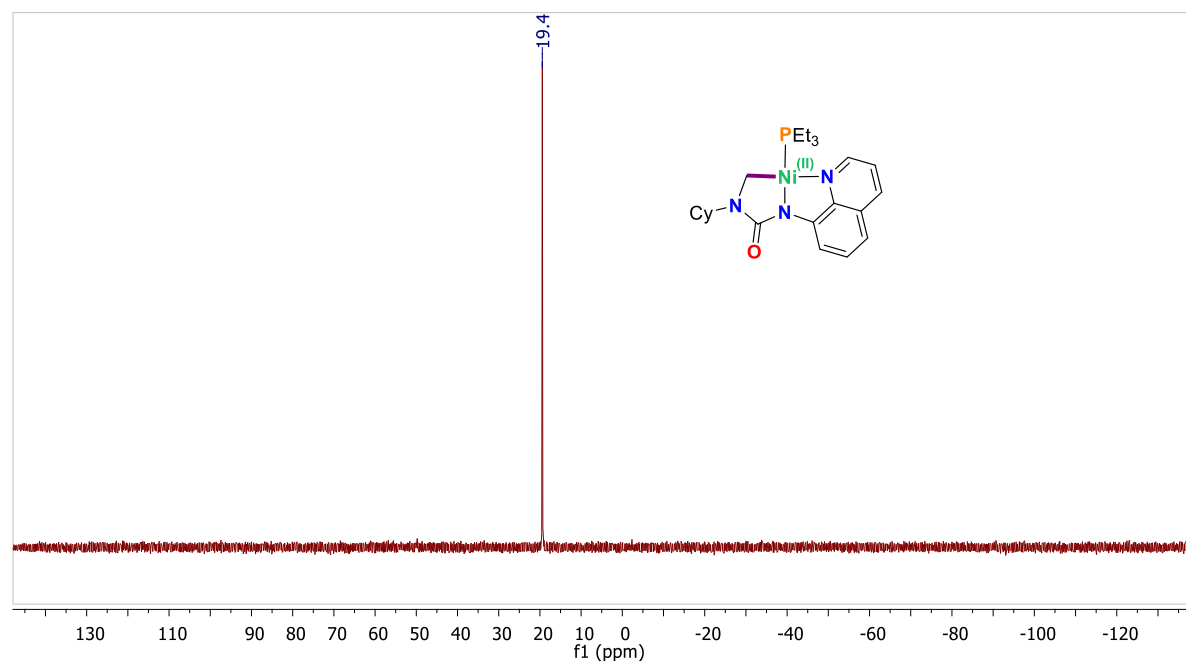


Figure A.2.7. $^{31}\text{P}\{^1\text{H}\}$ NMR spectrum of (2.2-Ni) (162 MHz, $\text{d}_6\text{-DMSO}$, 298K)

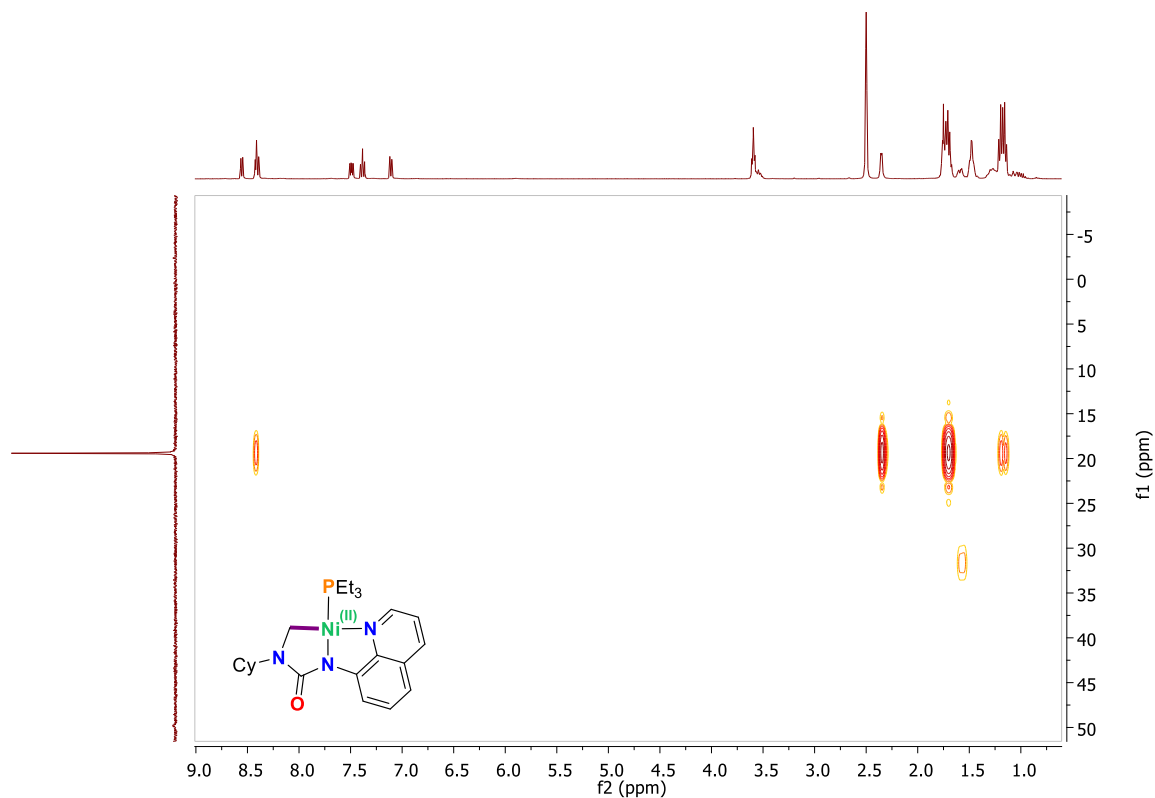


Figure A.2.8. ^1H - ^{31}P (HMBC) NMR spectrum of (2.2-Ni) (400 MHz, d_6 -DMSO, 298K)

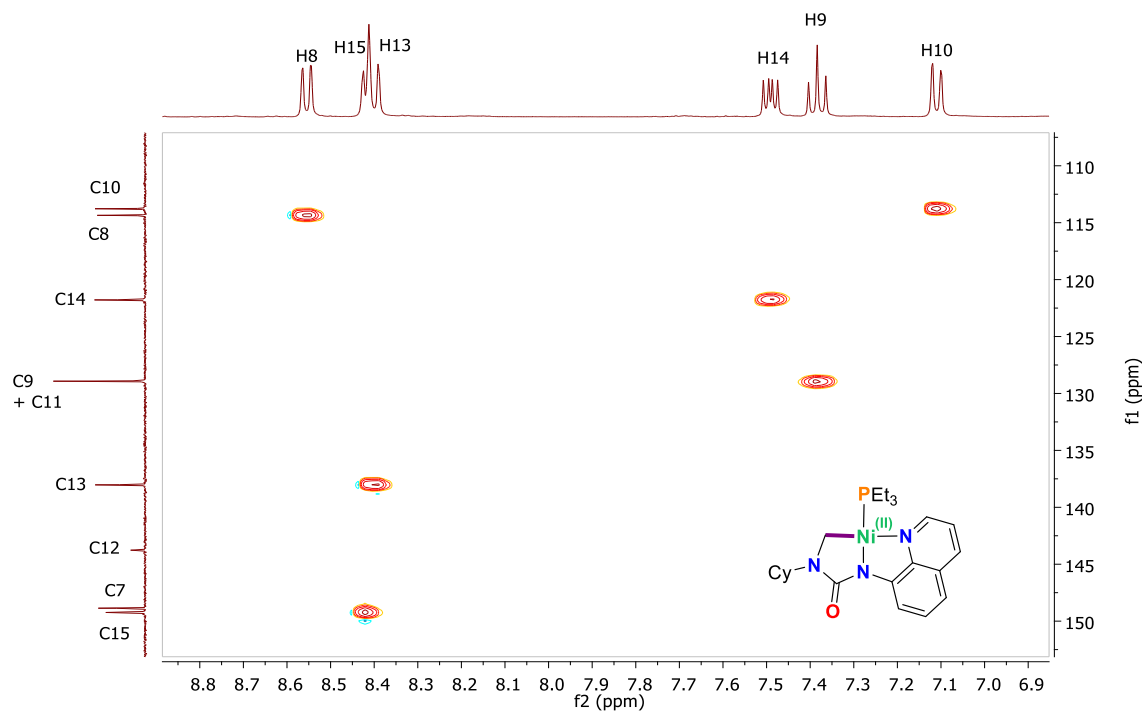


Figure A.2.9. ^{13}C - ^1H (HSQC-edited) NMR spectrum (expanded) of (2.2-Ni) (400 MHz, d_6 -DMSO, 298K)

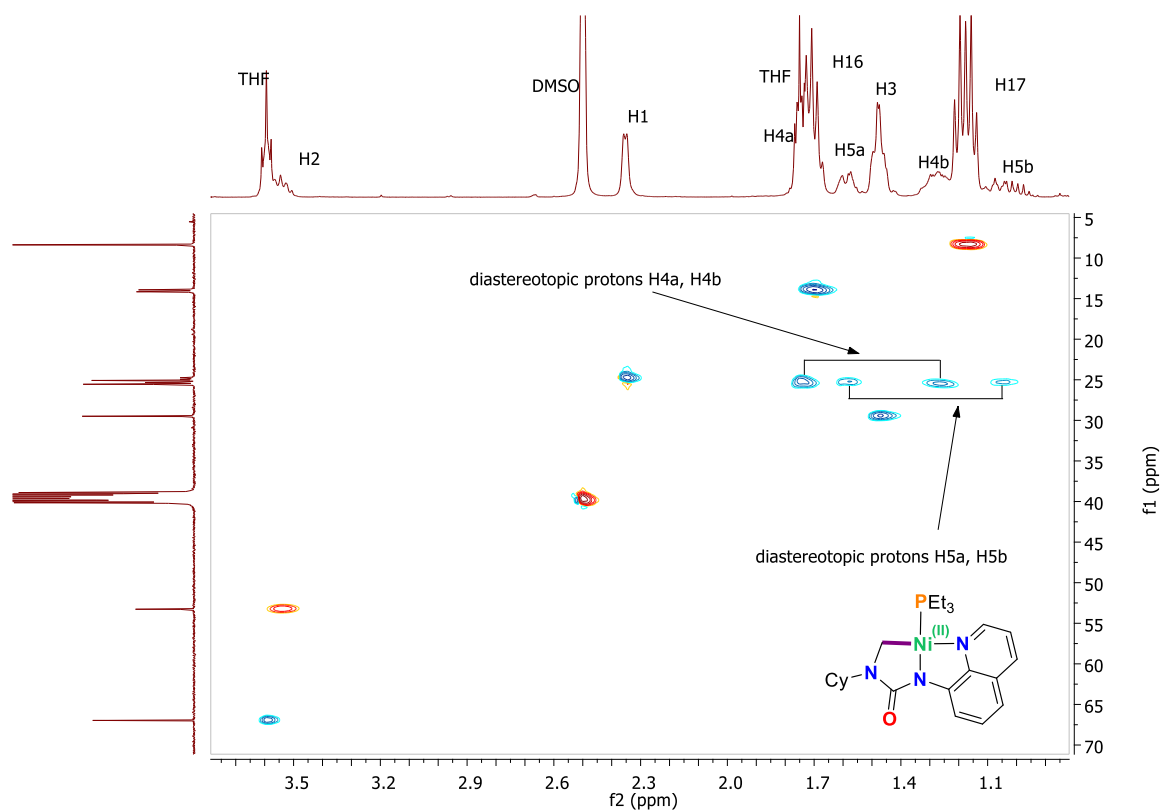


Figure A.2.10. ^{13}C - ^1H (HSQC-edited) NMR spectrum (expanded) of (2.2-Ni) (400 MHz, d_6 -DMSO, 298K)

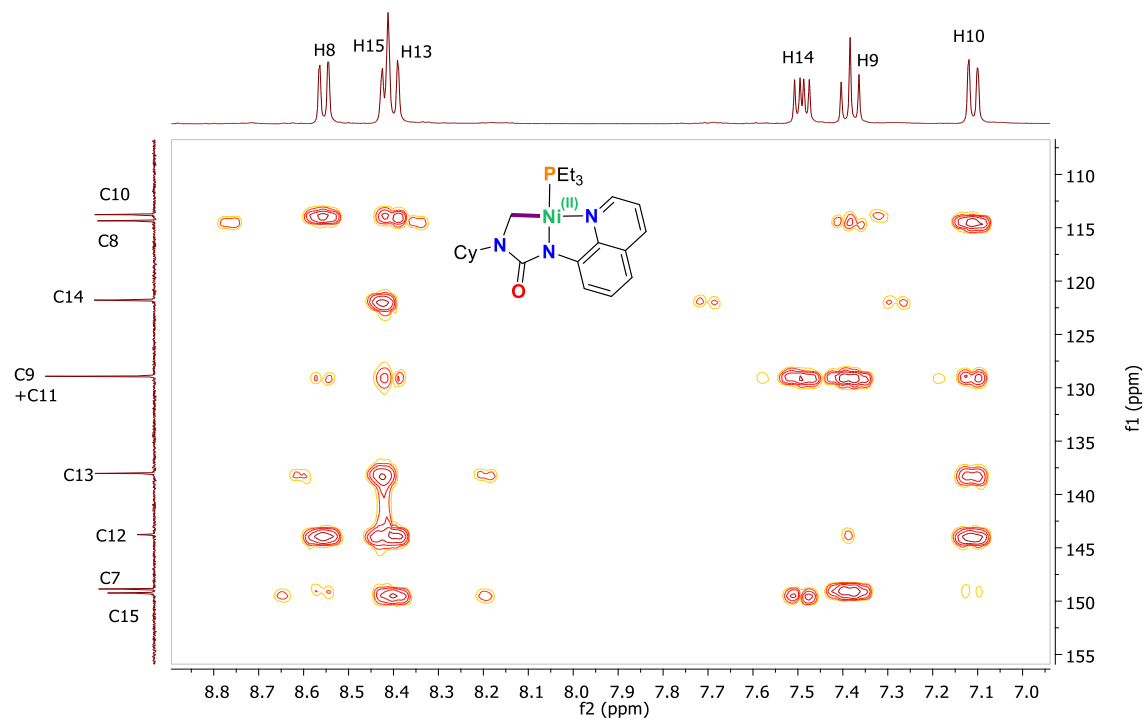


Figure A.2.11. ^{13}C - ^1H (HMBC) NMR spectrum (expanded) of (2.2-Ni) (400 MHz, d_6 -DMSO, 298K)

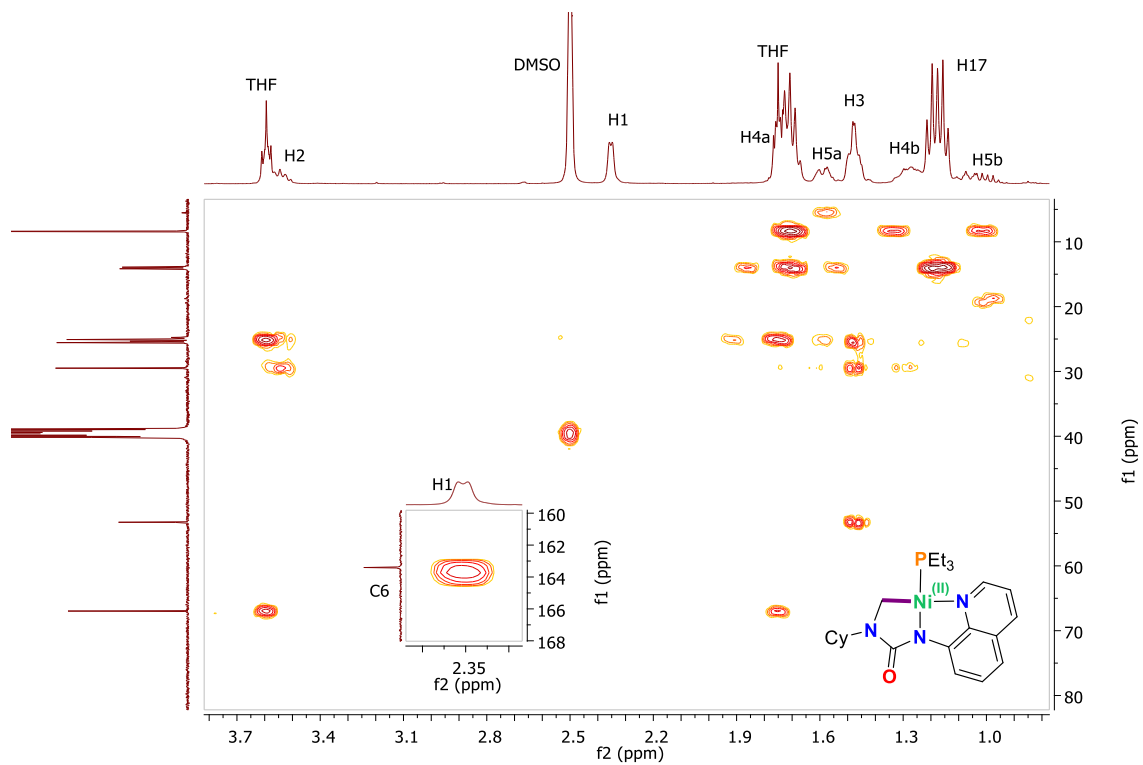


Figure A.2.12. ^{13}C - ^1H (HMBC) NMR spectrum (expanded) of (2.2-Ni) (400 MHz, d_6 -DMSO, 298K)

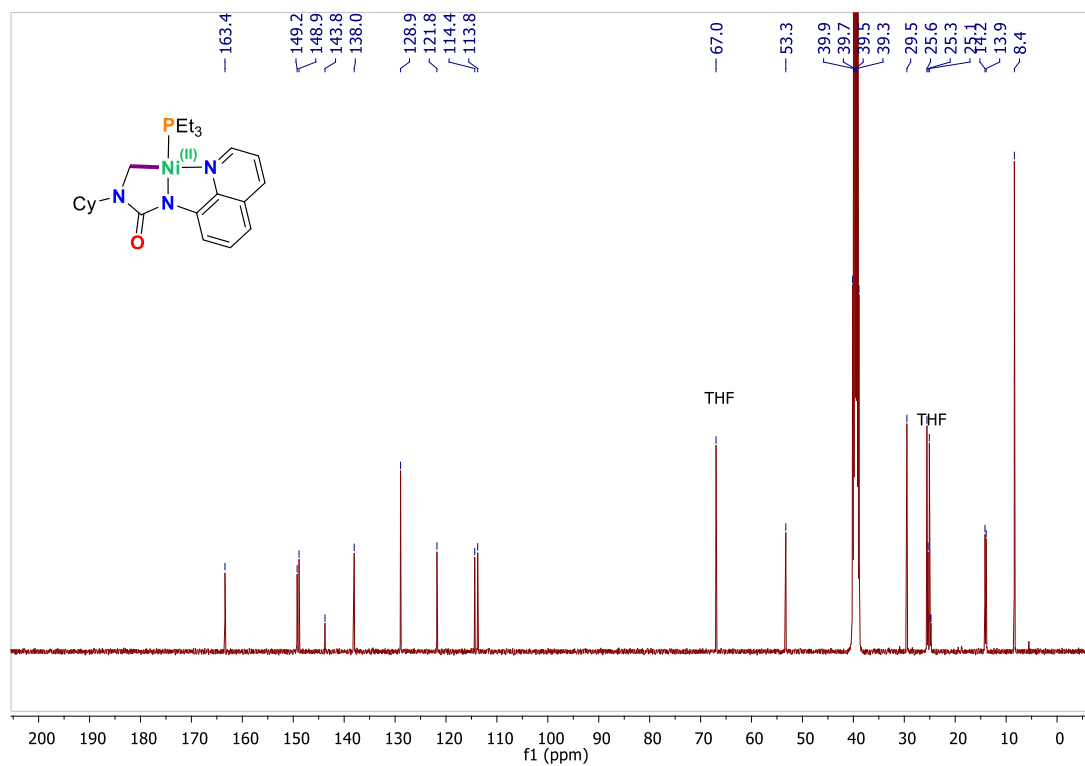
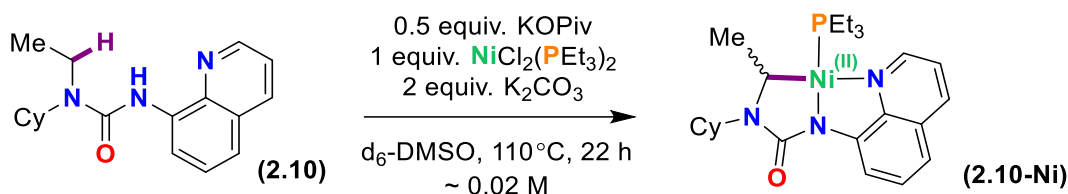


Figure A.2.13. $^{13}\text{C}\{^1\text{H}\}$ NMR spectrum of (2.2-Ni) (101 MHz, d_6 -DMSO, 298K)

Examples of In situ NMR Spec. Characterization of Nickelated Complexes

See *J. Am. Chem. Soc.* **2018**, *140*, 12602-12610] for remainder of spectra.



Characteristic signals of (2.10-Ni):

^1H NMR (400 MHz, $\text{d}_6\text{-DMSO}$) δ 8.46 (dd, $J = 7.8, 0.8$ Hz, 1H), 8.38 (eclipsed, 2H), 7.45 (dd, $J = 8.1, 5.0$ Hz, 1H), 7.37 (apparent t, $J = 7.9$ Hz, 1H), 7.08 (d, $J = 7.4$ Hz, 1H), ~ 3.42 (m, N-CH(Cy), 1H), ~ 2.68 (m, Ni-CH, 1H), 1.37 (d, $J = 6.2$ Hz, Ni-CH-CH₃, 3H). ^{13}C - ^1H (HSQC, HMBC) NMR (400 MHz, $\text{d}_6\text{-DMSO}$) δ ~ 163.5 (N(C=O)N), ~ 54.4 (N-CH(Cy)), ~ 37.1 (Ni-CH), ~ 22.9 (Ni-CH-CH₃). ^{31}P NMR (162 MHz, $\text{d}_6\text{-DMSO}$) δ 18.3 (s, Ni-PEt₃).

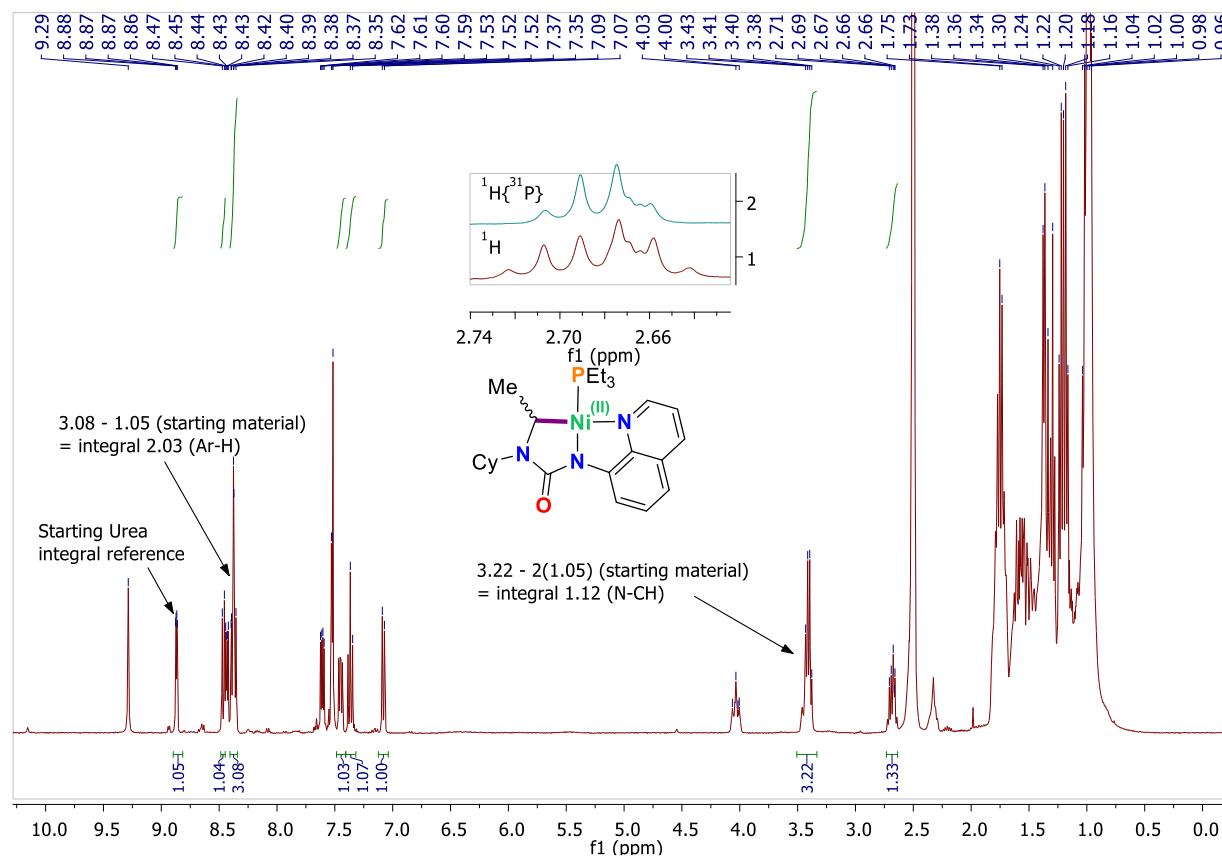


Figure A.2.14. In situ ^1H NMR spectrum of (2.10) and (2.10-Ni) (400 MHz, $\text{d}_6\text{-DMSO}$, 298K). The $^1\text{H}\{^{31}\text{P}\}$ NMR spectrum is shown in the inset.

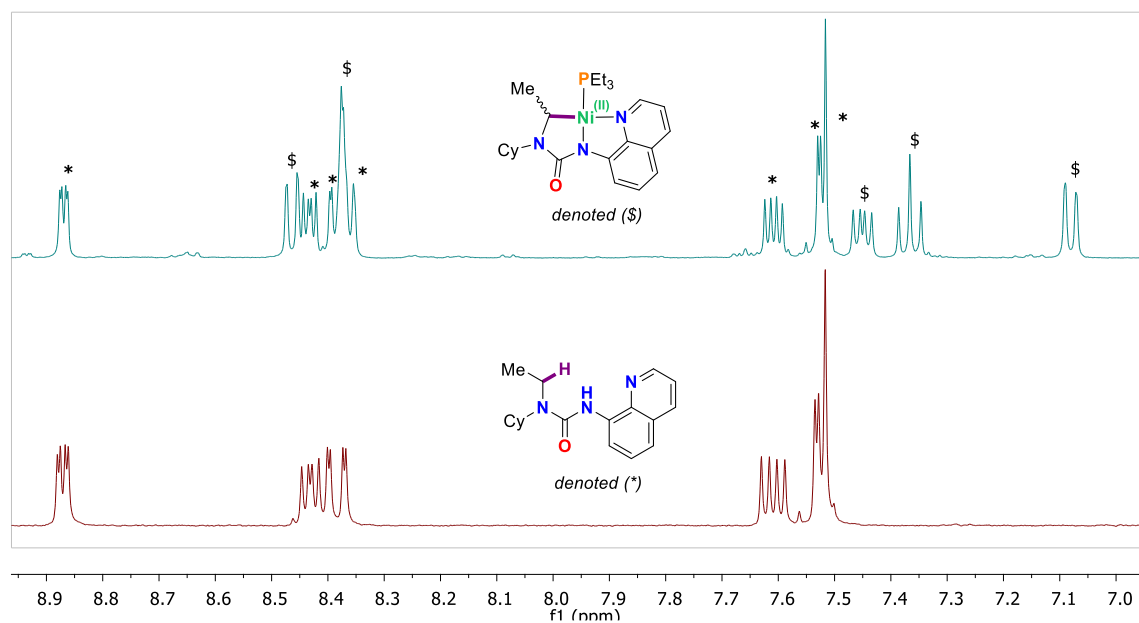


Figure A.2.15. Stacked ¹H NMR spectrum of (a) in situ reaction mixture containing (2.10, denoted *) and (2.10-Ni, denoted \$), and (b) isolated compound (2.10); (400 MHz, d₆-DMSO, 298K).

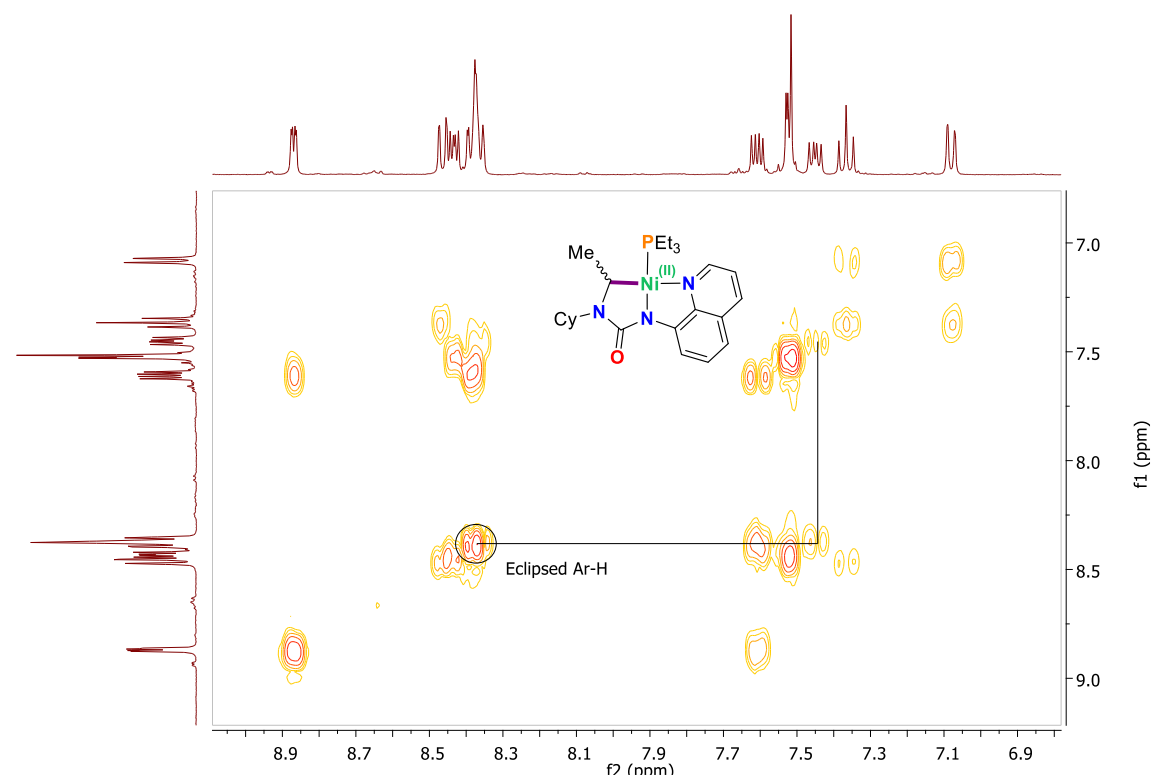


Figure A.2.16. In situ (expanded) ¹H COSY NMR spectrum of (2.10) and (2.10-Ni) (400 MHz, d₆-DMSO, 298K)

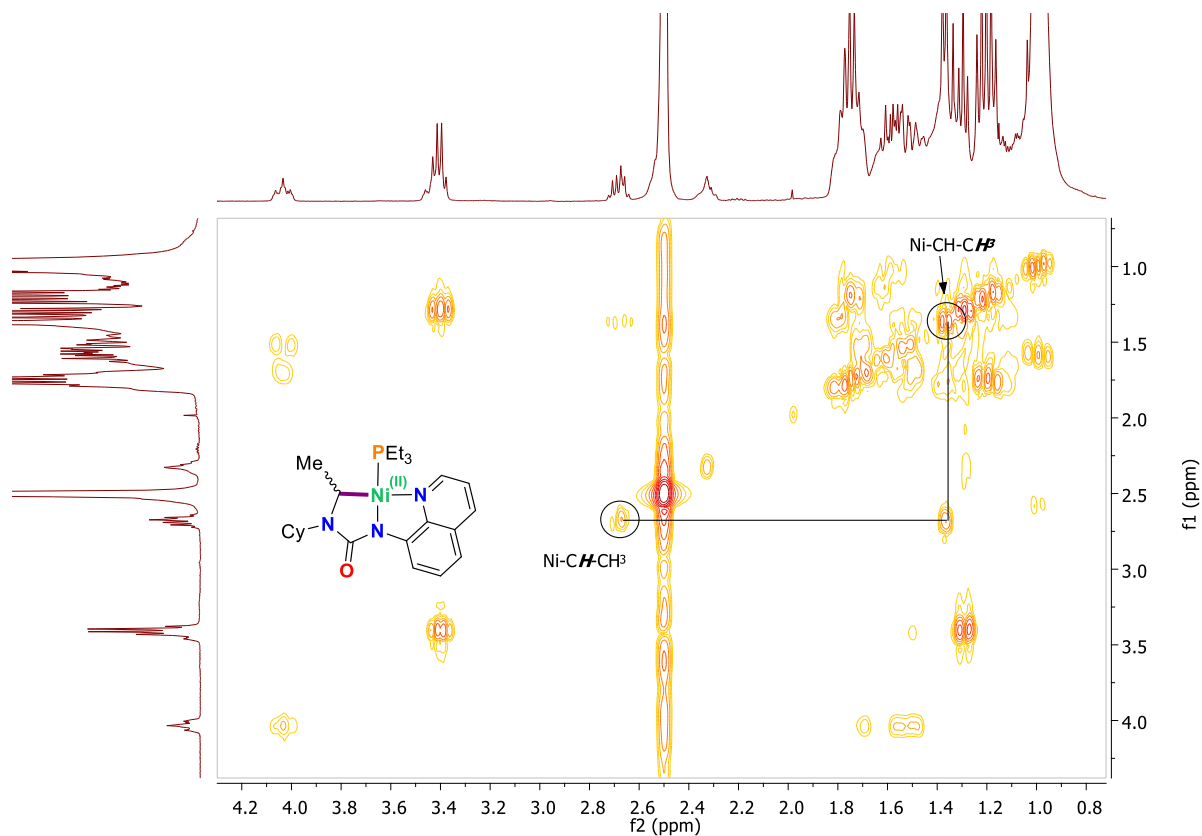


Figure A.2.17. In situ ¹H COSY NMR spectrum of (2.10) and (2.10-Ni) (400 MHz, d₆-DMSO, 298K)

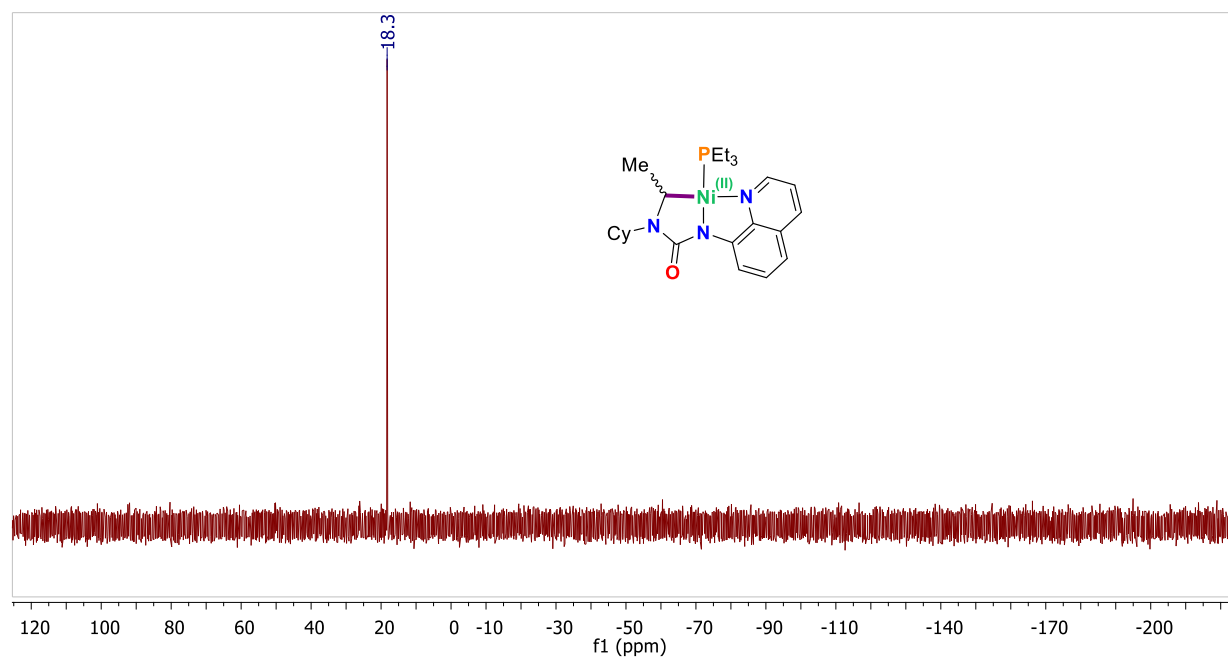


Figure A.2.18. In situ ³¹P{¹H} NMR spectrum of (2.10) and (2.10-Ni) (162 MHz, d₆-DMSO, 298K)

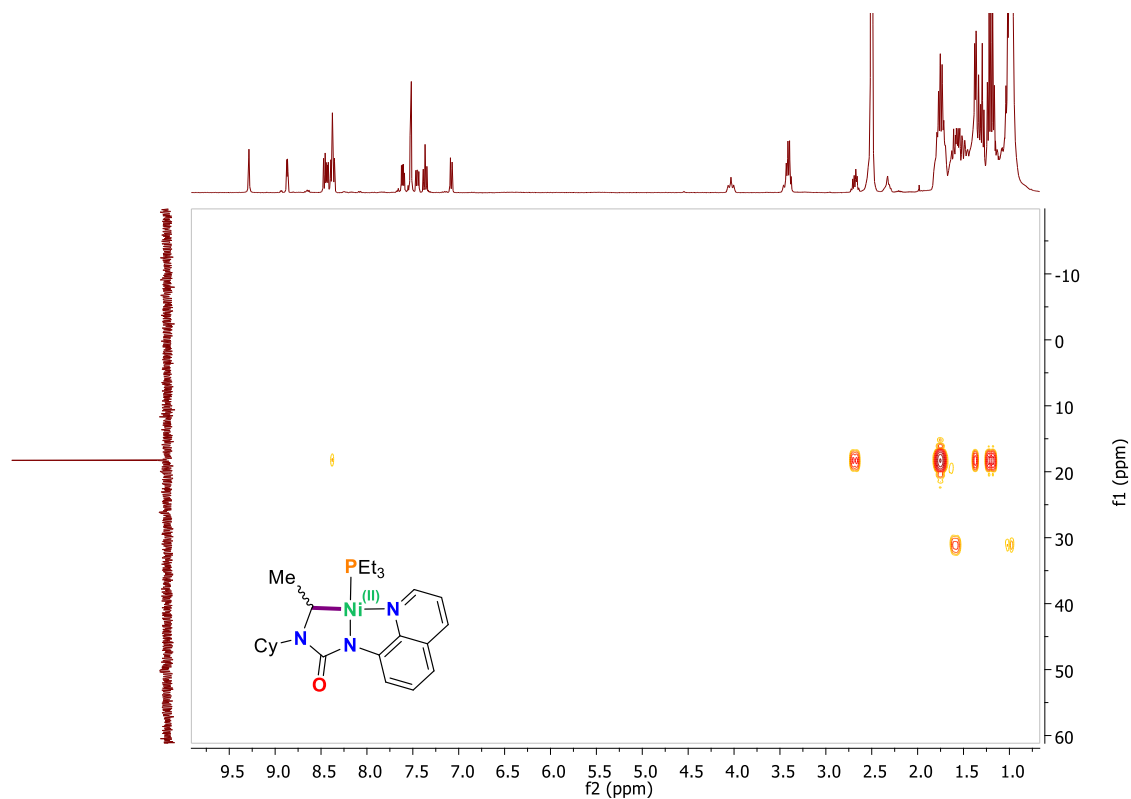


Figure A.2.19. In situ ^1H - ^{31}P (HMBC) NMR spectrum of (2.10) and (2.10-Ni) (400 MHz, $\text{d}_6\text{-DMSO}$, 298K)

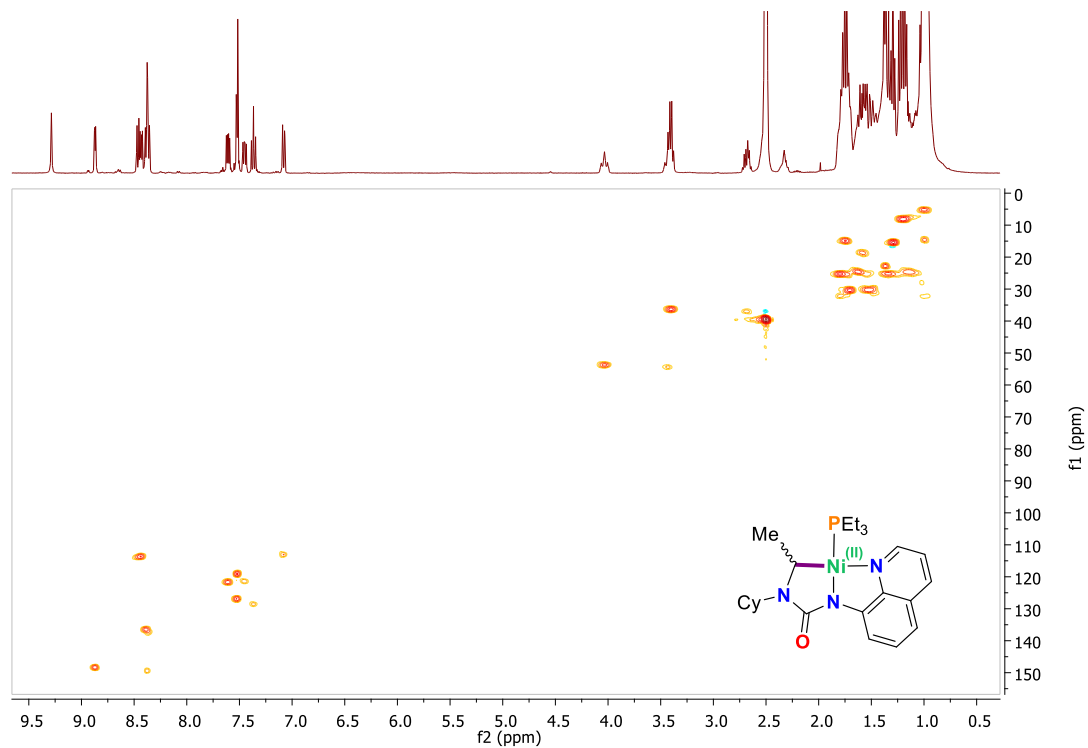


Figure A.2.20. In situ ^{13}C - ^1H (HSQC-edited) NMR spectrum of (2.10), (2.10-Ni) (400 MHz, $\text{d}_6\text{-DMSO}$, 298K)

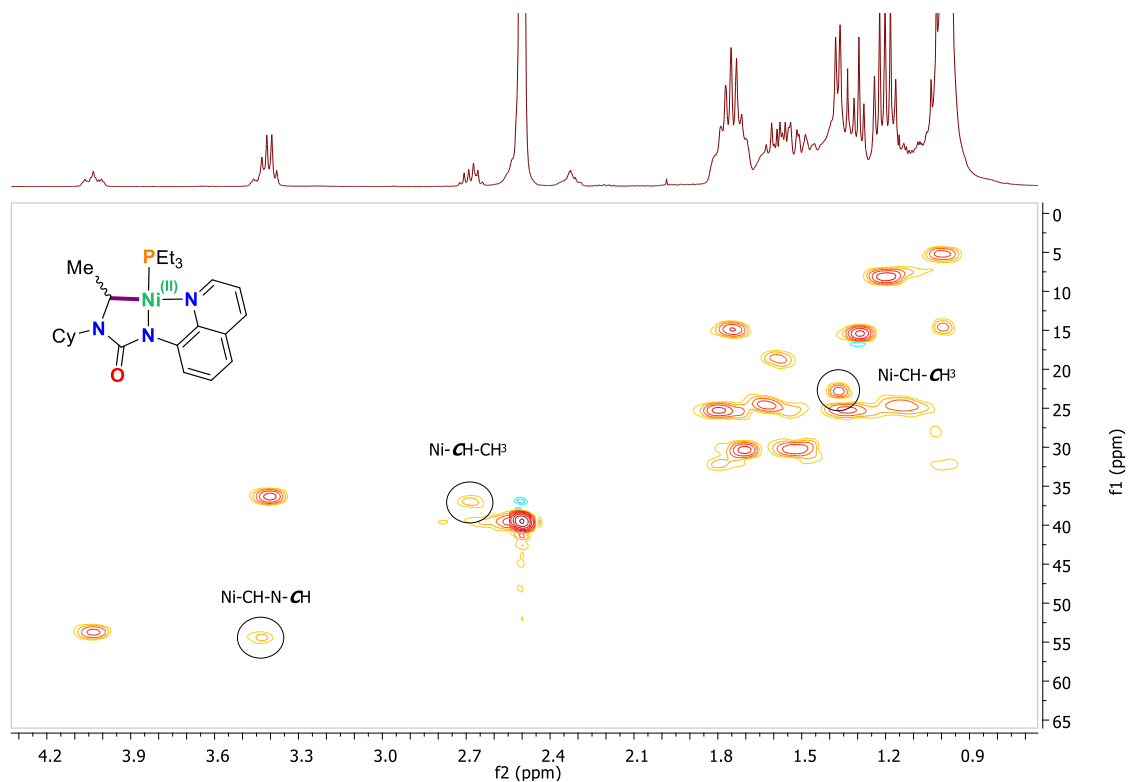


Figure A.2.21. In situ ^{13}C - ^1H (HSQC) NMR spectrum of (2.10) and (2.10-Ni) (400 MHz, d_6 -DMSO, 298K).

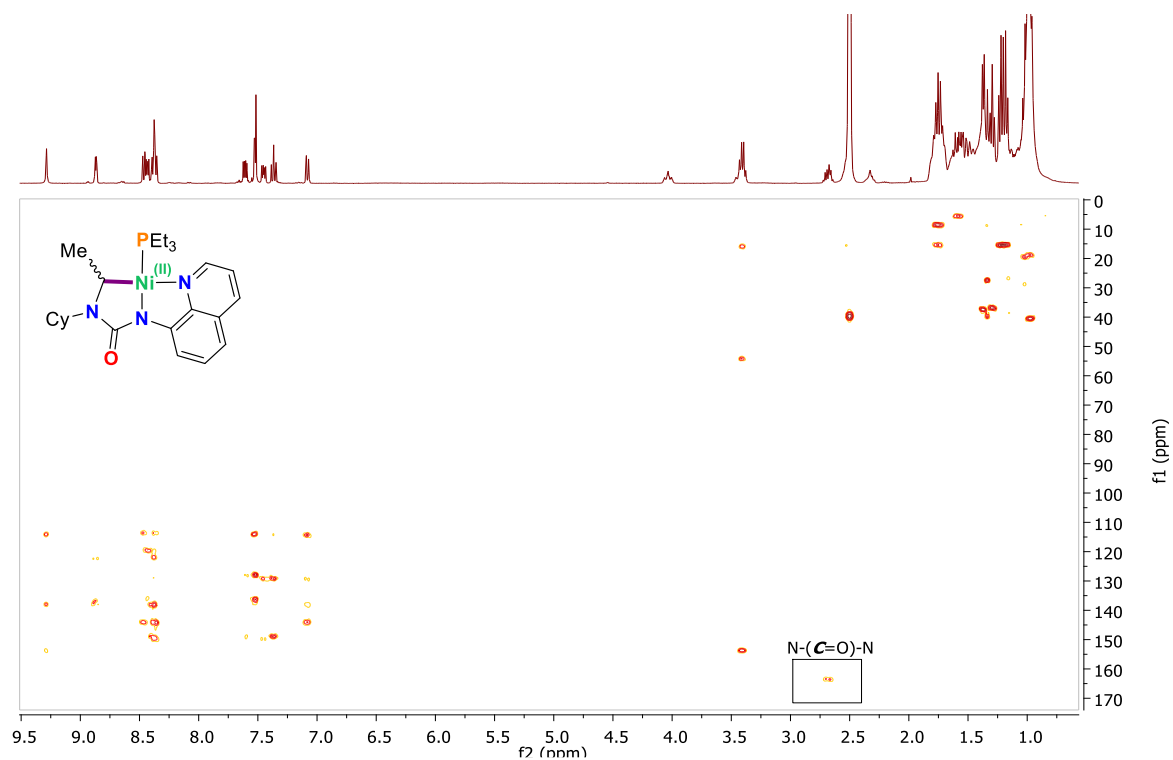
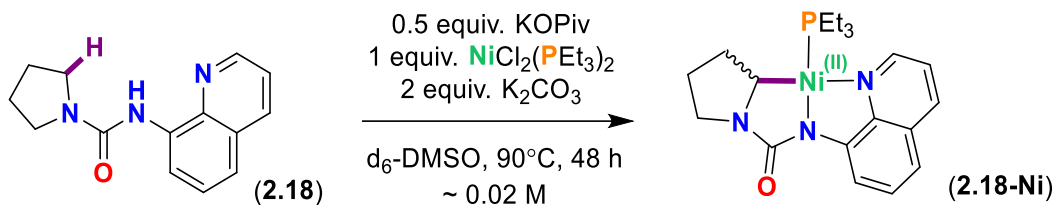


Figure A.2.22. In situ ^{13}C - ^1H (HMBC) NMR spectrum of (2.10) and (2.10-Ni) (400 MHz, d_6 -DMSO, 298K).



Characteristic signals of (2.18-Ni):

^1H NMR (400 MHz, $\text{d}_6\text{-DMSO}$) δ 8.51 (d, $J = 7.7$ Hz, 1H), 8.43 (d, $J = 6.2$ Hz, 1H), 7.40 (app. t, $J = 7.9$ Hz, 1H), 7.14 (d, $J = 7.8$ Hz, 1H), 3.37-3.25 (m, 1H), 2.80-2.70 (m, 1H), 2.33-2.25 (m, Ni-CH, 1H). ^{13}C - ^1H (HSQC, HMBC) NMR (400 MHz, $\text{d}_6\text{-DMSO}$) δ ~ 166.3 (N(C=O)N), ~ 44.0 (Cd), ~ 43.7 (Ca), ~ 30.8 (Cb), ~ 24.5 (Cc) ^{31}P NMR (162 MHz, $\text{d}_6\text{-DMSO}$) δ 19.0 (s, Ni- PEt_3).

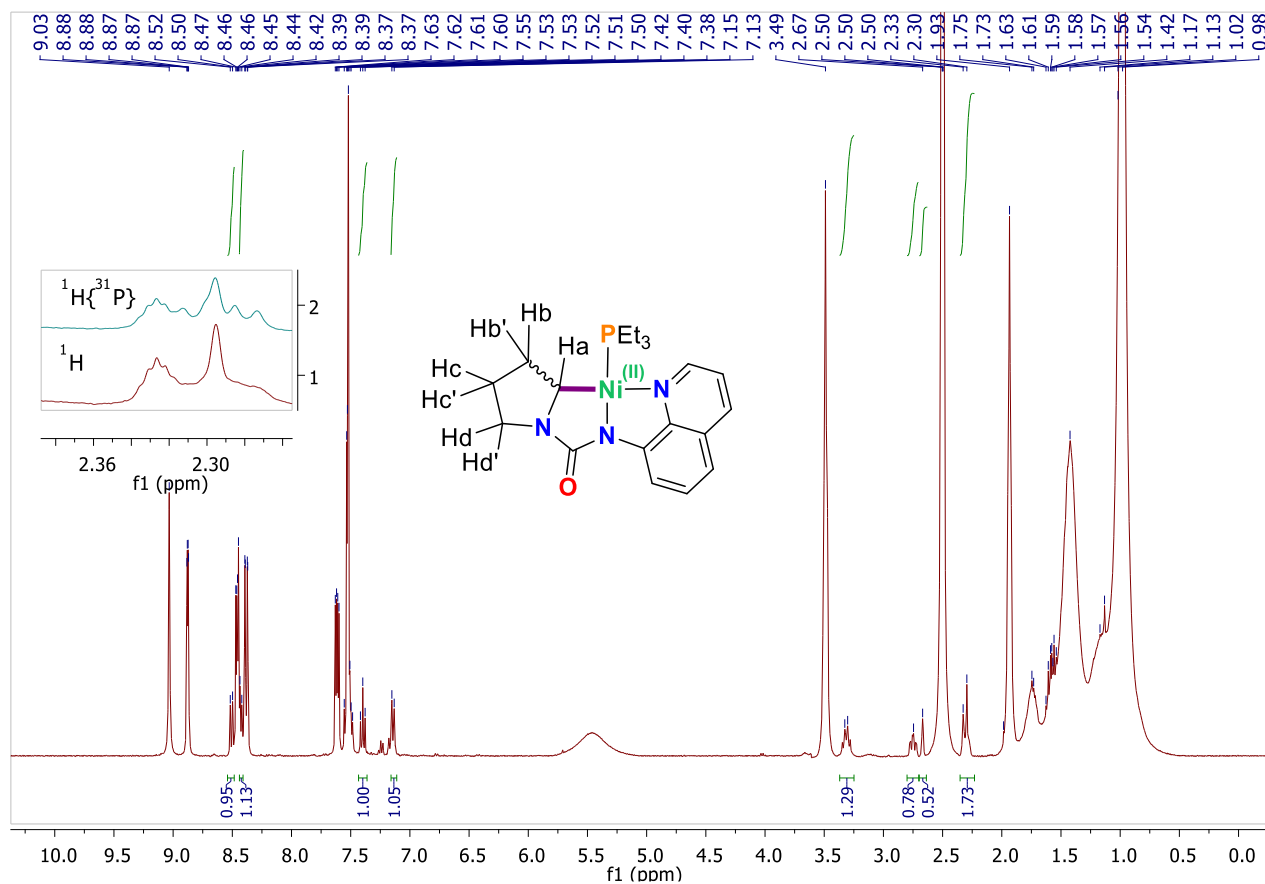


Figure A.2.23. In situ ^1H NMR spectrum of (2.18) and (2.18-Ni) (400 MHz, $\text{d}_6\text{-DMSO}$, 298K). The $^1\text{H}\{^{31}\text{P}\}$ NMR spectrum is shown in the inset.

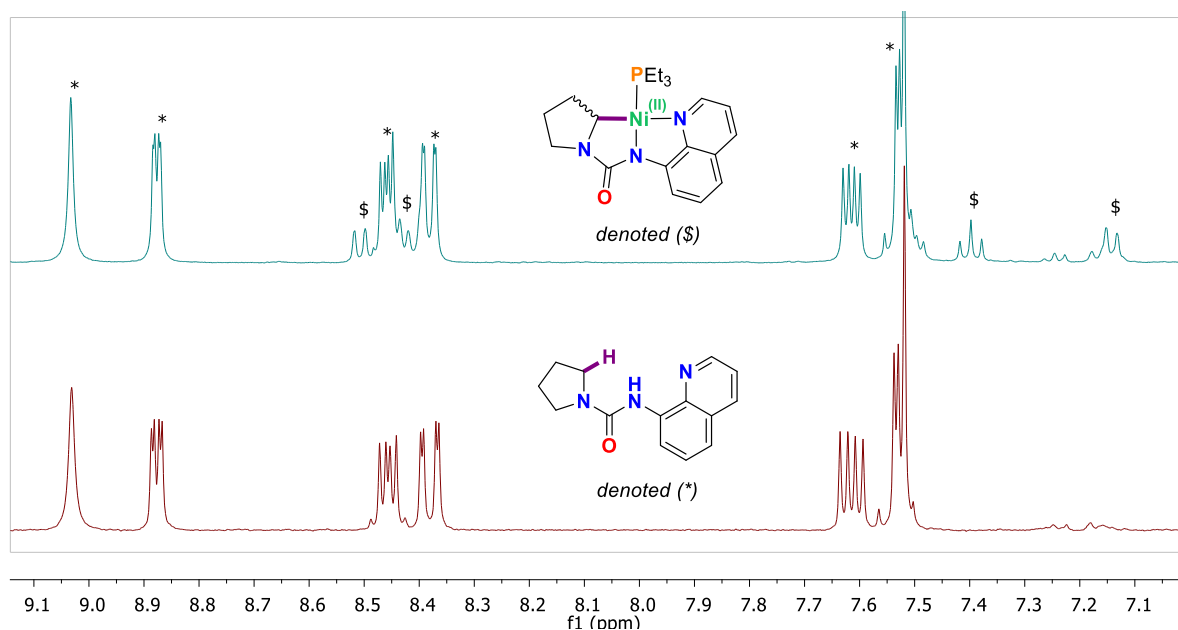


Figure A.2.24. Stacked ^1H NMR spectrum of (a) in situ reaction mixture containing (2.18, denoted *) and (2.18-Ni, denoted \$), and (b) isolated compound (2.18); (400 MHz, $\text{d}_6\text{-DMSO}$, 298K).

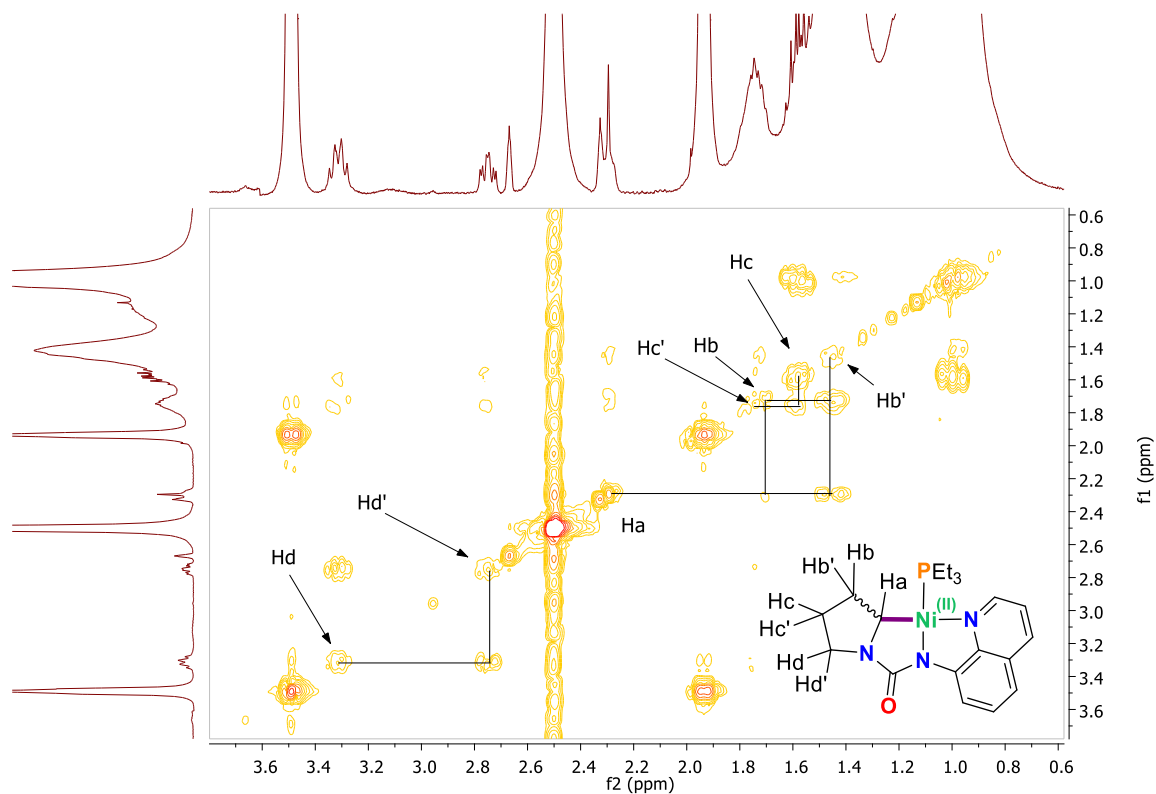


Figure A.2.25. In situ (expanded) ^1H COSY NMR spectrum of (2.18) and (2.18-Ni) (400 MHz, $\text{d}_6\text{-DMSO}$, 298K).

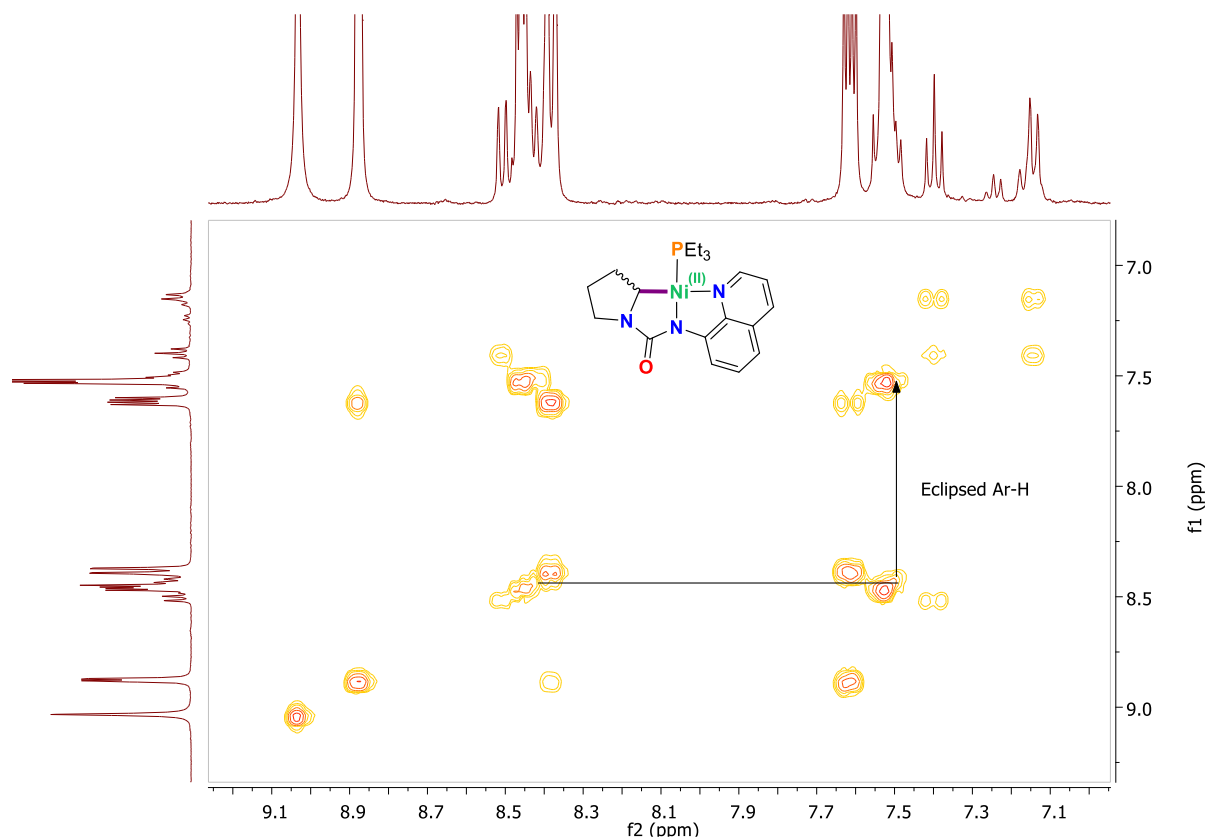


Figure A.2.26. In situ ^1H COSY NMR spectrum of (2.18) and (2.18-Ni) (400 MHz, $\text{d}_6\text{-DMSO}$, 298K)

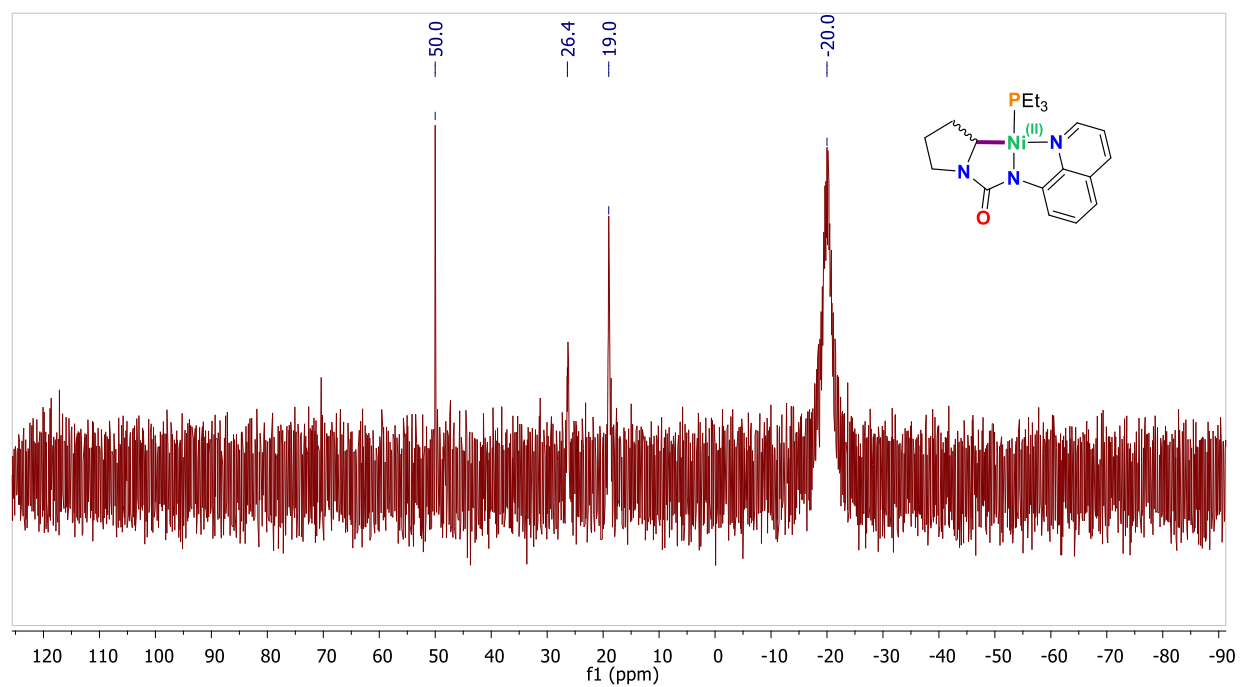


Figure A.2.27. In situ $^{31}\text{P}\{^1\text{H}\}$ NMR spectrum of (2.18) and (2.18-Ni) (162 MHz, $\text{d}_6\text{-DMSO}$, 298K).

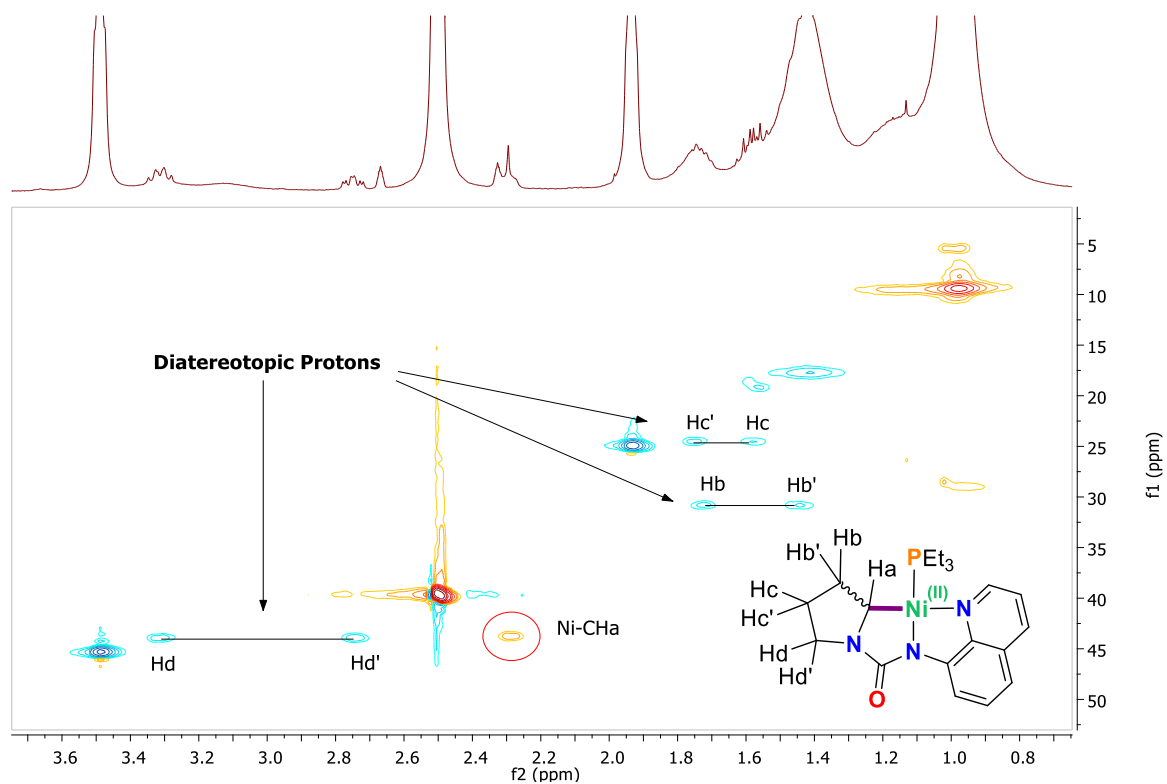


Figure A.2.28. In situ ^{13}C - ^1H (HSQC-edited) NMR spectrum of (2.18), (2.18-Ni) (400 MHz, d_6 -DMSO, 298K).

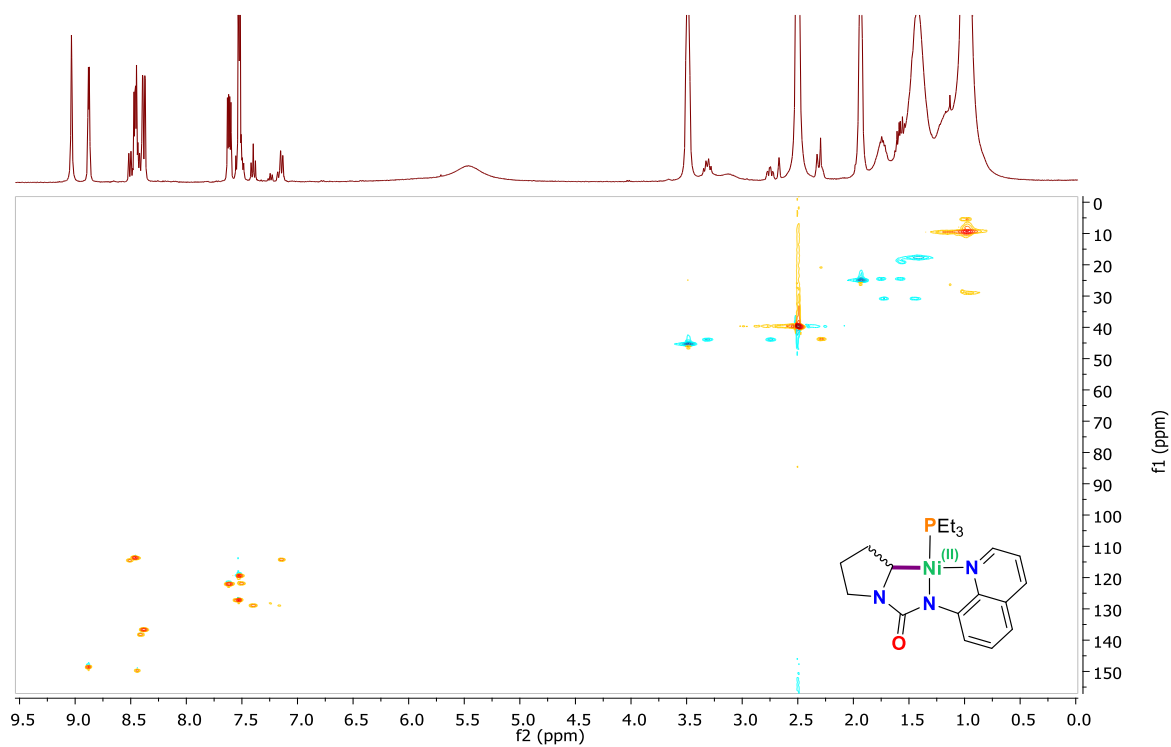


Figure A.2.29. In situ ^{13}C - ^1H (HSQC-edited) NMR spectrum of (2.18), (2.18-Ni) (400 MHz, d_6 -DMSO, 298K).

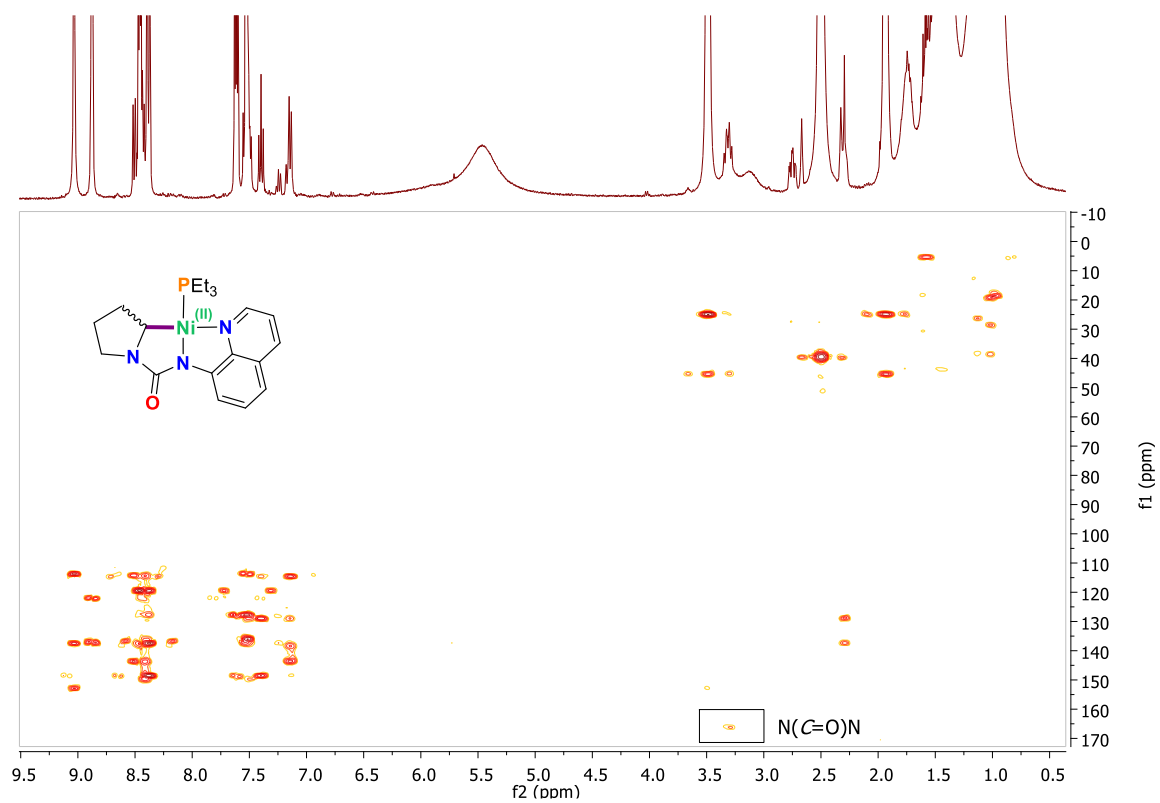
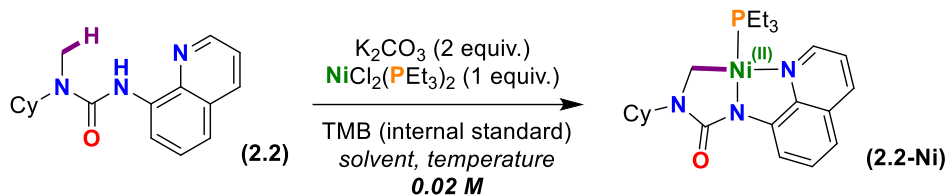


Figure A.2.30. In situ ^{13}C - ^1H (HMBC) NMR spectrum of (2.18) and (2.18-Ni) (400 MHz, d_6 -DMSO, 298K).

Example of reaction progress kinetics, Experimental Setup



In a glovebox, urea (**2.2**) (4.0 mg, 0.014 mmol), K_2CO_3 (3.9 mg, 0.028 mmol), and $\text{NiCl}_2(\text{PEt}_3)_2$ (5.1 mg, 0.014 mmol) were weighed into separate 5 mL scintillation vials. These components were mixed with solvent (0.7 mL), and added to a J-Young NMR tube for spectroscopic analysis.

TMB was weighed as standard solutions in each solvent (mass%) (1.0-1.7 mg, 0.0060-0.0010 mmol).

In the case of reactions in DMSO:

TMB was weighed as a 2.24% (mass %) solution in d_6 -DMSO.

$\text{NiCl}_2(\text{PEt}_3)_2$ was weighed as a 2.45% (mass %) solution in d_6 -DMSO.

KOPiv was weighed as a 1.08% (mass %) solution in d_6 -DMSO.

Notes: All ^1H NMR spectra in a kinetic series were processed in an identical manner. In the presence of nickel, substrates (**2.10**) and (**2.17** to **2.20**) are fluxional at higher temperatures, precluding accurate integrations using variable-temperature (VT) NMR studies. Thus, these kinetic data were collected by heating intervals using an oil-bath. All other kinetic data sets for substrates were obtained using VT-NMR studies.

Example of reaction progress kinetics, ^1H NMR spectra:

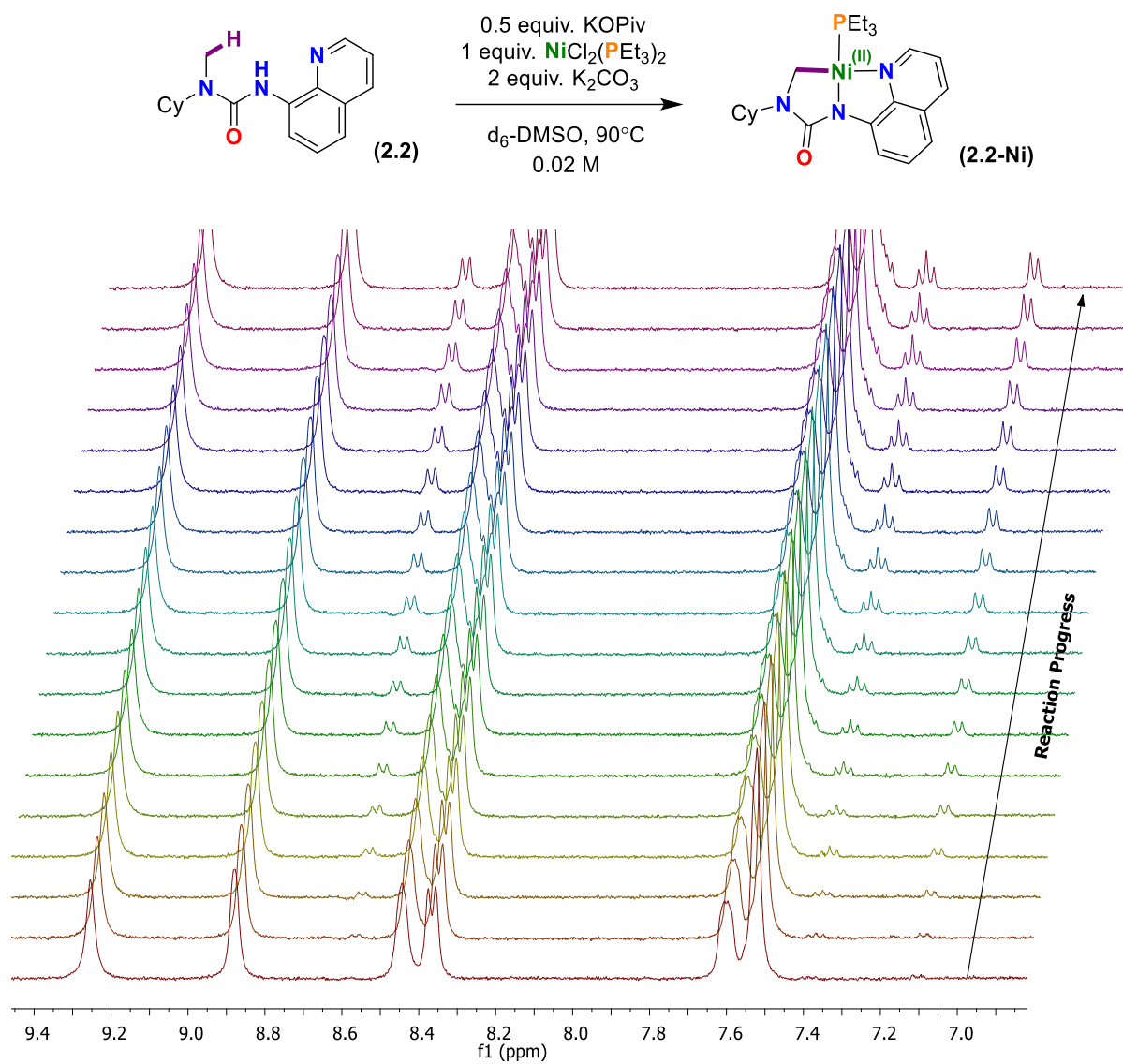


Figure A.2.31. In situ ^1H NMR spectra showing reaction progress of (2.2) converting to (2.2-Ni) (400 MHz, $\text{d}_6\text{-DMSO}$, 298K).

Example of Solvent Effects

(i) Dimethylsulfoxide (DMSO)

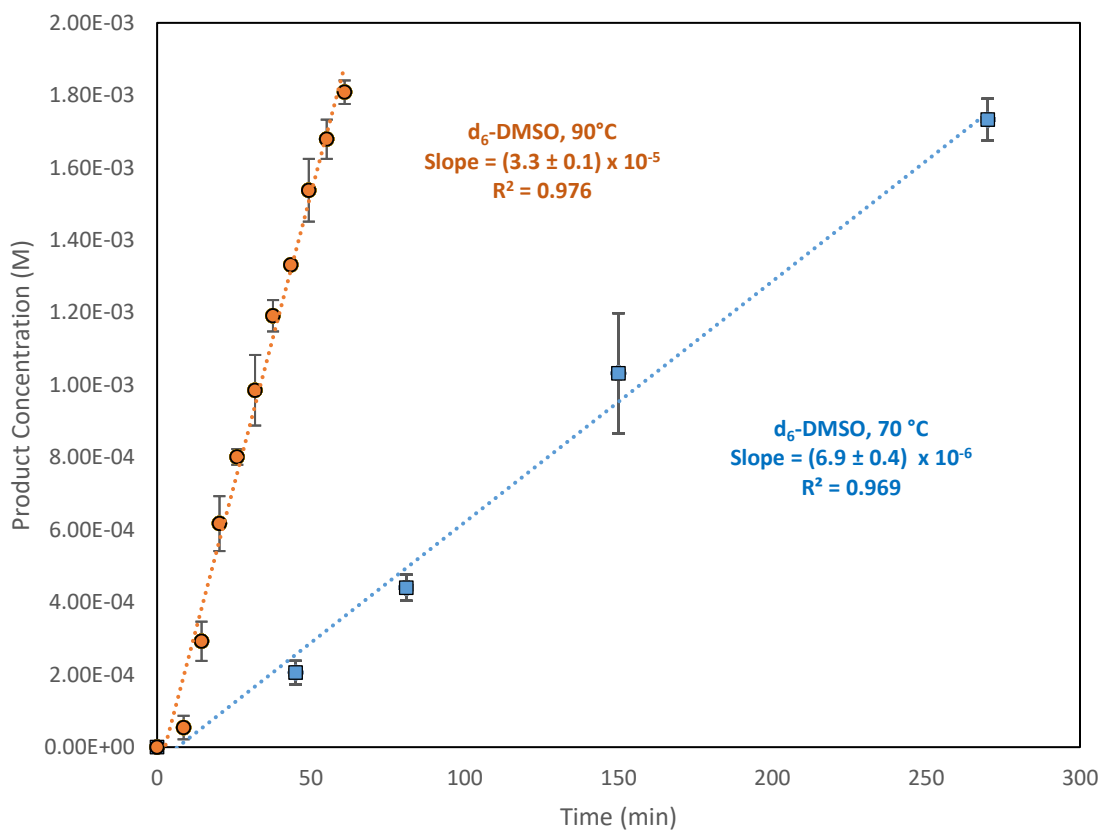
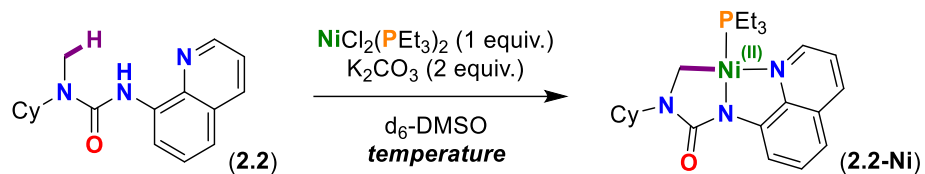


Figure A.2.32. Kinetic profile for conversion of (2.2) to (2.2-Ni) in d_6 -DMSO over time (M/min).

Example of Additive Effects

Other additive effects of (2.2) to (2.2-Ni)

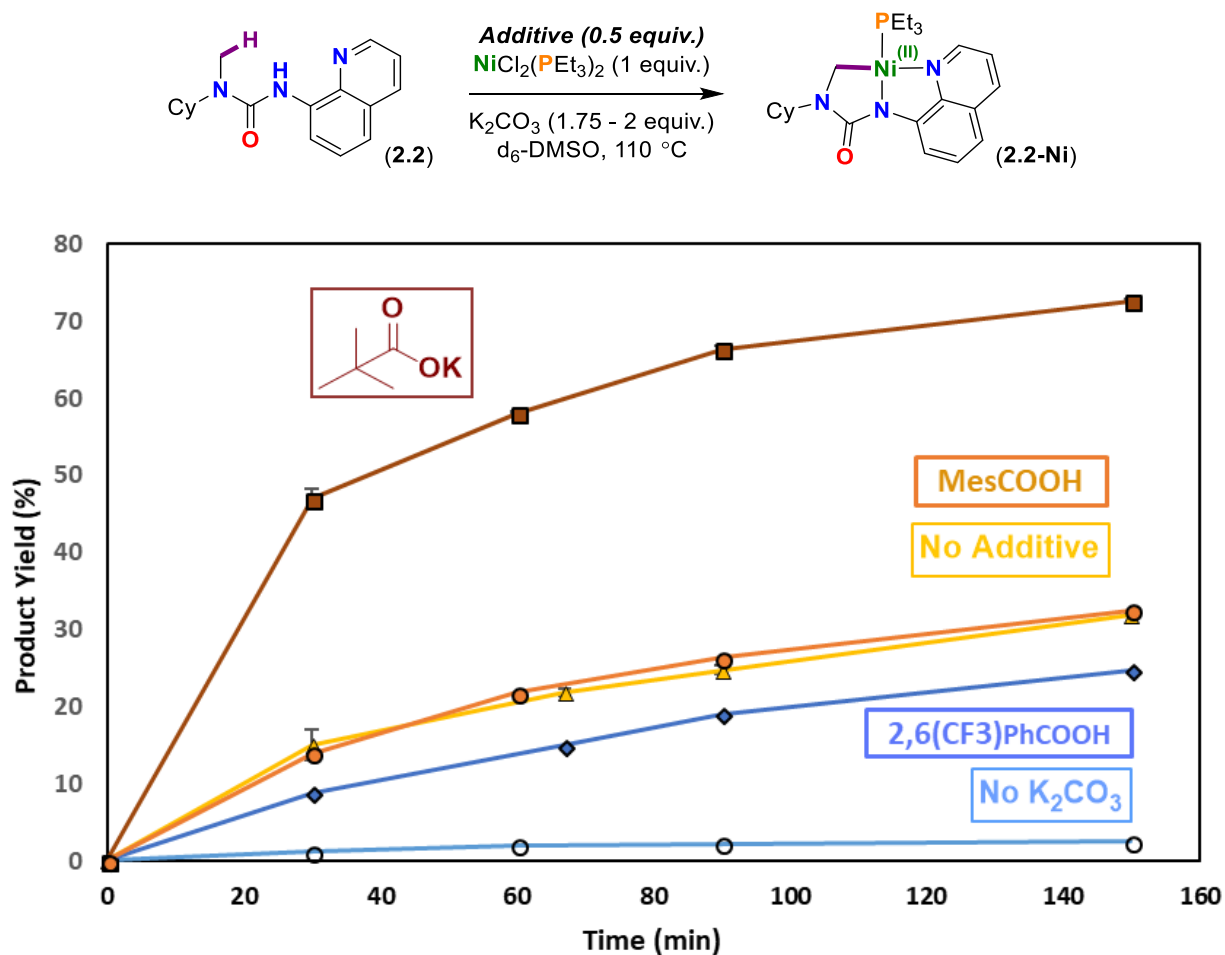


Figure A.2.33. For (i) acid additives, 2.0 molar equivalents K_2CO_3 , (ii) potassium salts, 1.75 molar equivalents K_2CO_3 . **Legend:** \circ No additive, or K_2CO_3 , Δ K_2CO_3 added (no additive); \bullet 2,4,6-trimethylbenzoic acid additive; \blacklozenge 2,6-bis(trifluoromethyl)benzoic acid additive; \blacksquare KOPiv additive.

Examples of Substituent Effects

See *J. Am. Chem. Soc.* **2018**, *140*, 12602-12610] for remainder of kinetic plots

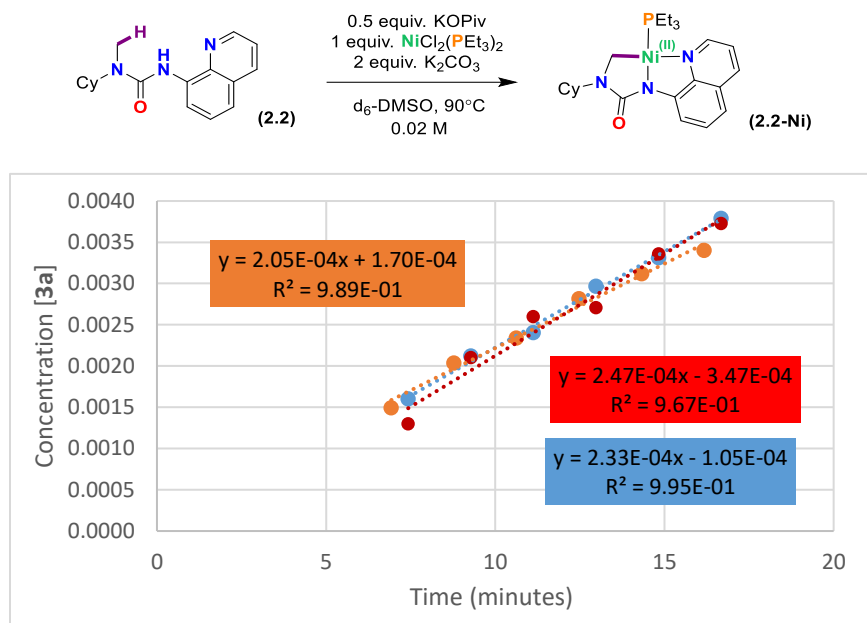


Figure A.2.34. Kinetic profile for conversion of (2.2) to (2.2-Ni) over time (M/min).

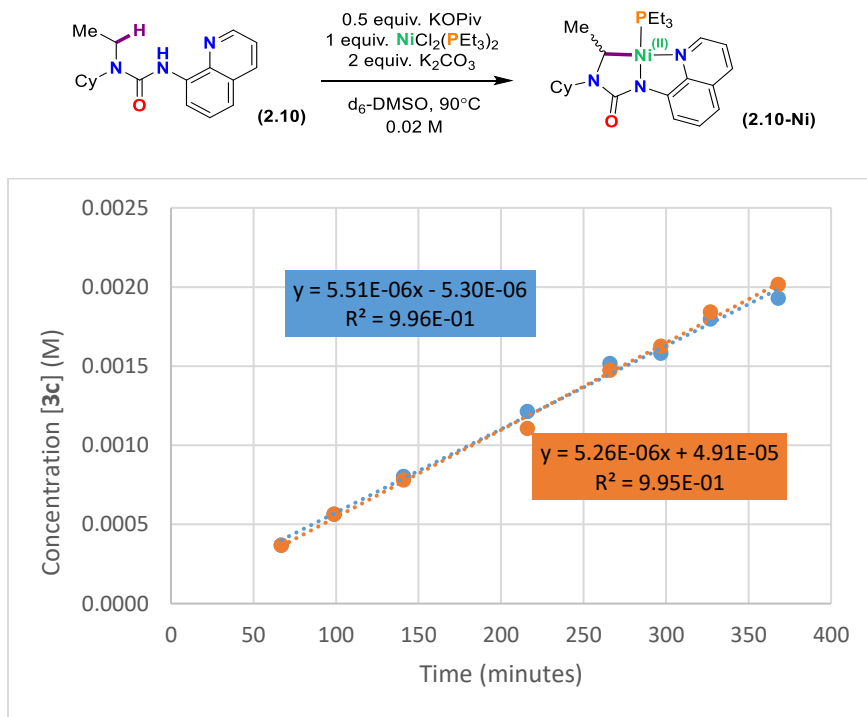


Figure A.2.35. Kinetic profile for conversion of (2.10) to (2.10-Ni) over time (M/min).

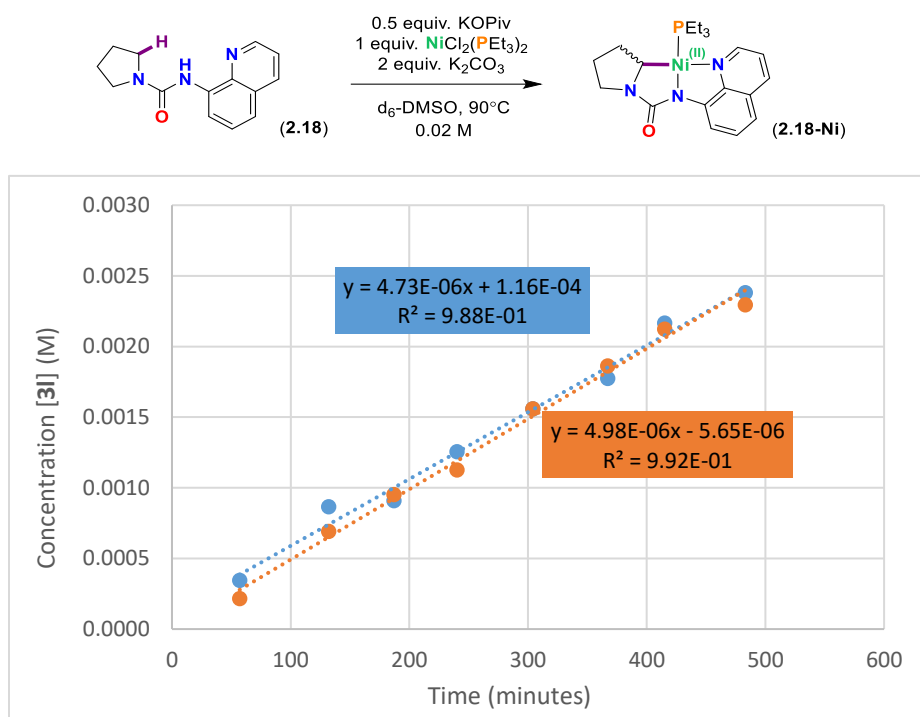
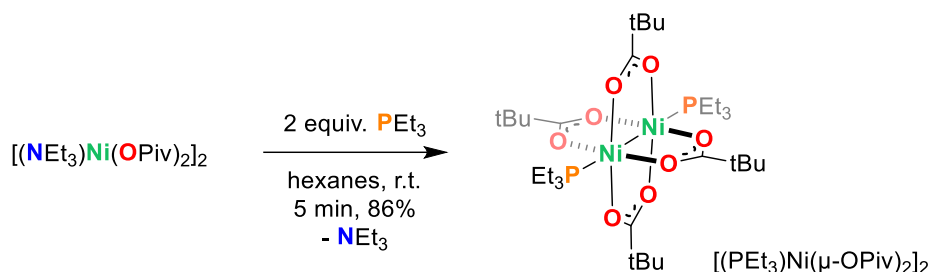


Figure A.2.36. Kinetic profiles for conversion of (2.18) to (2.18-Ni) over time (M/min).

Mechanistic Experiments

Synthesis and Characterization of Ni(II) Paddlewheel $[(\text{PEt}_3)\text{Ni}(\mu\text{-OPiv})_2]_2$



In a glovebox, $[(\text{NEt}_3)\text{Ni}(\text{OPiv})_2]_2$ ^[266] (500 mg, 0.690 mmol) was weighed into a 20 mL scintillation vial, to which hexanes (4 mL) and a stir bar were added. The contents were then stirred for 1 minute at room temperature. During this period, PEt_3 (180 mg, 1.52 mmol) was weighed into a 5 mL scintillation vial and diluted with hexanes (2 mL). The phosphine-hexanes solution was then added dropwise to the solution of nickel(II) over a period of 1 minute. After 5 minutes of stirring at room temperature, the contents were filtered through Celite[®] into a 20 mL scintillation vial, and cooled in the glovebox freezer (-35°C) to afford large X-ray quality green crystals of $[(\text{PEt}_3)\text{Ni}(\mu\text{-OPiv})_2]_2$ in 5 minutes. The vial was decanted, and the crystals were dried in vacuo to afford analytically pure $[(\text{PEt}_3)\text{Ni}(\mu\text{-OPiv})_2]_2$ (86%, 450 mg, 0.59 mmol).

^1H NMR (400 MHz, 25°C , C_6D_6): δ 31.92 (br s, 12H), 3.67 (br s, 36H), 1.02 (br s, 18H). **EI-MS (m/z):** no characteristic fragments were observed. **Evans Method (C_6D_6 , 25°C):** $\mu_{\text{eff}} = 2.4 \mu_{\text{B}}$. **Anal. Calcd.** for $\text{C}_{32}\text{H}_{66}\text{Ni}_2\text{O}_8\text{P}_2$ (758). C, 50.69%; H, 8.77%. Found: C, 51.00%; H, 9.01.

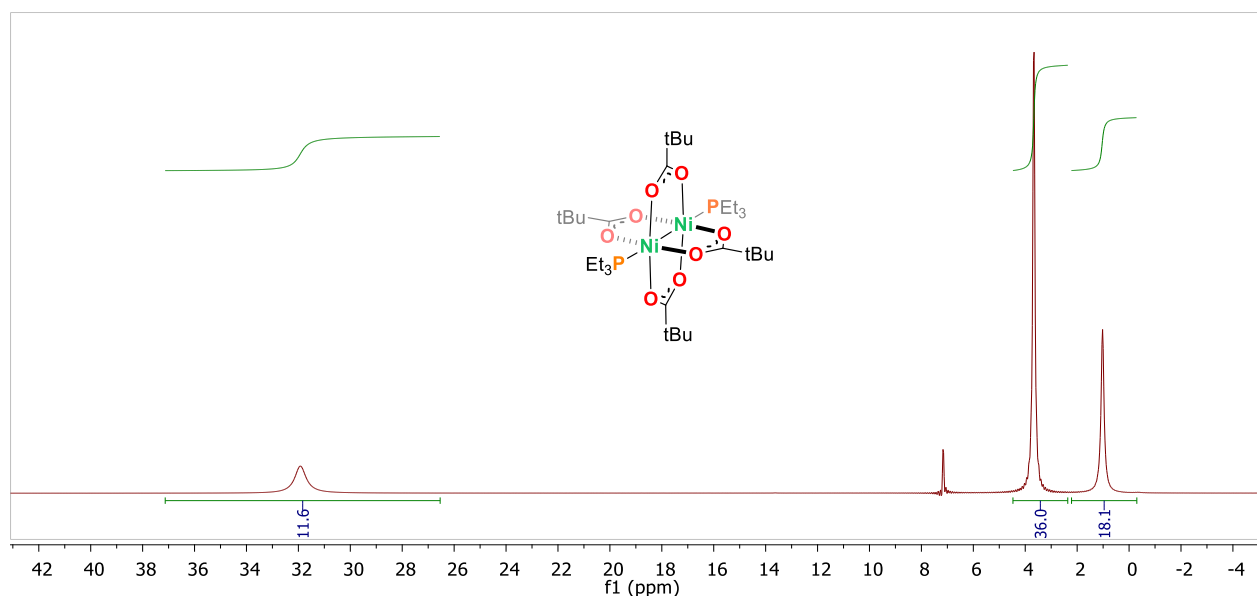


Figure A.2.37. $[(\text{PEt}_3)\text{Ni}(\mu\text{-OPiv})_2]_2$; *paramagnetic* ^1H NMR (400 MHz, C_6D_6 , 298K)

In situ Characterization of Complex $[(\text{PEt}_3)\text{Ni}(\mu\text{-OPiv})_2]_2$ from $\text{NiCl}_2(\text{PEt}_3)_2$

Below are stacked sets of NMR spectra for three samples:

Sample 1: $\text{NiCl}_2(\text{PEt}_3)_2$

Sample 2: $[(\text{PEt}_3)\text{Ni}(\mu\text{-OPiv})_2]_2$ synthesized independently

Sample 3: $\text{NiCl}_2(\text{PEt}_3)_2 + 2$ equiv. KOPiv ; mixed at room temperature

The stacked spectrum are shown in $\text{d}_6\text{-DMSO}$ & C_6D_6 and separated into stacks of ^1H , ^1H paramagnetic, and $^{31}\text{P}\{^1\text{H}\}$ stacked spectra. Additionally, pictures of the samples are shown beside the spectra.

Samples in d₆-DMSO:

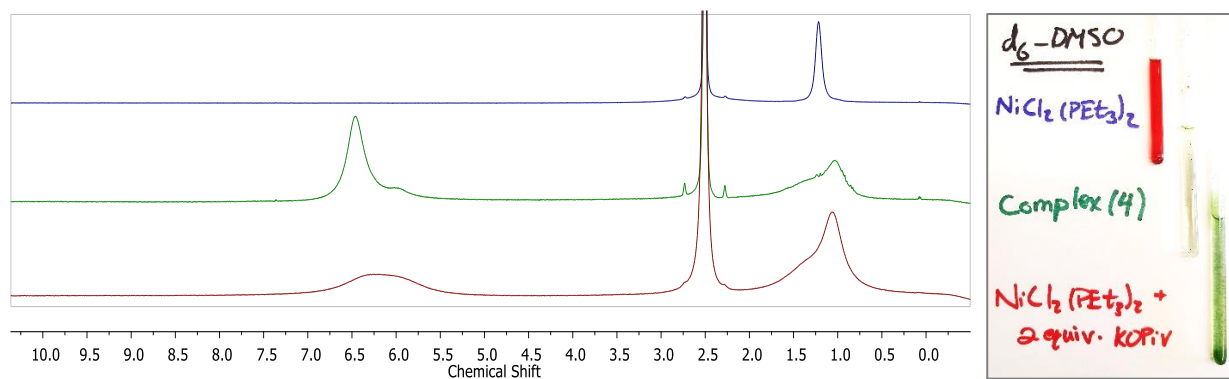


Figure A.2.38. ¹H NMR (300 MHz, d₆-DMSO, 298K)

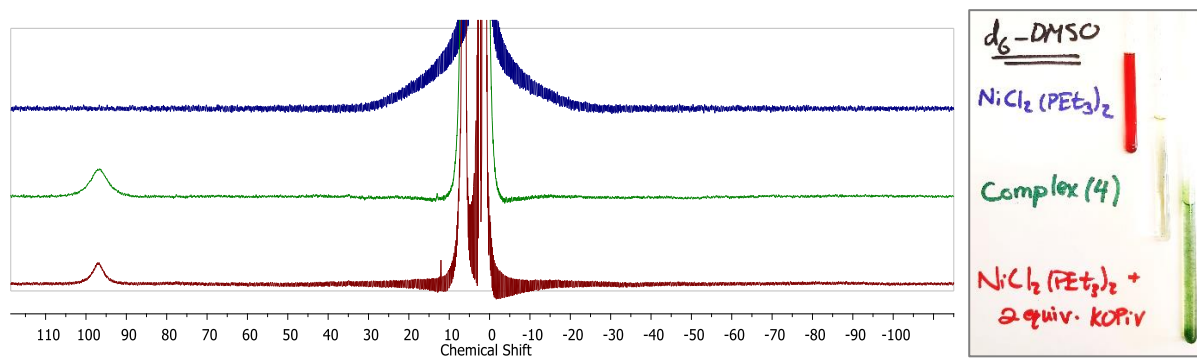


Figure A.2.39. ¹H paramagnetic NMR (300 MHz, d₆-DMSO, 298K)

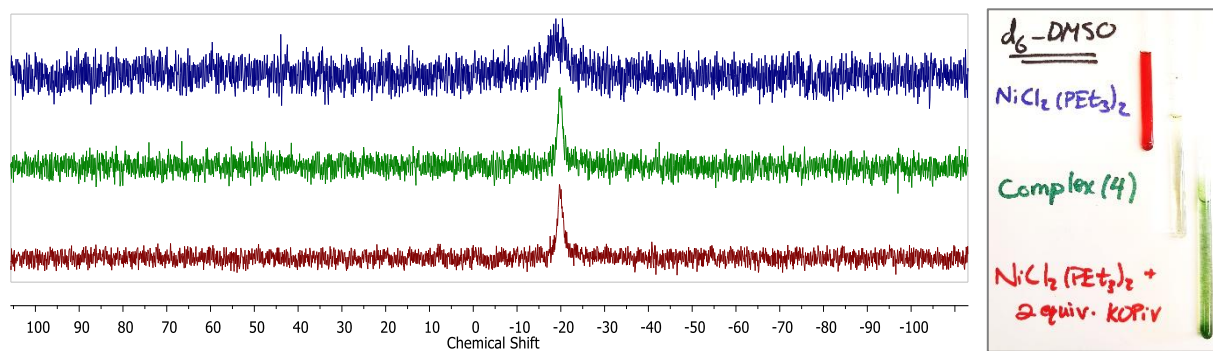


Figure A.2.40. ¹H NMR (300 MHz, d₆-DMSO, 298K)

Samples in C₆D₆:

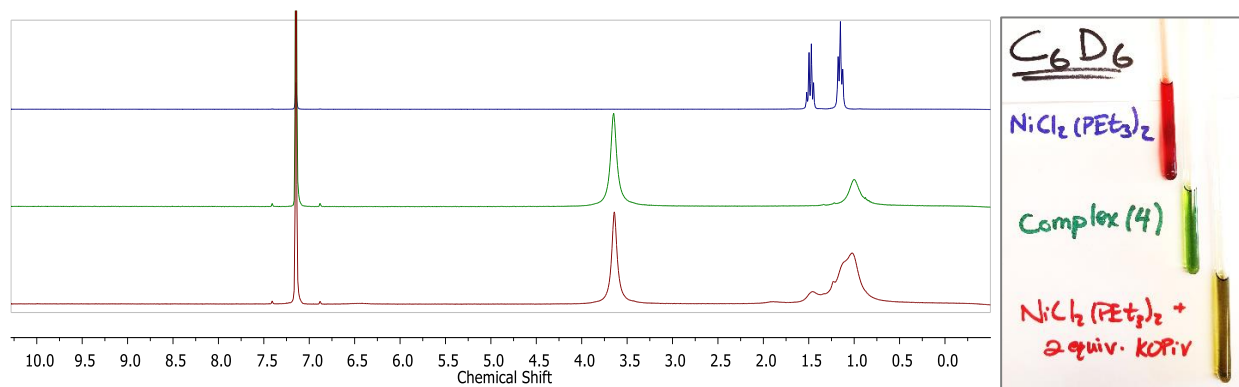


Figure A.2.41. ¹H NMR (300 MHz, C₆D₆, 298K)

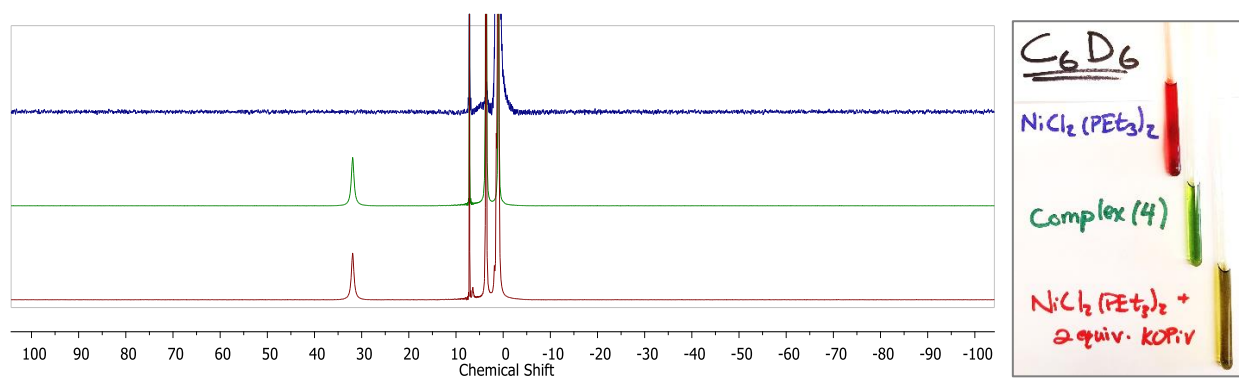


Figure A.2.42. ¹H paramagnetic NMR (300 MHz, C₆D₆, 298K)

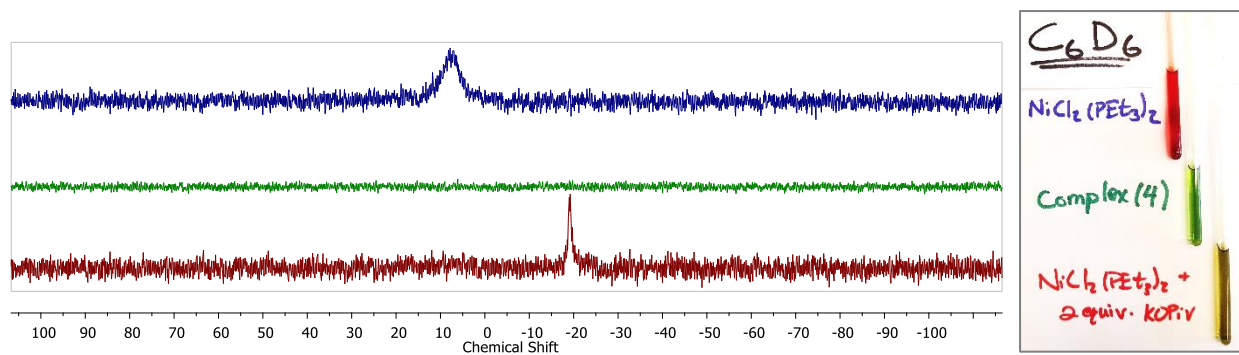


Figure A.2.43. ³¹P{¹H} NMR (300 MHz, C₆D₆, 298K)

Additional Discussion of Above Spectra Figures A.2.39 to A.2.44:

It is clear from both the samples in d_6 -DMSO and C_6D_6 that $[(PEt_3)Ni(\mu-OPiv)_2]_2$ is produced upon mixing $NiCl_2(PEt_3)_2$ and KOPIV (2 equiv.). Additionally, in C_6D_6 also samples are soluble, yet in d_6 -DMSO $[(PEt_3)Ni(\mu-OPiv)_2]_2$ is only very slightly soluble, and it crashes out as a green solid from mixtures of $NiCl_2(PEt_3)_2$.

Samples 1-3 in d_6 -DMSO:

Figure A.2.39: The broad peaks between 5.5-7.0 ppm are not visible in the starting material $NiCl_2(PEt_3)_2$ (Sample 1) but are visible in both $[(PEt_3)Ni(\mu-OPiv)_2]_2$ (Sample 2) and the in situ reaction of $NiCl_2(PEt_3)_2 + 2$ equiv. KOPIV (Sample 3). A similar trend is clear from the broadening from 0.5-2.0 ppm in Samples 2&3.

Figure A.2.40: The broad signal at ~ 97 ppm is not visible in the starting material $NiCl_2(PEt_3)_2$ (Sample 1) but is visible in both $[(PEt_3)Ni(\mu-OPiv)_2]_2$ (Sample 2) and the in situ reaction of $NiCl_2(PEt_3)_2 + 2$ equiv. KOPIV (Sample 3).

Figure A.2.41: Of note is the free PEt_3 ($\delta - 20$) observed in the phosphorus NMR spectra for all three samples in d_6 -DMSO. This suggests that DMSO plays a part in dissociating phosphine from nickel in both $NiCl_2(PEt_3)_2$ and in $[(PEt_3)Ni(\mu-OPiv)_2]_2$.

Samples 1-3 in C_6D_6 :

Figure A.2.42: The broad peak at ~ 3.7 ppm which corresponds to the pivalate methyl groups, is not visible in the starting material $NiCl_2(PEt_3)_2$ (Sample 1) but is visible in $[(PEt_3)Ni(\mu-OPiv)_2]_2$ and the in situ reaction of $NiCl_2(PEt_3)_2 + 2$ equiv. KOPIV (Sample 3). A similar trend can be seen for the broad signal at ~ 1.0 ppm.

Figure A.2.43: The broad peak at ~ 32 ppm which corresponds to the PEt_3 (CH_2) groups, is not visible in the starting material $NiCl_2(PEt_3)_2$ (Sample 1) but is visible in $[(PEt_3)Ni(\mu-OPiv)_2]_2$ and the in situ reaction of $NiCl_2(PEt_3)_2 + 2$ equiv. KOPIV (Sample 3).

Figure A.2.44: Unlike in d_6 -DMSO, all the nickel products are soluble in C_6D_6 . Thus, $NiCl_2(PEt_3)_2$ (Sample A) shows a broad signal at ~ 9 -10 ppm, $[(PEt_3)Ni(\mu-OPiv)_2]_2$, shows no signal, and Sample 3 shows free PEt_3 as expected from dimer formation of $[(PEt_3)Ni(\mu-OPiv)_2]_2$ in situ from $NiCl_2(PEt_3)_2$.

Example of Protonations of (2.2-Ni) – ^1H NMR Experiments

Protonation with 1-AdCOOH:

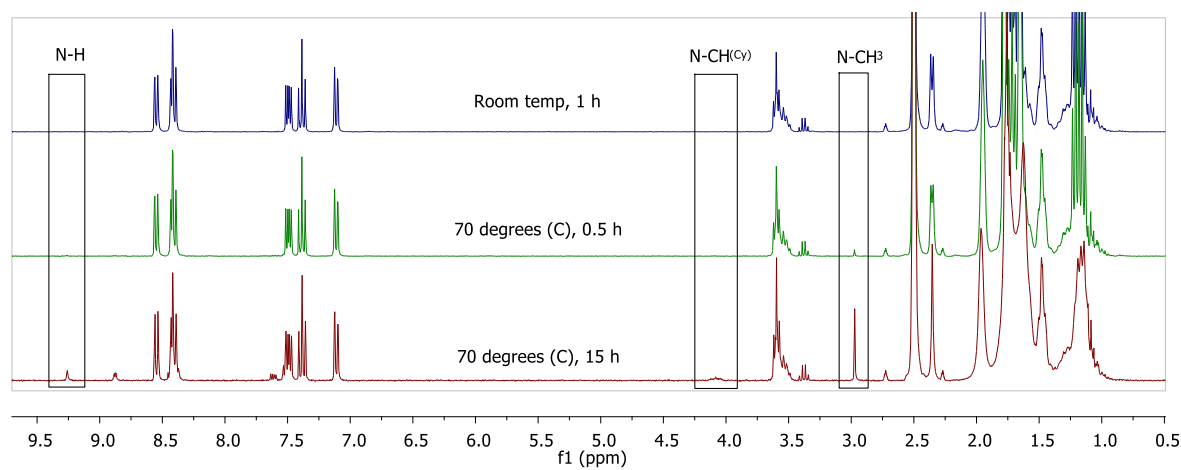
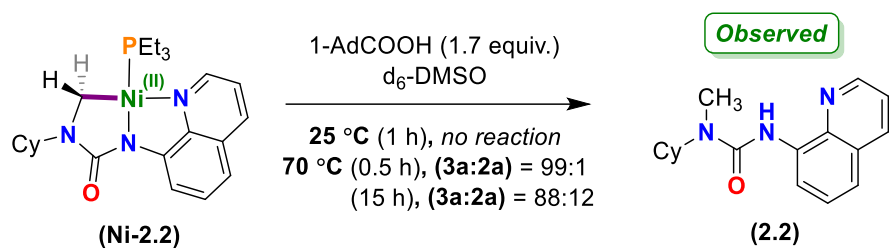
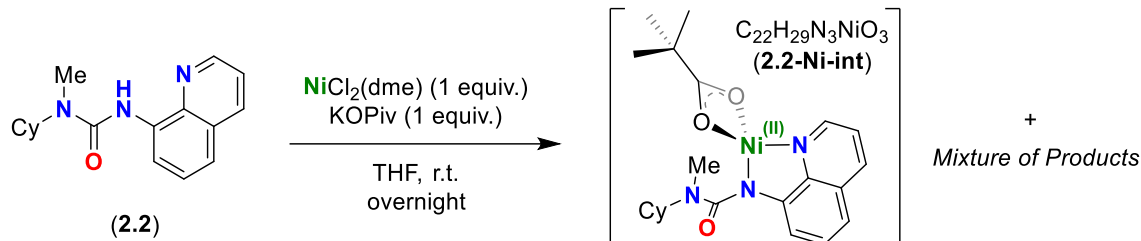


Figure A.2.44. ^1H NMR (300 & 400 MHz, $\text{d}_6\text{-DMSO}$, 298K)

Observation of (2.2-Ni-int) – ESI-MS & ¹H NMR experiments



A mixture of (2.2) (46 mg, 0.16 mmol), $\text{NiCl}_2(\text{dme})$ (50 mg, 0.16 mmol), KOPiv (23 mg, 1 equiv.), and K_2CO_3 (100 mg, 4.5 equiv.) were weighed into a 20 mL vial and stirred at room temperature overnight in a glovebox. In the morning, the volatiles were removed *in vacuo*, and the mixture was filtered with hexanes (15 mL) into a fresh 20 mL vial. The solution was concentrated to ~4 mL hexanes and cooled to -35 °C overnight to form a precipitate. The next morning, the precipitate were filtered onto a frit in the glovebox, then dried under vacuum to give a crude yellow-brown solid which was analyzed without purification.

¹H NMR of Mixture:

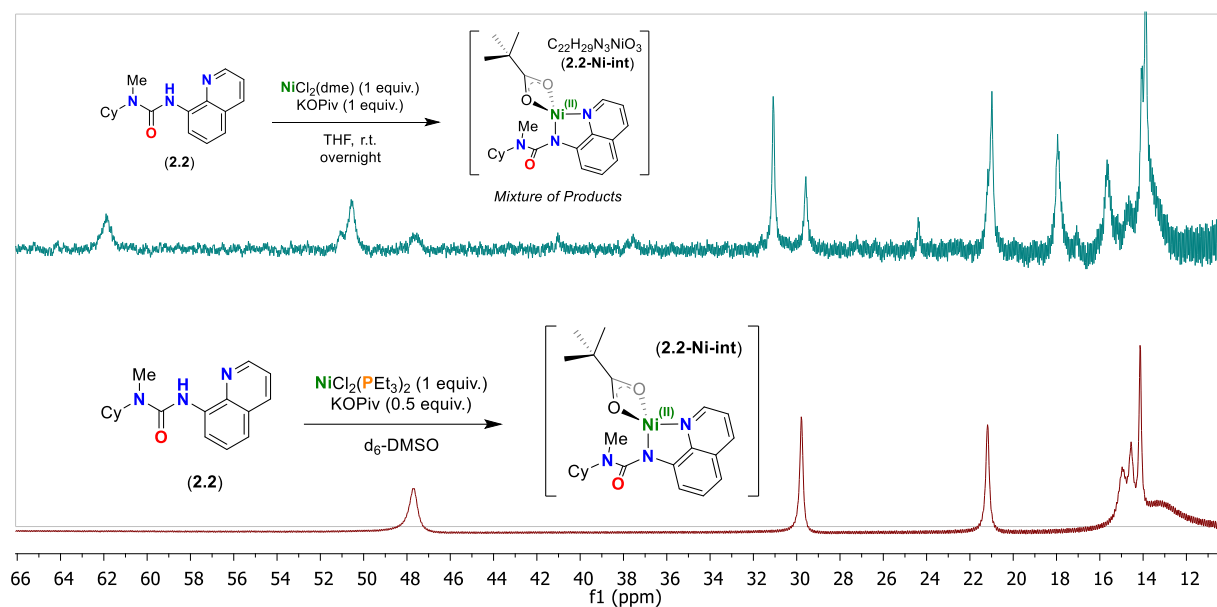
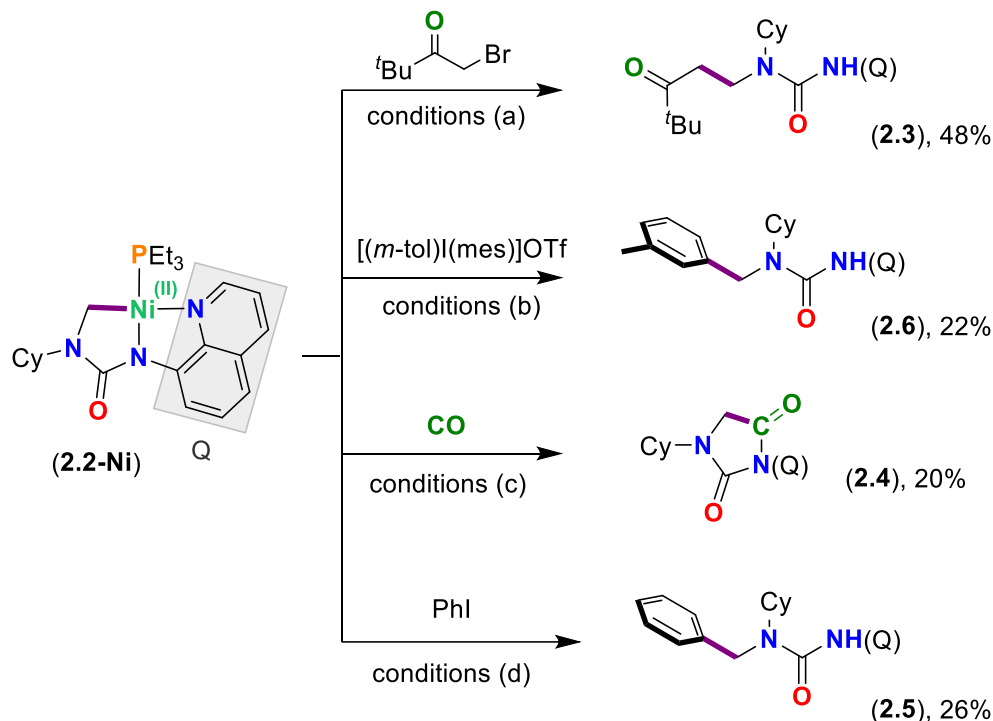


Figure A.2.45. paramagnetic ¹H NMR (top spectrum 300 MHz, bottom spectrum 400 MHz, d₆-DMSO, 298K)

Functionalization of Isolated (2.2-Ni)



General Procedure:

In a glovebox, complex (2.2-Ni), TMB (0.33 equiv.), and the coupling partner (3 equiv.) and the functionalization partner were each weighed into one-dram vials as standard solutions in *d*₈-toluene. These solutions were then added to a J-Young tube and diluted to ~ 600 μL . The tubes were then sealed and removed from the glovebox, and heated in oil baths. Reaction progress was monitored by NMR spectroscopy until consumption of (2.2-Ni) or coupling partner. The reactions were quenched with water, dried in vacuo, and analyzed in CDCl_3 solutions by ^1H NMR spec.

Functionalization Conditions:

Conditions (a): (2.2-Ni) (4.6 mg, 0.01 mmol), 1-bromopinacolone (5.4 mg, 0.03 mmol), *tol-d*₈ (0.02 M), 70 °C, 1 h

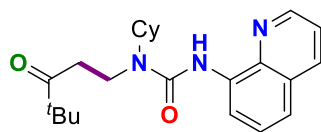
Conditions (b): (2.2-Ni) (4.6 mg, 0.01 mmol), (3-Methylphenyl)(2,4,6-trimethylphenyl)iodonium triflate (14.6 mg, 0.03 mmol), *tol-d*₈ (0.02 M), 70 °C, 1 h..

Conditions (c): (2.2-Ni) (8 mg, 0.014 mmol), CO (1 atm, Schlenk line), *tol-d*₈ (0.02 M), 110 °C, 20 h.

Conditions (d): (2.2-Ni) (4.6 mg, 0.01 mmol), PhI (6.1 mg, 0.03 mmol), *tol-d*₈ (0.02 M), 120 °C, 1 h.

Characterization of Functionalization Products:

1-cyclohexyl-1-(4,4-dimethyl-3-oxopentyl)-3-(quinolin-8-yl)urea (2.3)

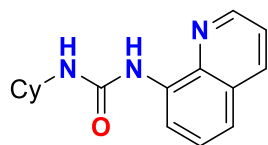


Synthesis for Isolation: (2.2-Ni) (109 mg, 0.19 mmol), 1-bromopinacolone (36 mg, 0.2 mmol), tol-d_8 (0.2 M), 70° C, 2 h, **Purification:** Following a standard work-up, the organic residue was subject to column chromatography (Hex:EtOAc, 10:1 to 3:1)

to afford (2.3) as a white solid, **Yield** = 59% (42 mg, 0.11 mmol). **^1H NMR (300 MHz, CDCl_3)** δ 9.39 (br s, 1H), 8.69 (dd, J = 4.2, 1.6 Hz, 1H), 8.56 (dd, J = 7.7, 1.0, 1H), 8.12 (dd, J = 8.3, 1.5 Hz, 1H), 7.50 (app. t, J = 8.0 Hz, 1H), 7.43-7.35 (m, 2H), 4.24-4.04 (m, 1H), 3.72-3.57 (m, 2H), 3.08-2.93 (m, 2H), 1.93-1.78 (m, 4H), 1.77-1.62 (m, 1H), 1.60-1.35 (m, 4H), 1.23-1.04 (m, 1H), 1.18 (s, 9H). **$^{13}\text{C}\{^1\text{H}\}$ NMR (75 MHz, CDCl_3)** δ 214.6, 154.8, 147.8, 138.7, 136.5, 136.2, 128.1, 127.8, 121.5, 119.5, 114.9, 44.3, 38.4, 37.6, 31.5, 26.4, 26.1, 25.6. **HRMS** (ESI) m/z calculated for $\text{C}_{23}\text{H}_{32}\text{N}_3\text{O}_2$ $[\text{M}+\text{H}]^+$: 382.2495; found: 382.2501

Side products from above (Ureas 2.7, 2.8):

1-cyclohexyl-3-(quinolin-8-yl)urea (2.7)

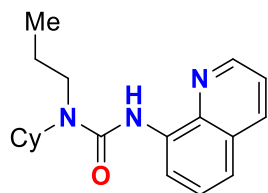


Synthesis for Isolation: See above, **Purification:** See above isolated as a white solid,

Yield = 34% (17 mg, 0.06 mmol). **^1H NMR (300 MHz, CDCl_3)** δ 8.92 (br s, 1H), 8.73 (dd, J = 4.2, 1.6 Hz, 1H), 8.54 (dd, J = 7.7, 1.1 Hz, 1H), 8.13 (dd, J = 8.3, 1.6 Hz, 1H), 8.0

(vir. t, J = 8.0 Hz, 1H), 7.45-7.34 (m, 2H), 4.84 (d, J = 7.8 Hz, 1H), 3.82-3.63 (m, 1H), 2.10-1.98 (m, 2H), 1.80-1.55 (m, 3H), 1.51-1.06 (m, 6H). **$^{13}\text{C}\{^1\text{H}\}$ NMR (75 MHz, CDCl_3)** δ 154.5, 147.7, 138.3, 136.6, 136.1, 128.2, 127.8, 121.5, 119.5, 114.9, 49.4, 33.9, 25.7, 25.1. **HRMS** (ESI) m/z calculated for $\text{C}_{16}\text{H}_{20}\text{N}_3\text{O}_2$ $[\text{M}+\text{H}]^+$: 270.1606; found: 270.1598.

1-cyclohexyl-1-propyl-3-(quinolin-8-yl)urea (2.8)



Synthesis for Isolation: See above, **Purification:** See above isolated as a light-yellow oil,

Yield = ~2-3% (~2 mg, 0.005 mmol, ~80-90% pure). **Independent Synthesis:** *see below*.

^1H NMR (400 MHz, CDCl_3) δ 9.44 (br s, 1H), 8.76 (dd, J = 4.2, 1.3 Hz, 1H), 8.58 (d, J = 7.7 Hz, 1H), 8.14 (dd, J = 8.2, 1.1 Hz, 1H), 7.56-7.33 (m, 3H), 4.20 (m, 1H), 3.33-3.29 (m,

2H, N- CH_2), 1.06 (t, J = 7.4 Hz, 3H). **LC-MS** (ESI) m/z calculated for $\text{C}_{19}\text{H}_{27}\text{N}_3\text{O}_1$ $[\text{M}+\text{H}]^+$: 312.2; found: 312.2.

Independent Synthesis

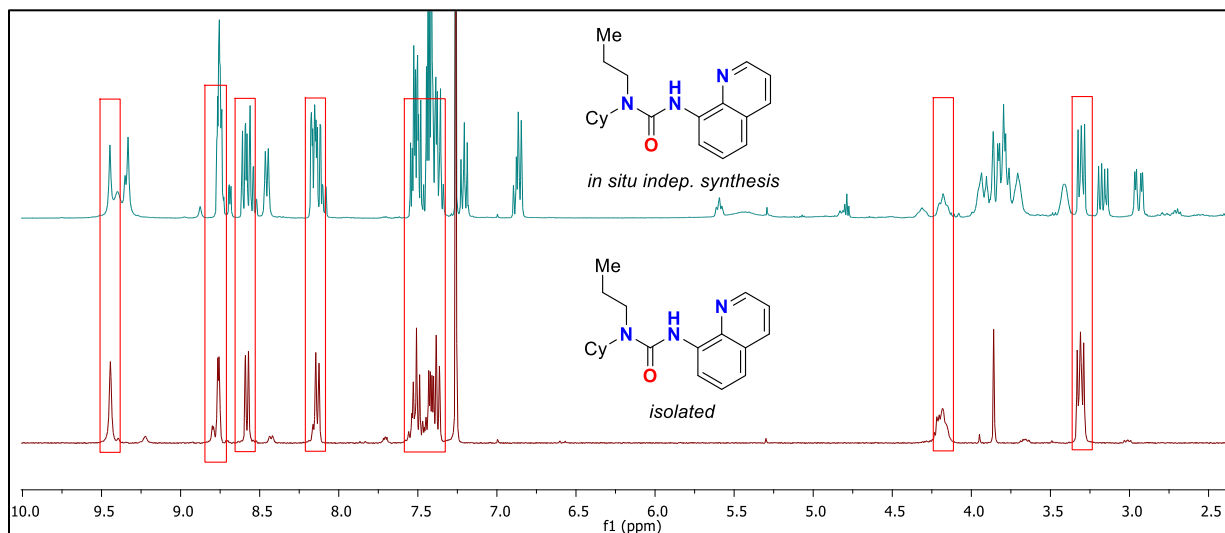
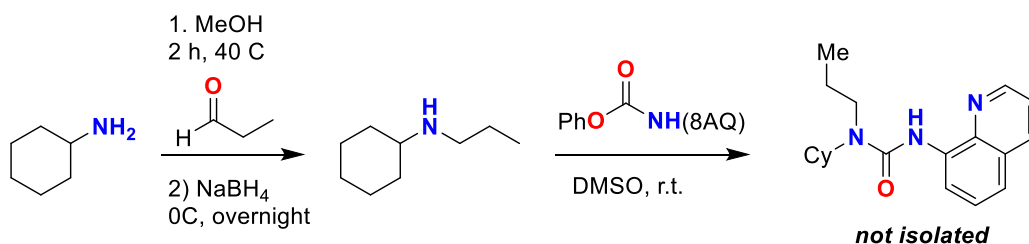
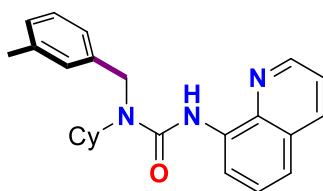


Figure A.2.46. ^1H NMR of compound **2.8** from independent synthesis and from isolation.

1-cyclohexyl-1-(3-methylbenzyl)-3-(quinolin-8-yl)urea (**2.6**)

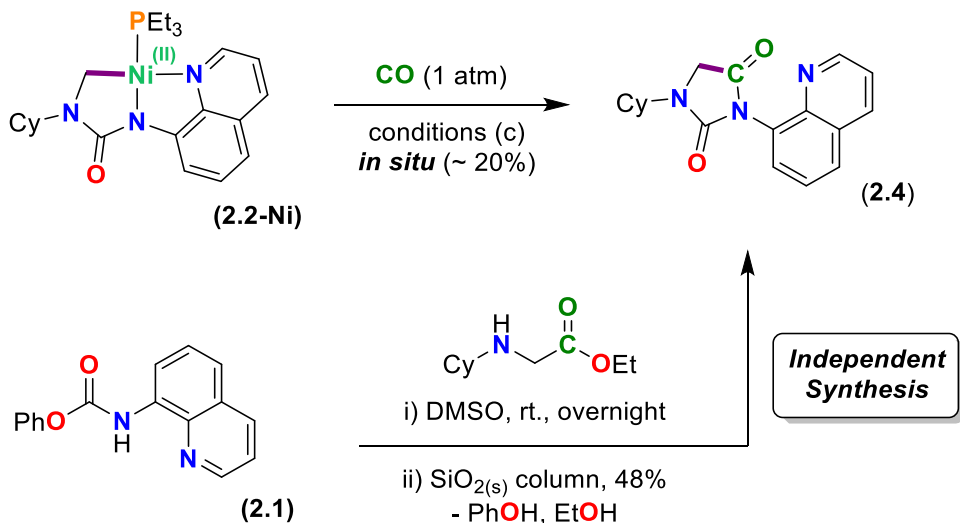


Synthesis for Isolation: (**2.2-Ni**) (76 mg, 0.13 mmol), (3-Methylphenyl)(2,4,6-trimethylphenyl)iodonium triflate (66 mg, 0.14 mmol), DMSO- d_6 (0.2 M), 110°C , 24 h, **Purification:** Following a standard work-up, the organic residue was subject to column chromatography (Hex:EtOAc, 10:1) to afford (**2.6**) as an off-white solid,

Yield = 23% (~ 90% pure, 12 mg, 0.032 mmol). ^1H NMR (400 MHz, CDCl_3) δ 9.32 (br s, 1H), 8.56 (d, J = 7.8 Hz, 1H), 8.51 (d, J = 4.2 Hz, 1H), 8.06 (dd, J = 8.2, 1.3 Hz, 1H), 7.38 (app. t, J = 8.0 Hz, 1H), 7.37-7.30 (m, 2H), 7.27 (eclipsed by solvent, 1H), 7.25-7.22 (m, 2H), 7.10-7.04 (m, 1H), 4.63 (s, 2H), 4.42-4.27 (m, 1H), 2.34 (s, 3H), 2.01-1.91 (m, 2H), 1.90-1.79 (m, 2H), 1.76-1.63 (m, 1H), 1.53-1.42 (m, 4H), 1.26 (s, unknown impurity, 4H), 1.18-1.02 (m, 1H). $^{13}\text{C}\{^1\text{H}\}$ NMR (101 MHz, CDCl_3) δ 155.8, 147.6, 138.8, 138.3, 136.5, 136.2, 128.6, 128.0, 128.0, 127.7,

127.6, 124.0, 121.3, 119.4, 115.0, 55.4, 46.7, 31.6, 29.8, 26.2, 25.8, 21.7. **HRMS** (ESI) m/z calculated for $C_{24}H_{28}N_3O_2$ [M+H]⁺: 374.2232; found: 374.2231

1-cyclohexyl-3-(quinolin-8-yl)imidazolidine-2,4-dione (2.4)



Independent Synthesis: Phenyl quinolin-8-ylcarbamate^[264] (637 mg, 2.41 mmol) was weighed into a 20-mL vial in the air. DMSO (3 mL) and a stir bar were added to the same vial and the contents were stirred vigorously. *N*-Cyclohexyl-ethylglycinate^[267] (447 mg, 2.41 mmol) was weighed into a 5-mL vial, and to that vial DMSO (1 mL) was added. The resulting solution of *N*-Cyclohexyl-ethylglycinate/DMSO was then added dropwise to the 20-mL vial while stirring. The vial was then capped and stirred overnight at room temperature. Reaction progress was monitored by TLC to confirm consumption of the carbamate. Upon completion, the contents of the reaction vial were added to an separation funnel. The contents were diluted with Et₂O (50 mL) and washed with distilled water (5 x 20 mL). The organic layer was then washed with brine, filtered, and were then dried using rotary evaporation. The reaction was then purified using a silica column (100% DCM). The mixture was eluted with 1 column volume of 100% DCM to elute all starting materials and by-products. Finally, the column was eluted with (8% MeOH, 92% DCM) to elute the desired product (**2.4**). The fractions containing the desired product were dried using rotary evaporation. To the resulting oil was added hexanes (5 mL), and the suspension was sonicated for 1 h. The resulting pale-yellow suspension was filtered over filter paper on a Buchner funnel. The solids were washed with cold hexanes (5 mL), dried in *vacuo* and collected to yield the desired product as a pale-yellow solid (360 mg, 1.16 mmol, 48%).

¹H NMR (400 MHz, CDCl₃): δ = 8.90 (dd, $J_{\text{H,H}} = 4.2, 1.7$ Hz, 1H), 8.18 (dd, $J_{\text{H,H}} = 8.3, 1.7$ Hz, 1H), 7.91 (dd, $J_{\text{H,H}} = 8.2, 1.4$ Hz, 1H), 7.69 (dd, $J_{\text{H,H}} = 7.3, 1.5$ Hz, 1H), 7.63-7.60 (m, 1H), 7.42 (dd, $J_{\text{H,H}} = 8.3, 4.2$ Hz, 1H), 4.23 (d, $^2J_{\text{H,H}} = 17.4$ Hz, 1H), 4.11-4.03 (m, 1H) 4.06 (d, $^2J_{\text{H,H}} = 17.4$ Hz, 1H), 2.03-2.00 (m, 1H), 1.96-1.94 (m, 1H), 1.88-1.86 (m, 1H), 1.73-1.70 (m, 1H), 1.52-1.36 (m, 4H), 1.22-1.11 (m, 1H). **¹³C{¹H} NMR (101 MHz, 25°C, CDCl₃):** δ = 170.32, 155.71, 151.06, 144.21, 136.23, 130.07, 129.88, 129.72, 129.40, 126.21, 121.98, 51.50, 46.46, 30.88, 30.85, 25.48, 25.40. **HRMS** (ESI) m/z calculated for C₁₈H₂₀N₃O₂ [M+H]⁺: 310.1556; found: 310.1549

Sample of NMR Spectra of Described Compounds

see *J. Am. Chem. Soc.* **2018**, *140*, 12602-12610 for all other ^1H and $^{13}\text{C}\{^1\text{H}\}$ spectra.

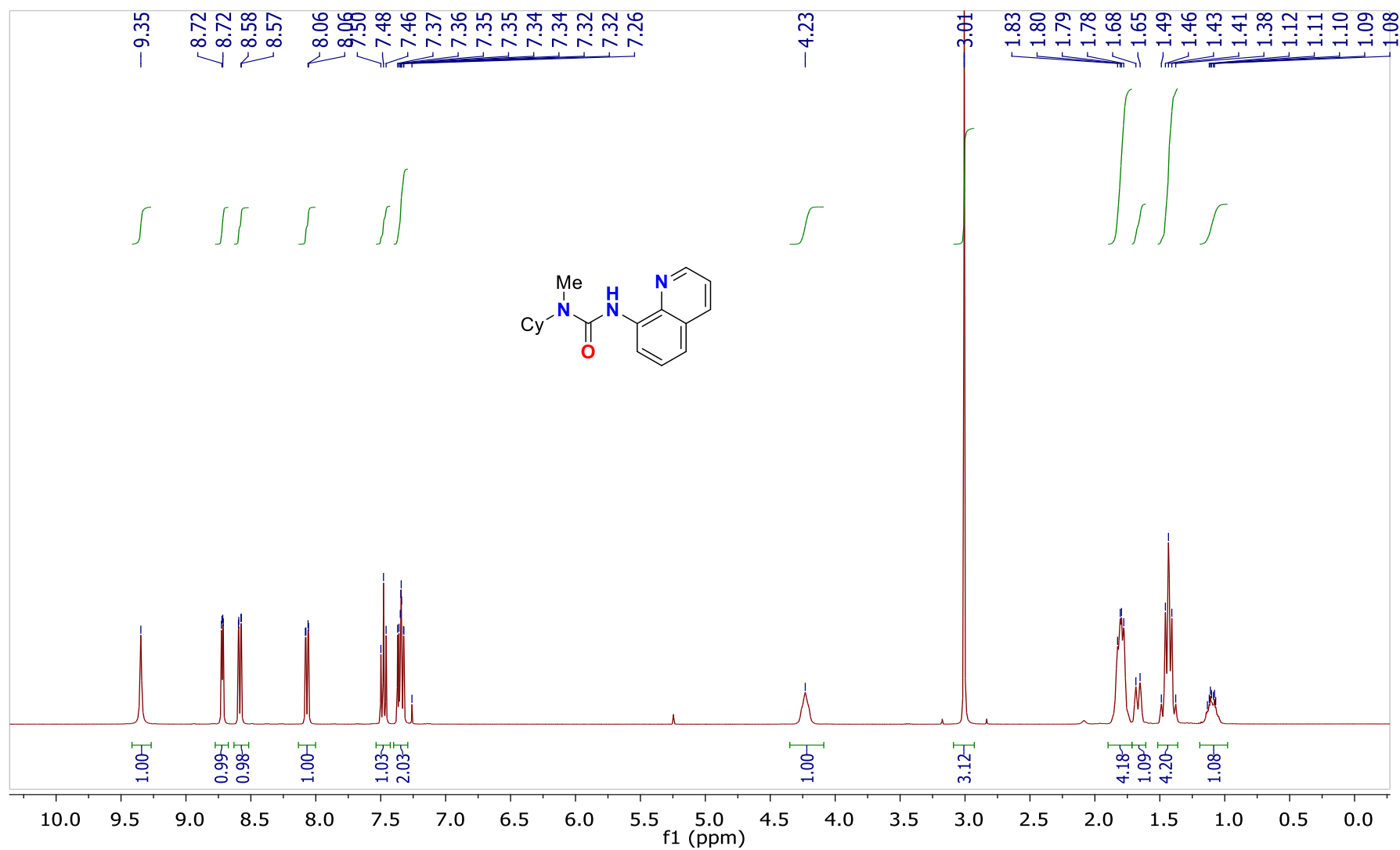


Figure A.2.47. Compound (2.2); ^1H NMR (400 MHz, CDCl_3 , 298K).

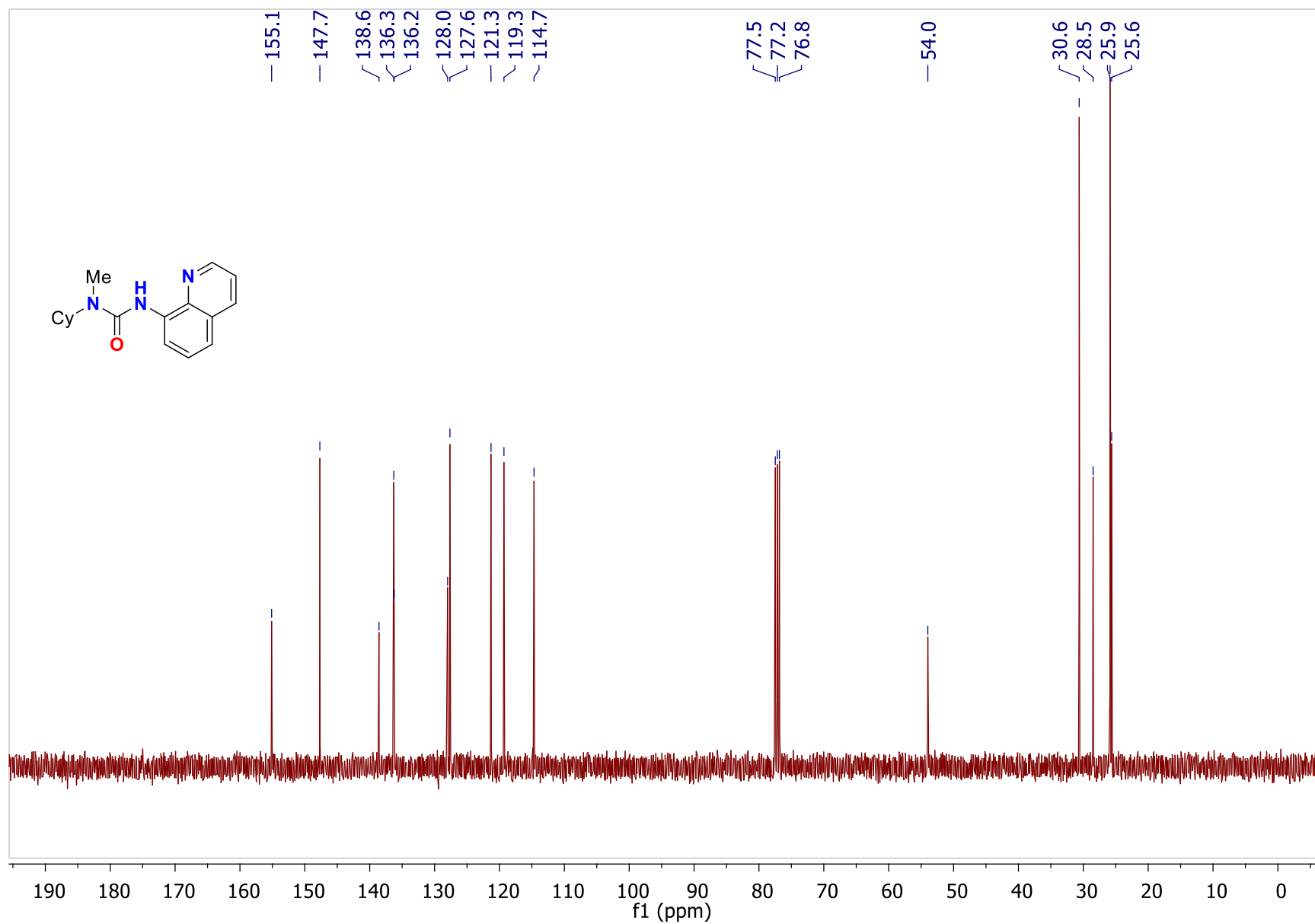


Figure A.2.48. Compound (2.2); $^{13}\text{C}\{^1\text{H}\}$ NMR (101 MHz, CDCl_3 , 298K)

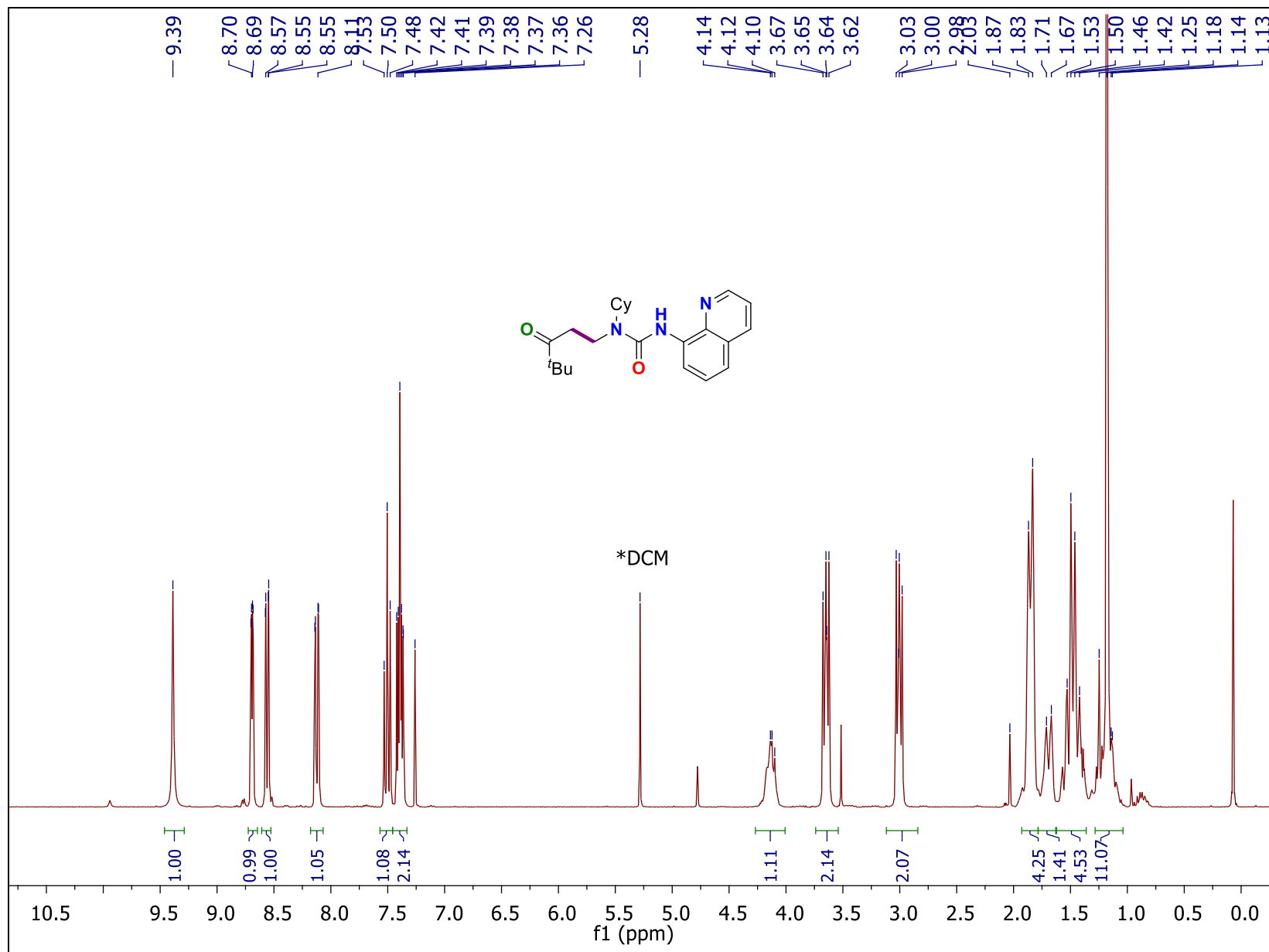


Figure A.2.49. Compound (2.3); ¹H NMR (400 MHz, CDCl₃, 298K)

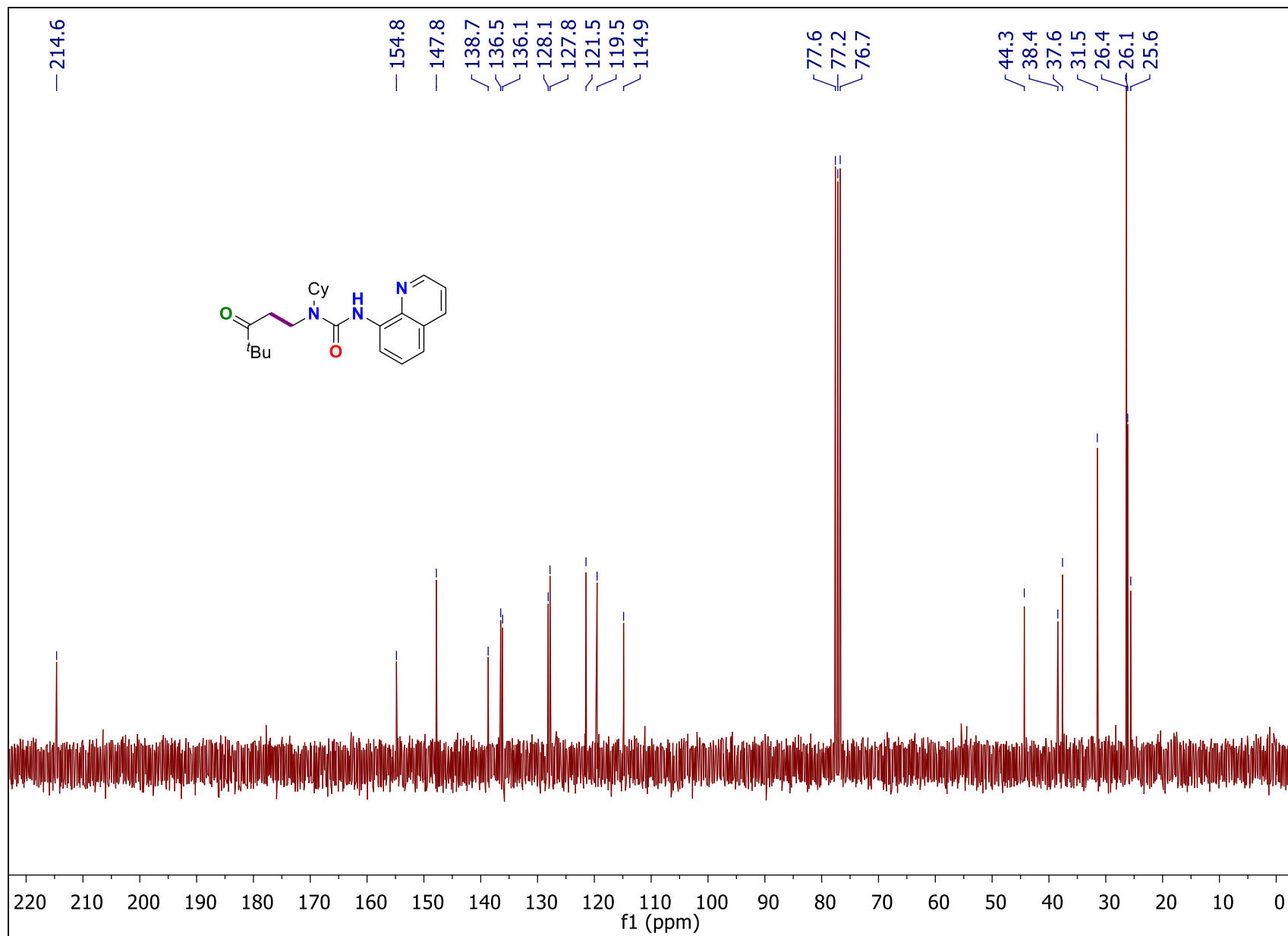


Figure A.2.50. Compound (2.3); $^{13}\text{C}\{^1\text{H}\}$ NMR (101 MHz, CDCl_3 , 298K)

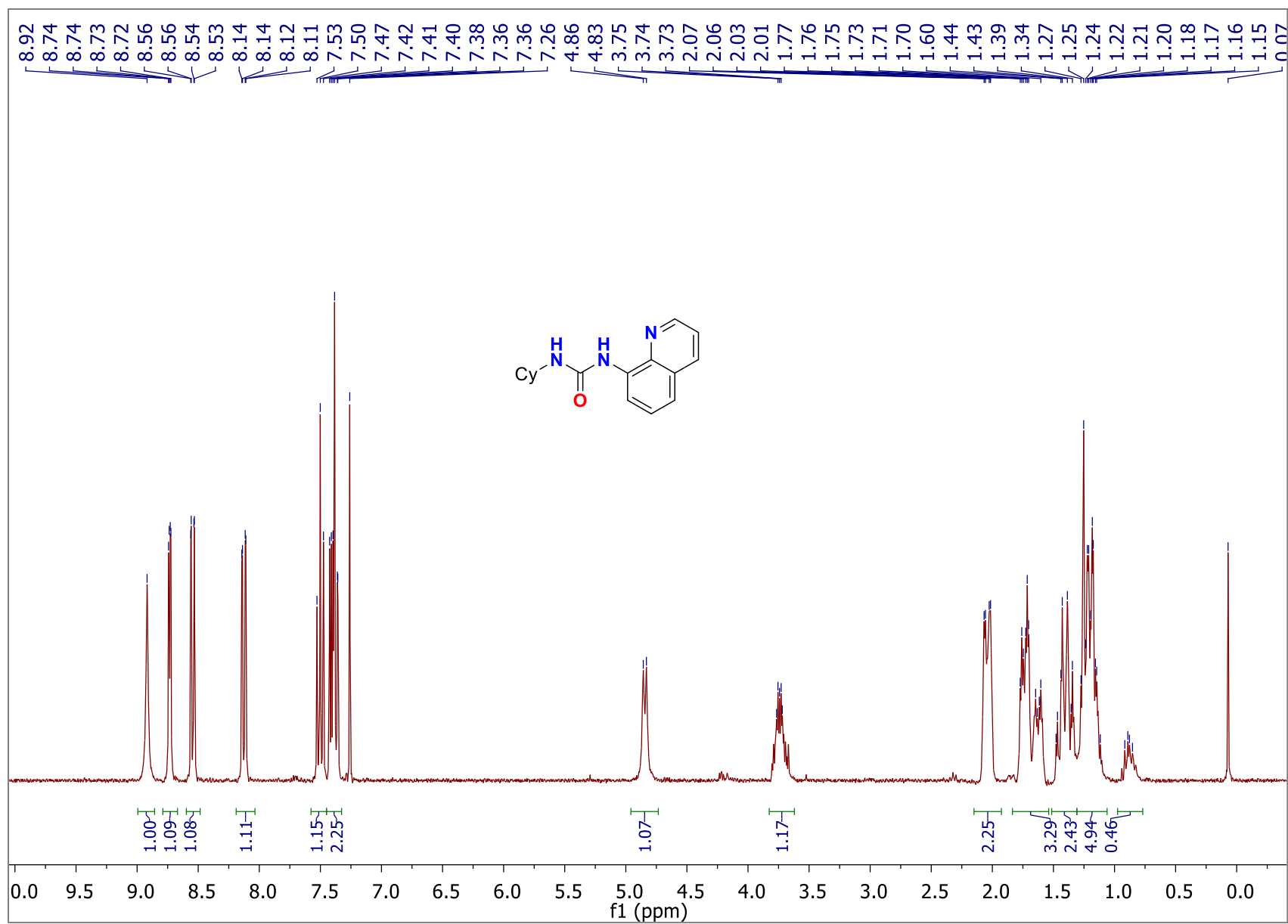


Figure A.2.51. Compound (2.7); ¹H NMR (300 MHz, CDCl₃, 298K)

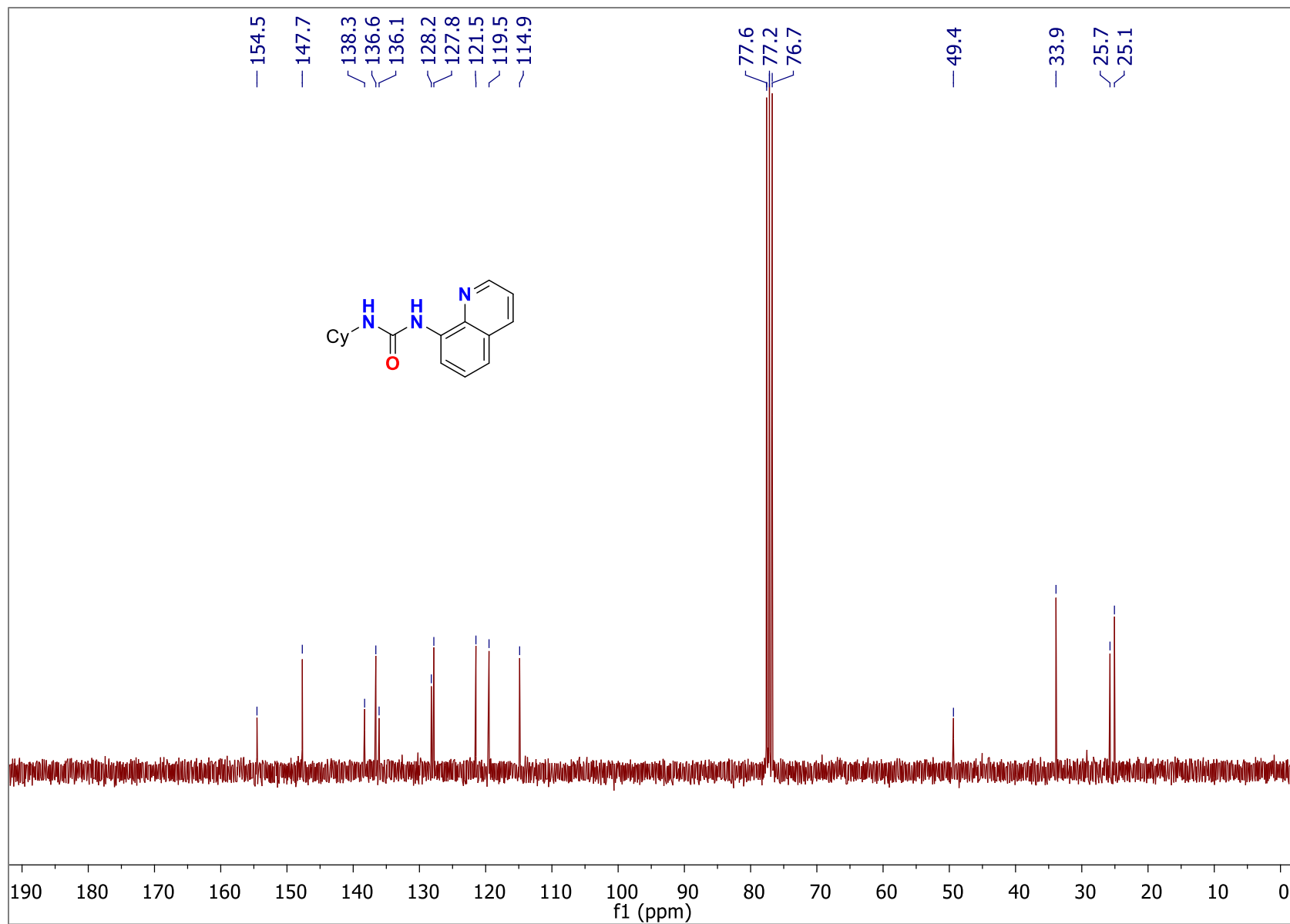


Figure A.2.52. Compound (2.7); ¹³C{¹H} NMR (75 MHz, CDCl₃, 298K)

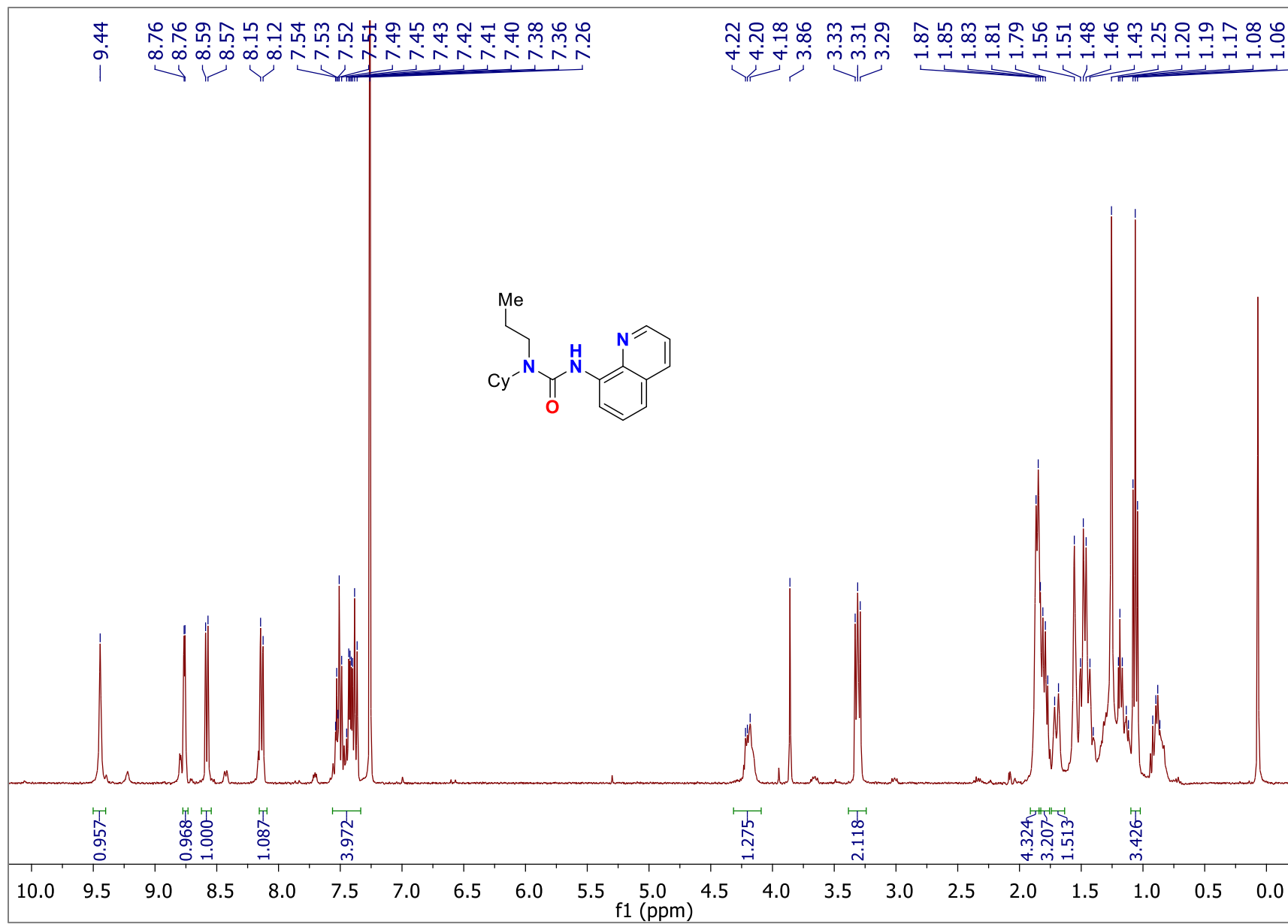


Figure A.2.53. Compound (2.8); ¹H NMR (300 MHz, CDCl₃, 298K)

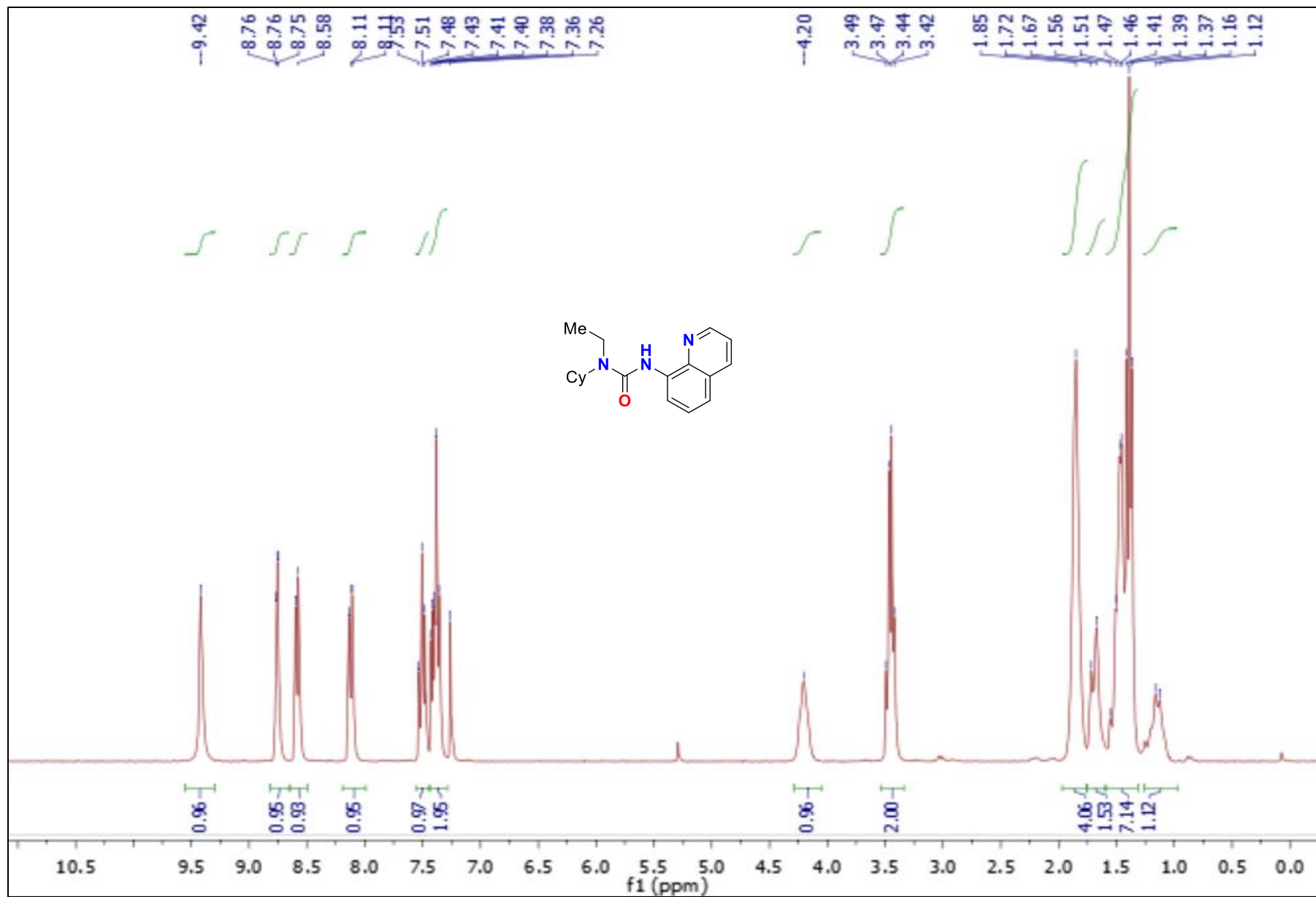


Figure A.2.54. Compound (2.10); ¹H NMR (300 MHz, CDCl₃, 298K)

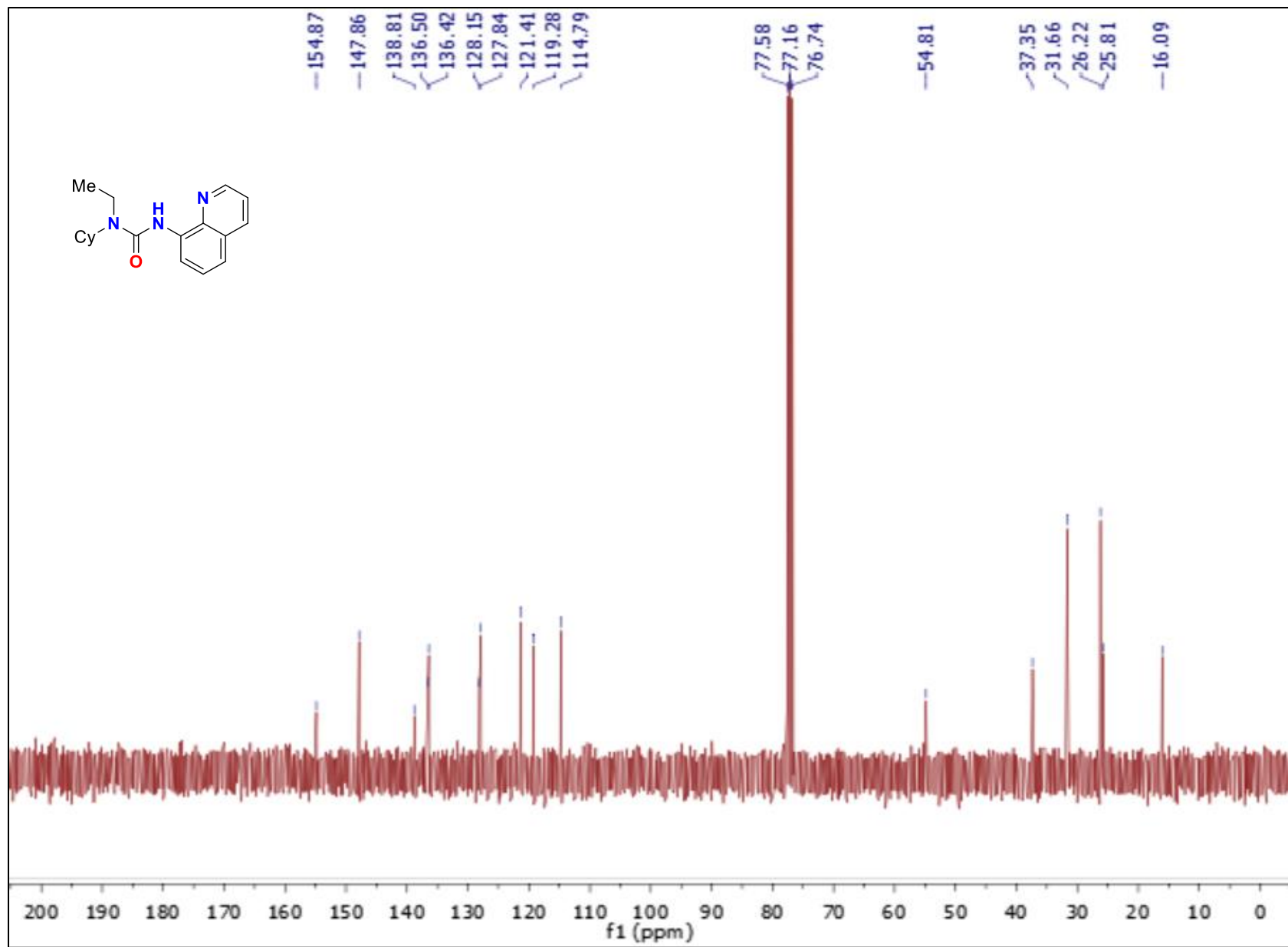


Figure A.2.55. Compound (2.10); $^{13}\text{C}\{^1\text{H}\}$ NMR (75 MHz, CDCl_3 , 298K)

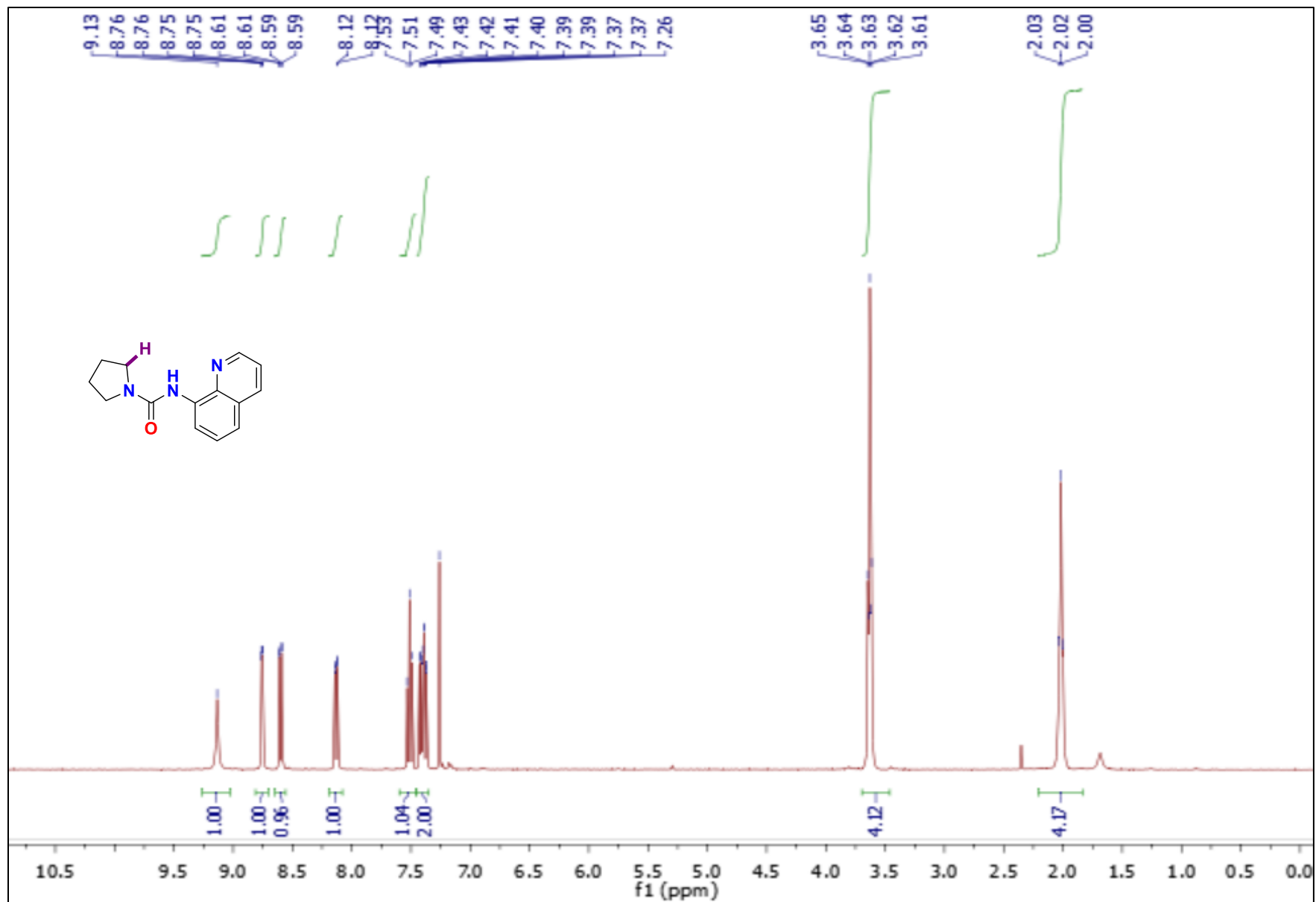


Figure A.2.56. Compound (2.18); ¹H NMR (300 MHz, CDCl₃, 298K)

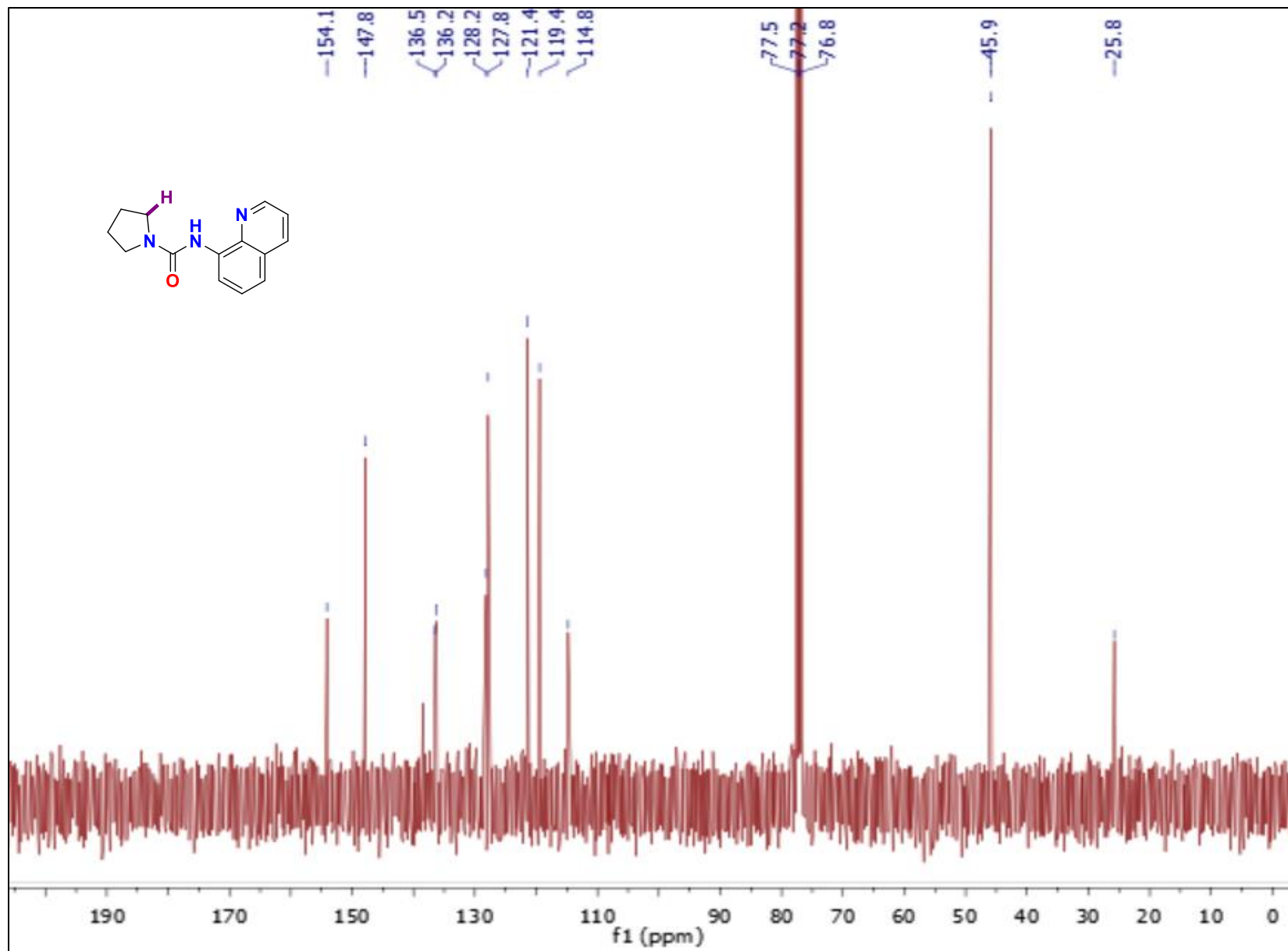


Figure A.2.57. Compound (2.18); $^{13}\text{C}\{^1\text{H}\}$ NMR (101 MHz, CDCl_3 , 298K)

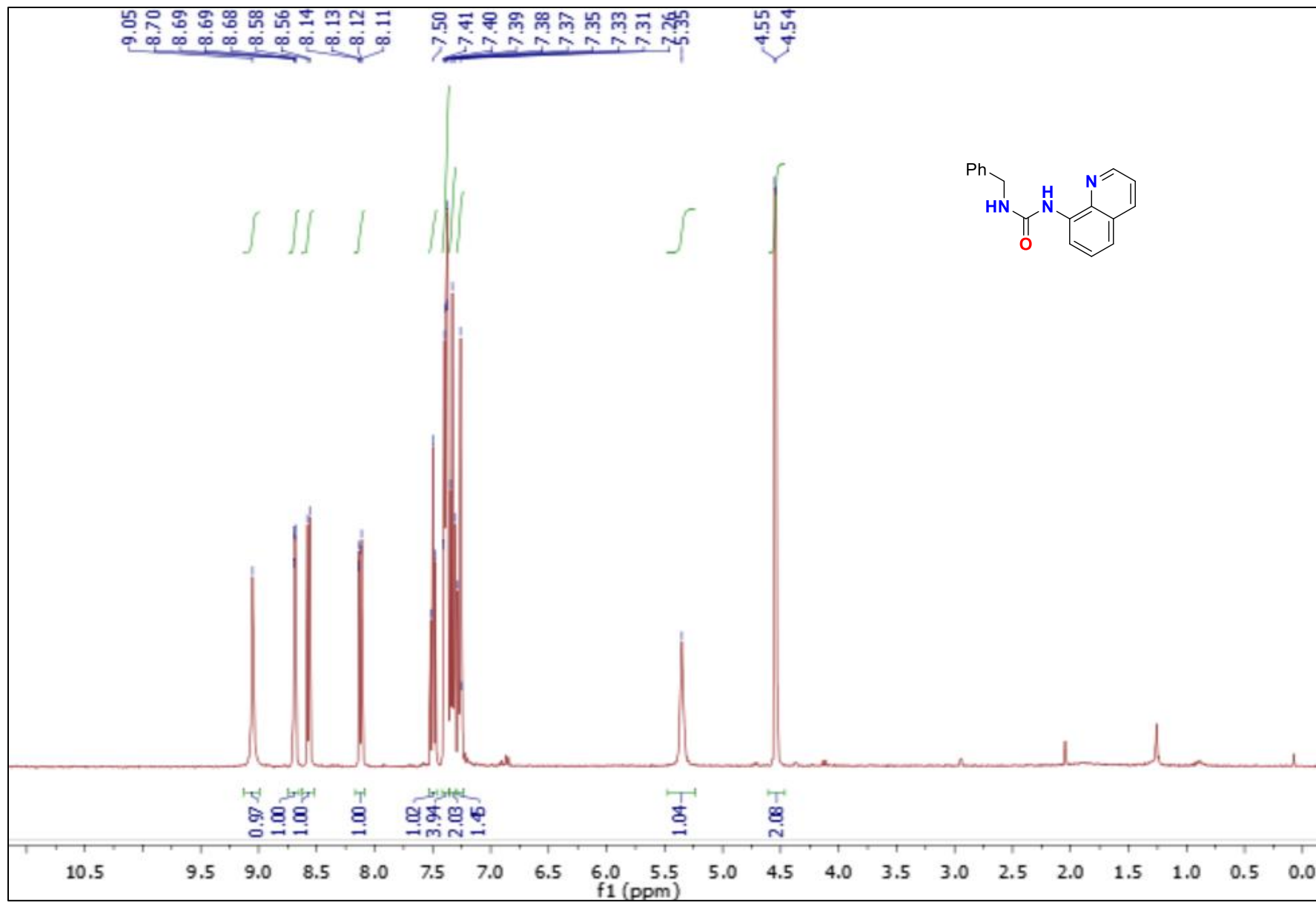


Figure A.2.58. Compound (2.21); ¹H NMR (400 MHz, CDCl₃, 298K)

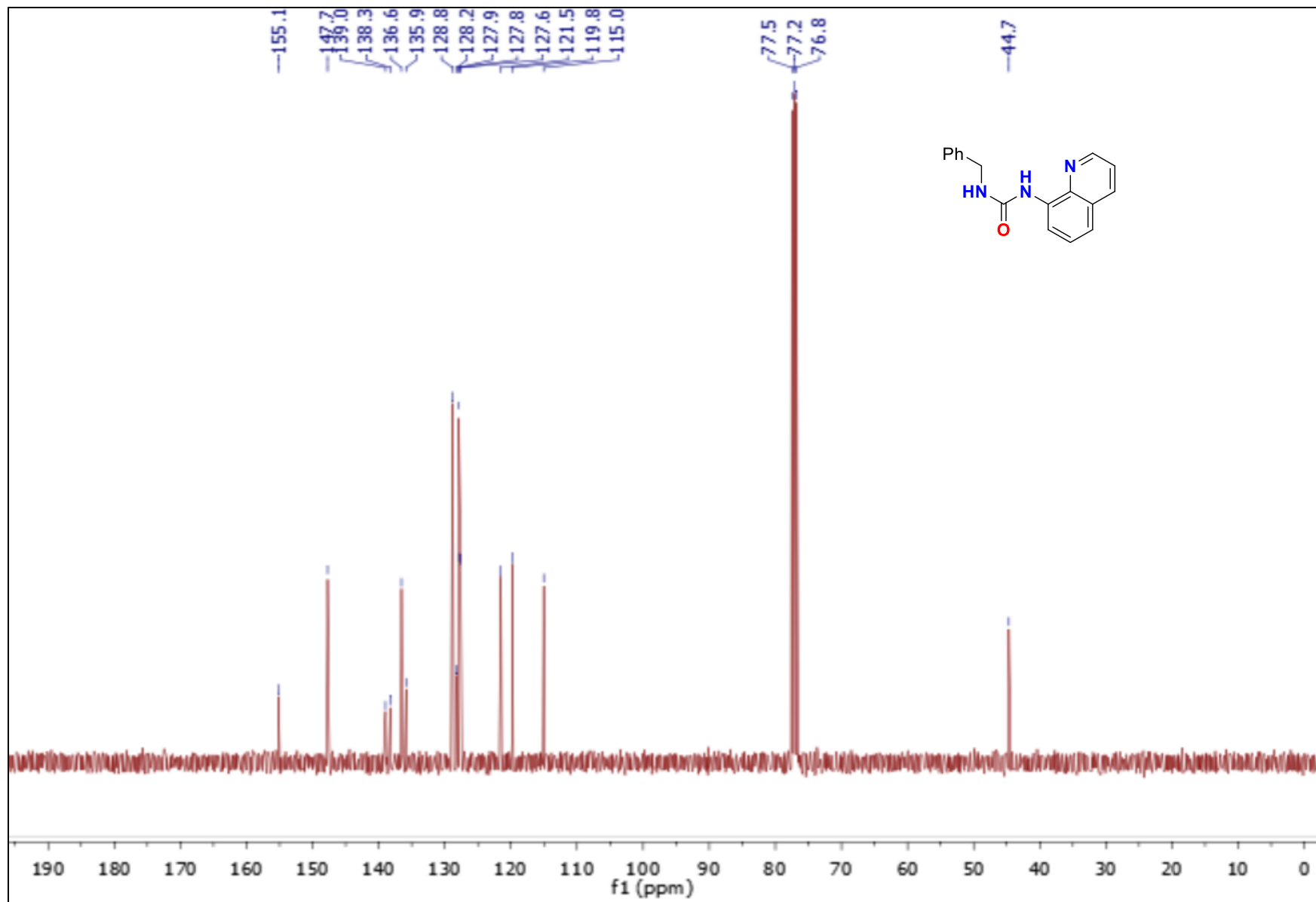


Figure A.2.59. Compound (2.21); ¹³C{¹H} NMR (101 MHz, CDCl₃, 298K)

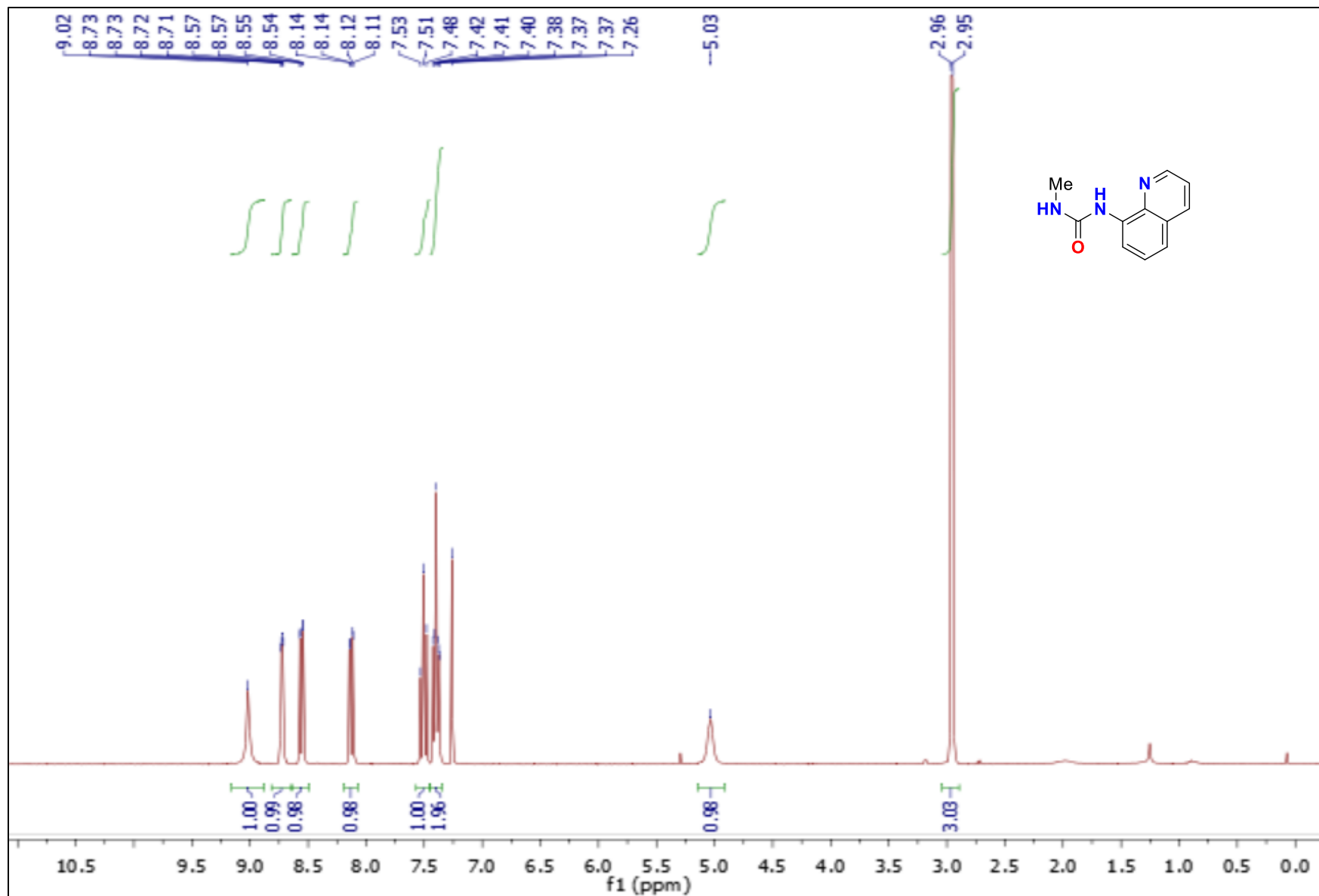


Figure A.2.60. Compound (2.22); ¹H NMR (300 MHz, CDCl₃, 298K)

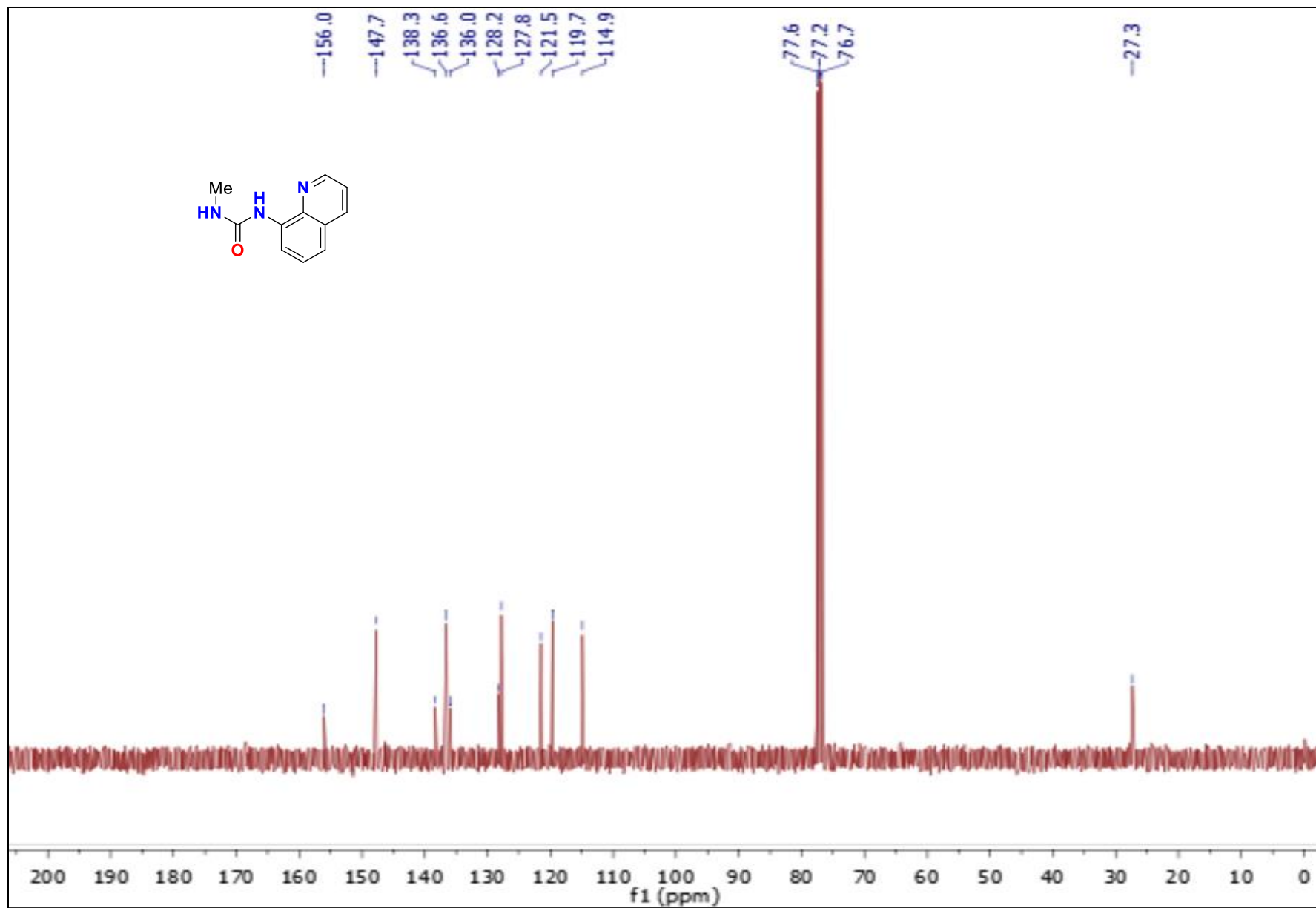


Figure A.2.61. Compound (2.22); $^{13}\text{C}\{^1\text{H}\}$ NMR (75 MHz, CDCl_3 , 298K)

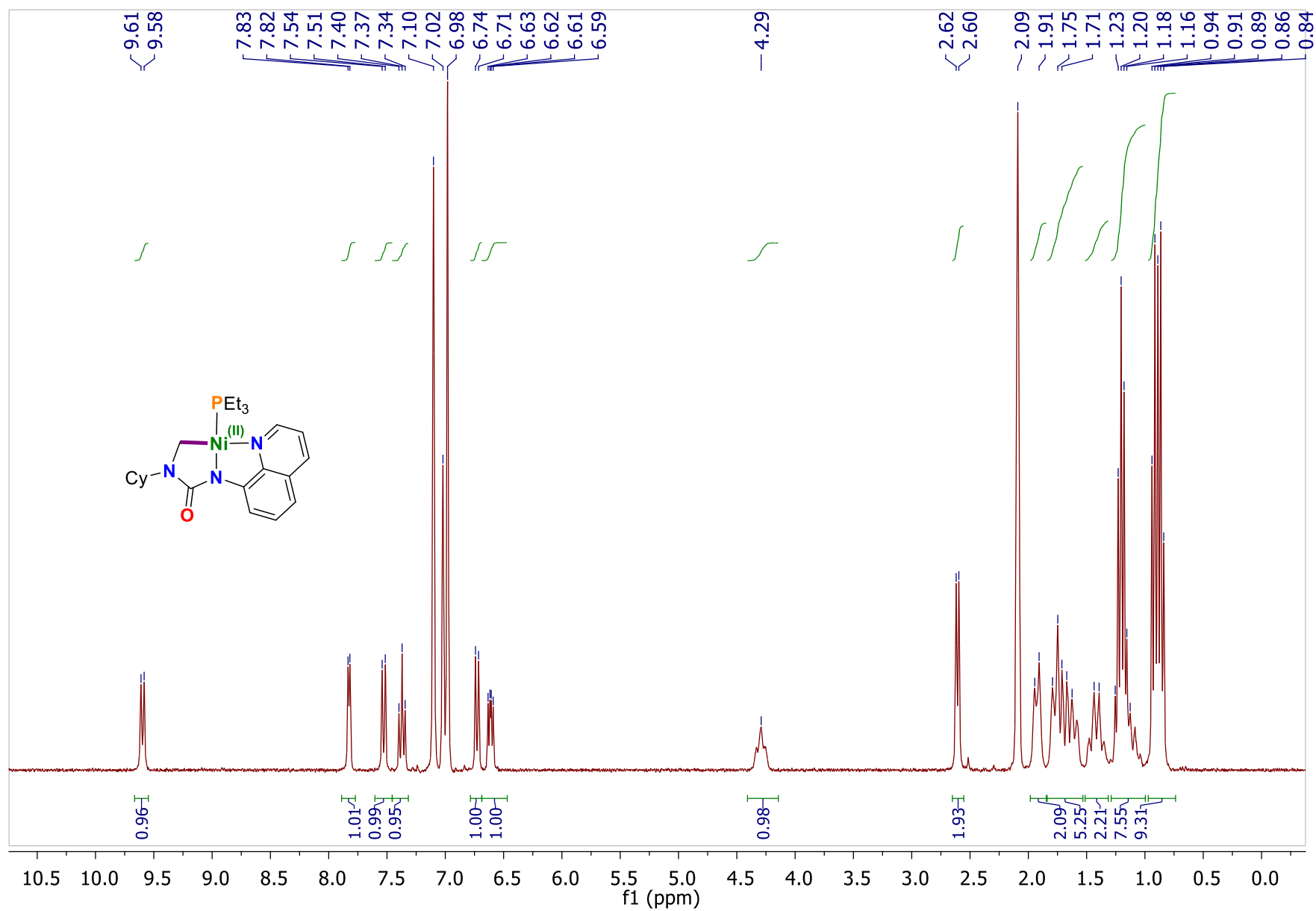


Figure A.2.62. Compound (2.2-Ni); ^1H NMR (400 MHz, $\text{d}_8\text{-tol}$, 298K)

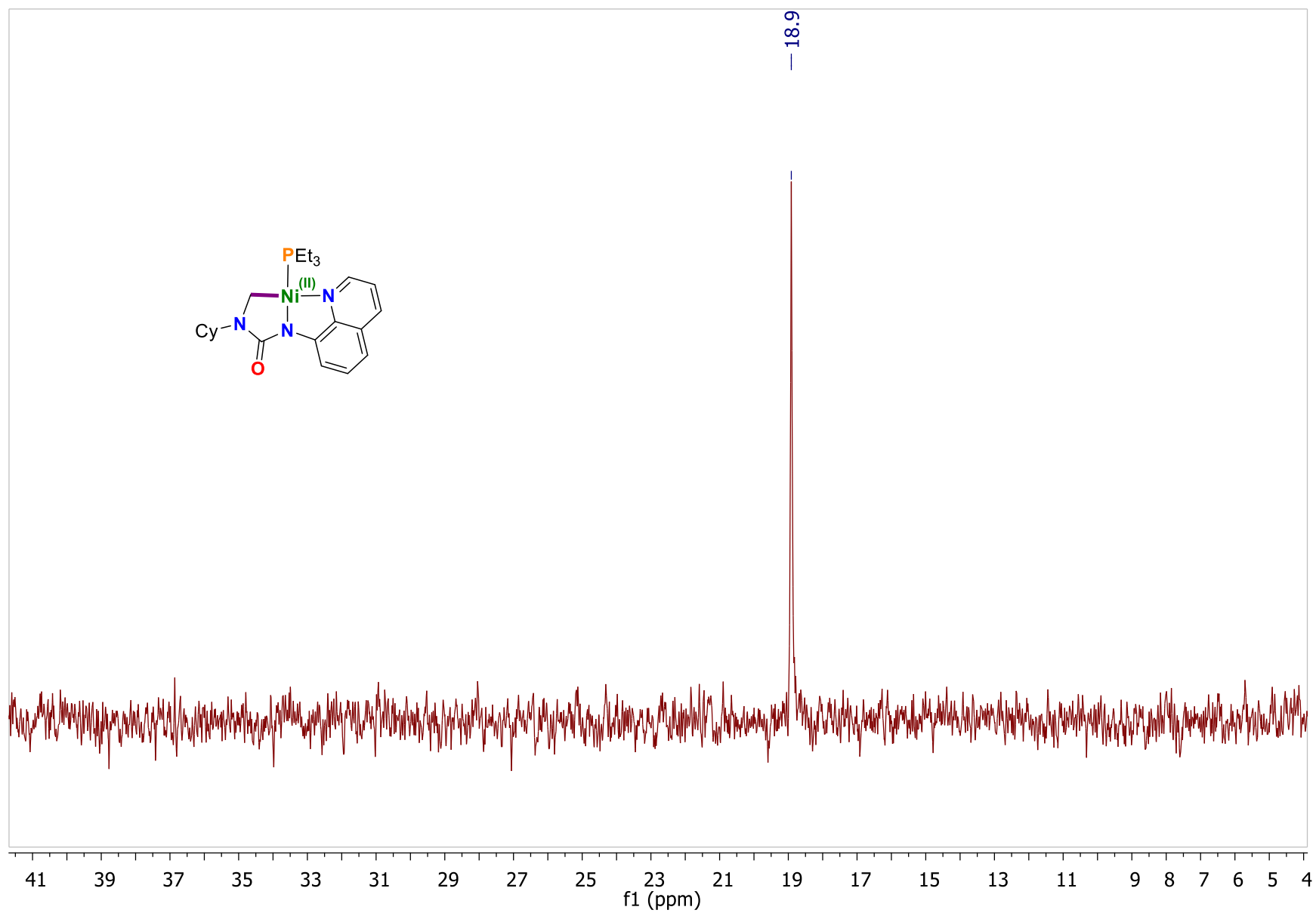


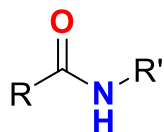
Figure A.2.63. Compound (2.2-Ni); $^{31}\text{P}\{^1\text{H}\}$ NMR (162 MHz, d_8 -tol, 298K)

Other Ni-C(*sp*³) Bond Lengths

Reference	Length (Å)
Piers ^[161]	2.000(3)
Piers ^[161]	1.981(5)
Piers ^[161]	1.978(2)
Piers ^[161]	1.973(2)
Piers ^[162]	2.043(4)
Piers ^[162]	2.030(8)
Iluc ^[163]	1.966(3)
Hofmann ^[164]	1.957(3)
Hofmann ^[164]	1.953(3)
Hofmann ^[164]	1.968(3)
Hofmann ^[164]	1.960(5)
Hofmann ^[164]	1.958(2)
Hofmann ^[164]	1.959(2)
Hofmann ^[164]	1.969(2)
Hofmann ^[164]	1.956(2)
Average	1.977
Median	1.968

A.3 Experimental Data for Chapter 3

The amides from chapter 3 are synthesized as below:



3.1 (R = tBu, R' = Dipp)^[209]

3.2 (R = Ph, R' = Dipp)^[268]

3.3 (R = 3,5-bis(CF₃)C₆H₃, R' = Dipp)^[269]

3.4 (R = Ph, R' = iPr)^[270]

3.5 (R = tBu, R' = iPr)^[207]

3.6 (R = MeCy, R' = iPr)^[271]

3.7 (R = d₃-MeCy, R' = iPr)^[272]

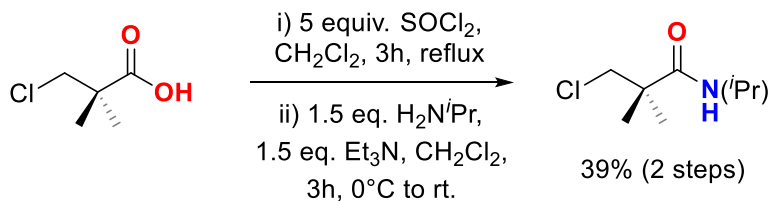
3.8 (R = tBu, R' = cyclopropyl)^[273]

3.9 (R = Cy, R' = iPr)^[274]

3.10 (R = iPr, R' = iPr)^[275]

3.11 (R = Et, R' = iPr)^[276]

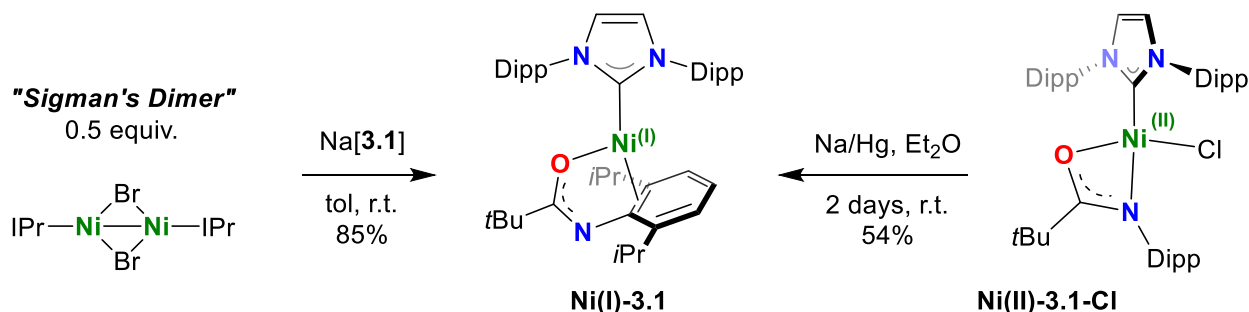
3.12 (R = 3-chloro,2-dimethylpropyl, R' = iPr)^[203]



Amide **3.12** is described in the literature; however the characterization data is not listed.

¹H NMR (400 MHz, 25°C, C₆D₆): δ = 5.21 (bs, HN(ⁱPr), 1H), 4.13 (2 x overlapping sept, ³J_{H,H} = 6.6 Hz, N-*i*Pr(CH), 1H), 3.40 (s, Cl(CH₂)C(CH₃)₂, 2H), 0.97 (s, Cl(CH₂)C(CH₃)₂, 6H), 0.91 (d, ³J_{H,H} = 6.6 Hz, N-*i*Pr(CH₃)₂, 6H). **¹H NMR (300 MHz, 25°C, ds-tol):** δ = 5.08 (bs, HN(ⁱPr), 1H), 4.05 (2 x overlapping sept, ³J_{H,H} = 6.6 Hz, N-*i*Pr(CH), 1H), 3.32 (s, Cl(CH₂)C(CH₃)₂, 2H), 0.94 (s, Cl(CH₂)C(CH₃)₂, 6H), 0.89 (d, ³J_{H,H} = 6.6 Hz, N-*i*Pr(CH₃)₂, 6H). **¹³C{¹H} NMR (101 MHz, 25°C, C₆D₆):** 173.3 (C=O), 53.3 (Cl(CH₂)), 43.80 (Cl(CH₂)C(CH₃)₂), 41.7 (N-*i*Pr(CH)), 23.3

(Cl(CH₂)C(CH₃)₂), 22.5 (N-*i*Pr(CH₃)₂). **HRMS** (EI) *m/z* calculated for C₈H₁₆ClNO [M]⁺: 177.09204; found: 177.09155.

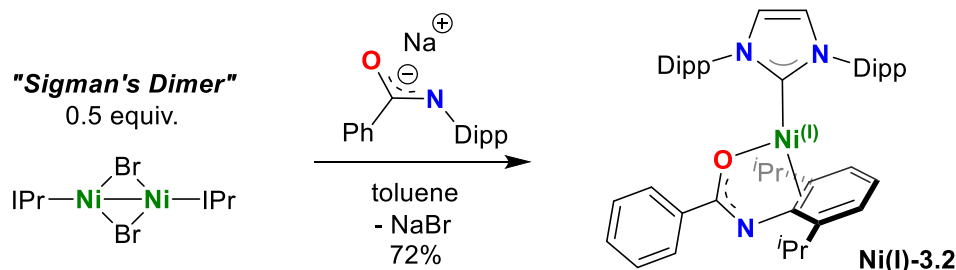


Method A: In a glovebox, **Ni(II)-3.1-Cl** (119 mg, 0.160 mmol) was weighed into a 5 mL vial. Diethyl ether (4.5 mL) was added to the vial, and the resulting purple solution was added to a 20 mL vial containing Na/Hg (0.5 % by Na, 1.1 eq.). A stir bar was added, and the mixture was stirred vigorously for 2 days. Diethyl ether (10 mL) was added, and the yellow solution was filtered through Celite® into a 20 mL vial. The volatiles were removed in vacuo, dissolved in minimal toluene, layered with 10 mL hexanes and cooled to -35°C overnight. Paramagnetic yellow crystals formed overnight, and the solid samples of **Ni(I)-3.1** were decanted and dried (61 mg, 54% - multiple crops). X-ray quality crystals were prepared by slow diffusion of hexanes into a concentrated solution of **Ni(I)-3.1** in toluene at -35°C.

By Salt Metathesis: In a glovebox, solid Na[3.1] (53.8 mg, 0.190 mmol) was added at room temperature to a 20 mL vial containing a stirring solution of [Ni(μ-Br)(iPr)]₂ (Sigman's Dimer) (100 mg, 0.0948 mmol) in toluene (10 mL). The contents were stirred overnight (~12 h), and in the morning removed from the stir plate and allowed to settle for 5 minutes. The supernatant was filtered through Celite®, and the remaining solids were dissolved in toluene and filtered until no solid remained. The filtered toluene was divided equally into 2 vials (10 mL each) and layered with hexanes. Paramagnetic yellow crystals of **Ni(I)-3.1** formed overnight at -35°C (114 mg, 85% - multiple crops) and were collected by decanting the vials, washing with cold hexanes (0.5 mL), and removal of volatiles *in vacuo*. The solid **Ni(I)-3.1** was characterized by NMR by comparing to a sample of **Ni(I)-3.1** prepared by reduction.

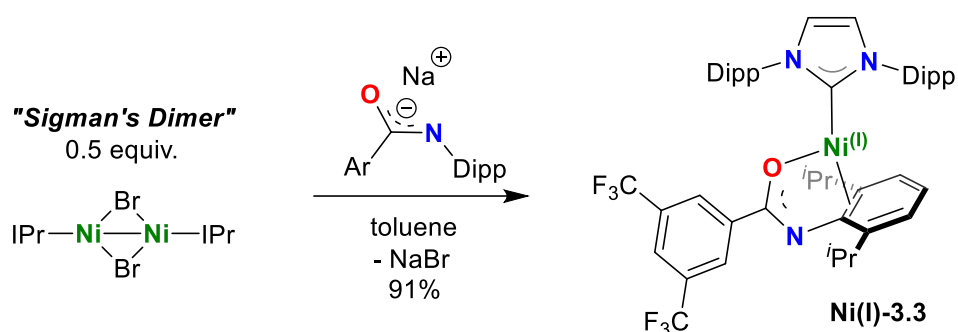
¹H NMR (400 MHz, 25°C, C₆D₆): δ = 32.6, 27.6, 17.2, 12.0, 10.7, 5.3, 4.98, 1.78, -0.27. **Evans Method (C₆D₆, 25°C):** μ_{eff} = 1.71 μ_B. **EI-MS (*m/z*):** 706 [M]⁺. *Elemental analysis suggests the incorporation of toluene in samples*

of **Ni(I)-3.1** prepared by either method. Additionally, a toluene molecule was found in the crystal structure, and consistently in the NMR of dried samples. Crushing crystals and extended drying continually led to analytical data consistent with approximately 0.5 equiv. toluene incorporation. **Anal. Calcd.** for $C_{44}H_{62}N_3NiO$ (706). C, 74.68%; H, 8.83%; N, 5.94%. **Anal. Calcd.** for $C_{47.5}H_{66}N_3NiO$ (753 for 0.5 equiv. toluene). C, 75.69%; H, 8.83%; N, 5.57%. Found: C, 75.71%; H, 8.56%; N, 5.24%.



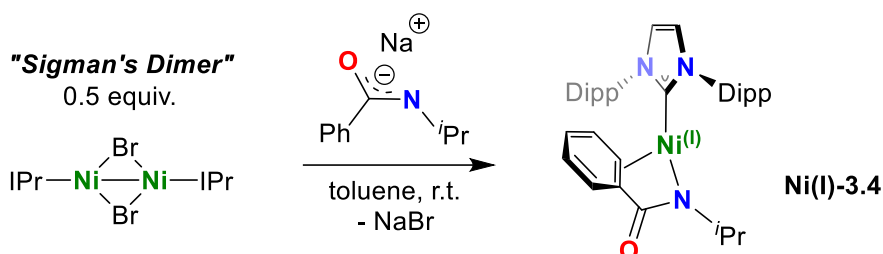
Ni(I)-3.2: In a glovebox, Sigman's Dimer (100 mg, 0.0948 mmol) was added as a solid at room temperature to a 20 mL vial containing a stirring solution of Na[**3.2**] (57.6 mg, 0.190 mmol) in toluene (10 mL). The contents were stirred overnight (~12 h), and in the morning removed from the stir plate and allowed to settle for 5 minutes. The supernatant was filtered through Celite®, and the remaining solids were dissolved in toluene (10 mL) and filtered until no solid remained. The filtered toluene was divided equally into 2 vials (10 mL each) and layered with hexanes. Paramagnetic yellow crystals of **Ni(I)-3.2** formed overnight at $-35^{\circ}C$ (99 mg, 72% - multiple crops) and were collected by decanting the vials, washing with cold hexanes (0.5 mL), and removal of volatiles *in vacuo*. X-ray quality crystals were prepared by slow diffusion of hexanes into a concentrated solution of **Ni(I)-3.2** in toluene at $-35^{\circ}C$.

1H NMR (400 MHz, $25^{\circ}C$, C_6D_6): δ = 31.28, 27.87, 14.17, 12.51, 10.53, 7.52, 7.16, 6.65, 6.49, 6.24, 5.42, 4.97, 4.50, 2.34, 1.94, 1.58, -0.18. **Evans Method (C_6D_6 , $27^{\circ}C$):** μ_{eff} = 1.96 μ_B . **EI-MS (m/z):** 726 [M]⁺. **Anal. Calcd.** for $C_{46}H_{58}N_3NiO$ (726). C, 75.93%; H, 8.03%; N, 5.77%. Found: C, 76.14%; H, 8.39%; N, 5.20%. *Analytical Data not sufficient for publication.*



Ni(I)-3.3: In a glovebox, Sigman's Dimer (50 mg, 0.0474 mmol) was added as a solid at room temperature to a 20 mL vial containing a stirring solution of Na[**3.3**] (41.7 mg, 0.948 mmol) in toluene (4 mL). The contents were stirred for 2 h, and subsequently the volatiles were removed in vacuo. The orange-yellow residue was taken up in minimal hexanes (5 mL) and the solution was filtered through Celite®. The solution was then cooled in the glovebox freezer at -35°C overnight. Paramagnetic yellow crystals of **Ni(I)-3.3** formed overnight (74 mg, 91% - multiple crops) and were collected by decanting the vial, washing with cold hexanes (0.5 mL), and removal of volatiles *in vacuo*. X-ray quality crystals were prepared by storing hexane solutions of **Ni(I)-3.3** at -35°C.

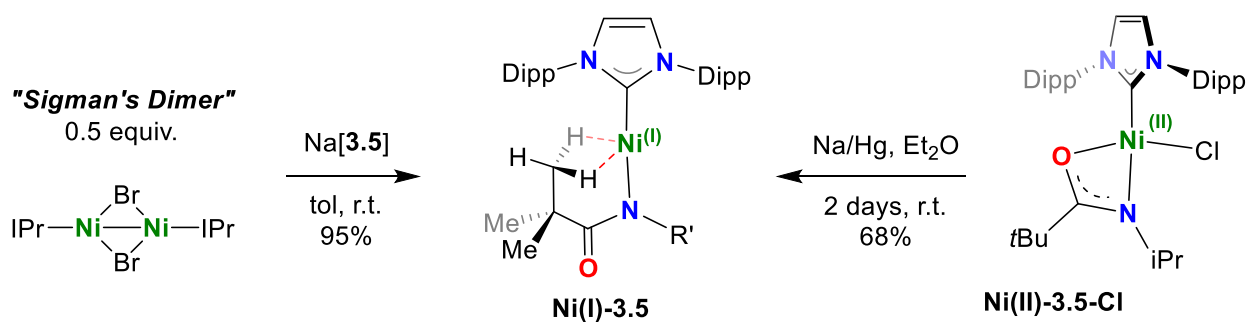
¹H NMR (300 MHz, 25°C, C₆D₆): δ = 29.54, 14.36, 4.72, 1.57, 0.29. **Evans Method (C₆D₆, 25°C):** μ_{eff} = 1.62 μ_B .



Ni(I)-3.4: In a glovebox, Sigman's Dimer (40 mg, 0.0379 mmol) was added as a solid at room temperature to a 20 mL vial containing a stirring slurry of Na[**3.4**] (14 mg, 0.0759 mmol) in toluene (5 mL). The contents were stirred overnight (~12 h), and in the morning removed from the stir plate and allowed to settle for 5 minutes. The supernatant was filtered through Celite®, and the remaining solids were dissolved in toluene (~2-3 mL) and filtered until no solid remained. The filtered toluene was divided equally into 2 vials and layered with hexanes. Paramagnetic yellow crystals of **Ni(I)-3.4** formed overnight at -35°C (27 mg, 59%) and were collected by decanting the vials, washing with cold

hexanes (0.5 mL), and removal of volatiles *in vacuo*. X-ray quality crystals were prepared by slow diffusion of hexanes into a concentrated solution of **Ni(I)-3.4** in toluene at -35°C.

¹H NMR (300 MHz, 25°C, C₆D₆): δ = 26.15, 16.64, 14.77, 11.41, 9.20, 6.95, 4.93, 4.35, 3.45, 2.73, 1.90, 0.06, -1.81, -14.47. **Evans Method (C₆D₆, 25°C):** μ_{eff} = 2.01 μ_B . **EI-MS (m/z):** 608 [M]⁺. **Anal. Calcd.** for C₄₆H₅₈N₃NiO (726). C, 72.91%; H, 7.94%; N, 6.89%. Found: C, 72.64%; H, 8.09%; N, 6.70%.

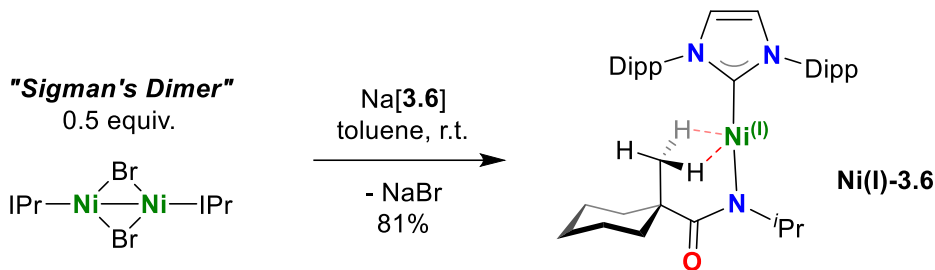


(IPr) Ni(κ^3 -N,bis(*H*₂Me)-N(*i*Pr)C(O)^{*t*Bu}) (Ni(I)-3.5): In a glovebox, **Ni(II)-3.5-Cl** (100 mg, 0.160 mmol) was weighed into a 5 mL vial. Diethyl ether (4.5 mL) was added to the vial, and the resulting purple solution was added to a 20 mL vial containing Na/Hg (0.5 % by Na, 1.1 eq.). A stir bar was added, and the mixture was stirred vigorously for 2 days. Diethyl ether (10 mL) was added, and the yellow solution was filtered through Celite® into a 20 mL vial. The volatiles were removed *in vacuo*, dissolved in minimal toluene, layered with 10 mL hexanes and cooled to -35°C overnight. Paramagnetic yellow crystals formed overnight, and the solid samples of **Ni(I)-3.5** were decanted and dried (64 mg, 68% - multiple crops). X-ray quality crystals were prepared by slow diffusion of hexanes into a concentrated solution of **Ni(I)-3.5** in toluene at -35°C

By Salt Metathesis: In a glovebox, [Ni(μ -Br)(IPr)]₂ (Sigman's Dimer) (100 mg, 0.0948 mmol) was added as a solid at room temperature to a 20 mL vial containing a stirring solution of Na[3.5] (31.5 mg, 0.190 mmol) in toluene (10 mL). The contents were stirred overnight (~12 h), and in the morning removed from the stir plate and allowed to settle for 5 minutes. The supernatant was filtered through Celite®, and the remaining solids were dissolved in toluene (10 mL) and filtered until no solid remained. The filtered toluene was divided equally into 2 vials (10 mL each) and layered with hexanes. Paramagnetic yellow crystals formed overnight at -35°C (106 mg, 95% - multiple crops) and

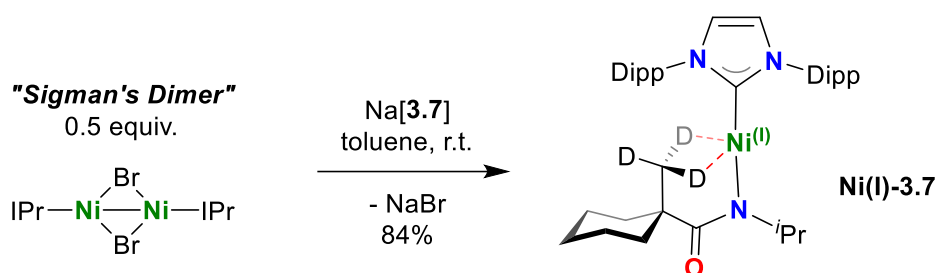
were collected by decanting the vials, washing with cold hexanes (0.5 mL), and removal of volatiles *in vacuo*. Solid **6** was characterized by NMR by comparing to a sample of **Ni(I)-3.5** prepared by reduction.

¹H NMR (400 MHz, 25°C, C₆D₆): δ = 68.4, 26.5, 14.8, 8.94, 8.74, 4.77, 2.94, 1.98. **Evans Method (C₆D₆, 27°C K):** μ_{eff} = 1.87 μ_B . **EI-MS (m/z):** 588 [M]⁺. **Anal. Calcd.** for C₃₅H₅₂N₃NiO (588). C, 71.31%; H, 8.89%; N, 7.13%. Found: C, 71.06%; H, 8.94%; N, 6.92%.



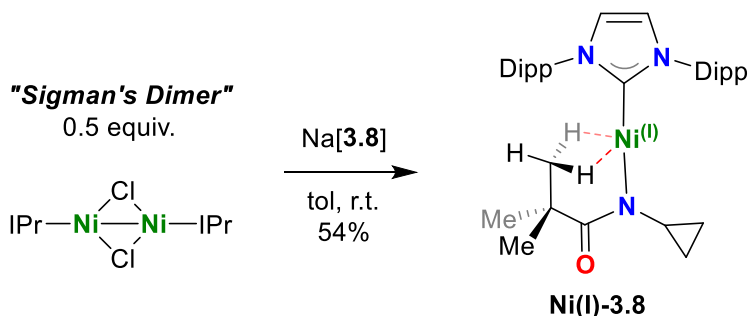
Ni(I)-3.6: In a glovebox, Sigman's Dimer (70 mg, 0.066 mmol) was added as a solid at room temperature to a 20 mL vial containing a stirring solution of Na[**3.6**] (27.2 mg, 0.132 mmol) in toluene (5 mL). The contents were stirred overnight (~12 h), and in the morning removed from the stir plate and allowed to settle for 5 minutes. The supernatant was filtered through Celite®, and the remaining solids were dissolved in toluene (5 mL) and filtered until no solid remained. The filtered toluene was divided equally into 2 vials (5 mL each) and layered with hexanes. Paramagnetic yellow crystals of **Ni(I)-3.6** formed overnight at -35°C (67.1 mg, 0.107 mmol, 81% - multiple crops) and were collected by decanting the vials, washing with cold hexanes (0.5 mL), and removal of volatiles *in vacuo*. X-ray quality crystals were prepared by slow diffusion of hexanes into toluene solutions of **Ni(I)-3.6** in toluene at -35°C.

¹H NMR (400 MHz, 25°C, d₈-tol): δ = 28.01, 17.51, 14.98, 9.11, 8.26, 5.12, 4.22, 2.36, 1.81, 1.24, 0.04, -0.99. **Evans Method (C₆D₆, 27°C):** μ_{eff} = 2.17 μ_B . **EI-MS (m/z):** 628 [M]⁺. **Anal. Calcd.** for C₃₈H₅₆N₃NiO (628). C, 72.50%; H, 8.97%; N, 6.67%. Found: C, 72.24%; H, 9.00%; N, 6.45%.



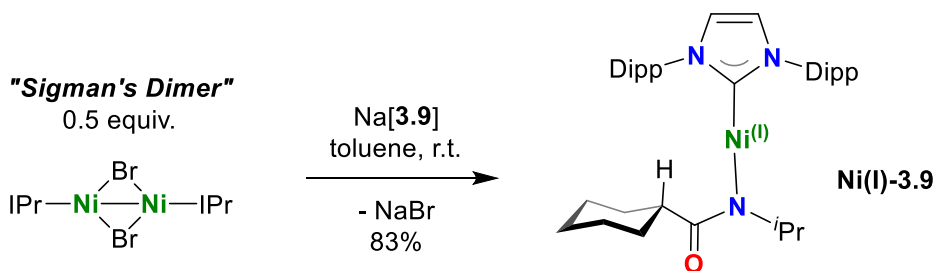
Ni(I)-3.7: In a glovebox, Sigman's Dimer (70 mg, 0.066 mmol) was added as a solid at room temperature to a 20 mL vial containing a stirring solution of Na[3.7] (27.7 mg, 0.132 mmol) in toluene (5 mL). The contents were stirred overnight (~12 h), and in the morning removed from the stir plate and allowed to settle for 5 minutes. The supernatant was filtered through Celite®, and the remaining solids were dissolved in toluene (5 mL) and filtered until no solid remained. The filtered toluene was divided equally into 2 vials (5 mL each) and layered with hexanes. Paramagnetic yellow crystals of **Ni(I)-3.7** formed overnight at -35°C (70 mg, 0.111 mmol, 84% - multiple crops) and were collected by decanting the vials, washing with cold hexanes (0.5 mL), and removal of volatiles *in vacuo*.

¹H NMR (400 MHz, 25°C, *ds*-tol): δ = 28.01, 17.51, 14.98, 9.11, 8.26, 5.12, 4.22, 2.36, 1.81, 1.24, 0.04, -0.99. **EI-MS (m/z):** 631 [M]⁺. **Anal. Calcd.** for C₃₈H₅₃D₃N₃NiO (631). C, 72.15%; H, 9.40%; N, 6.64%. Found: C, 71.76%; H, 9.15%; N, 6.42%. *Analytical Data not sufficient for publication.*



Ni(I)-3.8: In a glovebox, [Ni(μ-Cl)(IPr)]₂ (Sigman's Dimer) (83 mg, 0.086 mmol) was weighed into a 5 mL vial. Na[3.8] (33.7 mg, 0.206 mmol) was weighed into a 20 mL vial and a stir bar was added. THF (3 mL) was added to each vial, and the THF-Na[3.8] vial was stirred for 5 minutes at room temperature. Sigman's dimer was then added dropwise, to the stirring THF solution of Na[3.8] over a period of 15 min. After 30 minutes the THF mixture was filtered through Celite®, and volatiles were removed *in vacuo*. The orange residue was then washed with cold Et₂O (1

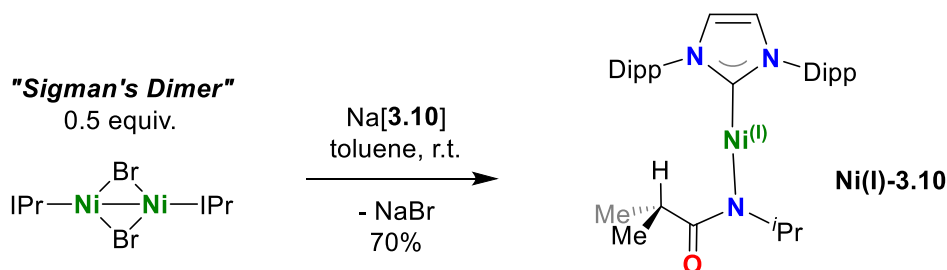
mL) and hexanes (1 mL). Toluene (10 mL) was added to the vial, a stirring bar was added, and the mixture was stirred for 5 minutes at room temperature. This mixture was then filtered through Celite® and layered with cold hexanes. Yellow crystals of **Ni(I)-3.8** formed after two nights at -35°C (55 mg, 54%, 0.094 mmol, 2 crops), which were collected by decanting the vial, washing with cold hexanes (0.5 mL), and drying *in vacuo*. X-ray quality crystals were prepared by slow diffusion of hexanes into a concentrated solution of **Ni(I)-3.8** in toluene at -35°C. **N.B.** *Complex Ni(I)-3.8 reacts with Sigman's Dimer to produce myriad products. Thus, Sigman's Dimer must be added to Na[3.8] in THF dropwise to avoid a high concentration of Sigman's Dimer in solution. Using higher equivalents of Na[3.8] (1.5 to 10 equiv.) resulted in contaminated material.* **¹H NMR (400 MHz, 25°C, C₆D₆)** δ 64.41, 30.80, 15.03, 9.31, 8.38, 4.36, 2.43, 2.04, 1.86, -11.70. **Evans Method (C₆D₆, 25°C):** $\mu_{\text{eff}} = 1.6 \mu_B$. **EI-MS (m/z):** 585 [M-1]⁺. **Anal. Calcd.** for C₃₅H₅₀N₃NiO (587). C, 71.56%; H, 8.58%; N, 7.15%. Found: C, 71.55%; H, 8.53%; N, 7.08%.



Ni(I)-3.9: In a glovebox, Sigman's Dimer (50 mg, 0.0474 mmol) was added as a solid at room temperature to a 20 mL vial containing a stirring solution of Na[3.9] (18.1 mg, 0.0948 mmol) in toluene (5 mL). The contents were stirred overnight (~12 h), and in the morning removed from the stir plate and allowed to settle for 5 minutes. The supernatant was filtered through Celite®, and the remaining solids were dissolved in toluene (10 mL) and filtered until no solid remained. The filtered toluene was divided equally into 2 vials (10 mL each) and layered with hexanes. Paramagnetic yellow crystals of **Ni(I)-3.9** formed overnight at -35°C (26.2 mg, 45% - single crop) and were collected by decanting the vials, washing with cold hexanes (0.5 mL), and removal of volatiles *in vacuo*. X-ray quality crystals were prepared by slow diffusion of hexanes into a concentrated solution of **Ni(I)-3.9** in toluene at -35°C.

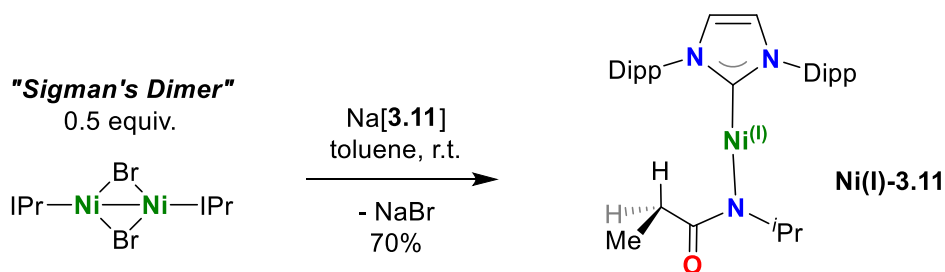
¹H NMR (300 MHz, 25°C, C₆D₆): δ(ppm) = 52.46, 32.35, 31.04, 27.01, 20.49, 15.20, 7.16, 4.96, 3.55, 2.79, 2.30, 1.90, 0.44, 0.29, -1.09, -2.28, -4.65, -5.14, -5.53, -5.77, -6.41, -15.35, -20.90. **Evans Method (C₆D₆, 24°C):** $\mu_{\text{eff}} =$

2.12 μ_B . **EI-MS** (m/z): 614 $[M]^+$. **Anal. Calcd.** for $C_{37}H_{54}N_3NiO$ (614). C, 72.20%; H, 8.84%; N, 6.83%. Found: C, 71.97%; H, 8.55%; N, 6.75%.



Ni(I)-3.10: In a glovebox, $[Ni(\mu-Br)(IPr)]_2$ (Sigman's Dimer) (105 mg, 0.099 mmol) was added as a solid at room temperature to a 20 mL vial containing a stirring solution of Na[3.10] (30 mg, 0.198 mmol) in toluene (10 mL). The contents were stirred overnight (~12 h), and in the morning removed from the stir plate and allowed to settle for 5 minutes. The supernatant was filtered through Celite®, and the remaining solids were dissolved in toluene (10 mL) and filtered until no solid remained. The filtered toluene solution was reduced to ~10 mL *in vacuo* and layered with hexanes. Paramagnetic yellow crystals of **Ni(I)-3.10** formed over two nights at $-35^\circ C$ (79 mg, 70%) and were collected by decanting the vial, washing with cold hexanes (0.5 mL), and removal of volatiles *in vacuo*. X-ray quality crystals were prepared by slow diffusion of hexanes into a concentrated solution of **Ni(I)-3.10** in toluene at $-35^\circ C$.

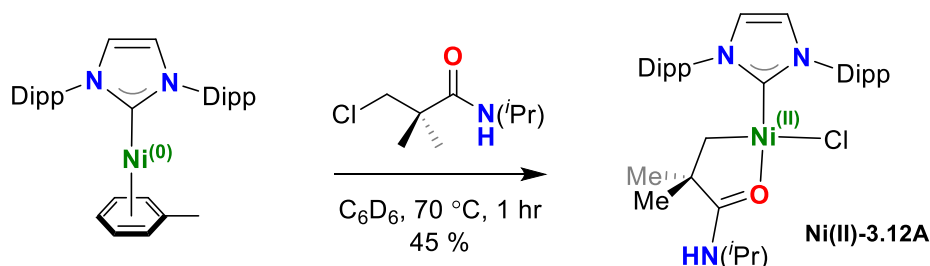
1H NMR (400 MHz, $25^\circ C$, C_6D_6) δ 44.04, 27.79, 27.07, 19.05, 15.06, 12.64, 10.34, 7.55, 4.94, 3.58, 2.57, 1.90, -2.80, -4.50, -5.66, -9.27. **Evans Method (C_6D_6 , $25^\circ C$):** $\mu_{eff} = 2.20 \mu_B$. **EI-MS** (m/z): 574 $[M]^+$. **Anal. Calcd.** for $C_{34}H_{50}N_3NiO$ (574). C, 70.96%; H, 8.76%; N, 7.30%. Found: C, 70.71%; H, 8.83%; N, 7.24%



Ni(I)-3.11: In a glovebox, Sigman's Dimer (40 mg, 0.0379 mmol) was added as a solid at room temperature to a 20 mL vial containing a stirring slurry of Na[3.11] (10.4 mg, 0.0759 mmol) in toluene (5 mL). The contents were stirred overnight (~12 h), and in the morning removed from the stir plate and allowed to settle for 5 minutes. The supernatant was filtered through Celite®, and the remaining solids were dissolved in toluene (~2-3 mL) and filtered until no solid

remained. The filtered toluene was divided equally into 2 vials and layered with hexanes. Paramagnetic yellow crystals of **Ni(I)-3.11** formed overnight at -35°C (29 mg, 68%) and were collected by decanting the vials, washing with cold hexanes (0.5 mL), and removal of volatiles *in vacuo*. X-ray quality crystals were prepared by slow diffusion of hexanes into a concentrated solution of **Ni(I)-3.11** in toluene at -35°C .

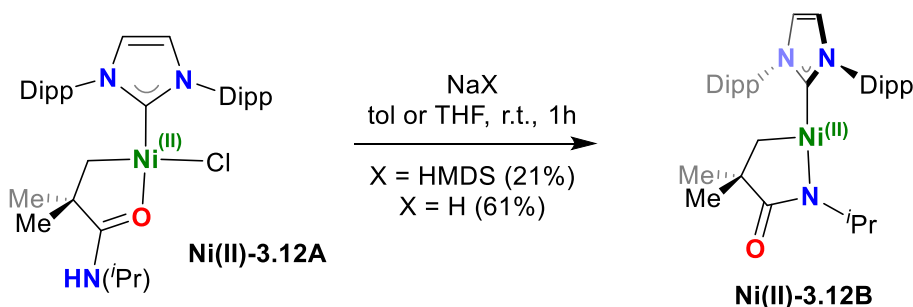
^1H NMR (400 MHz, 25°C , C_6D_6): δ = 49.26, 46.95, 29.08, 27.95, 19.21, 15.32, 15.14, 13.90, 13.04, 10.16, 4.83, 4.43, 3.29, 2.47, 1.86, -2.96, -4.97, -5.97, -11.02, -58.21. **Evans Method (C_6D_6 , 25°C):** μ_{eff} = 2.06 μB . **EI-MS (m/z):** 560 $[\text{M}]^+$. **Anal. Calcd.** for $\text{C}_{33}\text{H}_{48}\text{N}_3\text{NiO}$ (561). C, 70.60%; H, 8.62%; N, 7.48%. Found: C, 66.24%; H, 7.74%; N, 6.59%. *Analytical Data not sufficient for publication.*



Ni(II)-3.12A: In a glovebox, $(\text{iPr})\text{Ni}(\eta_6\text{-toluene})$ (205 mg, 0.428 mmol) and amide **3.12** were each weighed into separate 1-dram vials. The solids were then suspended in benzene (~ 2 mL) and introduced to a J-Young NMR tube. After removing the sealed J-Young from the glovebox, the mixture was heated in an oil bath at 70°C overnight. The J-Young tube was then re-introduced to the glovebox, and the mixture was dried *in vacuo*. The residue was then taken up in minimal toluene and filtered through a Celite® plug. Layering with hexanes forms analytically pure **Ni(II)-3.12A** (115 mg, 45% - multiple crops) over several days. X-ray quality crystals were obtained from concentrated samples of **Ni(II)-3.12A** in toluene with slow diffusion of hexanes.

^1H NMR (400 MHz, 25°C , C_6D_6): δ = 7.39-7.28 (m, $m\text{-Ar}_{\text{IPr}}\text{-H}$, 4H), 7.24 (d, $^3J_{\text{H,H}}$ = 6.0 Hz, $p\text{-Ar}_{\text{IPr}}\text{-H}$, 2H), 6.53 (s, $\text{CH}=\text{CH}$, 2H), 6.45 (bs, $\text{HN}(\text{iPr})$, 1H), 4.05 (sept, $^3J_{\text{H,H}}$ = 6.0 Hz, $\text{Ar}_{\text{IPr}}\text{-iPr}(\text{CH})$, 2H), 3.53 (sept, $^3J_{\text{H,H}}$ = 6.8 Hz, $\text{N-iPr}(\text{CH})$, 1H), 2.76 (d, $^3J_{\text{H,H}}$ = 6.0 Hz, $\text{Ar}_{\text{IPr}}\text{-iPr}(\text{CH})$, 2H), 1.81 (d, $^3J_{\text{H,H}}$ = 6.0 Hz, $\text{Ar}_{\text{IPr}}\text{-iPr}(\text{CH}_3)$, 6H), 1.45 (d, $^3J_{\text{H,H}}$ = 6.0 Hz, $\text{Ar}_{\text{IPr}}\text{-iPr}(\text{CH}_3)$, 6H), 1.12 (d, $^3J_{\text{H,H}}$ = 6.0 Hz, $\text{Ar}_{\text{IPr}}\text{-iPr}(\text{CH}_3)$, 6H), 1.03 (d, $^3J_{\text{H,H}}$ = 6.0 Hz, $\text{Ar}_{\text{IPr}}\text{-iPr}(\text{CH}_3)$, 6H), 0.90 (s, $(\text{C}=\text{O})\text{C}(\text{CH}_3)_2$, 6H), 0.72 (d, $^3J_{\text{H,H}}$ = 6.8 Hz, $\text{N-iPr}(\text{CH}_3)$, 6H), 0.49 (s, $\text{H}_2\text{C-Ni}$, 2H). **$^{13}\text{C}\{^1\text{H}\}$ NMR (101 MHz, 25°C , C_6D_6):** 188.2(C=O), 181.4($\text{C}_{\text{IPr}}\text{-Ni}$), 148.6($o\text{-C}_{\text{Ar}1}$), 145.4($o\text{-C}_{\text{Ar}2}$), 137.7(N-iC_{Ar}), 129.9($m\text{-C}_{\text{Ar}}$), 125.4($m\text{-C}_{\text{Ar}}$).

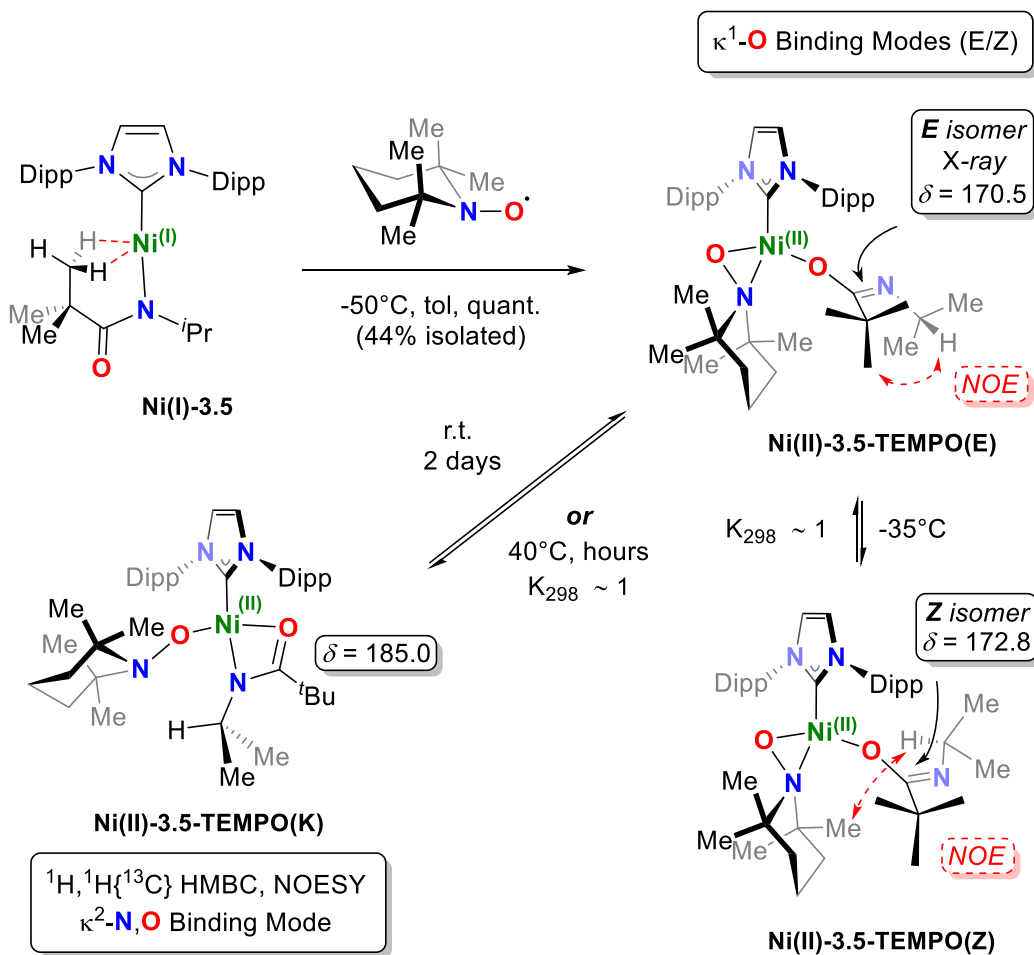
C_{Ar} , 124.2(HC=CH), 123.4(p - C_{Ar}), 48.5((C=O)C(CH₃)₂), 42.5(N- i Pr(CH)), 29.1(Ar- i Pr(CH)), 28.6(Ar- i Pr(CH)), 28.2((C=O)C(CH₃)₂), 26.6(Ar- i Pr(CH₃)), 26.4(Ar- i Pr(CH₃)), 24.0(Ar- i Pr(CH₃)), 22.9(Ar- i Pr(CH₃)), 22.2 (overlapped - (N- i Pr(CH₃)), (H₂C-Ni)). **EI(m/z):** 623 [M]⁺. *Elemental analysis suggests the incorporation of toluene in samples of Ni(II)-3.12A. Additionally, toluene molecules were found in the crystal structure, and consistently in the NMR of dried samples. Crushing crystals and extended drying continually led to analytical data consistent with approximately 0.5 equiv. toluene incorporation* **Anal. Calcd.** for C₃₅H₅₂ClN₃NiO (623). C, 67.27%; H, 8.39%; N, 6.72%. **Anal. Calcd.** for C_{38.5}H₅₆ClN₃NiO (671 for 0.5 equiv. toluene). C, 68.91%; H, 8.41%; N, 6.26%. Found (avg. of 2 runs): C, 69.05%; H, 8.56%; N, 6.34%



Ni(II)-3.12B (w/ NaHMDS): In glovebox, **Ni(II)-3.12A** (30 mg, 0.048 mmol) was weighed into a 1-dram vial. To this vial was added toluene (~ 2 mL) and a stir bar. This solution was stirred at room temperature to fully dissolved **Ni(II)-3.12A** which does not happen readily. During this process, NaHMDS (8.8 mg, 0.048 mmol) was weighed into a 1-dram vial and dissolved in minimal toluene (~ 1 mL). The toluene solution of NaHMDS was then added slowly to the vial of **Ni(II)-3.12A** dropwise. After 1 hour, the mixture was filtered through Celite® into a 1-dram vial, which was placed into a 4 dram vial which contained ~ 4 mL hexanes. Over a period of 2-3 days, **Ni(II)-3.12B** precipitates as a blue semi-crystalline solid (6 mg, 21%).

Ni(II)-3.12B (w/ NaH): In glovebox, **Ni(II)-3.12A** (26 mg, 0.042 mmol) was weighed into a 1-dram vial. To this vial was added THF (~ 2 mL) and a stir bar. NaH (2.0 mg, 0.042 mmol) was weighed into a 1-dram vial and dissolved in minimal THF (~ 1 mL). The THF solution of NaH was then added slowly to the vial of **Ni(II)-3.12A** dropwise. After 1 hour, the mixture dried in vacuo and taken up in diethyl ether. This solution was then filtered through Celite® and dried in vacuo to give **Ni(II)-3.12B** as a blue semi-crystalline solid (15 mg, 61%).

^1H NMR (400 MHz, 25°C , C_6D_6): δ = 7.19 (t, $^3J_{\text{H,H}}$ = 8.1 Hz, $p\text{-Ar}_{\text{IPr}}\text{-H}$, 2H), 7.06 (d, $^3J_{\text{H,H}}$ = 7.8 Hz, $m\text{-Ar}_{\text{IPr}}\text{-H}$, 4H), 6.34 (s, $\text{CH}=\text{CH}$, 2H), 3.86 (sept, $^3J_{\text{H,H}}$ = 6.4 Hz, $\text{N-}i\text{Pr}(\text{CH})$, 1H), 2.93 (sept, $^3J_{\text{H,H}}$ = 6.8 Hz, $\text{Ar}_{\text{IPr}}\text{-}i\text{Pr}(\text{CH})$, 4H), 1.59 (d, $^3J_{\text{H,H}}$ = 6.8 Hz, $\text{Ar}_{\text{IPr}}\text{-}i\text{Pr}(\text{CH}_3)$, 12H), 1.15 (s, $(\text{C}=\text{O})\text{C}(\text{CH}_3)_2$, 6H), 1.07 (s, $\text{H}_2\text{C-Ni}$, 2 H), 1.03 (d, $^3J_{\text{H,H}}$ = 6.8 Hz, $\text{Ar}_{\text{IPr}}\text{-}i\text{Pr}(\text{CH}_3)$, 12H), 0.53 (d, $^3J_{\text{H,H}}$ = 6.4 Hz, $\text{N-}i\text{Pr}(\text{CH}_3)$). **$^{13}\text{C}\{^1\text{H}\}$ NMR (101 MHz, 25°C , C_6D_6):** 182.5($\text{C}=\text{O}$), 181.9($\text{C}_{\text{IPr}}\text{-Ni}$), 146.0($o\text{-C}_{\text{Ar}}$), 135.2($\text{N-}i\text{C}_{\text{Ar}}$), 130.6($p\text{-C}_{\text{Ar}}$), 124.7($m\text{-C}_{\text{Ar}}$), 123.7($\text{HC}=\text{CH}$), 46.5($(\text{C}=\text{O})\text{C}(\text{CH}_3)_2$), 44.4($\text{N-}i\text{Pr}(\text{CH})$), 29.1($\text{Ar-}i\text{Pr}(\text{CH})$), 28.1($(\text{C}=\text{O})\text{C}(\text{CH}_3)_2$), 25.1($\text{Ar-}i\text{Pr}(\text{CH}_3)$), 23.9($\text{Ar-}i\text{Pr}(\text{CH}_3)$), 22.9($\text{N-}i\text{Pr}(\text{CH}_3)$), 18.1($\text{H}_2\text{C-Ni}$). **EI(m/z):** 587 $[\text{M}]^+$. **Anal. Calcd.** for $\text{C}_{35}\text{H}_{51}\text{N}_3\text{NiO}$ (587). C, 71.43%; H, 8.74%; N, 7.14%. Found: C, 71.07%; H, 8.62%; N, 7.33%



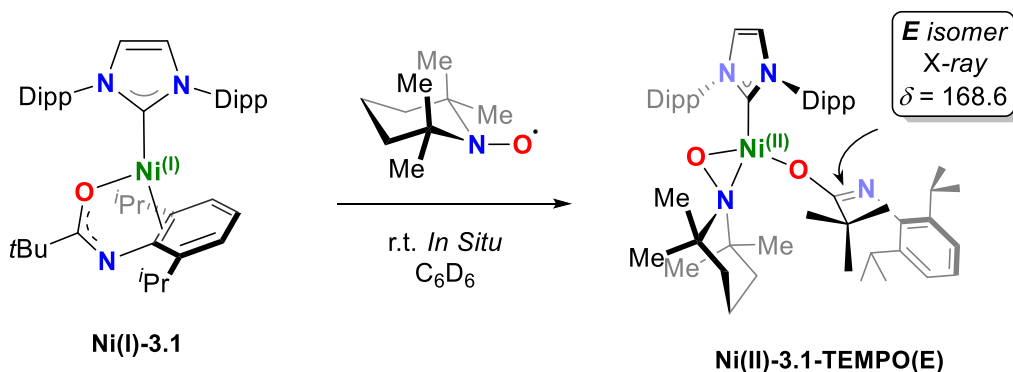
Ni(II)-3.5-TEMPO(E/Z/K):

NMR Scale Reactions:

Method A (-50 °C, GB cold-well): In a glove-box, **Ni(I)-3.5** (10 mg, 0.017 mmol) and TEMPO (2.6 mg, 0.017 mmol) were weighed into separate 1-dram vials. D₈-toluene (~0.3 mL) was then added to each vial, and the solutions were cooled in a glovebox cold-well for 1 hour. A J-Young NMR tube was also cooled in the cold-well, and the components were then mixed, and added the NMR tube. The NMR tube was then sealed, and quickly removed from the box before being submerged in an isopropanol/dry-ice bath. The cooled NMR tube was then brought to the NMR facility and introduced to the NMR spectrometer which was pre-cooled to -50 °C.

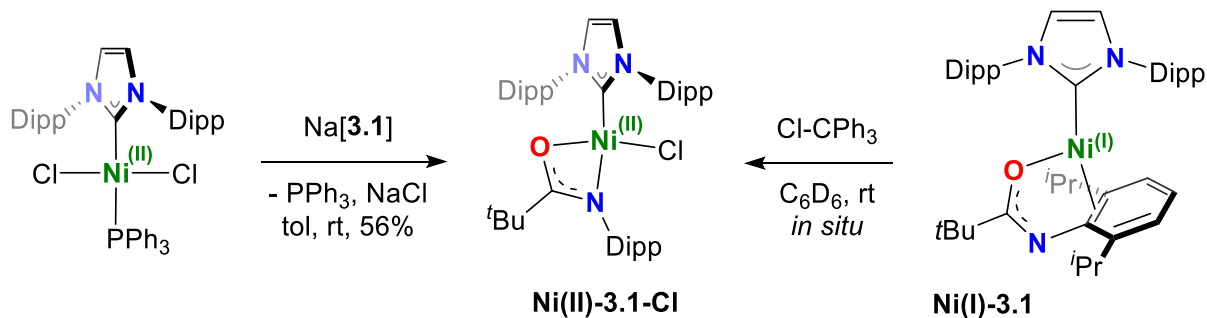
Method B: (room temp): Same as method A, but simply mixed at room temperature.

See NMR spectra



Ni(II)-3.1-TEMPO(E): In a glovebox, **Ni(I)-3.1** (10 mg, 0.015 mmol) and TEMPO (2.3 mg, 0.015 mmol) were weighed into separate 1-dram vials. D₈-toluene (~0.3 mL) was then added to each vial, and the solutions were then mixed, and added to a J-Young NMR tube. The NMR tube was then sealed and removed from the glovebox and analyzed immediately by NMR spectroscopy.

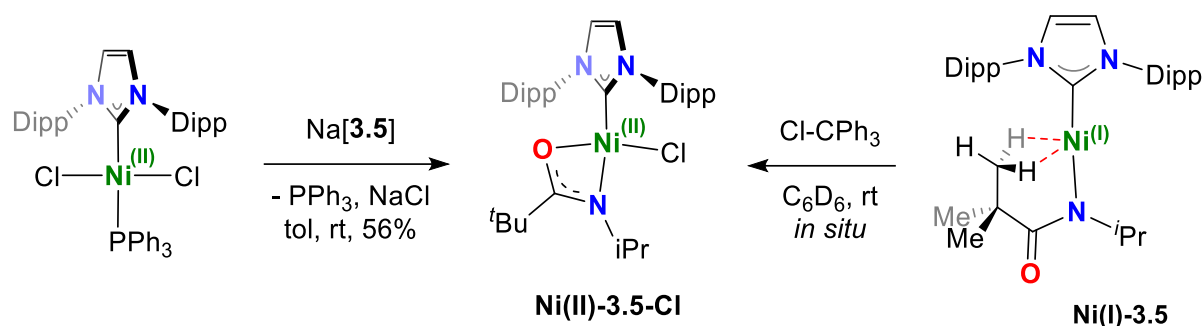
See NMR spectra



Ni(II)-3.1-Cl from **Ni(IPr)(PPh₃)Cl₂**: In a glovebox, Ni(IPr)(PPh₃)Cl₂ (300 mg, 0.384 mmol) and Na[**3.1**] (109 mg, 0.384 mmol) were added into separate 50 mL Schlenk flasks. The flasks were sealed and introduced onto a Schlenk line following established procedures and dry THF (2 x 15 mL) was added to each flask with stirring. Na[**3.1**] was then added by cannula to Ni(IPr)(PPh₃)Cl₂ at room temperature in a dropwise fashion to avoid bis-complexation of the ligand. After stirring for 2 hours, the reaction mixture was filtered *via* cannula filtration into a dried and degassed 50 mL Schlenk flask. Following removal of volatiles *in vacuo*, the evacuated flask was re-introduced into the glovebox where the residue was extracted with minimal ether, filtered through Celite®, and volatiles were removed *in vacuo*. Hexanes (2 mL) was added to the purple-red solids and the mixture was cooled overnight at -35°C overnight. The hexanes were decanted, and the resulting purple solids were washed with cold hexanes (2 x 2 mL) to produce an analytically pure powder of **Ni(II)-3.1-Cl** (161 mg, 56%). X-ray quality crystals were grown by evaporation of a concentrated ether solutions of **Ni(II)-3.1-Cl**.

Ni(II)-3.1-Cl from **Ni(I)-3.1**: In a glovebox, **Ni(I)-3.1** (10 mg, 0.015 mmol) and Cl-CPh₃ (4.2 mg, 0.015 mmol) were weighed into separate 1-dram vials. C₆D₆ (0.6 mL) was then added to the vial containing Cl-CPh₃, and the solution was added to **Ni(I)-3.1** and added to a J-Young NMR tube. The NMR tube was then sealed and removed from the glovebox and analyzed immediately by NMR spectroscopy. Only **Ni(II)-3.1-Cl** was observed; no paramagnetic signals of **Ni(I)-3.1** were observed.

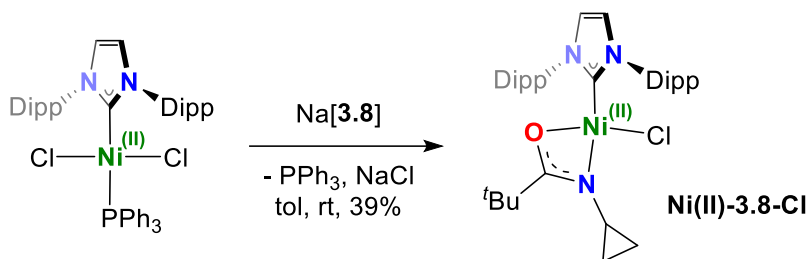
¹H NMR (400 MHz, 25°C, C₆D₆): δ = 7.45–7.42 (dd, ³J_{H,H} = 6.2, 9.0 Hz, *p*-Ar_{IPr}-H, 2H), 7.39 (d, ³J_{H,H} = 6.2 Hz, *m*-Ar_{IPr}-H, 2H), 7.38 (d, ³J_{H,H} = 9.0 Hz, *m*'-Ar_{IPr}-H, 2H), 6.97 (dd, ³J_{H,H} = 7.0, 8.1 Hz, *p*-Ar_{Am}-H, 1H), 6.88 (d, ³J_{H,H} = 7.5 Hz (avg. 7.0, 8.1 Hz), *m,m*'-Ar_{IPr}-H, 2H), 6.49 (s, CH=CH, 2H), 3.77 (sept, ³J_{H,H} = 6.8 Hz, Ar_{Am}-iPr(CH), 2H), 3.05 (sept, ³J_{H,H} = 6.7 Hz, Ar_{IPr}-iPr(CH), 4H), 1.60 (d, ³J_{H,H} = 6.7 Hz, Ar_{IPr}-iPr(CH₃), 12H), 1.44 (d, ³J_{H,H} = 6.8 Hz, Ar_{Am}-iPr(CH₃), 6H), 1.30 (d, ³J_{H,H} = 6.8 Hz, Ar_{Am}-iPr'(CH₃), 6H), 1.04 (d, ³J_{H,H} = 6.7 Hz, Ar_{IPr}-iPr'(CH₃), 12H), 0.75 (s, *t*Bu, 9H). **¹³C{¹H} NMR (101 MHz, 25°C, C₆D₆)** δ = 187.60(C=O), 162.27(C_{IPr}-Ni), 147.19, 143.08, 136.72, 136.18, 130.39(*p*-C_{Ar(IPr)}), 125.35(*p*-C_{Ar(Am)}), 124.90(HC=CH), 124.23(*m*-C_{Ar(IPr)}), 122.72(*m*-C_{Ar(Am)}), 41.26(CMe₃), 28.93(Ar_{IPr}-iPr(CH), Ar_{Am}-iPr(CH)), 27.61(*t*Bu(CH₃)), 26.18(Ar_{IPr}-iPr(CH₃)), 25.41(Ar_{Am}-iPr(CH₃)), 23.17(Ar_{IPr}-iPr(CH₃)), 22.97(Ar_{Am}-iPr(CH₃)). **EI-MS (m/z):** 741 [M]⁺. **Anal. Calcd.** for C₄₄H₆₂ClN₃NiO (741). C, 71.11%; H, 8.41%; N, 5.65%. Found: C, 71.43%; H, 8.40%; N, 5.63%.



Ni(II)-3.5-Cl from **Ni(IPr)(PPh₃)Cl₂** In a glovebox, Ni(IPr)(PPh₃)Cl₂ (700 mg, 0.897 mmol) and Na[3.5] (148 mg, 0.897 mmol) were added into separate 50 mL Schlenk flasks. The flasks were sealed and introduced onto a Schlenk line following established procedures and dry THF (15 mL) was added to each flask with stirring. Na[3.5] was then added by cannula to Ni(IPr)(PPh₃)Cl₂ at room temperature in a dropwise fashion to avoid bis-complexation of the ligand. After stirring for 2 hours, the reaction mixture was filtered *via* cannula filtration into a dried 50 mL Schlenk flask. Following removal of volatiles *in vacuo*, the evacuated flask was re-introduced into the glovebox where the residue was extracted with ether, filtered through Celite® and cooled overnight at -35°C to produce analytically pure purple crystals of **Ni(II)-3.5-Cl** (426 mg, 76%). The crystals were washed with cold hexanes (1 mL) and dried *in vacuo*. X-ray quality crystals of **Ni(II)-3.5-Cl** were obtained by slow diffusion of hexanes into a saturated toluene solution.

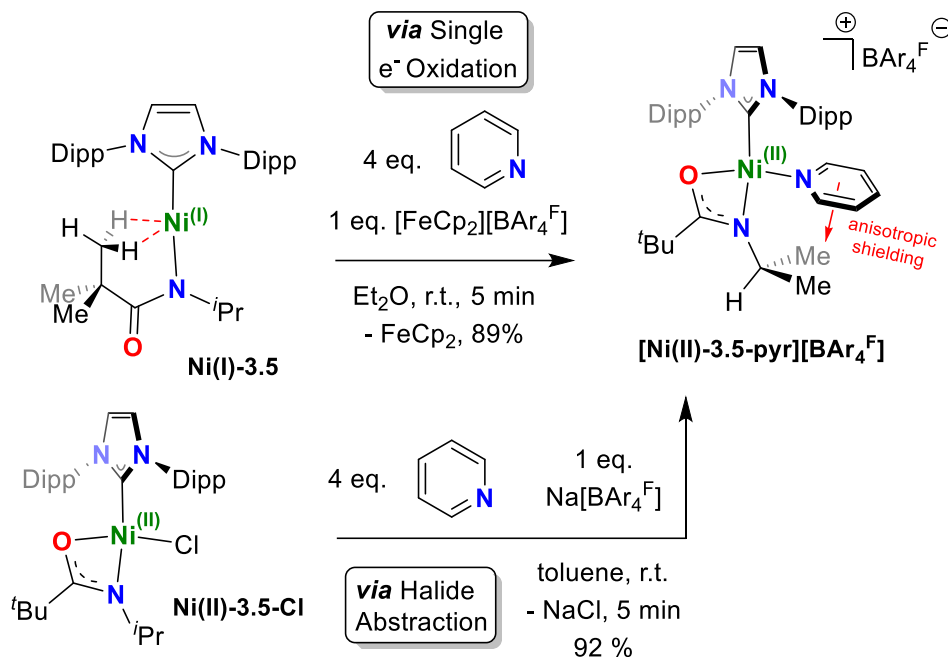
Ni(II)-3.5-Cl from **Ni(I)-3.5**: In a glovebox, **Ni(I)-3.5** (10 mg, 0.017 mg) and Cl-CPh₃ (4.8 mg, 0.017 mmol) were weighed into separate 1-dram vials. C₆D₆ (0.6 mL) was then added to the vial containing Cl-CPh₃, and the solution was added to **Ni(I)-3.5** and added to a J-Young NMR tube. The NMR tube was then sealed and removed from the glovebox and analyzed immediately by NMR spectroscopy. Only **Ni(II)-3.5-Cl** was observed; no paramagnetic signals of **Ni(I)-3.5** were observed.

¹H NMR (600 MHz, 25°C, C₆D₆): δ = 7.35–7.33 (m, Ar-*H*, 6H), 6.46 (s, CH=CH, 2H), 3.13 (sept, ³*J*_{H,H} = 6.7 Hz, Ar-*i*Pr(CH), 4H), 3.01 (sept, ³*J*_{H,H} = 6.3 Hz, N-*i*Pr(CH), 1H), 1.70 (d, ³*J*_{H,H} = 6.7 Hz, Ar-*i*Pr(CH₃), 12H), 1.06 (d, ³*J*_{H,H} = 6.7 Hz, Ar-*i*Pr(CH₃), 12H), 1.03 (d, ³*J*_{H,H} = 6.3 Hz, N-*i*Pr(CH₃), 6H), 0.75 (s, *t*Bu, 9H). **¹³C{¹H} NMR (151 MHz, 25°C, C₆D₆):** δ = 186.5(C=O), 164.1(C_{IPr}-Ni), 147.0(*o*-C_{Ar}), 136.2(N-*i*C_{Ar}), 130.3(*p*-C_{Ar}), 124.6(HC=CH), 124.3(*m*-C_{Ar}), 45.91(N-*i*Pr(CH)), 39.03(CMe₃), 28.94(Ar-*i*Pr(CH)), 27.22(*t*Bu(CH₃)), 26.09(Ar-*i*Pr(CH₃)), 23.68(Ar-*i*Pr(CH₃)), 23.09(N-*i*Pr(CH₃)). **EI-MS (m/z):** 623. **Anal. Calcd.** for C₃₅H₅₂ClN₃NiO (623). C, 67.27%; H, 8.39%; N, 6.72%. Found: C, 67.28%; H, 8.45%; N, 6.67%.



Ni(II)-3.8-Cl: In a glovebox, Ni(IPr)(PPh₃)Cl₂ (100 mg, 0.128 mmol) was weighed into a 20 mL vial. A stirring bar and THF (3 mL) were added to the same vial, and the red solution was stirred. Na[**3.8**] (20.2 mg, 0.123 mmol) was then weighed into a 5 mL vial, and subsequently THF (2 mL) was added. The clear solution of Na[**3.8**] in THF was then added dropwise to the red solution of Ni(IPr)(PPh₃)Cl₂ in THF at room temperature over a period of 5 minutes. After stirring for 20 minutes, the reaction mixture was filtered through Celite® into a 20 mL vial. Following removal of volatiles *in vacuo*, the red-purple residue was dissolved in Et₂O (~1.5 mL), filtered through Celite®, and cooled overnight at -35°C to produce analytically pure and X-ray quality purple crystals of **Ni(II)-3.8-Cl**. The crystals were washed with cold hexanes (1 mL) and dried *in vacuo* (30 mg, 39%, 0.048 mmol). *See the X-ray section (below).* **N.B.** Dissolving fresh crystals of **Ni(II)-3.8-Cl** affords ¹H and ¹³C{¹H} NMR spectra analogous to complex **Ni(II)-3.5-Cl**. However, solutions of **Ni(II)-3.8-Cl** in C₆D₆ decompose over time (overnight ~10%) to multiple unknown diamagnetic and paramagnetic products. *See ¹H NMR spectra (Figure S24) which show the decomposition over time.*

¹H NMR (400 MHz, 25°C, C₆D₆): δ = 7.35–7.32 (m, Ar-H, 6H), 6.49 (s, CH=CH, 2H), 3.07 (sept, ³J_{H,H} = 6.8 Hz, Ar-*i*Pr(CH), 4H), 2.07 (m, ³J_{H,H} = 3.5, 3.9 Hz, N-cyp(CH), 1H), 1.67 (d, ³J_{H,H} = 6.8 Hz, Ar-*i*Pr(CH₃), 12H), 1.04 (d, ³J_{H,H} = 6.7 Hz, Ar-*i*Pr(CH₃), 12H), 0.85 (m, N-cyp(H_BH_AC-C'H_AH_B), 2H), 0.84 (s, *t*Bu, 9H), 0.09 (m, ³J_{H,H} = 6.3 Hz, N-cyp(H_BH_AC-C'H_AH_B), 2H). **¹³C{¹H} NMR (101 MHz, 25°C, C₆D₆):** δ = 189.8(C=O), 147.0(*o*-C_{Ar}), 136.3(N-*i*C_{Ar}), 130.4(*p*-C_{Ar}), 125.4(HC=CH), 124.4(*m*-C_{Ar}), 39.5(CMe₃), 28.9(Ar-*i*Pr(CH)), 28.6(N-cyp(CH)), 27.1(*t*Bu(CH₃)), 26.1(Ar-*i*Pr(CH₃)), 23.7(Ar-*i*Pr(CH₃)), 7.8(N-cyp(CH₂)). *The carbene C_{IPr}-Ni resonance was not detected.* **EI-MS (m/z):** 621 **Anal. Calcd.** for C₃₅H₅₀ClN₃NiO (623). C, 67.48%; H, 8.09%; N, 5.69%. Found: C, 67.73%; H, 8.31%; N, 5.69%.

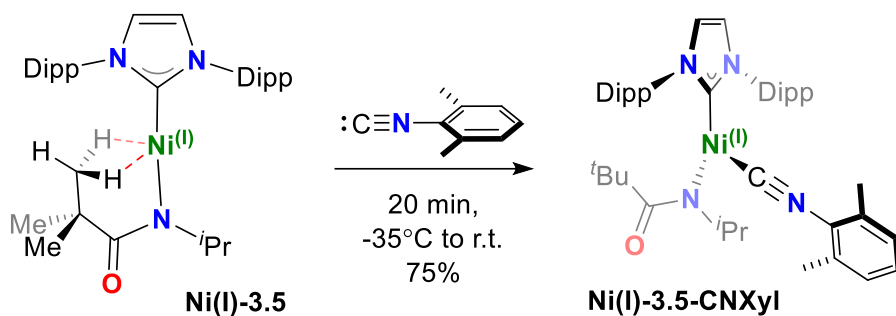


$[\text{Ni(II)-3.5-pyr}][\text{BAR}_4\text{F}]$: In a glovebox, complex **Ni(I)-3.5** (20 mg, 0.034 mmol) in diethyl ether (1 mL) was added to solution of $[\text{Cp}_2\text{Fe}][\text{BAR}_4\text{F}]$ (39.2 mg, 0.034 mmol) in diethyl ether (1 mL) in a 20 mL vial. The solution was stirred with a magnetic stir bar for 2 minutes at room temperature. Pyridine (~ 1 drop) was added to this solution and the mixture was stirred for an additional minute. This diethyl ether solution was filtered through Celite® into a new vial, and the volatiles were removed *in vacuo*. The resulting residue was then washed with hexanes (3 x 2 mL). The orange residue remaining was dissolved in minimal diethyl ether (~ 1 mL) and filtered through Celite® into a 5 mL vial. Removing the volatiles gives **$[\text{Ni(II)-3.5-pyr}][\text{BAR}_4\text{F}]$** as an orange solid (46 mg, 0.030 mmol, 89%). Ether solutions carefully layered with hexanes, and cooled -35°C afford X-ray quality orange crystals of **$[\text{Ni(II)-3.5-pyr}][\text{BAR}_4\text{F}]$** over two nights.

By Chloride Abstraction: In a glovebox, a solution of complex **Ni(II)-3.5-Cl** (21.2 mg, 0.034 mmol) in 1.0 mL diethyl ether was added to a solution of $\text{Na}[\text{BAR}_4\text{F}]$ (33 mg, 0.034 mmol) and pyridine (~ 1 drop) in diethyl ether (1 mL). This diethyl ether solution was stirred for 5 minutes, then filtered through Celite® into a new vial, and the volatiles were removed *in vacuo*. The resulting residue was then washed with hexanes (3 x 2 mL). The orange residue remaining was dissolved in minimal diethyl ether (~ 1 mL) and filtered through Celite® into a 5 mL vial. Removing the volatiles gives **$[\text{Ni(II)-3.5-pyr}][\text{BAR}_4\text{F}]$** as an orange solid (47.5 mg, 0.031 mmol, 92%).

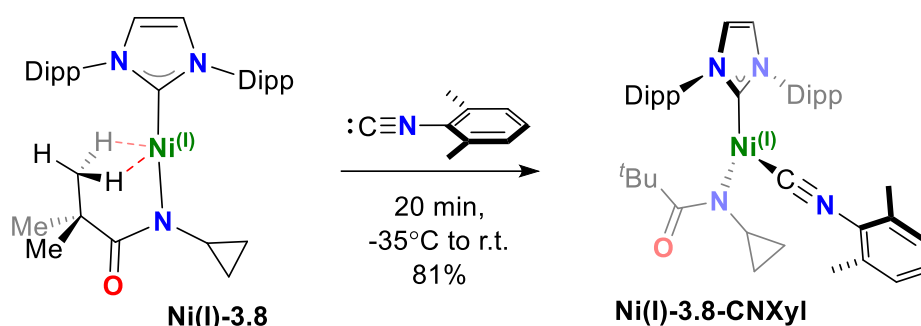
¹H NMR (400 MHz, 25°C, C₇D₈): δ = 8.29 (s, *o*-Ar_{BAr4}-H, 8H), 7.74 (d, ³*J*_{H,H} = 5.2 Hz, *o*-Ar_{pyr}-H, 2H), 7.76 (s, *p*-Ar_{BAr4}-H, 4H), 7.21 (t, ³*J*_{H,H} = 7.7 Hz, *p*-Ar_{IPr}-H, 2H), 7.04 (³*J*_{H,H} = 7.7 Hz, *m*-Ar_{IPr}-H, 4H), 6.56 (t, ³*J*_{H,H} = 7.8 Hz, *p*-Ar_{pyr}-H, 1H), 6.30 (s, CH=CH, 2H), 6.21 (t, ³*J*_{H,H} = 6.8 Hz, *m*-Ar_{pyr}-H, 2H), 2.75 (sept, ³*J*_{H,H} = 6.4 Hz, N-*i*Pr(CH), 1H), (sept, ³*J*_{H,H} = 6.8 Hz, Ar-*i*Pr(CH), 4H), 1.23 (d, ³*J*_{H,H} = 6.8 Hz, Ar-*i*Pr(CH₃), 12H), 0.90 (d, ³*J*_{H,H} = 6.8 Hz, Ar-*i*Pr(CH₃), 12H), 0.52 (s, ^{*t*}Bu, 9H), -0.17 (d, ³*J*_{H,H} = 6.4 Hz, N-*i*Pr(CH₃), 6H).

¹H-¹³C{¹H} HMBC (400MHz, 25°C, C₇D₈): δ = 192.3(C=O)

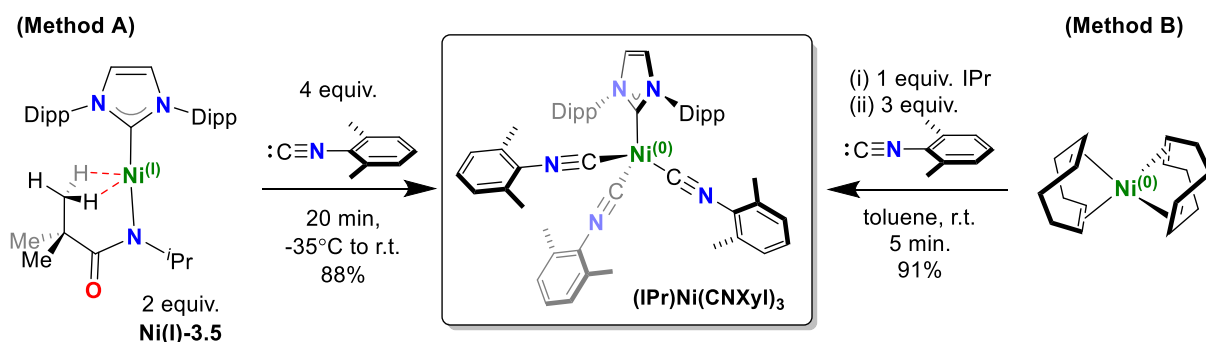


Ni(I)-3.5-CNXYl: In a glovebox, complex **Ni(I)-3.5** (41.7 mg, 0.0707 mmol) was weighed into a 20 mL vial. A stir bar was added to the vial and the solid was dissolved in toluene (8 mL). The isocyanide :C≡N(2,6-dimethylbenzene) (9.3 mg, 0.707 mmol) was weighed into a 5 mL vial and dissolved in toluene (4 mL). Both vials were cooled to -35°C in a glovebox freezer. The isocyanide solution was then added dropwise to the (cooled) stirring solution of **Ni(I)-3.5**. After 20 minutes, the solution was subject to vacuum until ~ 6 mL of the orange toluene solution remained. The solution was filtered through Celite®, layered with hexanes, and cooled to -35°C. Orange X-ray quality crystals of **Ni(I)-3.5-CNXYl** (38.3 mg, 75%) were collected after 2 days. *Inferior yields (i.e. 20%) were obtained when the isocyanide was added at room temperature, or when the isocyanide was added all at once to Ni(I)-3.5.*

¹H NMR (400 MHz, 25°C, C₆D₆): δ = 26.81, 25.00, 15.33, 13.30, 12.42, 8.92, 7.82, 4.79, 3.69, 2.44, 0.93, -3.36, -7.40, -10.47. **FT-IR (Nujol):** 2724, 2036, 1522, 1456, 1377, 1204, 1168, 935, 802, 722, 694 (cm⁻¹). **Evans Method (C₆D₆, 27°C):** μ_{eff} = 1.58 μ_B. **EI-MS (m/z):** 718 [M-1]⁺. **Anal. Calcd.** for C₄₆H₅₈N₃NiO (726). C, 75.93%; H, 8.03%; N, 5.77%. Found: C, 76.14%; H, 8.39%; N, 5.20%.

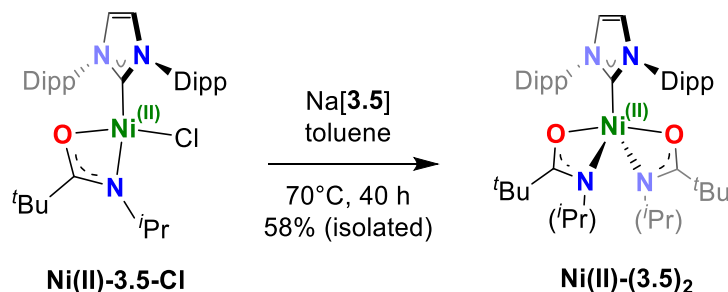


Ni(I)-3.8: In a glovebox, complex **Ni(I)-3.8** (17.6 mg, 0.0300 mmol) was weighed into a 20 mL vial. A stir bar was added to the vial and the solid was dissolved in toluene (3 mL). The isocyanide CNXYl (4.0 mg, 0.0300 mmol) was weighed into a 5 mL vial and dissolved in toluene (1 mL). Both vials were cooled to -35°C in a glovebox freezer. The isocyanide solution was then added dropwise to the (cooled) stirring solution of **Ni(I)-3.8**. After 20 minutes, the solution was subject to vacuum until ~ 3 mL of the orange toluene solution remained. The solution was filtered through Celite[®], layered with hexanes (~ 4 mL), and cooled to -35°C . Orange semi-crystalline material of **Ni(I)-3.8-CNXYl** (17.5 mg, 81%) is collected after 2 days. *N.B.* If disturbed, semi-crystalline material of **Ni(I)-3.8-CNXYl** will not precipitate. Like complex **Ni(I)-3.5-CNXYl**, the ^1H NMR spectrum is very broad. ^1H NMR (400 MHz, 25°C , C_6D_6): $\delta = 13.06$, 7.75, 3.79, 1.17, -3.23 FT-IR (Nujol, dilute): $2054\text{ (cm}^{-1}\text{)}$. Evans Method (C_6D_6 , 25°C): $\mu_{\text{eff}} = 1.6\ \mu_{\text{B}}$. EI-MS (m/z): 718 $[\text{M}+1]^+$. Anal. Calcd. for $\text{C}_{46}\text{H}_{58}\text{N}_3\text{NiO}$ (719). C, 73.54%; H, 8.28%; N, 7.80%. Found: C, 73.89%; H, 8.31%; N, 7.44%.



(IPr)Ni(CNXYl)₃: **Method A** – In a glovebox, complex **Ni(I)-3.5** (40 mg, 0.068 mmol) was weighed into a 20 mL vial. A stir bar was added to the vial and the solid was dissolved in toluene (5 mL). The isocyanide CNXYl (17.8 mg, 0.136 mmol) was then weighed into a 5 mL vial and dissolved in toluene (2 mL). Both vials were cooled in a glovebox

freezer (-35°C) for 15 minutes. The isonitrile solution was then added dropwise to the (cooled) stirring solution of **Ni(I)-3.5**. After 20 minutes, the volatiles were removed *in vacuo*. The residue was taken up in minimal hexanes, filtered through Celite® and cooled to -35°C overnight. Orange, X-ray quality crystals of **(IPr)Ni(CNXyl)₃** (25 mg, 88% based on **Ni(I)-3.5**, 0.0297 mmol) were collected from two crops. **Method B** – In a glovebox, Ni(COD)₂ (60 mg, 0.218 mmol) was weighed into a 20 mL vial. IPr (84 mg, 0.218 mmol) and CNXyl (85 mg, 0.654 mmol) were then weighed into two separate 5 mL vials. A stirring bar was added to the 20 mL vial, and the contents were dissolved in toluene (4 mL). To both 5 mL vials were added toluene (2 mL). The IPr and CNXyl solutions, in that order, were then added dropwise to the stirring Ni(COD)₂ solution at room temperature. After 5 minutes, the volatiles were removed *in vacuo*, and the residue was dissolved in minimal hexanes. The solution was filtered through Celite® and cooled to -35°C overnight. Orange crystals of **(IPr)Ni(CNXyl)₃** (167 mg, 91%, 0.199 mmol) were collected overnight. **¹H NMR (300 MHz, 25°C, C₆D₆):** δ = 7.15-7.10 (m, *m,p*-Ar_{IPr}-H, 6H), 6.85-6.75 (m, *m,p*-Ar_{CNXyl}-H, 9H), 6.70 (s, CH=CH, 2H), 3.27 (sept, ³J_{H,H} = 6.9 Hz, Ar_{IPr}-iPr(CH), 4H), 2.25 (s, Ar_{CNXyl}-(CH₃), 18H), 1.48 (d, ³J_{H,H} = 6.9 Hz, Ar_{IPr}-iPr(CH₃), 12H), 1.17 (d, ³J_{H,H} = 6.9 Hz, Ar_{IPr}-iPr(CH₃), 12H). **¹³C{¹H} NMR (75 MHz, 25°C, C₆D₆):** 206.27 (C_{IPr}-Ni), 181.15 (Ni-C_{CNXyl}), 146.48 (*o*-C_{Ar(IPr)}), 139.76 (*i*-C_{Ar(IPr)}), 133.19 (*o*-C_{Ar(CNXyl)}), 132.61 (*i*-C_{Ar(CNXyl)}), 128.85 (*p*-(H)C_{Ar(IPr)}), ~127.50 (HSQC – under C₆D₆, *m*-(H)C_{Ar(CNXyl)}), 124.53 (*p*-(H)C_{Ar(CNXyl)}), 123.68 (*m*-(H)C_{Ar(IPr)}), 122.57 (HC=CH), 28.83 (Ar_{IPr}-iPr(CH)), 25.30 (Ar_{IPr}-iPr(CH₃)), 23.46 (Ar_{IPr}-iPr(CH₃)), 19.58 (Ar_{CNXyl}-CH₃). **FT-IR (Nujol):** 2060, 1960, 1590 (cm⁻¹) **EL-MS (m/z):** 577 [M-(CNXyl)₂]⁺. **Anal. Calcd.** for C₅₄H₆₃N₅Ni (839). C, 77.14%; H, 7.55%; N, 8.33%. Found: C, 77.31%; H, 7.56%; N, 8.18%.

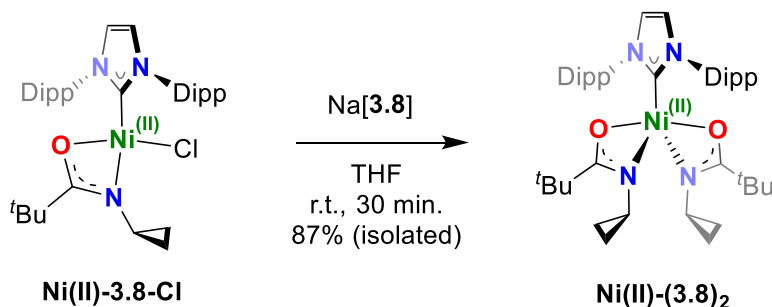


Ni(II)-(3.5)₂: In a glovebox, **Ni(II)-3.5-Cl** (109 mg, 0.174 mmol) was weighed into a 5 mL vial. Similarly, Na[3.5] was weighed (33 mg, 0.202 mmol) into another 5 mL vial. The contents of both vials were added as solids into a 5 mL Teflon™ sealed Schlenk bomb. The leftover solids were rinsed into the bomb with toluene (2 mL x 2). A stirring

bar was added, the bomb was sealed and brought out of the glovebox, and the contents were stirred at 70°C for 40 h. The bomb was then brought back into the glovebox, and the mixture was filtered through Celite® into a 20 mL vial. Following removal of volatiles in vacuo, the residue was taken up in Et₂O (2 mL) and filtered through Celite® into another 20 mL vial. The Et₂O solution was then left to evaporate in the freezer overnight to afford semi-crystalline material. Washing quickly with cold hexanes (1 mL) and drying under high vacuum affords **Ni(II)-(3.5)₂** as a brown solid (74 mg, 58%, 0.101 mmol). X-ray quality crystals were grown by evaporation of concentrated Et₂O solutions of **Ni(II)-(3.5)₂** at room temperature.

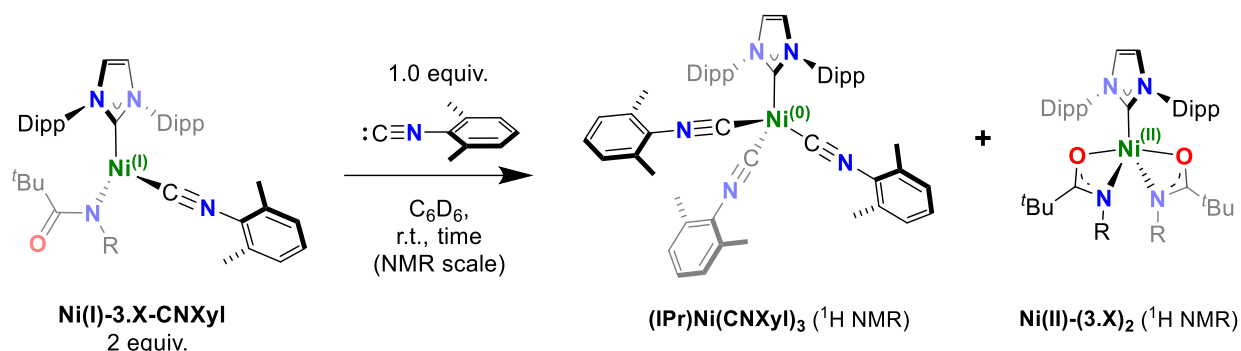
Notes: Compound **Ni(II)-(3.5)₂** may be reasonably integrated. The high solubility of **Ni(II)-(3.5)₂** in hydrocarbon solvents is responsible for the low yield. Washing with hexanes is necessary to remove some proteoligand.

¹H NMR (400 MHz, 25°C, C₆D₆): δ = 25.1, 19.6, 19.3, 17.5, 12.4 (tBu, 18 H), 9.33, 9.01, 6.24, 3.38, 1.94, -0.58, -7.43, -10.5. **Evans Method (C₆D₆, 25°C):** μ_{eff} = 3.03 μ_B. **Evans Balance (25°C):** μ_{eff} = 3.21 μ_B. **EI-MS or ESI(+)-MS:** No molecular ion or characteristic fragmentation patterns were found. **Anal. Calcd.** for C₄₃H₆₈N₄NiO₂ (732). C, 70.58%; H, 9.37%; N, 7.66%. Found: C, 70.42%; H, 9.74%; N, 7.18%.



Ni(II)-(3.8)₂: In a glovebox, complex **Ni(II)-3.8-Cl** (55 mg, 0.088 mmol) was weighed into a 20 mL vial, and a stirring bar was added. Na[3.8] was weighed (14.3 mg, 0.088 mmol) into a 5 mL vial, then added as a solid to the 20 mL vial containing **Ni(II)-3.8-Cl**. THF was added (2 mL) to the solids and the contents were stirred at room temperature for 30 minutes. The volatiles were removed in vacuo, and the resulting residue was taken up in Et₂O (~3 mL) and filtered through Celite® into a 20 mL vial. The Et₂O solution was then left to evaporate in the freezer overnight to afford semi-crystalline material. Washing quickly with cold hexanes (1 mL) and drying under high vacuum affords complex **Ni(II)-(3.8)₂** as a brown solid (56 mg, 87%, 0.077 mmol). X-ray quality crystals were grown by evaporation of concentrated Et₂O solutions of **Ni(II)-(3.8)₂**. See the X-ray section (below).

^1H NMR (400 MHz, 25°C , C_6D_6): δ = 126.71, 33.44, 10.03, 7.63, 7.40, 7.04, 4.62, 0.87, -1.56. **Evans Method** (C_6D_6 , 25°C): μ_{eff} = 3.07 μB . **EI-MS**: 726 $[\text{M}]^+$. **Anal. Calcd.** for $\text{C}_{43}\text{H}_{64}\text{N}_4\text{NiO}_2$ (728). C, 70.97%; H, 8.87%; N, 7.70%. Found: C, 71.01%; H, 8.62%; N, 7.52%.



Reaction of complex Ni(I)-3.5-CNXYl or Ni(I)-3.8-CNXYl with CNXYl:

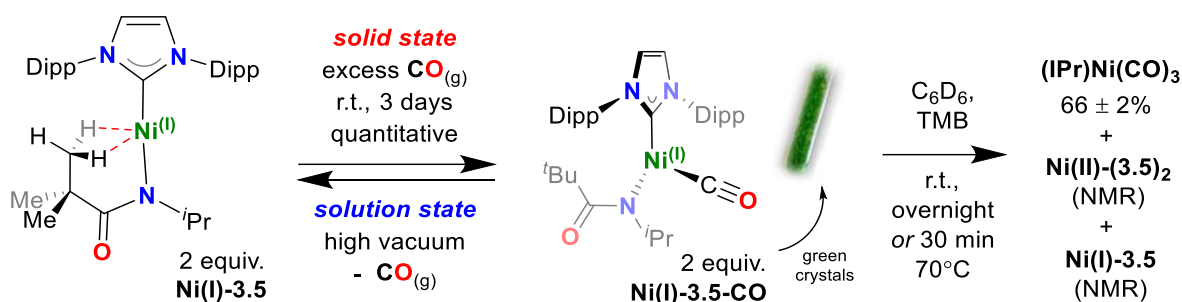
In a glovebox, crystalline complex **Ni(I)-3.X-CNXYl** (6 mg, 0.008 mmol), CNXYl (0.6 mg, 0.005 mmol), and TMB (1.5 -1.7mg, 0.08-0.01 mmol) are each weighed into 5 mL vials. C_6D_6 was added to the vials containing **Ni(I)-3.X-CNXYl** and CNXYl, and the solutions were cooled to -35°C in a glovebox freezer. Upon thawing, the CNXYl solution was added to the solution of **Ni(I)-3.X-CNXYl**, and the contents were mixed with the vial containing TMB, added to a J. Young NMR tube. The NMR tube was sealed and removed from the box. The contents of the reaction were monitored by ^1H NMR spectroscopy, showing the formation of **(IPr)Ni(CNXYl)₃** (yield from internal standard) and **Ni(II)-(3.X)₂** over a period of time.

(R = iPr) Complex 2-CNXYl: 70°C , 4h (quantitative) *or* 25°C , 14 days (without IS)

Run # 1: 96%, **Run # 2:** 86%

(R = cyclopropyl) Complex 7-CNXYl: 25°C , 14 days (**7-CNXYl** and **9** decompose if heated)

Run # 1: 70%, **Run # 2:** 74%



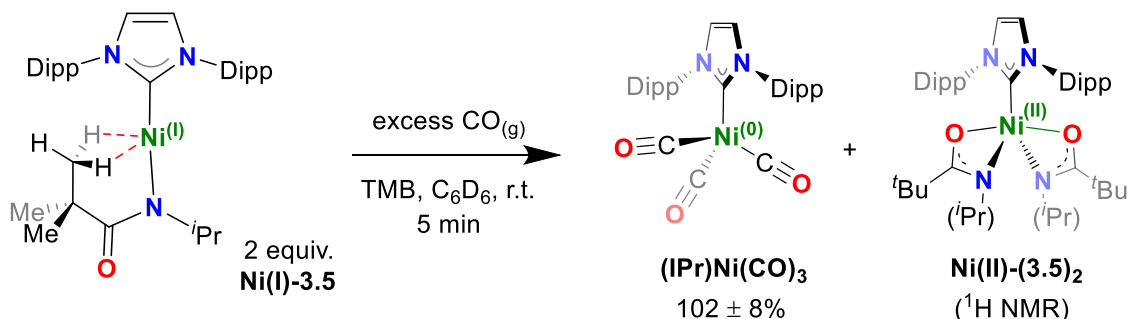
Ni(I)-3.5-CO: In a glovebox, crystalline **Ni(I)-3.5** is added to a J. Young NMR tube. The NMR tube was sealed and removed from the box. A J. Young adaptor was then connected to a Schlenk line. Following the standard three vacuum-nitrogen cycles, the contents of the J. Young were subject to vacuum. The gas line was then purged with CO for ~15 minutes. The contents of the J. Young were then subject to CO via the purged gas line. After closing the manifold, the J. Young was sealed. Over a period of 3 days, the crystals turn lime green (see above), signaling the formation of complex **Ni(I)-3.5-CO**. The tube was re-introduced to the Schlenk line, and the headspace of the tube was filled with $\text{N}_{2(g)}$ following standard vacuum-nitrogen cycles. The tube was then brought into a glovebox and the solid contents were transferred into a 20mL scintillation vial.

^1H NMR (300 MHz, 25°C , C_6D_6): $\delta = 7.62, 5.06, 3.15, 1.34, 1.24, -0.88$. **FT-IR (Nujol):** 2054, 1997, 1992, 1978, 1970, 1563, 1556, 1541 (cm^{-1}). **EI-MS (m/z):** 589 $[\text{M-CO}]^+$. **Anal. Calcd.** for $\text{C}_{36}\text{H}_{52}\text{N}_3\text{NiO}_2$ (617). C, 70.02%; H, 8.49%; N, 6.80%. Found (*best result*): C, 71.12%; H, 8.50%; N, 6.39%.

Reversibility studies: In a glovebox, a small sample of complex **Ni(I)-3.5-CO** (~5 mg) was subject to high vacuum as a solid. After several hours, the sample was dissolved in d_8 -toluene. Complex **Ni(I)-3.5** was not visible by ^1H NMR spectroscopy. The same sample was then dried by removal of volatiles *in vacuo*. The yellow residue was taken up in d_8 -toluene for analysis by ^1H NMR spectroscopy. In this case, only complex **Ni(I)-3.5** is visible, while **Ni(I)-3.5-CO** is no longer observed.

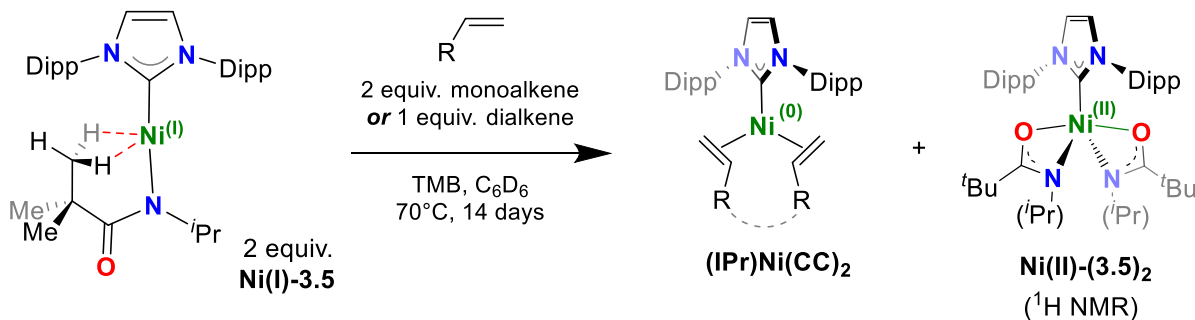
Disproportionation studies: In a glovebox, complex **Ni(I)-3.5-CO** (6.0 mg, 0.0097 mmol) and TMB (1.7 mg, 0.01 mmol) were weighed into scintillation vials (5 mL), dissolved in C_6D_6 (0.5 mL), mixed with a pipette, and added to a J. Young NMR tube. The NMR tube was then heated for 30 minutes at 70°C in an oil bath. The contents were then analyzed by NMR spectroscopy, showing the disappearance of **Ni(I)-3.5-CO**, and the formation of **(IPr)Ni(CO) $_3$** , **Ni(II)-(3.5) $_2$** , and **Ni(I)-3.5**. TMB was used as an internal standard for calculation of NMR yields of **3-CO** for the

duplicated runs: **Run # 1:** 68%, **Run # 2:** 64%. **Note:** this reaction also proceeds at room temperature overnight (~16 h).



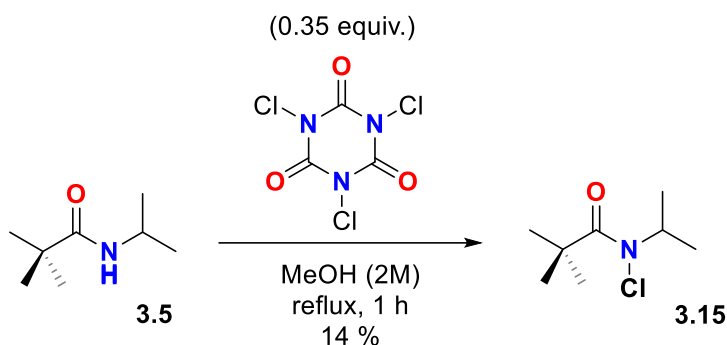
Reaction of Complex Ni(I)-3.5 with $\text{CO}_{(g)}$ in Solution:

In a glovebox, complex **Ni(I)-3.5** (8.8 mg, 0.015 mmol) and TMB (1.5 mg, 0.0089 mmol) were weighed into scintillation vials (5 mL), dissolved in C_6D_6 (0.5 mL), mixed with a pipette, and added to a J. Young NMR tube. The NMR tube was sealed and removed from the glovebox. The J. Young adaptor was then connected to a Schlenk line using the proper procedure. Following standard vacuum-nitrogen cycles, the contents of the J. Young were frozen with $\text{N}_2(l)$ and subjected to vacuum. The gas line was then purged with $\text{CO}_{(g)}$ for ~15 minutes. The contents of the J. Young were then subject to CO via the purged gas line. After closing the manifold, the J. Young was sealed. As the contents of the J. Young thawed, a rapid color change was observed in the J. Young (yellow to brown), signaling formation of complexes **Ni(I)-3.5-CO** and **Ni(II)-(3.5)₂**. The contents were immediately (5 min.) analyzed by NMR spectroscopy, showing the disappearance of **Ni(I)-3.5**, and the formation of **Ni(I)-3.5-CO** and **Ni(II)-(3.5)₂**. TMB was used as an internal standard for calculation of NMR yields of **Ni(I)-3.5-CO** for duplicate runs: **Run # 1:** 110%, **Run # 2:** 94%.



Reaction of Complex Ni(I)-3.5 with alkenes:

In a glovebox, complex **Ni(I)-3.5** (10 mg, 0.017 mmol), olefin (2 equivalent monoolefin *or* 1 equivalent diolefin), and TMB (1.0 mg, 0.006 mmol) were each weighed into scintillation vials (5 mL). To one vial was added C₆D₆ (0.84 mL), mixed with a pipette, and added to a J. Young NMR tube. The NMR tube was sealed and removed from the glovebox. The tube was then heated at 70°C in an oil bath. Reaction progress was monitored by ¹H NMR spectroscopy, using TMB as an internal standard.

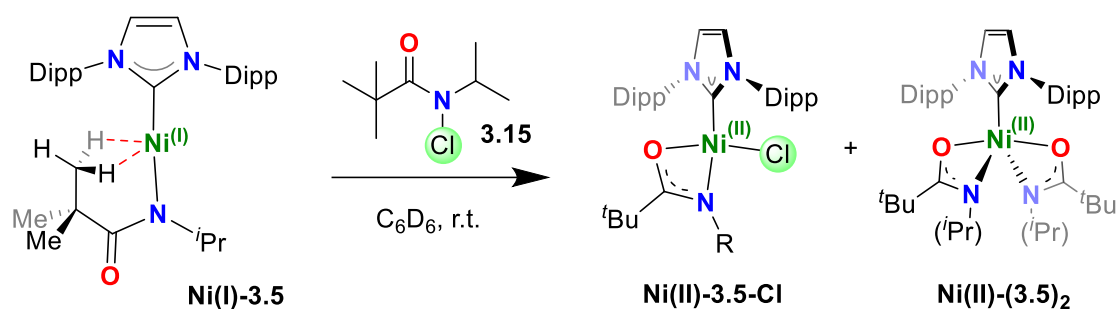


Synthesized according to a modified literature procedure.^[277]

3.15: Amide **3.5** (1140 mg, 7.96 mmol), trichloroisocyanuric acid (650 mg, 2.8 mmol), and MeOH (40 mL, approx. 2M) were added to a 100 mL round-bottom flask equipped with a stirring bar. The methanol solution was stirred for 30 minutes, at which time the solution was filtered, and concentrated by rotary evaporation. The residue was loaded on a silica-gel column/plug (15% EtOAc in hexanes) and subjected to column chromatography. The product **3.15** is eluted as the first compound, and is collected as a clear, colorless oil (100 mg, 0.56 mmol, 14%).

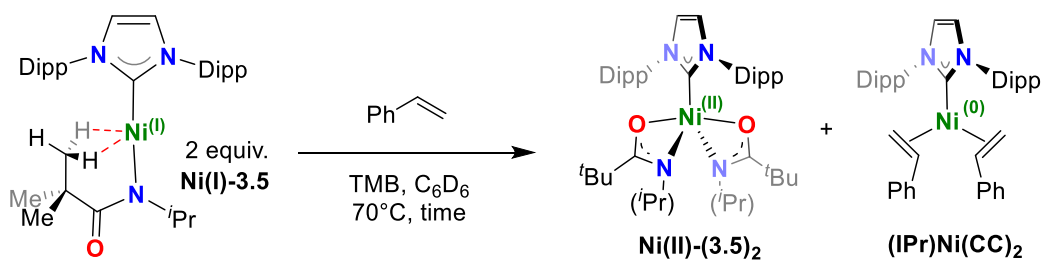
Notes: *In our hands, compound 3.15 decomposes considerably during the drying processes required to bring 3.15 into the glovebox (i.e. drying as a hexanes solution over mol. sieves). Thus, reactions with Ni(I)-3.5 do not go to full conversion.*

¹H NMR (400 MHz, 25°C, C₆D₆): δ = 4.87 (sept, ³J_{H,H} = 6.4 Hz, N-*i*Pr(CH), 1H), 1.28 (s, (s, ^tBu, 9H), 0.95 (d, ³J_{H,H} = 6.4 Hz, N-*i*Pr(CH₃)₂, 6H). **¹³C{¹H} NMR (101 MHz, 25°C, C₆D₆):** 178.3 (C=O), 51.4, 40.2, 27.7, 19.3. **ESI(+)-MS:** m/z calculated for C₈H₁₆ClNO [M]⁺: 177.0999; found: 177.0997. **TLC:** R_f = 0.8, 15% EtOAc in hexanes.



Reaction of complex Ni(I)-3.5 with 3.15:

In a glovebox, complex **Ni(I)-3.5** (6 mg, 0.008 mmol) and **3.15** (0.6 mg, 0.005 mmol) are each weighed into 5 mL vials. Deuterated solvent (C_6D_6 , 0.3 mL x 2) was added to each vial, and the solutions were mixed with a pipette, and the resulting brown solution was added to a J. Young NMR tube. The NMR tube was sealed and removed from the box. The contents of the reaction were monitored by ^1H NMR spectroscopy, showing the formation of **Ni(II)-3.5-Cl** and **Ni(II)-(3.5)₂**, along with unreacted **Ni(I)-3.5**.



In a glovebox, complex **[1]** (2.0-14.7 mg, 0.017-0.025 mmol), TMB (1.0-1.5 mg, 0.0059-0.0089 mmol), and olefin (3.5-24.6 mg, 0.021-0.146 mmol) were each weighed into 5 mL vials as (Method A) freshly made weight percentage solutions in C_6D_6 or as (Method B) neat reagents. The solutions were mixed, and C_6D_6 was added to one vial to make up the remaining 800 mg (0.84 mL). The contents of all the vials were then mixed together with a pipette. The solution was then added to a J. Young NMR tube, brought out of the glovebox, and heated at 70°C in an oil bath. Reaction progress was monitored by ^1H NMR spectroscopy, using TMB as an internal standard (See example of the ^1H NMR spectra of a kinetic run below). The order of reaction for the Nickel(I) complex **[1]** and olefin (styrene) for the described disproportionation reaction were calculated from initial rates (~2-10% conversion) of the following kinetic

experiments. The ill-defined region between 0-2% has been omitted from analysis, and is currently being investigated. We hypothesize a small concentration of impurity contributes to this initial product spike.

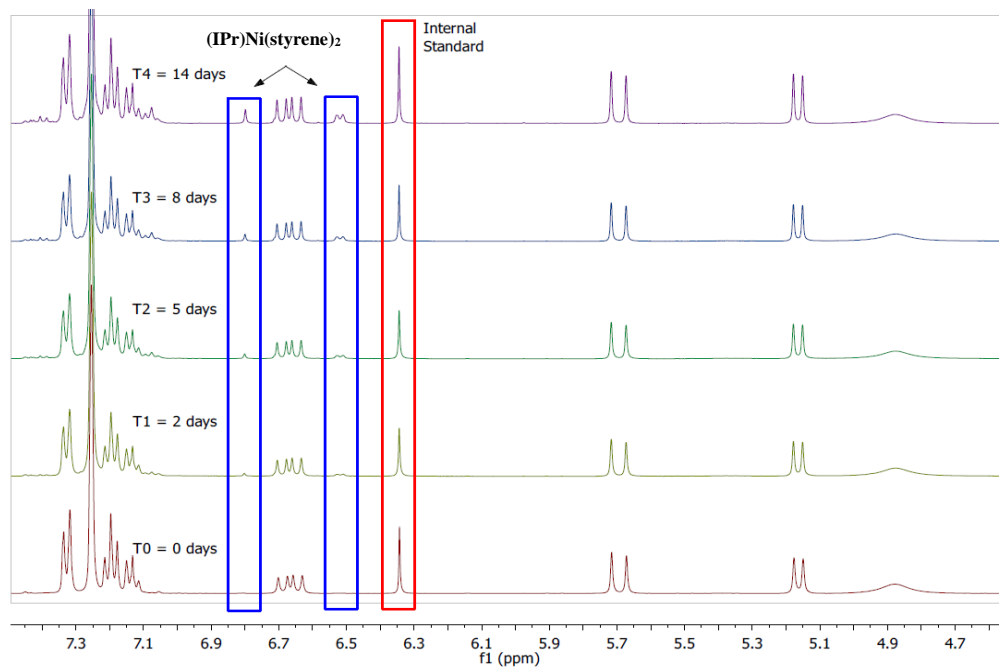


Figure A.3.64. Example of ^1H NMR spectra (C_6D_6 , 400MHz, 298K) for kinetic run: Experiment (a) $[\text{I}]_{\text{initial}} = 0.02\text{M}$, $[\text{styrene}]_{\text{initial}} = 0.04\text{M}$, $[\text{TMB}] = 0.007\text{M}$.

Kinetic Experiments Varying $[\text{styrene}]$:

Constants across experiments (a)-(d):

$[\text{Ni(I)-3.5}]_{\text{initial}} = 0.02\text{M}$, $[\text{TMB}] = 0.007\text{M}$, $\text{Volume}_{\text{C}_6\text{D}_6} = 0.84\text{ mL}$ (800 mg)

Variables:

Experiment (a) 3.5 mg styrene, $[\text{styrene}]_{\text{initial}} = 0.04\text{M}$ [~ 2 equiv. relative to $[\text{Ni(I)-3.5}]$]

Experiment (b) 8.9 mg styrene, $[\text{styrene}]_{\text{initial}} = 0.10\text{M}$ [~ 5 equiv. relative to $[\text{Ni(I)-3.5}]$]

Experiment (c) 17.8 styrene, [**styrene**_{initial}] = 0.20M [~10 equiv. relative to [Ni(I)-3.5]]

Experiment (d) 24.6 mg styrene, [**styrene**_{initial}] = 0.28M [~14 equiv. relative to [Ni(I)-3.5]]

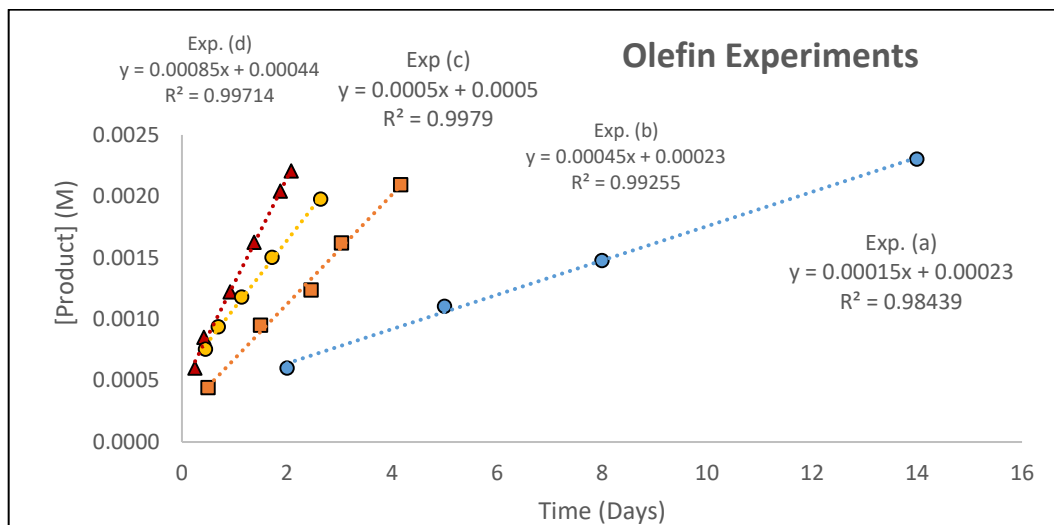


Figure A.3.65. Kinetic data for experiments (a)-(d). See description [above](#) for experimental procedure.

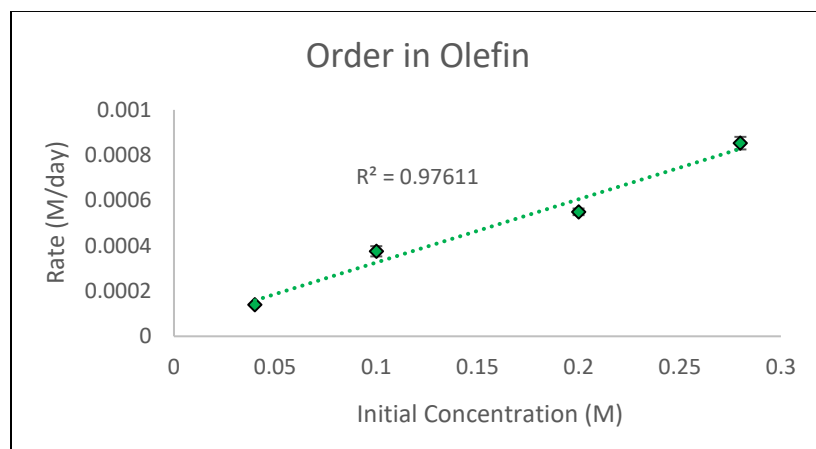


Figure A.3.66. Plot of olefin equivalents vs rate of reaction. Error bars for each rate were determined through regression analysis of the raw data for duplicated runs.

Kinetic Experiments Varying [Ni(I)-3.5]:

Constants across experiments (v)-(w):

[styrene]_{initial} = 0.28M, [TMB] = 0.007M, Volume_{C6D6} = 0.84 mL (800 mg)

Variables:

Experiment (w) 2.0 mg complex [Ni(I)-3.5], [Ni(I)-3.5]_{initial} = 0.004M

Experiment (x) 5.0 mg complex [Ni(I)-3.5], [Ni(I)-3.5]_{initial} = 0.01M

Experiment (y) 10.0 mg complex [Ni(I)-3.5], [Ni(I)-3.5]_{initial} = 0.02M [this is the same as Exp (d)]

Experiment (z) 14.8 mg complex [Ni(I)-3.5], [Ni(I)-3.5]_{initial} = 0.03M

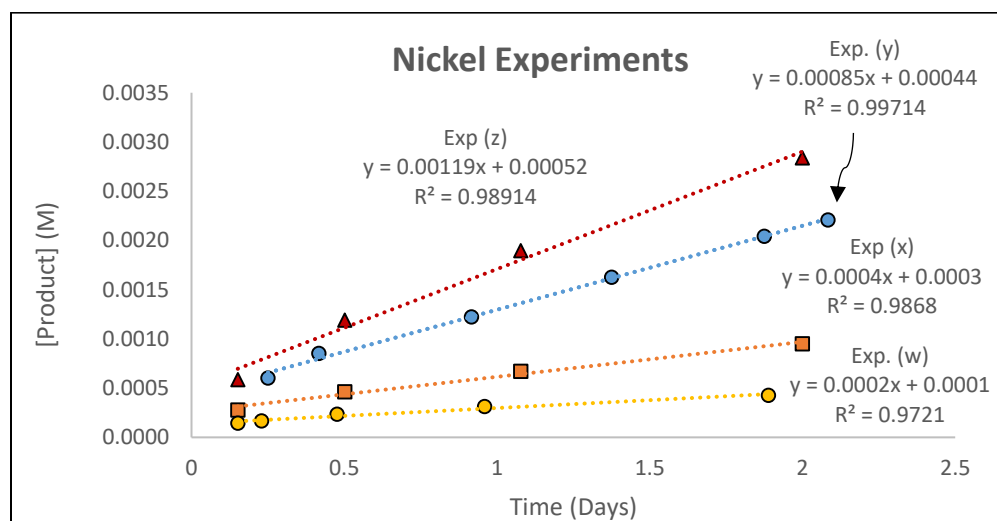


Figure A.3.67. Raw kinetic data for experiments (w)-(z). See description above for experimental procedure.

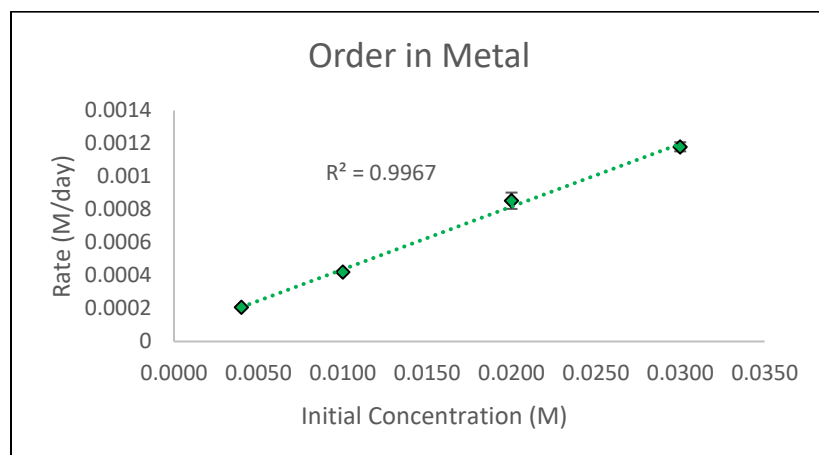
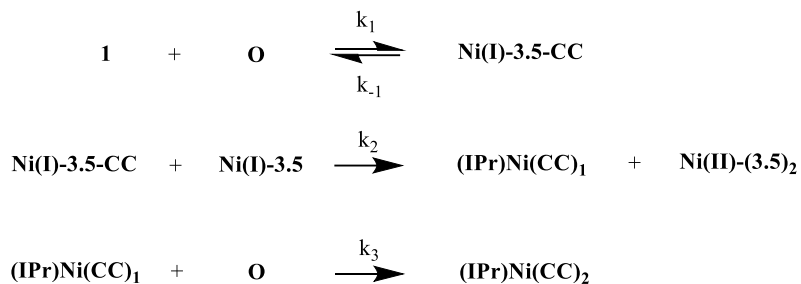


Figure A.3.68. Plot of initial nickel concentration [Ni(I)-3.5] vs. rate of reaction. Error bars for each rate were determined through regression analysis of the raw data for duplicated runs.

Derivation of Rate Law:

Elementary Steps:



Assumptions:

- 1) Unsaturated $(\text{IPr})\text{Ni}(\text{CC})_1$ should be very transient (i.e. k_3 is very large). Furthermore, $(\text{IPr})\text{Ni}(\text{CC})_1$ is not observed.

$$\frac{d[(\text{IPr})\text{NiCC}_1]}{dt} = \frac{d[(\text{IPr})\text{NiCC}_2]}{dt} = k_2[\text{Ni(I)3.5}][\text{Ni(I)3.5CC}]$$

- 2) Steady state assumption for complex Ni(I)-3.5-CC ; i.e. $[\text{Ni(I)-3.5-CC}]$ is small and constant, and k_1 is small.

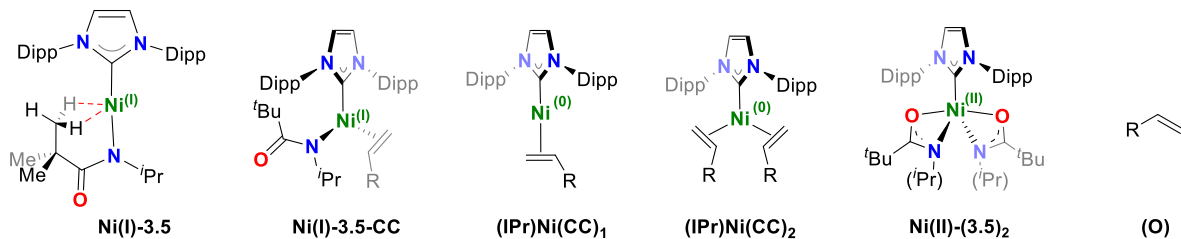
$$\frac{d[\text{Ni(I)3.5CC}]}{dt} = k_1[\text{Ni(I)3.5}][\text{O}] - k_2[\text{Ni(I)3.5CC}][\text{Ni(I)3.5}] - k_{-1}[\text{Ni(I)3.5CC}] = 0$$

$$[\text{2CC}] = \frac{k_1[\text{Ni(I)3.5}][\text{O}]}{k_{-1} + k_2[\text{Ni(I)3.5}]}$$

Thus, our derived rate law becomes:

$$\frac{d[(\text{IPr})\text{NiCC}_2]}{dt} = \frac{k_1 k_2 [\text{Ni(I)3.5}]^2 [\text{O}]}{k_{-1} + k_2 [\text{Ni(I)3.5}]}$$

LEGEND:



Calculation of Amidate Dynamics in Ni(II)-(3.5)₂

We based our calculations for the amidate dynamics on two sets of coalescing peaks:

Peak Set # 1 (tBu singlets @ δ -19.35, -18.13)

$$\Delta\nu_1 = 490 \text{ Hz}$$

$$T_C \approx -71 \text{ }^\circ\text{C} = 202.15 \text{ K}$$

$$k_{c1} = 2.22(490) \text{ s}^{-1}$$

$$= 1088 \text{ s}^{-1}$$

$$\Delta G_1^\ddagger = 19.14 (212.15) (10.32 + \log(212.15/1088))$$

$$= 37102 \text{ J/mol}$$

$$= 8.9 \text{ kcal/mol}$$

Peak Set # 2 (singlets @ δ -3.73, -5.70)

$$\Delta\nu_2 = 730 \text{ Hz}$$

$$T_C \approx -61 \text{ }^\circ\text{C} = 212.15 \text{ K}$$

$$k_{c2} = 2.22(730) \text{ s}^{-1}$$

$$= 1621 \text{ s}^{-1}$$

$$\Delta G_2^\ddagger = 19.14 (212.15) (10.32 + \log(212.15/1621))$$

$$= 38319 \text{ J/mol}$$

$$= 9.2 \text{ kcal/mol}$$

$$\text{Avg } \Delta G^\ddagger = 9.0 \pm 0.1 \text{ kcal/mol}$$

Sample of NMR Spectra of Described Compounds

see *Angew. Chem. Int. Ed.* **2016**, 55, 13290-13295 and *Organometallics* **2018**, 37, 1392-1399 for all other ^1H and $^{13}\text{C}\{^1\text{H}\}$ spectra.

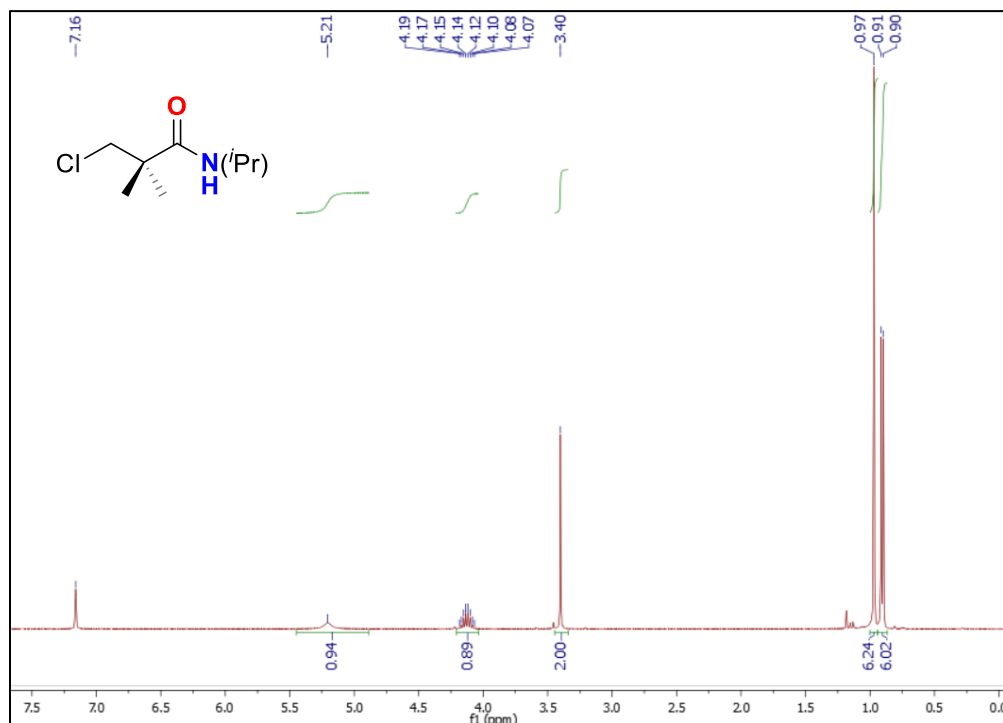


Figure A.3.69. ^1H NMR (400 MHz, 25°C, C_6D_6) of amide 3.12.

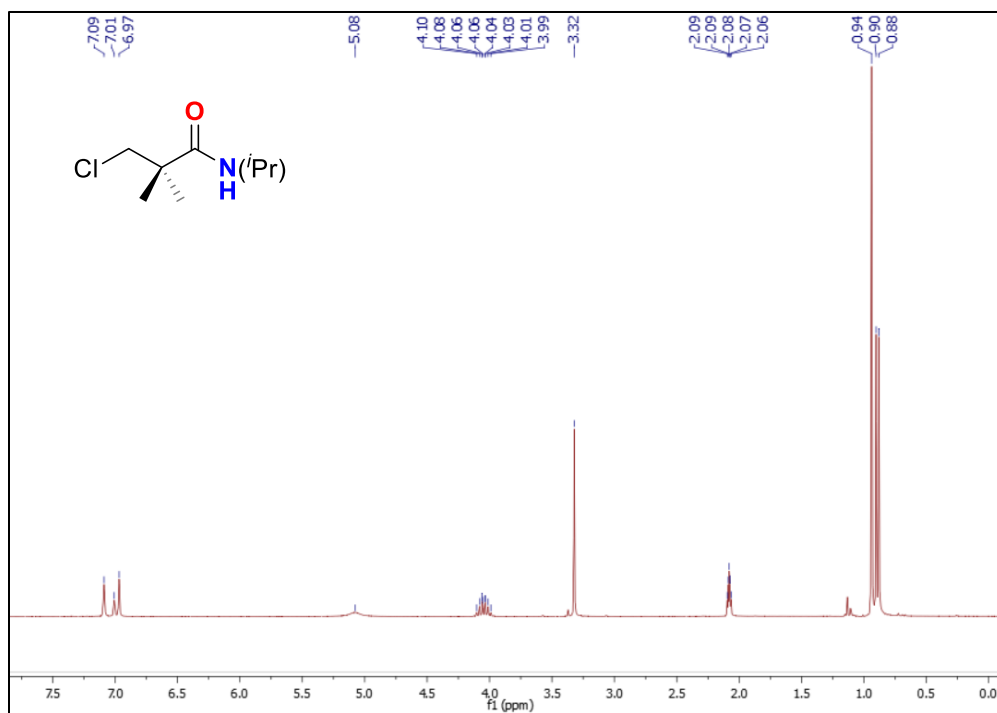


Figure A.3.70. ¹H NMR (300 MHz, 25°C, C₇D₈) of amide 3.12.

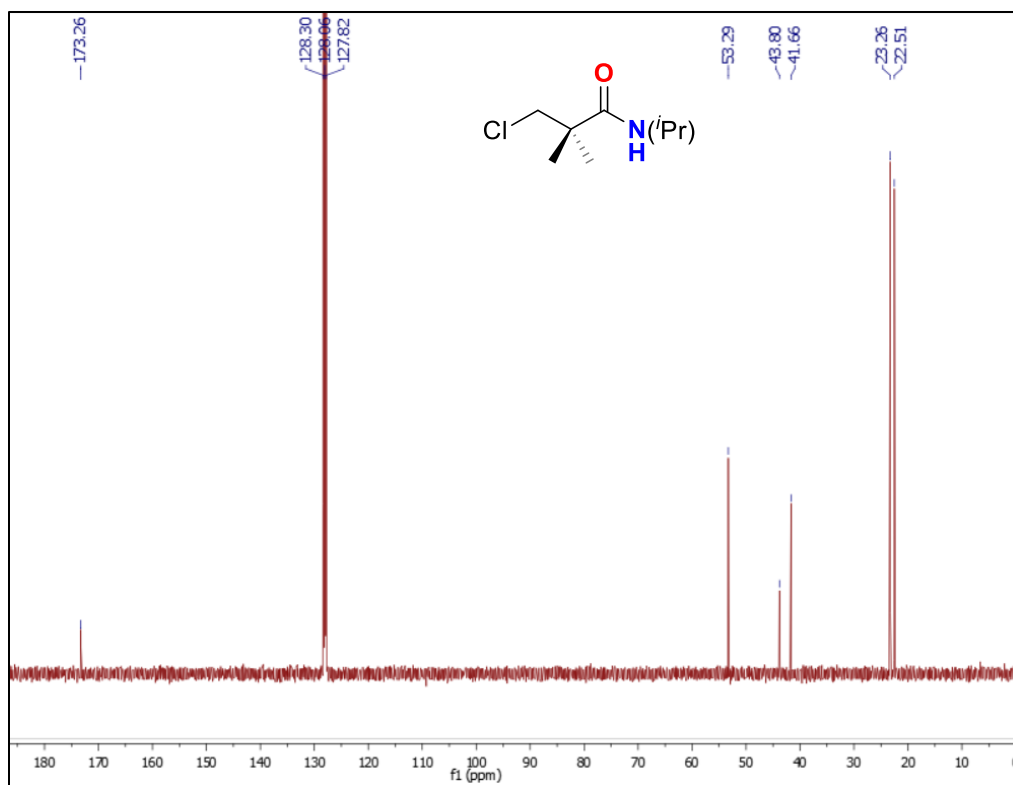


Figure A.3.71. ¹³C NMR (101 MHz, 25°C, C₆D₆) of amide 3.12.

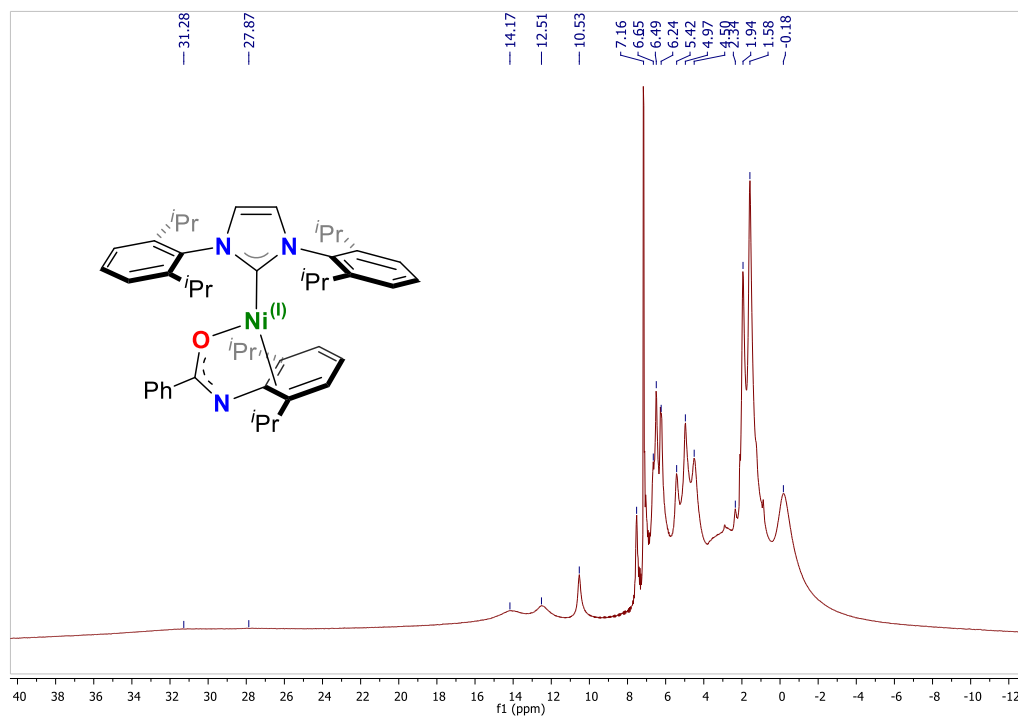


Figure A.3.72. ¹H NMR (400 MHz, 25°C, C₆D₆) of Ni(I)-3.2.

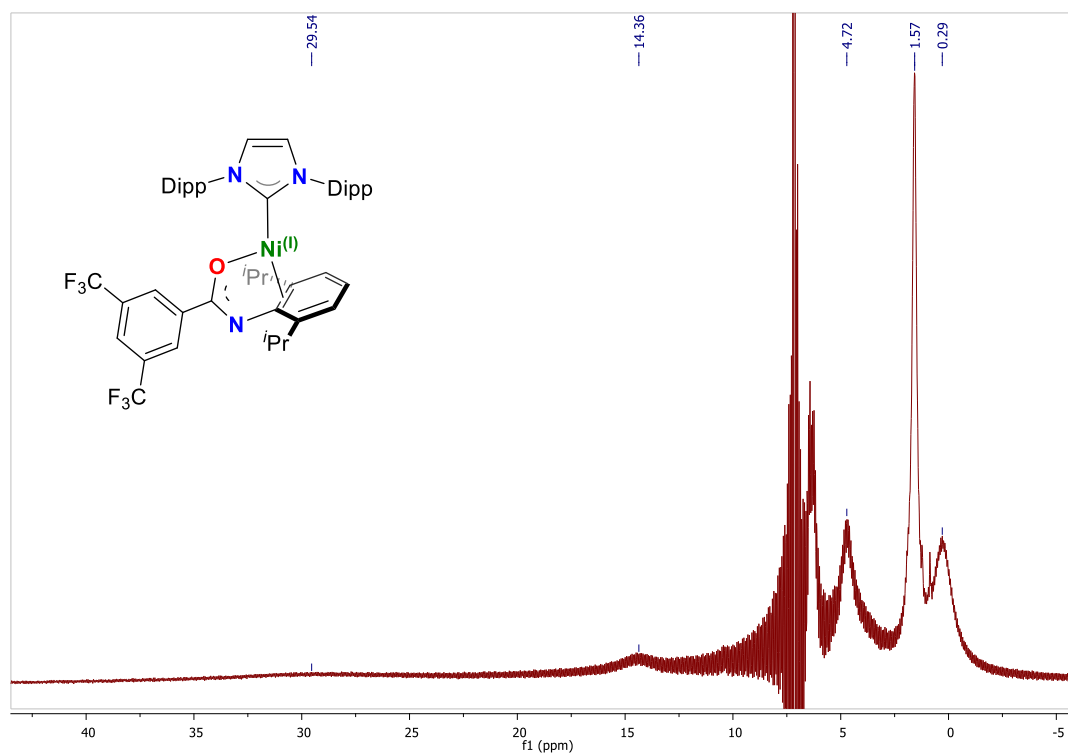


Figure A.3.73. ¹H NMR (400 MHz, 25°C, C₆D₆) of Ni(I)-3.3.

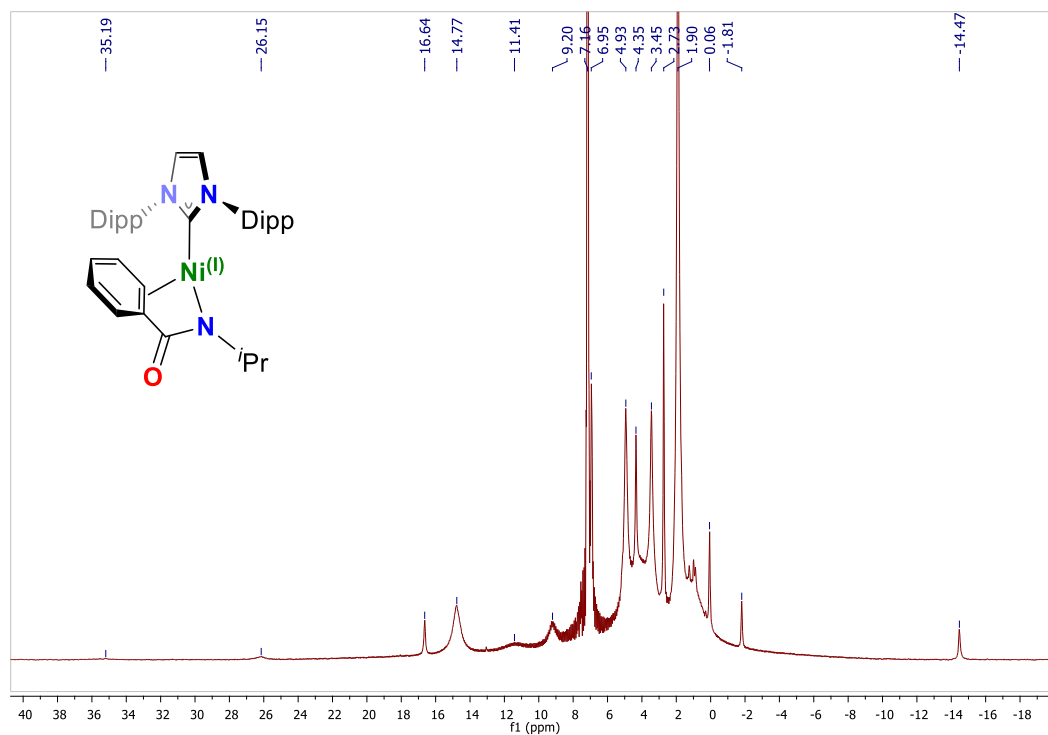


Figure A.3.74. ¹H NMR (400 MHz, 25°C, C₆D₆) of Ni(I)-3.4.

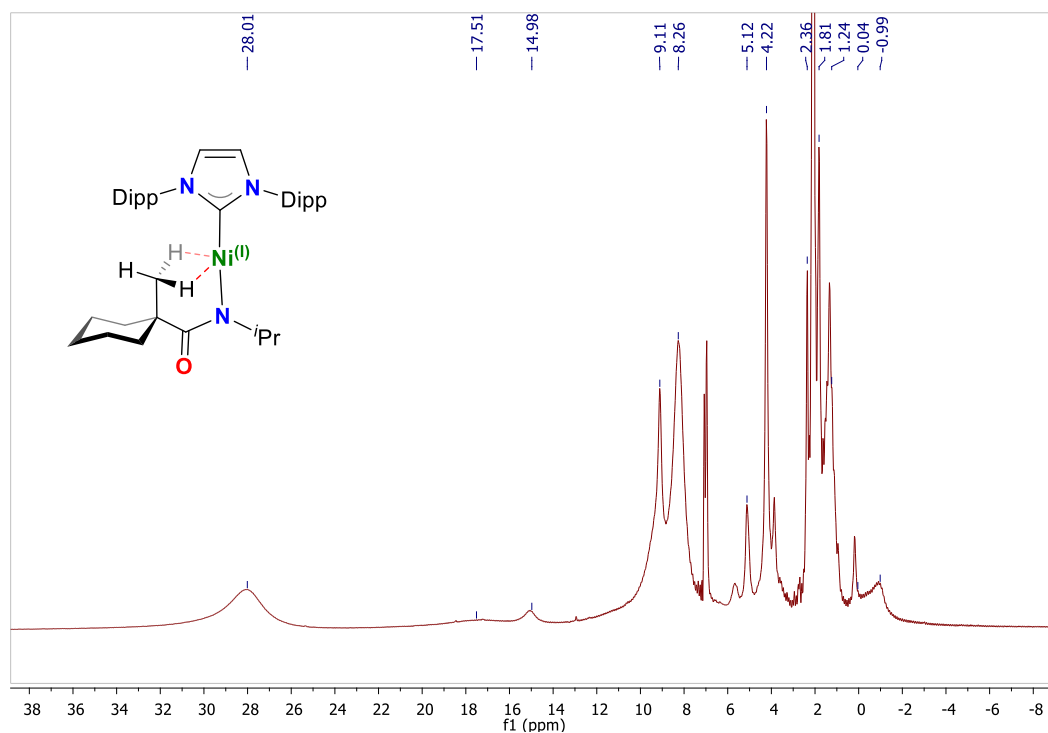


Figure A.3.75. ¹H NMR (400 MHz, 25°C, C₆D₆) of Ni(I)-3.6.

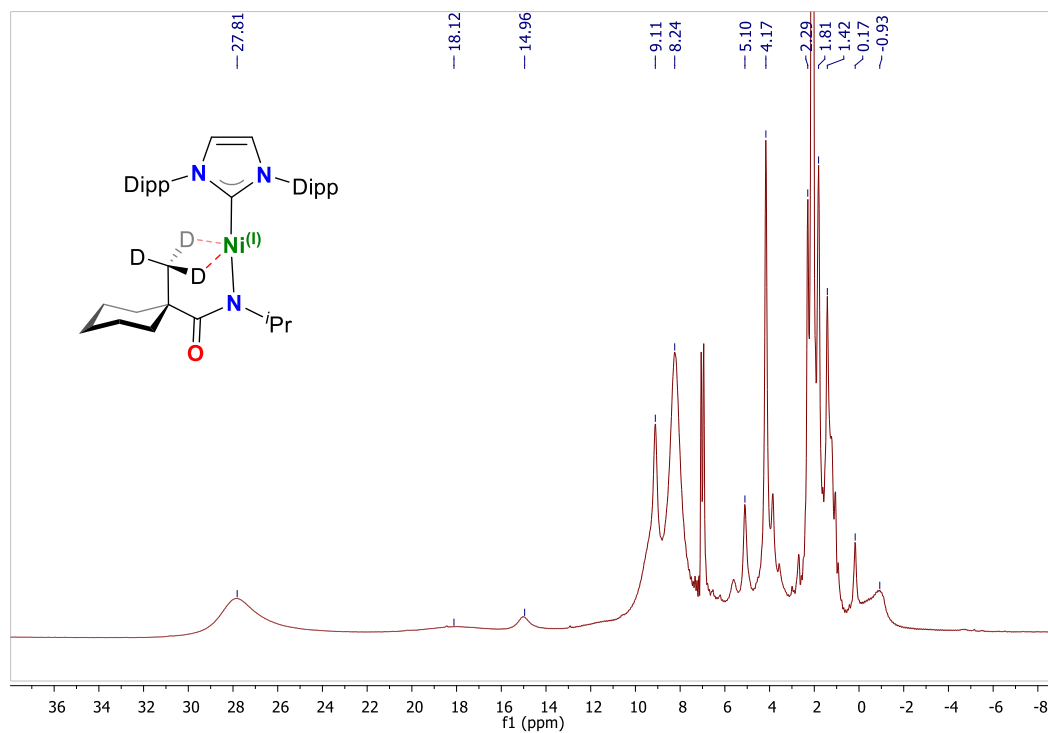


Figure A.3.76. ¹H NMR (400 MHz, 25°C, C₆D₆) of Ni(I)-3.7.

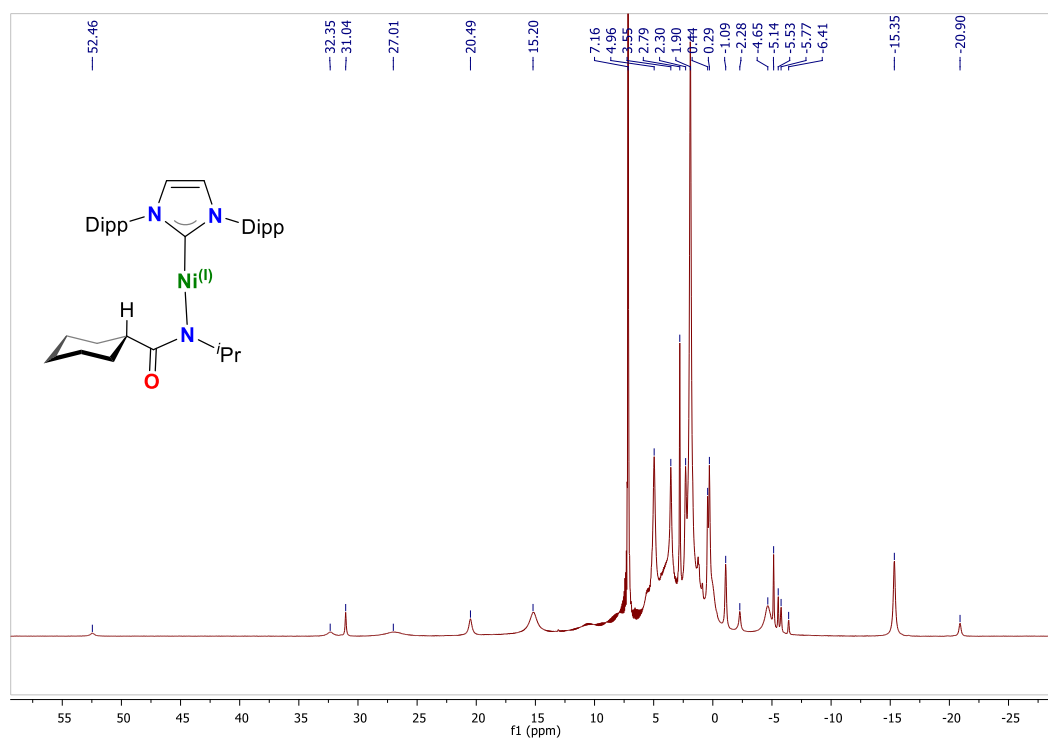


Figure A.3.77. ¹H NMR (400 MHz, 25°C, C₆D₆) of Ni(I)-3.9.

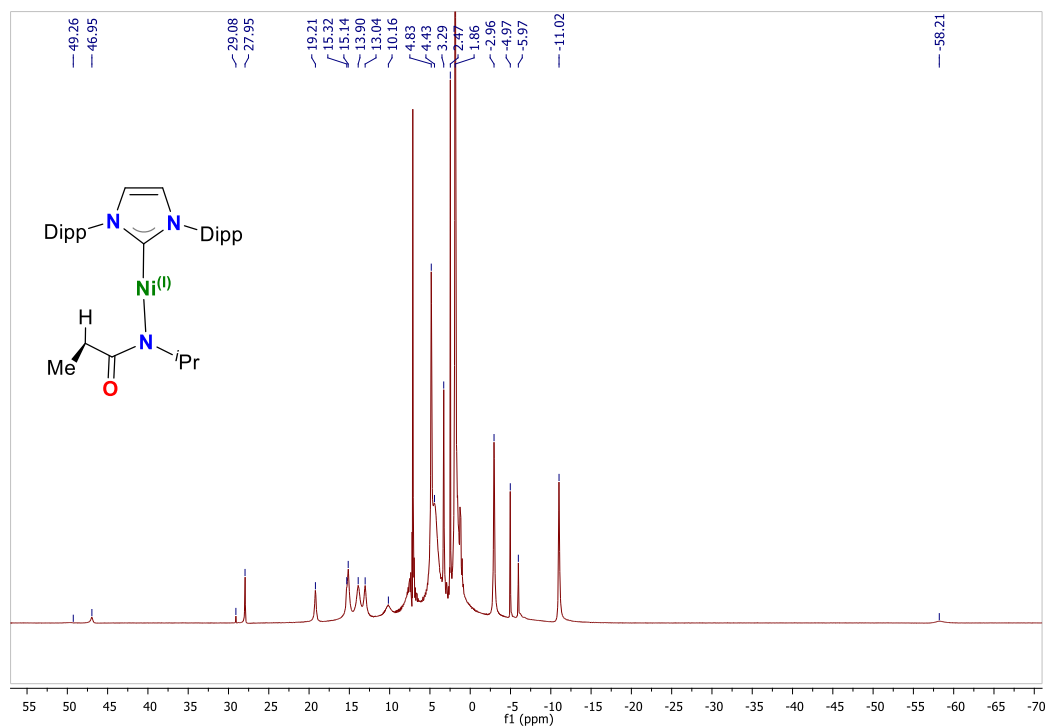


Figure A.3.78. ^1H NMR (400 MHz, 25°C , C_6D_6) of Ni(I)-3.11.

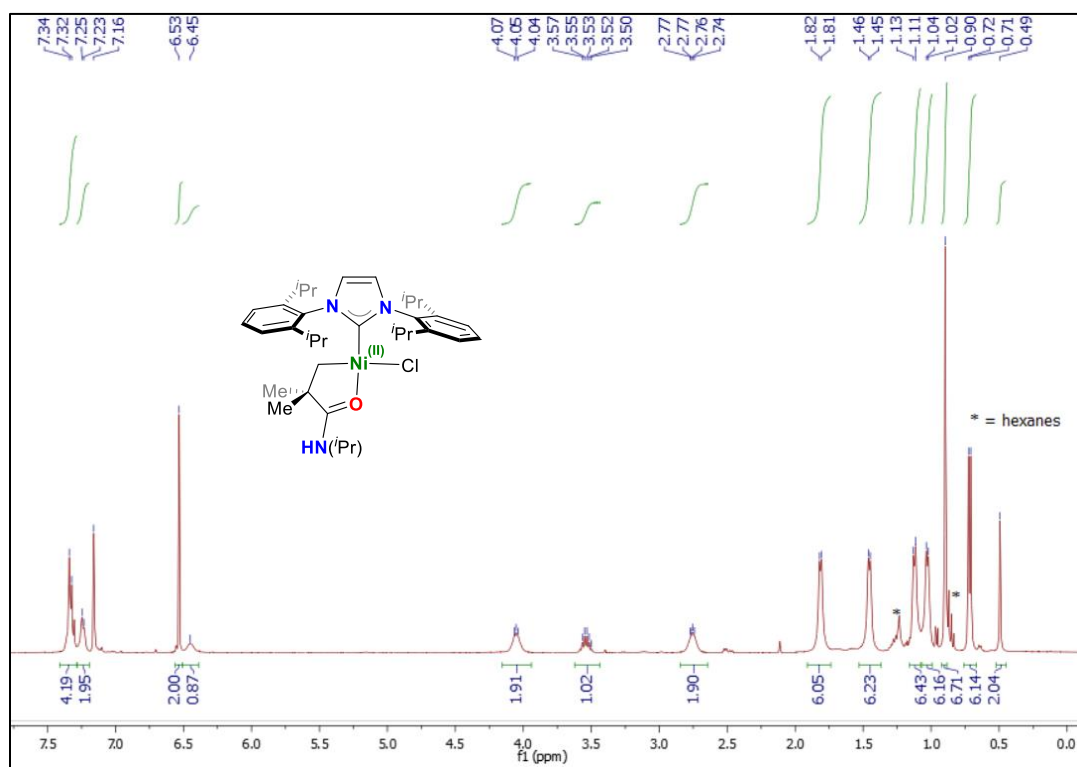


Figure A.3.79. ^1H NMR (400 MHz, 25°C , C_6D_6) of Ni(II)-3.12A.

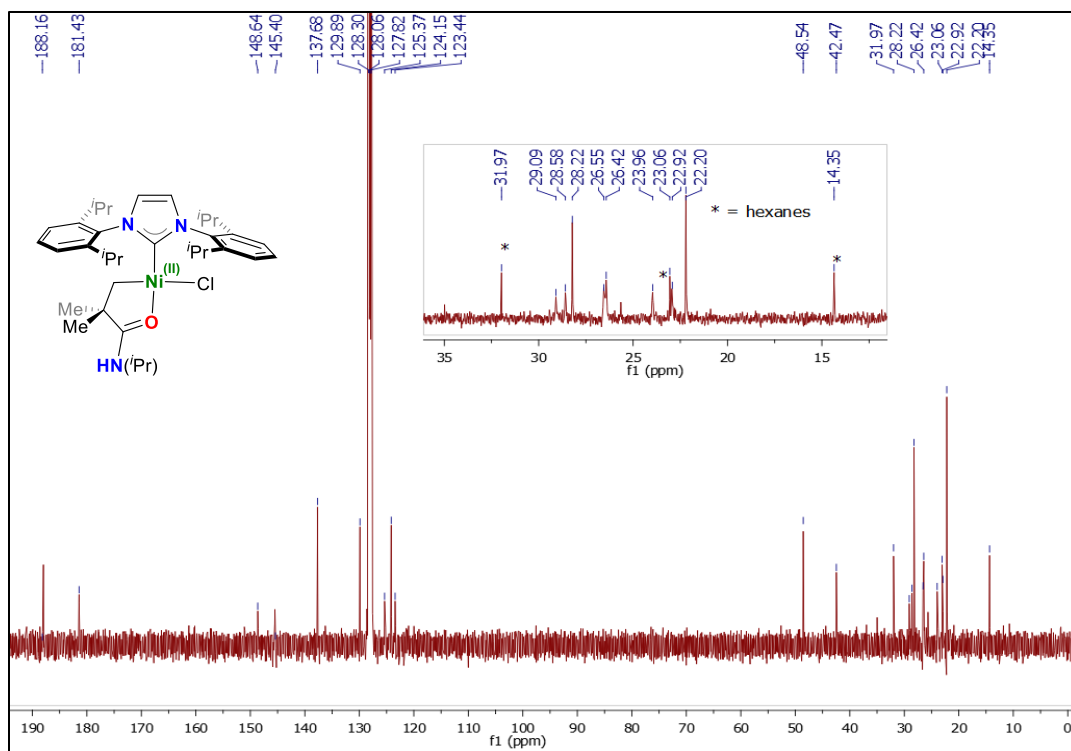


Figure A.3.80. ¹³C NMR (101 MHz, 25°C, C₆D₆) of Ni(II)-3.12A.

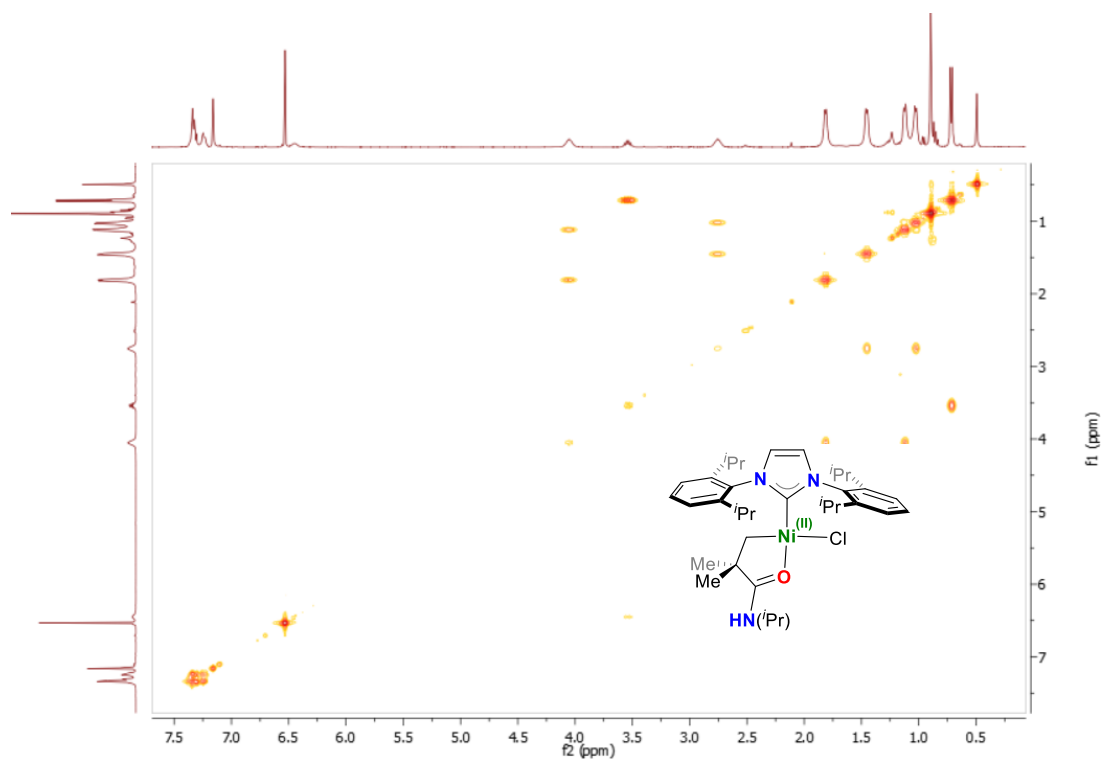


Figure A.3.81. ¹H-¹H COSY NMR (400 MHz, 25°C, C₆D₆) of Ni(II)-3.12A.

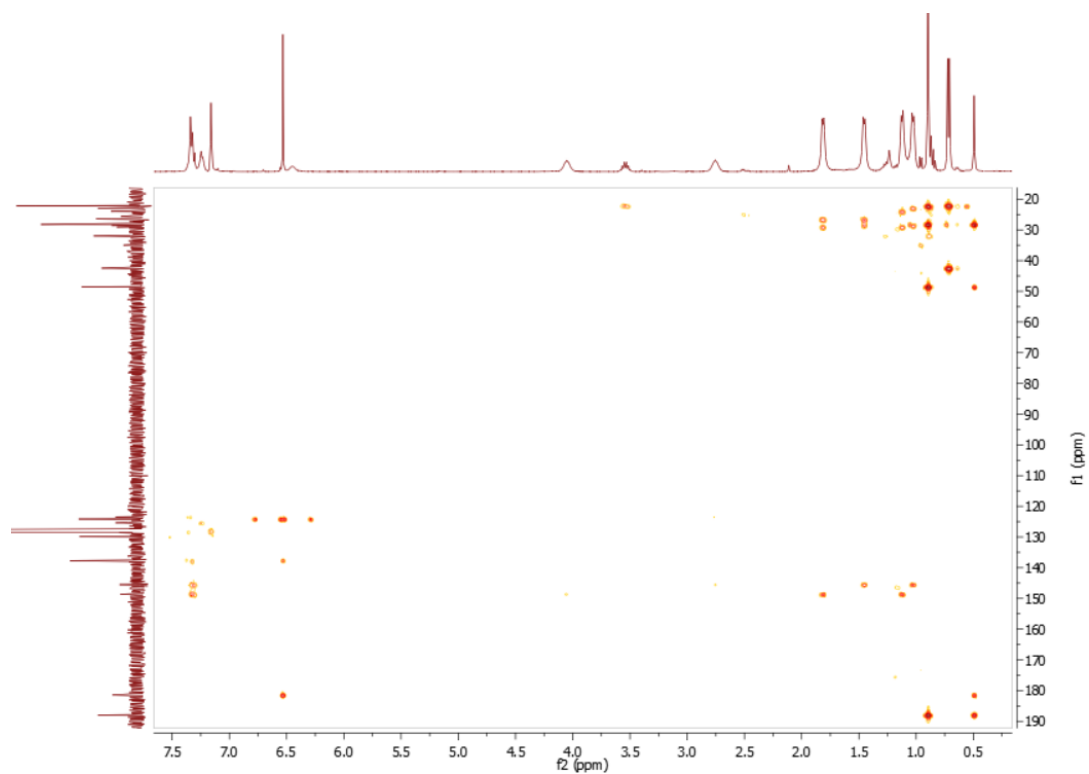


Figure A.3.82. ^1H - ^{13}C HMBC NMR (400 MHz, 25°C, C_6D_6) of Ni(II)-3.12A.

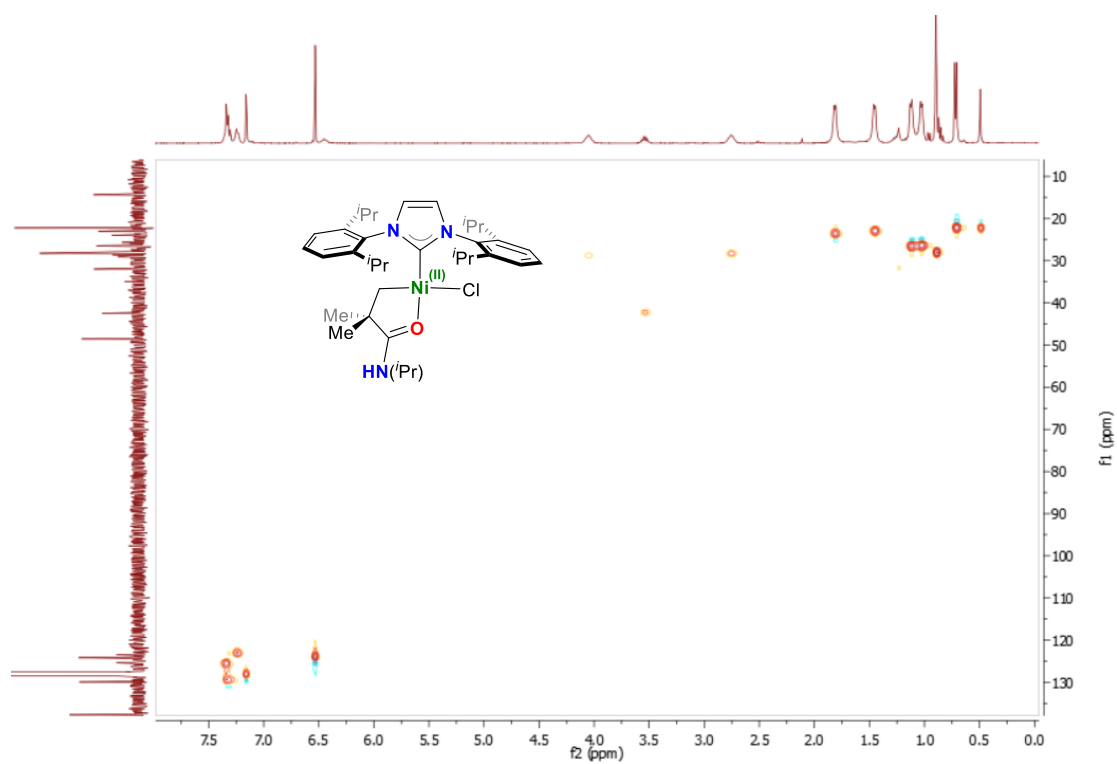


Figure A.3.83. ^1H - ^{13}C HSQC NMR (400 MHz, 25°C, C_6D_6) of Ni(II)-3.12A.

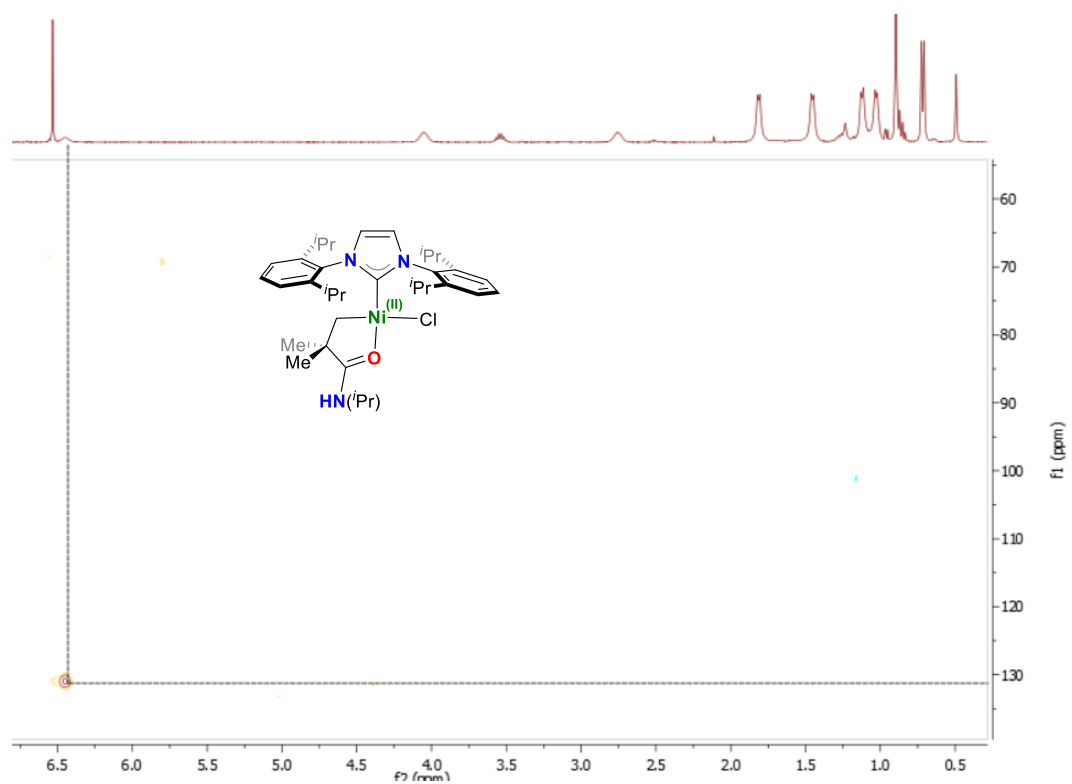


Figure A.3.84. ^1H - ^{15}N HSQC NMR (400 MHz, 25°C, C_6D_6) of Ni(II)-3.12A.

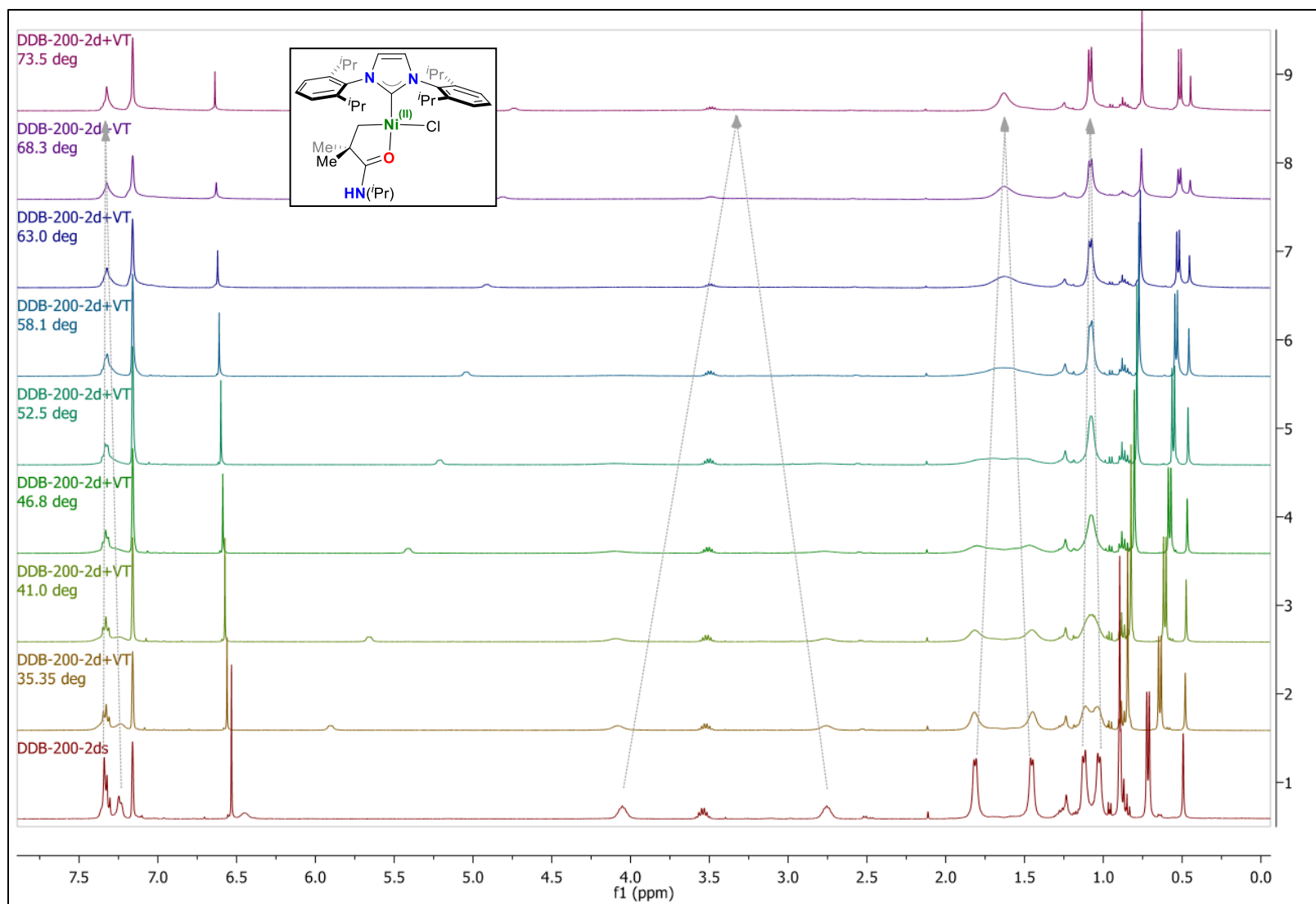


Figure A.3.85. Variable temperature ^1H NMR (400 MHz, 25°C , C_6D_6) of $\text{Ni}(\text{II})$ -3.12A.

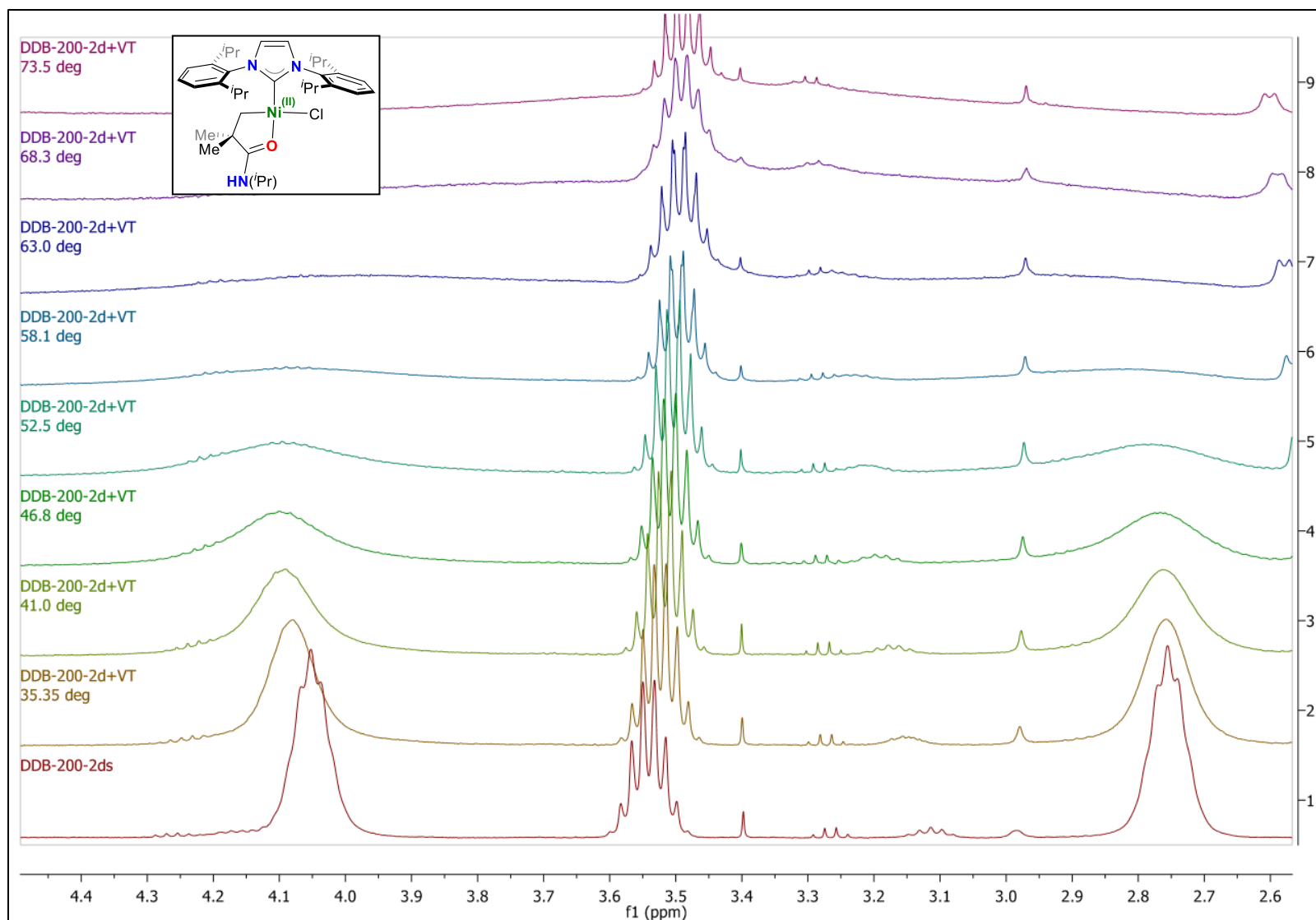


Figure A.3.86. Variable temperature ^1H NMR (400 MHz, 25°C , C_6D_6) of Ni(II)-3.12A.

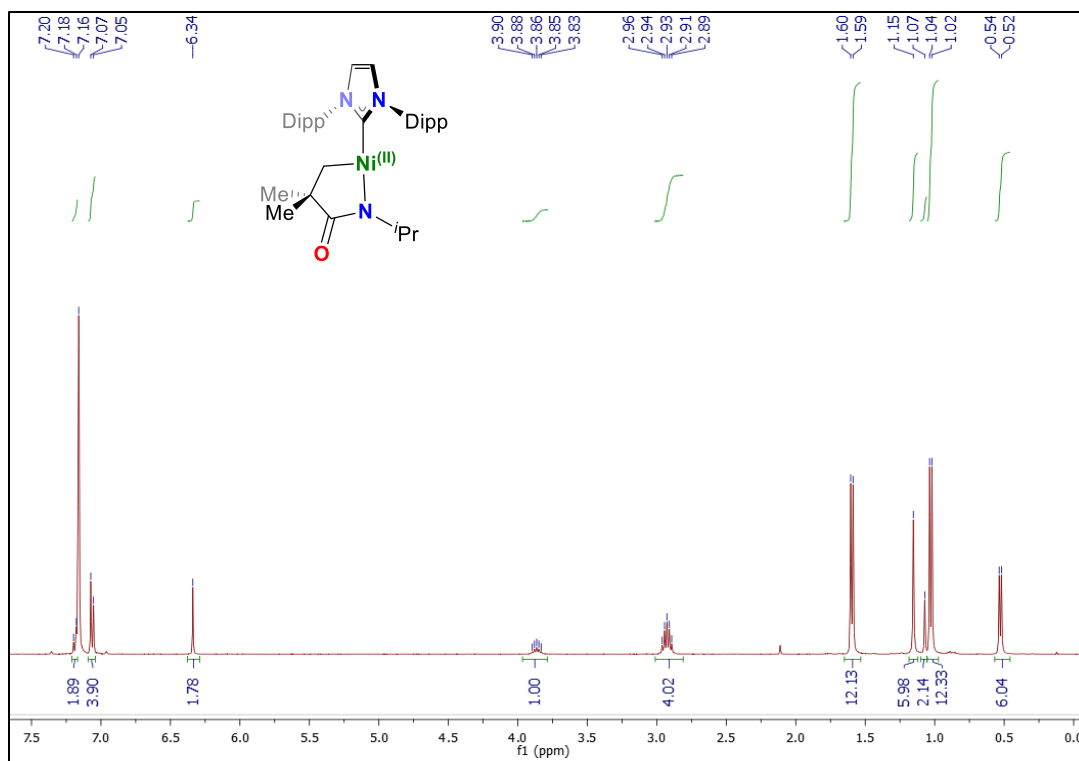


Figure A.3.87. ^1H NMR (400 MHz, 25°C , C_6D_6) of Ni(II)-3.12B.

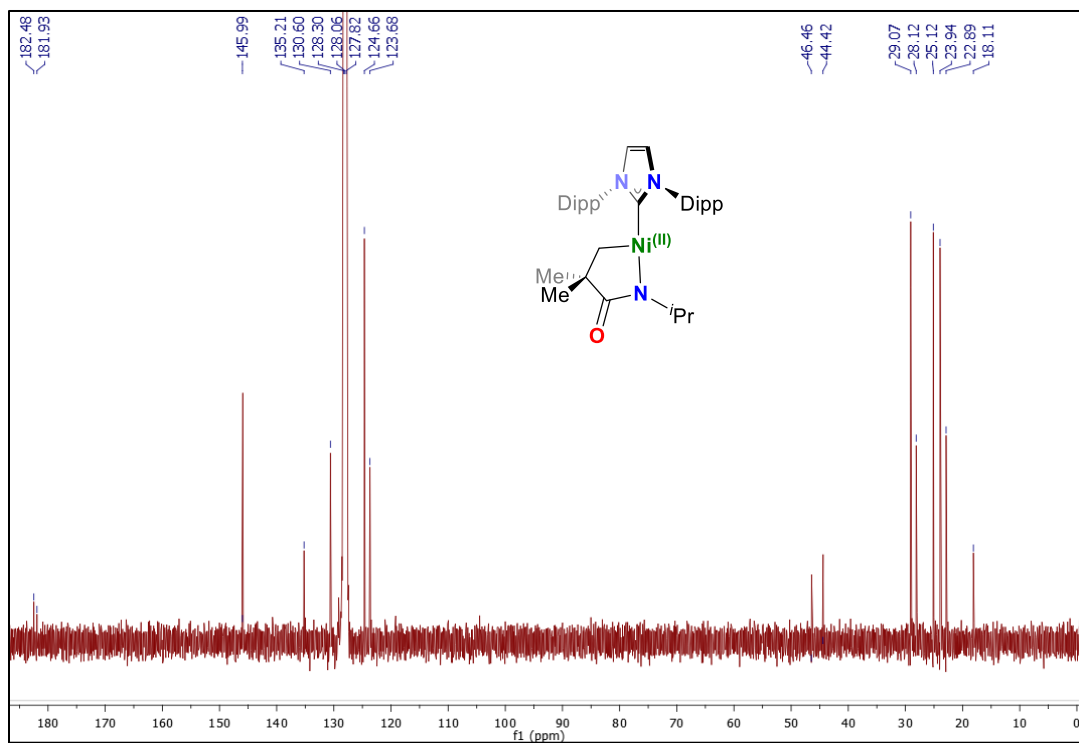


Figure A.3.88. ^{13}C NMR (101 MHz, 25°C , C_6D_6) of Ni(II)-3.12B.

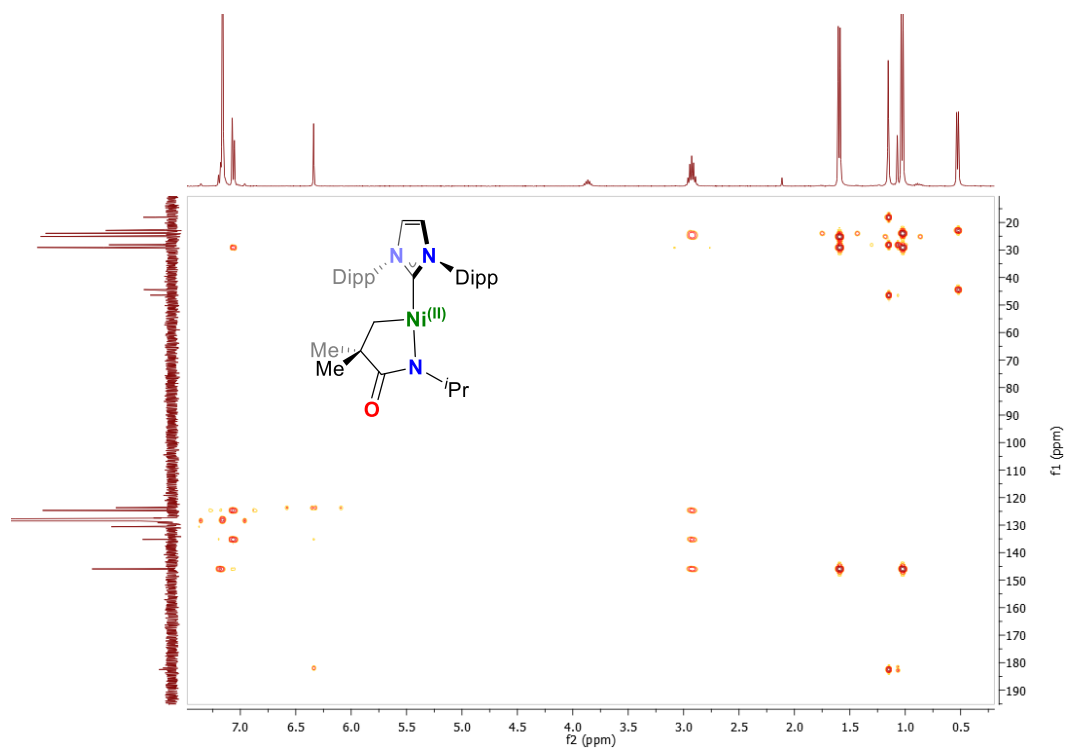


Figure A.3.89. ^1H - ^{13}C HMBC NMR (400 MHz, 25°C , C_6D_6) of Ni(II)-3.12B.

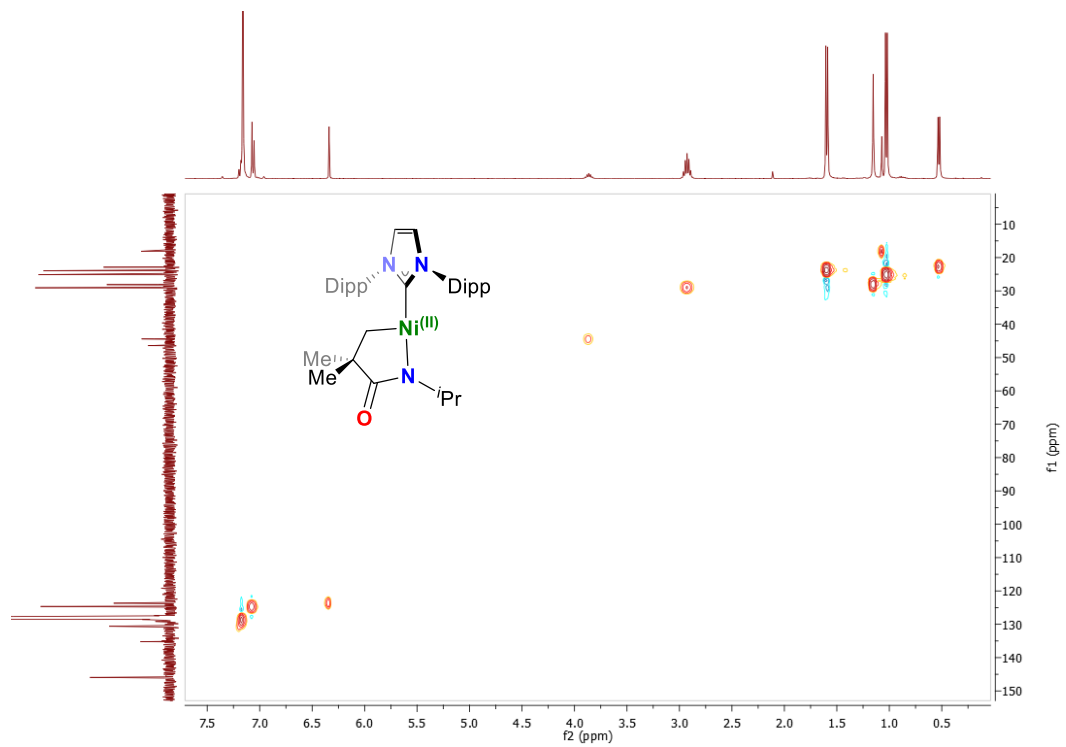


Figure A.3.90. ^1H - ^{13}C HSQC NMR (400 MHz, 25°C , C_6D_6) of Ni(II)-3.12B.

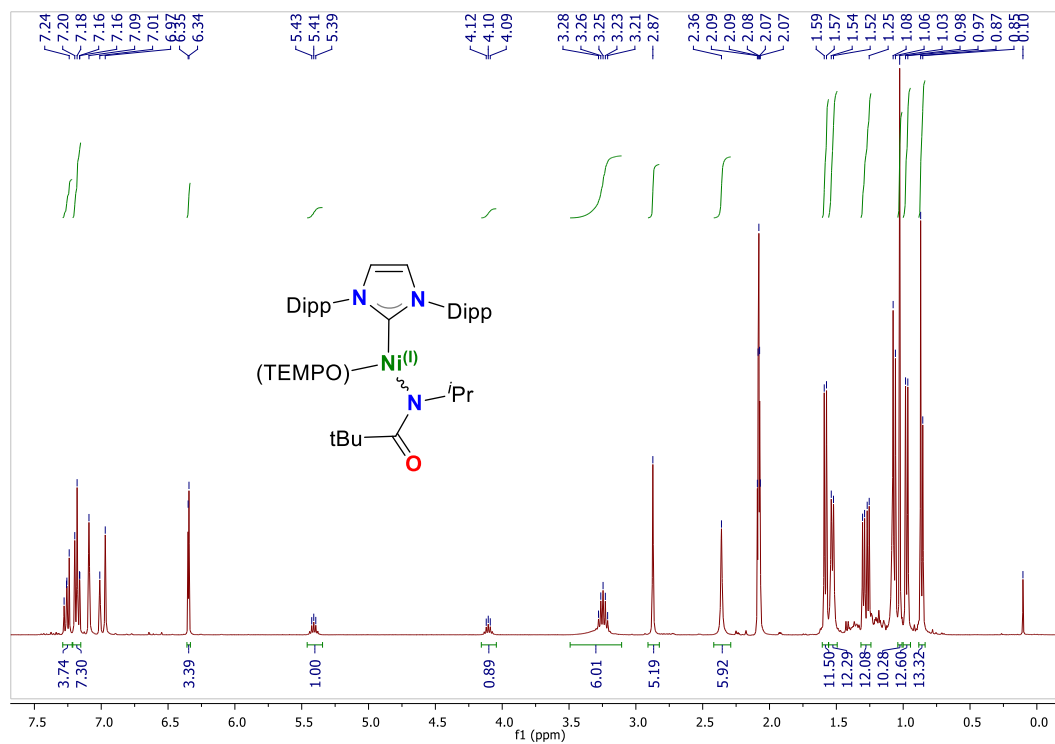


Figure A.3.91. ¹H NMR (400 MHz, 25°C, C₆D₆) of Ni(II)-3.5-TEMPO(E/Z)

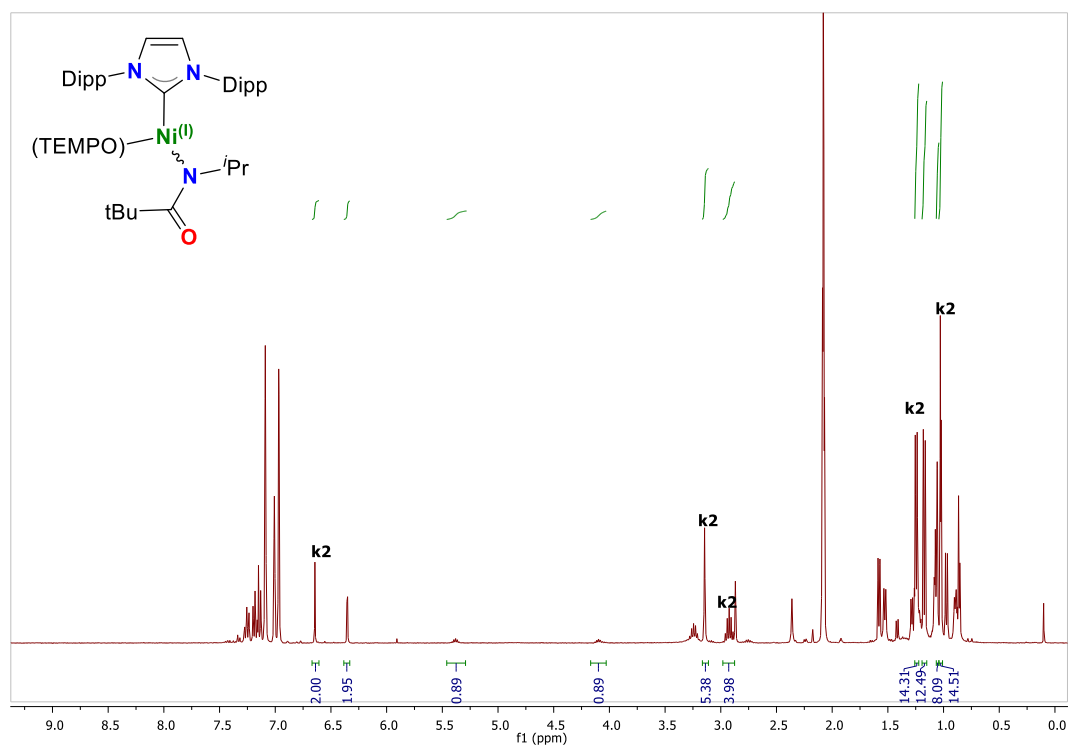


Figure A.3.92. ¹H NMR (400 MHz, 25°C, C₆D₆) of Ni(II)-3.5-TEMPO(E/Z/K)

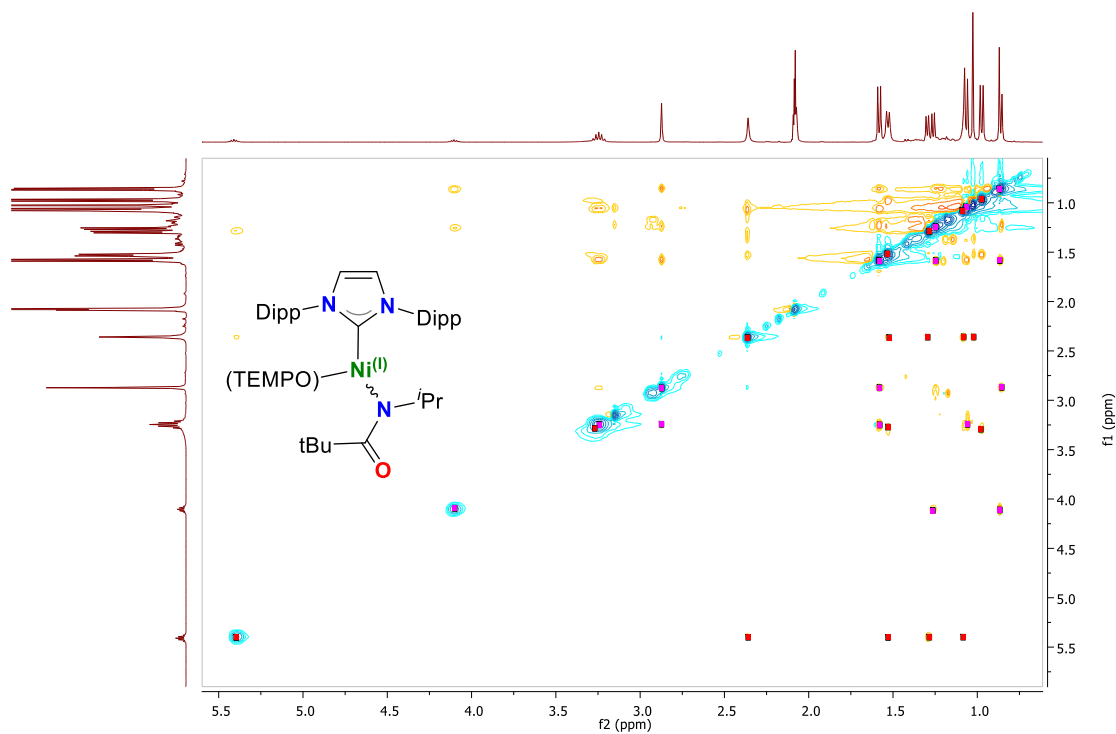


Figure A.3.93. ^1H - ^1H NOESY NMR (400 MHz, 25°C, C_6D_6) of Ni(II)-3.5-TEMPO(E/Z)

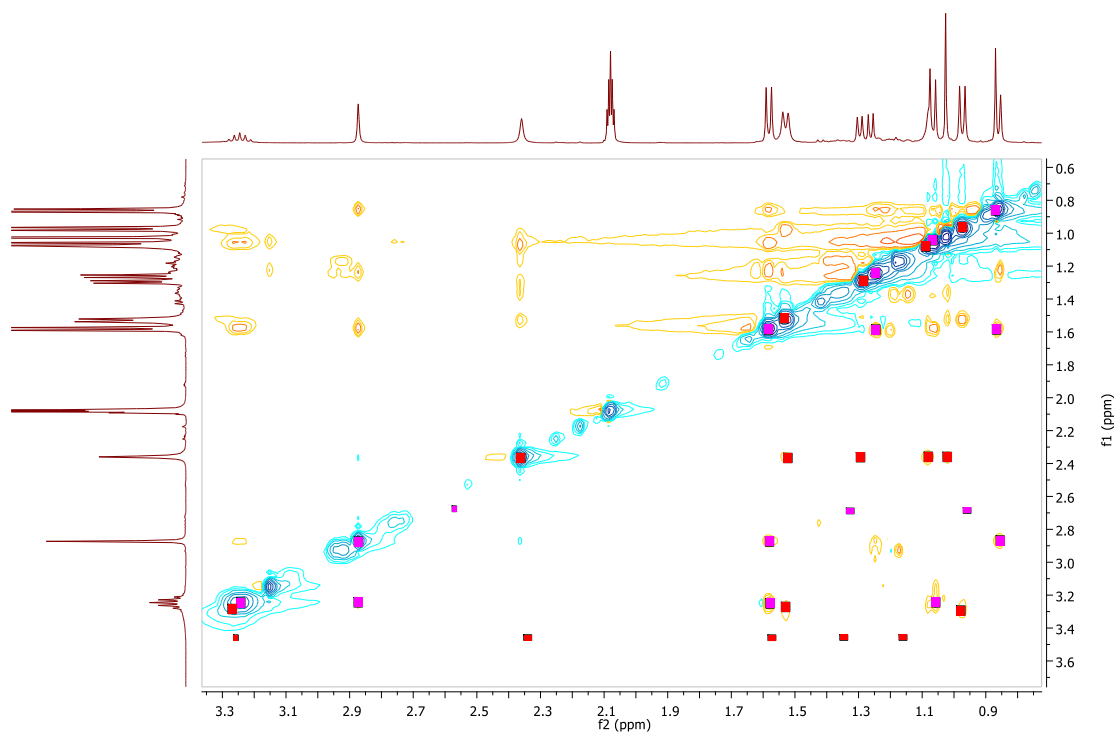


Figure A.3.94. ^1H - ^1H NOESY NMR (400 MHz, 25°C, C_6D_6) of Ni(II)-3.5-TEMPO(E/Z)

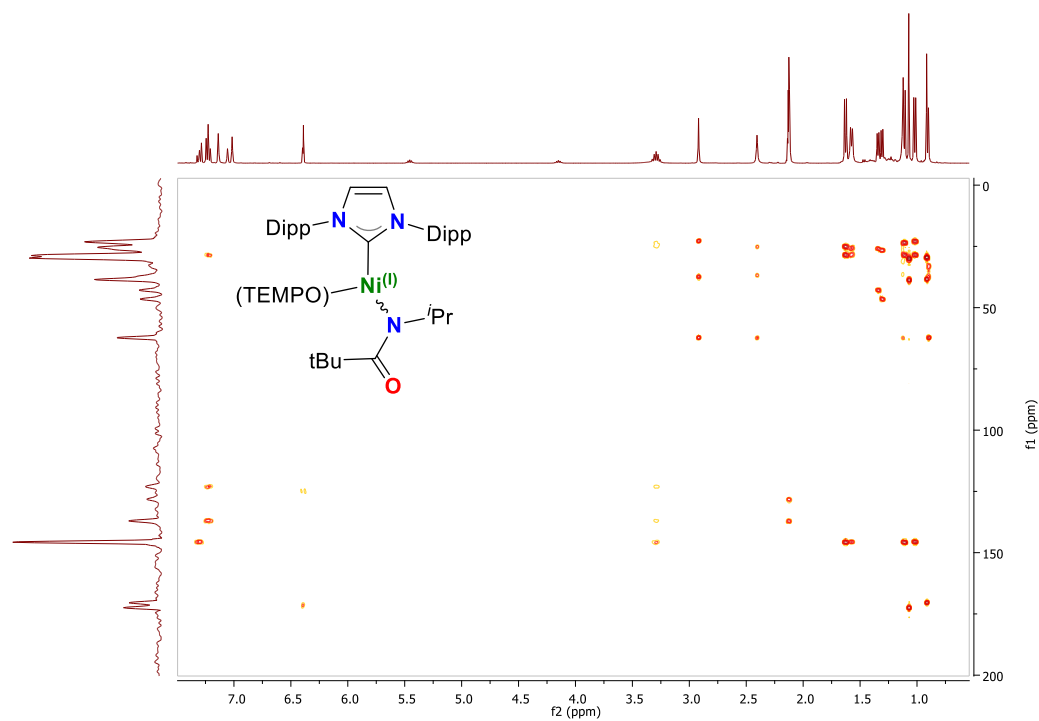


Figure A.3.95. ^1H - ^{13}C HMBC NMR (400 MHz, 25°C , C_6D_6) of Ni(II)-3.5-TEMPO(E/Z)

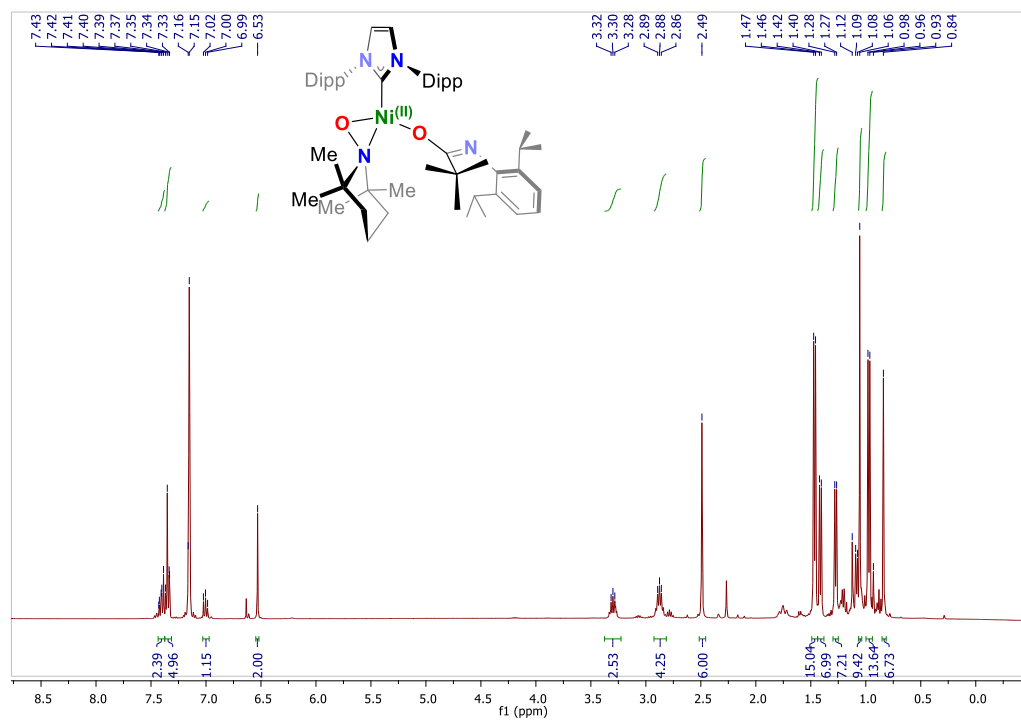


Figure A.3.96. ^1H NMR (400 MHz, 25°C , C_6D_6) of Ni(II)-3.1-TEMPO

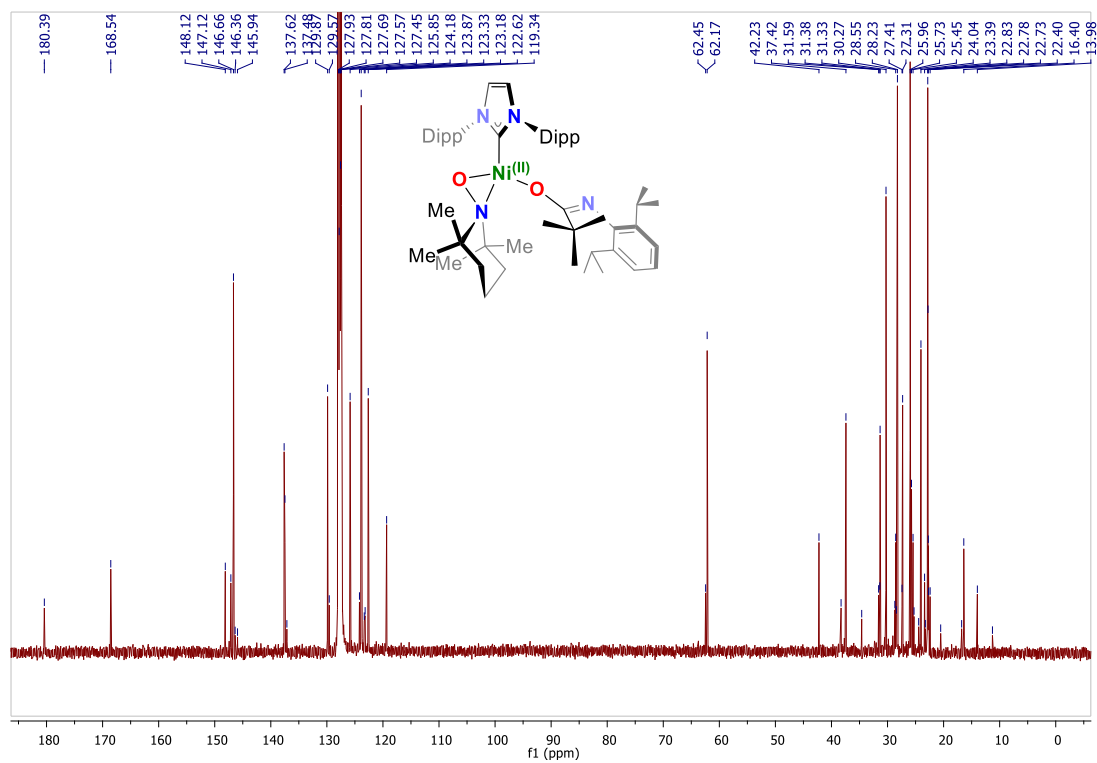


Figure A.3.97. $^{13}\text{C}\{^1\text{H}\}$ NMR (101 MHz, 25°C, C_6D_6) of Ni(II)-3.1-TEMPO

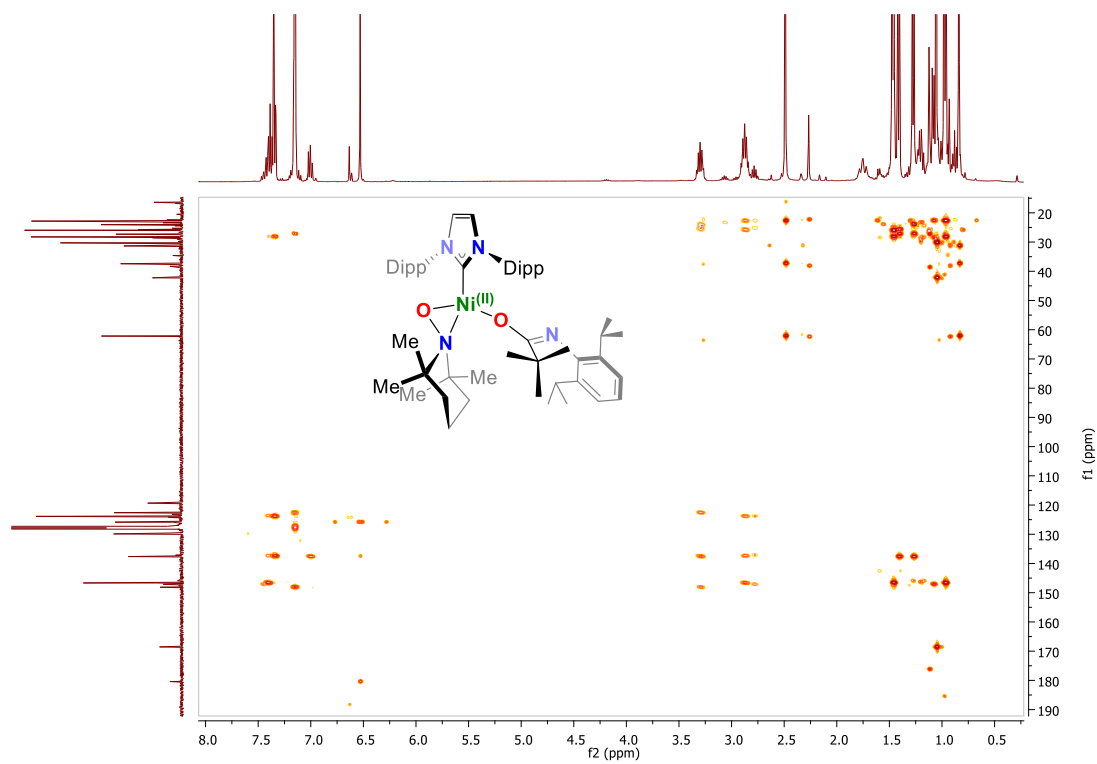
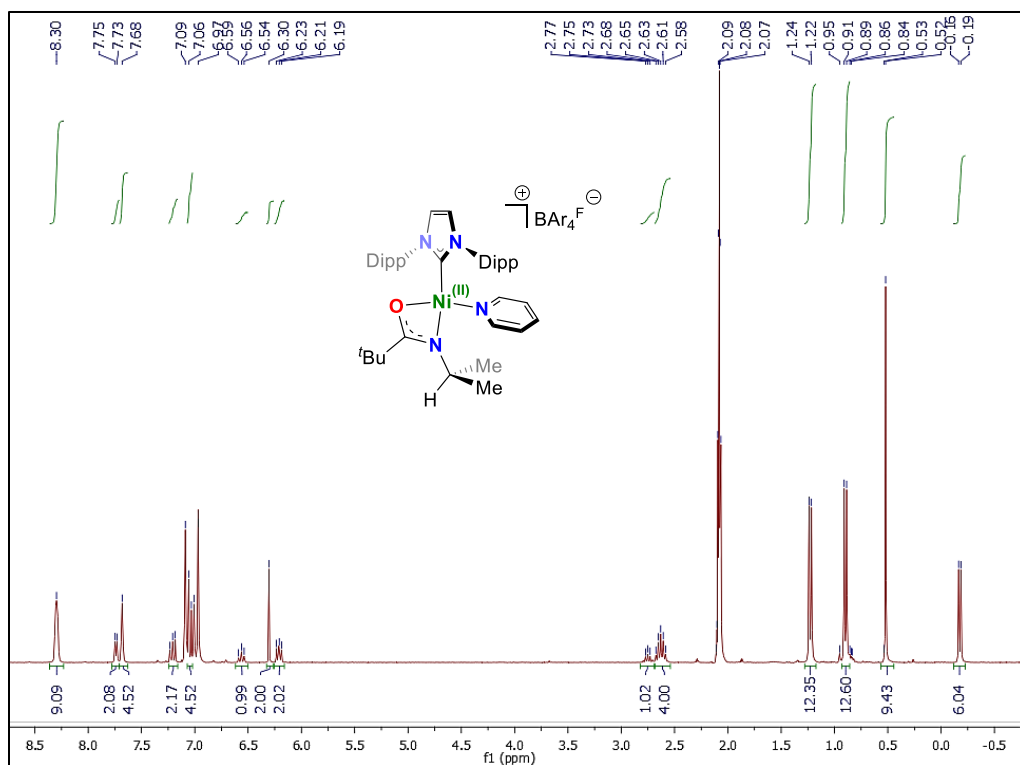


Figure A.3.98. ^1H - ^{13}C HMBC NMR (400 MHz, 25°C, C_6D_6) of Ni(II)-3.1-TEMPO



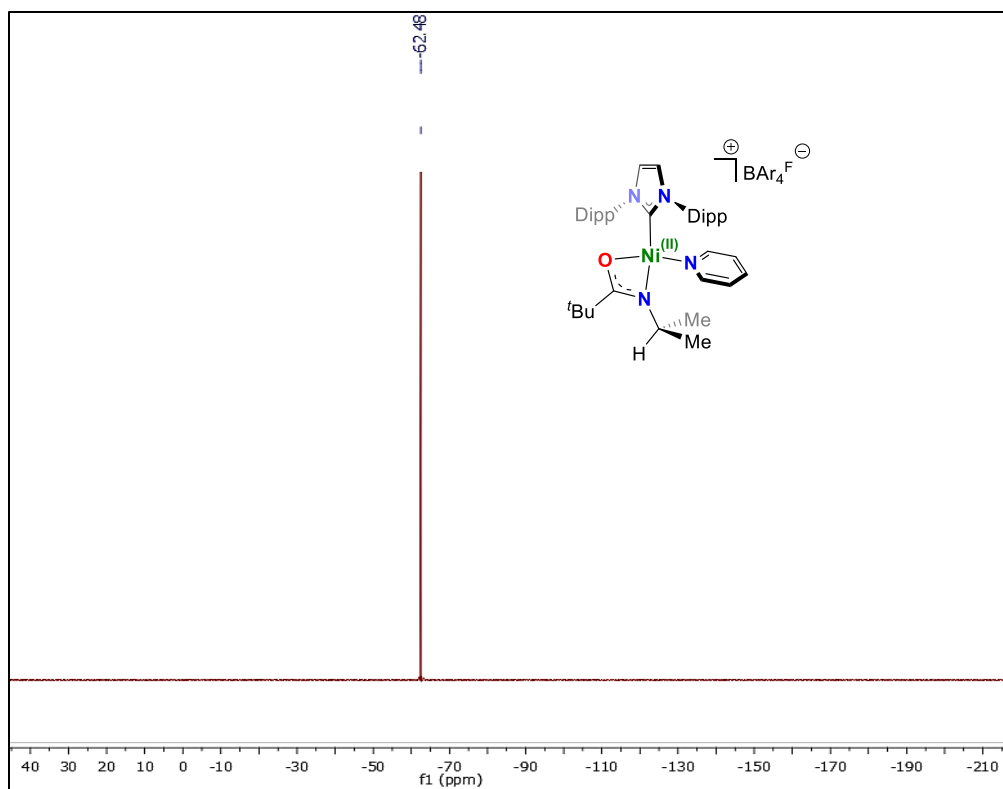


Figure A.3.101. $^{19}\text{F}\{^1\text{H}\}$ NMR (282 MHz, 25°C, C_7D_8) of $[\text{Ni}(\text{II})\text{-}3.5\text{-pyr}][\text{BAr}_4\text{F}]$.

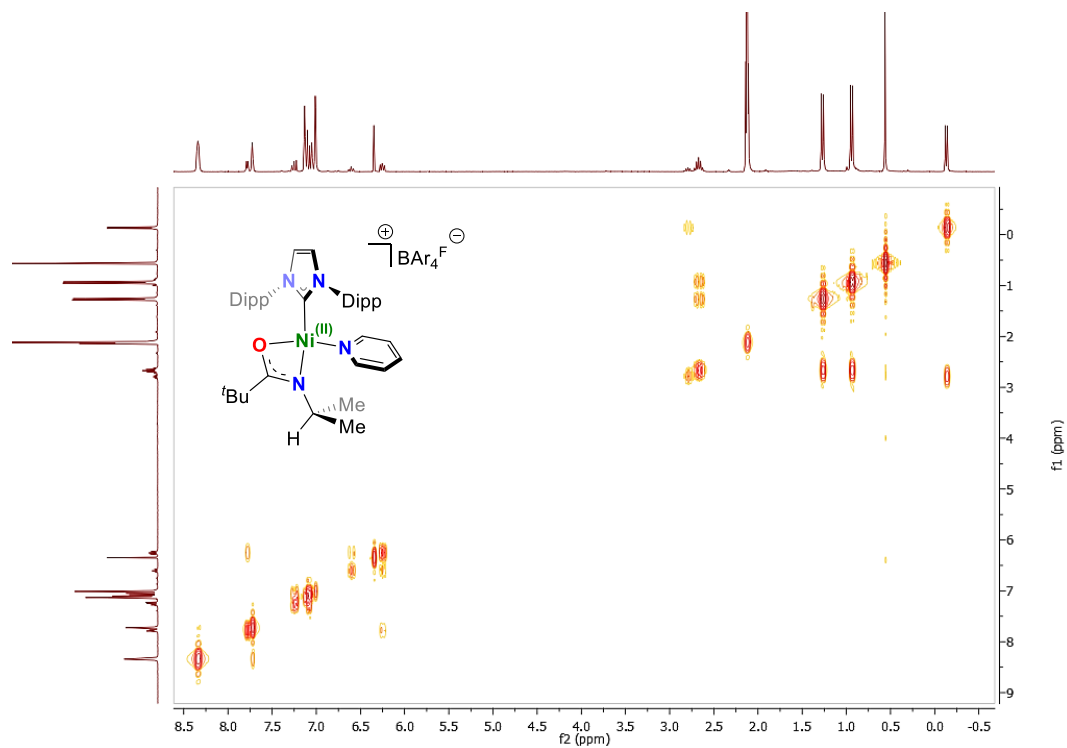


Figure A.3.102. $^1\text{H}\text{-}^1\text{H}$ COSY NMR (300 MHz, 25°C, C_7D_8) of $[\text{Ni}(\text{II})\text{-}3.5\text{-pyr}][\text{BAr}_4\text{F}]$.

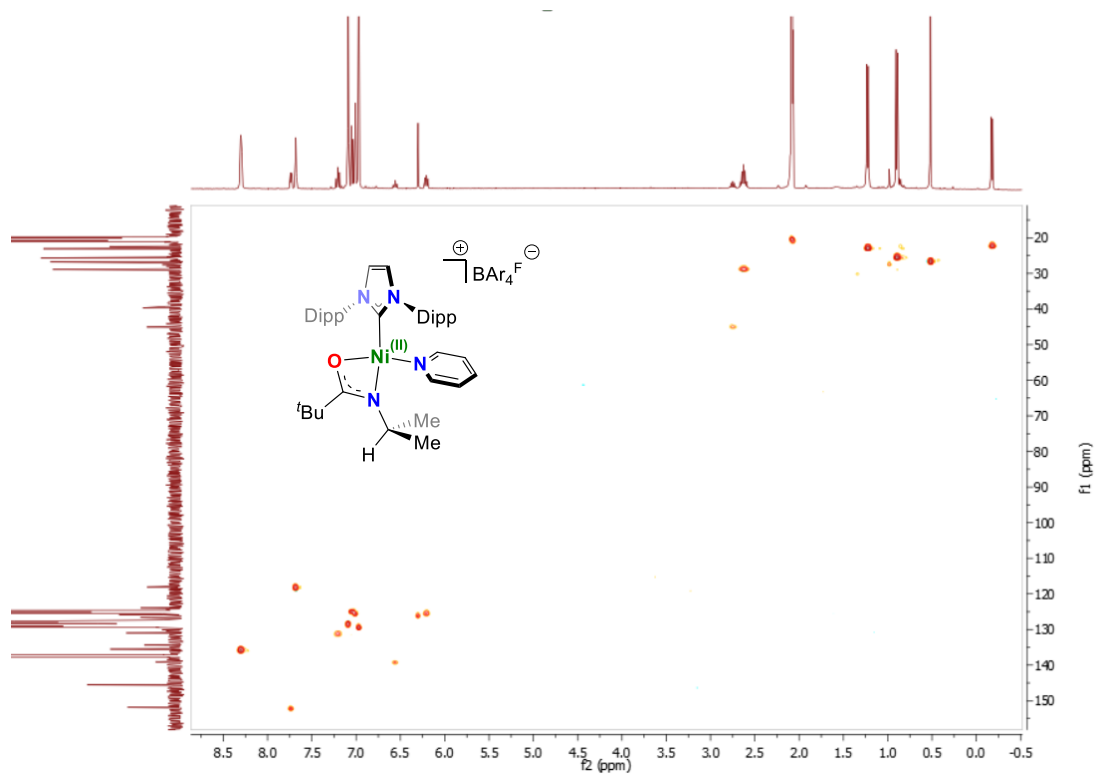


Figure A.3.103. ^1H - ^{13}C HSQC NMR (300 MHz, 25°C , C_7D_8) of $[\text{Ni}(\text{II})\text{-}3.5\text{-pyr}][\text{BAR}4\text{F}]$.

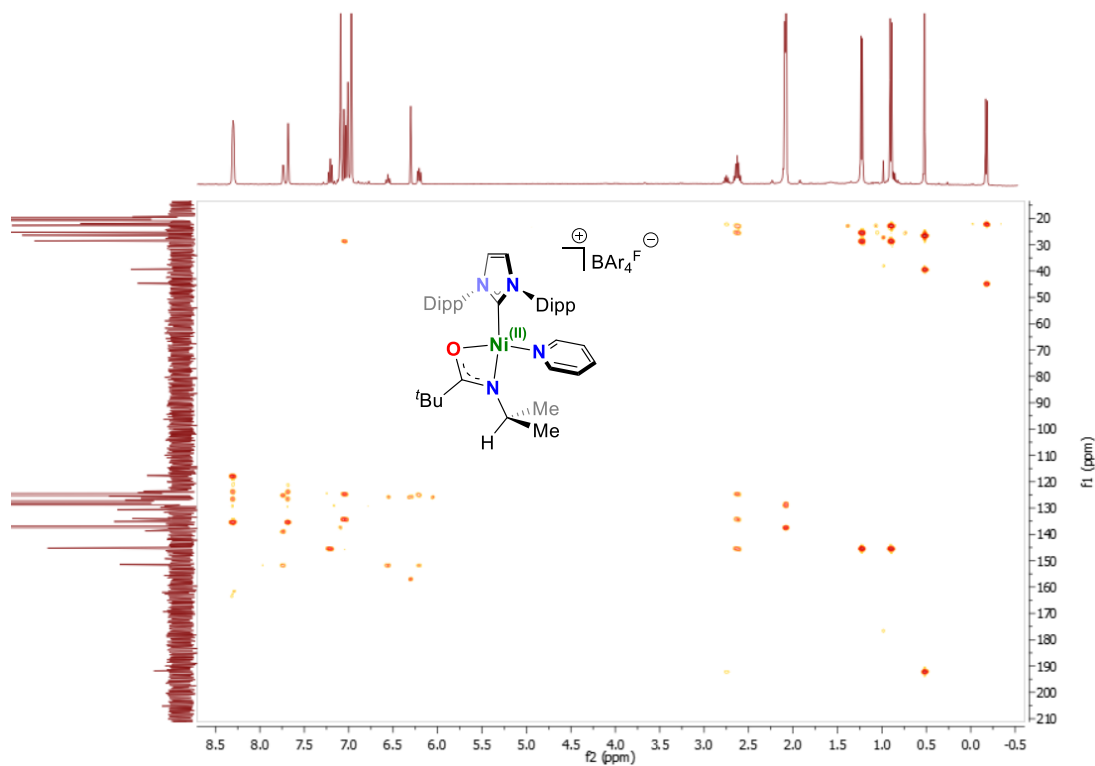


Figure A.3.104. ^1H - ^{13}C HMBC NMR (300 MHz, 25°C , C_7D_8) of $[\text{Ni}(\text{II})\text{-}3.5\text{-pyr}][\text{BAR}4\text{F}]$.

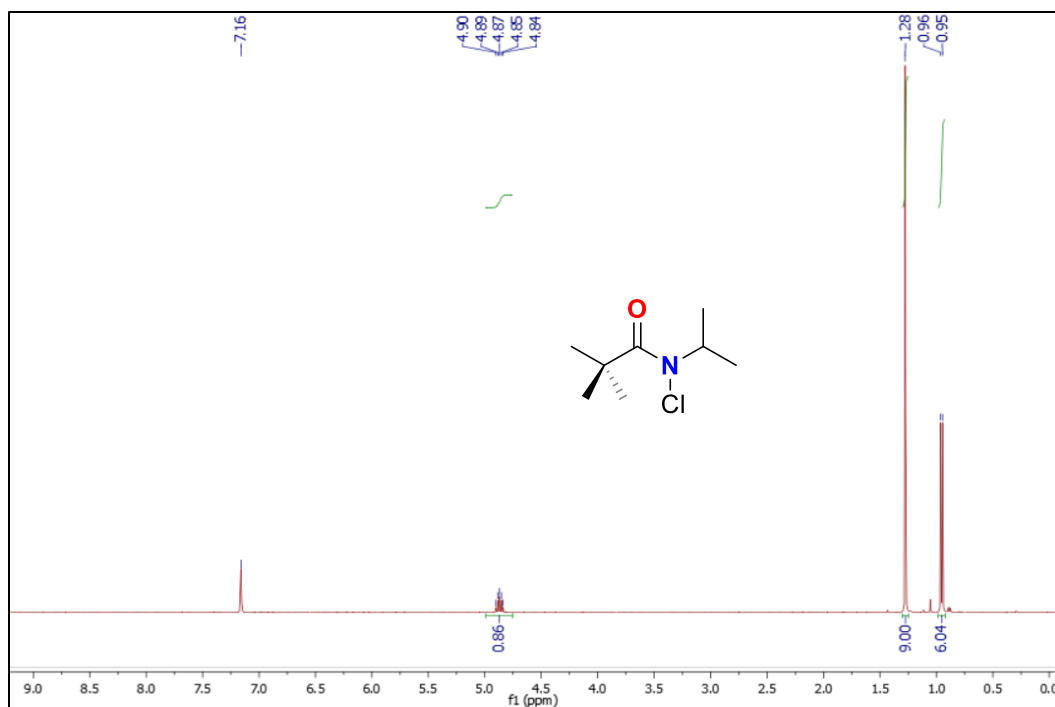


Figure A.3.105. ^1H NMR (400 MHz, 25°C , C_6D_6) of 3.15.

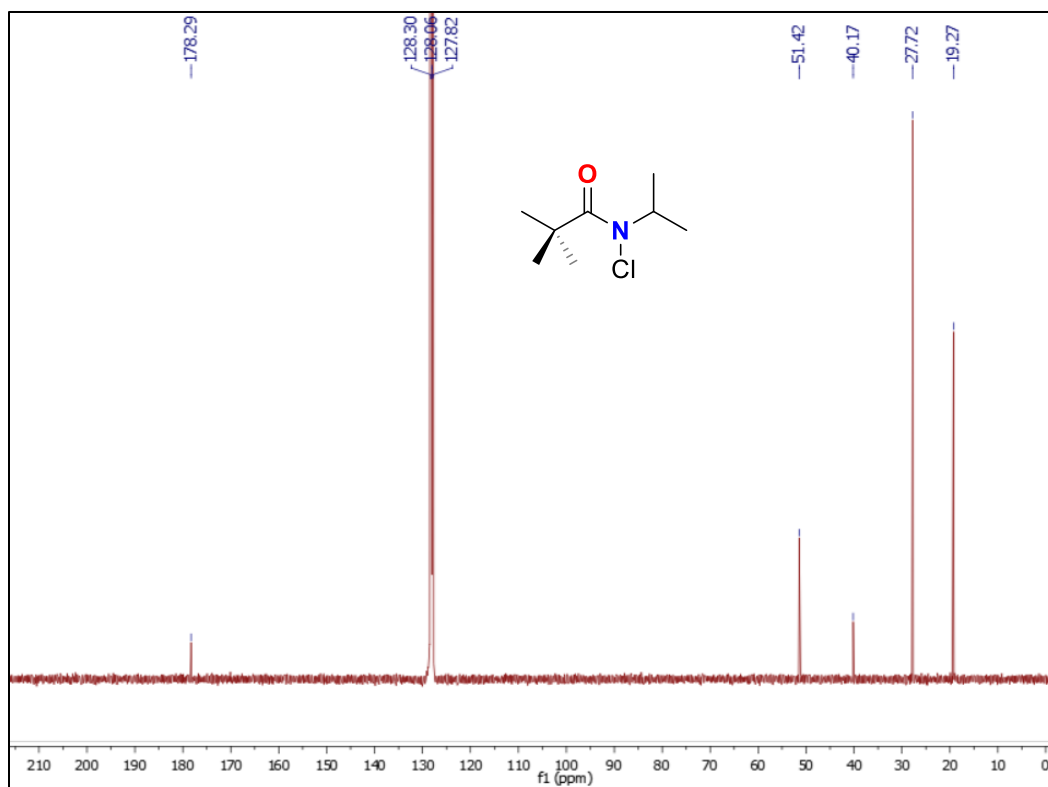
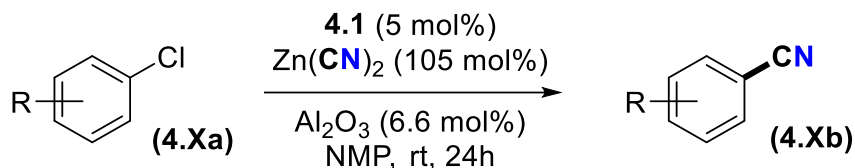


Figure A.3.106. ^{13}C NMR (101 MHz, 25°C , C_6D_6) of 3.15.

A.4 Experimental Data for Chapter 4

General Procedure for Cyanation of Aryl Chlorides

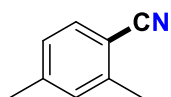


To a 10 mL Schlenk tube equipped with a Teflon stir bar was added **4.1** (38.2 mg, 0.05 mmol), Zn(CN)₂ (123.3 mg, 1.05 mmol), and Al₂O₃ (6.7 mg, 0.066 mmol). The Schlenk tube was sealed and the contents were evacuated on a Schlenk line for 1 h. After refilling and evacuating 3 times, the starting (hetero)aryl chloride (1 mmol) and solvent (NMP, 2.5 mL, 0.4 M) were added to the reaction flask under a flow of argon. Once the flask was resealed, it was stirred (~600 rpm) without heating for 24 h. The reaction contents were then added to a small (50 mL) separatory funnel. EtOAc (2 x 10 mL) was added to the reaction flask, then into the separatory funnel. The organic layer was then washed with distilled water (2 x 5 mL), and saturated brine (5 mL). Finally, a back extraction from the combined aqueous layers was performed with EtOAc (15 mL), and the organic layers were combined and dried over Na₂SO₄. After filtering through filter paper and concentrating the organic fractions to *ca.* 2 mL *in vacuo*, the crude mixture was adsorbed onto a small portion of silica gel for chromatography purposes. After removing the solvent from the silica-adsorbed product mixture *in vacuo*, the silica sample was then dry-loaded onto a silica column (Heptane or pentane/EtOAc, pentane/DCM), or Teledyne Isco Combiflash Rf, and the product was purified using standard flash-chromatographic techniques. Aqueous layers and all glassware were washed with solutions of Na_{2.10}O₃ with FeSO₄ prior to disposal. The resulting Na₄[FeCN₆] solutions were disposed of using accepted protocols.^[278]

Notes on Procedure:

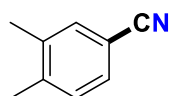
- Zn(CN)₂ is toxic and should only be handled with care.
- Larger Schlenk tubes may be used for the reaction, but care should be taken to wash the sides of the flask with solvent to ensure all reagents and catalyst enter reaction mixture.
- In our hands stirring was an important variable: stirring between 500-700 (rpm) gave optimal results during the screening process.

2,4-dimethylbenzonitrile (4.8b)



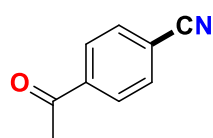
Column conditions 50:1 (pentane:EtOAc), average yield: 62%, [run 1: 78 mg, 59%, run 2: 85 mg, 65%]. The analytical data was consistent with literature.^[279] ¹H NMR (300 MHz, CDCl₃) δ 7.47 (d, *J*_{H,H} = 7.9 Hz, 1H), 7.12 (d, *J*_{H,H} = 0.7 Hz, 1H), 7.08 (dd, *J*_{H,H} = 7.9, 0.7 Hz, 1H), 2.49 (s, 3H), 2.37 (s, 3H); ¹³C{¹H} NMR (75 MHz, CDCl₃) δ 143.5, 141.7, 132.4, 131.0, 127.1, 118.5, 109.6, 21.7, 20.3.

3,4-dimethylbenzonitrile (4.9b)



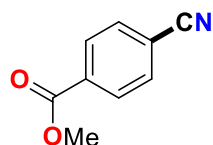
Column conditions 50:1 (heptane:EtOAc), average yield 97%, [run 1: 129 mg, 98%, run 2: 126 mg, 96%]. The analytical data was consistent with literature.^[279] ¹H NMR (300 MHz, CDCl₃) δ 7.37 (m, 2H), 7.20 (d, *J*_{H,H} = 7.7 Hz, 1H), 2.31 (s, 3H), 2.27 (s, 3H); ¹³C{¹H} NMR (75 MHz, CDCl₃) δ 142.6, 138.0, 132.9, 130.4, 129.7, 119.4, 109.6, 20.2, 19.6.

4-acetylbenzonitrile (4.10b)



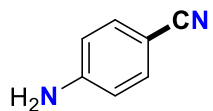
Column conditions 10:1 (pentane:EtOAc), average yield 96%, [run 1: 136 mg, 93%, run 2: 142 mg, 98%]. The analytical data was consistent with literature.^[241] ¹H NMR (300 MHz, CDCl₃) δ 8.04 (dd, *J*_{H,H} = 8.2, 1.9 Hz, 2H), 7.76 (dd, *J*_{H,H} = 8.2, 1.9 Hz, 2H), 2.64 (s, 3H); ¹³C{¹H} NMR (75 MHz, CDCl₃) δ 196.7, 140.0, 132.6, 128.8, 118.0, 116.5, 26.9.

methyl 4-cyanobenzoate (4.11b)



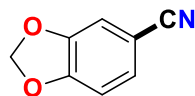
Column conditions 10:1 (pentane:EtOAc), average yield 95%, [run 1: 155 mg, 96%, run 2: 153 mg, 95%]. The analytical data was consistent with literature.^[280] ¹H NMR (300 MHz, CDCl₃) δ 8.12 (dd, *J*_{H,H} = 8.2, 1.9 Hz, 2H), 7.73 (dd, *J*_{H,H} = 8.2, 1.9 Hz, 2H), 3.94 (d, 3H); ¹³C{¹H} NMR (75 MHz, CDCl₃) δ 165.5, 134.0, 132.3, 130.2, 118.0, 116.5, 52.8.

4-aminobenzonitrile (4.12b)



Column conditions 1:1 (pentane:DCM), average yield 78%, [run 1: 95 mg, 80%, run 2: 89 mg, 75%]. The analytical data was consistent with literature.^[281] ¹H NMR (400 MHz, CDCl₃) δ 7.39 (dd, *J*_{H,H} = 9.1, 2.0 Hz, 2H), 6.64 (dd, *J*_{H,H} = 9.1, 2.0 Hz, 2H), 4.22 (s, 2H); ¹³C{¹H} NMR (101 MHz, CDCl₃) δ 150.6, 133.8, 120.3, 114.5, 100.0.

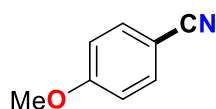
benzo[d][1,3]dioxole-5-carbonitrile (4.13b)



Column conditions 10:1 (pentane:EtOAc), average yield 91%, [**run 1**: 136 mg, 92%, **run 2**: 131 mg, 89%]. The analytical data was consistent with literature.^[241] **¹H NMR (300 MHz, CDCl₃)** δ

7.22 (ddd, $J_{\text{H,H}} = 8.1, 1.5, 1.4$ Hz, 1H), 7.02 (dd, $J_{\text{H,H}} = 1.4, 1.5$ Hz, 1H), 6.86 (dd, $J_{\text{H,H}} = 8.1, 0.5$ Hz, 1H), 6.06 (d, $J_{\text{H,H}} = 0.6$ Hz, 2H); **¹³C{¹H} NMR (75 MHz, CDCl₃)** δ 151.6, 148.1, 128.3, 119.0, 111.5, 109.2, 105.0, 102.3.

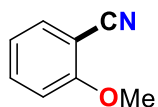
4-methoxybenzonitrile (4.14b)



Column conditions 10:1 (pentane:EtOAc), average yield 89%, [**run 1**: 119 mg, 90%, **run 2**: 118 mg, 88%]. The analytical data was consistent with literature.^[241] **¹H NMR (300 MHz, CDCl₃)** δ

7.56 (dd, $J_{\text{H,H}} = 9.6, 2.1$ Hz, 2H), 6.93 (dd, $J_{\text{H,H}} = 9.6, 2.1$ Hz, 2H), 3.84 (s, 3H); **¹³C{¹H} NMR (75 MHz, CDCl₃)** δ 162.9, 134.0, 119.3, 114.8, 103.9, 55.6.

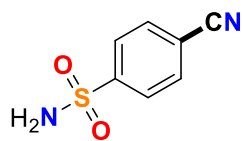
2-methoxybenzonitrile (4.15b)



Combiflash separation, (heptane:EtOAc, gradient – up to 30% EtOAc), average yield 69%, [**run 1**: 91 mg, 68%, **run 2**: 92 mg, 69%]. The analytical data was consistent with literature.^[282] **¹H NMR (400 MHz, CDCl₃)** δ

7.53 (m, 2H), 6.99 (m, 2H), 3.92 (s, 3H); **¹³C{¹H} NMR (101 MHz, CDCl₃)** δ 161.3, 134.5, 133.8, 120.8, 116.6, 111.4, 101.8, 56.1.

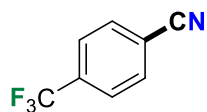
4-cyanobenzenesulfonamide (4.16b)



Combiflash separation, (heptane:EtOAc, gradient – up to 100% EtOAc), average yield 91%, [**run 1**: 160 mg, 88%, **run 2**: 171 mg, 94%]. The analytical data was consistent with literature.^[239] **¹H NMR (300 MHz, DMSO)** δ

8.07 (d, $J_{\text{H,H}} = 8.3$ Hz, 2H), 7.98 (d, $J_{\text{H,H}} = 8.3$ Hz, 2H), 7.66 (s, 2H); **¹³C{¹H} NMR (75 MHz, DMSO)** δ 148.0, 133.3, 126.5, 117.9, 114.4.

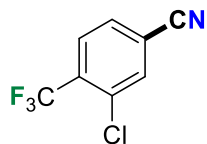
4-trifluoromethylbenzonitrile (4.17b)



Combiflash separation, (heptane:EtOAc, gradient – up to 20% EtOAc), average yield 69%, [**run 1**: 125 mg, 73%, **run 2**: 113 mg, 66%]. The analytical data was consistent with literature.^[281] **¹H**

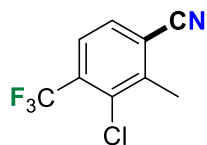
NMR (300 MHz, CDCl₃) δ 7.81 (d, $J_{\text{H,H}} = 8.4$ Hz, 2H), 7.76 (d, $J_{\text{H,H}} = 8.4$ Hz, 2H); **¹³C{¹H} NMR (75 MHz, CDCl₃)** δ 134.9 (q, $J_{\text{F,C}} = 32.8$ Hz), 132.8, 126.3 (q, $J_{\text{F,C}} = 3.6$ Hz), 123.2 (q, $J_{\text{F,C}} = 273.8$ Hz), 117.6, 116.2; **¹⁹F{¹H} NMR (282 MHz, CDCl₃)** δ -63.1.

3-chloro-4-trifluoromethylbenzonitrile (4.18b)



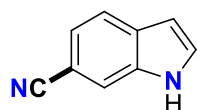
Column conditions 20:1 (heptane:EtOAc), average yield 63%, [**run 1**: 132 mg, 64%, **run 2**: 127 mg, 62%]. ^1H NMR (300 MHz, CDCl_3) δ 7.83 (m, 2H), 7.69 (m, 1H); $^{13}\text{C}\{^1\text{H}\}$ NMR (75 MHz, CDCl_3) δ 134.8, 133.9, 132.7 (q, $J_{\text{F,C}} = 32.7$ Hz), 130.5, 128.6 (q, $J_{\text{F,C}} = 5.3$ Hz), 122.0 (q, $J_{\text{F,C}} = 274.0$ Hz), 117.4, 116.3. $^{19}\text{F}\{^1\text{H}\}$ NMR (282 MHz, CDCl_3) δ -63.1. HRMS (EI) m/z calculated for $\text{C}_8\text{H}_3\text{ClF}_3\text{N}$ $[\text{M}]^+$: 204.99006; found: 204.99020.

3-chloro-2-methyl-4-trifluoromethylbenzonitrile (4.19b)



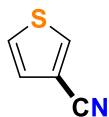
Column conditions 50:1 (heptane:EtOAc), average yield 92%, [**run 1**: 202 mg, 92%, **run 2**: 204 mg, 93%]. ^1H NMR (300 MHz, CDCl_3) δ 7.64 (m, 2H), 2.66 (s, 3H); $^{13}\text{C}\{^1\text{H}\}$ NMR (75 MHz, CDCl_3) δ 142.6, 134.1, 133.3 (q, $J_{\text{F,C}} = 31.7$ Hz), 130.7, 125.6 (q, $J_{\text{F,C}} = 5.5$ Hz), 122.2 (q, $J_{\text{F,C}} = 274.5$ Hz), 118.16, 116.46, 19.34. $^{19}\text{F}\{^1\text{H}\}$ NMR (282 MHz, CD_2Cl_2) δ -63.1. HRMS (ESI-TOF) m/z calculated for $\text{C}_9\text{H}_5\text{ClF}_3\text{N}$ $[\text{M}-\text{H}]^-$: 217.99899; found: 217.99865.

1H-indole-6-carbonitrile (4.20b)



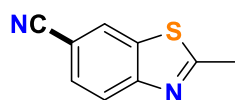
Column conditions 5:1 (heptane:EtOAc), average yield 70%, [**run 1**: 100 mg, 70%, **run 2**: 100 mg, 70%]. The analytical data was consistent with literature.^[283] ^1H NMR (400 MHz, CDCl_3) δ 8.75 (s, 1H), 7.78 (m, 1H), 7.70 (d, $J_{\text{H,H}} = 8.2$ Hz, 1H), 7.43 (d, $J_{\text{H,H}} = 8.2, 1.4$ Hz, 1H), 7.35 (dd, $J = 8.2, 1.4$ Hz, 1H), 6.63 (m, 1H); $^{13}\text{C}\{^1\text{H}\}$ NMR (101 MHz, CDCl_3) δ 134.7, 131.3, 128.3, 122.8, 121.6, 120.9, 116.2, 104.2, 103.5.

3-cyanothiophene (4.21b)



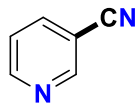
Column conditions 25:1 (heptane:EtOAc), average yield 72%, [**run 1**: 79 mg, 72%, **run 2**: 80 mg, 73%]. The analytical data was consistent with literature.^[281] ^1H NMR (400 MHz, CDCl_3) δ 7.95 (dd, $J_{\text{H,H}} = 3.0, 1.2$ Hz, 1H), 7.44 (dd, $J_{\text{H,H}} = 5.1, 3.0$ Hz, 1H), 7.30 (dd, $J_{\text{H,H}} = 5.1, 1.2$ Hz, 1H); $^{13}\text{C}\{^1\text{H}\}$ NMR (101 MHz, CDCl_3) δ 135.5, 128.7, 127.4, 115.2, 110.6.

2-methylbenzo[d]thiazole-6-carbonitrile (4.22b)



Combiflash separation, (heptane:EtOAc, gradient – up to 70% EtOAc), average yield 86%, [**run 1**: 145 mg, 83%, **run 2**: 155 mg, 89%]. The analytical data was consistent with literature.^[284] ^1H NMR (300 MHz, CDCl_3) δ 8.18 (s, 1H), 7.89 (d, $J_{\text{H,H}} = 1.5$ Hz, 1H), 7.54 (m, 1H), 2.85 (d, $J_{\text{H,H}} = 1.6$ Hz, 3H); $^{13}\text{C}\{^1\text{H}\}$ NMR (75 MHz, CDCl_3) δ 169.8, 153.1, 140.7, 127.2, 126.5, 122.6, 118.9, 109.7, 20.3.

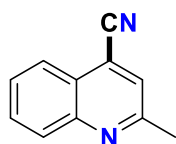
3-cyanopyridine (4.23b)



Column conditions 5:1 (heptane:EtOAc), average yield 68%, [**run 1**: 70 mg, 67%, **run 2**: 72 mg, 69%].

The analytical data was consistent with literature.^[285] **¹H NMR (300 MHz, CDCl₃)** δ 8.90 (dd, $J_{\text{H,H}} = 2.1, 0.8$ Hz, 1 H), 8.82 (dd, $J_{\text{H,H}} = 5.0, 1.6$ Hz, 1 H), 7.98 (dd, $J_{\text{H,H}} = 8.0, 1.9$ Hz, 1 H), 7.45 (ddd, $J_{\text{H,H}} = 8.0, 5.0, 0.9$ Hz, 1 H); **¹³C{¹H} NMR (75 MHz, CDCl₃)** δ 153.2, 152.6, 139.4, 123.8, 116.6, 110.3.

2-methylquinoline-4-carbonitrile (4.24b)



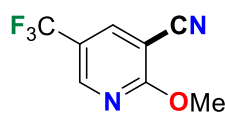
Combiflash separation, (heptane:EtOAc, gradient – up to 40% EtOAc), average yield 94%, [**run**

1: 161 mg, 96%, **run 2**: 156 mg, 93%]. The analytical data was consistent with literature.^[285] **¹H**

NMR (300 MHz, CDCl₃) δ 8.10 (m, 2H), 7.81 (m, 1H), 7.67 (m, 1H), 7.61 (s, 1H), 2.79 (s, 3H);

¹³C{¹H} NMR (75 MHz, CDCl₃) δ 158.5, 147.9, 131.2, 129.6, 128.3, 126.0, 124.8, 124.1, 119.0, 115.8, 25.3.

2-methoxy-5-(trifluoromethyl)nicotinonitrile (4.24b)



Combiflash separation, (pentane:EtOAc, gradient – up to 60% EtOAc), average yield 76%,

[**run 1**: 151 mg, 75%, **run 2**: 157 mg, 78%]. **¹H NMR (300 MHz, CDCl₃)** δ 8.62 (dq, $J_{\text{H,H}} =$

2.5 Hz, $J_{\text{H,F}} = 0.89$ Hz, 1H), 8.10 (d, $J_{\text{H,H}} = 2.5$ Hz, 1H), 4.13 (s, 3H); **¹³C{¹H} NMR (75 MHz,**

CDCl₃) δ 165.9, 149.1 (q, $J_{\text{F,C}} = 4.0$ Hz), 140.1 (q, $J_{\text{F,C}} = 3.2$ Hz), 122.9 (q, $J_{\text{F,C}} = 271.6$ Hz), 120.4 (q, $J_{\text{F,C}} = 34.5$ Hz),

113.8, 97.5, 55.6. **¹⁹F{¹H} NMR (282 MHz, CDCl₃)** δ -61.3. **HRMS (EI)** m/z calculated for C₈H₅O₁F₃N₂ [M]⁺:

202.03485; found: 202.03446.

Other Solvent Combinations

Using the following list of solvents/solutions, no product (0%) was observed by GC-MS under reaction conditions similar to those used in Table 4.1, entry 4.

- Toluene, acetone, dichloromethane, Water, n-BuOH, DMSO, CH₃CN, 1,4-dioxane, DME
- Water:THF (1:1)
- Water:NMP (1:4, 2:3)
- *N,N,N'*-tetramethylurea
- NMP:solvent (1:9)
 - solvent = acetonitrile, toluene, n-BuOH, THF, DCM, acetone, water

Representative Spectra of Complex 4.1

In our hands the synthesis of complex **4.1** was consistent with literature methods.^[254] Moreover, the catalytic efficiency was reliable from multiple syntheses of **4.1**. Below are representative ^1H (300MHz, C_6D_6 , 298K) and ^{31}P (121.5 MHz, C_6D_6 , 298K) NMR spectra.

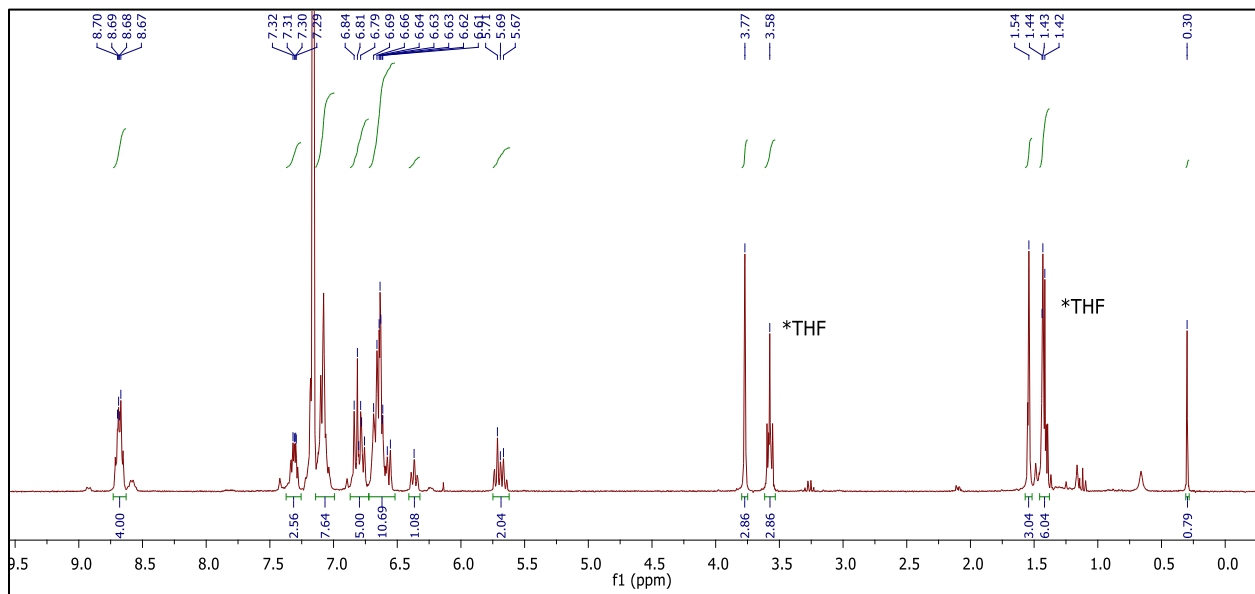


Figure A.4.107. ^1H NMR spectrum (300MHz, C_6D_6 , 298K) of complex **4.1**.

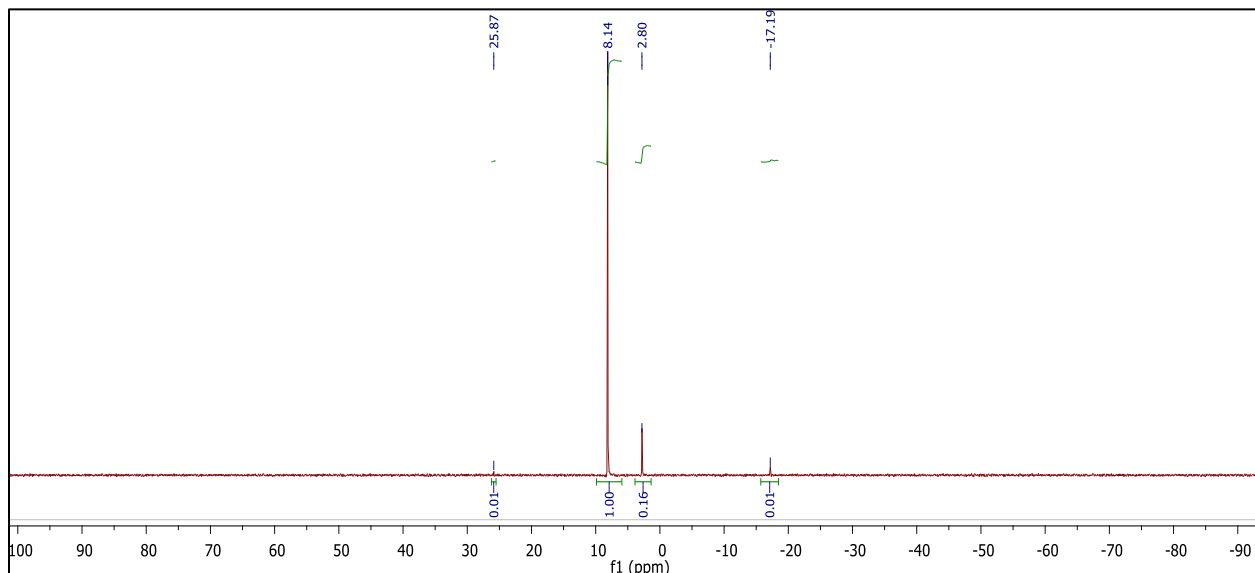


Figure A.4.108. $^{31}\text{P}\{^1\text{H}\}$ NMR spectrum (121.5MHz, C_6D_6 , 298K) of complex **4.1**.

Representative NMR Spectra of Nitrile Products

see *Org. Biol. Chem.* **2017**, *15*, 4291-4294 for remainder of ^1H and $^{13}\text{C}\{^1\text{H}\}$ spectra.

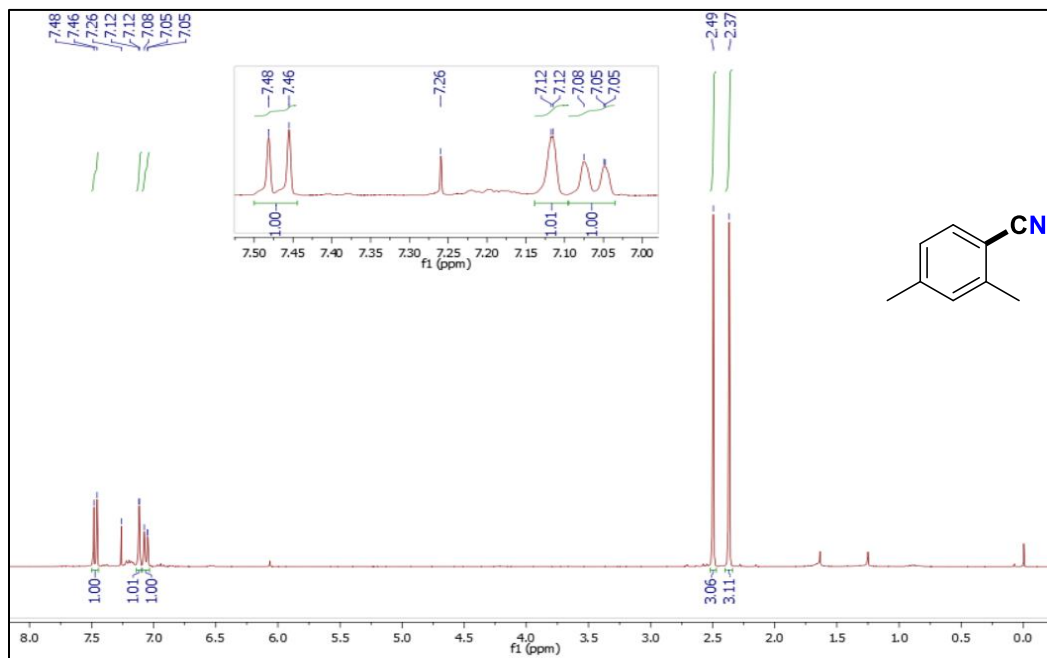


Figure A.4.109. ^1H NMR spectrum (300 MHz, CDCl_3) of compound (4.8b)

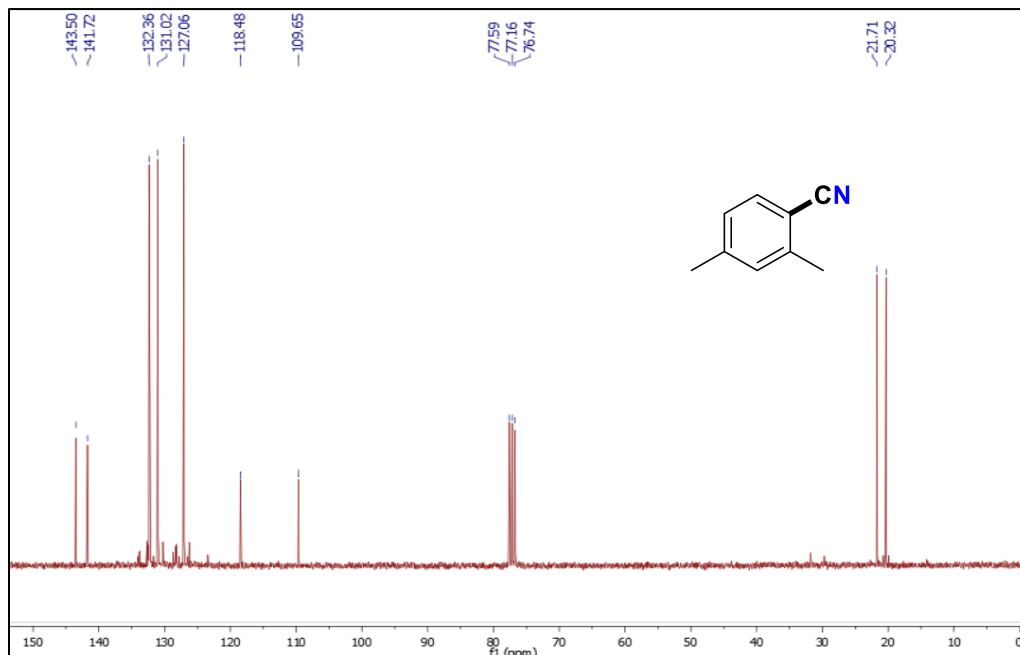


Figure A.4.4. $^{13}\text{C}\{^1\text{H}\}$ NMR spectrum (75 MHz, CDCl_3) of compound (4.8b)

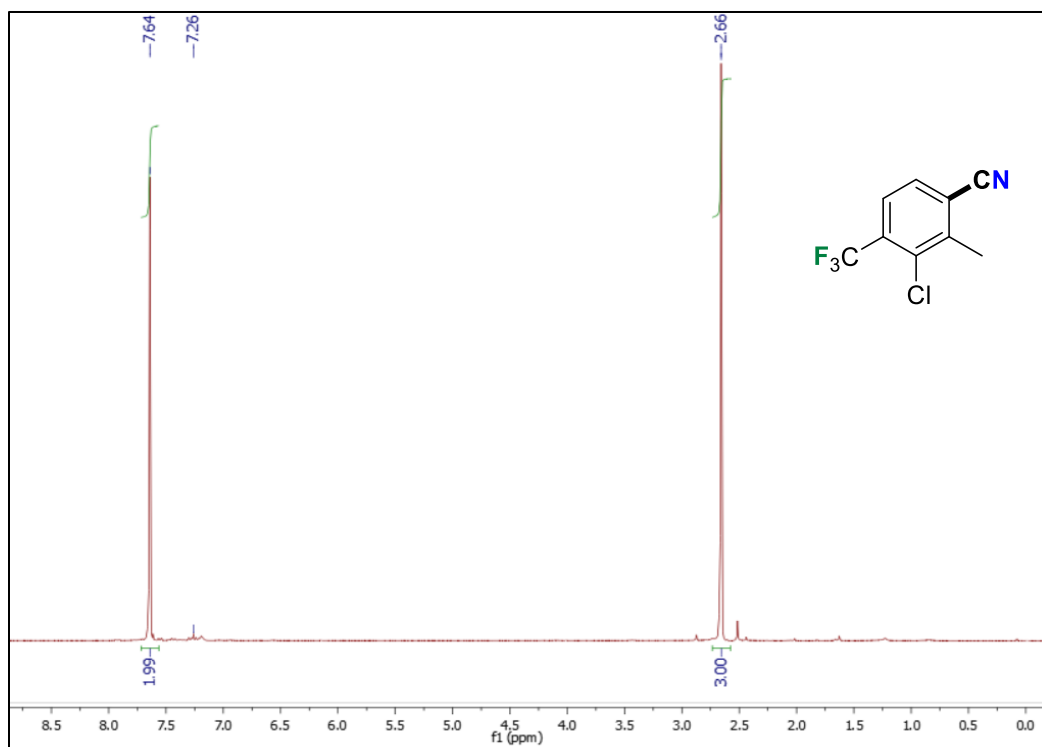


Figure A.4.110. ¹H NMR spectrum (300 MHz, CDCl₃) of compound (4.19b)

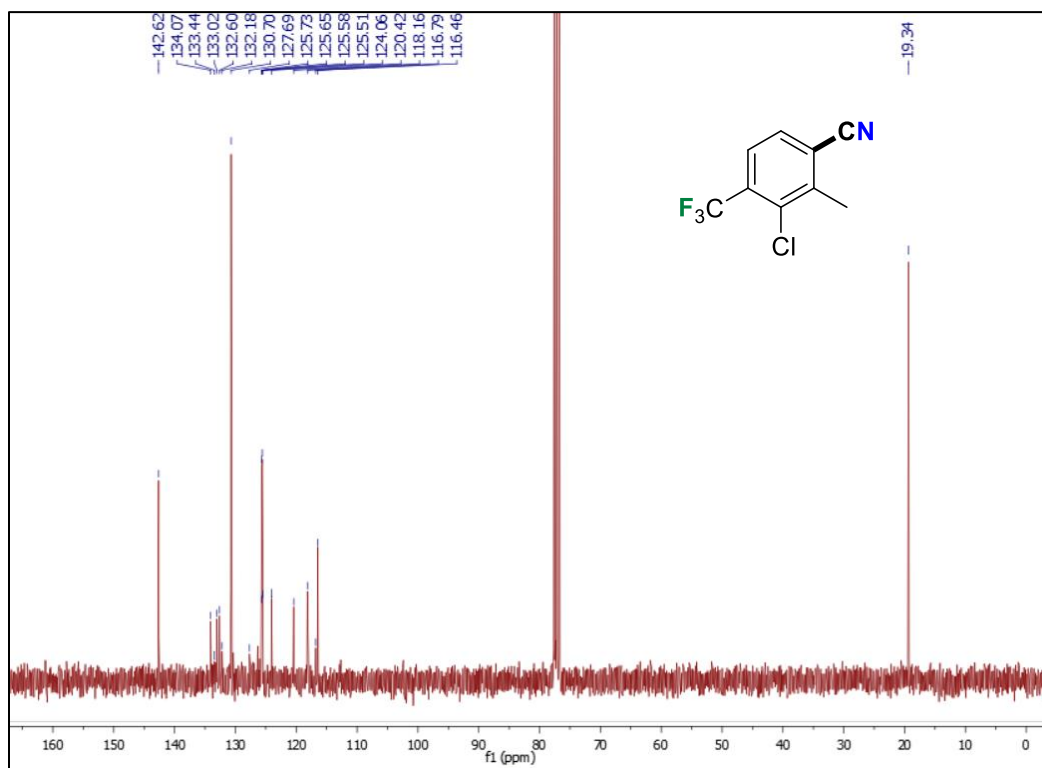


Figure A.4.111. ¹³C{¹H} NMR spectrum (75 MHz, CDCl₃) of compound (4.19b)

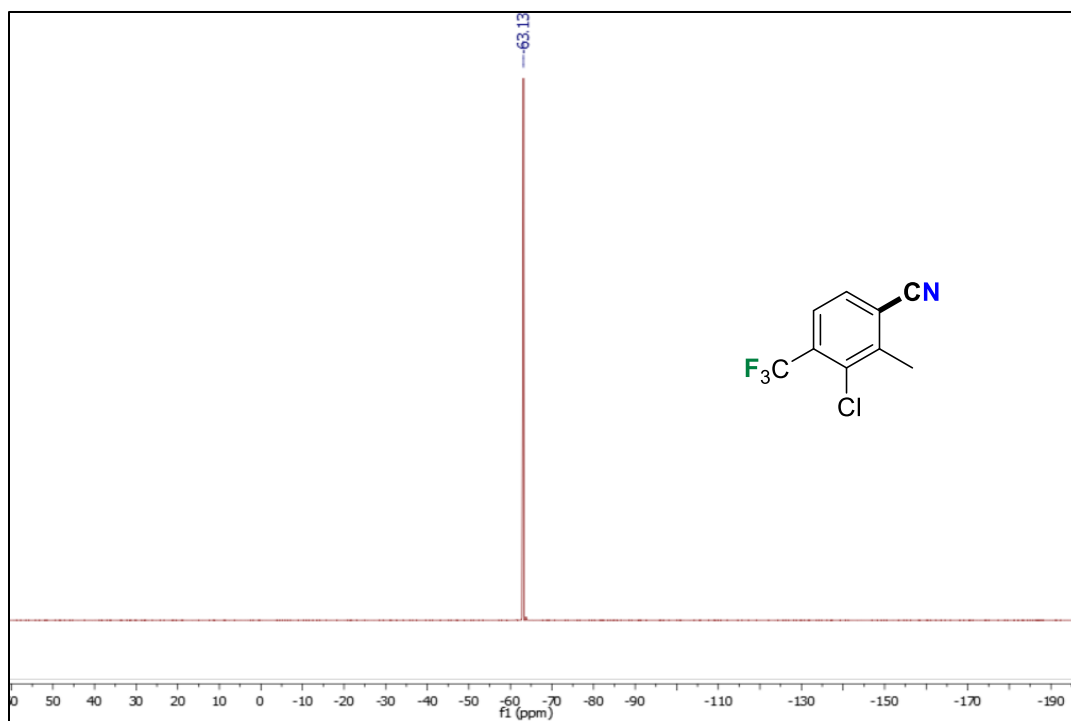


Figure A.4.112. $^{19}\text{F}\{^1\text{H}\}$ NMR spectrum (282 MHz, CDCl_3) of compound (4.19b)

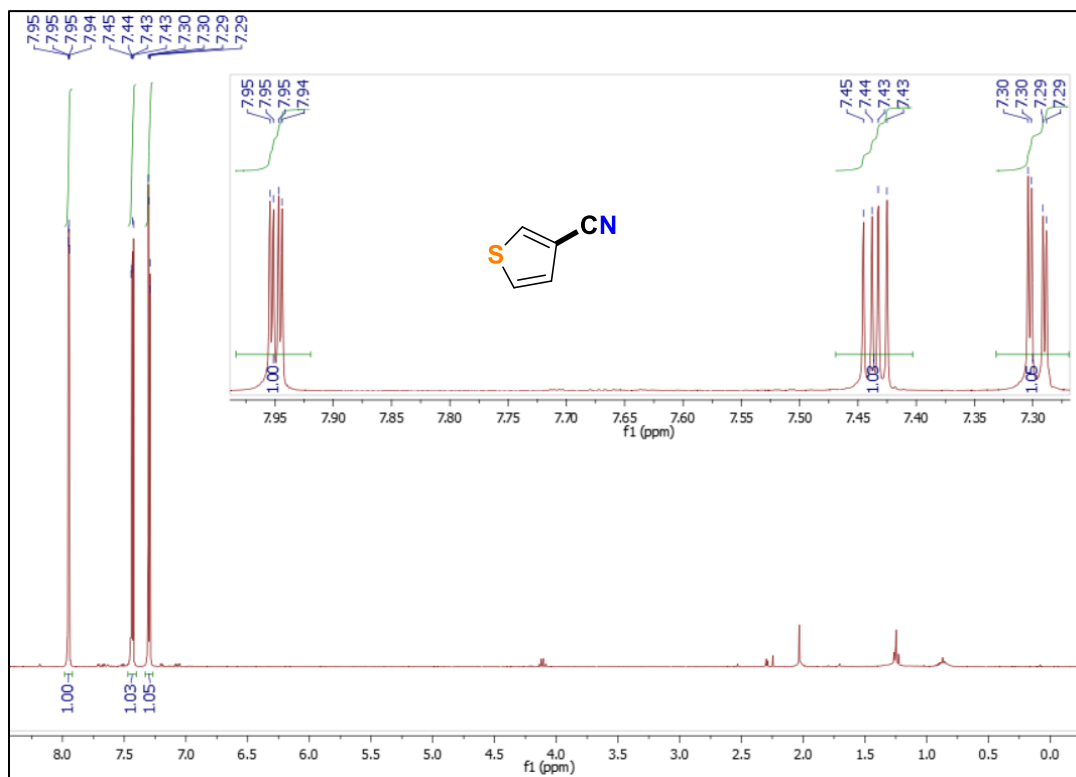


Figure A.4.113. ^1H NMR spectrum (400 MHz, CDCl_3) spectrum of compound (4.21b)

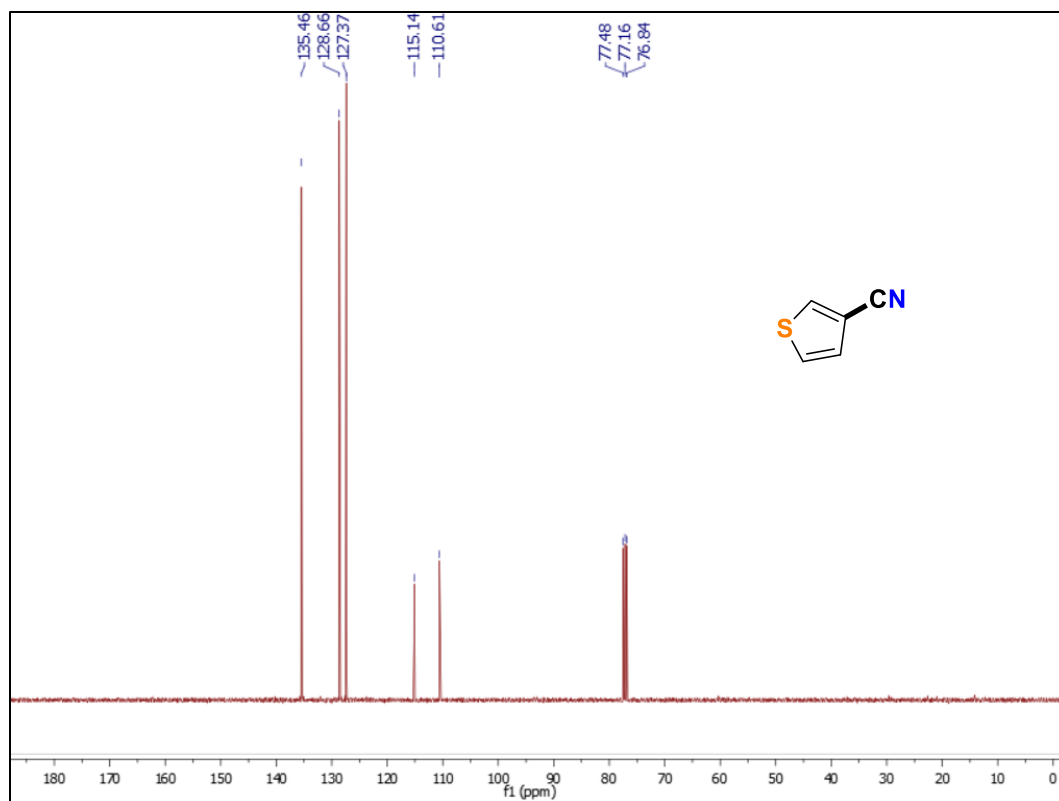
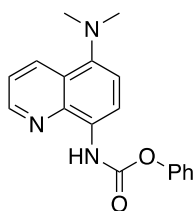


Figure A.4.114. $^{13}\text{C}\{^1\text{H}\}$ NMR spectrum (101 MHz, CDCl_3) spectrum of compound (4.21b)

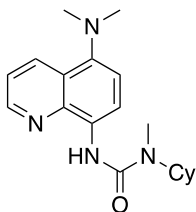
A.5 Experimental Data for Chapter 5

Phenyl (5-(dimethylamino)quinolin-8-yl)carbamate



The carbamate was synthesized following a procedure adapted from literature. To a stirred solution of *N*⁵,*N*⁵-dimethylquinoline-5,8-diamine (0.3745 g, 2 mmol, 1 equiv.) and triethylamine (0.56 mL, 4 mmol, 2 equiv.) in THF (15 mL) at 0 °C phenylchloroformate (0.26 mL, 2.1 mmol, 1.05 equiv.) was added drop-wise over 5 minutes, under inert atmosphere. The resulting solution was allowed to stir at room temperature for 12 h to generate a heterogeneous mixture. Upon completion, the solvent was removed under reduced pressure and the solid obtained was diluted with ethyl acetate and sat. aq. NaHCO₃. The organic layer was separated and the aqueous layer was extracted with ethyl acetate (x3). The combined organic layers were washed with brine, dried over anhydrous sodium sulfate, filtered and concentrated under reduced pressure. The compound was purified by column chromatography (75:25 - Hex:EtOAc) to afford a yellow solid in 84%. **¹H NMR** (400 MHz; CDCl₃): 9.41 (d, *J* = 0.2 Hz, 1H), 8.83 (dd, *J* = 4.2, 1.7 Hz, 1H), 8.60-8.58 (m, 1H), 8.35-8.33 (m, 1H), 7.48 (dd, *J* = 8.4, 4.2 Hz, 1H), 7.44-7.39 (m, 2H), 7.27 (t, *J* = 2.4 Hz, 1H), 7.25-7.24 (m, 1H), 7.14 (d, *J* = 8.4 Hz, 1H), 2.86 (s, 6H). **¹³C NMR** (101 MHz; CDCl₃): δ 151.9, 151.0, 148.2, 145.5, 139.5, 133.2, 129.8, 129.5, 125.7, 124.0, 121.9, 120.9, 115.17, 115.14, 45.6. HRMS (ESI⁺) *m/z* calc'd for C₁₈H₁₈N₃O₂ [M+H⁺]: 308.1399; found: 308.1400.

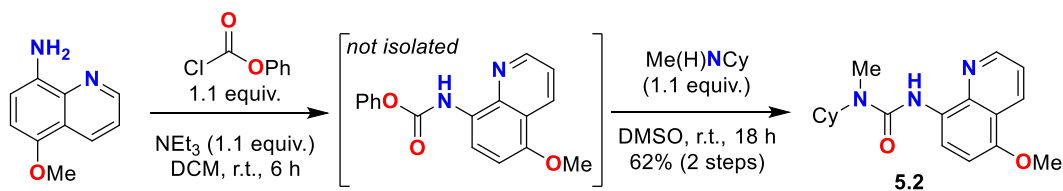
1-Cyclohexyl-3-(5-(dimethylamino)quinolin-8-yl)-1-methylurea (5.1)



The urea was synthesized following a procedure adapted from literature. To a stirred solution of phenyl (5-(dimethylamino)quinolin-8-yl)carbamate in DMSO was added a solution of *N*-methylcyclohexanamine also in DMSO. The resulting solution was allowed to stir at room temperature for 18 h. Upon completion, the reaction solution was diluted with ethyl acetate and washed with successive aliquots of distilled water (x5). The organic layer was washed with brine, dried over anhydrous sodium sulfate, filtered and concentrated under reduced pressure. The compound was purified by column chromatography (7:3 - Hex:EtOAc) to afford a yellow oil in 69% (This oil slowly solidifies over a few months). **¹H NMR** (400 MHz; CDCl₃): 9.21 (s, br, 1H), 8.75 (dd, *J* = 4.2, 1.7 Hz, 1H), 8.56 (d, *J* = 8.1 Hz, 1H), 8.46 (d, *J* = 8.4 Hz, 1H), 7.42 (dd, *J* = 8.5, 4.2 Hz, 1H), 7.13 (d, *J* = 8.4 Hz, 1H), 4.28-4.20 (m, 1H), 3.03 (s, 3H), 2.83 (s, 6H), 1.85-1.80 (m, 4H), 1.71-1.68 (m, 1H), 1.52-1.40 (m, 4H), 1.17-1.08 (m, 1H). **¹³C NMR** (101 MHz; CDCl₃): δ 155.4, 147.6,

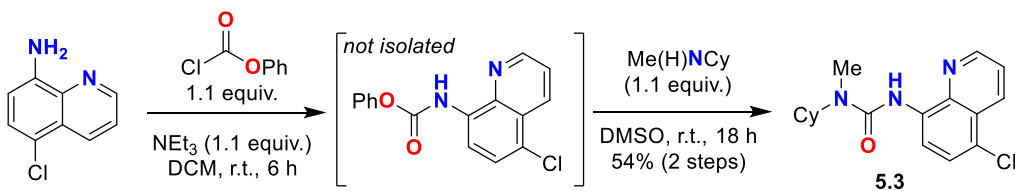
143.8, 139.7, 133.0, 132.0, 124.0, 120.5, 115.7, 114.8, 54.0, 45.7, 30.8, 28.6, 26.0, 25.8. HRMS (ESI+) m/z calc'd for $C_{19}H_{27}N_4O$ $[M+H]^+$: 327.2185; found: 327.2184.

1-cyclohexyl-3-(5-methoxyquinolin-8-yl)-1-methylurea (**5.2**)



Synthesis: Synthesized according to a modified literature procedure:^[204,264] the carbamate was prepared from 5-methoxyquinolin-8-amine^[286] (157 mg, 0.9 mmol), phenyl chloroformate (156 mg, 1 mmol), and triethylamine (101 mg, 1 mmol) in DCM (~ 5 mL). Following the reaction, the DCM was removed on a rotary evaporator, and the residue was used directly in the next reaction. DMSO (1-2 mL) was added to the residue, along with *N*-methylcyclohexylamine (115 mg, 1 mmol). After 18 hours, the reaction was diluted with water (20 mL) and extracted with EtOAc (3 x 15 mL). Removal of the EtOAc on a rotary evaporator followed by crystallization from cold EtOAc afforded urea **5.2** as a yellow solid. **Yield** = 62% (176 mg, 0.56 mmol). **¹H NMR (400 MHz, CDCl₃)** δ = 0.06 (br s, 1H), 8.79 (dd, J = 4.3, 1.7 Hz, 1H), 8.57 (dd, J = 8.3, 1.1 Hz, 1H), 8.47 (d, J = 8.5 Hz, 1H), 7.42 (dd, J = 8.4, 4.3 Hz, 1H), 6.85 (d, J = 8.5 Hz, 1H), 4.31-4.18 (m, 1H), 3.98 (s, 3H), 3.03 (s, 3H), 1.90-1.74 (m, 4H), 1.74-1.64 (m, 1H), 1.53-1.37 (m, 4H), 1.21-1.06 (m, 1H). **¹³C NMR (101 MHz, CDCl₃)** δ = 155.4, 148.8, 148.2, 139.2, 131.2, 129.7, 120.5, 120.4, 114.7, 104.9, 55.8, 53.8, 30.7, 28.4, 25.9, 25.7. **HRMS** (ESI) m/z calculated for $C_{18}H_{24}N_3O_2$ $[M+H]^+$: 314.1869; found: 314.1870.

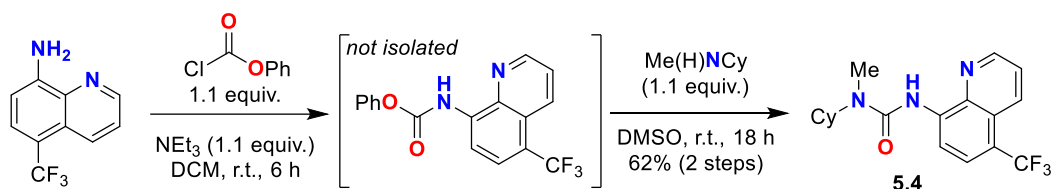
1-cyclohexyl-3-(5-chloroquinolin-8-yl)-1-methylurea (**5.3**)



Synthesis: Synthesized according to a modified literature procedure:^[204,264] the carbamate was prepared from 5-chloroquinolin-8-amine^[286] (500 mg, 2.8 mmol), phenyl chloroformate (490 mg, 3.1 mmol), and triethylamine (313 mg, 3 mmol) in DCM (~ 20 mL). Following the reaction, the DCM was removed on a rotary evaporator, and the

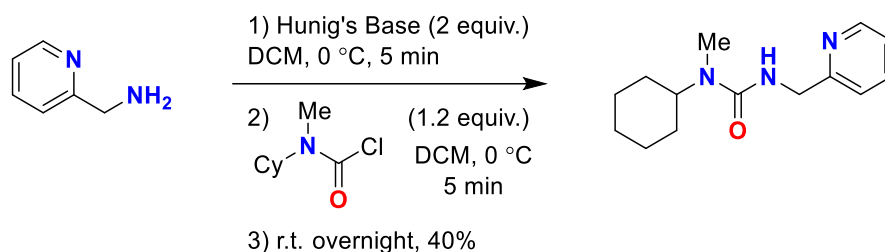
residue was used directly in the next reaction. DMSO (5 mL) was added to the residue, along with *N*-methylcyclohexylamine (350 mg, 3.1 mmol). After 18 hours, the reaction was diluted with water (50 mL) and extracted with EtOAc (3 x 30 mL). Removal of the EtOAc on a rotary evaporator followed by crystallization from cold EtOAc afforded urea **5.3** as an off-white solid. **Yield** = 54% (488 mg, 1.6 mmol). **¹H NMR (400 MHz, CDCl₃)** δ = 9.33 (br s, 1H), 8.82 (dd, *J* = 4.3, 1.6 Hz, 1H), 8.57 (dd, *J* = 8.5, 1.6 Hz, 1H), 8.53 (d, *J* = 8.5 Hz, 1H), 7.59 (d, *J* = 8.5 Hz, 1H), 7.56 (*J* = 8.6, 4.3 Hz, 1H), 4.31-4.12 (m, 1H), 3.05 (s, 3H), 1.94-1.75 (m, 4H), 1.75-1.64 (m, 1H), 1.56-1.36 (m, 4H), 1.20-1.04 (m, 1H). **¹³C NMR (101 MHz, CDCl₃)** δ = 155.1, 148.1, 139.0, 135.6, 133.9, 127.8, 126.1, 122.2, 122.2, 115.3, 54.2, 30.8, 28.7, 26.0, 25.8. **HRMS** (ESI) *m/z* calculated for C₁₇H₂₁ClN₃O [M+H]⁺: 318.1373; found: 318.1371.

1-cyclohexyl-1-methyl-3-(5-(trifluoromethyl)quinolin-8-yl)urea (**5.4**)



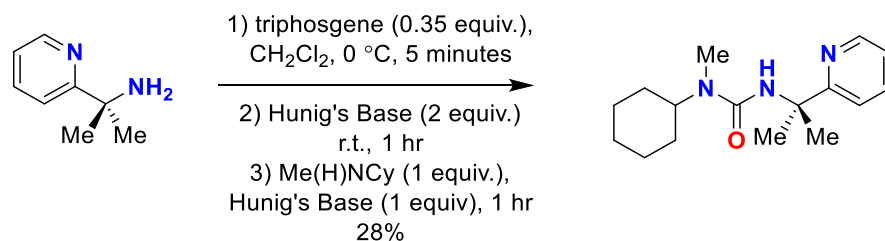
Synthesis: Synthesized according to a modified literature procedure:^[204,264] the carbamate was prepared from 5-methoxyquinolin-8-amine^[286] (127 mg, 0.60 mmol), phenyl chloroformate (108 mg, 0.7 mmol), and triethylamine (71 mg, 0.7 mmol) in DCM (~ 5 mL). Following the reaction, the DCM was removed on a rotary evaporator, and the residue was used directly in the next reaction. DMSO (1-2 mL) was added to the residue, along with *N*-methylcyclohexylamine (81 mg, 0.7 mmol). After 18 hours, the reaction was diluted with water (20 mL) and extracted with EtOAc (3 x 15 mL). Removal of the EtOAc on a rotary evaporator followed by crystallization from cold EtOAc afforded urea **5.4** as a white solid. **Yield** = 42% (88 mg, 0.25 mmol). **¹H NMR (400 MHz, CDCl₃)** δ = 9.61 (br s, 1H), 8.85 (dd, *J* = 4.2, 1.4 Hz, 1H), 8.61 (d, *J* = 8.3 Hz, 1H), 8.53-8.48 (dm, *J* = 8.7, 1.6 Hz, 1H), 7.89 (d, *J* = 8.4 Hz, 1H), 7.57 (dd, *J* = 8.7, 4.2 Hz, 1H), 4.32-4.11 (m, 1H), 3.06 (s, 3H), 1.94-1.76 (m, 4H), 1.76-1.65 (m, 1H), 1.57-1.37 (m, 4H), 1.22-1.05 (m, 1H). **¹³C NMR (101 MHz, CDCl₃)** δ = 154.7, 148.1, 139.9, 138.3, 133.2 (q, *J* = 2.2 Hz), 126.9 (q, *J* = 5.9 Hz), 124.6 (q, *J* = 272.5 Hz), 124.3, 122.5, 117.3 (q, *J* = 30.7 Hz), 112.2, 54.2, 30.6, 28.6, 25.8, 25.6. **¹⁹F{¹H} (282 MHz, CDCl₃)** δ = 58.7. **HRMS** (ESI) *m/z* calculated for C₁₈H₂₁F₃N₃O [M+H]⁺: 352.1637; found: 352.1639.

1-cyclohexyl-1-methyl-3-(pyridin-2-ylmethyl)urea (5.5)



Synthesis: Pyridin-2-ylmethanamine (165 mg, 1.53 mmol) was weighed into a round bottom flask. Hunig's base (400 mg, 3.06 mmol) was added to the same round bottom flask. A stir bar was added, and the contents were dissolved in dichloromethane (15 mL). The flask was then cooled with an ice bath while stirring. Cyclohexyl(methyl)carbamic chloride (300 mg, 1.71 mmol) was weighed into a vial and dissolved in dichloromethane (5 mL). The carbamic chloride was then added dropwise to the cooled solution of amines. The solution was then warmed to room temperature and stirred overnight. **Purification:** The contents were then added to a separatory funnel, to which aqueous HCl (1M, 50 mL) was also added. The aqueous layer was washed with DCM (2 x 15 mL) in the separatory funnel, then neutralized to pH 8 with NaHCO₃ in an Erlenmeyer flask. The organics were then extracted from the aqueous layer with DCM (2 x 30 mL), dried over magnesium sulfate, and dried on a rotary evaporator. The residue was taken up in DCM (~ 0.5 mL), and diluted with hexanes (~ 4 mL). Crystals of **5.5** formed overnight in a freezer. **Yield** = 40% (151 mg, 0.61 mmol). **¹H NMR (400 MHz, CDCl₃)** δ = 8.51 (d, J = 4.8, 1H), 7.64 (app. td, J = 7.7, 1.7 Hz, 1H), 7.30 (d, J = 7.8 Hz, 1H), 7.17 (ddd, 7.2, 5.2, 1H), 5.67 (bs, 1H), 4.54 (d, J = 4.9 Hz, 2H), 4.05 (m, 1H), 2.79 (s, 3H), 1.86-1.55 (m, 5H), 1.44-1.28 (m, 4H), 1.17-0.99 (m, 1H). **¹³C NMR (101 MHz, CDCl₃)** δ = 158.1, 158.1, 148.9, 136.8, 122.4, 122.2, 53.9, 46.0, 30.7, 28.2, 25.9, 25.8. **HRMS (ESI)** m/z calculated for C₁₄H₂₁N₃ONa [M+Na]⁺: 270.1582; found: 270.1581.

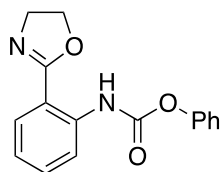
1-cyclohexyl-1-methyl-3-(2-(pyridin-2-yl)propan-2-yl)urea (5.6)



Synthesis: Synthesized according to an adapted literature procedure^[287] with 2-pyridin-2-yl)isopropyl amine (200 mg, 1.47 mmol) and *N*-methylcyclohexylamine 166 mg, 1.47 mmol). **Purification:** Workup as in literature procedure; purified by a silica plug (1:1 EtOAc/hexanes) to afford **5.6** as a clear oil. **Yield** = 28% (115 mg, 0.42 mmol).

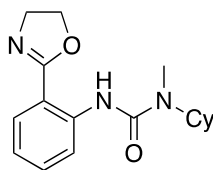
¹H NMR (400 MHz, CDCl₃) δ = 8.49 (ddd, J = 4.9, 1.7, 0.9 Hz, 1H), 7.68 (app. td, J = 7.8, 1.8 Hz, 1H), 7.42 (d, J = 8.1 Hz, 1H), 7.15 (ddd, 7.4, 4.9, 0.9 Hz, 1H), 6.72 (bs, 1H), 4.03 (m, 1H), 2.81 (s, 3H), 1.90-1.76 (m, 2H), 1.75 (s, 6H), 1.72-1.59 (m, 3H), 1.44-1.28 (m, 4H), 1.17-0.99 (m, 1H). **¹³C NMR (101 MHz, CDCl₃)** δ = 166.1, 157.3, 147.7, 137.0, 121.6, 119.7, 56.4, 53.4, 30.8, 28.6, 28.3, 26.0, 25.8. **HRMS (ESI)** m/z calculated for C₁₆H₂₆N₃O [M+H]⁺: 276.2076; found: 276.2073.

Phenyl (2-(4,5-dihydrooxazol-2-yl)phenyl)carbamate



The carbamate was synthesized following a procedure adapted from literature. To a stirred solution of 2-(4,5-dihydrooxazol-2-yl)aniline (0.6664 g, 4.1 mmol, 1 equiv.) and triethylamine (1.2 mL, 8.2 mmol, 2 equiv.) in THF (30 mL) at 0 °C phenylchloroformate (0.54 mL, 4.3 mmol, 1.05 equiv.) was added drop-wise over 5 minutes, under inert atmosphere. The resulting solution was allowed to stir at room temperature for 18 h to generate a heterogeneous mixture. Upon completion, the solvent was removed under reduced pressure and the solid obtained was diluted with ethyl acetate and sat. aq. NaHCO₃. The organic layer was separated, and the aqueous layer was extracted with ethyl acetate (x3). The combined organic layers were washed with brine, dried over anhydrous sodium sulfate, filtered and concentrated. Phenyl (2-(4,5-dihydrooxazol-2-yl)phenyl)carbamate was used for the following step without further purification.

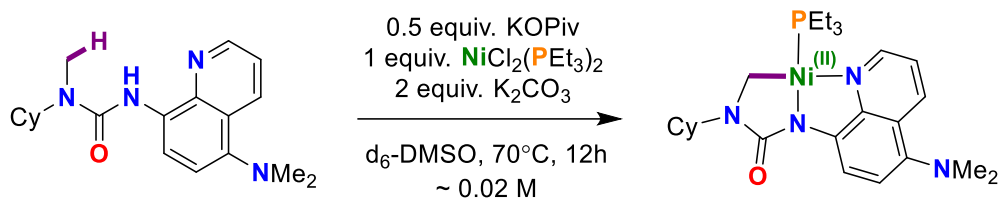
1-Cyclohexyl-3-(2-(4,5-dihydrooxazol-2-yl)phenyl)-1-methylurea (5.7)



The urea was synthesized following a procedure adapted from literature. To a stirred solution of phenyl (2-(4,5-dihydrooxazol-2-yl)phenyl)carbamate (1.0485, 3.7 mmol, 1 equiv.) in DMSO (5 mL) was added a solution of *N*-methylcyclohexylamine (0.48 mL, 3.7 mmol, 1 equiv.) also in DMSO (5 mL). The resulting solution was allowed to stir at room temperature for 18 h. Upon completion, the reaction solution was diluted with ethyl acetate and washed with successive aliquots of distilled water (x5). The organic layer was washed with brine, dried over anhydrous sodium sulfate, filtered and concentrated under reduced

pressure. The compound was purified by column chromatography (gradient 1:1 - Hex:EtOAc to 100% EtOAc to 95:5 – EtOAc:Et₃N) to afford **5.7** white solid in 6%. **¹H NMR** (400 MHz; CDCl₃): 10.26 (s, br, 1H), 8.12 (dd, *J* = 8.0, 1.3 Hz, 1H), 7.59 (ddd, *J* = 8.1, 7.2, 1.3 Hz, 1H), 7.22 (ddd, *J* = 8.0, 7.2, 0.8 Hz, 1H), 7.10 (d, *J* = 8.1 Hz, 1H), 4.21-4.17 (m, 2H), 2.78-2.75 (m, 2H), 2.44 (s, 3H), 2.42-2.39 (m, 1H), 1.81-1.74 (m, 4H), 1.61-1.58 (m, 1H), 1.25-1.15 (m, 4H), 1.10-1.03 (m, 1H). **¹³C NMR** (101 MHz; CDCl₃): δ 162.5, 152.4, 138.8, 135.0, 128.5, 123.4, 115.1, 114.8, 63.1, 50.5, 39.5, 38.7, 29.0, 26.4, 26.1. HRMS (ESI+) *m/z* calc'd for C₁₇H₂₄N₃O₂ [M+H⁺]: 302.1869; found: 302.1868.

Spectroscopic Data for Cyclometalated Ureas



Characteristic signals of (5.1-Ni):

¹H NMR (400 MHz, d₆-DMSO) δ 8.60 (d, *J* = 8.3 Hz, 1H), 8.48-8.39 (m, 2H), 7.50 (dd, *J* = 7.2, 4.6 Hz 1H), 7.1 (d, *J* = 8.3 Hz, 1H), 3.51 (m, 1H), 2.70 (s, N-(CH₃)₂, 6H), 2.32 (s, Ni-CH₂, 2H). **¹³C-¹H (HSQC, HMBC) NMR (400 MHz, d₆-DMSO)** δ ~ 163.5 (N(C=O)N), ~ 52.9 (N-CH(Cy)), ~ 45.3 (N-(CH₃)₂), ~ 24.4 (Ni-CH₂). **³¹P NMR (162 MHz, d₆-DMSO)** δ 18.1 (s, Ni-PEt₃).

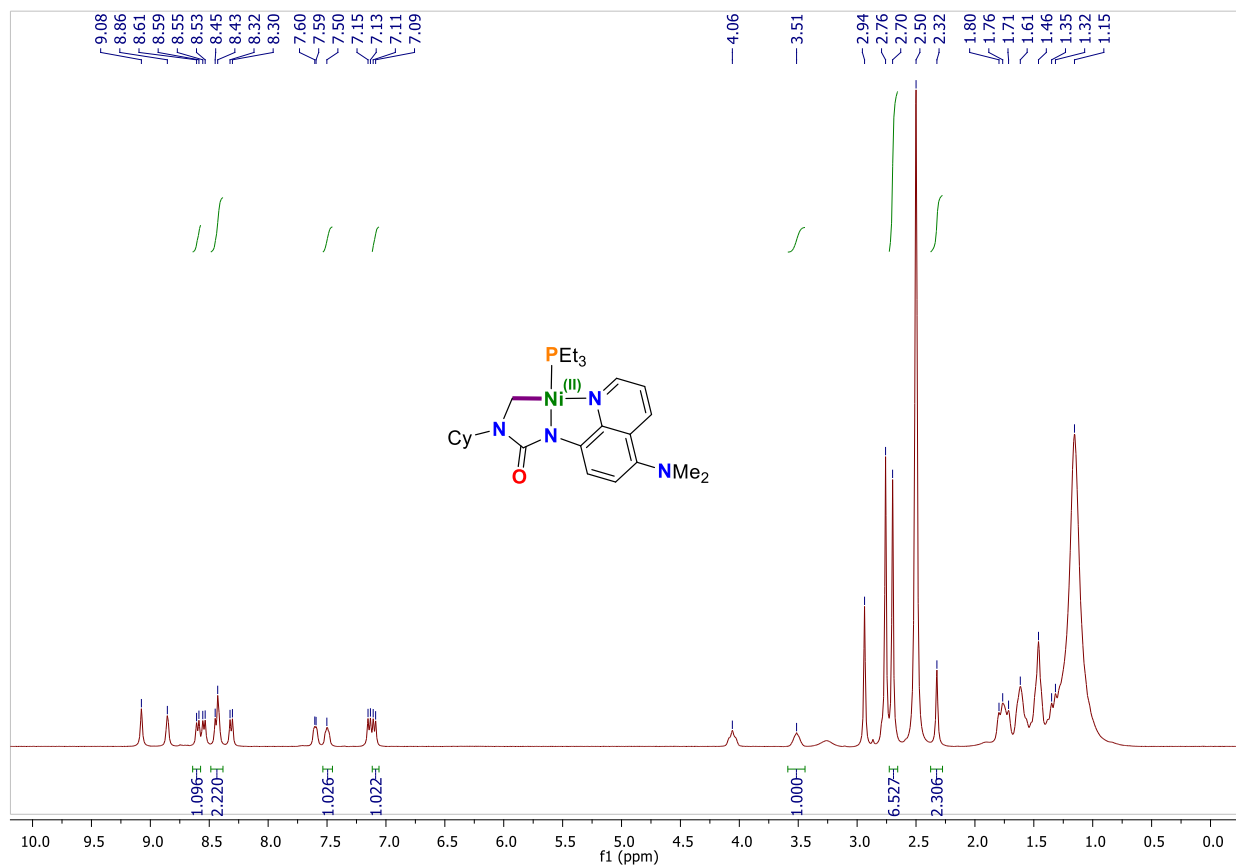


Figure A.5.115. In situ ¹H NMR spectrum of (5.1) and (5.1-Ni) (400 MHz, d₆-DMSO, 298K).

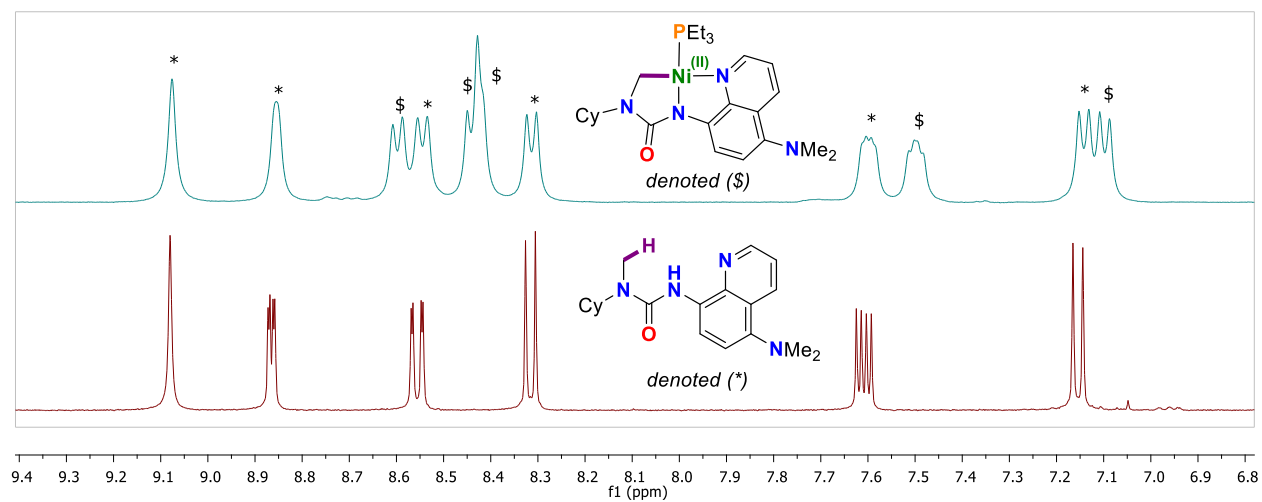


Figure A.5.116. Stacked ^1H NMR spectrum of (a) in situ reaction mixture containing (5.1, denoted *) and (5.1-Ni, denoted \$), and (b) isolated compound (5.1); (400 MHz, $\text{d}_6\text{-DMSO}$, 298K).

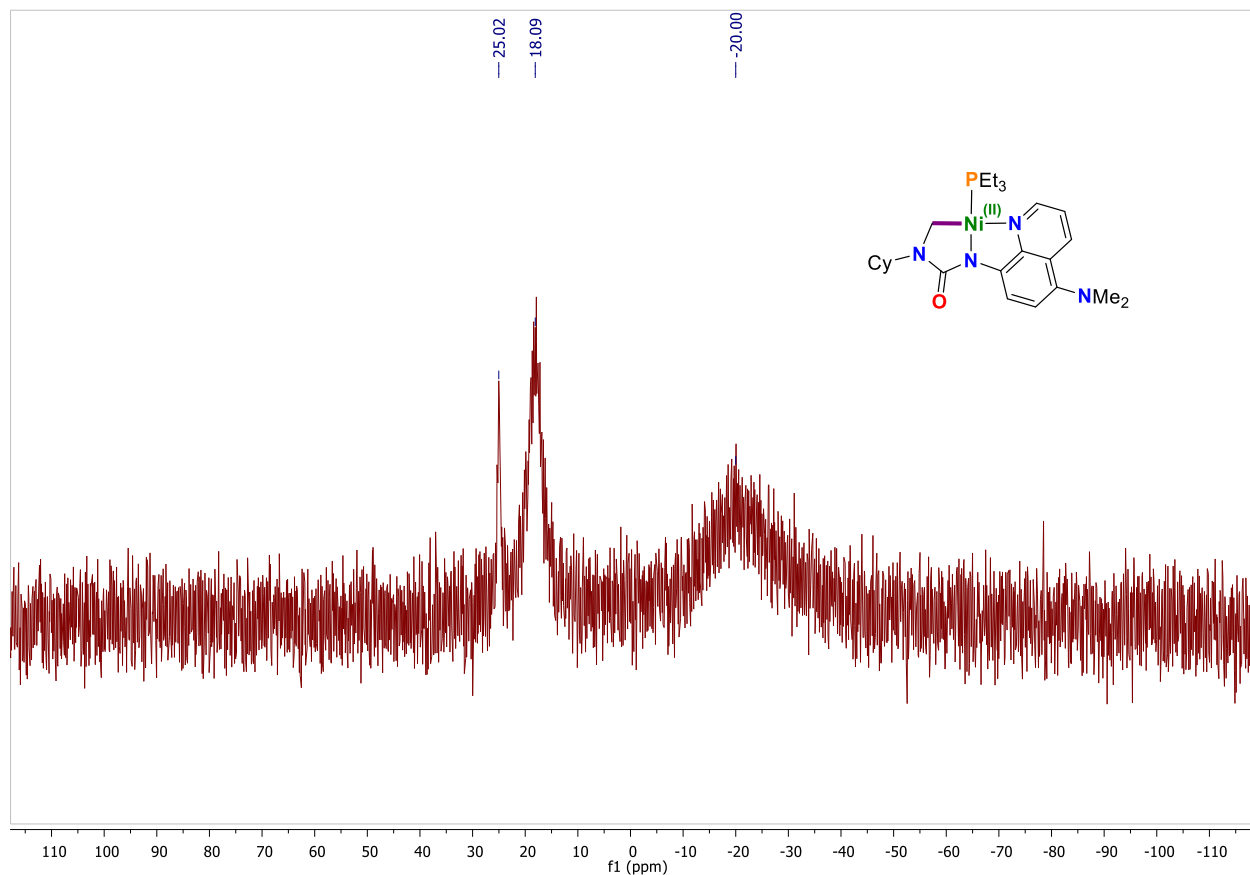


Figure A.5.117. In situ $^{31}\text{P}\{^1\text{H}\}$ NMR spectrum of (5.1) and (5.1-Ni) (162 MHz, $\text{d}_6\text{-DMSO}$, 298K)

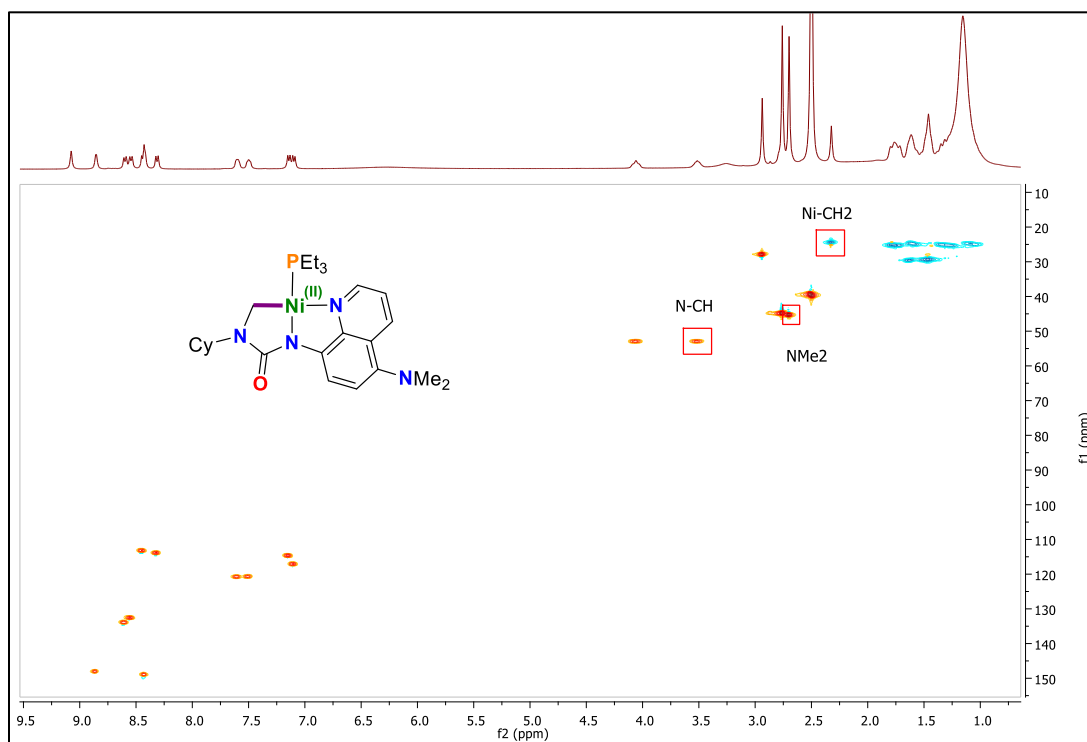


Figure A.5.118. In situ ^{13}C - ^1H (HSQC-edited) NMR spectrum of (5.1) & (5.1-Ni) (400 MHz, d₆-DMSO, 298K).

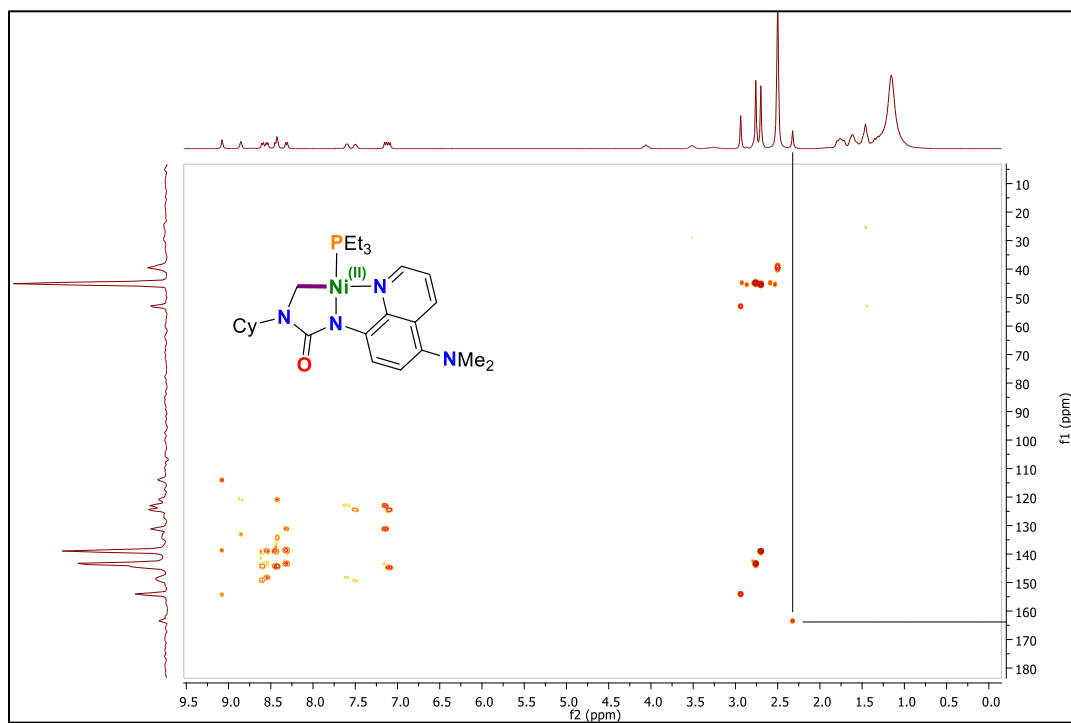
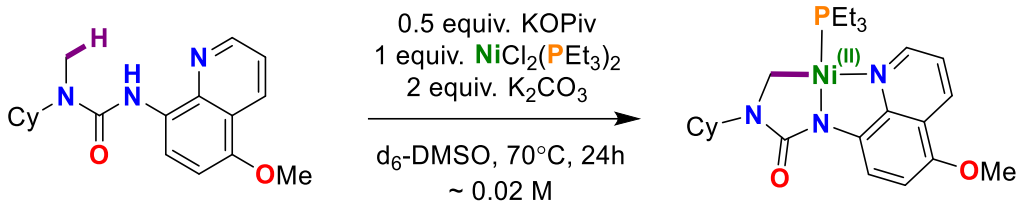


Figure A.5.119. In situ ^{13}C - ^1H (HMBC) NMR spectrum of (5.1) and (5.1-Ni) (400 MHz, d₆-DMSO, 298K)



Characteristic signals of (5.2-Ni):

^1H NMR (400 MHz, $\text{d}_6\text{-DMSO}$) δ 8.57 (d, $J = 8.2$ Hz, 1H), 8.49-8.42 (m, 2H), 7.49 (dd, $J = 7.9, 4.9$ Hz 1H), 6.95 (d, $J = 8.6$ Hz, 1H), 3.88 (s, O-CH₃, 3H), 3.52 (m, 1H), 2.33 (s, Ni-CH₂, 2H). ^{13}C - ^1H (HSQC, HMBC) NMR (400 MHz, $\text{d}_6\text{-DMSO}$) δ ~ 163.9 (N(C=O)N), ~ 56.5 (O-CH₃), ~ 53.6 (N-CH(Cy)), ~ 25.1 (Ni-CH₂). ^{31}P NMR (162 MHz, $\text{d}_6\text{-DMSO}$) δ 18.8 (s, Ni-PEt₃).

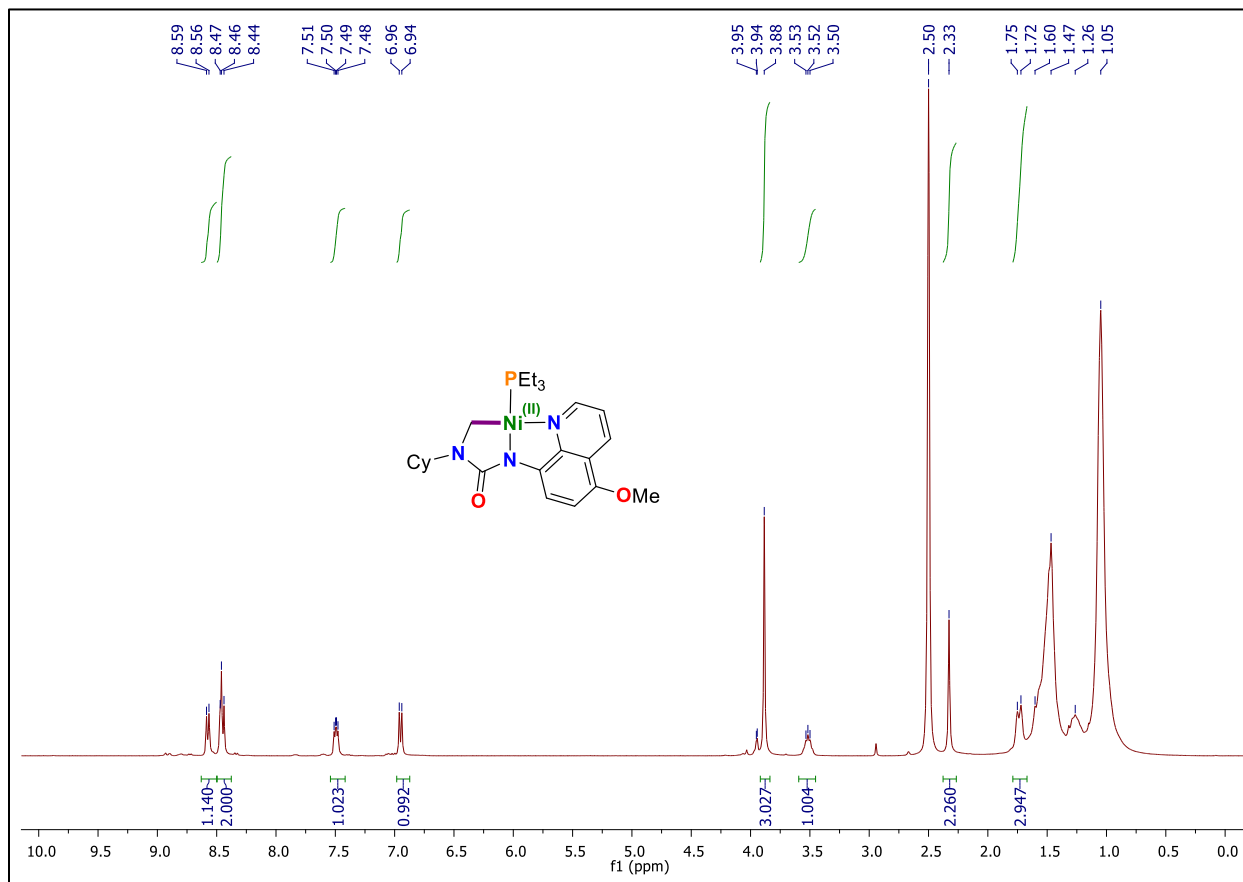


Figure A.5.120. In situ ^1H NMR spectrum of (5.2) and (5.2-Ni) (400 MHz, $\text{d}_6\text{-DMSO}$, 298K).

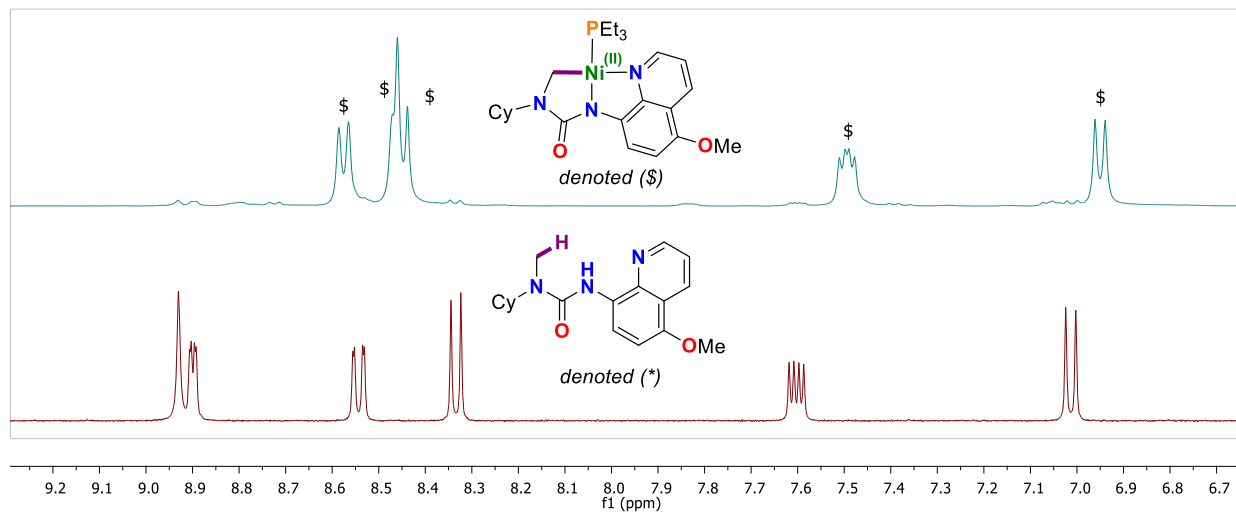


Figure A.5.121. Stacked ^1H NMR spectrum of (a) in situ reaction mixture containing (5.2, denoted *) and (5.2-Ni, denoted \$), and (b) isolated compound (5.2); (400 MHz, d_6 -DMSO, 298K).

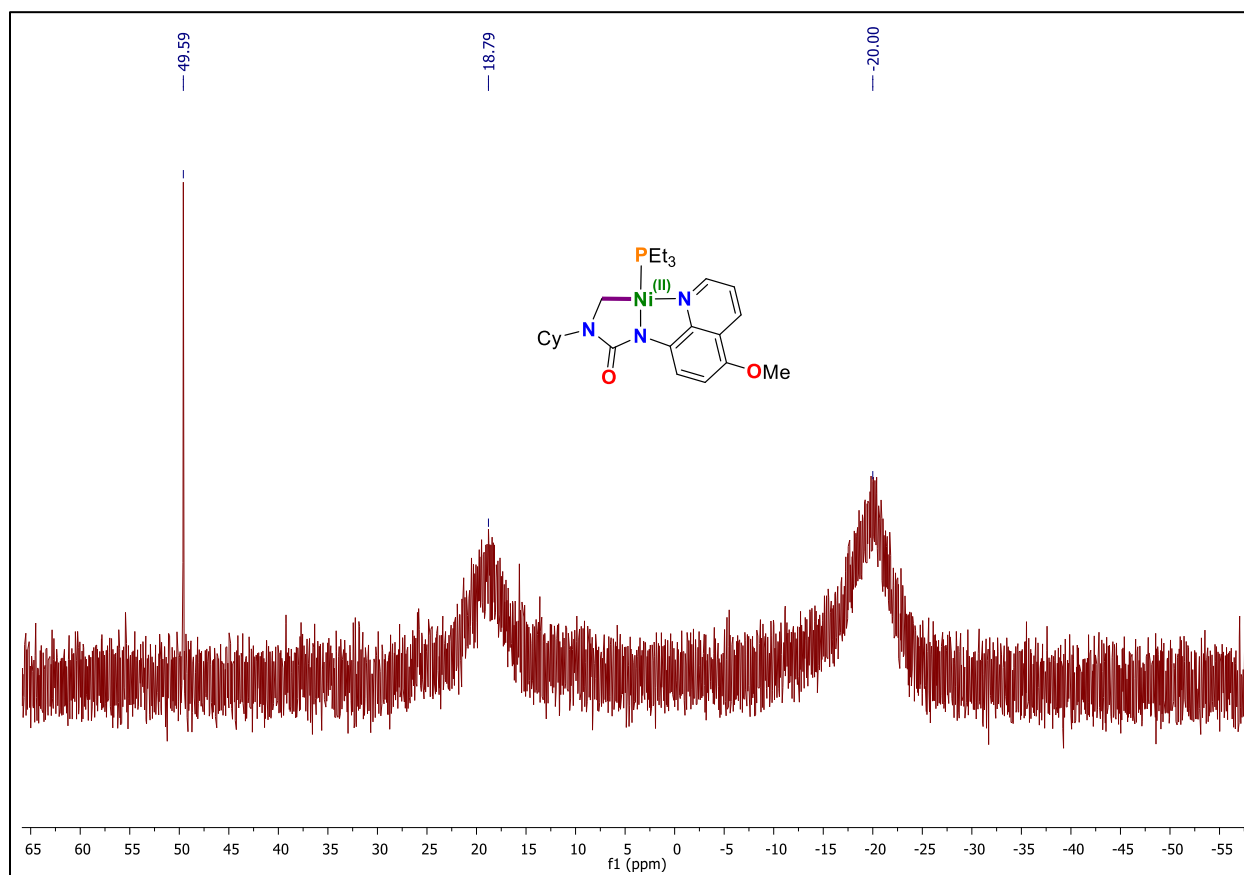


Figure A.5.122. In situ $^{31}\text{P}\{^1\text{H}\}$ NMR spectrum of (5.2) and (5.2-Ni) (162 MHz, d_6 -DMSO, 298K)

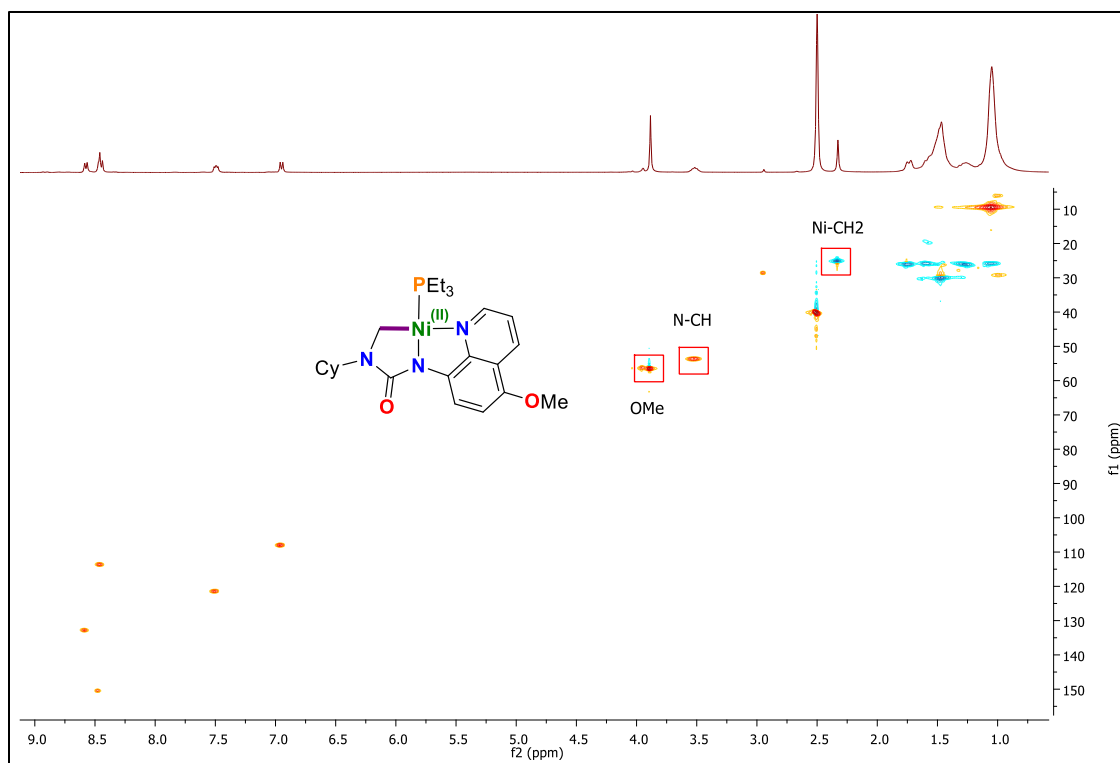


Figure A.5.123. In situ ^{13}C - ^1H (HSQC-edited) NMR spectrum of (5.2) & (5.2-Ni) (400 MHz, d₆-DMSO, 298K).

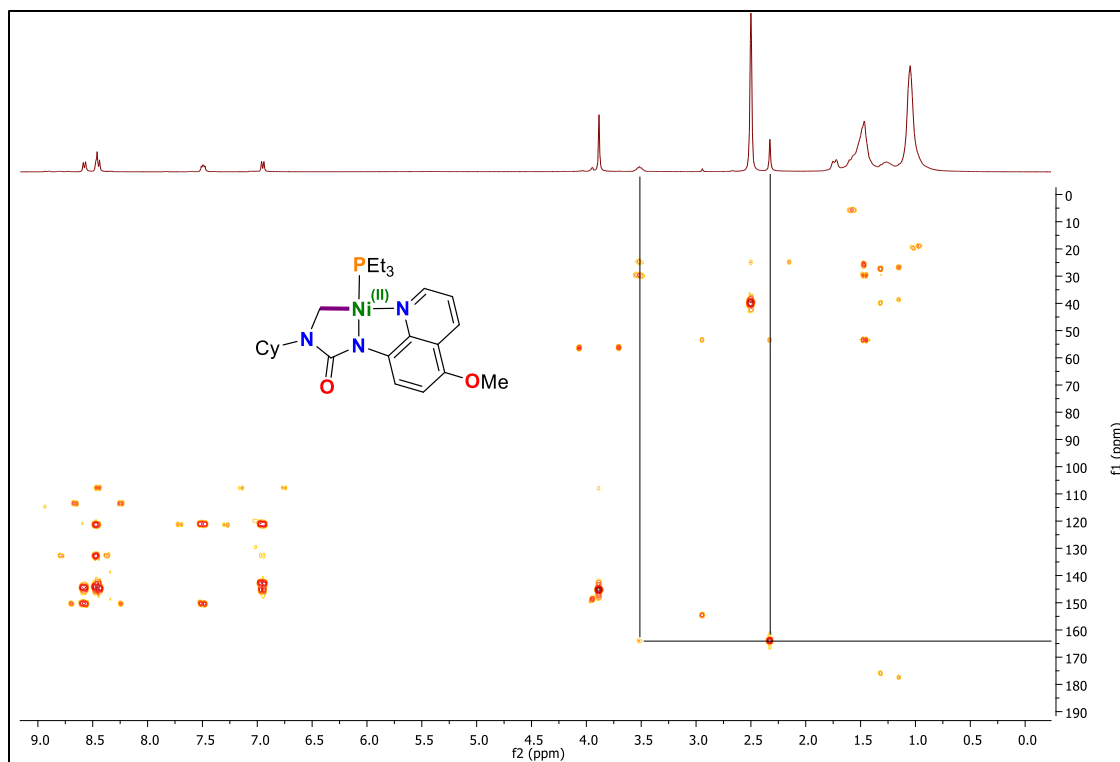
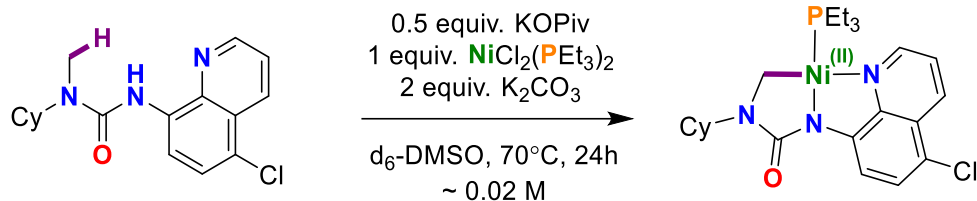


Figure A.5.124. In situ ^{13}C - ^1H (HMBC) NMR spectrum of (5.2) and (5.2-Ni) (400 MHz, d₆-DMSO, 298K)



Characteristic signals of (5.3-Ni):

^1H NMR (400 MHz, $\text{d}_6\text{-DMSO}$) δ 8.57 (d, ****overlapped with SM****, 1H), 8.53-8.47 (m, 2H), 7.65 (dd, $J = 8.4, 4.9$ Hz 1H), 7.53 (d, $J = 8.6$ Hz, 1H), 3.53 (m, 1H), 2.37 (s, Ni- CH_2 , 2H). ^{13}C - ^1H (HSQC, HMBC) NMR (400 MHz, $\text{d}_6\text{-DMSO}$) δ ~ 163.4 (N(C=O)N), ~ 55.2 (N-CH(Cy)), ~ 24.5 (Ni- CH_2).

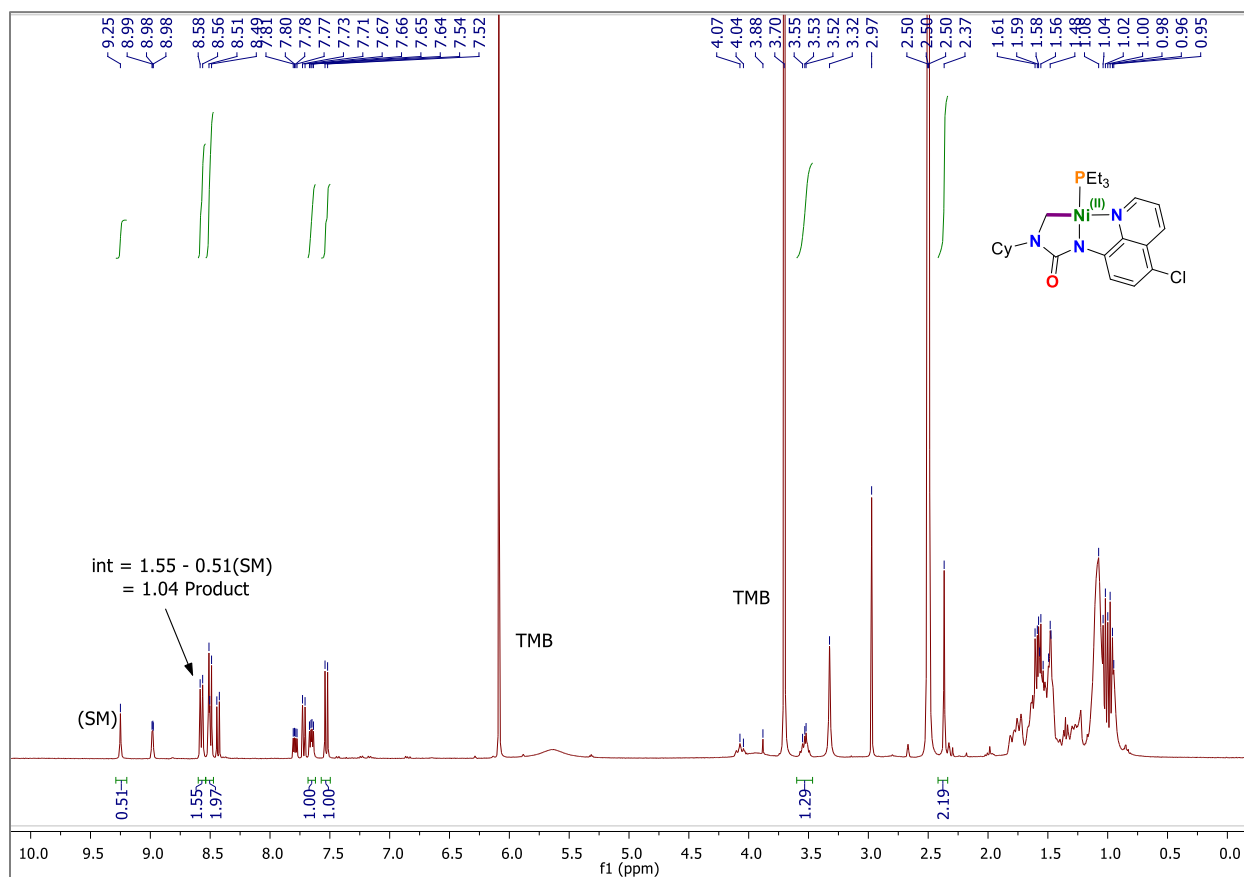


Figure A.5.125. In situ ^1H NMR spectrum of (5.3) and (5.3-Ni) (400 MHz, $\text{d}_6\text{-DMSO}$, 298K).

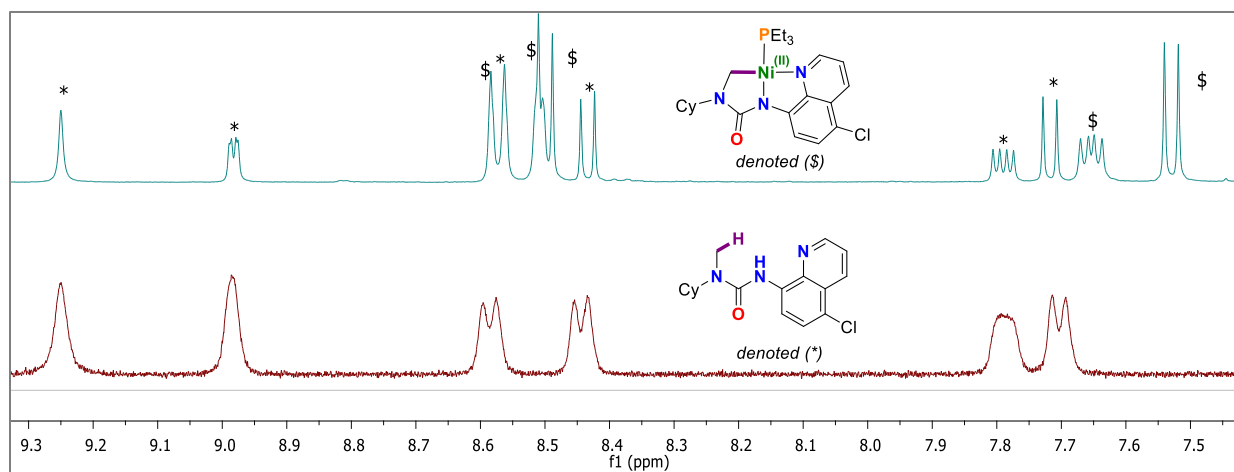


Figure A.5.126. Stacked ^1H NMR spectrum of (a) in situ reaction mixture containing (5.3, denoted *) and (5.3-Ni, denoted \$), and (b) isolated compound (5.3); (400 MHz, $\text{d}_6\text{-DMSO}$, 298K).

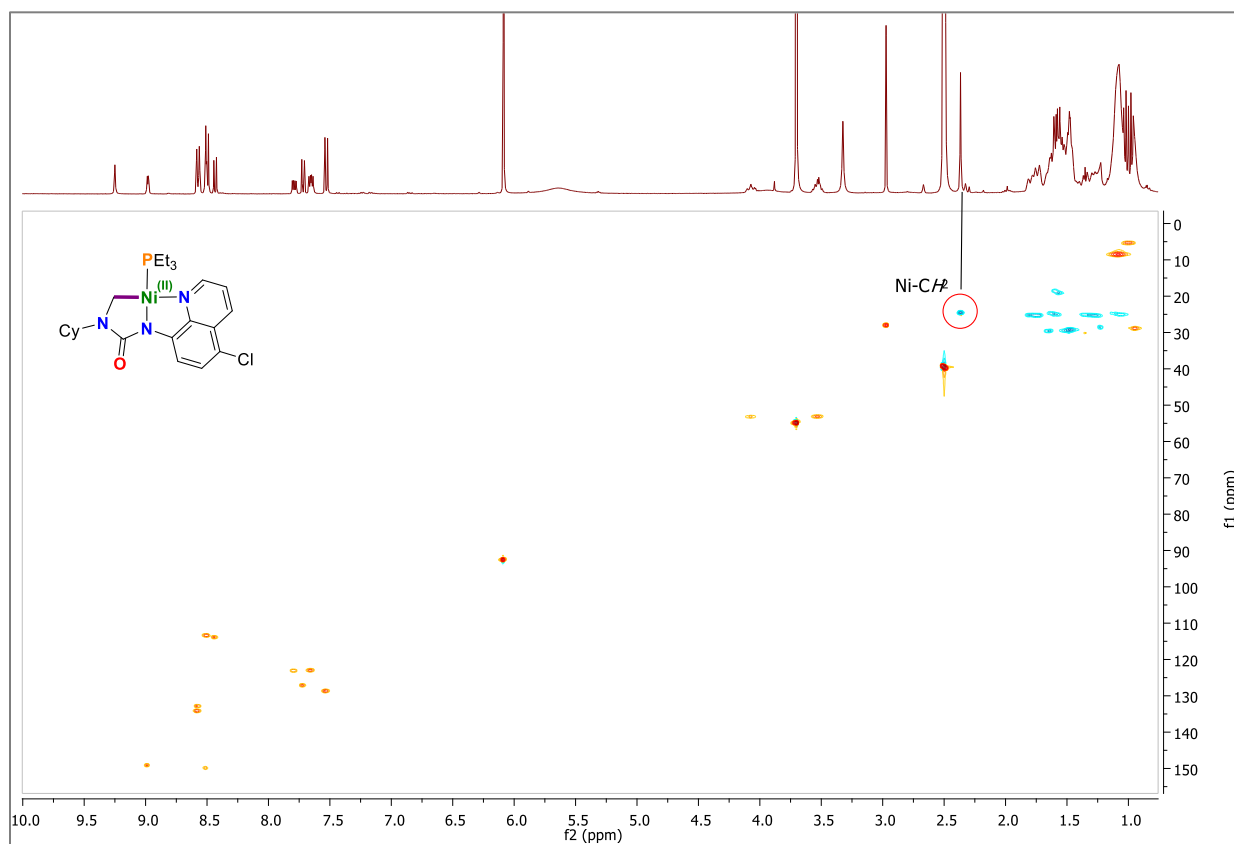


Figure A.5.127. In situ ^{13}C - ^1H (HSQC-edited) NMR spectrum of (5.3) & (5.3-Ni) (400 MHz, $\text{d}_6\text{-DMSO}$, 298K).

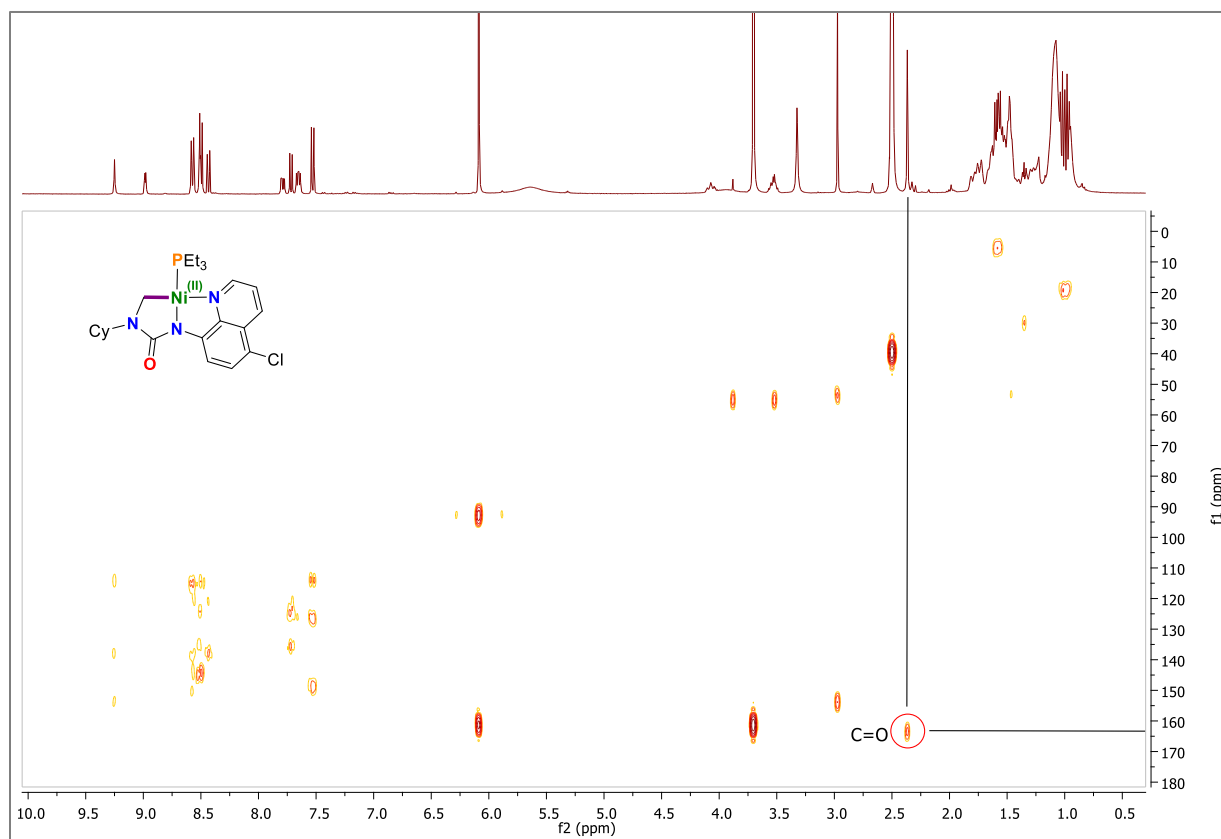
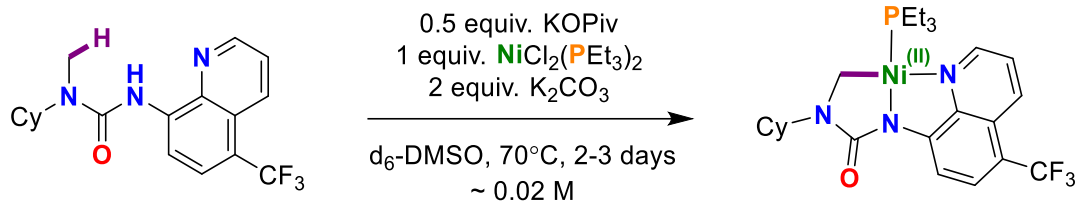


Figure A.5.128. In situ ^{13}C - ^1H (HMBC) NMR spectrum of (5.3) and (5.3-Ni) (400 MHz, d_6 -DMSO, 298K)



Characteristic signals of (5.4-Ni):

^1H NMR (400 MHz, $\text{d}_6\text{-DMSO}$) δ 8.59-8.46 (m, 3H), 7.80 (d, $J = 8.6$ Hz, 1H), 7.70 (dd, $J = 8.6, 5.2$ Hz 1H), 3.55 (m, 1H), 2.40 (s, Ni- CH_2 , 2H). ^{13}C - ^1H (HSQC, HMBC) NMR (400 MHz, $\text{d}_6\text{-DMSO}$) δ ~ 163.4 (N(C=O)N), ~ 53.9 (N-CH(Cy)), ~ 25.5 (Ni- CH_2).

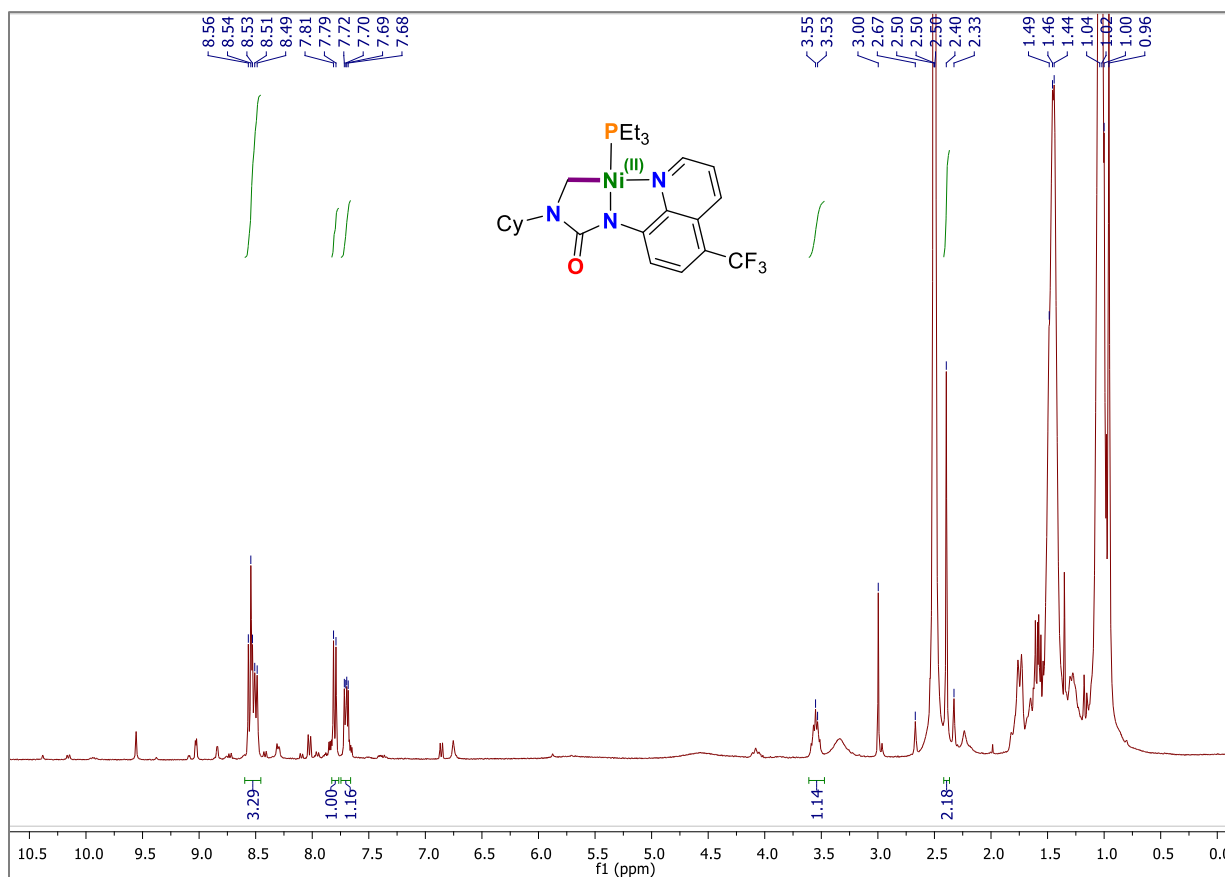


Figure A.5.129. In situ ^1H NMR spectrum of (5.4) and (5.4-Ni) (400 MHz, $\text{d}_6\text{-DMSO}$, 298K).

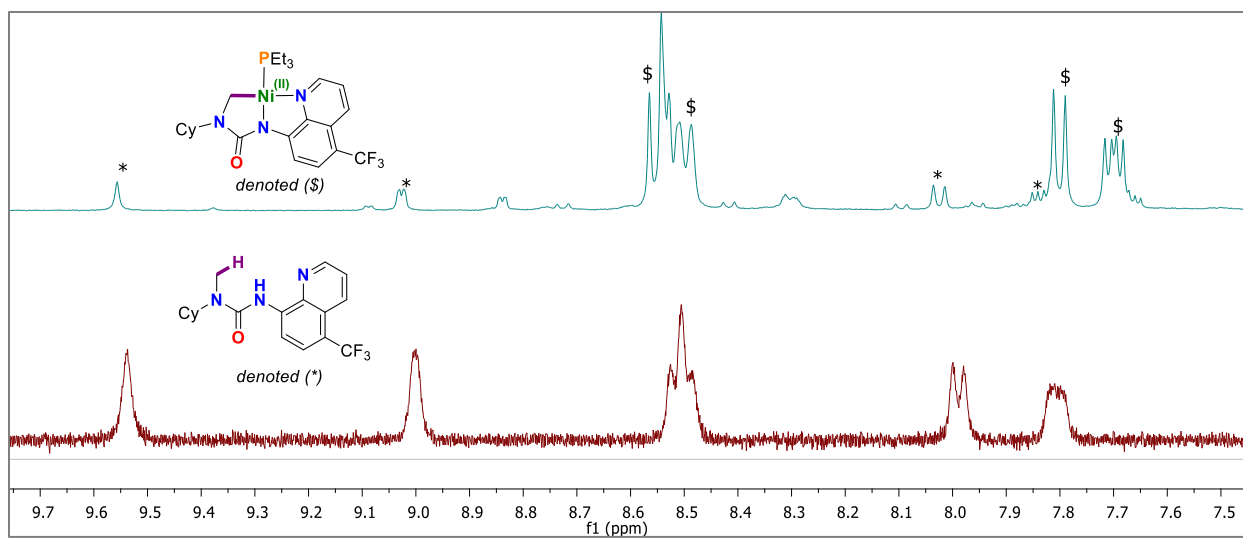


Figure A.5.130. Stacked ^1H NMR spectrum of (a) in situ reaction mixture containing (5.4, denoted *) and (5.4-Ni, denoted \$), and (b) isolated compound (5.4); (400 MHz, $\text{d}_6\text{-DMSO}$, 298K).

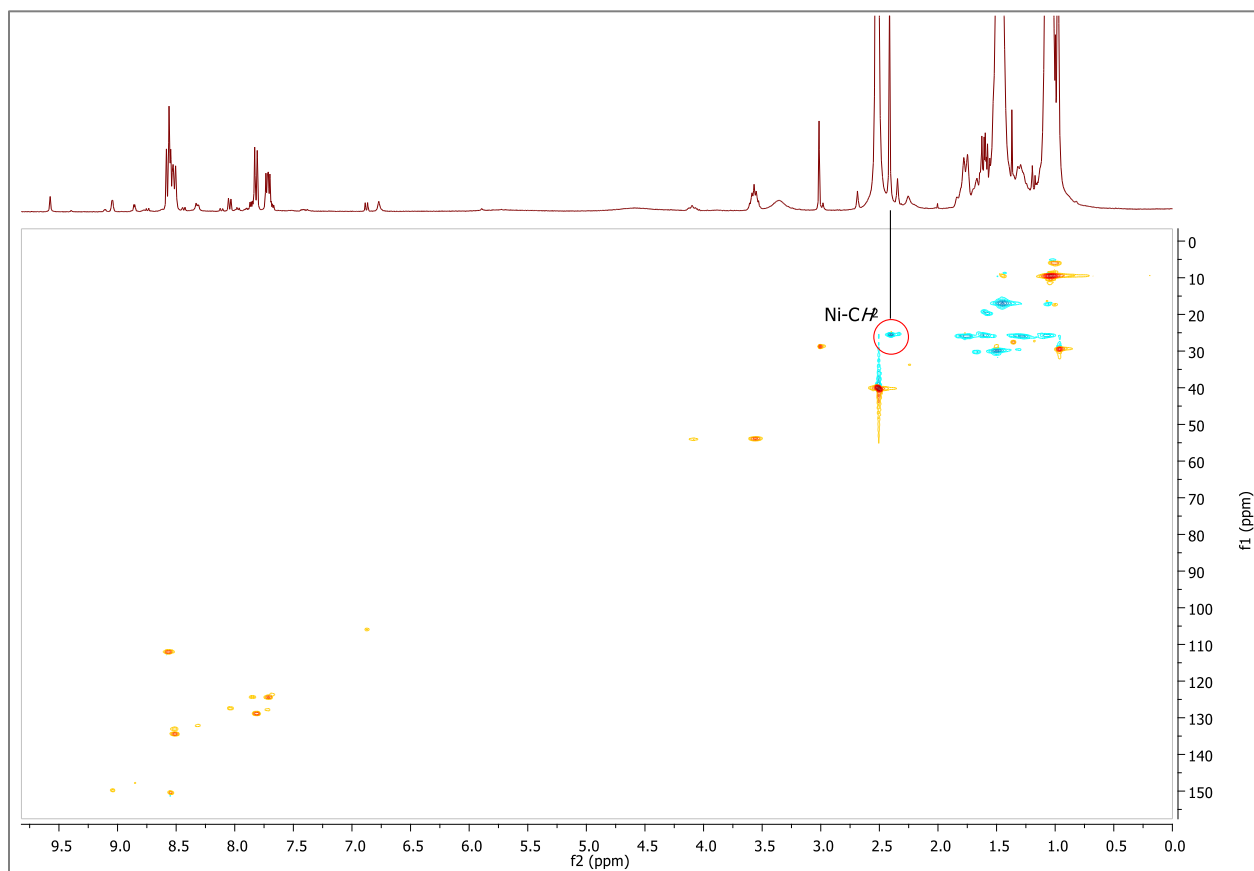


Figure A.5.131. In situ ^{13}C - ^1H (HSQC-edited) NMR spectrum of (5.4) & (5.4-Ni) (400 MHz, $\text{d}_6\text{-DMSO}$, 298K).

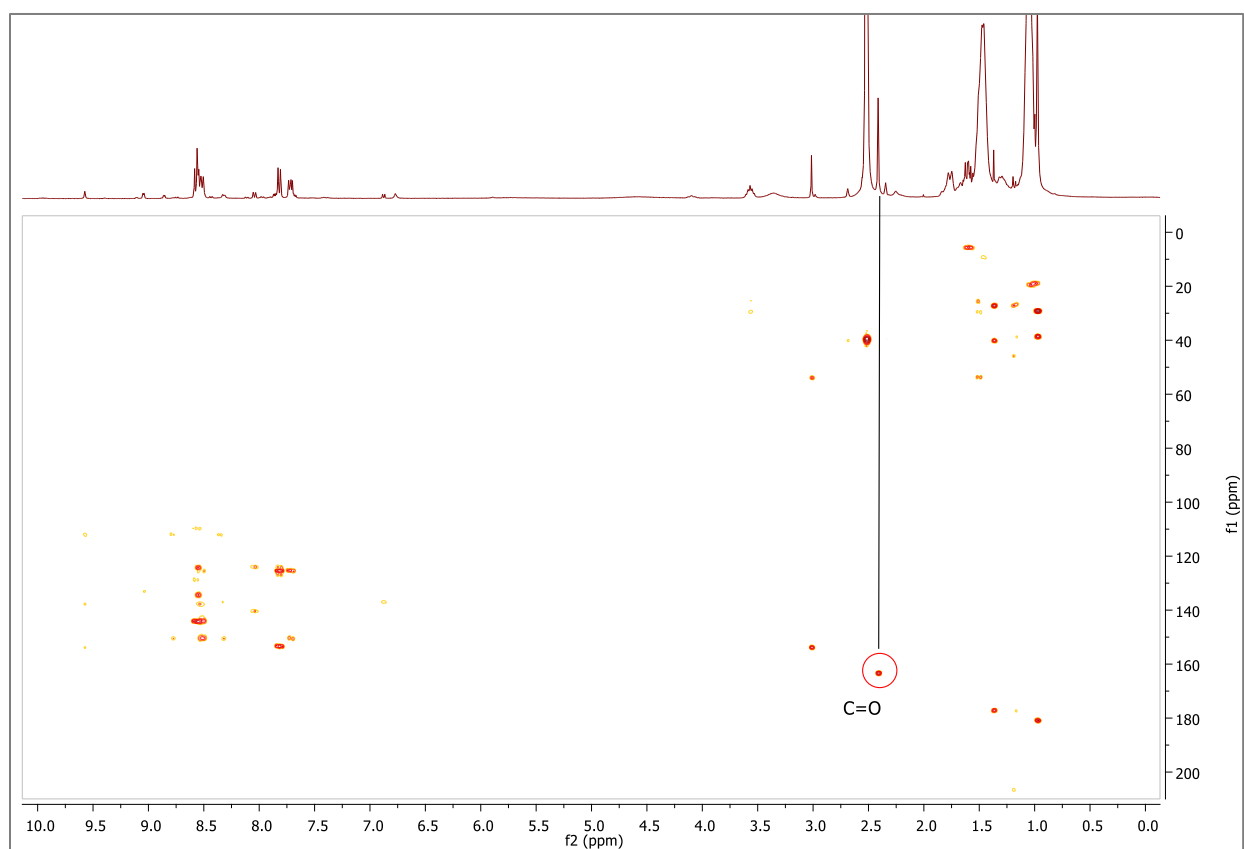
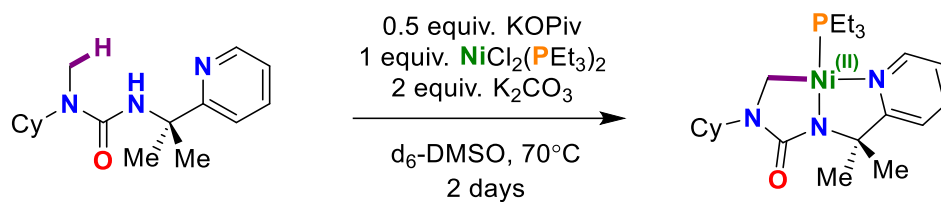


Figure A.5.132. In situ ^{13}C - ^1H (HMBC) NMR spectrum of (5.4) and (5.4-Ni) (400 MHz, d₆-DMSO, 298K)



Characterisitic signals of (5.6):

^1H NMR (400 MHz, $\text{d}_6\text{-DMSO}$) δ 8.08 (d, $J = 5.1$ Hz, 1H), 7.87 (app. t, $J = 7.4$ Hz, 1H), 7.48 (d, $J = 7.9$ Hz, 1H), 7.24 (d, $J = 6.2$ Hz, 1H), 3.42-3.26 (m, 1H), 2.11 (s, 2H), 1.65 (s, 6H). ^{13}C - ^1H (HSQC, HMBC) NMR (400 MHz, $\text{d}_6\text{-DMSO}$) δ ~ 166.0 (N(C=O)N), ~ 29.4 (N-C(CH₃)₂), ~ 25.5 (Ni-CH₂). ^{31}P NMR (162 MHz, $\text{d}_6\text{-DMSO}$) δ 18.5 (s, Ni-PEt₃).

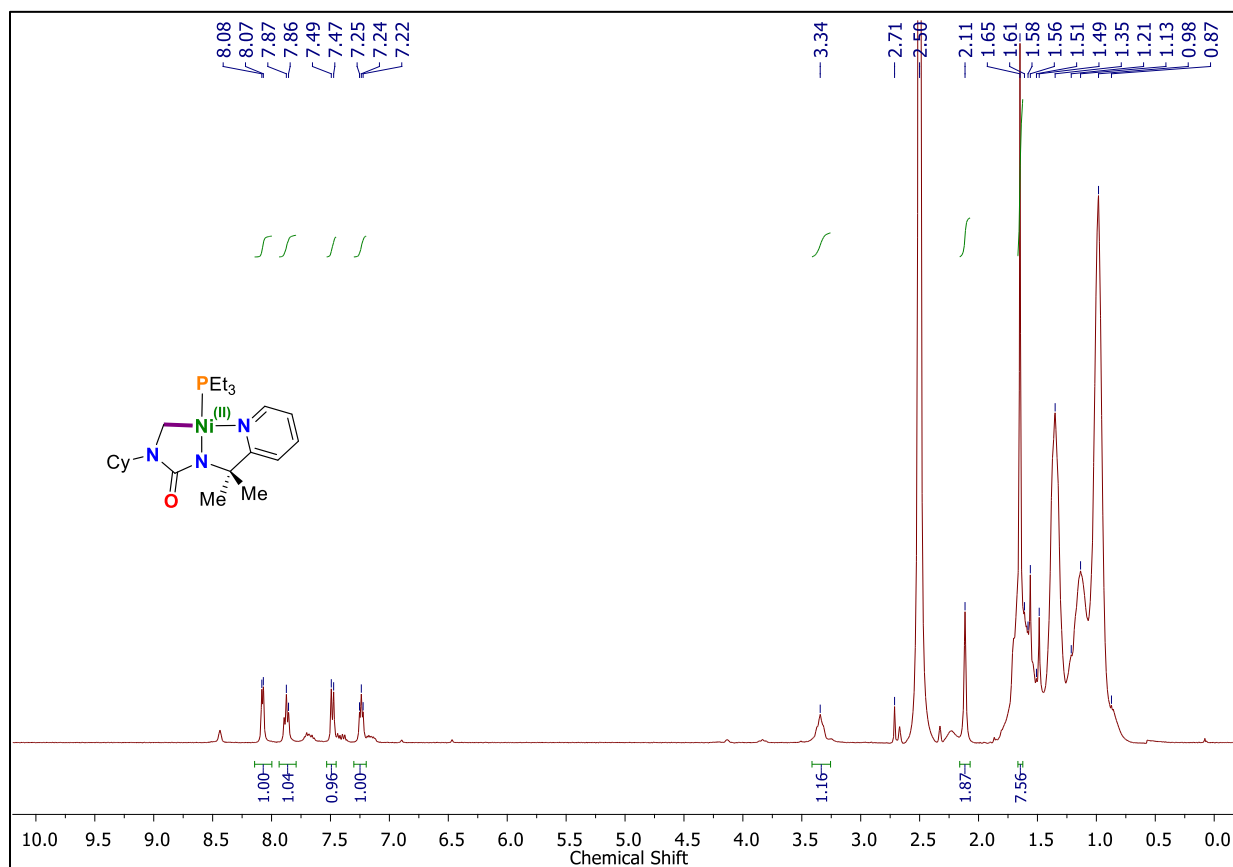


Figure A.5.133. In situ ^1H NMR spectrum of (5.6) and (5.6-Ni) (400 MHz, $\text{d}_6\text{-DMSO}$, 298K).

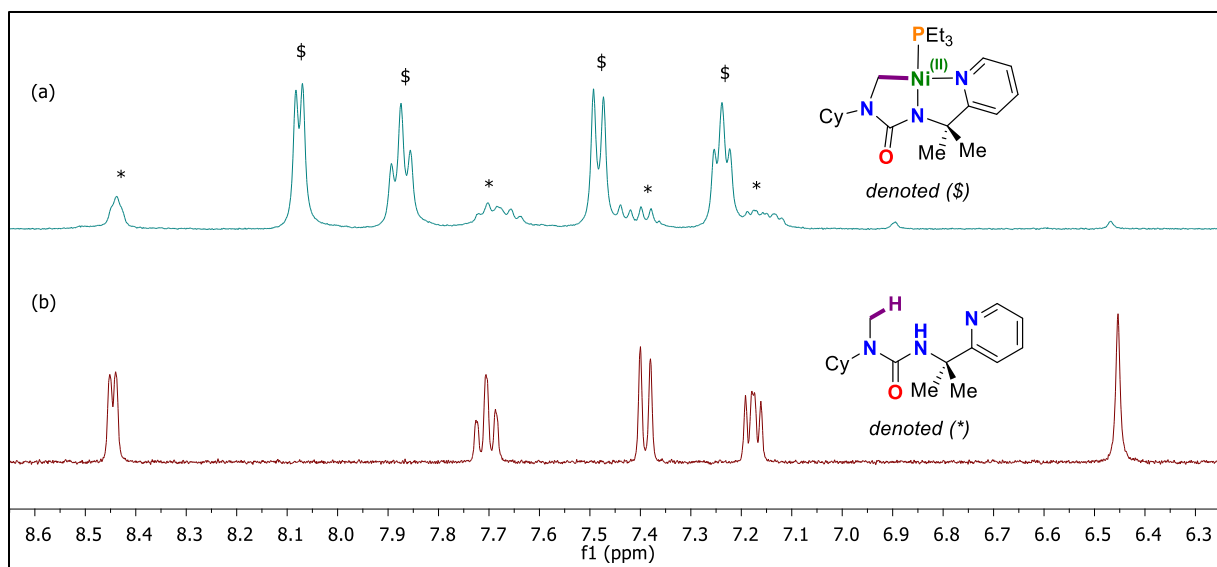


Figure A.5.134. Stacked ^1H NMR spectrum of (a) in situ reaction mixture containing (5.6, denoted *) and (5.6-Ni, denoted \$), and (b) isolated compound (5.6); (400 MHz, $\text{d}_6\text{-DMSO}$, 298K).

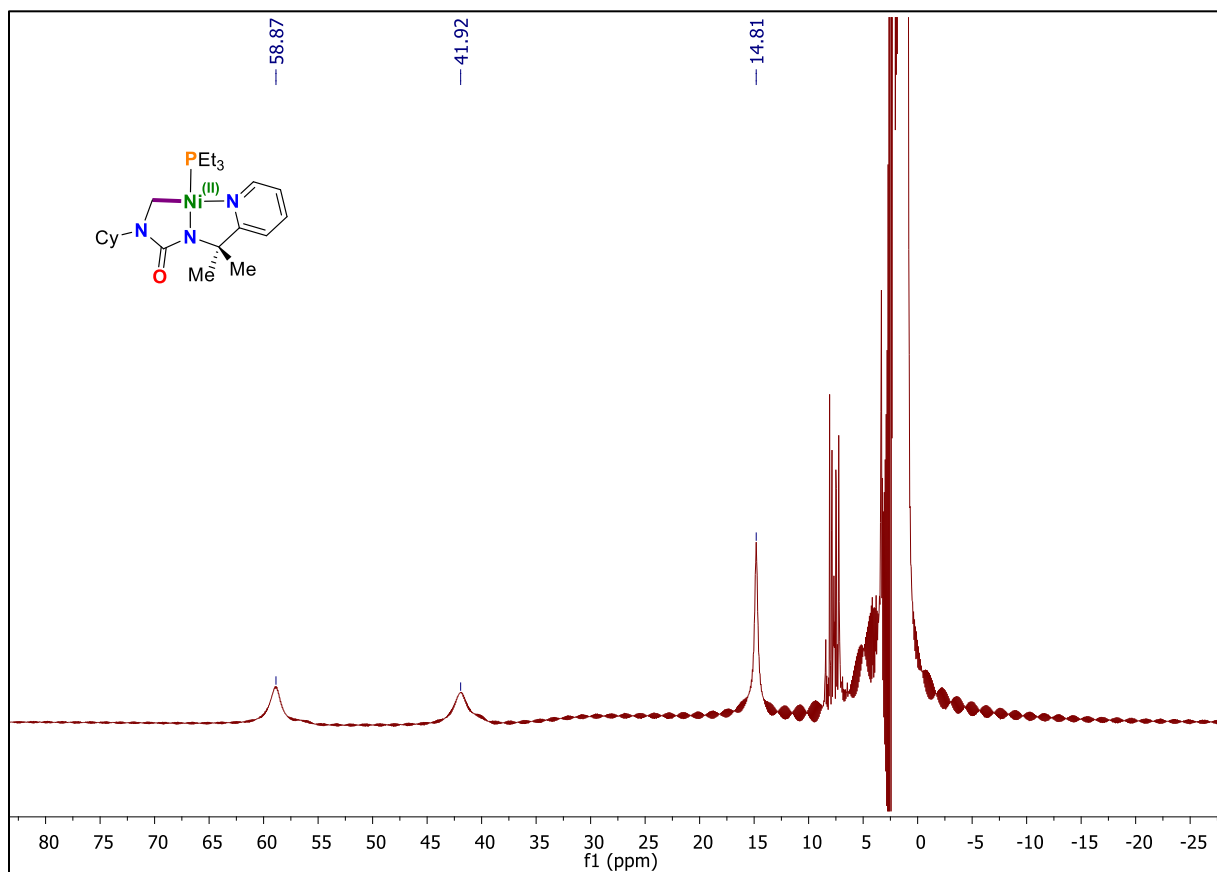


Figure A.5.135. In situ paramagnetic ^1H NMR spectrum of (5.6) and (5.6-Ni) (400 MHz, $\text{d}_6\text{-DMSO}$, 298K).

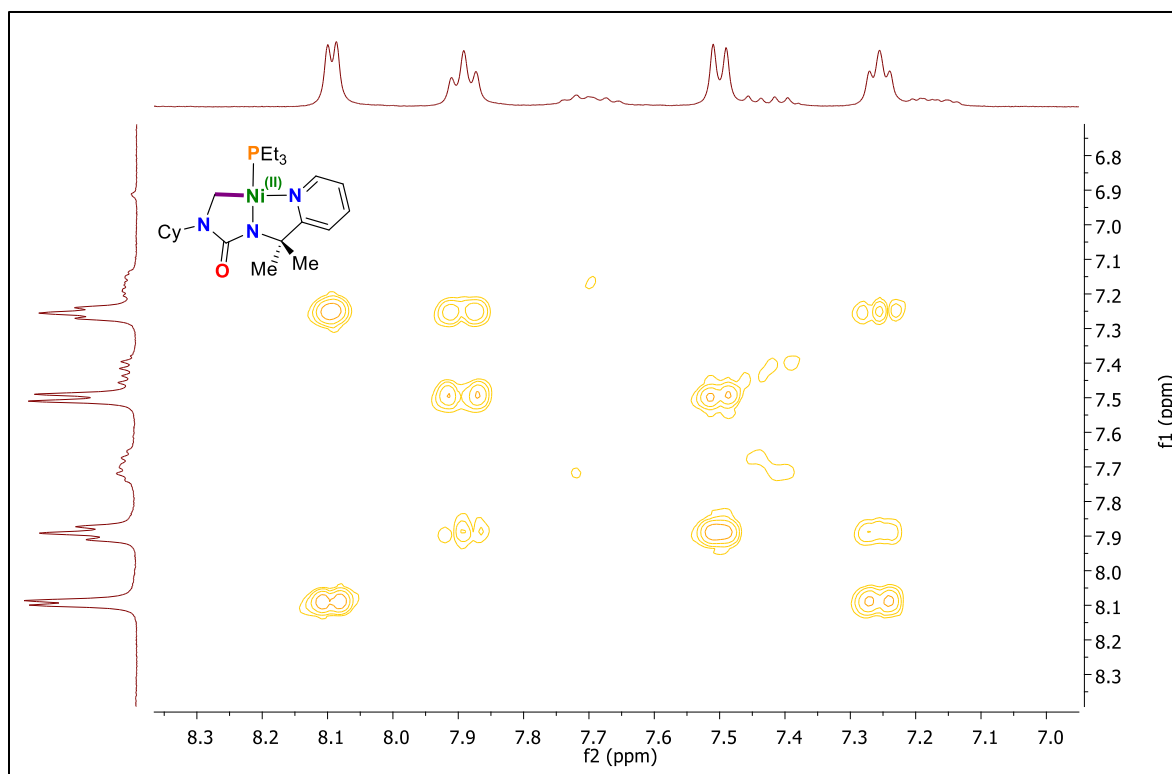


Figure A.5.136. In situ (expanded) ^1H -COSY NMR spectrum of (5.6) and (5.6-Ni) (300 MHz, d_6 -DMSO, 298K).

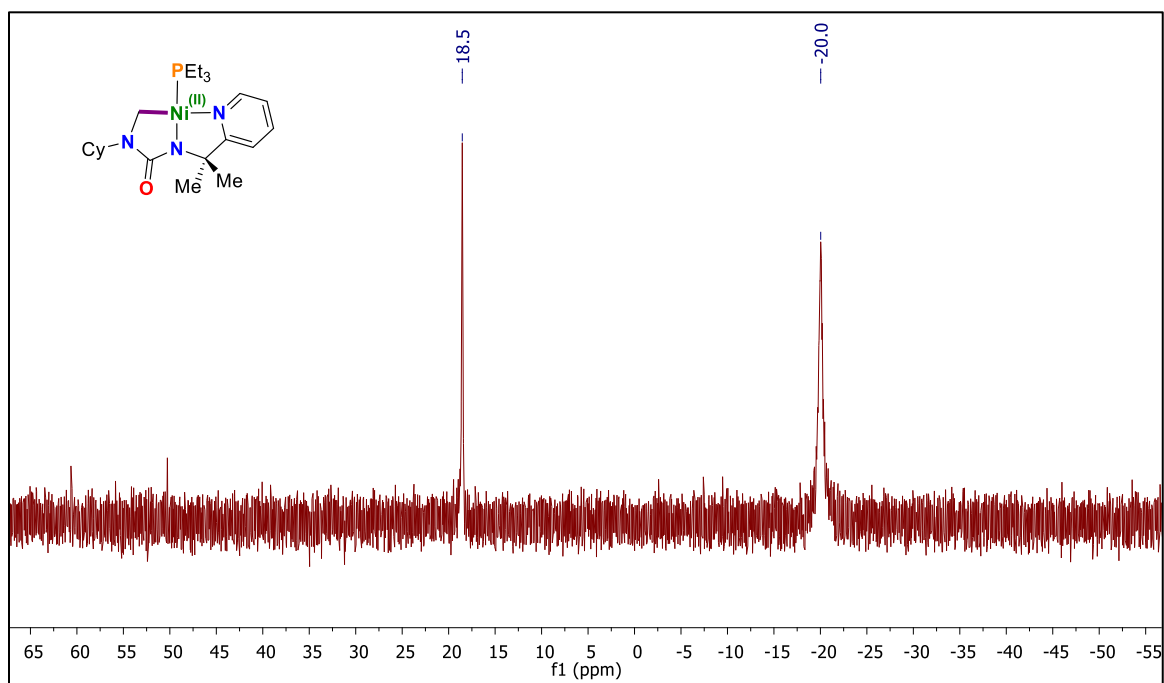


Figure A.5.137. In situ $^{31}\text{P}\{^1\text{H}\}$ NMR spectrum of (5.6) and (5.6-Ni) (162 MHz, d_6 -DMSO, 298K)

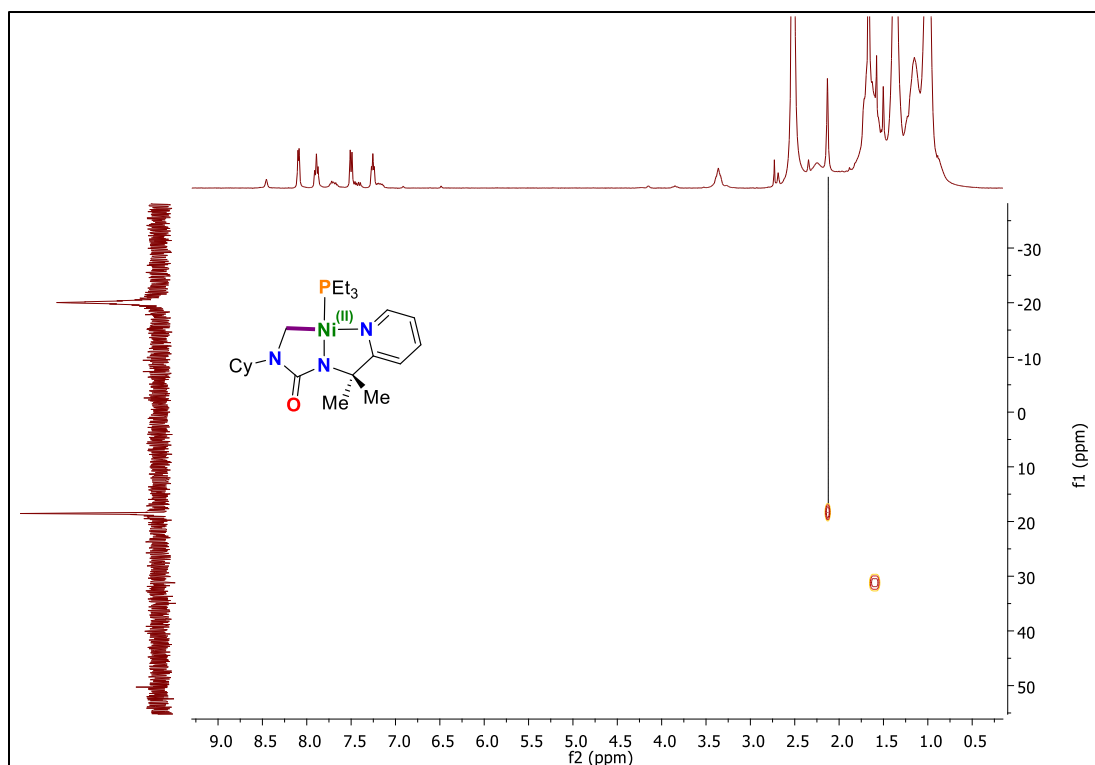


Figure A.5.138. In situ ^{31}P - ^1H HMBC NMR spectrum of (5.6) and (5.6-Ni) (162 MHz, d₆-DMSO, 298K)

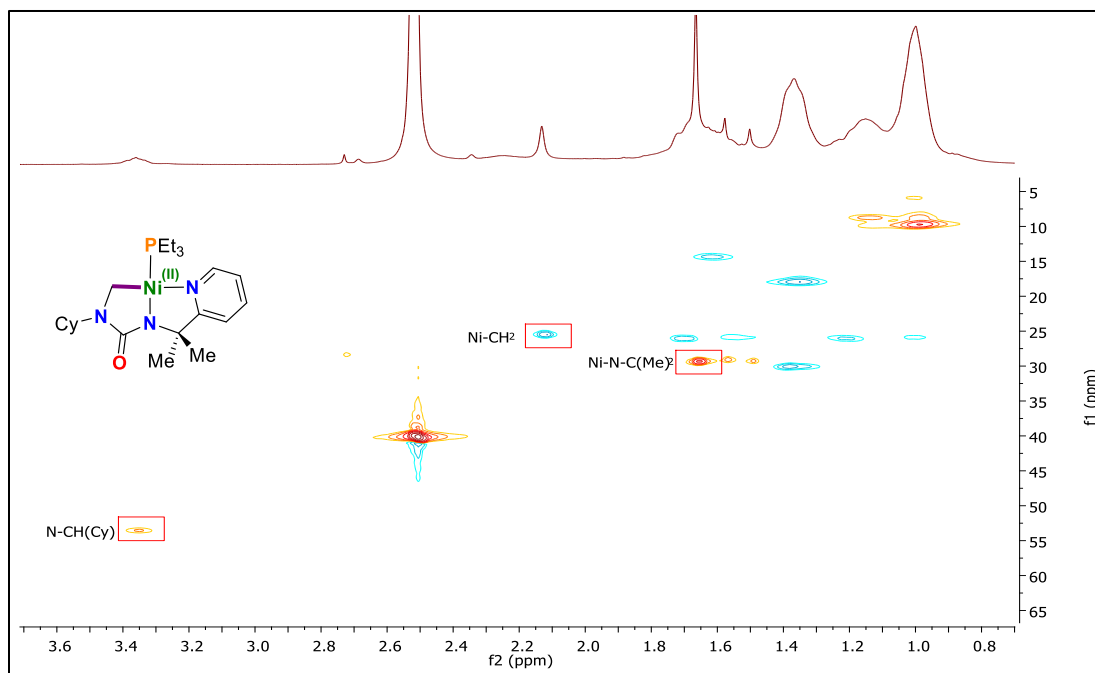


Figure A.5.139. In situ ^{13}C - ^1H (HSQC-edited) NMR spectrum of (5.6) and (5.6-Ni) (400 MHz, d₆-DMSO, 298K)

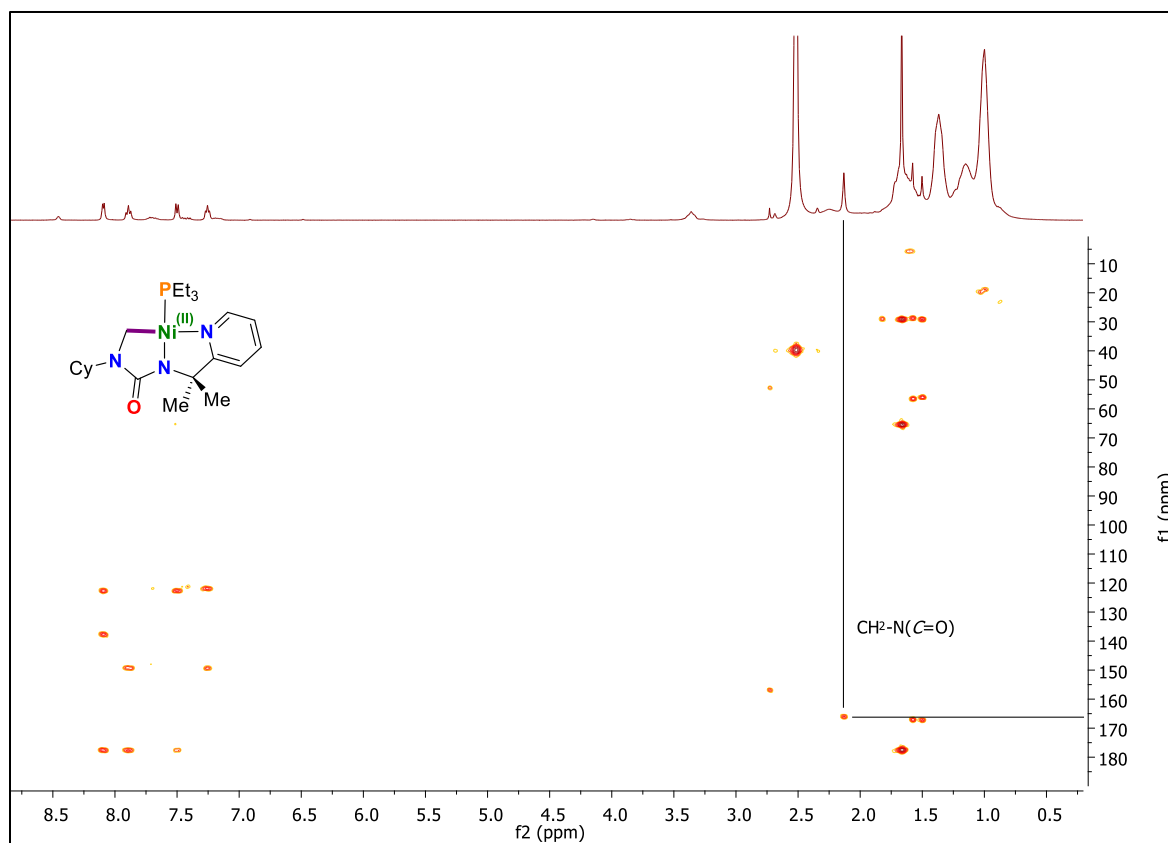


Figure A.5.140. In situ ^{13}C - ^1H (HMBC) NMR spectrum of (5.6) and (5.6-Ni) (400 MHz, d $_6$ -DMSO, 298K)

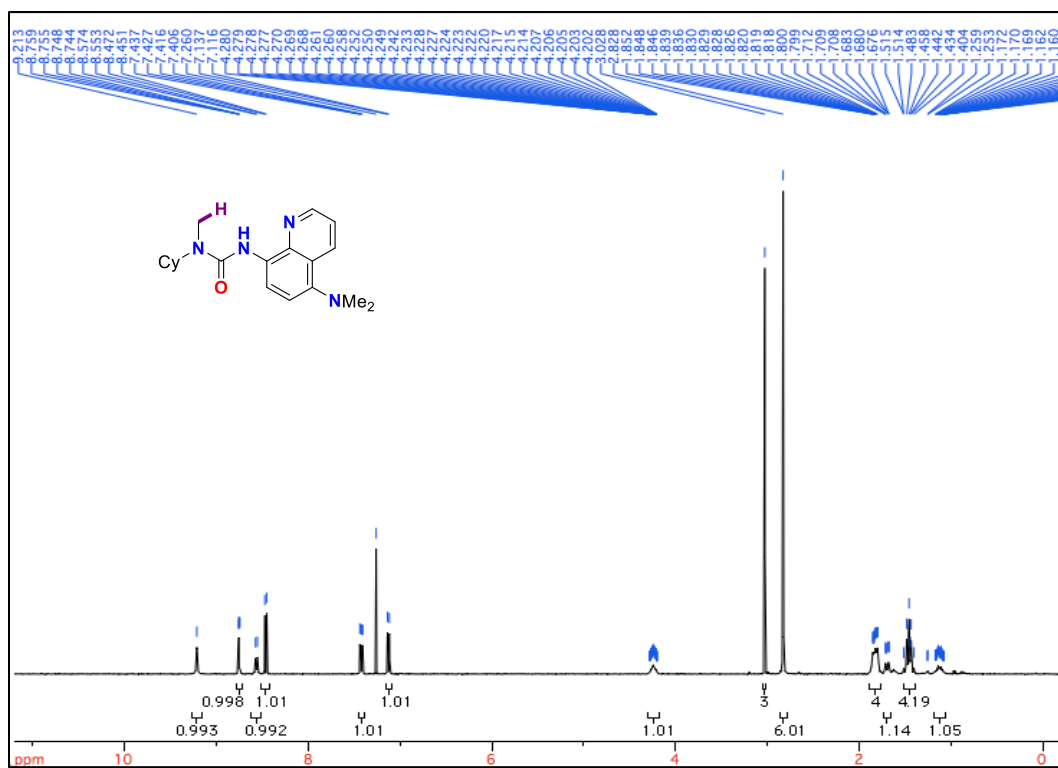


Figure A.5.141 ¹H NMR (400 MHz, CDCl₃, 298K) of 5.1

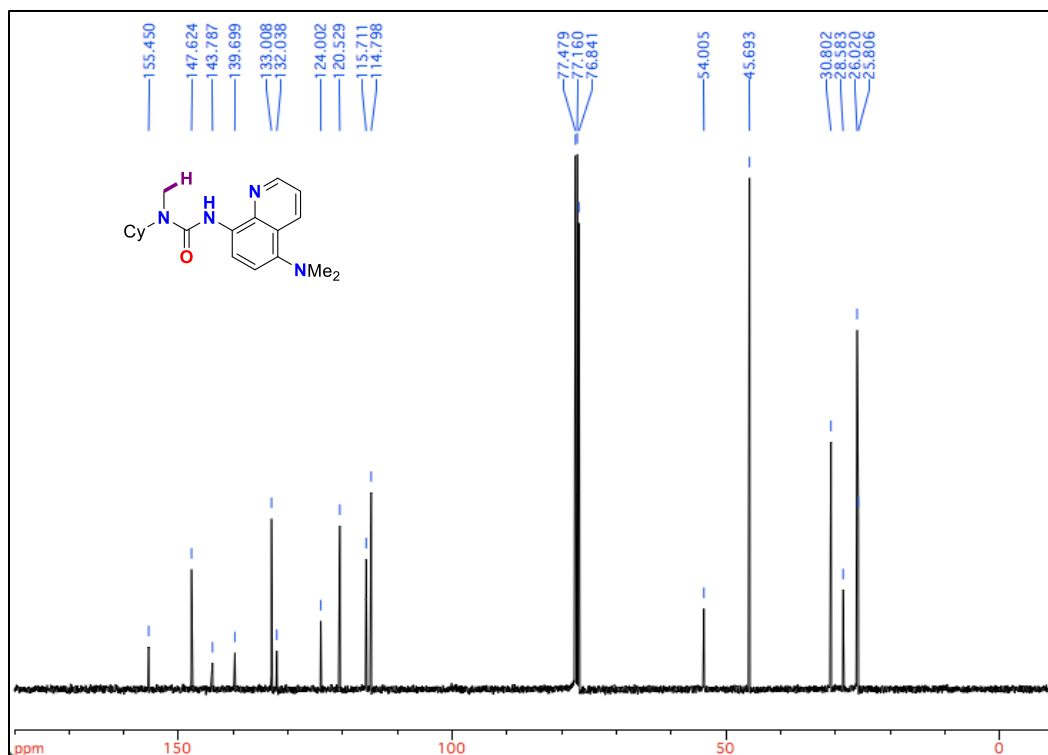


Figure A.5.142 ¹³C NMR (101 MHz, CDCl₃, 298K) of 5.1

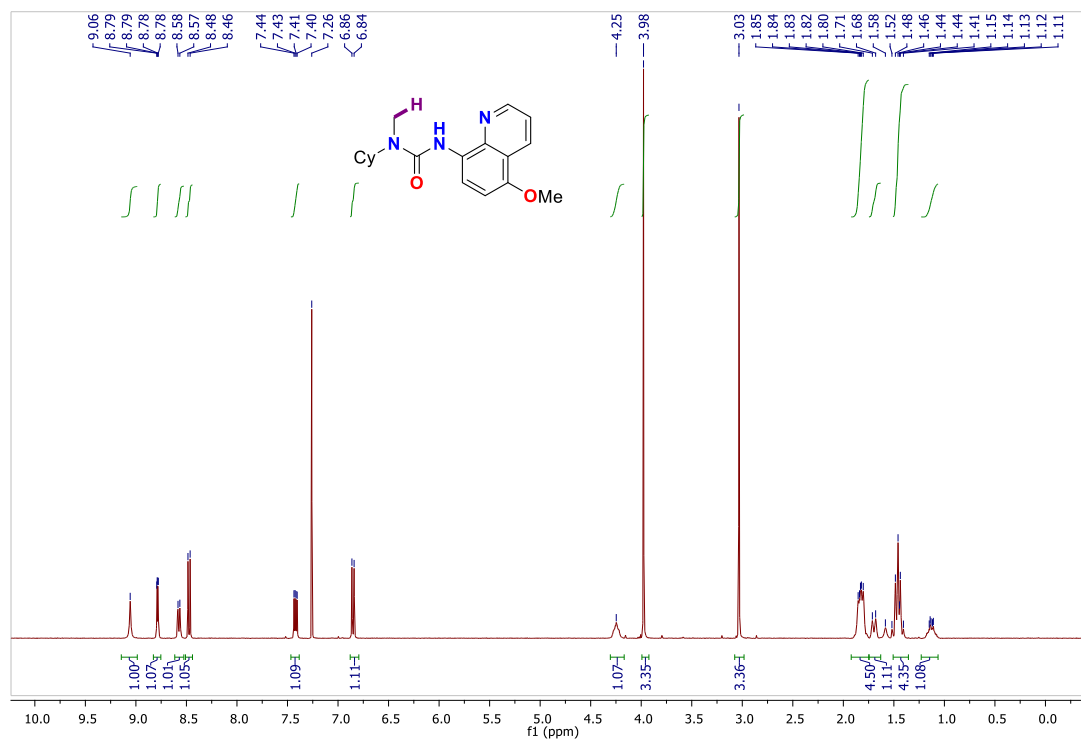


Figure A.5.143 ¹H NMR (400 MHz, CDCl₃, 298K) of 5.2

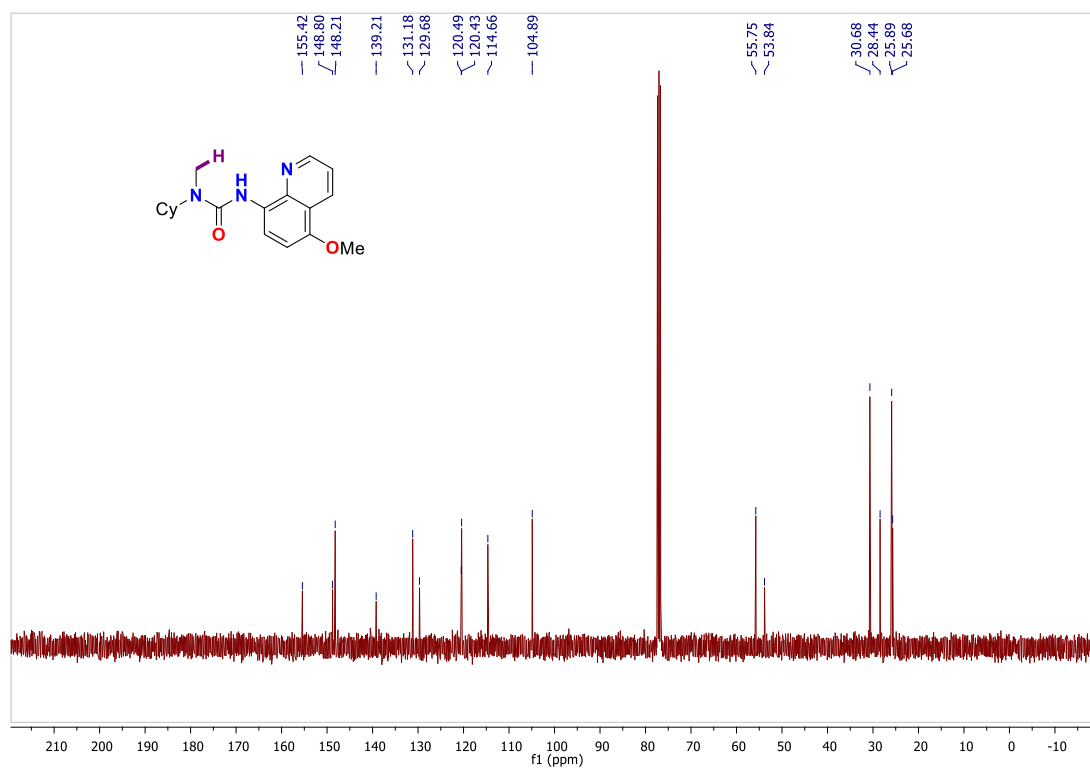


Figure A.5.144 ¹³C NMR (101 MHz, CDCl₃, 298K) of 5.2

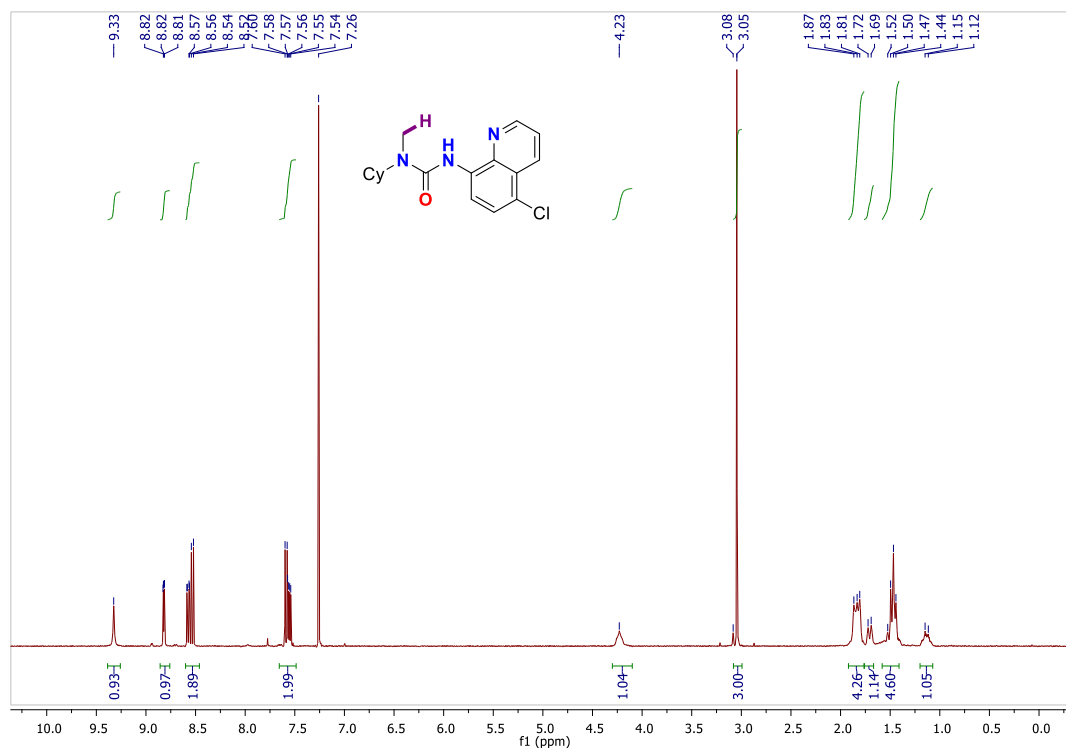


Figure A.5.145 ¹H NMR (400 MHz, CDCl₃, 298K) of 5.3

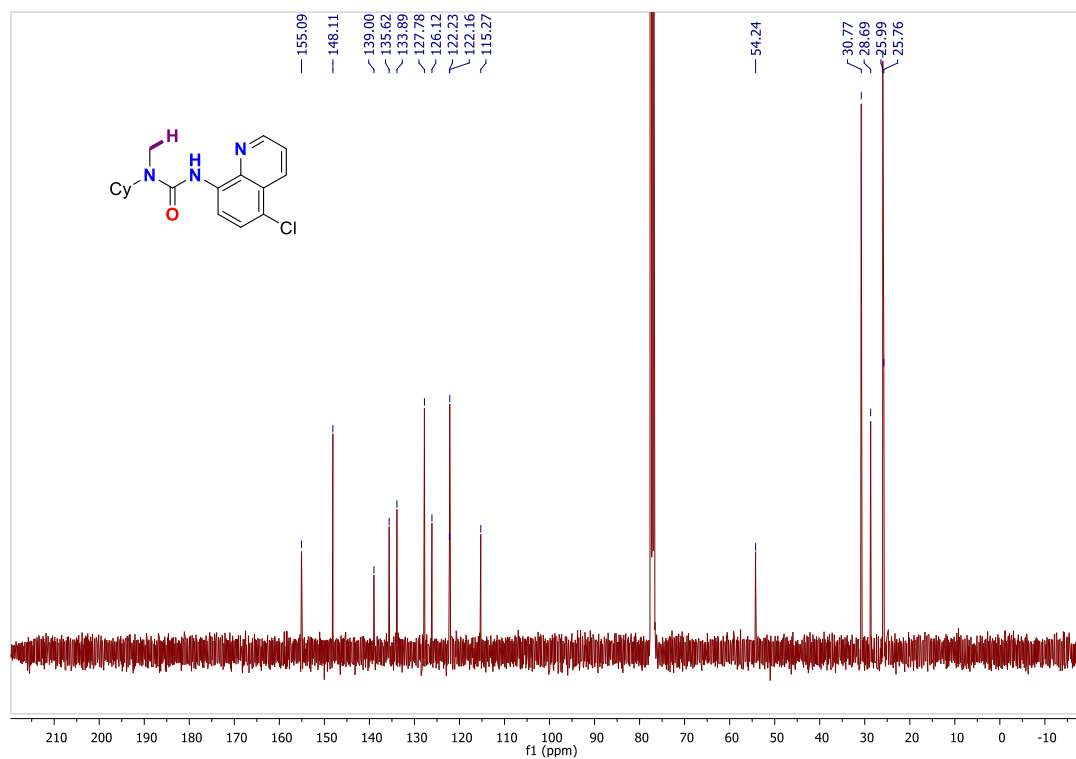


Figure A.5.146 ¹³C NMR (101 MHz, CDCl₃, 298K) of 5.3

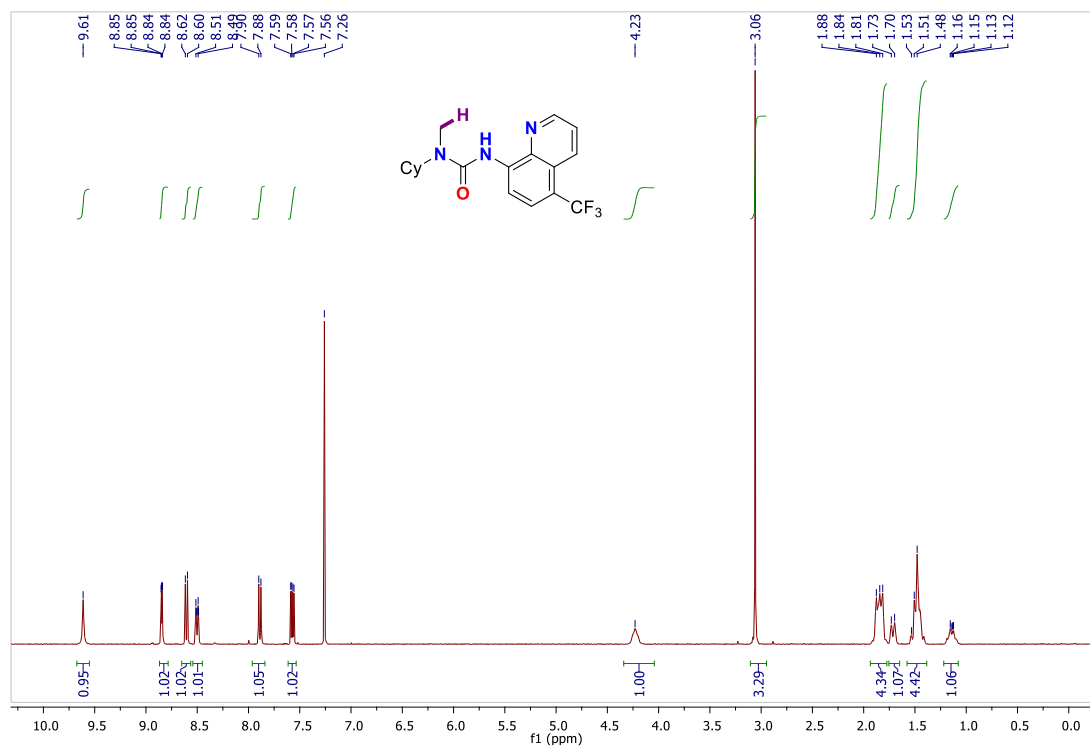


Figure A.5.147 ¹H NMR (400 MHz, CDCl₃, 298K) of 5.4

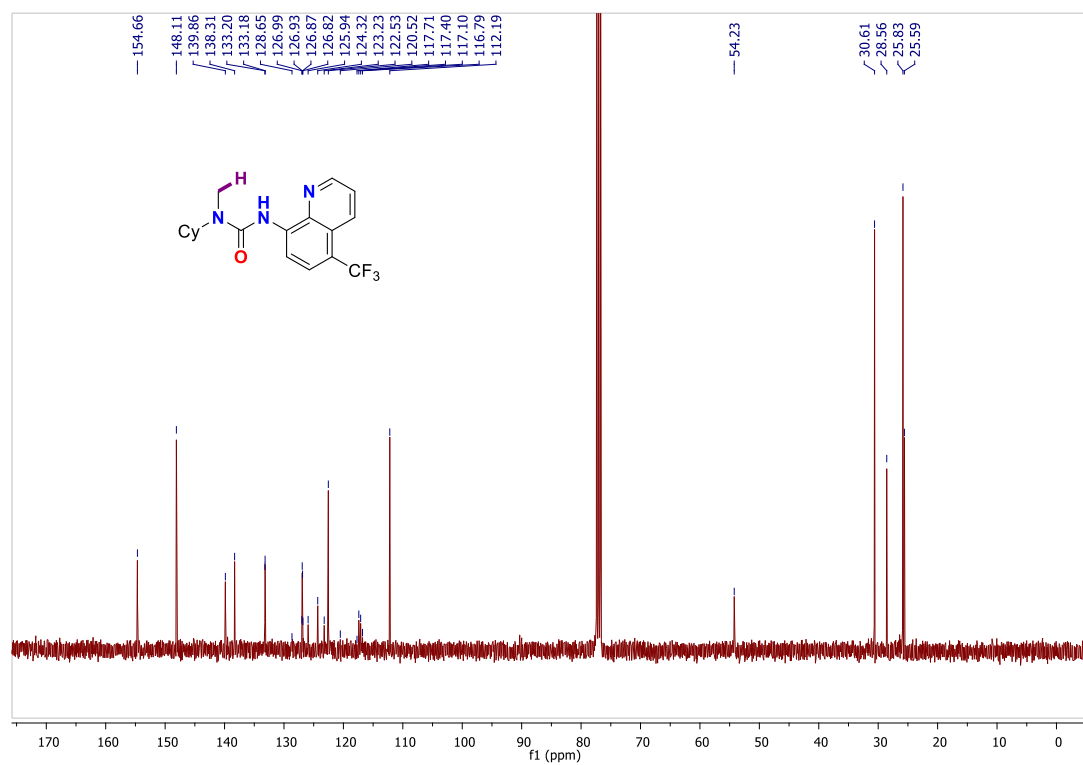


Figure A.5.148 ¹³C NMR (101 MHz, CDCl₃, 298K) of 5.4

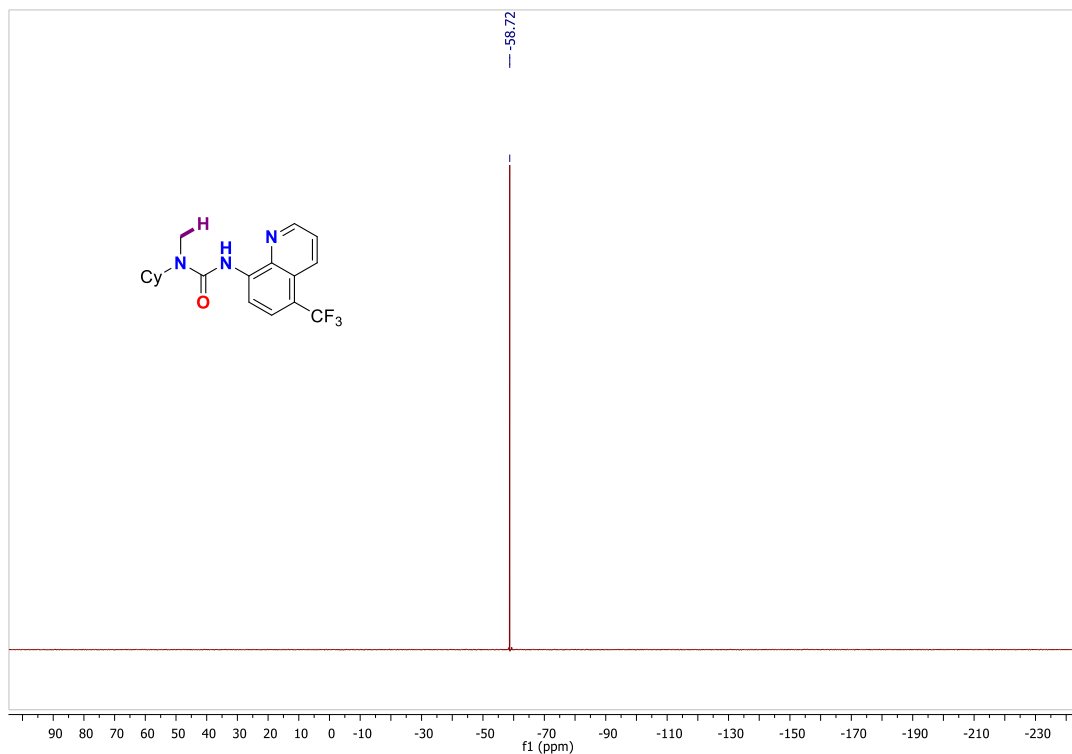


Figure A.5.149 ^{19}F NMR (282 MHz, CDCl_3 , 298K) of 5.4

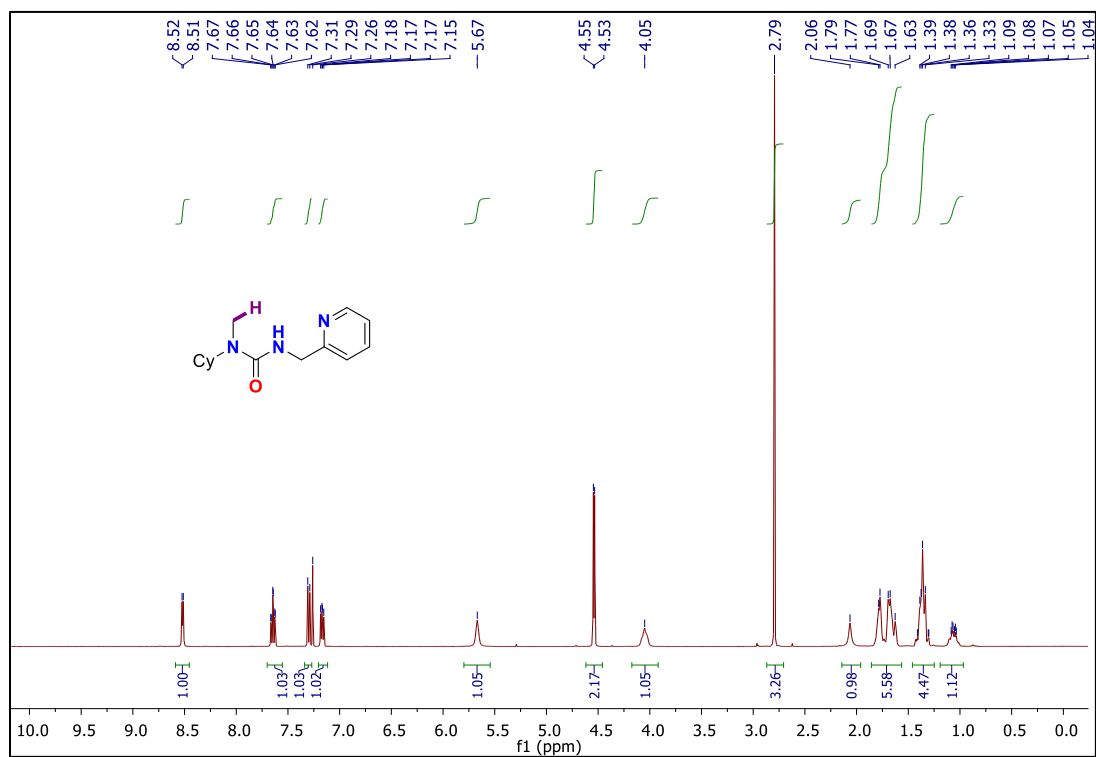


Figure A.5.150 ^1H NMR (400 MHz, CDCl_3 , 298K) of 5.5

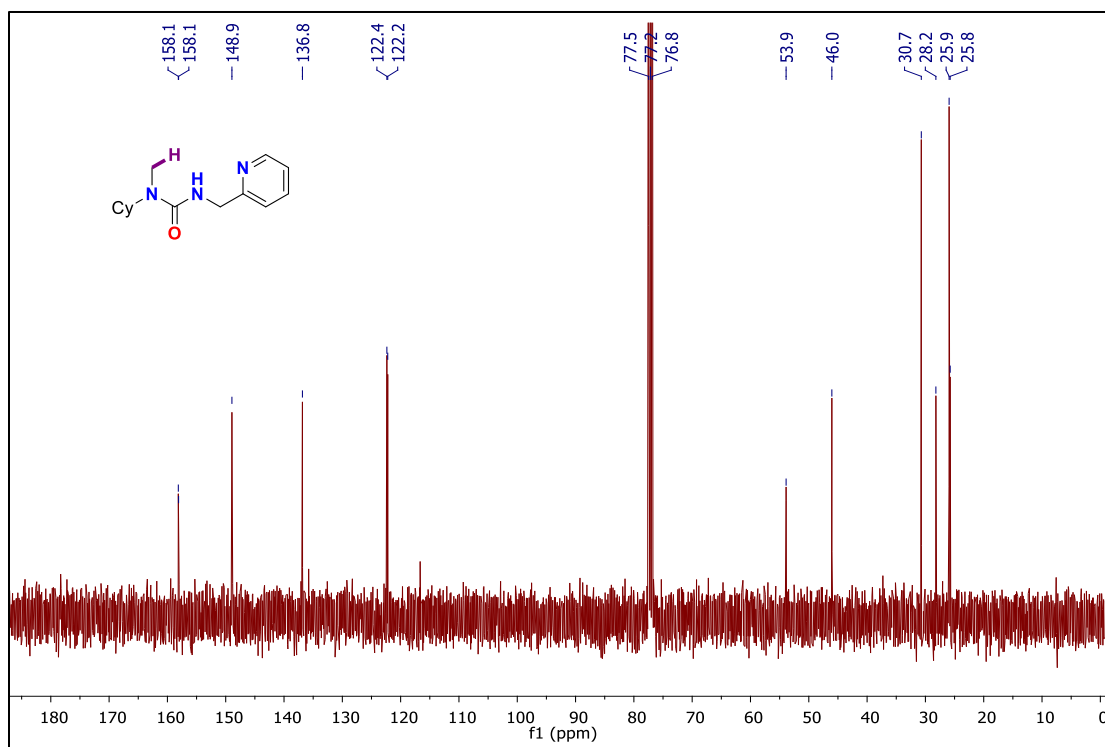


Figure A.5.151 ¹³C NMR (101 MHz, CDCl₃, 298K) of 5.5

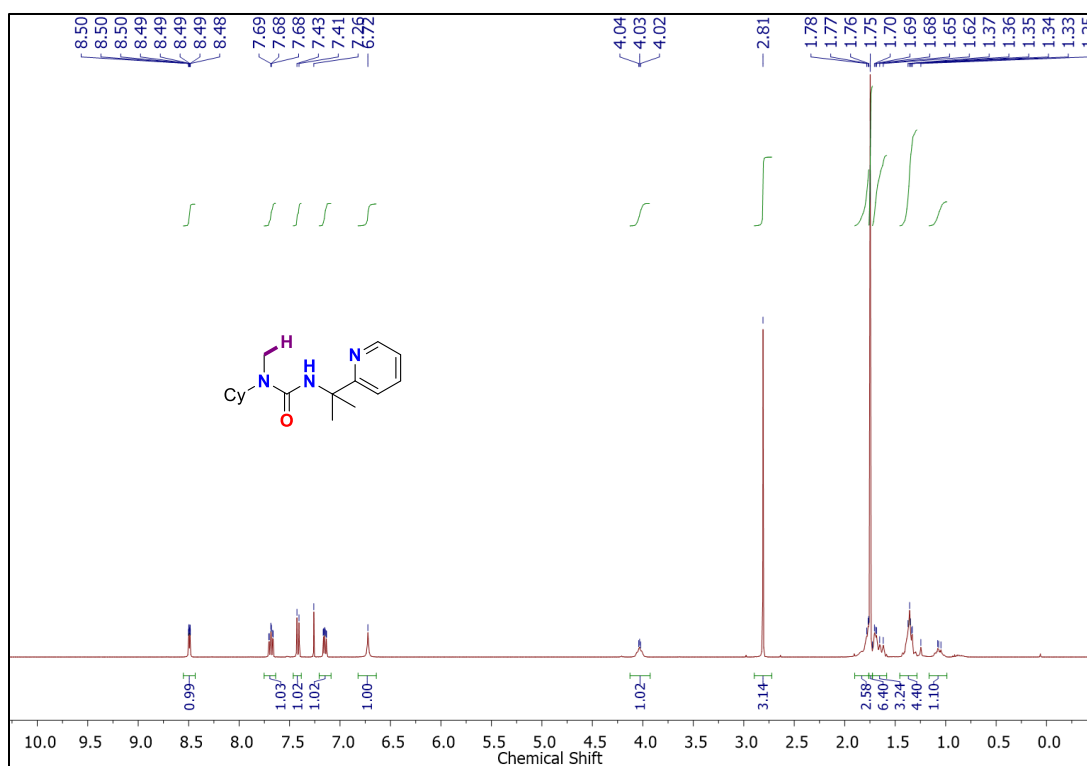


Figure A.5.152 ¹H NMR (400 MHz, CDCl₃, 298K) of 5.6

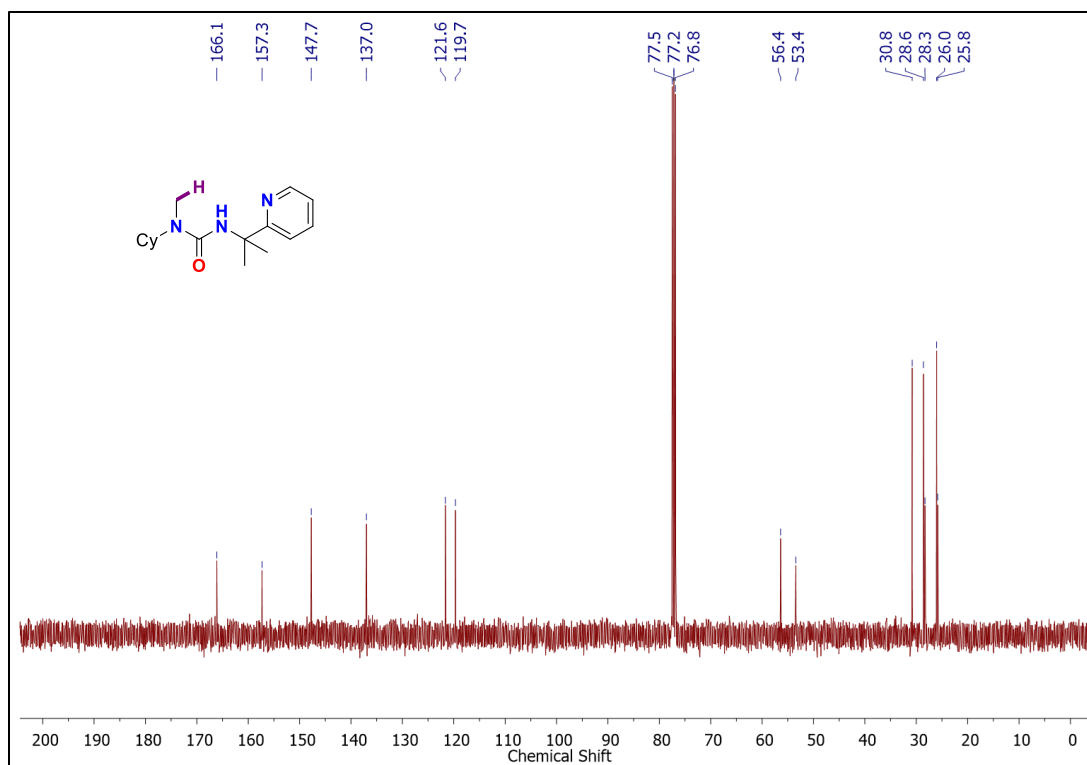


Figure A.5.153 ¹³C NMR (101 MHz, CDCl₃, 298K) of 5.6

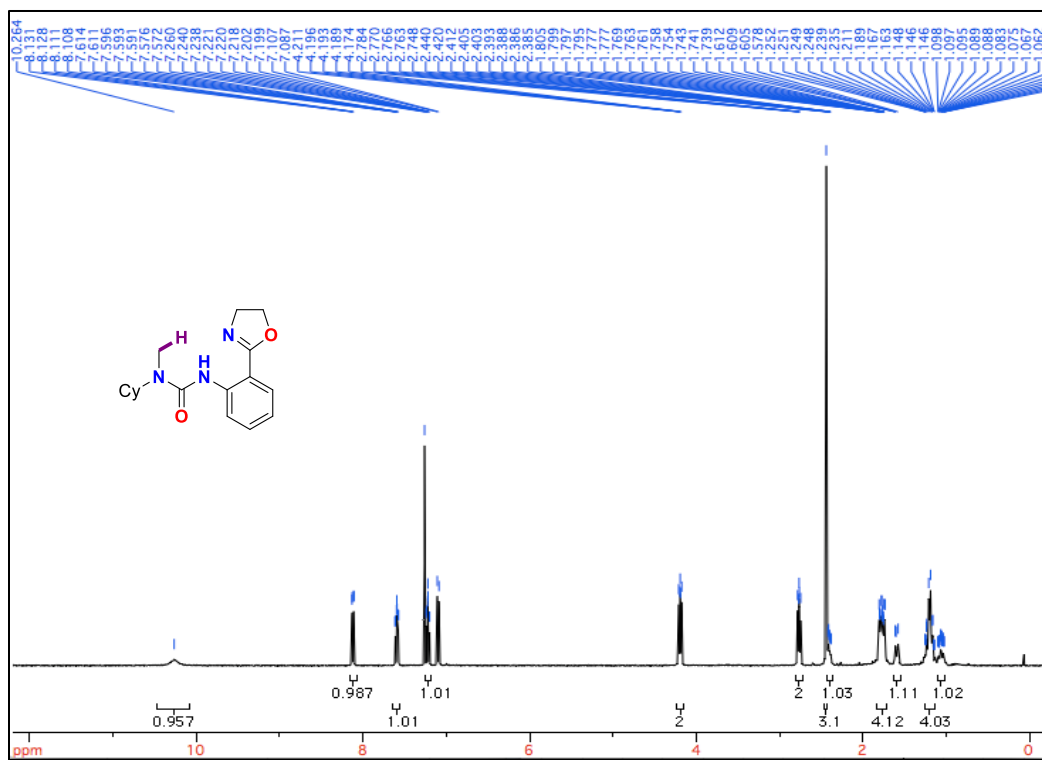


Figure A.5.154 ¹H NMR (400 MHz, CDCl₃, 298K) of 5.7

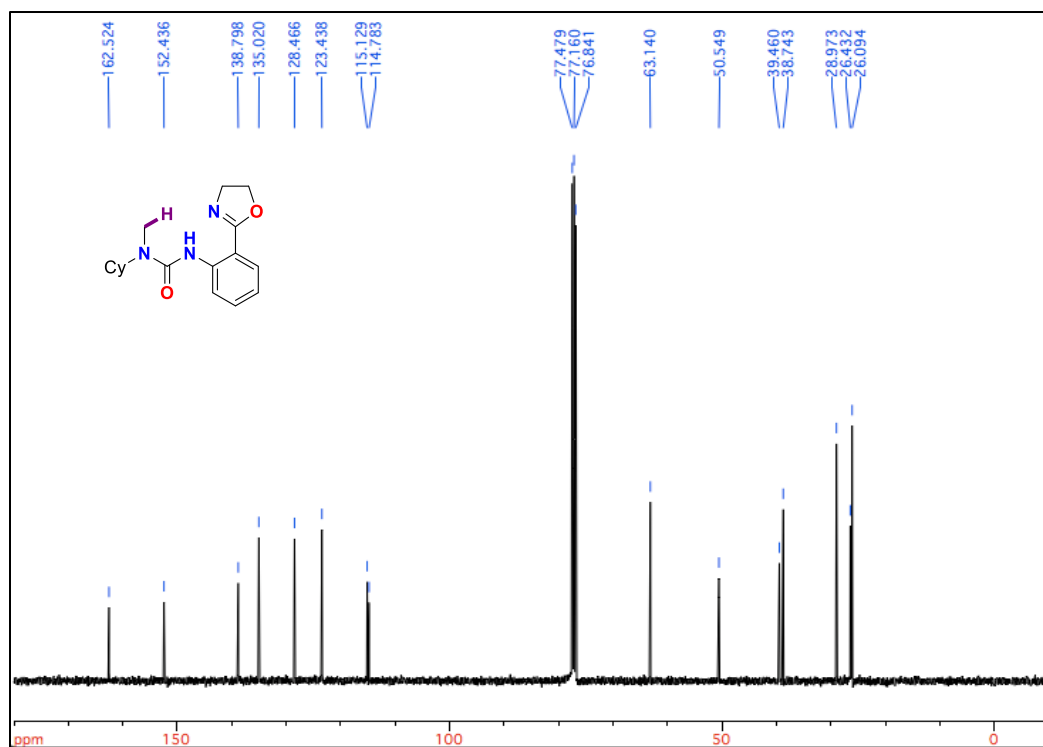


Figure A.5.155 ¹³C NMR (101 MHz, CDCl₃, 298K) of 5.7

Appendix B Crystallographic Tables

B.1 Chapter 2: Understanding Ni(II) Mediated C(sp³)-H Activation: Ureas as Model

Substrates

Data for **2.2**, **2.2-Ni**, and **[(PEt₃)Ni(μ-OⁱPiv)₂]₂** were collected using graphite-monochromated Mo Kα radiation (λ=0.71073 Å) on a Bruker APEX Duo diffractometer. This analysis was carried out at the Department of Chemistry, The University of British Columbia by Mr. Dawson Beattie. The structures were solved by intrinsic phasing (ShelXT) and refined by full-matrix least-squares procedures on F2 (SHELXL-2013)^[288] using the OLEX2 interface.^[289]

CCDC 1853556-1853558 contains the supplementary crystallographic data for Chapter 2. These data can be obtained free of charge from The Cambridge Crystallographic Data Centre via <https://www.ccdc.cam.ac.uk/structures>

Additional Notes on Refinement:

Urea (2.2): The structure is 90% complete. However, all other statistics are sufficient.

Complex (2.2-Ni): No notes.

[(PEt₃)Ni(μ-OⁱPiv)₂]₂: The asymmetric unit contains half of the nickel dimer. Growing the structure shows the complete structure. This grown structure is shown in the manuscript.

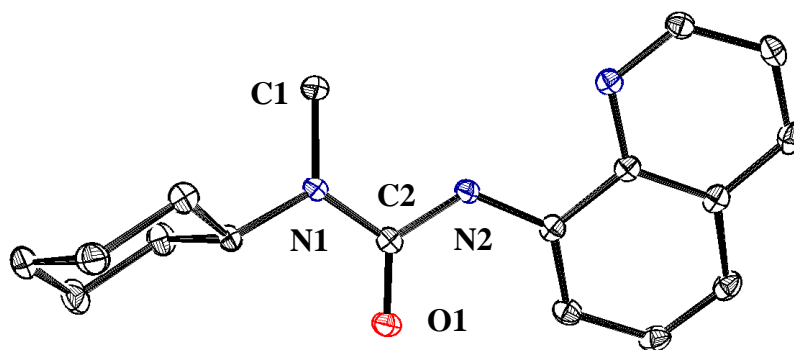


Figure B.1.156. ORTEP depiction of the solid-state structure of compound (**2.2**) (ellipsoids at 50% probability, hydrogens omitted). Selected bond lengths (Å) and angles (°): N1-C2 1.36153(7), C2-N2 1.38376(8), C2-O1 1.23146(10), C1-N1-C2 122.693(5), N1-C2-N2 114.660(6).

Compound	2.2	2.2-Ni
Empirical formula	C ₁₇ H ₂₁ N ₃ O	C _{26.5} H ₃₈ N ₃ NiOP
Formula weight	283.37	504.28
Temperature/K	90	90
Crystal system	trigonal	monoclinic
Space group	R-3	P2 ₁ /c
a/Å	27.062(2)	10.7609(5)
b/Å	27.062(2)	16.9421(7)
c/Å	10.3516(11)	28.0175(13)
α/°	90	90
β/°	90	99.6020(10)
γ/°	120	90
Volume/Å ³	6565.6(13)	5036.4(4)
Z	18	8
ρ _{calc} /g/cm ³	1.290	1.330
μ/mm ⁻¹	0.082	0.858
F(000)	2736.0	2152.0
Crystal size/mm ³	0.23 × 0.09 × 0.08	0.23 × 0.08 × 0.07
Radiation	MoKα (λ = 0.71073)	MoKα (λ = 0.71073)
2θ range for data collection/°	3.01 to 54.28	2.82 to 58.428
Index ranges	-33 ≤ h ≤ 34, -34 ≤ k ≤ 18, -13 ≤ l ≤ 13	-14 ≤ h ≤ 14, -12 ≤ k ≤ 23, -38 ≤ l ≤ 38
Reflections collected	18708	91204
Independent reflections	2960 [R _{int} = 0.0396, R _{sigma} = 0.0398]	13633 [R _{int} = 0.0607, R _{sigma} = 0.0444]
Data/restraints/parameters	2960/0/195	13633/0/593
Goodness-of-fit on F ²	1.043	1.103
Final R indexes [I ≥ 2σ (I)]	R ₁ = 0.0355, wR ₂ = 0.0867	R ₁ = 0.0532, wR ₂ = 0.0955
Final R indexes [all data]	R ₁ = 0.0450, wR ₂ = 0.0901	R ₁ = 0.0790, wR ₂ = 0.1062
Largest diff. peak/hole / e Å ⁻³	0.24/-0.18	1.15/-0.89

Compound	[(PEt₃)Ni(μ-OPiv)₂]₂
Empirical formula	C ₃₂ H ₆₆ Ni ₂ O ₈ P ₂
Formula weight	758.20
Temperature/K	90
Crystal system	monoclinic
Space group	P2 ₁ /c
a/Å	9.9146(6)
b/Å	17.8444(12)
c/Å	12.4027(8)
α /°	90
β /°	109.0940(10)
γ /°	90
Volume/Å ³	2073.6(2)
Z	2
ρ_{calc} /cm ³	1.214
μ /mm ⁻¹	1.025
F(000)	816.0
Crystal size/mm ³	0.2 \times 0.19 \times 0.09
Radiation	MoK α (λ = 0.71073)
2 θ range for data collection/°	4.158 to 60.984
Index ranges	-14 \leq h \leq 14, -23 \leq k \leq 25, -17 \leq l \leq 17
Reflections collected	24248
Independent reflections	6312 [R _{int} = 0.0366, R _{sigma} = 0.0341]
Data/restraints/parameters	6312/0/279
Goodness-of-fit on F ²	1.008
Final R indexes [$I \geq 2\sigma(I)$]	R ₁ = 0.0256, wR ₂ = 0.0599
Final R indexes [all data]	R ₁ = 0.0375, wR ₂ = 0.0630

B.2 Chapter 3: Preparation of Low-Coordinate Ni(I) Amidate Complexes and Reactivity of Ni(I) Complexes Towards C(sp³)-H Activation

The crystallographic data for **3.1**, **Ni(II)-3.1-Cl**, **Ni(II)-3.5-Cl**, **Ni(I)-3.1**, **Ni(I)-3.5**, **Ni(I)-3.10**, and **Ni(I)-3.5-CNXYl** has been published as: *Angew. Chem. Int. Ed.* **2016**, 55, 13290-13295. Likewise, the data for **(IPr)Ni(CNXYl)₃**, **Ni(II)-(3.5)₂**, **Ni(I)-3.8**, **Ni(II)-3.8-Cl**, and **Ni(II)-(3.8)₂** has been published as: *Organometallics* **2018**, 37, 1392-1399.

Ni(I)-3.2, **Ni(I)-3.3**, **Ni(I)-3.4**, **Ni(I)-3.6**, **Ni(I)-3.9**, **Ni(I)-3.11**, **Ni(II)-3.12A**, **Ni(II)-3.5-TEMPO(E)**, and **[Ni(II)-3.5-pyr][BAr^F]** were collected using graphite-monochromated Mo K α radiation ($\lambda=0.71073$ Å) on a Bruker APEX Duo or X8 diffractometer. The analyses was carried out at the Department of Chemistry, The University of British Columbia by Dr. Marcus Drover or Mr. Dawson Beattie. Dr. Brian Patrick was also helpful with structural refinements. The structures were solved by intrinsic phasing (ShelXT) and refined by full-matrix least-squares procedures on F2 (SHELXL-2013)^[288] using the OLEX2 interface.^[289]

Additional Notes on Refinement:

Ni(I)-3.2: The structure is 88% complete and is of very poor quality. Only connectivity may be reasoned.

Ni(I)-3.3: No notes.

Ni(I)-3.4: Disorder was modelled successfully in the amidate and all isopropyl groups. However, the structure is still somewhat poor quality.

Ni(I)-3.6: The hydrogen atoms were found in the electron density map.

Ni(I)-3.9: Disorder was modelled successfully in IPr isopropyl groups.

Ni(I)-3.11: Disorder was modelled partially in the amidate and toluene molecules. However, the structure is still somewhat poor quality.

Ni(II)-3.12A: Four independent molecules of **Ni(II)-3.12A** crystallize together, with hydrogen bonding between the structures (Cl --- H-N). Only a single structure is shown. Solvent is also omitted.

Ni(II)-3.5-TEMPO(E): These crystals diffract well, but the structure is only 66% complete. However, although the structure is poor, connectivity may be reasoned.

[Ni(II)-3.5-pyr][BAr^F]: The CF₃ groups were modelled successfully.

Complex Ni(II)-3.8-Cl:

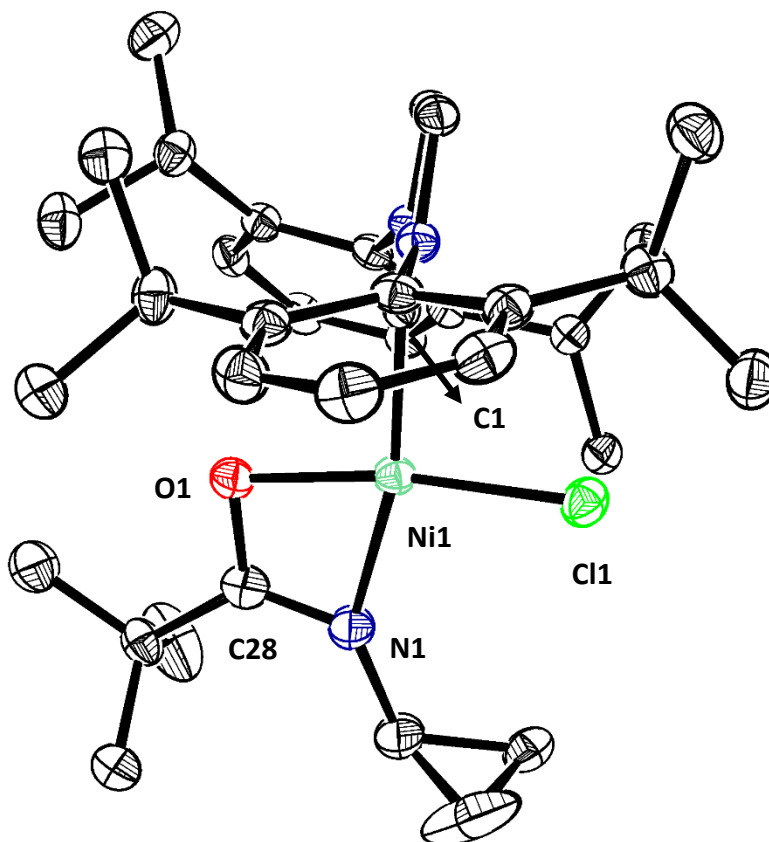


Figure B.2.157. ORTEP depiction of the solid-state structure of Ni(II)-3.8-Cl (ellipsoids at 50% probability, hydrogens omitted). Selected bond lengths (Å) and angles (°): Ni1-Cl1 2.1779(7), Ni1-N1 1.942(2), Ni1-C28 2.322(3), C28-N1 1.301(3), C28-O1 1.311(3), N1-Ni1-Cl1 163.39(10), O1-Ni1-Cl1 171.21(5), O1-Ni1-N1 68.42(8).

Complex Ni(II)-(3.8)₂:

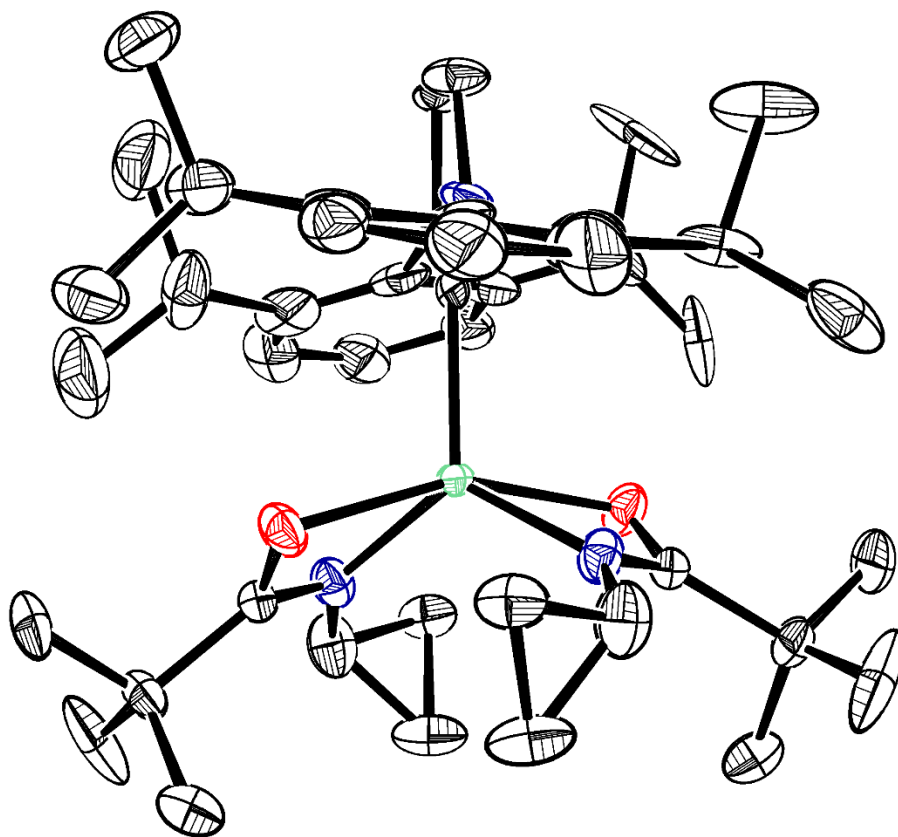


Figure B.2.158. ORTEP depiction of the solid-state structure of (Λ)- Ni(II)-(3.8)₂ (ellipsoids at 50% probability, hydrogens omitted).

Compound	Ni(I)-3.2	Ni(I)-3.3
Empirical formula	C ₅₃ H ₆₆ N ₃ NiO	C ₄₈ H ₅₆ F ₆ N ₃ NiO
Formula weight	819.79	863.66
Temperature/K	296.15	273.15
Crystal system	monoclinic	orthorhombic
Space group	Pc	Pbca
a/Å	24.277(6)	17.6723(7)
b/Å	9.743(3)	21.0009(9)
c/Å	20.892(6)	23.4629(10)
α /°	90	90
β /°	111.975(7)	90
γ /°	90	90
Volume/Å ³	4583(2)	8707.9(6)
Z	4	8
$\rho_{\text{calc}}/\text{g/cm}^3$	1.188	1.318
μ/mm^{-1}	0.464	0.511
F(000)	1764	3640
Radiation	MoK α (λ = 0.71073)	MoK α (λ = 0.71073)
2 θ range for data collection/°	1.808 to 50.864	3.472 to 56.366
Index ranges	-27 \leq h \leq 29, -11 \leq k \leq 11, -25 \leq l \leq 25	-11 \leq h \leq 23, -27 \leq k \leq 24, -31 \leq l \leq 28
Reflections collected	33219	43574
Independent reflections	13989 [R _{int} = 0.0540, R _{sigma} = 0.0782]	10612 [R _{int} = 0.0349, R _{sigma} = 0.0311]
Data/restraints/parameters	13989/915/956	10612/0/572
Goodness-of-fit on F ²	1.079	1.031
Final R indexes [I \geq 2 σ (I)]	R ₁ = 0.1969, wR ₂ = 0.5057	R ₁ = 0.0380, wR ₂ = 0.0927
Final R indexes [all data]	R ₁ = 0.1995, wR ₂ = 0.5071	R ₁ = 0.0522, wR ₂ = 0.0997
Largest diff. peak/hole / e Å ⁻³	5.17/-2.97	0.75/-0.48
Flack parameter	-0.001(11)	N.A.

Compound	Ni(I)-3.4	Ni(I)-3.6
Empirical formula	C ₃₇ H ₄₈ N ₃ NiO	C ₃₈ H ₅₆ N ₃ NiO
Formula weight	609.49	629.56
Temperature/K	296.15	90
Crystal system	monoclinic	monoclinic
Space group	Cc	P2 ₁ /c
a/Å	22.7749(9)	9.3273(13)
b/Å	10.8820(4)	17.223(2)
c/Å	16.3049(6)	21.432(3)
α /°	90	90
β /°	122.3950(10)	94.644(3)
γ /°	90	90
Volume/Å ³	3412.1(2)	3431.7(8)
Z	4	4
ρ_{calc} /cm ³	1.186	1.219
μ /mm ⁻¹	0.6	0.598
F(000)	1308	1364
Crystal size/mm ³	0.27 × 0.23 × 0.19	0.57 × 0.12 × 0.04
Radiation	MoK α (λ = 0.71073)	MoK α (λ = 0.71073)
2 θ range for data collection/°	2.958 to 50.718	3.038 to 56.018
Index ranges	-27 ≤ h ≤ 26, -13 ≤ k ≤ 6, -19 ≤ l ≤ 19	-10 ≤ h ≤ 12, -22 ≤ k ≤ 22, -27 ≤ l ≤ 28
Reflections collected	12635	32923
Independent reflections	6063 [R _{int} = 0.0215, R _{sigma} = 0.0339]	8266 [R _{int} = 0.0536, R _{sigma} = 0.0468]
Data/restraints/parameters	6063/480/510	8266/0/399
Goodness-of-fit on F ²	1.015	1.02
Final R indexes [I ≥ 2 σ (I)]	R ₁ = 0.0395, wR ₂ = 0.0874	R ₁ = 0.0374, wR ₂ = 0.0808
Final R indexes [all data]	R ₁ = 0.0590, wR ₂ = 0.0984	R ₁ = 0.0610, wR ₂ = 0.0897
Largest diff. peak/hole / e Å ⁻³	0.38/-0.25	0.47/-0.37
Flack parameter	0.011(17)	N.A.

Compound	Ni(I)-3.9	Ni(I)-3.11
Empirical formula	C ₃₇ H ₅₄ N ₃ NiO	C ₄₀ H _{54.09} N ₃ NiO
Formula weight	615.54	652.03
Temperature/K	90	296.15
Crystal system	monoclinic	monoclinic
Space group	P2 ₁ /n	Cc
a/Å	9.4012(6)	20.929(2)
b/Å	20.5882(13)	10.8744(9)
c/Å	18.0158(13)	17.9491(17)
α /°	90	90
β /°	94.096(2)	114.986(4)
γ /°	90	90
Volume/Å ³	3478.1(4)	3702.7(6)
Z	4	4
ρ_{calc} /cm ³	1.175	1.17
μ /mm ⁻¹	0.589	0.557
F(000)	1332	1406
Crystal size/mm ³	0.19 × 0.17 × 0.17	-
Radiation	MoK α (λ = 0.71073)	MoK α (λ = 0.71073)
2 θ range for data collection/°	3.956 to 58.254	2.504 to 52.892
Index ranges	-12 ≤ h ≤ 12, -28 ≤ k ≤ 20, -24 ≤ l ≤ 24	-26 ≤ h ≤ 26, -13 ≤ k ≤ 13, -22 ≤ l ≤ 22
Reflections collected	39295	29338
Independent reflections	9351 [R _{int} = 0.0521, R _{sigma} = 0.0472]	7624 [R _{int} = 0.0288, R _{sigma} = 0.0278]
Data/restraints/parameters	9351/6/419	7624/296/427
Goodness-of-fit on F ²	1.008	1.087
Final R indexes [I ≥ 2 σ (I)]	R ₁ = 0.0378, wR ₂ = 0.0798	R ₁ = 0.0445, wR ₂ = 0.1046
Final R indexes [all data]	R ₁ = 0.0612, wR ₂ = 0.0877	R ₁ = 0.0566, wR ₂ = 0.1155
Largest diff. peak/hole / e Å ⁻³	0.48/-0.26	1.26/-0.52
Flack parameter	N.A.	0.001(8)

Compound	Ni(II)-3.12A	Ni(II)-3.5-TEMPO(E)
Empirical formula	C ₁₈₂ H ₂₅₆ Cl ₄ N ₁₂ Ni ₄ O ₄	C ₄₈ H ₈₀ N ₄ NiO ₃
Formula weight	508.77	819.87
Temperature/K	296.15	273.15
Crystal system	triclinic	triclinic
Space group	P-1	P-1
a/Å	17.3299(16)	11.719
b/Å	17.8309(17)	11.752
c/Å	32.981(3)	18.14
α /°	103.970(2)	83.47
β /°	93.918(2)	76.88
γ /°	94.147(2)	73.7
Volume/Å ³	9825.2(16)	2331.7
Z	2	2
ρ_{calc} /g/cm ³	1.032	1.168
μ /mm ⁻¹	0.481	0.459
F(000)	3288	896
Crystal size/mm ³	0.44 × 0.42 × 0.15	-
Radiation	MoK α (λ = 0.71073)	MoK α (λ = 0.71073)
2 θ range for data collection/°	2.364 to 54.438	3.616 to 58.278
Index ranges	-22 ≤ h ≤ 22, -22 ≤ k ≤ 22, -42 ≤ l ≤ 42	-8 ≤ h ≤ 14, -15 ≤ k ≤ 16, -24 ≤ l ≤ 22
Reflections collected	161708	8999
Independent reflections	43540 [R _{int} = 0.0459, R _{sigma} = 0.0504]	8359 [R _{int} = 0.0884, R _{sigma} = 0.2914]
Data/restraints/parameters	43540/1570/1909	8359/0/244
Goodness-of-fit on F ²	1.018	1.753
Final R indexes [I ≥ 2 σ (I)]	R ₁ = 0.0601, wR ₂ = 0.1538	R ₁ = 0.3285, wR ₂ = 0.6126
Final R indexes [all data]	R ₁ = 0.0821, wR ₂ = 0.1659	R ₁ = 0.3737, wR ₂ = 0.6517
Largest diff. peak/hole / e Å ⁻³	1.39/-0.62	6.77/-6.17

Compound	[Ni(II)-3.5-pyr][BAr ₄ ^F]
Empirical formula	C ₇₂ H ₆₉ BF _{23.96} N ₄ NiO
Formula weight	1531.12
Temperature/K	90
Crystal system	monoclinic
Space group	P2 ₁ /n
a/Å	13.012(8)
b/Å	14.770(10)
c/Å	36.76(2)
α/°	90
β/°	90.112(10)
γ/°	90
Volume/Å ³	7064(8)
Z	4
ρ _{calc} /g/cm ³	1.44
μ/mm ⁻¹	0.385
F(000)	3143
Crystal size/mm ³	-
Radiation	MoKα (λ = 0.71073)
2θ range for data collection/°	2.216 to 53.25
Index ranges	-15 ≤ h ≤ 16, -17 ≤ k ≤ 13, -44 ≤ l ≤ 43
Reflections collected	35077
Independent reflections	12879 [R _{int} = 0.0708, R _{sigma} = 0.1061]
Data/restraints/parameters	12879/862/969
Goodness-of-fit on F ²	1.085
Final R indexes [I ≥ 2σ (I)]	R ₁ = 0.0999, wR ₂ = 0.2308
Final R indexes [all data]	R ₁ = 0.1436, wR ₂ = 0.2499
Largest diff. peak/hole / e Å ⁻³	0.68/-0.70

Appendix C DFT Analysis

C.1 Chapter 3: Preparation of Low-Coordinate Ni(I) Amidate Complexes and Reactivity of Ni(I) Complexes Towards C(sp³)-H Activation

The geometry optimization for **6** was performed without restrictions in Gaussian 09^[13] at the PBE0-D3/6-31G(*d,p*) level of theory^[14] with the inclusion of Grimme's dispersion corrections^[15]. The LANL2DZ effective core potential (ECP) and associated basis set augmented by a *f*-polarization function^[16] was used for Ni. A single point calculation at the PBE0-D3/6-311+G(2*d,p*) level of theory (SDD+*f* for Ni) was performed on the optimized geometry to obtain orbitals for further analysis. Natural Bond Order (NBO) calculations were performed in using the standalone NBO 6.0 program^[17] after generating the appropriate *.47 input files using NBO 3.0 as implemented in Gaussian 09. Atoms in Molecules (AIM) analysis was performed using AIMALL.^[18] To probe whether the change in geometry on going from the solid-state structure to the gas phase optimized structure significantly affected the nature of the CH₂...Ni interaction, an additional calculation was performed. The location of hydrogen atoms in **6** were optimized starting from a structure generated from the X-Ray crystallographic heavy atoms coordinates. The non-hydrogen atom positions were frozen during the calculation. No significant elongation of the C-H bonds was observed, and therefore we limit our discussion to the freely optimized geometry of **6**. Table S1 compares C-H and Ni-H bond lengths calculated in free and constrained optimizations as well as the experimental values determined *via* diffraction. For consistency, the numbering scheme used in the computational data is consistent with that assigned to the solid-state structure of **6**.

For more information see SI of: *Angew. Chem. Int. Ed.* **2016**, 55, 13290-13295